University of Newcastle upon Tyne

Department of Civil Engineering

A FRACTURE MECHANICS STUDY OF UNASSISTED AND WATER JET ASSISTED ROCK DISC CUTTING

by

XUANLIANG ZHAO

A thesis submitted in partial fulfilment of the requirement for the Degree of Doctor of Philosophy in the Faculty of Engineering at the University of Newcastle upon Tyne

January, 1989

ABSTRACT

The work presented in the thesis introduces the use of the principles of fracture mechanics on the mechanism of rock breakage by disc cutters with and without water jet assistance. The work may be divided into five major parts:

1. Rock fracture tests; The values of fracture toughness are measured from three different directions of the rock blocks by three different testing methods: radially cracked ring specimens, three point bend specimens and short bar specimens. The effect of moisture on the fracture toughness was also investigated.

2. Indentation tests; A primary study of the use of a disc cutter as a type of indenter has been carried out. These tests provided a parameter, contact pressure, for predicting the disc cutting forces and understanding the fragmentation of the rock during cutting.

3. Water jet assisted disc cutting tests; The factors influenced the performance of water jet assisted disc cutting were investigated, including: a) The pressure of the water jet; b) The position of the water jet nozzle; c) The cutting speed; and d) The spacing distance and penetration depths.

4. Theoretical analysis of disc forces; Based on a widely accepted assumption, a simple mathematical model was developed for the relationships between the cutting forces. The indentation fracture theories were used to predict the performance of disc cutting. A further use of the predictor equations in the water jet assisted cutting was also investigated.

5. The analysis of stress distribution beneath the disc cutter; Boundary element method was used in the investigation of the stress distribution beneath the disc cutter. The effects of geometries of the disc cutters, spacing distance, penetration depth were also considered.

ACKNOWLEDGEMENTS

The author would like to thank:

Dr. E.K.S. Passaris, lecturer in Geotechnical Engineering, and Dr. A. Rispin, former lecturer in Geotechnical Engineering, for providing the opportunity to carry out the research and for their supervision and encouragement.

Prof. C.J.F.P. Jones, head of the Department of Geotechnical Engineering, and Mrs J.Y. Butterfield, assistant in British Council, for their valuable help.

British Council, Fuxin Mining Institute (China), and The Britain - China Educational Trust for supporting him financially during his study.

Mr. J. Jack for his friendship and help in checking the manuscript.

Mr. T. Shepherdson and his staff, for their cheerful assistance.

Dr. J. Zhao, Dr. D. Wen, Dr. G. Xiao (former students in Geotechnical Engineering), Mr. M. Chen (student in Geology), and Mr. D. Jiao (student in Mining Engineering) for their help and friendship.

The author also wishes to express his sincere appreciation with love to his wife, Ju Qiu, and son, Yi Zhao, for their understanding, patience, assistance and encouragement.

CONTENTS

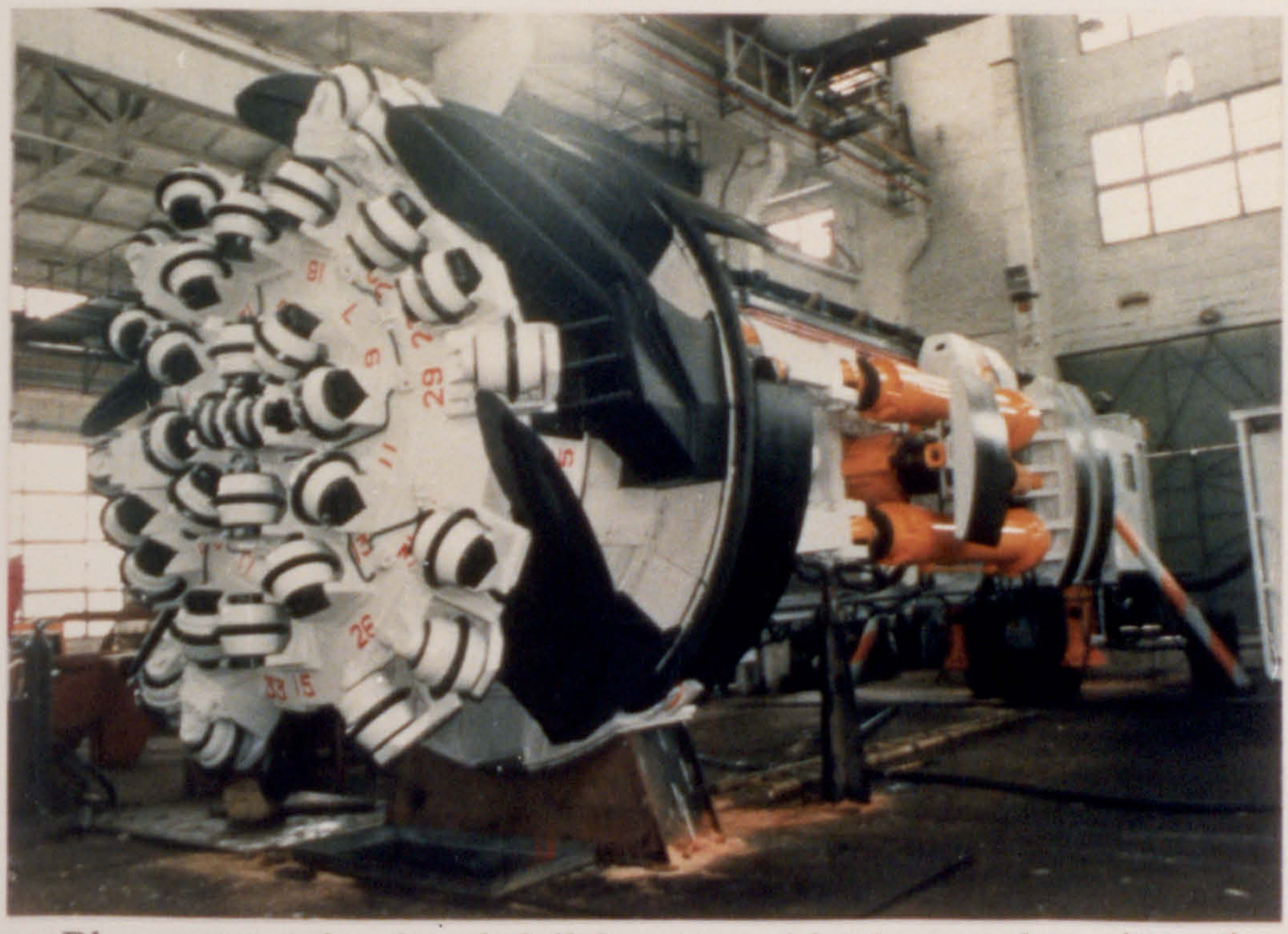

Plate 1.0.1 A hard rock full-face tunnel boring machine (TBM) made in China

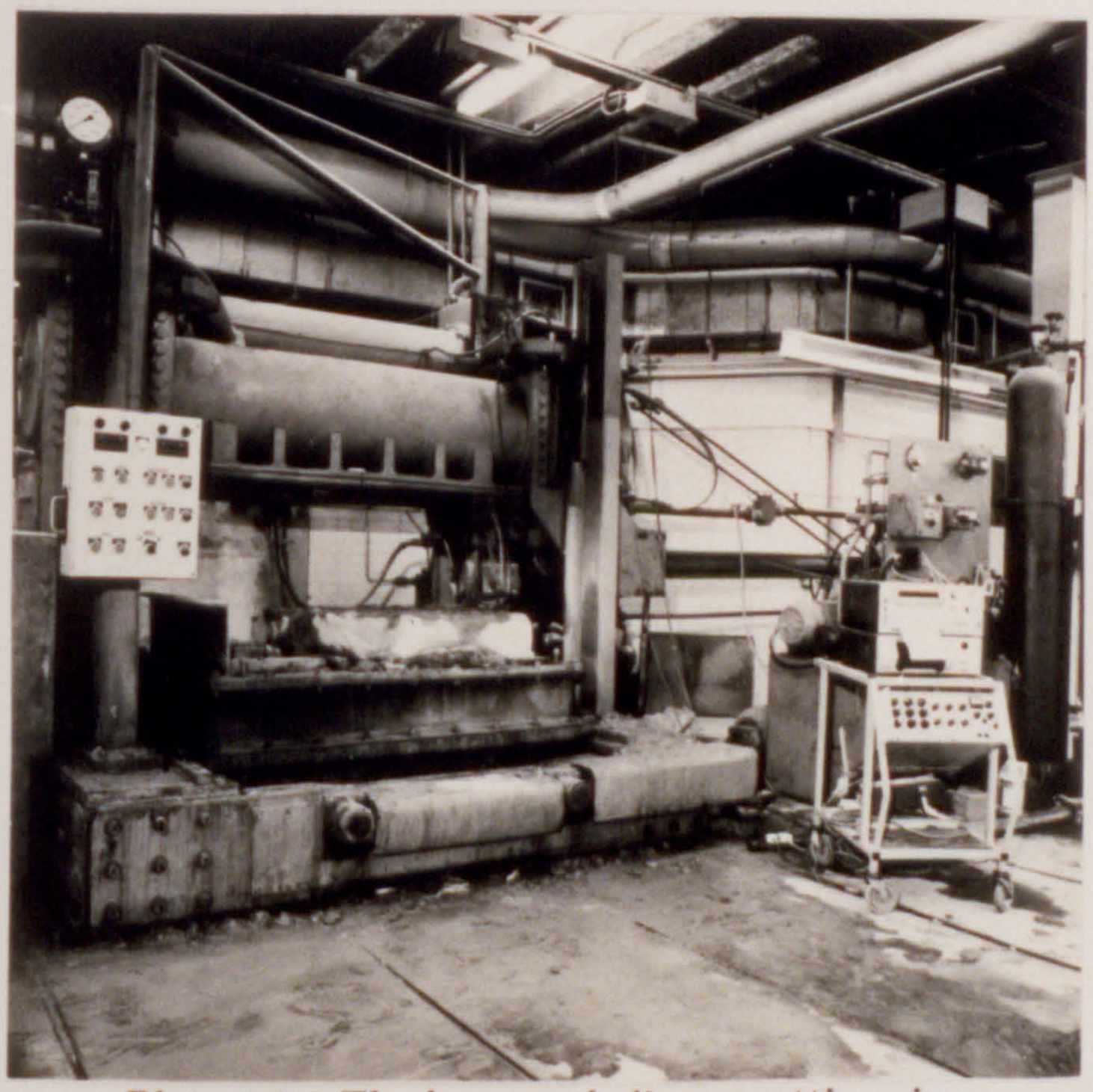

Plate 1.0.2 The large scale linear cutting rig

Chapter 1

INTRODUCTION

This chapter presents the purpose and scope of the research into the application of rock fracture mechanics on water jet assisted and mechanical rock cutting. The contents of this research, are directly linked to the most current tunnel boring machines (TBM's) developments.

The greatly increased demand for faster and cheaper methods of constructing underground openings, such as tunnels and shafts, has strained present-day excavation technology. Drilling and blasting, the so called "conventional method", is cyclic in nature and consists of several individual operations — drilling, blasting, and removal of the debris — which cannot be performed simultaneously. Thus, while the introduction of hydraulic drilling machines and smooth wall blasting techniques have improved the old method considerably, more and more mining and civil engineering tunnelling companies prefer to use continuous tunnelling machines.

There are two basic classes of machines concerned with excavation in solid ground:

1. full-face tunnel boring machines (TBM's) which cut the full face of the tunnel while being advanced continuously along the tunnel axis (see Plate 1.0.1). Machines in this class are capable of cutting circular cross sections or rectangular cross sections.

2. roadheaders which make a localised attack on the face with cutter heads substantially smaller than the dimensions of the face, sweeping across the face and

thus advancing incrementally. Machines in this class are capable of cutting non-circular cross sections.

The subject of the research project is the disc cutting tool as developed from that which was first applied to tunnel boring in 1953 by Jim Robbins. Now, this type of cutter is widely used in tunnel boring machines (TBM's) for full-face tunnel excavation, as well as shaft boring machines (SBM's) for mines shafts and the "Mobile Miner" for tunnels with a rectangular cross section.

Many of the most important changes in TBM technology over the past 30 years have been made in response to the increasing demand for these machines to bore tunnels through so called "hard" rocks rather than through the generally weaker and sedimentary rocks for which the first machines were designed. The advantages of using such a machine are obvious (Woodley, 1979):

1. the circular roadway section presents the strongest shape for resisting pressures;

2. the strata through which the machine is driven is relatively undisturbed and thereby the introduction of new rock stresses is minimised;

3. the smoothly cut profile distributes loads on supports more uniformly and hence lighter and cheaper supports can be used;

4. the danger of rockfalls is reduced as is that of handling explosives;

5. whilst on average, the drivage rates achieved are more often than not in line with those achieved with conventional methods, impressive rates have been achieved, e.g. maximum rates of 64 m/day and average rates of 43 m/day have been obtained in shales of 62 MPa compressive strength. Basically, the most modern TBM's are capable of achieving average progress rates which are three to six times greater than those which are obtained by conventional means.

All these point to the conclusion that as the years roll by more and more tunnels will be driven by TBM's and cost per metre will come down. It is no surprise then that eleven TBM's are to be used to drive the Channel Tunnel (Tunnels & Tunelling, May, 1988).

Such tunnelling machines, however, also have their limitations:

1. the high initial cost in many instances must be written off against a limited number of tunnel drivages. This factor in addition to the time and labour involved in the assembly and dismantling of the machine, makes them uneconomic in drivages shorter than around 3,000 m;

2. mechanical failure is costly in such sophisticated machines, for example, failure of the head bearings can involve extended downtime. This problem becomes more acute when the machine cuts through very hard rock.

3. the circular tunnel section can give rise to operational difficulties due to the resultant restricted floor width.

4. the machines can not be used to drive sharp curved tunnels.

Recent advances in high-pressure water jet technology can be effectively employed in mining and tunnelling. This new technology has been thought as the first significant development since the introduction of electrically powered underground mining machines in the 1930's and 1940's. Its role is seen mainly as an aid to mechanical cutting, whereby the high cutting forces and wear on mechanical cutters is reduced. The principal advantages of water jet assisted cutting relative to mechanical cutting are the higher progress rates, lower dust levels and reduced fines. More and more attention has been given to investigate and improve the efficiency of high-pressure water jet assisted mechanical tools cutting since the 1980's, and the

new roadheaders equiped with water jet have demonstrated the potential. However, the overall performance of high-pressure water jet assisted TBM's is the subject of financial cost. It has been observed that while the TBM assisted by water jets has technological advantages, it is not economical. Other disadvantages are related to system operation, reliability and safety.

Much research work aimed at improving the potential for and performance of cutting arrays has been carried out in USA, USSR, West Germany, South Africa, Japan, Australia and the United Kingdom. The work done for this Ph.D. project is undertaken in the Department of Geotechnical Engineering, at the University of Newcastle upon Tyne. The major objectives of the present work are the laboratory investigation of the performance of mechanical and water jet assisted disc cutting. Low pressure water jets are used to avoid the above mentioned disadvantages associated with high pressure cutting. An application of the principle of fracture mechanics in theoretical and experimental analysis of disc cutting is also presented.

This thesis comprises nine Chapters.

The previous work in the field of rock cutting with a disc cutter, involving theoretical and experimental analysis of mechanical disc cutting and water jet assisted disc cutting, is reviewed in the Chapter 2.

The experimental equipment and procedures are described in Chapter 3.

In Chapter 4, the measurements of fracture toughness for the rock materials used, are tabulated for further use in predicting the performance of TBM's. The methods for measuring the fracture toughness are studied.

It is believed that an improved understanding of the indentation technique — which is used in one way or another in most of today's mining, tunnelling and

drilling operations — will lead to an improvement in rock excavation technology. Therefore the study investigates the disc cutter as a type of indenter to (i) improve our understanding of the the fragmentation of the rock during cutting, and (ii) facilitate improved prediction of the performance of TBM's. The work on the indentation tests is described in Chapter 5, and their use to predict the performance of rock cutting is described in Chapter 7.

The rock cutting tests were carried out on both large and small scale linear cutting rigs (Plate 1.0.2), and results are presented in Chapter 6. The work included an evaluation of testing methods, mechanical and water jet assisted cutting, the effects of rock properties and so on.

For the water jet assisted cutting process, factors which influence the efficiency of water jet assisted disc cutting were investigated. Such factors considered were:

a. the pressure of water jets;

b. the position of water nozzles;

c. the speed of disc cutting;

d. the spacing distance and penetration depth.

An analysis of the mechanisms of rock cutting by mechanical tools only, by high pressure water jet assisted tools and by low pressure water jet assisted tools is also given in this chapter.

Roxborough (1985), has pointed out that some simple mathematical models for discs do reflect the observed trends and relationships and often fit the measured data reasonably well, but they are all scientificaly tentative in that they rely on unacceptable assumptions and sometimes reveal glaring inconsistencies. However, a simple mathematical model of disc cutting forces that has been developed as part of the undertaken research, is presented in Chapter 7. This model, in contract

with the simple mathematical models criticized by Roxborough (1985), is capable of predicting very acceptable conclusion between experimental results and predicted response. The principles of fracture mechanics is introduced in the analysis. The comparison of the model with experimental test data is presented, and a comparative study of rock fracture parameters with the results of field TBM performance is reported.

In Chapter 8, the use of boundary element method for analysis of the stress distribution beneath the disc cutter is described. The investigation phased in the effects of edge angle and the tip radius of the disc cutters, the penetration depth and spacing distance.

In Chapter 9, conclusions are drawn and further research in this field is suggested.

In addition to the nine Chapters there are six Appendices which show all the test data.

Chapter 2

LITERATURE REVIEW OF DISC CUTTING

2.1 THEORETICAL ANALYSIS OF CUTTER FORCES AND PERFORMANCE PREDICTION OF TBMS

2.1.1 Theoretical Analysis of Disc Forces

Crow (1975) pointed out that the stresses on the contact surface A_1 produced a thrust FT resisting the advance of the tunnel boring machine and the stresses on the contact surface A_2 produced a drag FR resisting the rotation of the cutterhead. (See Fig. 2.1.1). The stress σ_0 on the contact surfaces was assumed to be uniform and normal to the contact surface. This leads the conclusion that the thrust FT equals σ_0 times the projection of A_1 on a plane parallel to the rock face, and that the cutting force FR is proportional to the projection of A_2 on a plane transverse to the motion of the disc.

If the conical disc intercepts the rock face in a pair of parabolas, it can be proved that

$$FT = \frac{4\sqrt{2}}{3}\sqrt{p^3 R}\tan\frac{\theta}{2}\sigma_0 \qquad 2.1.1$$

$$FR = p^2 \tan\frac{\theta}{2}\sigma_0 \qquad 2.1.2$$

where

p = depth of penetration,

R = radius of the disc cutter,

θ = edge angle of the disc cutter.

The relationship of the stress σ_0 and unconfined compressive strength σ_c is

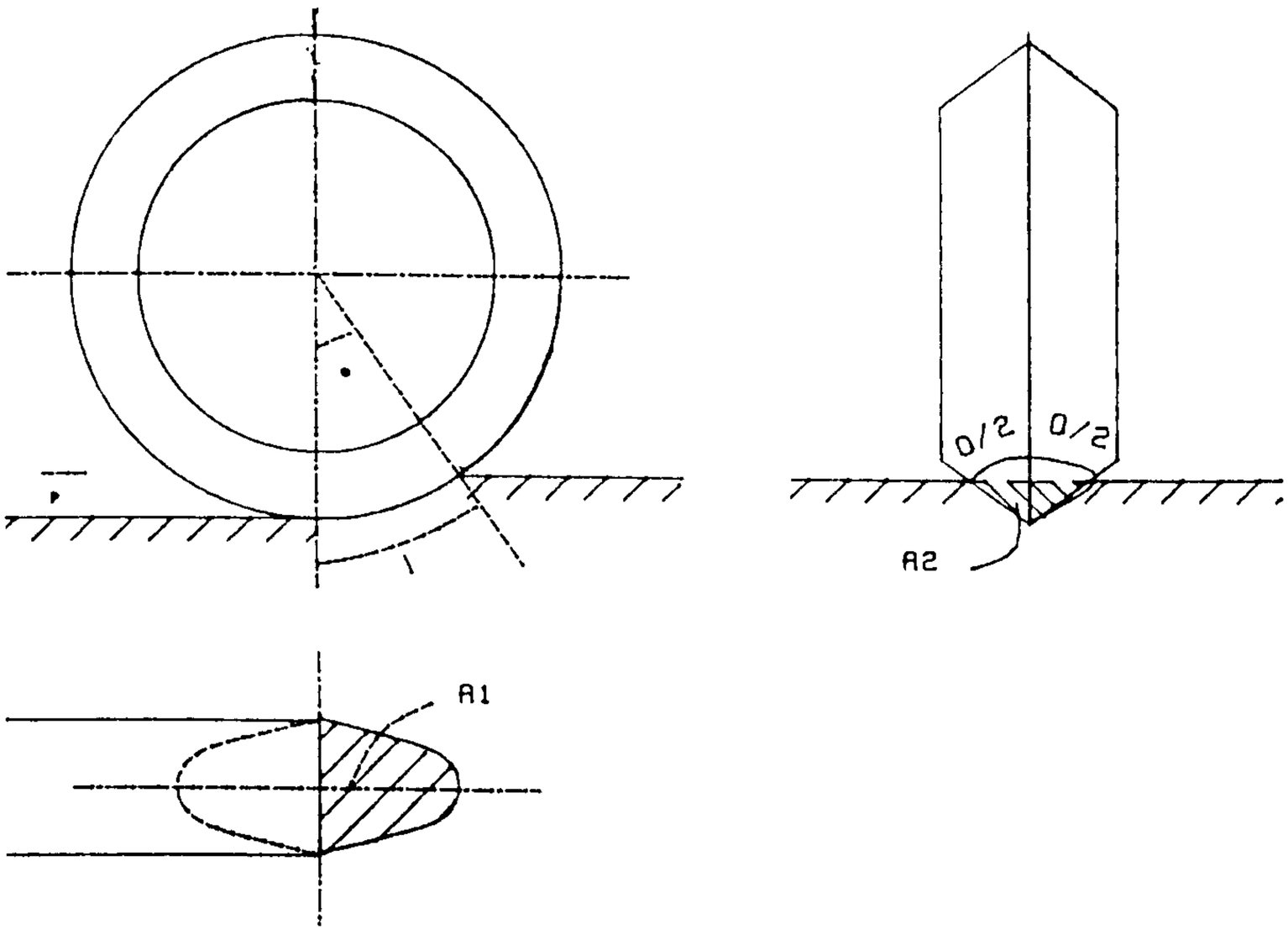

Fig. 2.1.1 Area of contact of a disc cutter with rock

given, as

$$\tan\frac{\theta}{2}\sigma_0 = 8\sigma_c \qquad 2.1.3$$

Thus the thrust force and cutting force are obtained:

$$FT = 15\sqrt{p^3}\sqrt{R}\sigma_c \qquad 2.1.4$$

$$FR = 8p^2\sigma_c \qquad 2.1.5$$

Roxborough's model (Roxborough and Phillips, 1975a) assumes that the resistance to penetration is essentially compressive and that the thrust force FT is equivalent to $\sigma_c \times A$, e.g. a compressive strength acting over the projected area of disc contact (Fig. 2.1.2). He also makes the assumption that the value of FT remains constant when the disc is made to roll. Fig. 2.1.3 represents a disc under the action of the two principal forces FT and FR. If the disc is free rolling and

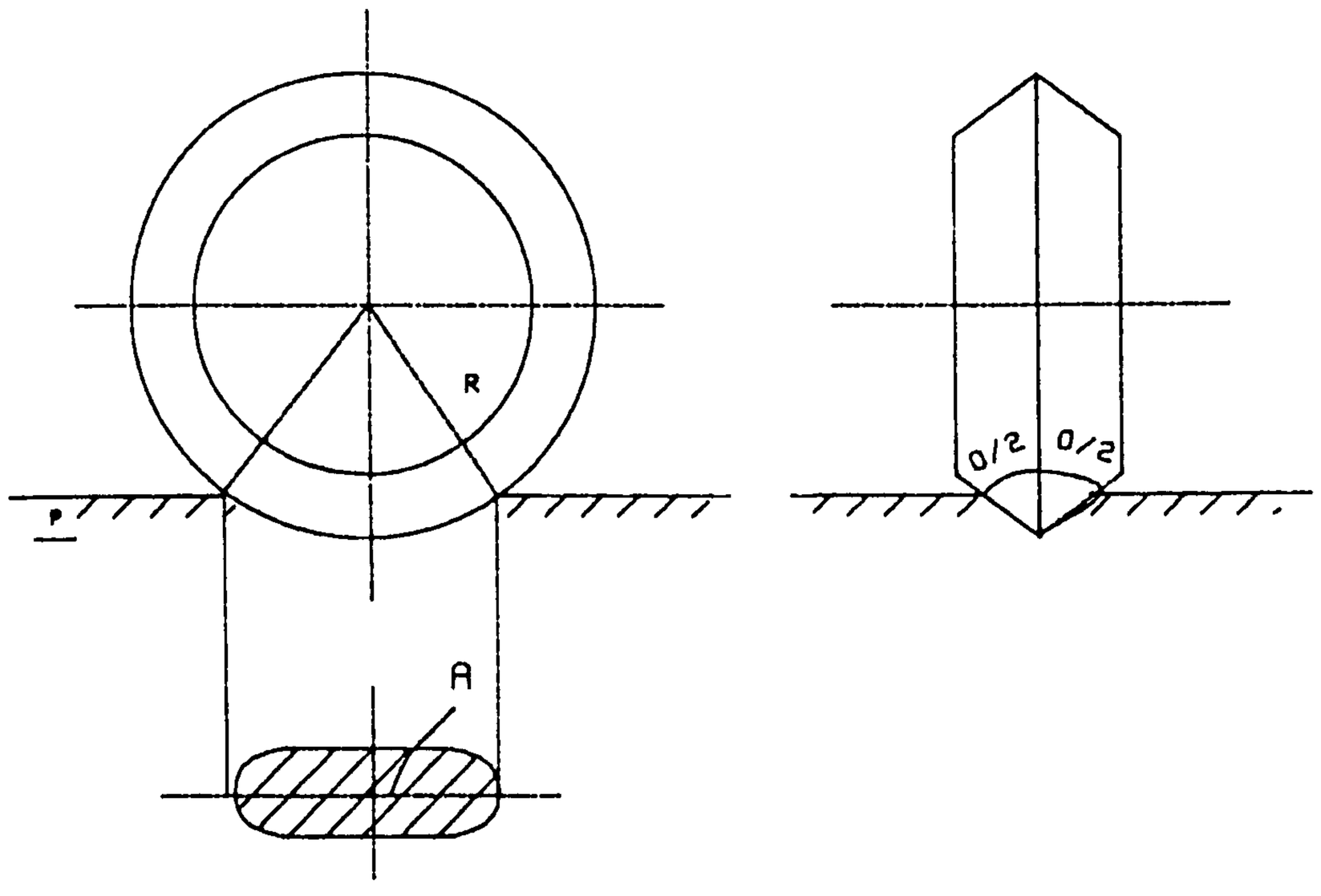

Fig. 2.1.2 Contact area of a disc cutter with rock

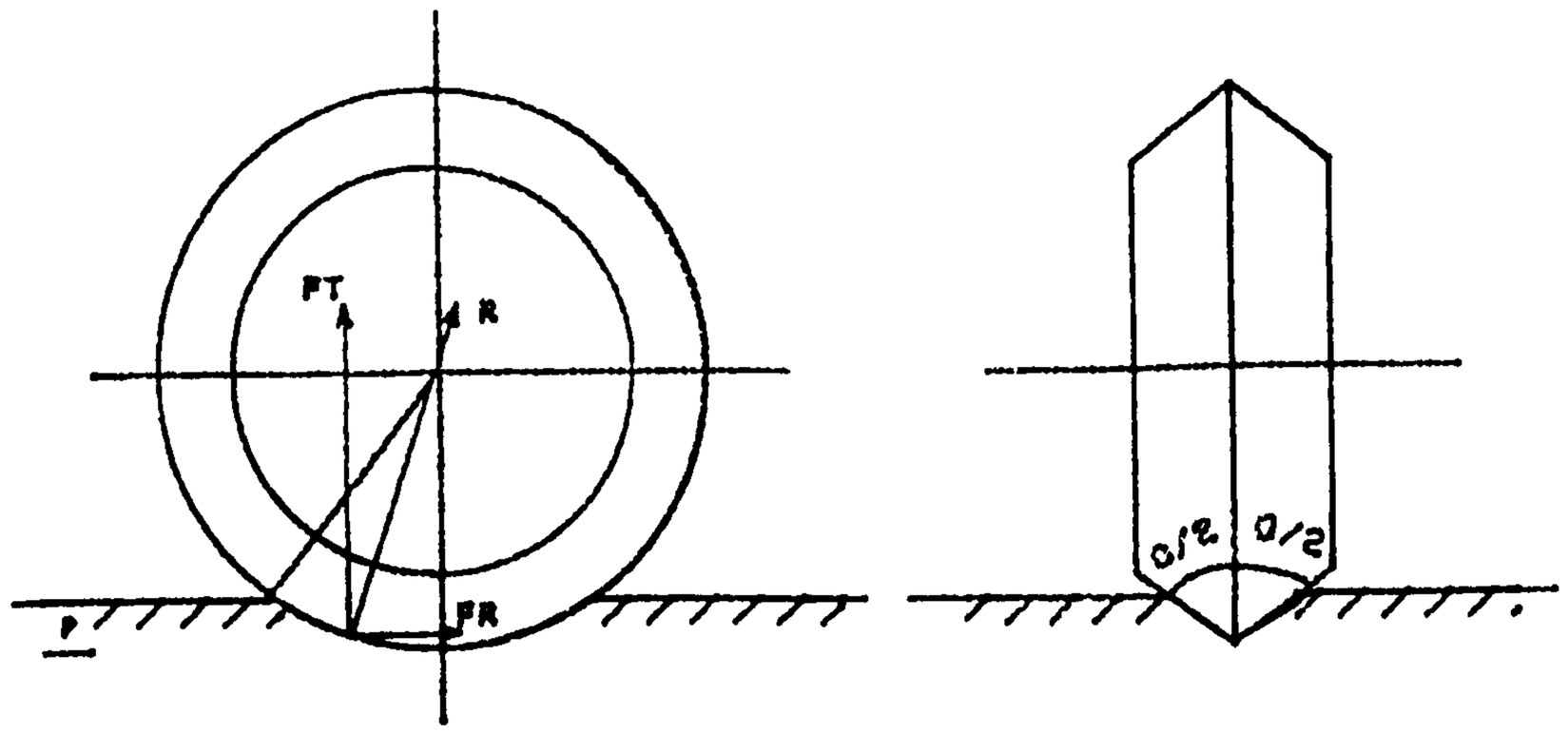

Fig. 2.1.3 The determination of the rolling force

neglecting friction, then the line of action of the resultant R must pass through the centre of rotation to satisfy the zero net torque condition. Thus, the thrust force is given as:

$$FT = 4p\sqrt{Dp - p^2}\tan\frac{\theta}{2}\sigma_c \qquad 2.1.6$$

where

D = diameter of the disc cutter;

and the rolling force:

$$FR = 4p^2\tan\frac{\theta}{2} \qquad 2.1.7$$

Furthermore, an expression for the optimum spacing, s, to penetration ratio (s/p) is derived as

$$\frac{s}{p} = \frac{\sigma_c}{\tau} \qquad 2.1.8$$

where

τ = shear strength of the rock.

Meijer (1977), however, pointed out that the agreement between theory and experiment indicated that the penetration strength was approximately 1.5 times the unconfined compression strength in this case.

Ozdemir et al. (1977), considering the effect of spacing, divided the predictor equation of thrust force into two parts, an intercept and a linear slope.

The intercept component is given as:

$$F_1 = \sigma_c A \qquad 2.1.9$$

where

A = area of contact of cutter with the rock measured at the level of rock surface.

This contact area is represented in Fig. 2.1.1 by the shaded portion of the cutter contact area.

The function constituting the linear portion of the predictor equation is based on a considerations of shear failure of the rock to the adjacent cut(s), and the side force exerted by the cutter to overcome the shear resistance:

$$F_2 = 2\tau s R\phi \tan\frac{\theta}{2} \qquad 2.1.10$$

where

$\phi = \cos^{-1}(\frac{R-p}{R})$.

The actual width of the chip(s) should be less than the value given by Eq. (2.1.10) considering the fact that the rock surrounding the penetrating edge of the cutter is locally crushed and the force required to shear this zone should be minute. Assuming the width of the crushed zone to be $2p\tan\frac{\theta}{2}$, Eq. (2.1.10) was replaced by

$$F_2 = 2\tau R\phi(s - 2p\tan\frac{\theta}{2})\tan\frac{\theta}{2} \qquad 2.1.11$$

Thus, incorporating the possible approximations into the equation yields:

$$FT = \sqrt{Dp^3}[\frac{4\sigma_c}{3} + 2\tau(\frac{s}{p} - 2\tan\frac{\theta}{2})]\tan\frac{\theta}{2} \qquad 2.1.12$$

Considering the disc condition as shown in Fig 2.1.4, the rolling force is given by

$$FR = [\sigma_c p^2 + \frac{4\tau\phi(s - 2p\tan\frac{\theta}{2})}{D(\phi - \sin\phi\cos\phi)}]\tan\frac{\theta}{2} \qquad 2.1.13$$

An attempt also was made by authors to predict the cutting forces of worn disc cutters.

For penetrations less than $r(1 - \sin\frac{\theta}{2})$, it gives

$$FT = \sqrt{Dp}[\frac{4}{3}\sigma_c d + 2\tau(s - 2d)\frac{\gamma - \sin\gamma\cos\gamma}{1 - \cos\gamma}] \qquad 2.1.14$$

where

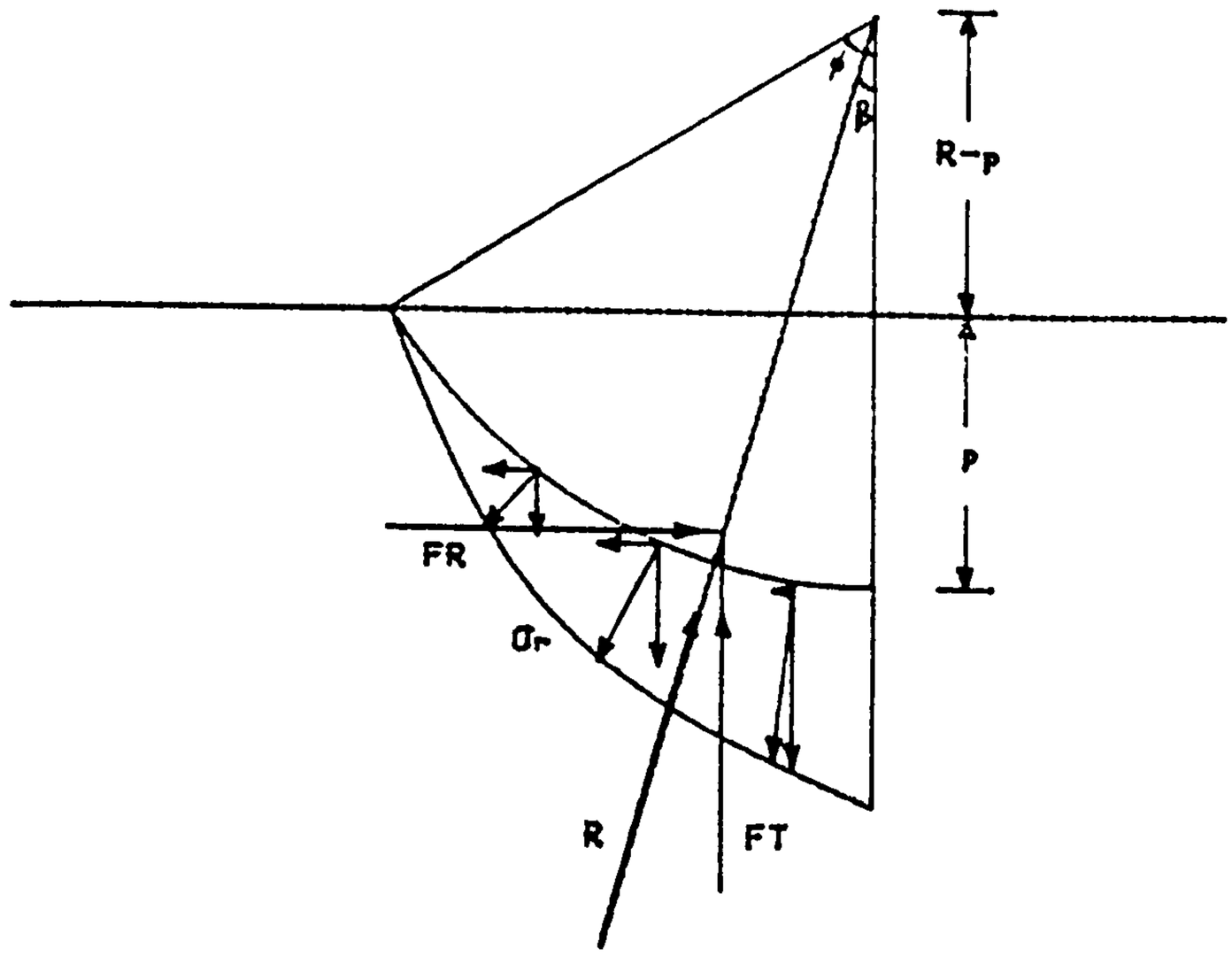

Fig. 2.1.4 Representation of the resultant force and its vertical and rolling components on the cutter-rock contact surface

r = radius of cutter tip,

$d = \sqrt{2rp - p^2}$,

$\gamma = cos^{-1}(\frac{r-p}{r})$.

and for for penetration greater than $r(1 - \sin\frac{\theta}{2})$, it is:

$$FT = \sqrt{Dp}[\frac{4}{3}\sigma_c d + 2\tau(s - 2d)]Z \qquad 2.1.14b$$

where

TL = cutter tip (radius) loss due to wear,

$d = (p + TL)\tan\frac{\theta}{2}$,

$Z = \frac{(r\cos\frac{\theta}{2}+d)(p-TL\sin\frac{\theta}{2})+R^2(\gamma-\sin\gamma\cos\gamma)}{p^2}$.

The existence of a wear surface does not influence the cutting coefficient and

its value for dull cutters is exactly the same as for sharp cutters. It is,

$$FR = FT \tan \beta \qquad 2.1.15$$

where

$\tan \beta = \frac{(1-\cos \phi)^2}{1-\sin \phi \cos \phi}$, cutting coefficient.

It should be noted that one of the most important assumptions made by the author, is that of the frictionless cutter/rock interface. Therefore, considering the possible effect of a cutter/rock interface with friction, Fig. 2.1.5 shows the effect on the resultant force R. Thus comparison with Fig. 2.1.6 (as given by the author) is to find that fv is equal to $FT/2$ but not $F_2/2$.

A recent report given by Sanio (1985), shows the prediction of the performance of disc cutter in anisotropic rock. It is assumed that the dominant chip forming mechanism of disc cutter is not due to shear failure but tensile. The formula is given as:

$$FT = Sk\sqrt{dsp} \tan \frac{\theta}{2} \qquad 2.1.16$$

$$FR = \frac{4}{5}\sqrt{\frac{p}{d}}FT \qquad 2.1.17$$

where

Sk = the cutting constant which has the dimension of a stress intensity factor of force/length$^{3/2}$.

In order to derive the empirical relation between the cutting coefficient Sk and the point load index Is from a wide range of experimental data, test results and in situ data of several other authors are considered in addition to data from Sanio's (1983) cutting tests and in situ measurements. It is given

$$Sk = f\sqrt{Is_{50}} \qquad 2.1.18$$

where

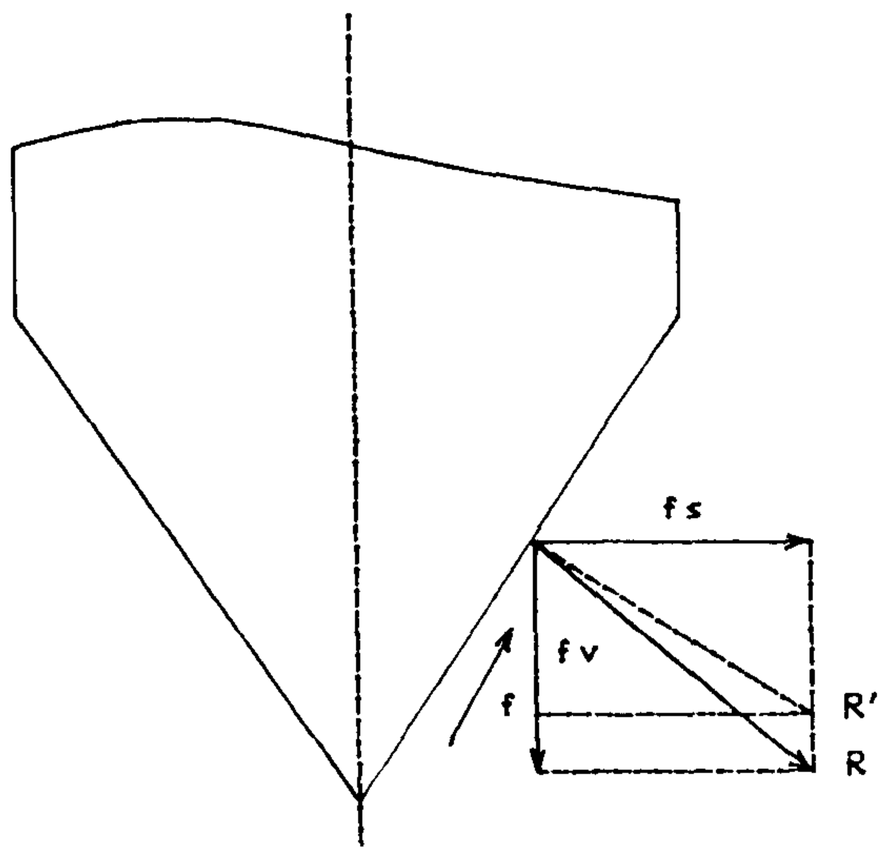

Fig. 2.1.5 Rotation of the resultant with the existence of rock-cutter friction

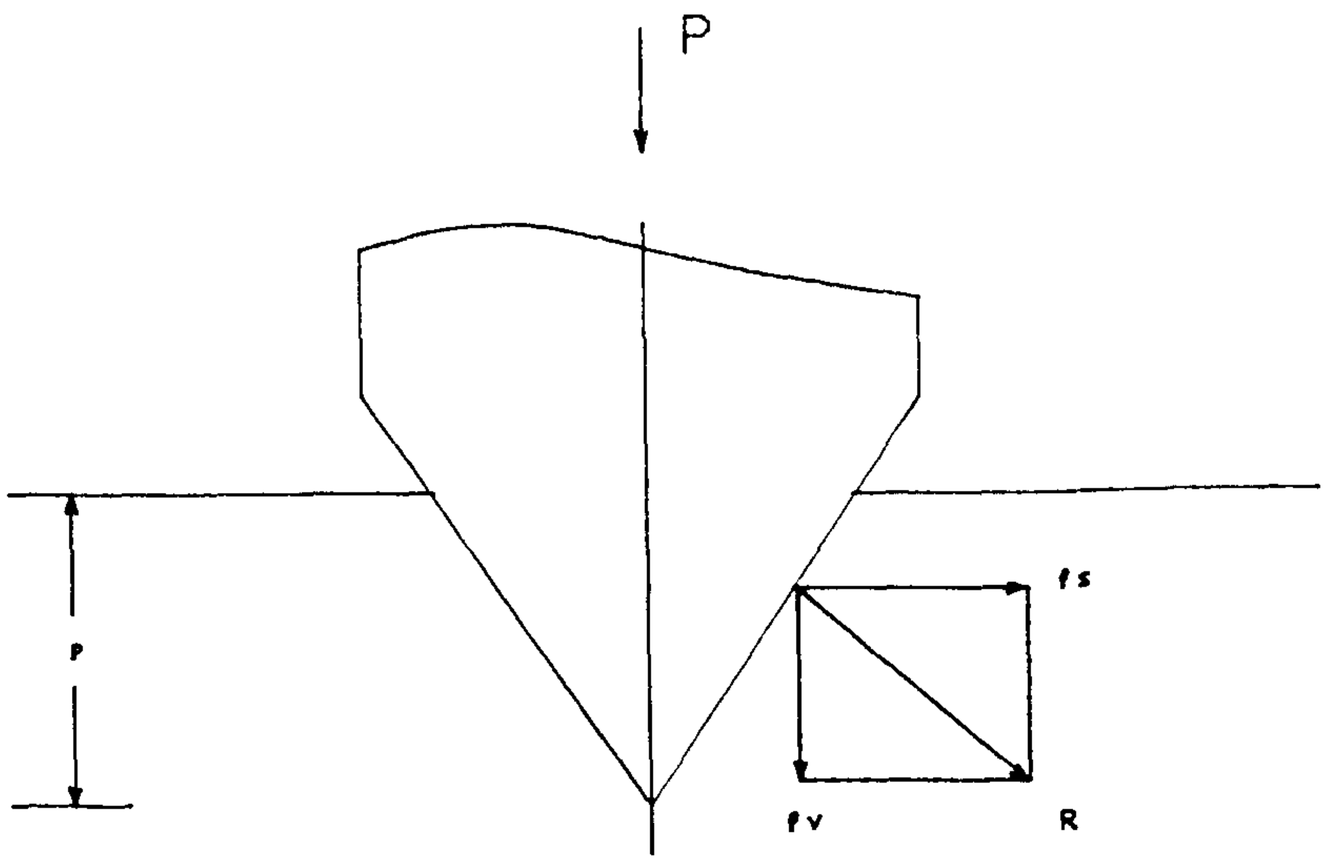

Fig. 2.1.6 Geometry of disc penetration

$f = 3/25$;

Is_{50} = point load index with core diameter of 50 mm.

In addition to the theoretical analysis, some researchers presented experimental methods for the prediction of disc cutter performance.

Nelson and Fong (1986) found that the prediction of disc cutter forces and force-penetration relationships was possible using fracture material properties. Laboratory measurements of G — critical crack driving force — could be used to estimate non-interactive cutter forces for selected cutter diameters and penetrations:

$$\frac{(FT)_{ni}}{p} = \frac{G}{3.8} \qquad 2.1.19$$

$$\frac{(FR)_{ni}}{p} = \frac{G}{4.2} \qquad 2.1.20$$

where

$(FT)_{ni}$ = non-interactive thrust force,

$(FR)_{ni}$ = non-interactive rolling force,

Rispin and Bilgin (1977) derived the equations for the prediction of the forces, yield and specific energy, from the disc penetration, edge angle and diameter, which were reported to be satisfactory.

The results from a single tool can be applied on the cutter head by summing the tool forces (Fauvel, 1981). Therefore, by considering only thrust and rolling forces, and assuming that the tools are normally mounted at equal groove spacings on a flat cutter head, the following relationships are obtained:

$$T_h = \sum_{n}^{1} FT \qquad 2.1.21$$

$$T_q = \sum_{n}^{1} (FR \times R) \qquad 2.1.22$$

$$s = \frac{d}{2}(n-1) \qquad 2.1.23$$

where

n = number of cutting tools,

T_h = total thrust force (mean),

T_q = total torque (mean).

Although the dynamic behaviour of a disc cutter is complex, its primary action is considered to be similar to that of a wedge penetrating a rock surface. Hence, some models proposed for drag picks are also applicable to disc cutters (Nishimatsu, 1972). However, though more mathematical derivation has been done, generally, such models do not agree with the experimental cutting results very well, suggesting that these models are not the favourite with disc cutting research.

2.1.2 Performance Prediction of TBM's

There are two main groups of methods for predicting the penetration rate of full face boring machines. Methods of the first group make use of the compressive strength, tensile strength, or shear strength of the rock to be bored; methods of the second group involve various indices obtained from indentation tests (Howarth, 1986). The methods of both groups are known to yield acceptable predictions. Some of the formulas used are given as follows:

Farmer and Glossop (1980)

$$P = \frac{624 F_n}{\sigma_t} \qquad 2.1.24$$

where

p = penetration per revolution, mm/rev,

F_n = average cutter force, kN,

σ_t = tensile strength, kPa,

$$V = \frac{29.4 F_n RPM D^2}{\sigma_t} \qquad 2.1.25$$

where

V = volume of rock excavated in unit time, m /h,

RPM = rotary speed, rev/min,

D = diameter of tunnel boring machine, m.

Graham (1976)

$$p = \frac{3940\ F_n}{\sigma_c} \qquad 2.1.26$$

where

σ_c = compressive strength, kPa.

Cassinelli et al. (1982)

$$v = -0.059\ PSR + 1.59 \qquad 2.1.27$$

where

v = TBM penetration rate, m/h,

RSR = rock support rating.

Bamford (1984)

$$P = 0.535S - 8.49 - 0.00344T - 0.000823N + 0.0137P \qquad 2.1.28$$

where

P = penetration rate, m/h,

S = Schmidt hammer hardness,

T = machine thrust force, t,

N = NCB cone indenter index, N/mm,

P = angle of shearing resistance, degrees,

Hughes (1986)

$$V = \frac{6p^{1.2}Nn}{\sigma_c{}^{1.2}r^{0.6}} \qquad 2.1.29$$

where

V = rate of advance, m/h,

p = thrust per disc periphery, kN,

N = speed of cutting head, rev/s,

n = average number of disc per kerf,

σ_c = unconfined compressive strength, MPa,

r = average radius of discs, m.

$$PW = 28.45D + 9.07D^2 \qquad 2.1.30$$

where

PW = power, kW,

D = TBM diameter, m.

Tarkoy and Hendron (1975)

$$FT = K_1 \times \sigma_c \qquad 2.1.31$$

or

$$FT = K_2 \times H_t \qquad 2.1.32$$

where

H_t = Total Hardness,

K_1 = 70,

K_2 = 100 to 500.

$$T = FT \times n \qquad 2.1.33$$

where

T = Total thrust, kN,

n = number of cutters.

$$FR = C_c \times FT \tag{2.1.34}$$

where

$$C_c = \begin{cases} 0.1 & \text{for hard rock,} \\ 0.15 & \text{for soft rock.} \end{cases}$$

$$t = \sum_{i=1}^{n} (FR \times R_i) \tag{2.1.35}$$

where

t = torque, kN-m,

R_i = radius or moment arm of each cutter, m.

Farmer et al. (1986; Farmer, 1987)

$$\frac{Pc}{VER} = \frac{\sigma_{cf}^2}{E} \tag{2.1.36}$$

where

P = cutting need power MW or MJ/s,

c = the power efficiency or transfer ratio,

VER = the volume excavation rate,

σ_{cf} = the rock strength,

E = deformation modulus or stiffness.

Athorn et al. (1983)

$$E = PS_oV \tag{2.1.37}$$

where

E = the energy input,

P = the surface energy required to satisfy unit area of new crack formed.

S_o = the area of new crack formed per unit volume of rock

V = the volume of rock affected.

2.2 DISC CUTTING TESTS

A considerable amount of experimental work has been performed in the area of rock breakage by various cutter tools, and different authors have used different test procedures and ways of analysis, the resulting main conclusions are very similar. In this section, the factors in the performance of disc cutting are reviewed.

2.2.1 Specific Energy

Specific energy — as the amount of energy required to remove a unit volume of rock — has been widely used as an important index to commend the efficiency of a rock cutting system. A system with the lowest value of specific energy is considered to be the most efficient.

A comparison of laboratory specific energy, as measured on a laboratory linear cutter and in-situ specific energy, measured on a full face tunnelling machine was made by Hustralid (1972). The results show that the laboratory specific energy is greater than that observed in the field, and that the relationship was approximately linear. The same conclusion was given by Rad (1975,a). The possible reason is that the ways of rock breakages are different between the laboratory tests and in-situ tests. The specific energy measured in the laboratory were from so called "single pass cutting tests", e.g., the cutting tests were performed on a smooth rock surface, but the specific energy measured in the field were on the rough rock surface and in a way "multiple cutting". The difference of these two cutting methods was discussed

by Kutter and Sanio (1983).

2.2.2 Penetration, Spacing Distance and s/p Ratio

Penetration is likely to be the most dominant variable in disc cutting. Several authors (Teale, 1964; Bruce and Morrell, 1976) have concluded that there is a linear relationship between penetration and thrust. Gaye (1972) also observed a linear increase in penetration with increasing thrust for a field machine. Yet, others (Rad and Olson, 1974) have concluded that the higher thrusts are more efficient for breaking rock in terms of volume of material excavated and minimum specific energy. Early work by Takaoka et al. (1973), however, showed that penetration increased at a decreasing rate with increasing normal cutter force.

The effect of cutting spacing was examined in greater depth by Rad and McGarry (1971), Rad (1975) and Rad and Olson (1974). A variety of rock was involved in the tests and a constant normal force, 31 kN (7,000 lb), was used in all experiments. They defined the behavior of cutting as several terms: critical spacing, at which adjacent grooves only just interact; optimum spacing, at which there is complete breakout between grooves and for which debris yield is a maximum and specific energy a minimum; and pre-optimum range of spacings, which covers the spacings smaller than the optimum. All tests were performed on the level trimmed surfaces of rocks. At the given level of thrust, it is seen that the optimum spacing is dependent on the rock type. The effect of multiple passes to achieve steady excavation was also investigated. With a constant normal force, a series of 15 equally spaced parallel grooves were made in Granite, and the material yield and specific energy reached steady state after five passes. Rad (1974) also carried out some tunnel boring experiments on the effects of spacing on the cutting forces.

Ozdemir et al. (1977) performed laboratory tests covering a wide range of

Table 2.2.1 Optimum s/p ratios for sharp disc cutters

Optimum s/p ratio	Cutter included angle θ [degree]				
	60	70	80	90	100
2.5	[88]			[88]	
3.0				[17,88]	
3.5	[122]			[122,88]	
4.0	[116,122]	[116]	[116]	[116,122]	[116]
4.5				[122,88]	
5.0	[121,87,39,122]			[110]	
5.5	[101]	[39]			[102]
6.0	[16,119,38,109]	[10,119,38,87]	[10,38]	[10,119,38,122]	[10,38]
7.5					[119]
8.0	[79]				[118]
8.5				[17]	
9.0	[79]				
11.0				[17]	

Table 2.2.2 Optimum s/p ratios for worn disc cutters

Optimum s/p ratio	Wear tip radius (mm)				
	1.0	1.5	2.0	2.5	3.0
5.0		[29]			
5.5	[101]60°	[29]			
6.0	[10]60°				
6.5			[101]60°		
7.0				[10]60°	[101]60°
7.5	[119]100°			[133]80°	
8.0	[118]				
8.5				[136]80°	
10.0				[134,136,146,133]80°	
12.0				[134,136]80°	
15.0				[134,34]80°	
16.5				[136]80°	
18.0				[136]80°	

s/p ratios and found that the cutter force continually increased with increasing s/p ratio. They suggested that the cutting spacing should be at or beyond the optimum, as closely spaced cutter were observed to cause unnecessary overcrushing of rock, thus requiring higher thrust levels to achieve a given penetration.

Introducing the work carried out in the Transport and Road Research Laboratory, Temporal et al. (1983) concluded that for the single pass cutting the minimum specific energy was obtained at a well defined value of s/p ratio for a given rock type. This s/p ratio was found to be independent of the tool penetration. However, they also noted that the specific energy at the most efficient s/p ratio was found to decrease asymptotically with increasing penetration. This indicated that a "critical" value of penetration existed beyond which no significant improvement in specific energy would occur.

Work to determine optimum s/p ratios has been undertaken by many investigators. A very recent report presented by Howarth and Bridge (1988) gave the optimum s/p ratios obtained from published results for sharp disc cutters and blunt disc cutters. Table 2.2.1 and Table 2.2.2 list these results and some unpublished results.

2.2.3 Cutter Geometry

For disc roller type cutters, the geometry is defined by the diameter and the edge angle. The analysis of laboratory tests results given by various authors has indicated that the edge angle has a significant effect on cutter performance, and that the cutter diameter has only a minor influence on the thrust force and virtually no effect on the rolling force. For a constant penetration with tools of increasing wedge angle, however, the critical s/p ratio was found to increase.

The effect of edge radius on the cutting performance of disc cutting was inves-

tigated by Bilgin (1977). He found that thrust and rolling forces increased considerably with edge radius, but this rate was reduced when using deeper penetrations. Specific energy remained almost constant with increasing edge radius for penetration depths greater than 2 mm, as bluntness causes an increase in yield.

2.2.4 Cutting Speed

The individual cutters of a boring machine traverse the rock surface at different linear velocities, because they are placed at various radii from the centre of the cutter head.

Thrust force, rolling force, rock yield and specific energy had shown no discernible change with cutting speeds over the range 50 - 200 mm/s by Roxborough and Phillips (1975,b) and over the range 0 - 1 m/s by Roxborough and Rispin (1973). Similar work was undertaken by Bilgin (1977).

With increased velocity of cutting up to approximately 254 mm/s, Ozdemir et al. (1977) observed increasing cutter forces. However, for velocities greater than 254 mm/s, the cutter forces appeared to be independent to cutting velocity. Since most field cutters operate at these higher range of velocities, They suggested that the cutting speed should not be a major consideration in attempting to develop basic cutter performance criteria. Samuel and Seow (1984) also come to the same conclusion from a full scale investigation of the performance of a TBM — thrust forces were found to be independent of cutting velocity.

2.2.5 Wear of Tools

Wear of the cutter tools is considered as a significant criterion in any tunnelling job, especially in hard rock. The reason is not only that the cutter costs can repre-

sent a considerable proportion of the total excavation costs, but their replacement also causes expensive down-time. Worn cutter tools also generated more heat and thereby reduce the energy transfer ratio. this is, in effect, is another cost.

Investigations into the wear of pick and drag tools are quite common, because of the ease with which weight reduction and flattening of tool tips can be made. In contract, work on tool wear of disc cutter has been relatively limited. The probable reasons for this are that the changes of tool weight and tool tip flattening of disc cutters are not very significant. Consequently, only comparative studies of rock cutting performance with new and worn disc cutters have been carried out. Rad (1975) used several blunt discs with different edge radius and found that a comparison of the worn diameters of disc cutters with the original diameters provided a good way in determining bluntness and wear. Ozdemir et al. (1977) observed that the degree to which wear increased the cutter forces was strongly dependent on the spacing of cuts. Kutter and Sanio (1982) pointed out that the optimum spacing of a worn disc cutter is smaller than that of a new disc. For constant thrust force, it is reported that the rate of penetration decreases considerably with progressive tool wear.

2.2.6 Rock Properties and Geological Conditions

The rock properties and geological conditions are the factors which relate most directly to the performance of the boring machines. Generally, the easily determined rock properties, such as the compressive strength, tensile strength, elastic modulus and indentation indices, have been taken as a measurement of boreability. Since the 1970's, rock cutting tests on a great variety of rock materials have produced a basic understanding of the relationships between rock properties and laboratory or field test results. A summary of this work is given in Table 2.2.3.

Table 2.2.3 Rock Property Matrix for Rock Cutting Tests

Rock Type	C.S. MPa	T.S. MPa	E GPa	B.D. g/cm	Ref.
Marrival Granite	174.0	10.0	–	2.62	[10,114]
Dolerite	340.0	27.5	–	2.91	[10,114]
Gregory Sandstone	50.0	3.5	–	2.65	[10,114]
Plas Gwilym Limestone	155.0	13.7	–	2.65	[10,114]
Shap Granite	155.0	10.8	–	2.63	[10,114]
Anhydrite	112.9	5.5	109.5	2.92	[10,114]
Dunhouse Sandstone	55.8	3.1	12.0	2.19	[10,114]
Four Fathom Limestone	127.3	7.5	105.1	2.66	[10,114]
Gypsum	45.0	2.8	50.0	2.26	[10,114]
Magnesium Limestone	84.9	6.2	20.6	2.63	[10,114]
Mansfield Sandstone	71.3	4.4	53.3	2.37	[10,114]
Bunter Sandstone 1	49.2	2.6	10.3	2.03	[120]
Bunter Sandstone 2	40.9	1.9	10.3	2.03	[120]
Springwell Sandstone	40.2	4.0	90.3	2.63	[79]
Tennessee Marble	71.4	5.6	19.9	2.69	[110,78,96]
Valders White Stone	108.4	3.8	20.2	2.55	[110,78]
Charcoal Granite	183.4	11.0	29.9	2.72	[110,96]
Jasper Quartzite	559.2	8.9	45.7	2.64	[110]
Indiana Limestone 1	62.9	4.6	24.1	2.30	[77]
Indiana Limestone 2	68.8	3.5	30.3	2.40	[77]
Kasota Stone	90.8	5.4	39.3	2.49	[77]
Norite	254.0	11.9	91.8	2.92	[29]
Fukushima Andesite	78.0	5.0	–	–	[141]
Kofu Andesite	168.0	12.7	–	–	[141]
Sawairi Granite	137.0	13.7	–	–	[141]
Chalk (dry)	35.42	1.58	–	–	[122]
Chalk (wet)	6.40	0.36	–	–	[122]

Note:

C.S. = Compressive Strength, E = Elastic moduli,

T.S. = Tensile Strength, B.D. = Bulk Density.

2.2.7 Tunnel Boring Machine Performance

While an examination of tunnel boring machine performance is not within the

scope of this dissertation, a review of this aspect is very helpful to an understanding of the relationships between the performance of tunnel boring machines and theoretical and laboratory studies. Note that the performance of a TBM concerned in this dissertation is only the performance of the machine cutting forces.

The use of a full scale machine to conduct experimental trials represents a considerable expenditure of funds for even the most modest programme of experiments. Therefore it is not surprising that the incidence of such trials is rare. Only six field research projects have been documented, according to Samuel and Seow (1984).

Instead of testing a full scale, instrumented machine, Dubugnon and Barendsen (1985) used a small scale model which modelled the TBM's or the cutter head down to a scale of 1/5 to 1/10. It was found that the thrust force FT on the disc cutter at full scale could be calculated from the small scale FT_0 by:

$$\frac{FT}{FT_0} = (\frac{D}{D_0})^{1.75} \qquad 2.2.1$$

where

D = linear dimension at full scale,

D_0 = linear dimension at small scale.

To closely simulate the operation and performance of field boring equipment, a 1.83m (6ft) diameter laboratory rotary cutting machine was designed and fabricated in the Colorado School of Mines (Ozdemir et al., 1983).

A great deal of research work has been undertaken to determine whether there are statistically significant correlations between the physical properties of rocks and machine performance. Unconfined compressive strength is the most commonly used because it is easily determined. It seems that other physical properties, such as grain hardness, interact with compressive strength to affect the rebound number. That perhaps is the reason that the Schmidt Hammer gives such good correlations with

machine performance in some rocks and a great deal of scatter in others (Bilgin, 1977). Tarkoy and Hendron (1975) defined the abrasiveness AR, abrasion hardness HA and total hardness TH as follows:

$$AR = \frac{1}{WL_d} \qquad 2.2.2$$

$$HA = \frac{1}{WL_s} \qquad 2.2.3$$

$$HT = HR\sqrt{HA} \qquad 2.2.4$$

where

WL_d = averaged weight loss of 4 abrasor discs, gm,

WL_s = averaged weight loss of 2 rock specimens, gm,

HR = Schmidt rebound number.

and found that there was a linear relationship between rock hardness and machine penetration rates. Also, it was concluded by Nelson et al. (1985) that a linear relationship existed in the fracture energy release rates of rocks and machine penetration rates. The details of this study will be discussed in Chapter 7.

A summary of developments in hard rock tunnel boring technique was presented by Dollinger (1983). He indicated that the major factors affected on the TBM performance are penetration depth, spacing distance, cutter dullness, cutter head design, rock strength, etc..

2.3 WATER JET ASSISTED MECHANICAL TOOLS CUTTING

Mining and tunnelling with high pressure water jet systems is a new technology and is thought of as the first significant development since the introduction of electrically powered underground mining machines in the 1930's and 1940's. There has been rapidly growing interest in the uses of high pressure water jets since the

early 1970's. Such interest ranges from the cleaning and descaling of various materials, for which water jet pressure is not more than 100 MPa, to the breaking of hard rock with pressure in excess of 1,500 MPa. A great deal of this interest can be attributed to the proceedings of International Symposium on Jet–Cutting Technology, first held in 1972, and the US Water Jet Conference, first held in 1981. As this project is only concerned with water jet assisted disc cutting, only the literature relating to this field is reviewed.

2.3.1 In U.S.A.

Since 1974, several laboratory tests of high pressure water jet to kerf hard rock followed by mechanical disc cutting have been conducted by the Colorado School of Mines and The Robbins Co., with financial supports from the US-Bureau of Mines and the National Science Foundation.

First, laboratory testing of rock samples from the field site was conducted in order to establish design parameters. The tunnel boring machine cutterhead equipped with water jets was then designed and constructed, and the necessary modifications to the tunnelling machine were performed. A report given by Wang et al. (1976) predicted that the tunnelling advance rate might be improved more than twice, with a potential economic saving 30 to 50%. It was also calculated in connection with two actual tunnelling projects in USA that a 10% increase in tunnelling speed would compensate the additional costs of water jet assistance, including energy consumption. A 50% increase in tunnelling speed would reduce the total costs of the project by about 25%.

Extensive testing was carried out by Ozdemir (Ozdemir, 1984; Ozdemir and Dollinger, 1984) using low pressure water jet to enhance the disc cutting performance. In cutting tests with sedimentary rocks, substantial increases of up to 40%

were achieved in depth of penetration when a jet were used to assist the disc cutter even at a pressure as low as 13.5 MPa (135 bar) (Ozdemir, 1986). Observed benefits relating to increased depth of penetration were great.

2.3.2 In W. Germany

Bergbau-Forschung GmbH, the central research institute of the German Coal Mining Industry, carried out full size tests for water jet assisted tunnel boring in German coal mines in 1978. The tests were performed with a tunnelborer of 2.6m diameter in an upper carboniferous sandstone-quarry near Dortmund in the Ruhr-District, in cooperation with a machine manufacturer, Wirth, and the US Department of Energy. The whole project was financially supported by the German government. The results of the tests, which were reported by Henneke and Knickmeyer (1979), have shown that the possible technical advantages of water jet asssistance on tunnel boring machines are as follows:

1. Lower forward thrust;
2. Lighter machine construction;
3. Easier machine transport;
4. Simplified machine assembly and dismantling;
5. Quicker underground machine resetting between subsequent driving sections;
6. Lower cutterhead drive;
7. Less cutter wear;
8. Effective dust suppression;
9. No sparking danger;
10. Reduced content of fines in cuttings.

As a subsequent step, high pressure water jets were used underground on a Mannesmann-Demag AG full-face tunnelling machine in 1983. Knickmeyer and Baumann (1983) summarized the results and experience to date with the novel

heading system. They found, in comparison with the conventional operation of cutting tools in particular, that either the high cutting force components required could be substantially reduced, or the rate of advance could be increased for the same thrust force. Besides, there were both positive effects on tool wear and important economic advantages.

Baumann and Heneke (1980) also indicated that the efficiency of cutting discs arranged on the drilling head of a full face tunnelling machine could be considerably improved by means of high pressure water jets. The reduction of the required power feed by more than 50% would, in turn, accommodate proportional decreases in machinery weight with all the other beneficial effects on the flexibility of such tunnelling system.

2.3.3 In USSR

Research on coal breakage by high pressure water jet with different types of cutters and disc cutters was undertaken at Skochinsky Institute of Mining. Kuzmich et al. (1982) found that the optimum correlation between depth of cut, formed by a thin high pressure water jet and the depth of cut formed by a mechanical tool was as follows:

$$\frac{P_{hm}}{P_m} = 1 - 0.4\sqrt{\frac{H_s}{H}} \qquad 2.3.1$$

where

P_{hm} = Hydromechanical cutting force, kN,

P_m = Mechanical cutting force, kN,

H_s = Depth of slot, mm,

H = Depth of cut, mm.

The efficiency of water jet assisted disc cutting was evaluated on the basis of the cutting forces and the mechanical specific energy. It was also found that better

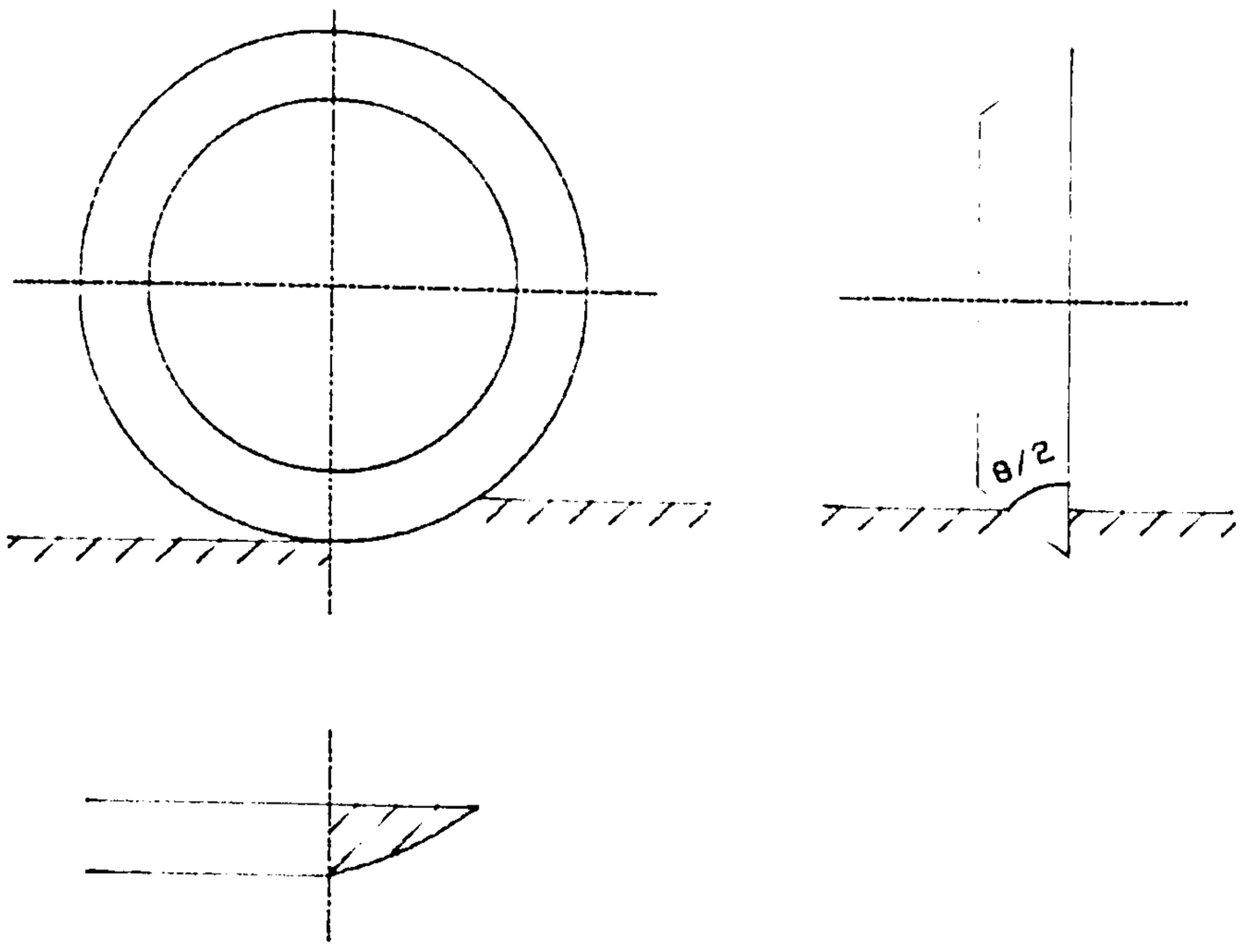

Fig. 2.3.1 The disc cutter with one-side sharpening angle

results would be obtained by using a disc cutter with a one-side sharpening angle (Fig. 2.3.1).

2.3.4 In Japan

The study of high pressure water jet cutting started in 1966 at the Railway Technical Research Institute, Japanese National Railways. The first experimental water jet cutting machine for hard rock cutting tests was built in 1967, A second was built in 1968. Cutting tests were carried out on many rock types, and Hoshino et al. (1972) conducted a series of cutting tests using disc cutters in conjunction with high speed water jets. The pre-cut grooves made by high speed water jet were in sides of disc cutters and spacing of the grooves was determined by the compressive strength of rock. Cutting forces were found to be only 50% - 20% that of cutting with a mechanical cutter only.

2.3.5 In South Africa

In 1976, Hood reported an investigation into the possible use of high pressure water jets as an aid to drag tool cutting. Using pressures of 10 - 50 MPa and a water flow rate of 30 l/min, he reported that the forces on the bit for the same available machine force were reduced to the extent that the depth of cut was increased from a maximum of 4.5 mm without high pressure jets to 10.5 mm using the jets.

A paper presented by Fenn et al. (1985) has shown that the use of low pressure water jets can enhance the performance of mechanical disc cutting in very hard rock, the assistance of water jet in this case resulting in reductions in the order of 40% in the forces on a free rolling cutter.

2.3.6 In United Kingdom

A very powerful excavating machine in the form of high pressure water jet assisted roadheader has been developed in United Kingdom (Plumpton and Tomlin, 1982), with much of the research work being undertaken at the University of Newcastle upon Tyne. The resulting reports, papers and Ph.D theses have shown that much improvement is possible using water jet assisted pick cutting.

In contrast with the research on water jet assisted pick tools, less attention has been paid to water jet assisted disc cutting. Only one report in this field — an M.Sc dissertation submitted by Moses (1985) — has been found. Using a single pass, constant penetration model, Moses carried out water jet assisted disc cutting tests on Springwell Sandstone. The depths of pre-cut slots cut by the water jets were equal to the depths of mechanical cutting penetrations. Compared with unassisted cutting, reductions of 32% to 69% were measured in the mean cutter forces during water jet assisted disc cutting tests.

Chapter 3

EXPERIMENTAL APPARATUS AND PROCEDURE

3.1 EXPERIMENTAL APPARATUS

A small scale linear cutting rig and a large scale linear cutting rig, with different pumping systems, were used in this study. The details of the small cutting rig and pumping system were given by Tecen (1982) and Moses (1985), and the large rig and pumping system were given by Fauvel (1981) and Fowell et al. (1985). Consequently, a brief description of the test equipment used is presented in this Chapter.

3.1.1 The Small Scale Linear Cutting Rig and Pumping System

The machine used in the cutting tests is a modified shaping machine with a forward stroke of 800 mm and a maximum in-line thrust force of 50 kN. A rock specimen of 500×500×300mm in size can be accommodated on the machine table and lowered and laterally traversed with respect to the cutting tool.

An Uraca three piston, positive displacement pump is used in the water jet assisted cutting test. It is powered by a continuously rated 30 horsepower electric motor, and delivers 8.62 l/min at a pressure of 48.28 MPa through a nozzle of 0.68 mm exit diameter. A 110.35 MPa Bourdon Tube type gauge monitored the pressure.

3.1.2 The Large Scale Linear Cutting Rig and Pumping System

The rig used is an instrumented 500 kN rock planer mounted on a sturdy frame

and four columns. There are two independent hydraulic systems, a main system and a clamping circuit system. The power required to operate the cutting tool is provided by the main system and the large clamps are operated by the clamping circuit to remove cutter backlash and increase cutter stiffness.

Two pumps are used to provide cutting forces, the high pressure pump with maximum cutting force upto 500 kN, and low pressure pump up to 80 kN. Because the low pressure pump was out of order, the high pressure pump is used in the investigation.

A brief summary of the rig specifications is as follows:

Maximum specimen size	1.5×1.0×1.0m
Maximum table travel	0.9 m
Speed of table traverse	0.34 m/min
Maximum cutter slide travel	0.6 m
Speed of cutter slide traverse	0.03 m/min
Maximum thrust force	500 kN
Maximum rolling force	
low	80 kN
high	500 kN
Maximum cutter stroke	2.0 m
Cutter speed	0.0–1.3 m/s

High pressure water supply unit used for the water jet was a 75 kW "hydroflo" pump with a maximum delivery pressure of 70 MPa.

The rig having been previously used for disc cutting tests between 1977 to 1981 (Fauvel, 1981), and then for water jet assisted drag bit cutting from 1982 to 1985 (Fowell et al., 1985), was cleaned and modified for this study, over a period of three

months.

3.1.3 Nozzles

A Nikonov type nozzle in silver steel, with 13° contraction angle and nozzle diameter of 0.68mm, was used.

3.1.4 Disc Cutters

For the small cutting machine system, a disc cutter with 150mm diameter and 60° edge angle was used in the test. It was machined from blanks of high carbon, high chrome, non-distorting steel and subsequently heat treated.

The cutter used in the large cutting machine had a 60° edge angle and a 2.5mm tip radius based on a nominal diameter disc of 300mm. It was made of tool steel and heat treated before grinding to the final dimension.

3.2 SAMPLE PREPARATION

3.2.1 Samples for Small Cutting Rig

Two rock samples, one Springwell Sandstone and one Whinstone were prepared by diamond sawing to approximate dimensions of 500×500×300mm. Araldite adhesive was used to stick the blocks to steel plates. The steel plates were cleaned, grinded and smoothed in preparation for the sample blocks.

3.2.2 Samples for Large Cutting Rig

Sample blocks with a size of 1×0.8×0.6m were used for large machine testing. The preparation of rock samples for the large cutting rig was much more involved and time consuming than the samples for the small machine. The procedure for

preparing the samples was as follows:

1. Put the rock block on the table of the cutting rig and fix a steel frame around the table using timbers between the block and the frame to firmly secure the sample block.

2. Shave the block surface level using a plate pick tool.

3. Turn the rock block over and shave another surface using procedures (1) and (2).

4. Bolt the sample plate with an array of projecting dowels to the table.

5. Drill a corresponding array of holes into the rock sample, and pour Araldite adhesive in the holes.

6. Use Araldite adhesive to stick the block to the steel plate.

Two hard rocks were involved in the disc cutting tests on the big cutting rig: Pennant Sandstone and Whinstone.

3.3 PARAMETER MEASUREMENTS

3.3.1 Triaxial Dynamometer and Data Recording System

Specifically designed instruments and triaxial dynamometers were used in both cutting machine systems for measuring the magnitudes and directions of the cutting forces during cutting tests. The strains induced by these forces were detected by strain gauges arranged in three full bridges on beams which support the tool holder. Details can be obtained from Fauvel (1981).

Electrical signals generated by the dynamometer were amplified and fed contin-

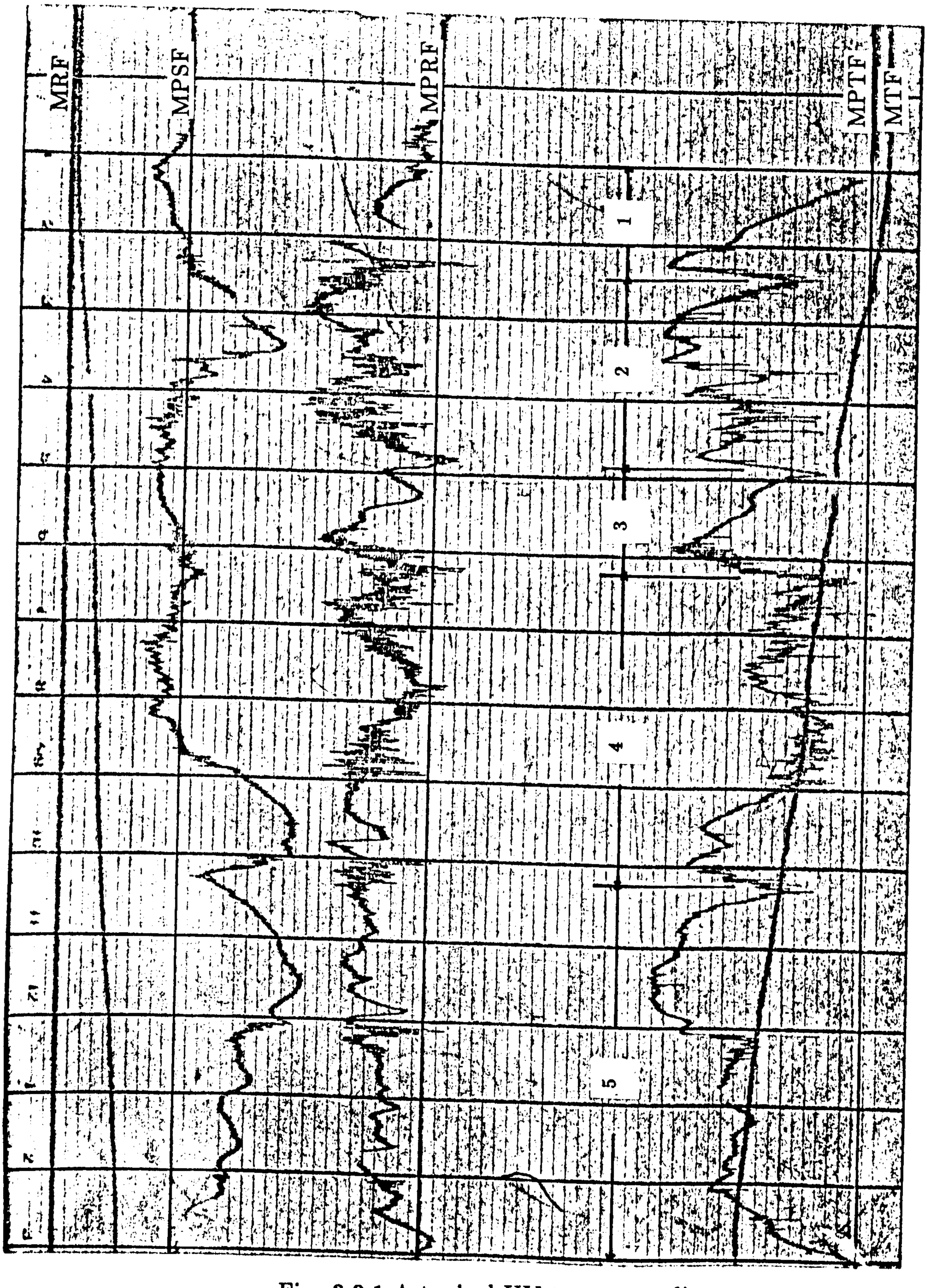

Fig. 3.3.1 A typical UV trace recording

uously to an UV recorder. Also the dynamic signals were electronically integrated simultaneously output to the UV recorder.

The recording instrumentation used was an SE4000 system with an Ultra-Violet chart recorder. The arrangement comprised three amplifiers and three integrators to form three channels for one each of the forces.

A typical UV recording shows six traces. Three are direct force/time traces to record peak forces, two are integrated force lines in respect to the mean thrust force and rolling force, and the sixth is a reference line (Fig. 3.3.1).

3.3.2 Calibration of the Dynamometers

The dynamometers were calibrated before the cutting tests, as the UV recorder cannot give directly the values of forces. Generally, the calibration procedure was as follows:

1. Calibrate the load cell in a pressure machine using a strain gauge box.

2. Set and adjust the UV recorder. Each channel carries various amplification and integration settings which allow a range of forces to be monitored.

3. Put the load cell between two steel ball, one of which is fitted to the tool holder and the other on a pyramidal plate which is bolted to the machine table.

4. Calibrate the thrust force and the rolling force separately by using a hydraulic ram to load the arrangement. The UV traces of the forces, meanwhile, are recorded by the UV recorder and the reading of the load cell, which has been calibrated already, is presented by the strain gauge box.

5. calculate the calibration constants.

The load cell used was a Type 405, Serial no. 143. Some results are given in Appendix A.

3.3.3 Volume of Rock Cut by Water Jet Assisted disc cutting

Generally speaking, the measurement of cut volume for unassisted cutting tests is quite easy, as the debris can be easily collected and weighted. However, for the water jet assisted cutting tests, there are associated difficulties, because it is not possible to collect the debris since most of it is washed away. Therefore, due to the impracticality of weighing the rock before and after each cutting test, and because of its size and relative immobility, another method of "cut volume" or "rock yield" measurement had to be found.

Several investigators have developed different methods to tackle the problem. One of them measured the cut volume by pouring a fine material of known density into cut. This method was adopted for the cutting tests on the small cutting rig, as the tests were done on smooth rock surfaces. The filler material used was a finely graded silica sand.

The same method of determining rock yield however was not appropriate to the big cutting rig using the multiple cutting method and so another method based on the angle of cutting grooves was used. The method has been used by Fenn et al. (1985), but no distribution was given in the way of the measurements.

In this study, the plasticine was used to model the shape of the groove. Five models were selected from each cut length. The angles of the grooves, then, were obtained by measuring the sections of the models (Plate 3.3.1).

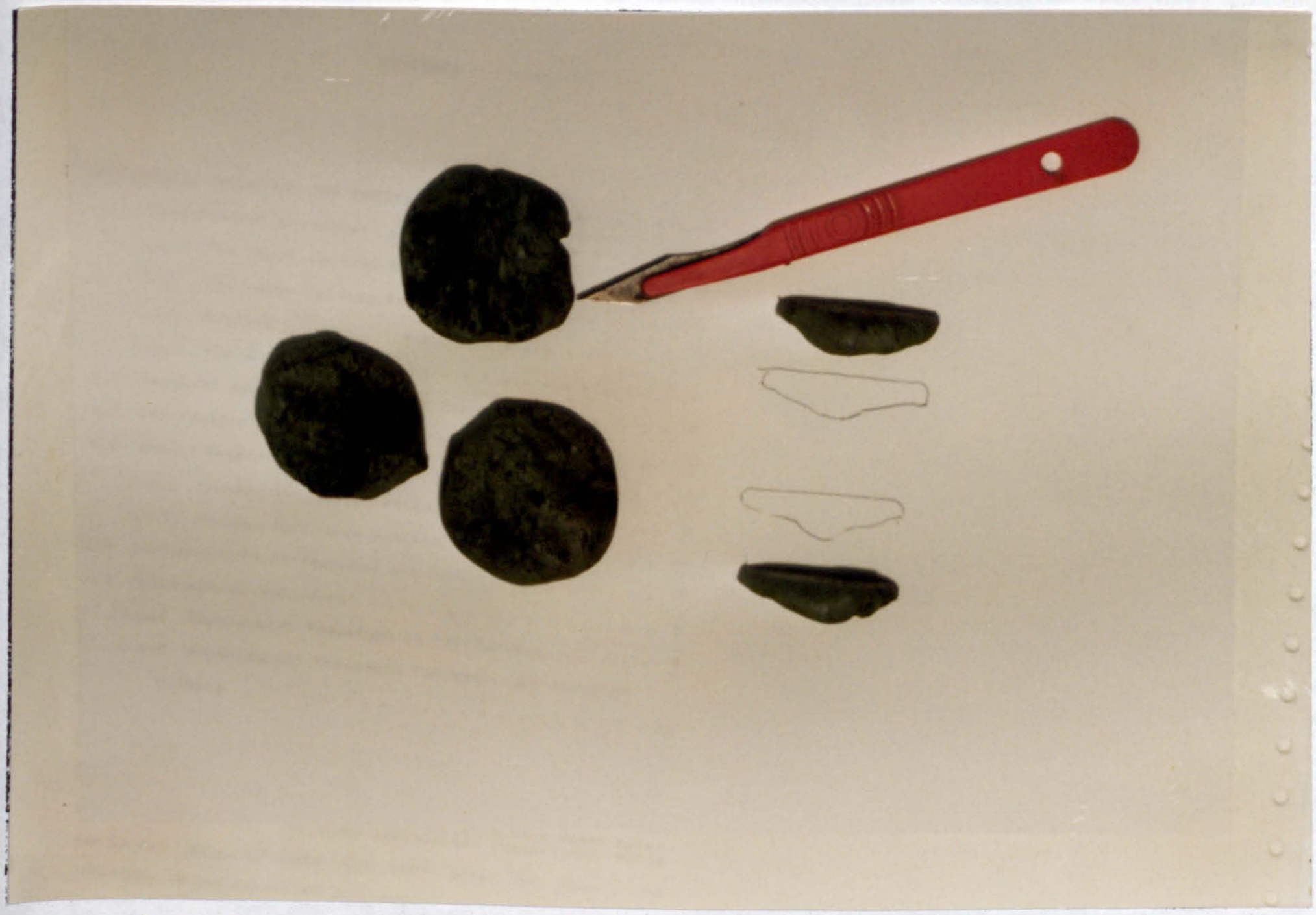

Plate 3.3.1 The determination of the groove angle

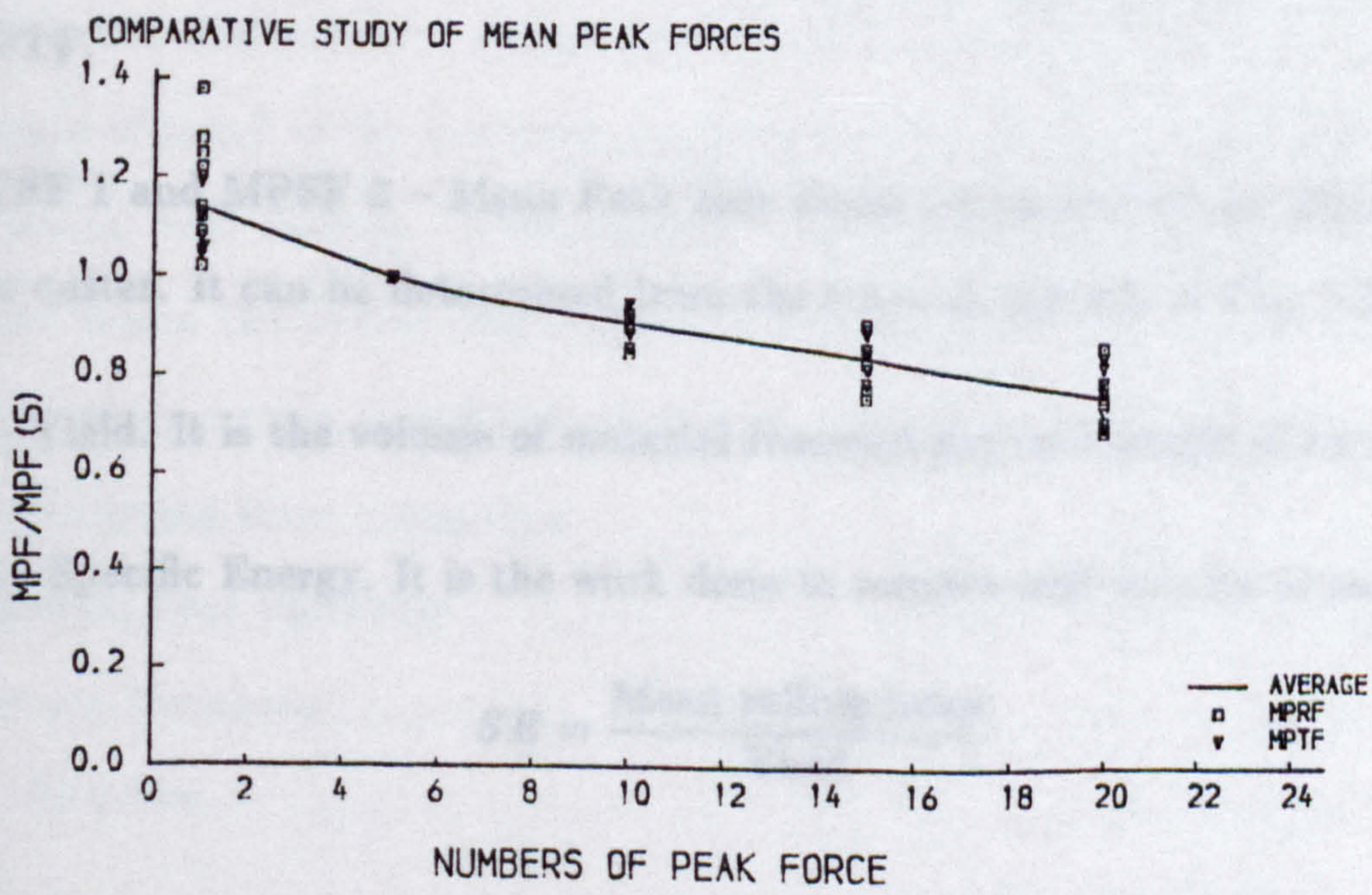

Fig. 3.4.1 The effect of selected numbers of peak forces on mean peak forces

3.4 EXPERIMENTAL PARAMETERS

Applying the appropriate calibration constants, the forces measured are defined as follows:

1. MTF – Mean Thrust Force. This is the average applied force required to penetrate the rock surface. It can be obtained directly from the slope of trace in the test results provided by UV recorder (Fig. 3.3.1)

2. MPTF – Mean Peak Thrust Force. It can be determined as the average of the five highest values of normal forces as shown in Fig. 3.3.1.

3. MRF – Mean Rolling Force. It is the average force required to force the disc rolling, and can be obtained directly from the slope of another trace in the results.

4. MPRF – Mean Peak Rolling Force. It can be obtained in the same way as MPTF.

5. MPSF 1 and MPSF 2 – Mean Peak Side Force acting on Left or Right of the disc cutter. It can be determined from the trace on the top of Fig. 3.3.1.

6. Q – Yield. It is the volume of material removed per unit length of cut.

7. SE – Specific Energy. It is the work done to remove unit volume of rock:

$$SE = \frac{\text{Mean rolling force}}{\text{Yield}} \qquad 3.4.1$$

It is important to acknowledge that in previous investigations, different authors determined mean forces in different ways. For example, Roxborough and Phillips (1975,b) determined the mean peak forces for a cut by measuring the peak value for each 0.1 second interval and averaging. But Kutter and Sanio (1982), and Snowdon

et al. (1982) used only peak forces.

If we examine Fig 3.3.1 carefully, it will be found the rock breakage by the disc cutter is cyclic with well defined periods. Furthermore, the effect of selected numbers of peak forces on the mean peak force measurement is investigated (Fig. 3.4.1). From 20 different cuts, the results show a proportional decrease with increased numbers of peak forces, suggesting that there is a regular relationship between the mean peak forces collected from different methods. The periods with forces of large magnitude in this study are 4 or 5. That is why the top five peak forces were selected and averaged as a mean peak force value in this study.

3.5 EXPERIMENTAL VARIABLES

To decide upon the variables and their levels to be considered is the first step in the design of any experimental programme. Because of the number of factors involved, it was impossible to examine every possible relationship. The potentially wide ranges of many of the variables precluded full investigations and particularly in mechanical tool cutting. Consequently, a selection was made of likely areas of interest where the option was available. The variables which were considered important when cutting rock with a water jet assisted disc cutter may be divided in to the following three categories:

a. Mechanical Tool Variables;

b. Water Jet Variables;

c. Rock Variables.

3.5.1 Mechanical Tool Variables

1. Test Methods

The aims of mechanical cutting tests are: (i) to compare with a theoretical analysis which will be given in Chapter 7, and (ii) to serve as the reference data for water jet assisted disc cutting tests.

Generally, there are two different test methods in rock cutting tests. One is the single cutting method, and other is the multiple cutting method. For the single cutting method, there are two different ways to perform the test — the disc tool cutting through the smooth surface of the rock example and cutting along the previous kerf. It has been found that different conclusions could be drawn from the results obtained by the different testing methods. For such reasons, attention is paid in this study to investigate the degree to which results are affected by the use of the different test methods. The effects of different test methods on water jet assisted disc cutting is also studied.

The purpose of multiple pass cutting is to closely simulate the relevant cutting conditions at a tunnel face. Also from the view point of laboratory tests, the multiple pass cutting method is easier to undertake, as there is no need of shaving the block level after every pass, and specially for hard rock cutting, a great deal of time is saved.

Single pass cutting, on the other hand, can provide the data which are more stable and more convenient for comparing with each other. But, as some authors have already pointed out, this phenomena is only relevant in softer rock cutting. For such reason, the single pass cutting method was only used with the small cutting machine system, and the cutting tests were conducted on smooth rock surfaces.

2. Spacing Distance and Penetration

For the unassisted disc cutting, the greatest benefit can be obtained by adjusting the ratio of spacing distance and penetration depth (s/p) in the region of 3 -

6. In fact the distances of cutters in the TBM's are all fixed. So, when the TBM's excavate in very hard rock, it is impossible to keep the machines driving with such s/p ratios, as too much thrust force is required. In the general case the ribs between the cutters are not broken during first cut, but only after several cuts. It is for that reason that it is called "multiple cutting".

It is a widely accepted view that the s/p ratio plays a very important role in improving the performance of TBM's driving in hard rock formations. However, with the advent of water jet assisted tunnel boring the practice has been simply to add water jets to TBM's whose s/p ratios were optimised for unassisted mechanical cutting. Therefore, it has been assumed that the optimum s/p ratio for unassisted cutting is also the optimum s/p ratio for water jet assisted cutting. No detailed investigation has been undertaken to support or deny the present assumption. Consequently, the purpose of this study to establish the possibility that the optimum s/p ratio for assisted cutting is different from that for unassisted cutting.

For the large machine tests, penetration depths of 2mm and 4mm were selected. In fact, a 6mm penetration depth was also planned, but abandoned when the required thrust force detached the rock sample from the steel plate. Thus spacing distances — 20mm, 40mm and 60mm were used to give s/p ratios of 5, 10, 15, 20, 30. This range of s/p ratios covers the region of optimum s/p ratios for unassisted cutting.

3.5.2 Water Jet Variables

1. Position of Water Jet Nozzle

Attention has been given to the influence of nozzle positions for water jet pressure assisted disc cutting by several workers. Wang et al. (1976) considered three different jet location arrangements: (1) jets under the cutters, (2) jets between

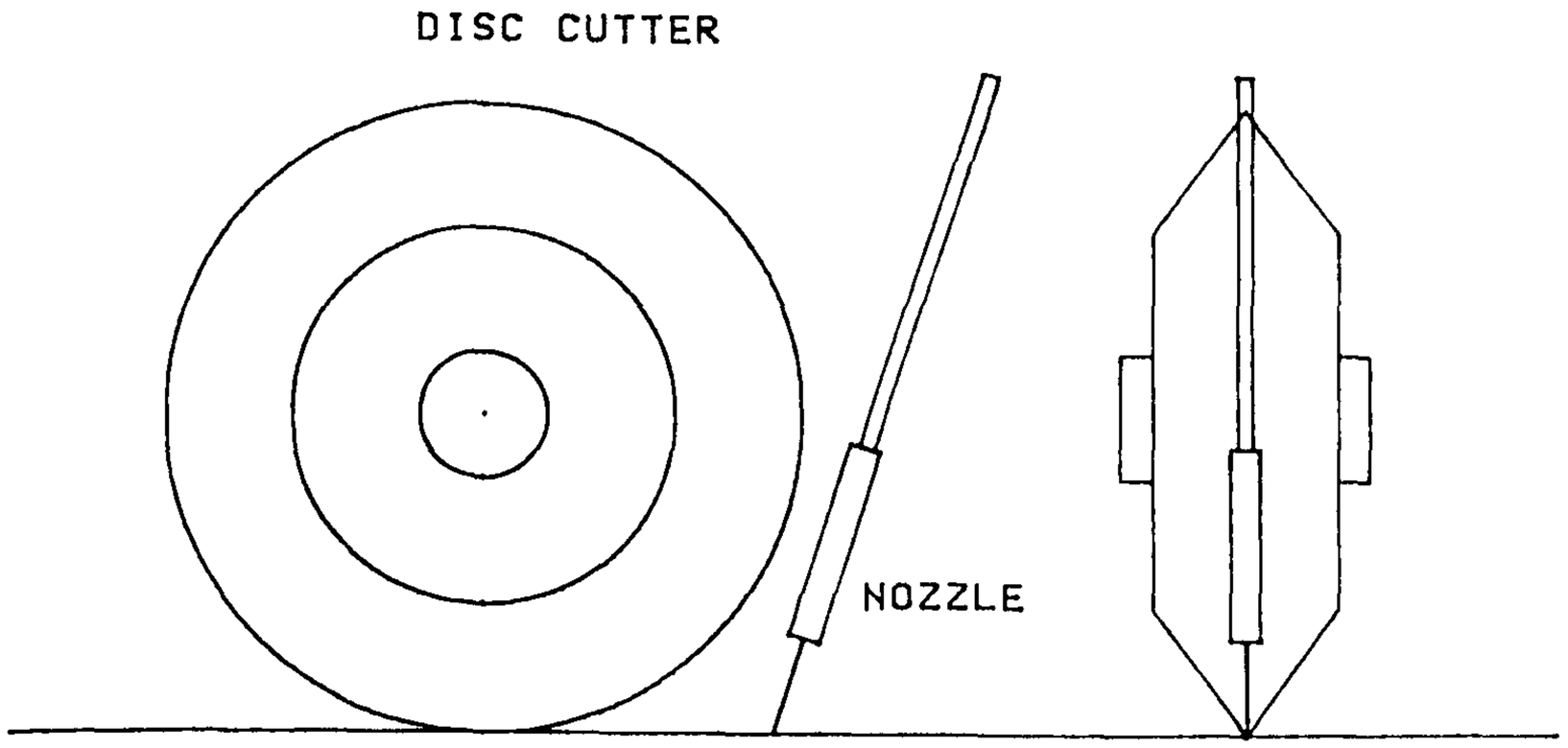

(a). Nozzle location No. 1 – in front of the cutter

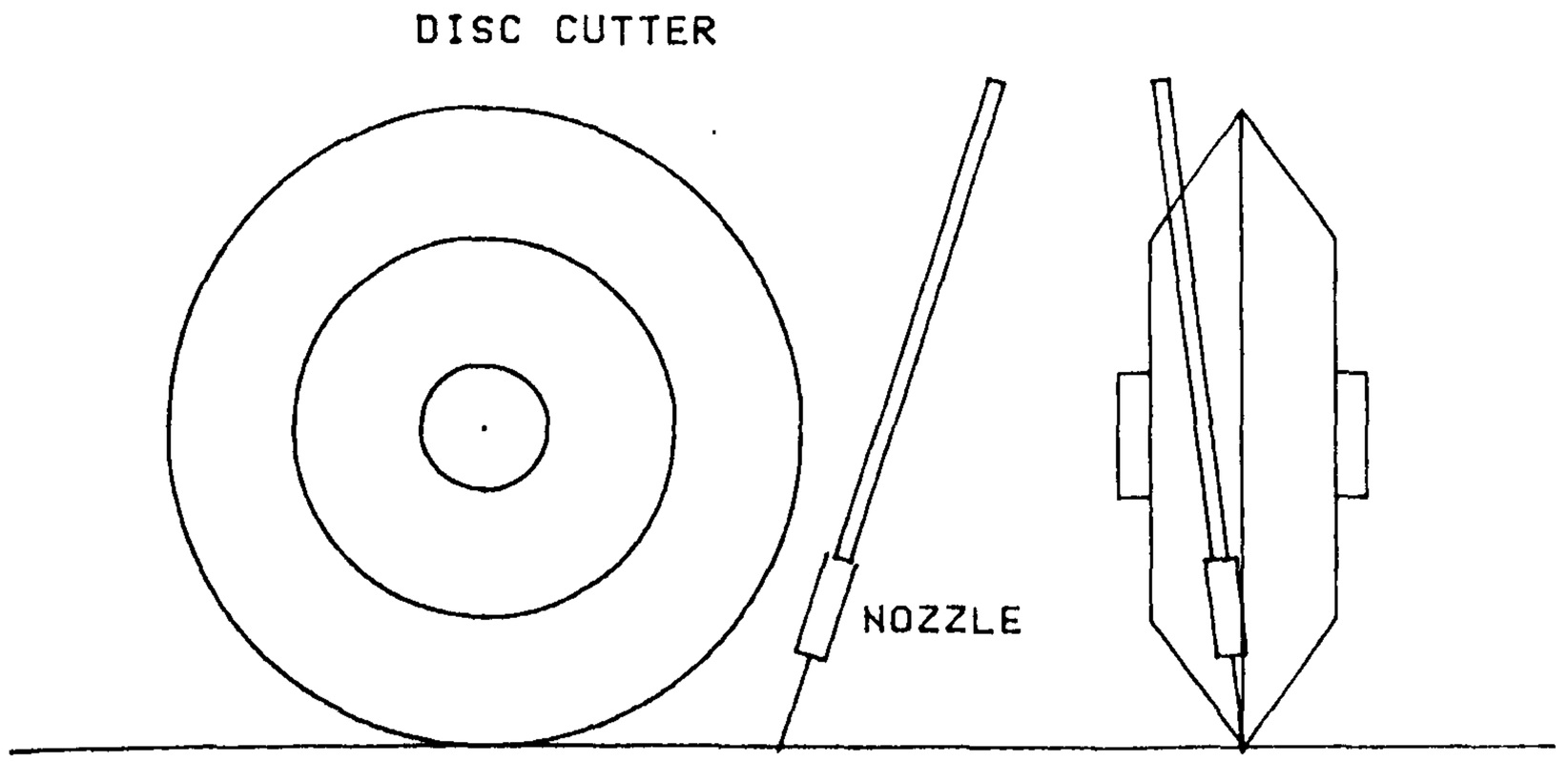

(b). Nozzle location No. 2 – in front of and besides the cutter

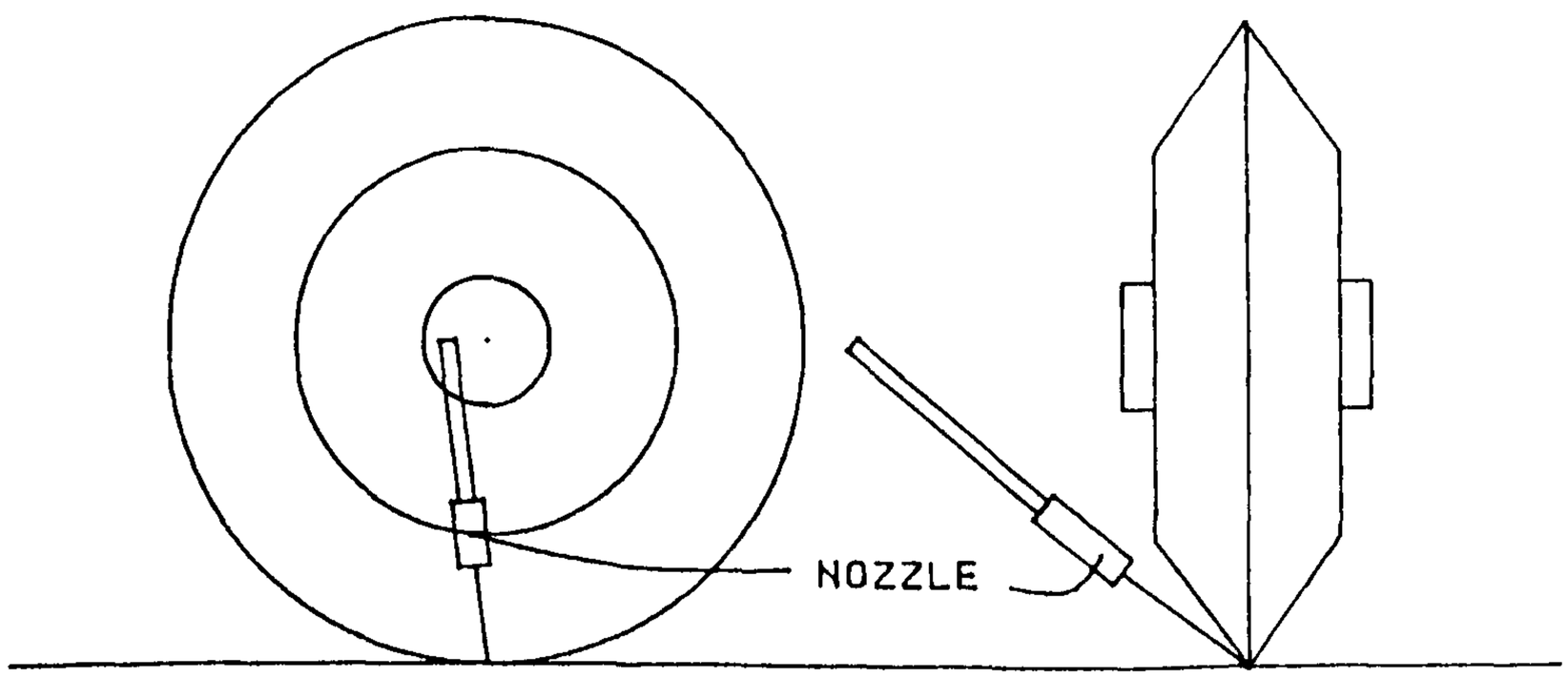

(c). Nozzle location No. 3 – besides the cutter

Fig. 3.5.1 Water jet locations

the cutters, and (3) jets both under and between the cutters. The results concluded that the first arrangement required the least horsepower and the third arrangement required the greatest horsepower for the same depth of mechanical penetration.

Several arrangements of jet locations with respect to the cutters were investigated in the field tests in W. Germany (Ozdemir 1984). The arrangement involving a more or less uniform distribution of jet nozzles over the cutterhead was found to produce the greatest benefit.

Other factors concerned with nozzle locations which affect the performance of water jet penetration are lead-on distance, stand-off distance and attack angle. But for the low-pressure water jet assisted disc cutting, the situation is quite different. The pressure of the jets is not powerful enough to make the kerfs on the rock surface. In such case, the first pattern of the nozzle locations cannot give much assistance to rock cutting. Consequently, locations of water jet nozzles were placed in the following positions: (i) in front of the cutter; (ii) in front of and besides the cutter and (iii) besides the cutter (Fig. 3.5.1). Only a single nozzle was used in every case. The position of nozzle between two grooves was excluded from the study because at low-pressure the jet was not able to make a kerf into the rock.

2. Water Jet Pressure

Four water jet pressures were used in the tests. They are: 13.79 MPa (2,000 psi), 27.58 MPa (4,000 psi), 41.37 MPa (6,000 psi) and 55.16 MPa (8,000 psi). Before water jet assisted disc cutting, cutting without the assistance of water jets, or so called unassisted cutting, was performed. The results obtained in the unassisted cutting can be used as reference data to compare with that obtained in water jet assisted disc cutting.

3. Cutting Speed

For the dry cutting, it has been observed that if the cutting speed is higher than 0.25 m/s, there is no influence of cutting speed to the cutting forces. At the same time it has been acknowledged for the high pressure water jet cutting, that the jet travelling speed is one of the most important factors directly involved in the depth of slots cut. Therefore, attention was taken in the study to examine the effect of cutting speeds of 0.25 m/s, 0.45 m/s, 0.6 m/s and 0.85 m/s.

3.5.3 Rock Variables

Laboratory investigation into the performance of tunnelling machines entails both rock cutting tests and rock material properties tests. Generally, the material properties' tests can be divided into two classes:

I. Geological properties — Petrographic and mineral properties;

II. Mechanical properties — Strength, Hardness.

1. Geological properties

Springwell Sandstone is composed predominantly of quartz fragments of medium grain size between 0.5mm and 0.75mm. Their poor rounding suggests an alluvial origin in which the grains had not been subjected to high energy conditions. Samples displayed a mono-quartz content of 87%, poly-quartz 3%, feldspar 5% and other 5%. It is light yellow in colour.

Quartz grains up to 1.0 mm in diameter from 70% of Pennant Sandstone. The remaining grains consist of equal proportions of feldspar crystals content of 7%, with a few flakes of muscovite. The rock is poorly sorted with a matrix of cemented clay minerals forming 20% of the total volume.

Whinstone is a dark-grey quartz-dolerite with a ground mass grain size that varies from 0.2 to 1.0 mm. A model analysis gives the following constitutents:

Table 3.5.1 Mechanical properties of rocks

mechanical property	Springwell Sandstone	Pennant Sandstone	Whinstone
uniaxial compressive strength (MPa)	40.22	197.17	268.05
tensile strength (MPa)	3.02	11.22	16.01
shear strength (MPa)	5.51	23.67	32.75
inner friction angle (Degree)	36.23	-	-
static elastic moduli (GPa)			
E(tan)	9.49	17.86	25.83
E(sec)	5.51	14.83	17.97
Poisson's ratio	0.28	0.23	0.18
Shore scleroscope hardness	40.88	75.3	84.8
Schmidt hammer rebound number	38.50	48.04	57.5
cone indentation test	1.98	4.25	6.41
bulk density (Mg/m^3)	2.18	2.68	2.88

feldspar 70%, mono-quartz 15% and other 15%.

2. Mechanical properties

The tests were carried out in the Rock Mechanics Laboratory, Department of Geotechnical Engineering. Rock samples were collected from the rock blocks used in the cutting tests, and subjected to certain testing procedures following guidelines prescribed in ISRM suggested methods (Brown, 1981).

The mechanical properties of Springwell Sandstone, Pennant Sandstone and Whinstone are listed in the Table 3.5.1.

3.6 EXPERIMENTAL PROCEDURES OF CUTTING TESTS

All of the tests were performed as relieved cutting under constant penetration mode, where the cutter penetration into the rock surface was held constant and

the cutter forces required to maintain the penetration depth, were measured and recorded. The laboratory test programmes for investigating the effectiveness of water jet assisted disc cutting were conducted on both the large and small linear cutting machines.

3.6.1 Cutting tests on Small Cutting Rig

The block of rock was stuck to a prepared steel plate with Araldite and allowed to cure for at least 24 hours. To allow warming up and settling down of any galvanometer drift, the UV recorder was switched on about 20 minutes before cutting. It was then necessary to select and position the galvanometer spots appropriately for each of the required force traces. Care was taken to ensure that the system was balanced before and after each run.

The variables studied in this experiment were penetration and spacing. After shaving the block level with a shaving tool, the bed was unbolted and raise so that the disc tool just came into contact with the level block surface and a zero reading was taken on the deformation dial gauge. The bed was then raised and locked to the required depth of cut, thereafter series of cuts were made cross the rock surface. At the end of each cut, the tool was reversed and the debris was collected and weighted.

The paper speed of the UV recorder was set to 125 mm/s and for every cut, cut number, amplification and integration time levels from UV recorder, depth of penetration, and weight of debris were recorded.

As noted previously, the jet nozzle for the tests was positioned directly in front of the cutter and oriented to impinge on the rock surface along the cutter path. Shaving and cutting procedures were adopted as for unassisted cutting tests. After checking the balance of the system, the pump was started. No cut is made until

the required water jet pressure was attained. At the end of each cut, the jet was turned off and the tool was brought back to its original position.

Grooves made on the rock by the tool were cleaned with a brush and fine silica sand was poured in. The sand was then levelled by scraping the rock surface with a steel ruler and any excess sand was returned to the sand container. Thereby the weight of sand used to full the groove was found by re-weighting the container and its remaining sand:

$$W_p = W_b - W_a \tag{3.6.1}$$

where

W_p = weight of the sand used to fill groove,

W_b = total weight of the container before cutting,

W_a = total weight of the container after the cutting.

Subsequently, the yield was calculated:

$$Y = \frac{W_p}{gL} \tag{3.6.2}$$

where

g= the density of the sand used,

L = the length of the groove measured.

Soluble oil was added to the water in 1 to 50 proportion by volume to prevent rusting to any part of the pump and the shaping machine. The same proportion was maintained throughout the water jet cutting experiments. Finally, the position of the nozzle in its holder was noted and the same position was used throughout the experimental programme.

3.6.2 Cutting tests on Large Cutting Rig

The measurement system for the large and small machine tests was identical.

The test procedure, however, was different, as distinct from the single pass method used in the small machine tests, a multi-pass method was used in the large machine tests.

The procedure of the cutting tests using the large machine was as follows:

1. As consistent measurements can only be obtained after a number of cutting passes, say five to six, a series of cuts were made across the rock surface at the required depth and spacing parameters before any efficient data on the cutter forces were measured.

2. Unassisted cuts made to give data for comparison.

3. Select and arrange jet patterns; also jet pressure and cutting speed.

4. Lower cutting tool by a further penetration increment into grooves previously produced by (2).

5. Make assisted cut and repeat with same depth of penetration and spacing distance for required number of cuts.

6. Model the groove angles with the plastic material.

7. Reset jet positions, jet pressure and cutting speed for next s/p ratio test condition and re-constitute rock sample surface.

The desired penetration of the cutter was set by hydraulically lowering the cutter holder frame. Thereafter, and after each cut, the plate holding the specimen was translated sideways with the amount of translation corresponding to desired spacing of cutters.

Chapter 4

ROCK FRACTURE TESTS

4.1 INTRODUCTION

Strength failures of load bearing structures can be either of the yielding dominant or fracture dominant types. Fracture mechanics is concerned almost entirely with fracture dominant failures. Griffith (1920) gave the first successful analysis of a fracture dominant problem. His well-known concept is based on the assumption that there is a simple energy balance, as represented by a decrease in elastic strain energy within the stressed body as the crack extends, countered by the energy needed to create the new crack surfaces. The Griffith's fracture theory was developed by Irwin (1957). Irwin also developed the concepts of energy release rate G and stress intensity K (or fracture energy and fracture toughness in common).

A fracture mechanics approach has recently been introduced in rock mechanics. It is believed that an understanding of the mechanics and mechanisms of rock fracture is a key element in solving a great many engineering problems involving geotechnical structures. As there are large differences in basic physical properties and engineering applications between rock and metallic materials, one should be very careful when adopting the principles, practice, sample preparation, and test methods of general fracture mechanics.

4.2 BASICS OF ROCK FRACTURE MECHANICS

4.2.1 The Griffith Energy Balance Approach

The major contribution of Griffith to the theoretical understanding of fracture

was his formulation of a criterion for the extension of an isolated plane crack in a stressed solid in terms of mechanical energy and thermodynamics. He modelled this system as a reversible thermodynamic process in which the crack would be in a state of equilibrium when the total free energy of the system was a minimum.

The total energy U of the through-cracked plate (Fig. 4.2.1) may be written as:

$$U = U_0 + U_a + U_e - F \qquad 4.2.1$$

where

U_0 = elastic energy of the loaded uncracked plate (a constant),

U_a = change in the elastic energy caused by introducing a crack in the plate,

U_e = change in the elastic surface energy caused by the formation of crack surfaces,

F = work performed by external forces.

For unit thickness the absolute value of U_a is given by

$$|U_a| = \frac{\pi\sigma^2 a^2}{E} \qquad 4.2.2$$

and U_e is equal to the product of the elastic surface energy of the material, γ_e, and the new surface area of crack:

$$U_e = 2(2a\ \gamma_e) \qquad 4.2.3$$

Crack growth instability will occur as soon as U no longer increases with increasing crack length, a. Thus the equilibrium condition for crack extension is obtained by setting dU/da equal to zero. Since U_0 is a constant, we have

$$\frac{d(U_a + U_e - F)}{da} = 0 \qquad 4.2.4$$

Equation (4.2.4) can be rearranged to give

$$\frac{d(F - U_a)}{da} = \frac{dU_e}{da} \qquad 4.2.5$$

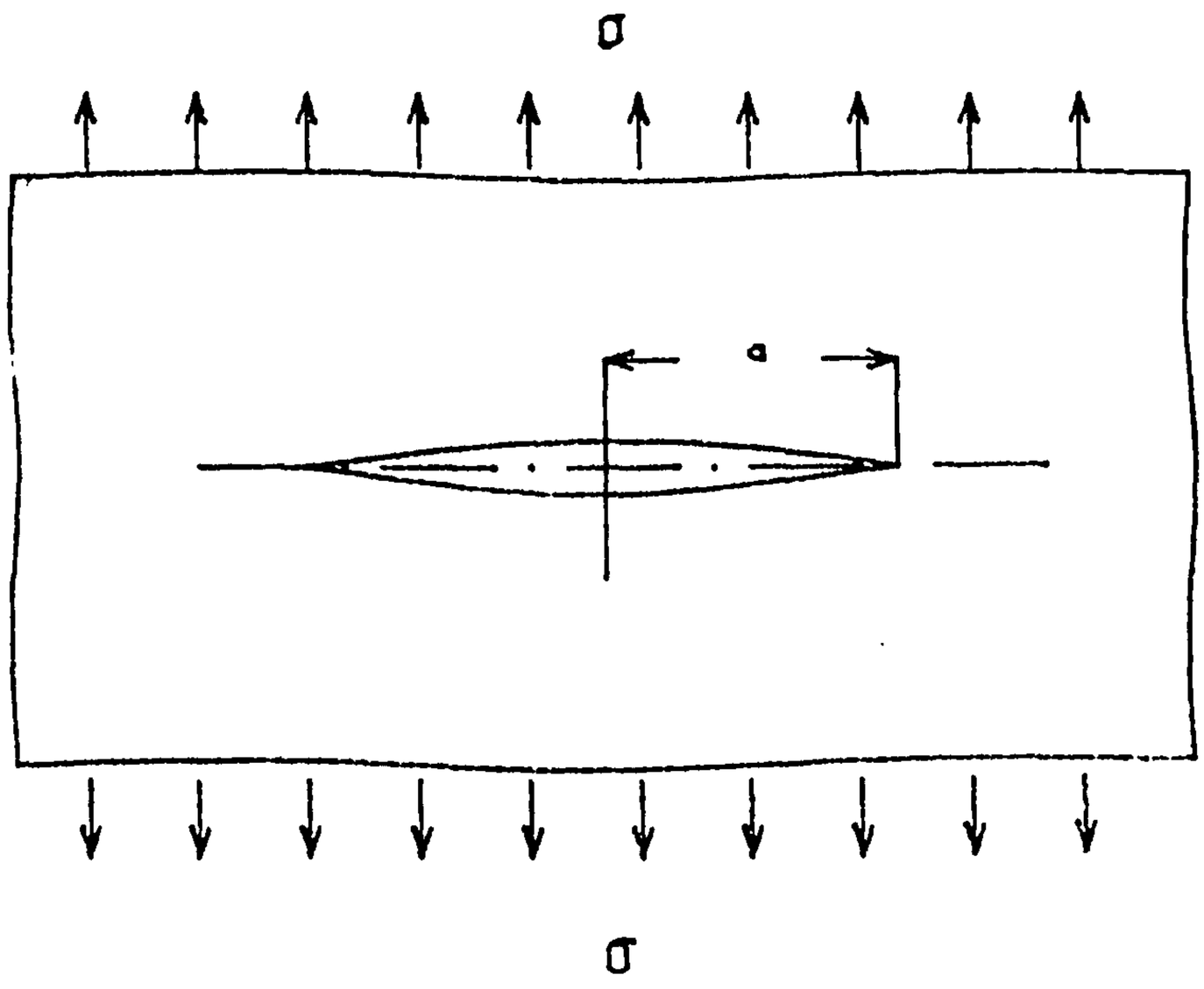

Fig. 4.2.1 A through-cracked plate

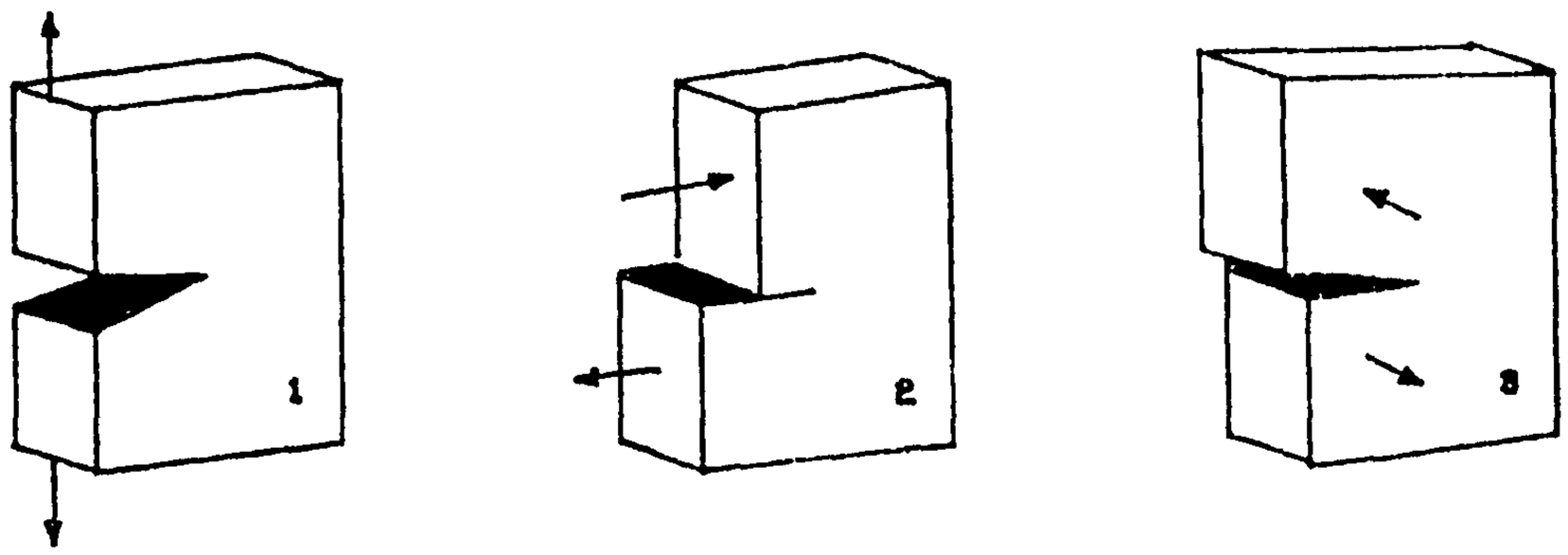

Fig. 4.2.2 The three models of loading

$$G = 2\Gamma \tag{4.2.6}$$

where

$G = \frac{d(F-U_a)}{da}$ mechanical energy release rate, and

$\Gamma = \frac{1}{2}\frac{dU_e}{da}$ fracture surface energy.

For constant displacement of the specimen edges (the so called fixed grip condition), the external forces do not perform work during the crack extension process (F=constant), thus $dF/da = 0$. Furthermore, as

$$U_a = -\frac{\pi\sigma^2 a^2}{E} \tag{4.2.7}$$

The instability condition for crack extension is

$$\frac{\pi\sigma^2 a}{E} = 2\gamma_e \tag{4.2.8}$$

4.2.2 The Stress Intensity Factor

The stress intensity factor is a parameter which appears from a straight forward analysis of stress at a crack tip. Before the discussion of stress field at the tip of a crack in a linear elastic body, one must first define a crack. Indeed, irrespective of the nature of the field, the stress systems in the vicinity of a crack tip may be considered as a combination of three simple modes of loading (Fig. 4.2.2).

In Mode 1, the opening mode, the crack surface displacements are perpendicular to the plane of the crack. In Mode 2, the sliding mode, the crack surface displacements occur in the plane of the crack and perpendicular to the leading edge of the crack. In Mode 3, the tearing mode, the crack surface displacements are also in the plane of the crack but parallel to the leading edge. Of these modes, Mode 1 is the predominant stress situation in many practical cases.

The derivations of elastic stress field equations for the Mode 1, Mode 2, and Mode 3 can be found in many textbooks on fracture mechanics, eg., Ewalds and

Wanhill (1984) and Williams (1984). The general form of the stress intensity factor K is given by

$$K = \sigma\sqrt{\pi a}\ f(\frac{a}{W}) \qquad 4.2.9$$

where $f(a/W)$ is a dimensionless parameter that depends on the geometries of the specimen and crack. For a through-cracked plate, $f(a/W) = 1$, so

$$K = \sigma\sqrt{\pi a} \qquad 4.2.10$$

4.2.3 The Fracture Toughness and J-integral

The importance of fracture mechanics is that it enables the derivation of a quantitative relationship between the applied stress necessary to cause failure in a structure or test piece, and the size of any defect or precrack that may be present. The quantity which must be measured to link these two parameters is a material's toughness, K. It is defined as the value of the stress intensity factor at which crack growth commences.

A similar parameter known as the fracture energy, G, is the energy consumed in producing a unit of crack surface. Since $K = \sigma\sqrt{\pi a}$ fracture energy and fracture toughness have the relationship:

$$G = \frac{K^2(1-\nu^2)}{E} \qquad 4.2.11$$

where

ν = Poisson's ratio,

E = Young's modulus.

For structural engineers, fracture toughness, as a failure criterion, can be used to determine how large a crack that a structure will tolerate at a certain load without failure, or, how large a fracture load is required to initiate fracture extension. But

for the mining and civil engineers, some applications of fracture toughness for rock are as follows:

1. a parameter for classification of rock material,

2. an index of fragmentation processes such as tunnel boring and model scale blasting, and

3. a material property in the modelling of rock fragmentation like hydraulic fracture, explosive stimulation of gas wells, radial explosive fracturing, and crater blasting as well as in stability analysis.

If there is extensive plasticity, G cannot be calculated from the elastic stress field because of the relatively large size of the crack tip plastic zone. The J-integral concept was introduced by Rice (1968) to provide a means of determining the energy release rate in such cases. Due to its path independence, J is a characteristic scalar measure of the conditions at the crack tip, much as the stress intensity factor in linear elastic fracture mechanics (LEFM). Therefore, the J-integral concept is limited to nonlinear elasticity conditions and to model plastic behaviour of a material. This is known as the deformation theory of plasticity. When applying the J-integral concept, however, it is important to remember that no unloading may occur in any part of a body, as the deformation behind the tip is irreversible.

For an elastic, not necessarily linear, material

$$J = G = \frac{d(F - U_a)}{da} \qquad 4.2.12$$

Note that for elastic behaviour $J = G$ by definition.

Now we may define the potential energy U_p as

$$U_p = U_0 + U_a - F \qquad 4.2.13$$

i.e.

$$U = U_p + U_e \qquad 4.2.14$$

Thus all of energy terms that may contribute to nonlinear elastic behaviour are included in U_p, except U_e since the change in elastic surface energy owing to crack extension is generally irreversible. Since U_0 is a constant, differentiation of U_p gives

$$\frac{dU_p}{da} = \frac{d(U_a - F)}{da} = -\frac{d(F - U_a)}{da} \qquad 4.2.15$$

so

$$J = -\frac{dU_p}{da} \qquad 4.2.16$$

The J-integral resistance measurements on rock have been carried out by Wilkening (1978), Schmidt and Lutz (1979), and Constin (1981).

4.2.4 Fracture Toughness Testing of Geological Materials

Fracture toughness is one of the key parameters in understanding brittle fracture. The standardized test methods of linear elastic fracture mechanics (LEFM), such as E399 in USA and BS5447 in United Kingdom, are based on conservative design criteria, since it is the prevention of failure that is usually desired in man-made structures. Some criteria of validity for fracture toughness — K_{Ic}, are quite stringent (Ouchterlony, 1982). For example, in E399,

1. the specimen size requirements:

   a. thickness$\leq 2.5\ (K_{\mathrm{Ic}}/\sigma_y)^2$

   b. crack length$\leq 2.5\ (K_{\mathrm{Ic}}/\sigma_y)^2$

2. specimen precracking requirements:

   a. K_{MAX} in fatigue$\leq 0.6\ K_{\mathrm{Ic}}$

   b. final crack length within 45 - 55% of depth W

c. local crack geometry

3. test procedure and interpretation:

a. 5% offset scant used to determine F_5 and F_Q from load vs displacement curves

b. $F_{MAX}/F_Q < 1.1$

c. loading rate.

All fracture toughness for rocks are invalid as most of the requirements for specimen configurations based on the standardized test methods are impossible to machine or impractical to perform on rocks. Also fatigue pre-cracks are very difficult to form on rock samples (Zhao, 1984). Until then, there was no standard method for the fracture toughness testing of rocks. Methods previously used in rock fracture tests have included the following:

– Short Bar, SB;

– Short Rod, SR;

– Double Cantilever Beam (Pulled), DCBP;

– Double Cantilever Beam (Wedge load), DCBW;

– Double Torstan, DT;

– Single Edge Notched Beam (or Three Point Bending) SENB-3PB;

– Single Edge Notched Round Bar (Three Point Bending) SENRB-3PB;

– Circumferentially Notched Round Bar (Pull), CENBP;

– Single Edge Notched Beam (Pulled), SENBP;

– Compact Tension, CT;

– Double Edge Notched Plate, DENP;

– Centre Notched Plate, CNP;

– Burst Test (Internally notched), BTI;

– Indentation Test, IT;

– Semi-Circular Disc, SCD; etc.

There are often large differences in published estimates of the fracture toughness obtained from tests on the same material, but using different testing techniques.

In recent years, there has been considerable interest in the use of Chevron-notched specimens in fracture tests, specially in fracture toughness testing of ceramics, rocks, high-strength metals and other brittle materials (Barker, 1977). The unique features of a Chevron-notched specimen over conventional fracture toughness specimens, are: (i) the extremely high-stress concentration at the tip of the Chevron notch, and (ii) the stress-intensity factor passing through a minimum as the crack grows (Newman, 1984). These features make the specimen smaller and a pre-cracking specimen is not needed. The fracture toughness can be evaluated from the maximum test load and a load-deformation curve is not needed for determination of effective load.

As rock is a natural material, some variation in measured values of fracture toughness is expected. Most rocks contain planar anisotropies like primary bedding, foliation, or micro crack sets, and nearly all rock types investigated for anisotropy show some effects on fracture toughness and energy measurements. Examples are shale (Kenner et al., 1984; Schmidt, 1977), coal (Kirby and Mazur, 1985; Klepaczko et al., 1984), limestone and granite (Ingrattea, 1981), sandstone and limestone (Hoagland et al., 1973; Schmidt, 1976), sandstone and marble (Atkinson, 1979), and granite (Peng and Johnson, 1972).

Thus, not only are the values of fracture toughness and energy of the rocks likely to be affected by the configuration of specimens, the loading geometry and crack length, they are also affected by the test environment as well. Generally, the fracture toughness in the presence of water is lower than that measured in air, eg., there is a 10% reduction in the Avils Point oil shale (Schmidt, 1977), a 33% reduction in Berea sandstone, 34% reduction in Salem limestone (Hoagland et al.,

1973) and a 5% reduction in Granite (Meredith, 1983). Other investigations have shown the effects of temperature (Hoagland et al., 1973).

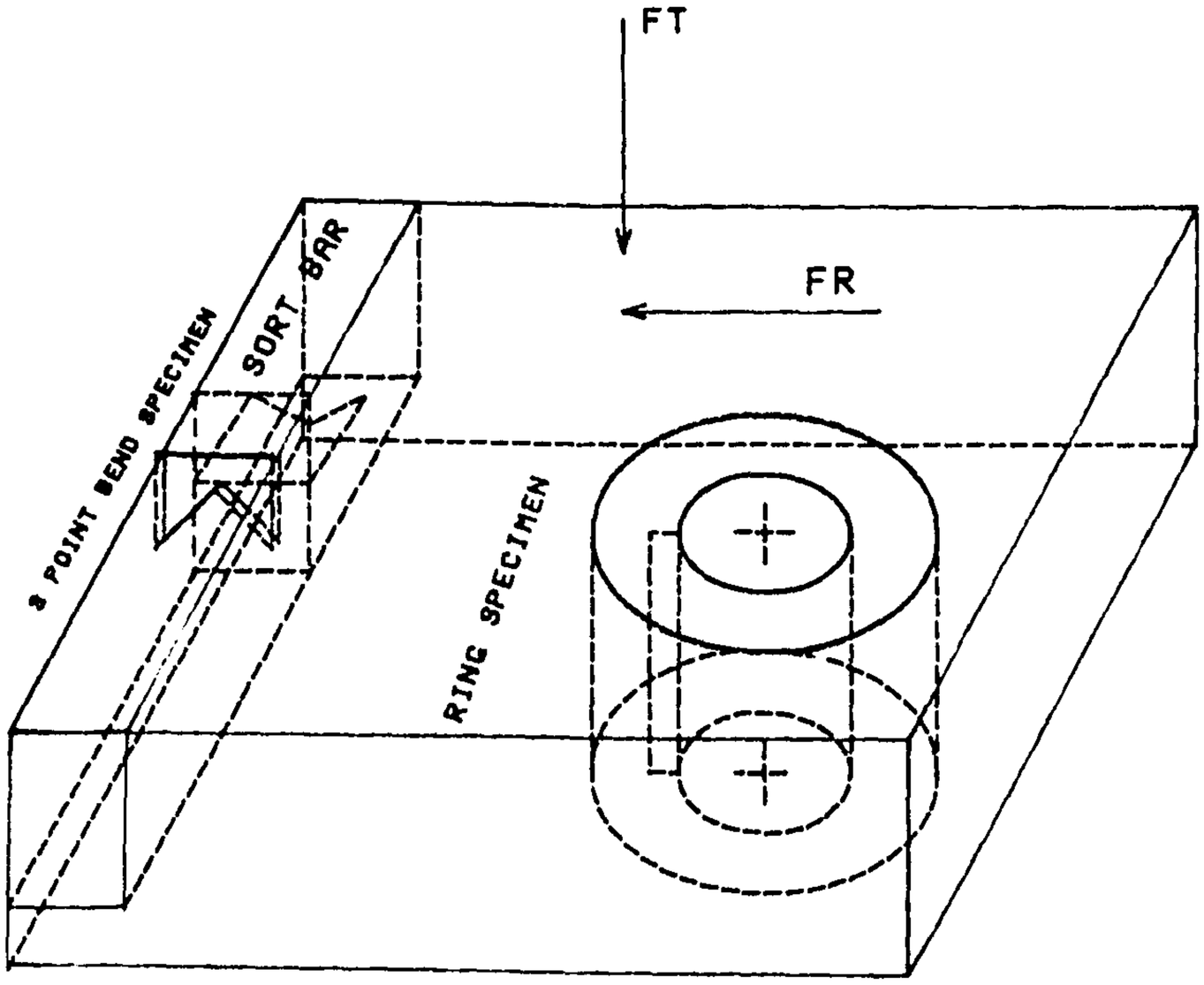

Fig. 4.2.3 The preparation of the specimens

Presented here are descriptions and results of fracture toughness for all three directions of rock materials used in the rock cutting tests. The methods of testing included: radially cracked, line loaded ring specimens, short bar specimens and Chevron-notched three points bend specimens. All of the specimens were from the rock blocks which were also used for rock cutting tests. The specimens were prepared as follows (Fig. 4.2.3):

1. the ring specimen to give the fracture toughness of cutting direction,
2. the three point bending specimen along the thrust and,
3. the short bar along the sides.

4.3 ROCK FRACTURE TOUGHNESS TESTS USING RADIALLY CRACKED, LINE LOADED RING SPECIMENS

Previous investigations into fracture toughness tests using radially cracked ring specimens have been carried out by Underwood et al. (1972), Jones (1974), Ahmad and Ashbaugh (1982), and Thompson et al. (1984). Jones (1974) considered cylindrical shells containing one and two cracks (Fig. 4.3.1) and having aspect ratios, $\rho = R_I/R_O$, (where R_I and R_O are the inner and outer radii of the ring), of 0.5, 0.8 and 0.9. For a single crack configuration of ρ=0.5 and compressive loading (Fig 4.3.1a), it was found that within a range of non-dimensional crack length $\alpha = a/(R_O - R_I)$ (where a is the crack length) of 0.5 to 0.65, the Mode 1 stress intensity factor, K_I, remains practically constant. But in configurations with $\rho \neq 0.5$, the constant K_I feature is not found. Using a finite element technique, an attempt was made by Ahmad and Ashbaugh (1982) to design a specimen for which K_I remains constant over a large range of non-dimensional crack lengths. The advantages of adopting this type of test are very clear and as follows:

1. specimens can be made directly from rock cores obtained during the geotechnical site investigation;

2. the fracture toughness is measured along the diametrical direction of the rock core, this being the most important direction for the purpose of designing a large range of engineering projects;

3. the specimens can be prepared without difficulty and no sophisticated special equipment is needed be employed for the test procedures.

The present study is aimed at applying this method to rock fracture tests.

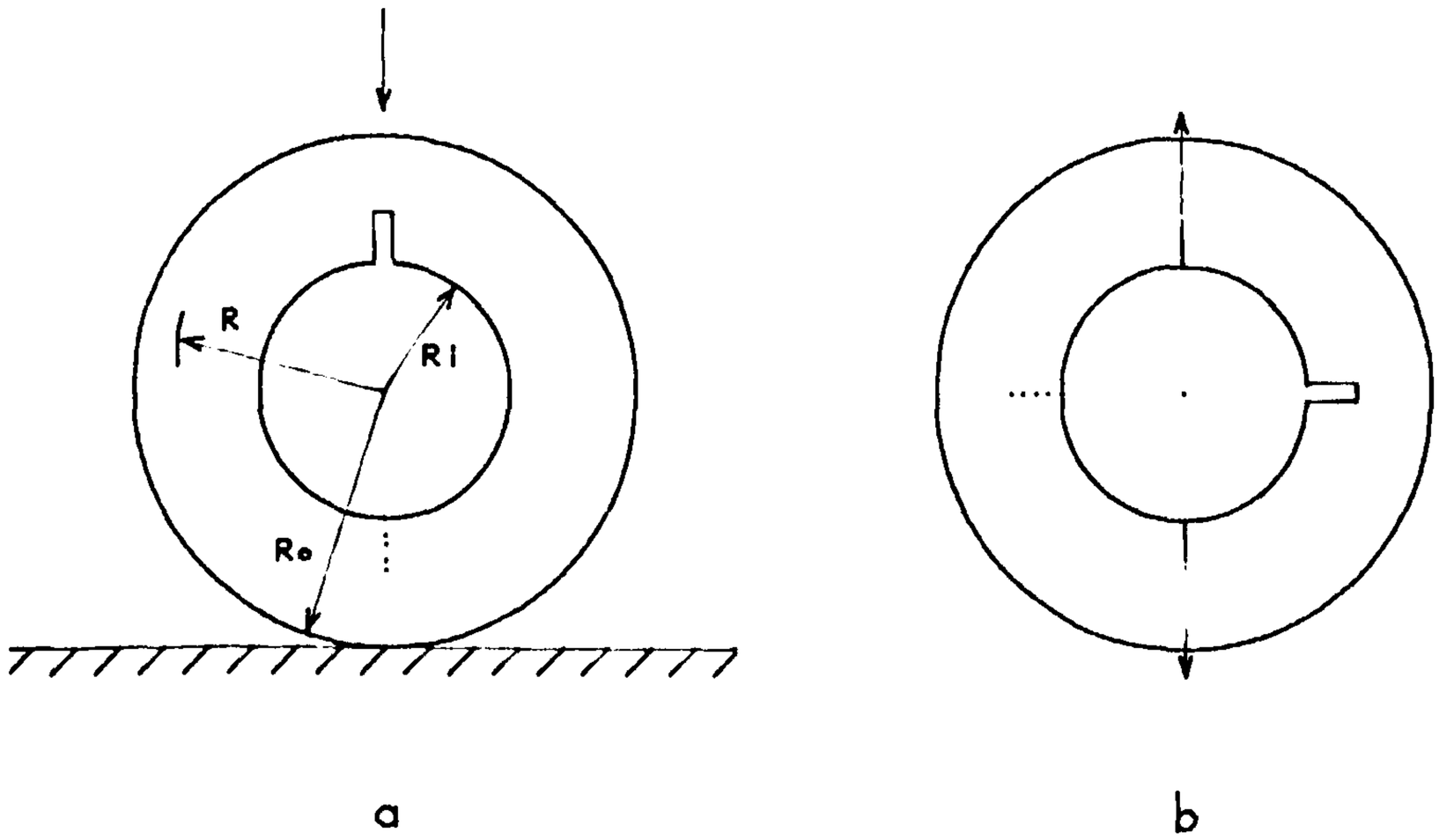

Fig. 4.3.1 Ring specimen

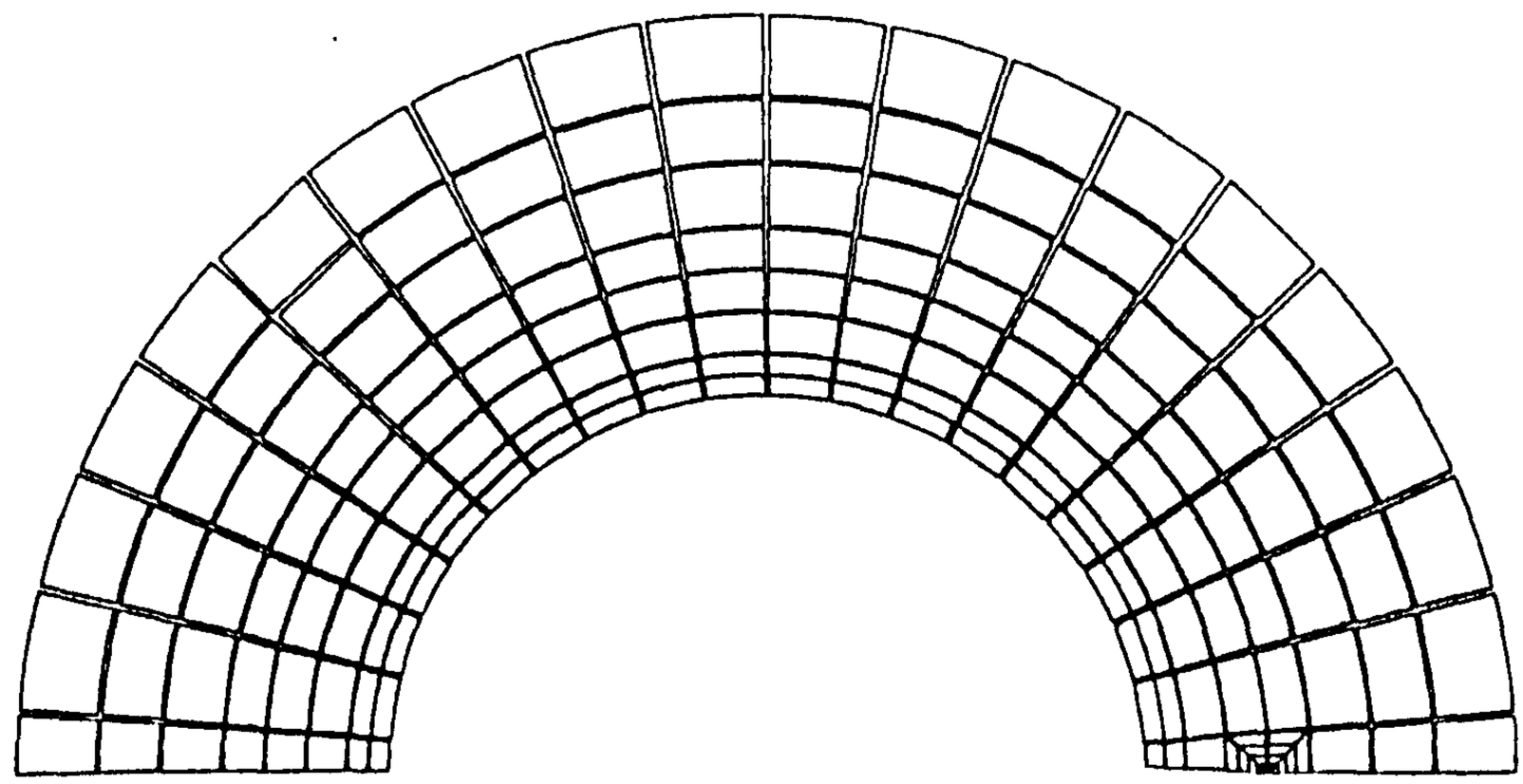

Fig. 4.3.2 Typical finite element mesh for single notch ring specimen

4.3.1 Determination of Stress Intensity Factors

As the theoretical analysis of the radially cracked ring specimens is very complex, some authors (Jones, 1974; Ahmad and Ashbaugh, 1982; Thompson et al., 1984) employed the finite element method for the determination of the stress intensity factors.

A standard package of finite element analysis, PAFEC, with eight noded, curved, isoparametric elements has been used in this study. The elements on the crack tip are six noded triangular elements as specially required by the package. The element size for the specimens was determined by refining the mesh until two successive runs were within 3% for K_I in the regions where comparisons were meaningful. Normally, the final mesh consisted of approximately 160 elements with 600 nodes. The typical mesh for PAFEC finite element analysis is shown in Fig. 4.3.2.

The finite element analysis results were non-dimensionalized using the following definitions (Ahmad and Ashbaugh, 1982):

Non-dimensional Mode I stress intensity factor

$$Y = \frac{K_I B\sqrt{R_O}}{P} \qquad 4.3.1$$

Non-dimensional load-line compliance

$$C(l - l) = \frac{BE\delta(l - l)}{P} \qquad 4.3.2$$

Non-dimensional crack-mouth compliance

$$C(m - m) = \frac{BE\delta(m - m)}{P} \qquad 4.3.3$$

Non-dimensional crack length

$$\alpha = \frac{a_0}{R_O - R_I} \qquad 4.3.4$$

Table 4.3.1 Non-dimensional stress intensity and load-line compliance

R_I/R_O	$a_0/(R_O - R_I)$	Y	$C(m-m)$
0.455	0.1	1.766	1.345
0.5	0.5	2.706	6.473
0.5	0.333	2.661	4.430
0.5	0.25	2.570	3.427
0.6	0.5	5.335	11.303
0.6	0.333	4.890	7.082

where

$\delta(m-m)$ = the displacement at the crack mouth (inner radius);

$\delta(l-l)$ = the total displacement between the two load points.

In order to determine any size effects affecting the fracture toughness measurements, different sizes of specimens were tested. Such specimens had the nominal outside diameters, D_O, of 100mm and 75mm, and internal diameter, D_I, 50mm and 45.5mm. The ratios of the length of cracks and width of the ring were 0.1, 0.25, 0.333, 0.5. Table 4.3.1 presents the results of finite element analysis for the various specimen geometries and crack lengths used in the study.

4.3.2 Test Procedures

The ring specimens were prepared, first by use of a small core drilling tool to effect the inside surface of the specimen, and then a bigger tool was used to effect outside surface of the specimen. Finally, the crack width of 1.5 mm was cut by a hacksaw, see Plate 4.3.1 (on top). Prior to testing, the specimens were dried at 110° C for 5 hours in order to minimize the possible effects of different in moisture content from one specimen to another.

The tests were carried out on a 100 kN servo-hydraulic, closed-loop testing

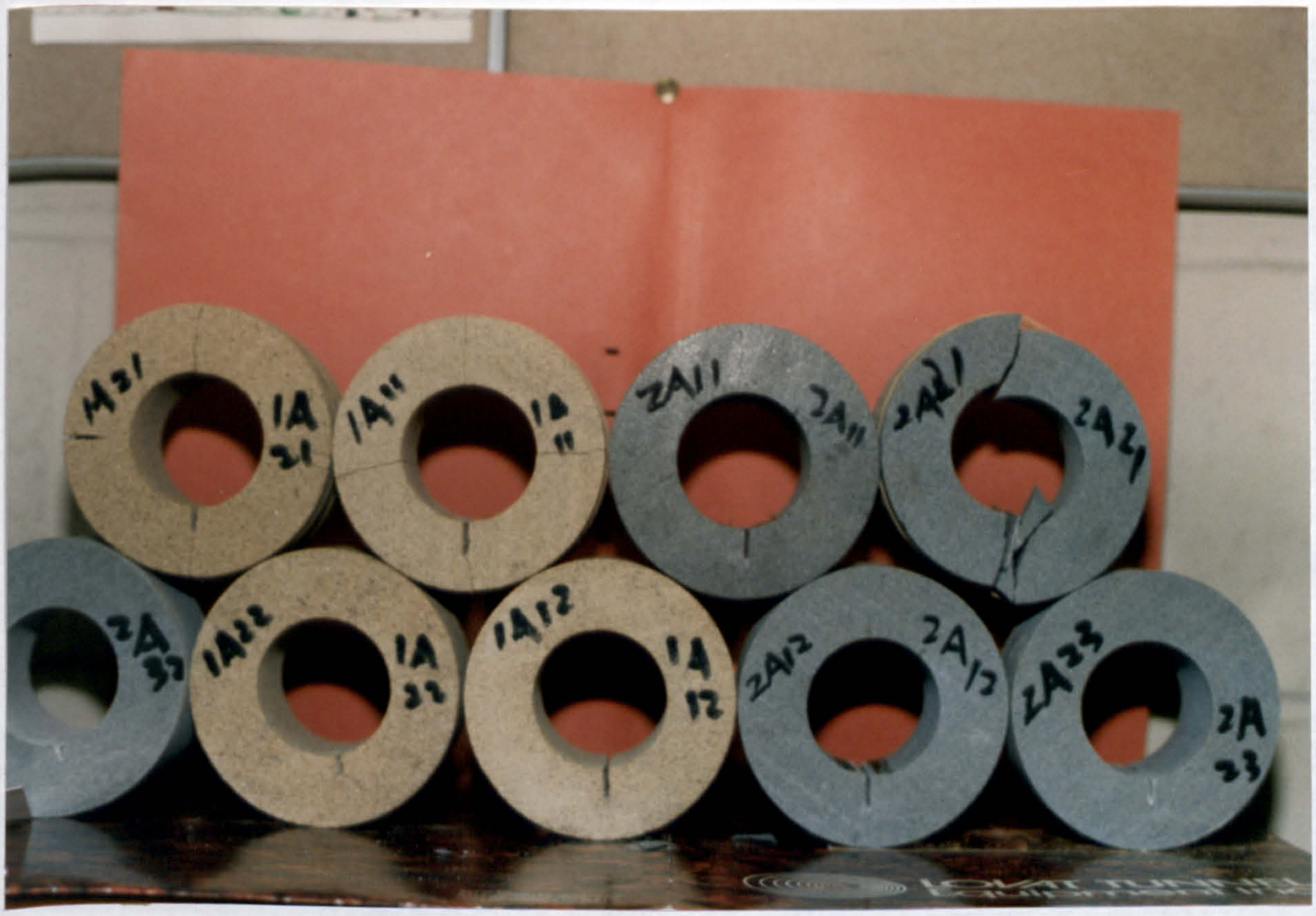

Plate 4.3.1 The ring specimens

machine. The load was read by a ring-shape transducer and recorded by a data-logger using an LVDT. Three LVDT's and two clip gauges were used to measure the displacements. One LVDT was used for measurement of loading point deformation, two for horizontal deformations and two clip gauges for crack open deformation (Plate 4.3.2). The clip gauges were made by the Department workshop based on the drawing provided by ASTM standard E399-78 (Fig. 4.3.3). These gauges were calibrated to the nearest 0.0025 m (0.0001 in). A pair of knife edges that support the gauges' arms and serving as displacement reference points, were attached to the specimens using adhesive prior to testing.

All data, which included the load magnitude, the load point displacement, two horizontal deformations, two crack open deformations, were stored in a data logger (Plate 4.3.3). The curves of load versus load point displacement, load vs horizontal displacement and load vs crack open deformation, were then drawn using GHOST

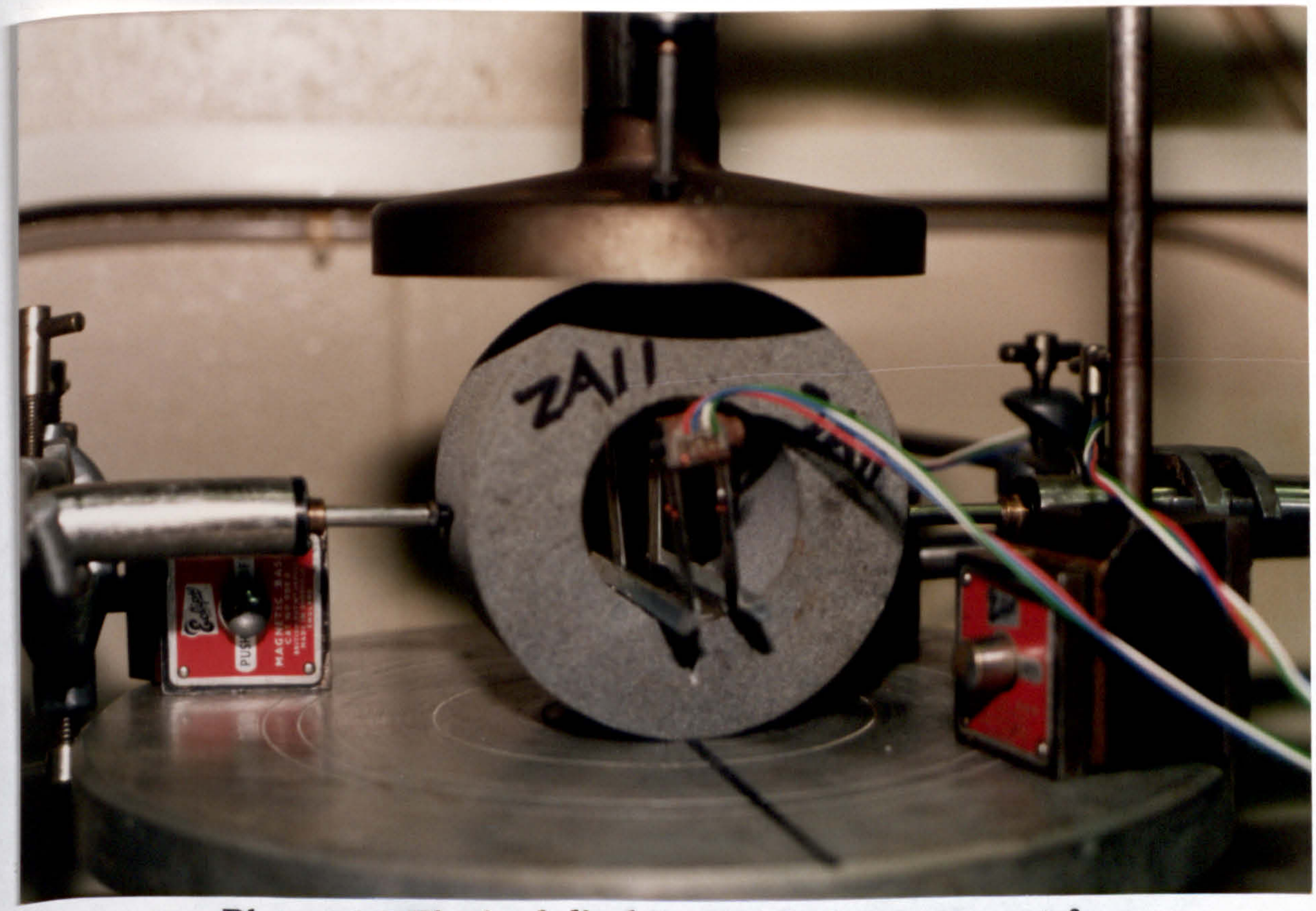

Plate 4.3.2 The load-displacement test arrangement for the ring specimens

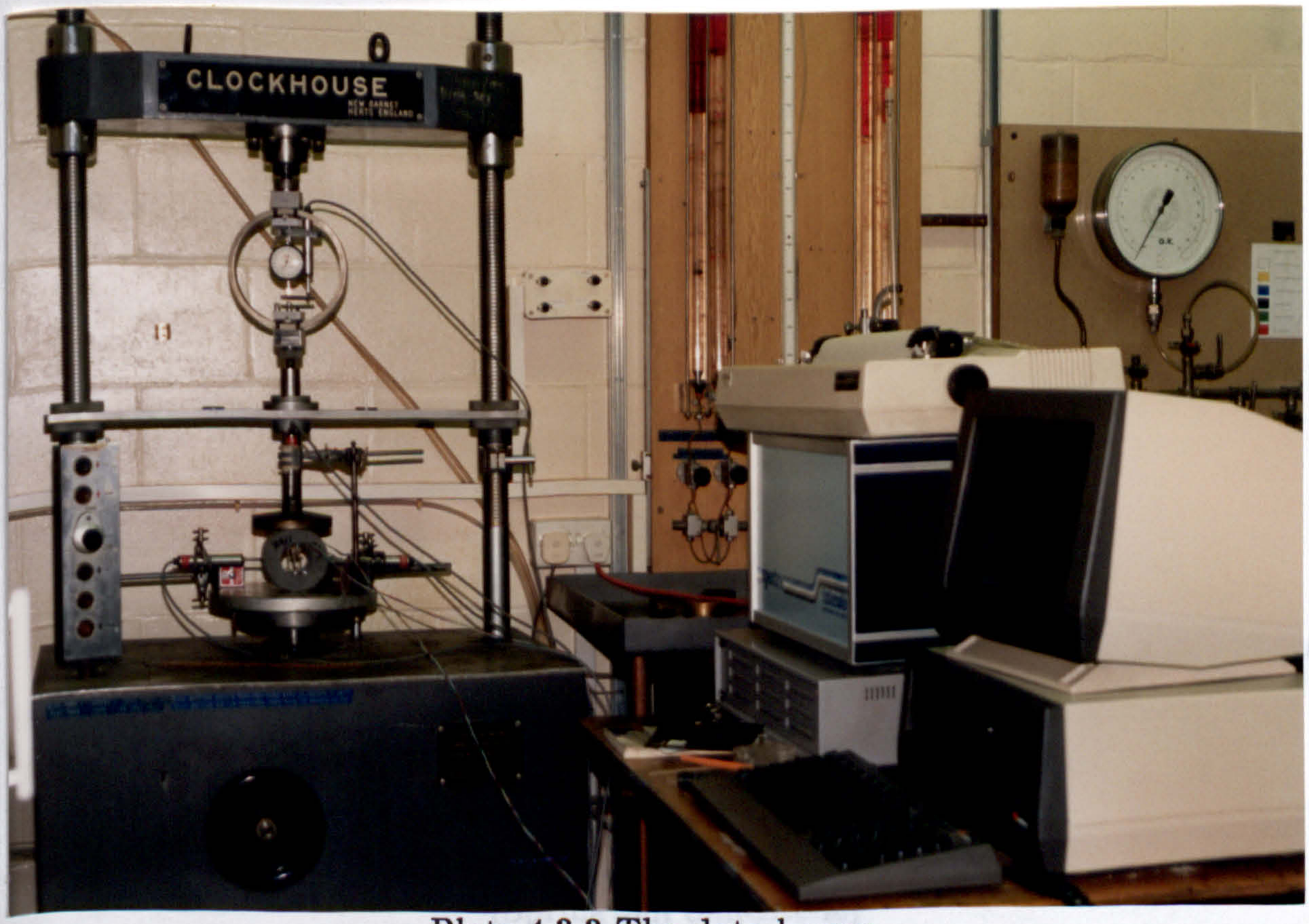

Plate 4.3.3 The data logger

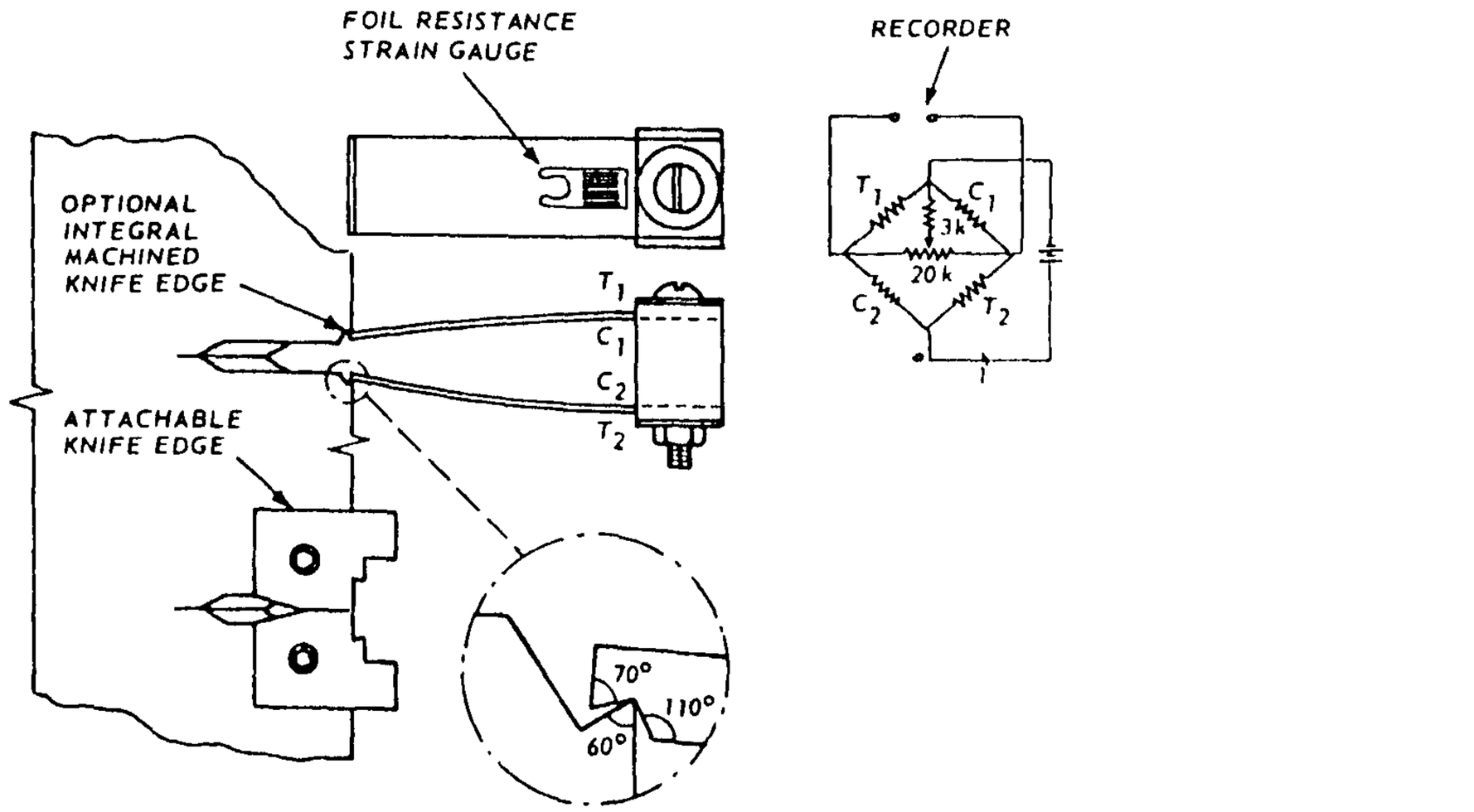

Fig. 4.3.3 Clip gauge and its attachment to the specimen

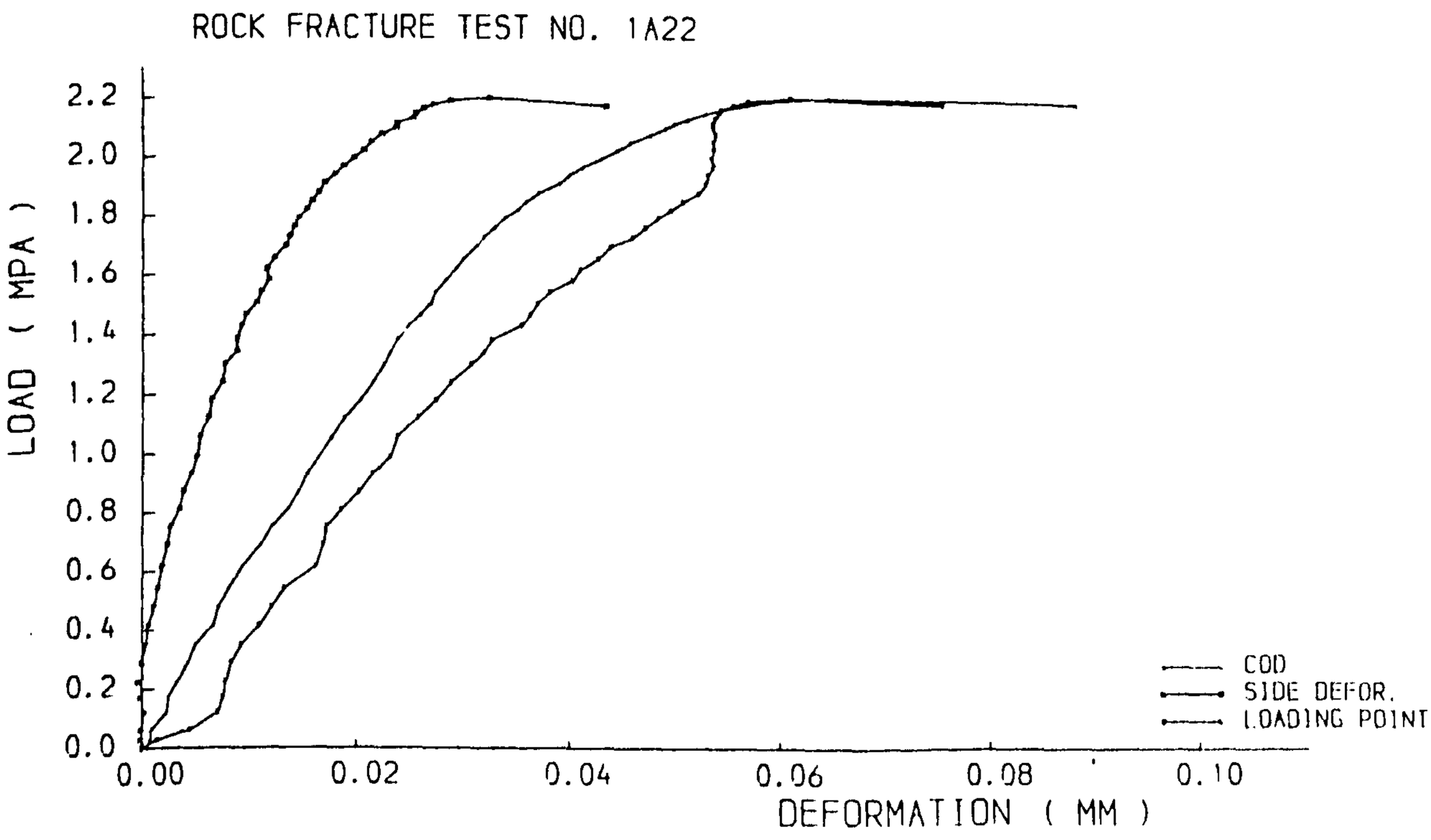

Fig. 4.3.4 Plots of load versus deformations for ring specimens (Springwell Sandstone)

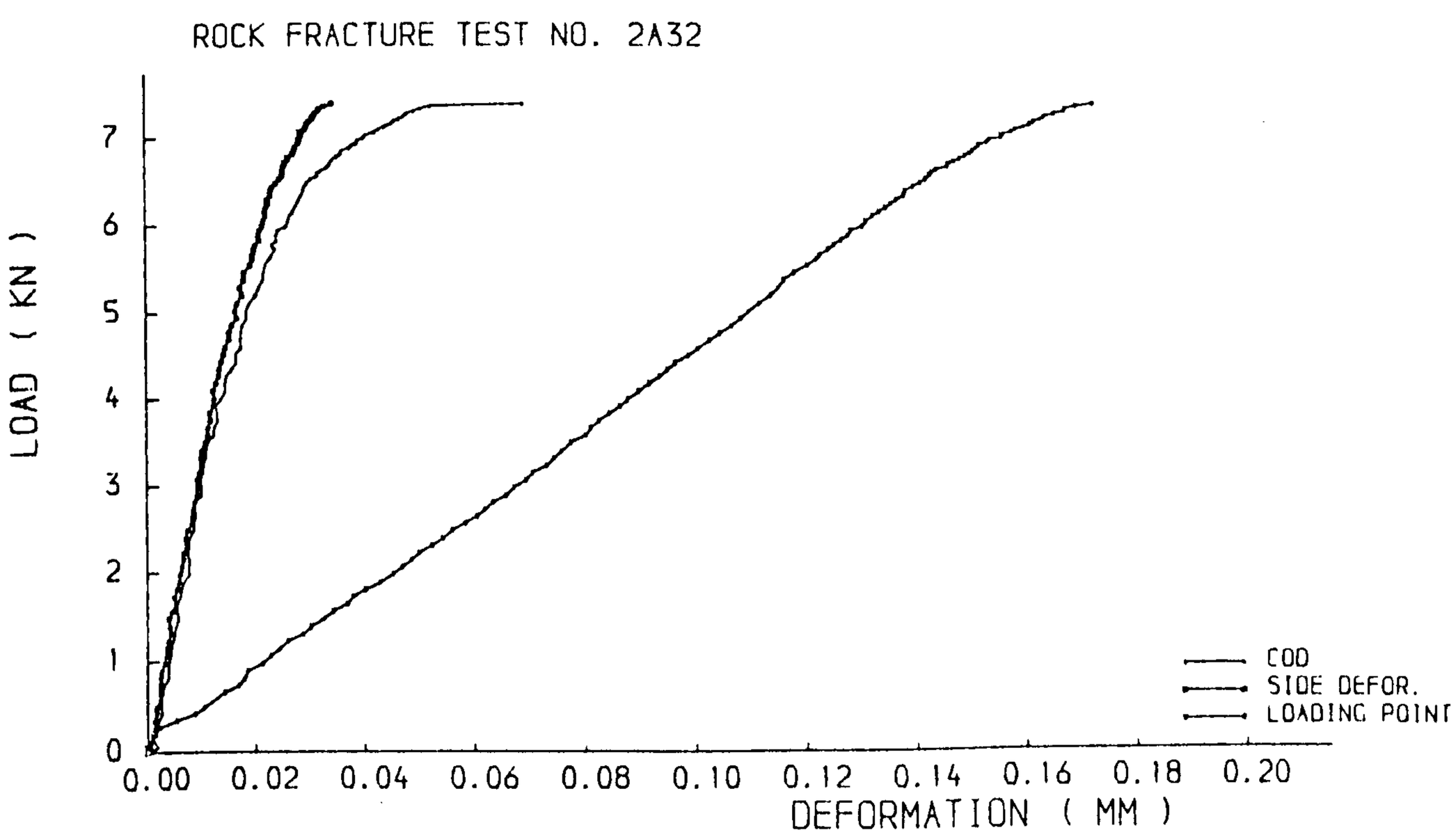

Fig. 4.3.5 Plots of load versus deformations for ring specimens (Pennant Sandstone)

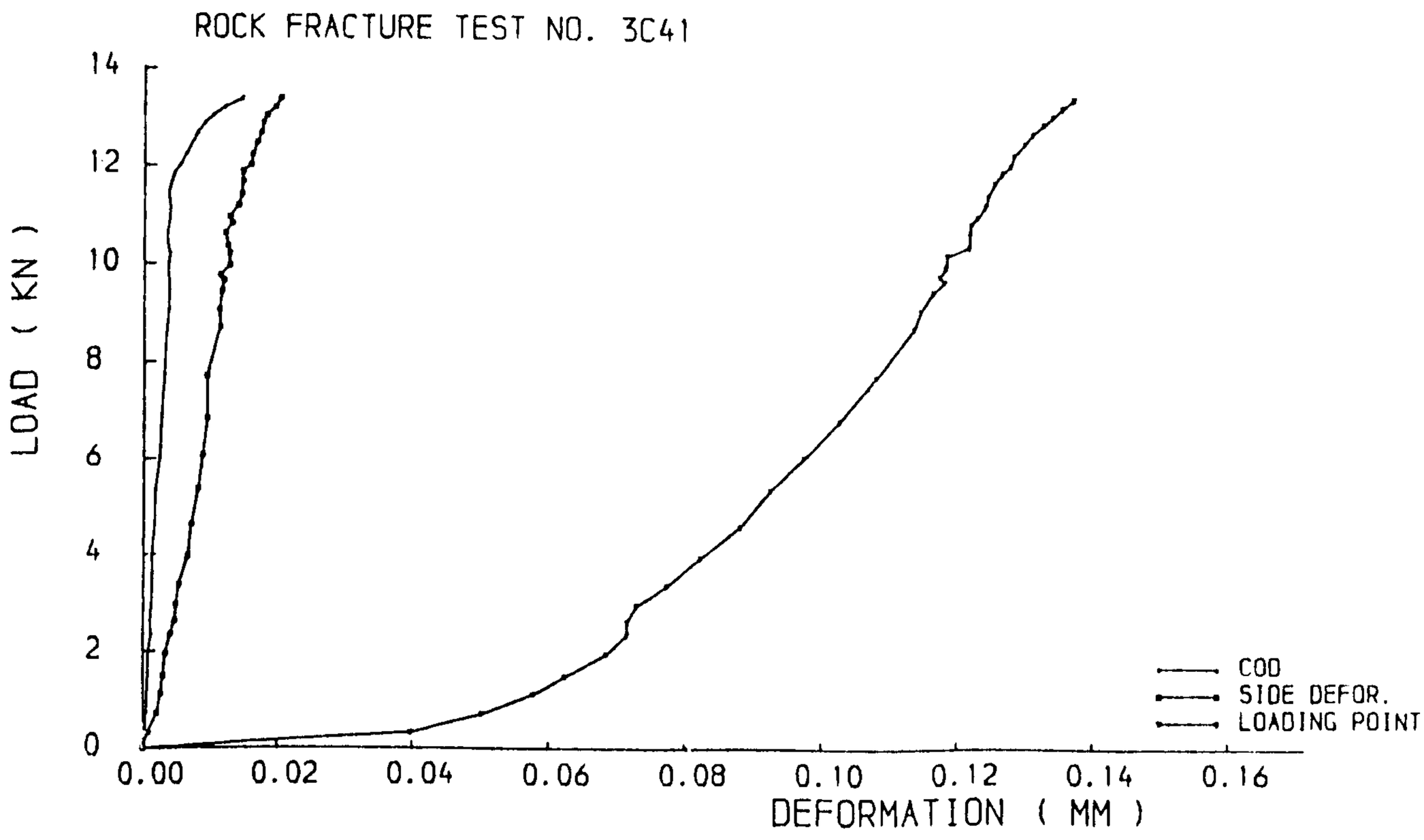

Fig. 4.3.6 Plots of load versus deformations for ring specimens (Whinstone)

– NUMAC main frame software package (Figs 4.3.4 - 4.3.6).

4.3.3 Results

The fracture toughness results obtained from the Springwell Sandstone, Pennant Sandstone and Whinstone for the radially cracked line loaded ring specimens are shown in Table 4.3.2. The first column of the specimen identification is the rock material where 1 is Springwell Sandstone, 2 Pennant Sandstone and 3 Whinstone. The second column is the specimens' geometry in which A is the ring with R_O=0.05m, R_I=0.025m, B is the ring with R_O=0.0375m, R_I=0.02275m, and C is the ring with R_O=0.05m, R_I=0.02275m. The third column is the non-dimensional crack length in which 1 is for α=0.5, 2 for α=0.3333, 3 for α=0.25 and 4 for α=0.1. The last column gives the specimen number.

4.3.4 Discussion

Plate 4.3.1 shows that the failure are straight alone the cracks when the specimens break and the energy stored in the testing machine is released. This causes the specimen to further fragment into four pieces (Plate 4.3.1 on top).

Figs 4.3.4 to 4.3.6 show the parametric plots of load versus displacement for each of three rocks. In each case, the specimen was loaded and unloaded twice to minimize the effect of contact between the load plates and the specimens. Then the specimen was slowly loaded with the table moving at a speed of 0.02 mm/min until the specimen broke. For the Springwell Sandstone, the displacement of the loading point initially increases linearly with load P and then there is a gradually increasing non-linearity until the specimen is finally broken. In the case of the Pennant Sandstone, the non-linearity only appears shortly before fast fracture. The Whinstone specimens, however, behave almost perfectly elastically, and break only after the maximum load is reached.

Table 4.3.2 Results of the fracture tests using radially cracked, line loaded ring specimens

Specimen iden. No	R_O m	R_I m	a_0 m	B m	P_{MAX} kN	K_{Ic} $MPa\sqrt{m}$
1A11	0.05	0.025	0.0125	0.05	2.02	0.49
1A12	0.05	0.025	0.0125	0.05	1.71	0.41
					$\overline{X} =$	0.45
1A21	0.05	0.025	0.00833	0.05	1.86	0.44
1A22	0.05	0.025	0.00833	0.05	2.18	0.52
					$\overline{X} =$	0.48
1B11	0.0375	0.02275	0.007375	0.0455	0.49	0.30
1B12	0.0375	0.02275	0.007375	0.0455	0.81	0.49
1B13	0.0375	0.02275	0.007375	0.0455	0.61	0.37
					$\overline{X} =$	0.39
1B21	0.0375	0.02275	0.004917	0.0455	0.78	0.44
1B22	0.0375	0.02275	0.004917	0.0455	0.52	0.29
					$\overline{X} =$	0.37
2A11	0.05	0.025	0.0125	0.05	6.90	1.67
2A12	0.05	0.025	0.0125	0.05	5.74	1.39
2A13	0.05	0.025	0.0125	0.05	7.23	1.75
					$\overline{X} =$	1.60
2A21	0.05	0.025	0.00833	0.05	6.83	1.63
2A22	0.05	0.025	0.00833	0.05	6.89	1.64
2A23	0.05	0.025	0.00833	0.05	6.03	1.43
					$\overline{X} =$	1.57
2A31	0.05	0.025	0.00625	0.05	7.16	1.65
2A32	0.05	0.025	0.00625	0.05	7.39	1.70
					$\overline{X} =$	1.68
2B11	0.0375	0.02275	0.007375	0.0455	2.33	1.41
2B12	0.0375	0.02275	0.007375	0.0455	2.45	1.48
2B13	0.0375	0.02275	0.007375	0.0455	2.89	1.75
					$\overline{X} =$	1.55
2B21	0.0375	0.02275	0.004917	0.0455	2.88	1.60
2B22	0.0375	0.02275	0.004917	0.0455	2.58	1.43
					$\overline{X} =$	1.52
3C41	0.05	0.02275	0.002725	0.05	13.40	2.12
3C42	0.05	0.02275	0.002725	0.05	12.70	2.01
3C43	0.05	0.02275	0.002725	0.05	12.90	2.04
					$\overline{X} =$	2.06

The results listed in Table 4.3.2 indicate that the average fracture toughness, K_{Ic}, determined from the ring specimens with R_O 0.05mm and R_I 0.025mm, differ from that with R_O 0.0375 mm and R_I 0.02275 mm by, at most, 25% for Springwell Sandstone and 9% for Pennant Sandstone. The fracture toughness obtained by bigger rings is higher than that for the smaller rings. For the same size of rings with different length of cracks, the values of fracture toughness are nearly the same. For example, the difference between the non-dimension crack lengths of 1/2 and 1/3 is about 3%.

4.4 THREE POINT BEND TESTS

4.4.1 Basic Relations

There are three ways to determine the stress intensity coefficient Y^* for the Chevron notched specimen.

1. experimental determination of Y^* based on a comparison with standard K_{Ic} values;

2. an analytical or semi-analytical approach based on the compliance and the stress intensity factor determined for specimens with straight cracks;

3. numerical stress analysis using three dimensional finite element or three dimensional boundary element analysis.

The first and the third ways should lead to more accurate values of Y^*, however, there is still a lot of work to do as each specimen geometry should be considered. For this reason, most researchers still use the second approach.

By using the energy approach of Linear Elastic Fracture Mechanics, Munz et

al. (1980) found that:

$$K_{Ic} = \frac{P_{MAX}}{B\sqrt{W}} Y^* \qquad 4.4.1$$

and

$$Y^* = \frac{1}{2} \frac{d\ C(\alpha)}{d\alpha} \frac{\alpha_1 - \alpha_0}{\alpha - \alpha_0} \qquad 4.4.2$$

where

$\alpha_0 = a_0/W$,

$\alpha_1 = a_1/W$,

$\alpha = a/W$,

$C(\alpha) = \frac{BE'\delta}{P}$, the dimensionless compliance of the specimen with the traperoidal crack front,

$E' = \frac{E}{1-\nu^2}$ for plane strain,

δ = load point displacement.

As a first approach, Munz assumed that dC/da for the Chevron notch is identical to that for a straight-through crack.

Thus,

$$Y^* = Y(\frac{\alpha_1 - \alpha_0}{\alpha - \alpha_0}) \qquad 4.4.3$$

Substitute Eq.(4.4.3) into critical condition $d\ Y^*/d\ \alpha = 0$, we obtain:

$$\frac{dY}{d\alpha} - \frac{1}{2} \frac{1}{\alpha - \alpha_0} Y = 0 \qquad 4.4.4$$

The dimensionless critical crack length α_c is the root of Eq. 4.4.4. Substituting α_c for α in Eq. (4.4.3), Y_m^* is obtained.

Following Eqs (4.4.3) and (4.4.4), Wu (1984) obtained the stress intensity factor coefficients for Chevron notched three point bend specimen (Fig. 4.4.1) as:

$$Y^* = d_0 + d_1\alpha_0 + d_2\alpha_0^2 + d_3\alpha_0^3 + d_4\alpha_0^4 + d_5\alpha_0^5 \qquad 4.4.5$$

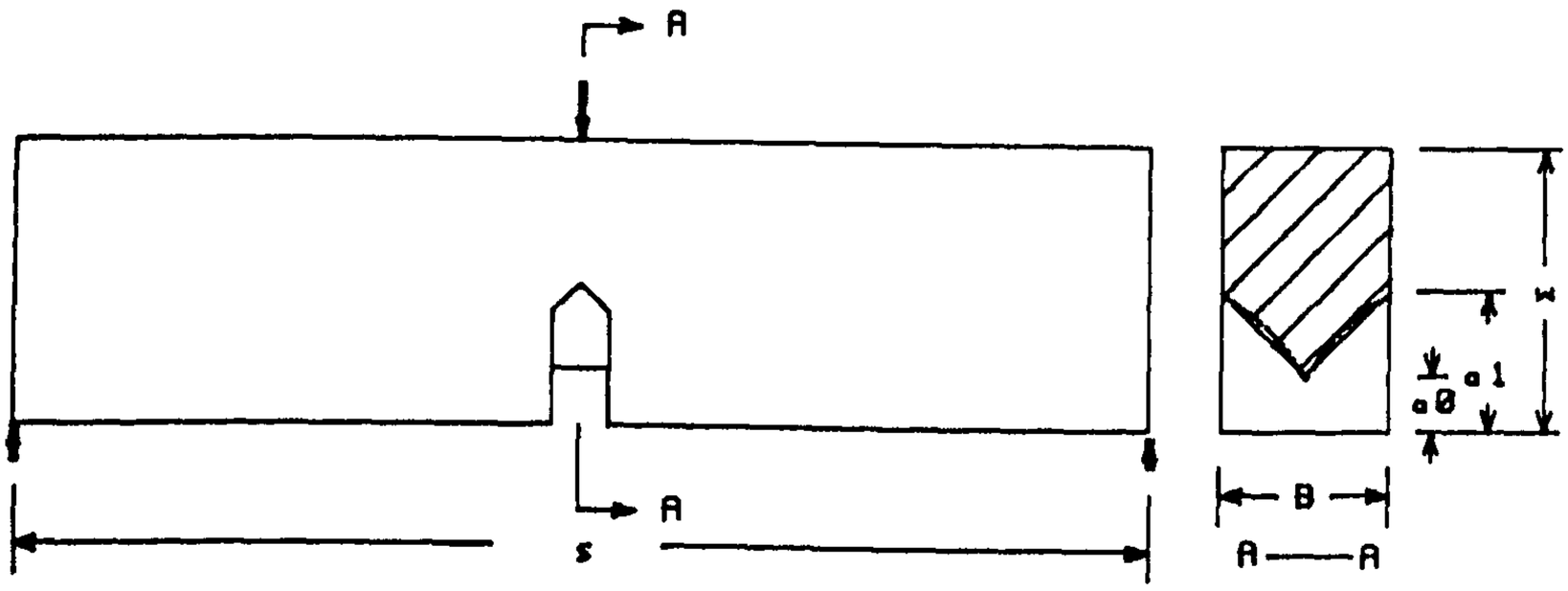

Fig. 4.4.1 The three point bend specimen

The $d's$ coefficients for chevron notch angle $\theta = 90°$ are:

$$d_0 = 2.809 \qquad d_1 = 44.51 \qquad d_2 = -269.6$$

$$d_3 = 1338 \qquad d_4 = -2736 \qquad d_5 = 2242$$

4.4.2 Test Procedure

In this study, specimens of dimension 190×45×30 mm were used. The specimens were cut from the same blocks of rocks as the ring specimens using a diamond saw with water coolant. They were then polished. The Chevron notchs were made by holding the specimen at the proper angle against a 127mm diameter diamond wheel saw for each of the two cuts. So, the resultant chevron had curved, rather than straight sides. The saw blade tip profile was semi-circular and produced a groove width of 1 mm, see Plate 4.4.1.

Plate 4.4.1 Three point bend specimens

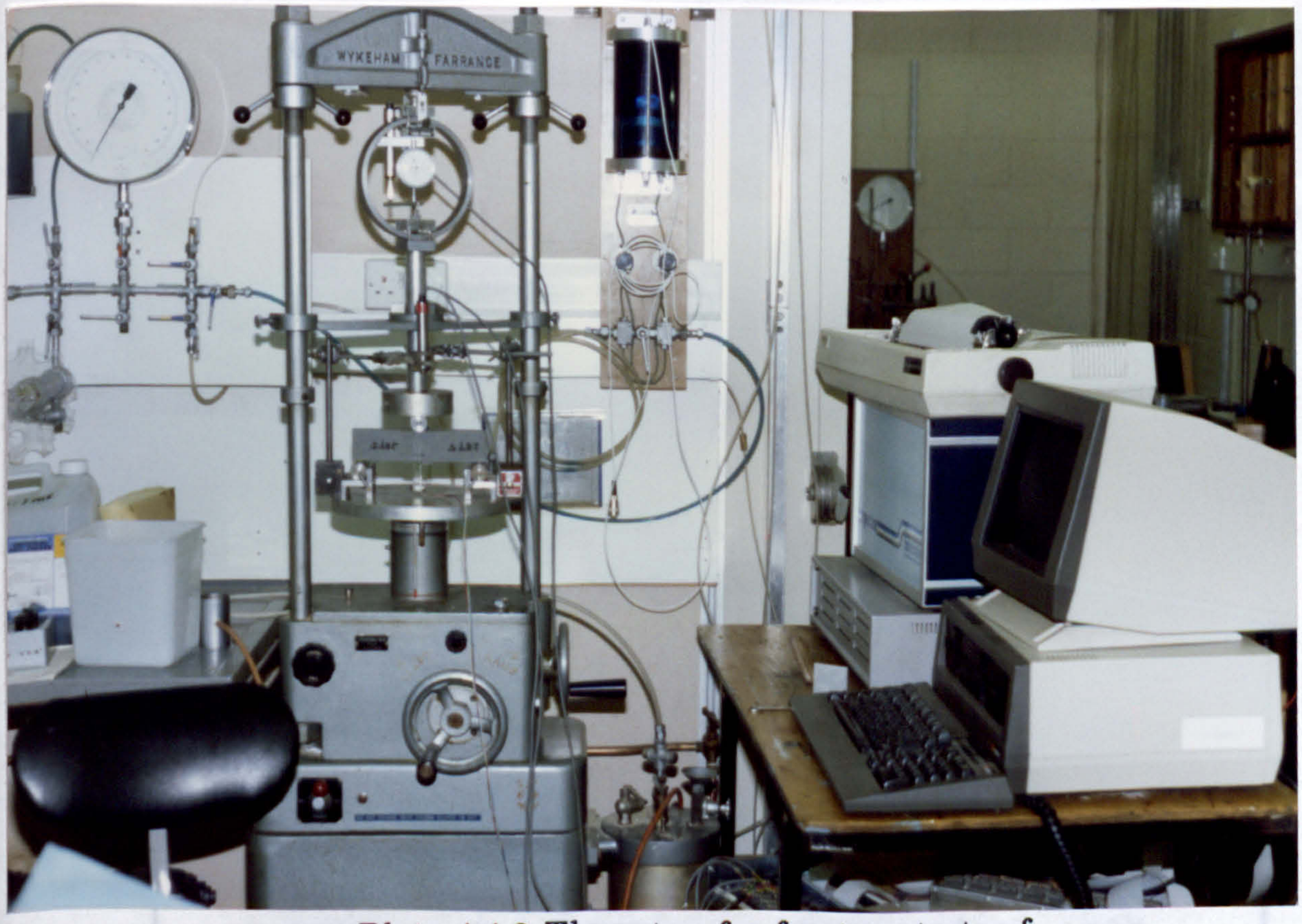

Plate 4.4.2 The setup for fracture tests of three point bend specimens

After dried at 110°C for 5 hours, the specimens were taken out and air-cooled. The tests were done using a 50 kN servo-hydraulic, closed-loop testing machine. The test fixture was designed to minimize frictional effects using support rollers to rotate outwards and to maintain rolling contact throughout the test. The rollers were initially positively positioned against stops that set the span length and were held in place by soft springs. The load point displacements and crack open displacements were recorded by a data-logger with one LVDT and one clip gauge (Plate 4.4.2).

4.4.3 Results

Table 4.4.1 shows the results for fracture toughness of three different rocks using the three point bend test. As mentioned previously, the first column represents the type of rock material, the last one the number of test specimen.

Table 4.4.1 Results of fracture tests using three-point bend specimens

Specimen Ident. No.	α_0	P_{MAX} kN	K_{Ic} $MPa\sqrt{m}$
1BT2	0.267	0.350	0.51
1BT3	0.256	0.317	0.45
1BT4	0.247	0.338	0.46
			$\overline{X}$= 0.47
2BT1	0.256	1.210	1.70
2BT5	0.242	1.150	1.54
2BT7	0.242	1.130	1.51
2BT8	0.233	1.100	1.42
			$\overline{X}$= 1.54
3BT1	0.242	1.350	1.81
3BT2	0.233	1.620	2.10
3BT3	0.256	1.540	2.17
3BT4	0.242	1.530	2.05
			$\overline{X}$= 2.03

4.4.4 Discussion

Plate 4.4.3 shows the fracture surfaces of the different rock specimens. During the fracture tests, the crack accelerates from its original position through the slow growth region, until a sharp transition to fast fracture occurs. Unlike steels, the stages of fracture are not identifiable from the fracture surface.

Typical load vs crack open displacement curves for three rocks are shown in Fig. 4.4.2, and load vs load-point displacement curves in Fig. 4.4.3. When crack propagations commence in the samples of Whinstone and Pennant Sandstone, the curves deviate from a straight line until a load maximum, P_{MAX}, is reached. At P_{MAX}, (e.g., Whinstone), or just a very short time after P_{MAX}, (e.g., Springwell Sandstone and Pennant Sandstone), the crack velocity reachs such a high value that the recorder can no longer follow the rapidly changing load and displacement. It is important to note that the specimen has not yet totally separated at the points of maximum loads.

The results for the three point bend specimens are in very good agreement with that for radially cracked, line loaded ring specimens. The difference being as follows:

1. Springwell Sandstone – 12.5%;
2. Pennant Sandstone – 2.3%; and
3. Whinstone – 1.2%.

4.5 SHORT BAR TESTS

4.5.1 Test Procedure

The short bar specimens were machined to the dimensions shown in Fig. 4.5.1. The ratio of width to diameter (W/B) was 2.0. The Chevron notch length at the

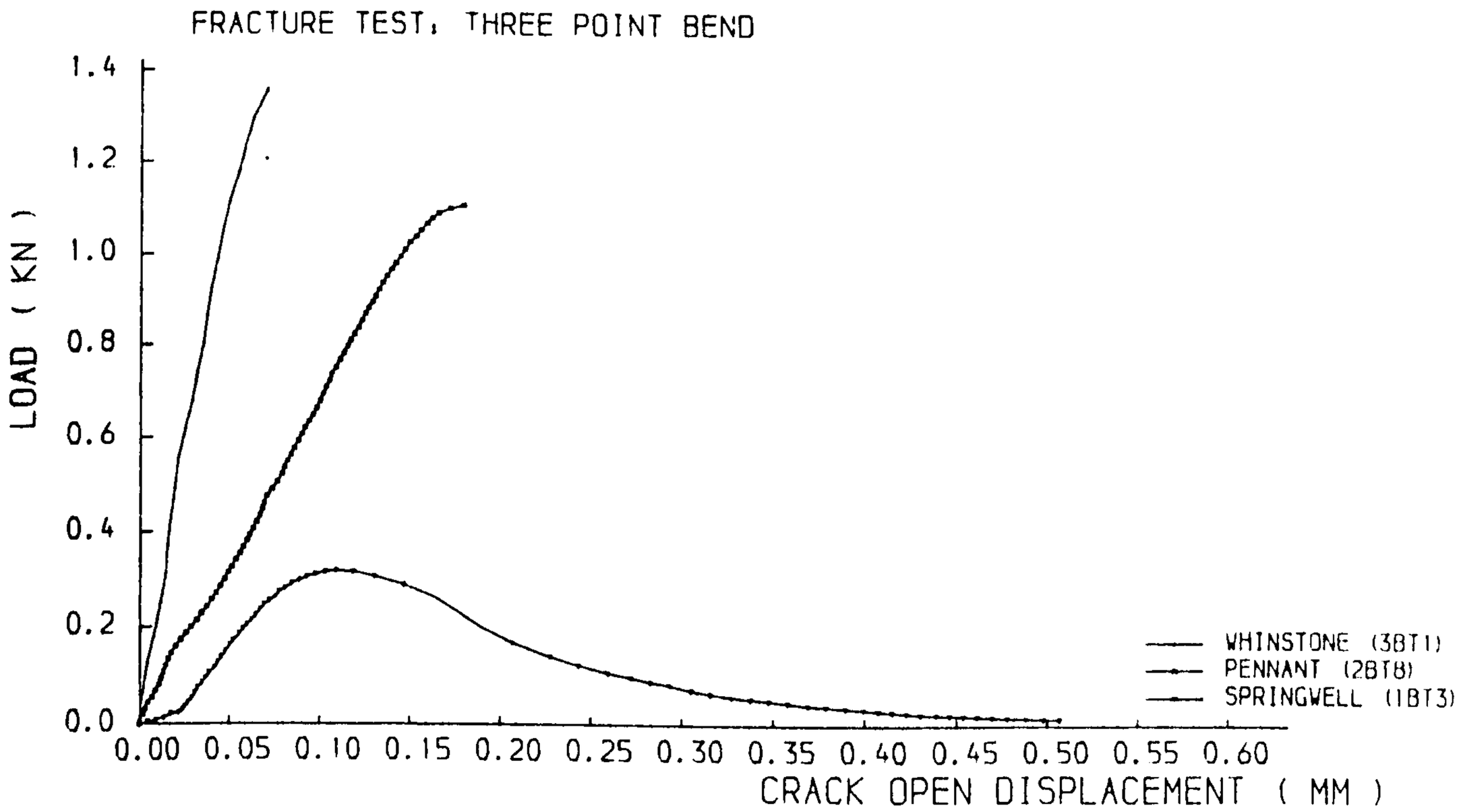

Fig. 4.4.2 Plots of load versus crack open displacements for three point bend specimens

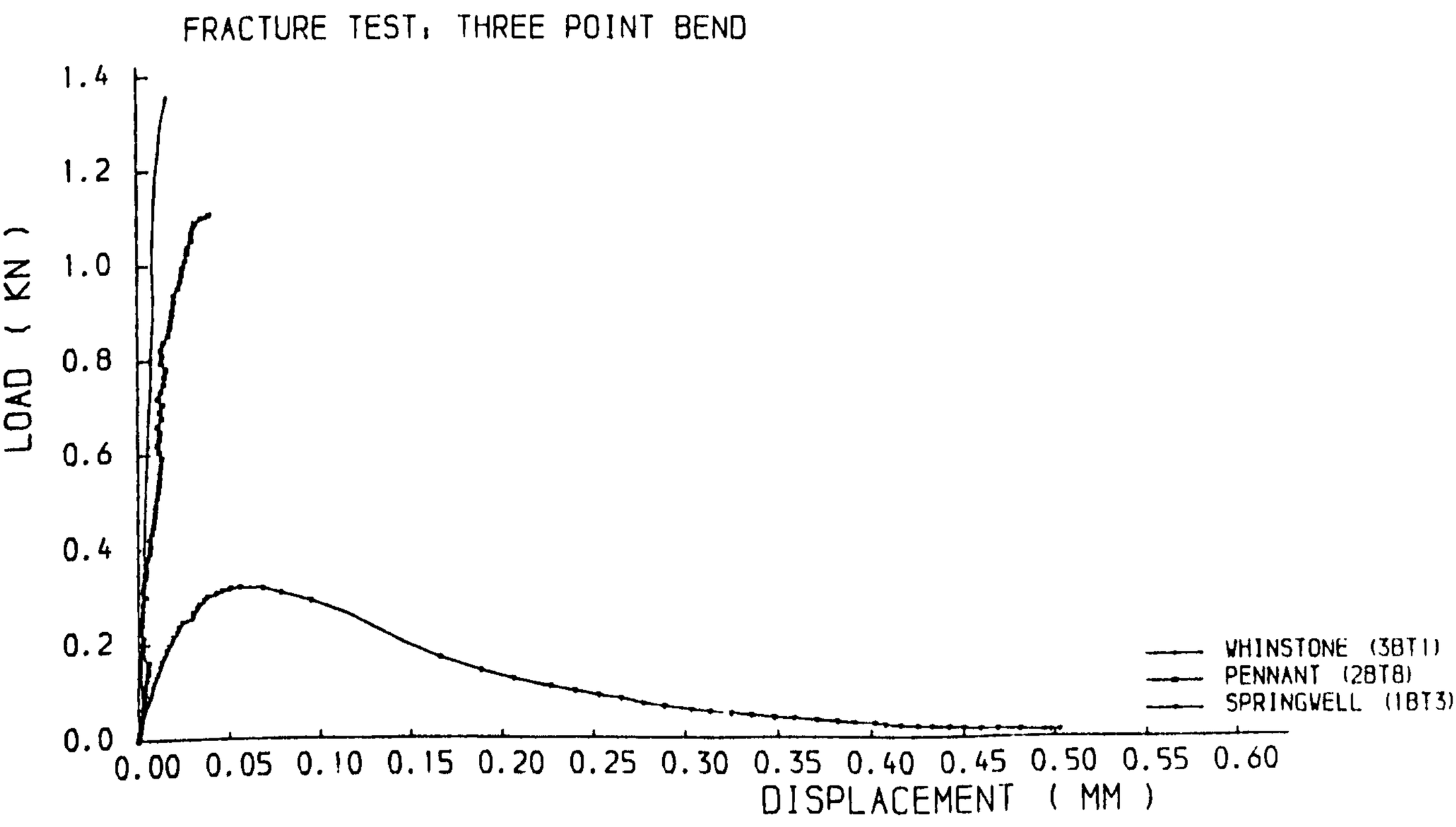

Fig. 4.4.3 Plots of load versus loading point displacements for three point bend specimens

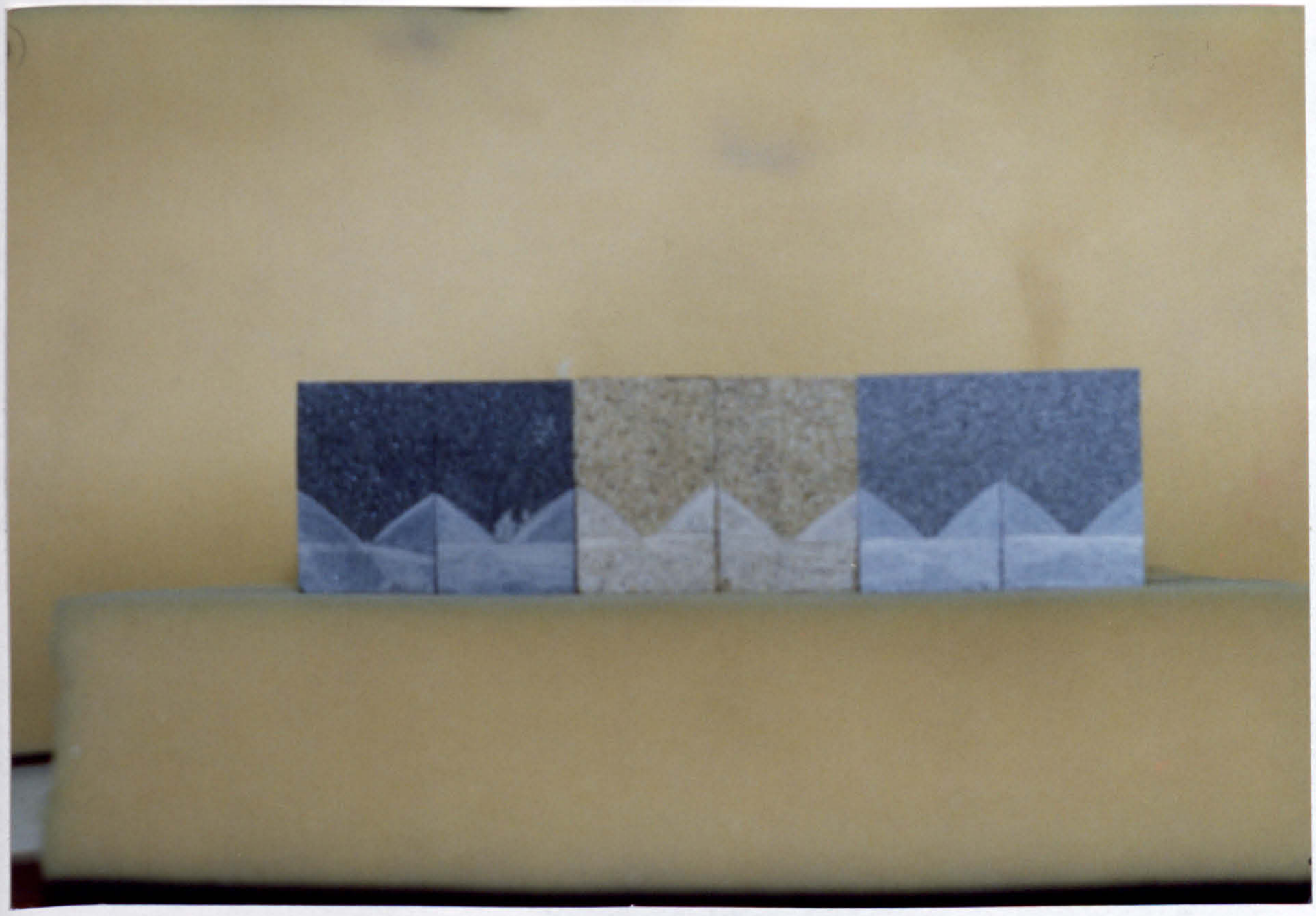

Plate 4.4.3 The crack surface of a three point bend specimen

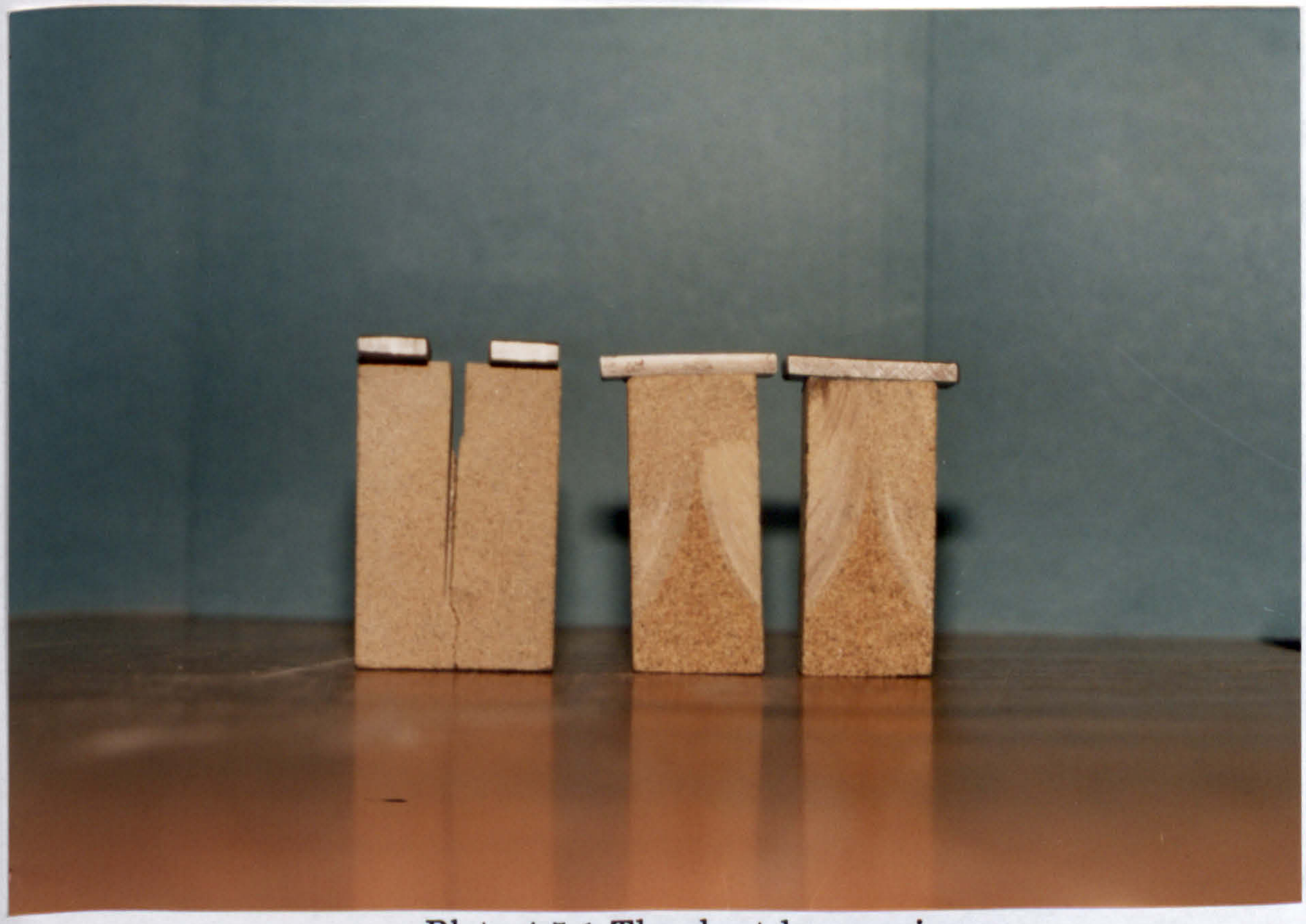

Plate 4.5.1 The short bar specimens

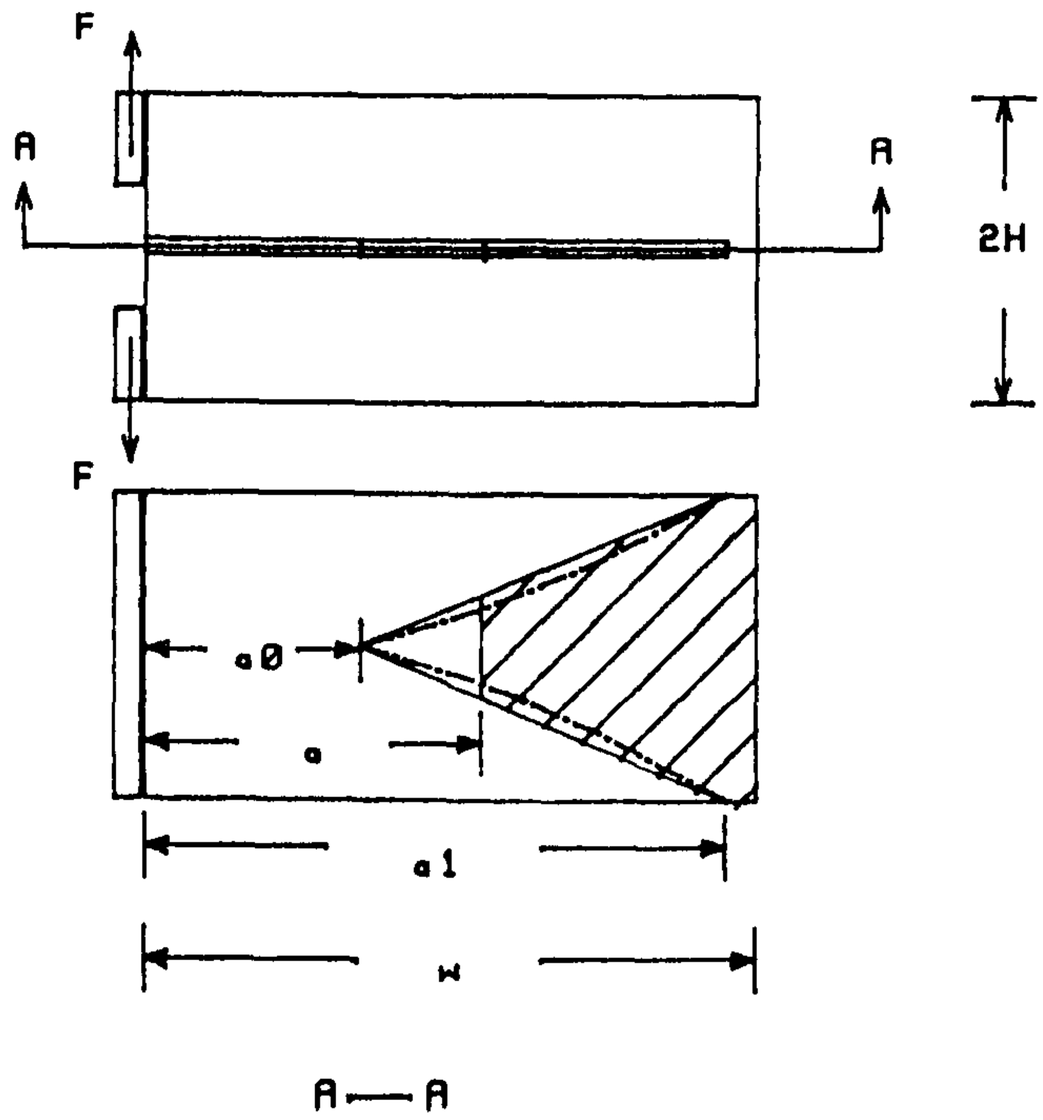

Fig. 4.5.1 Short bar specimen

specimen surface (α_1) was always equal to the specimen width (W), e.g. α_1=1. The Chevron angle θ was 48° in this investigation. The notchs were introduced by a diamond wheel to effect kerfs of 1.0mm width. Two aluminum alloy plates of dimension 57×13×5mm were glued using an epoxy resin to the top surface of the bar specimen to act as loading lines (Plate 4.5.1).

The specimens were dried at 110°C for 5 hours and then were divided in to two groups. The specimens in the first group were cooled in air, and the specimens in the second group were soaked in water for another 5 hours. All experiments were run in air, and the same test procedures were followed through all short bar fracture tests.

The test setup is shown in Plate 4.5.2. The apparatus was specially designed to comprise a vertical arrangement of a bar and a tube, with the bar effecting a

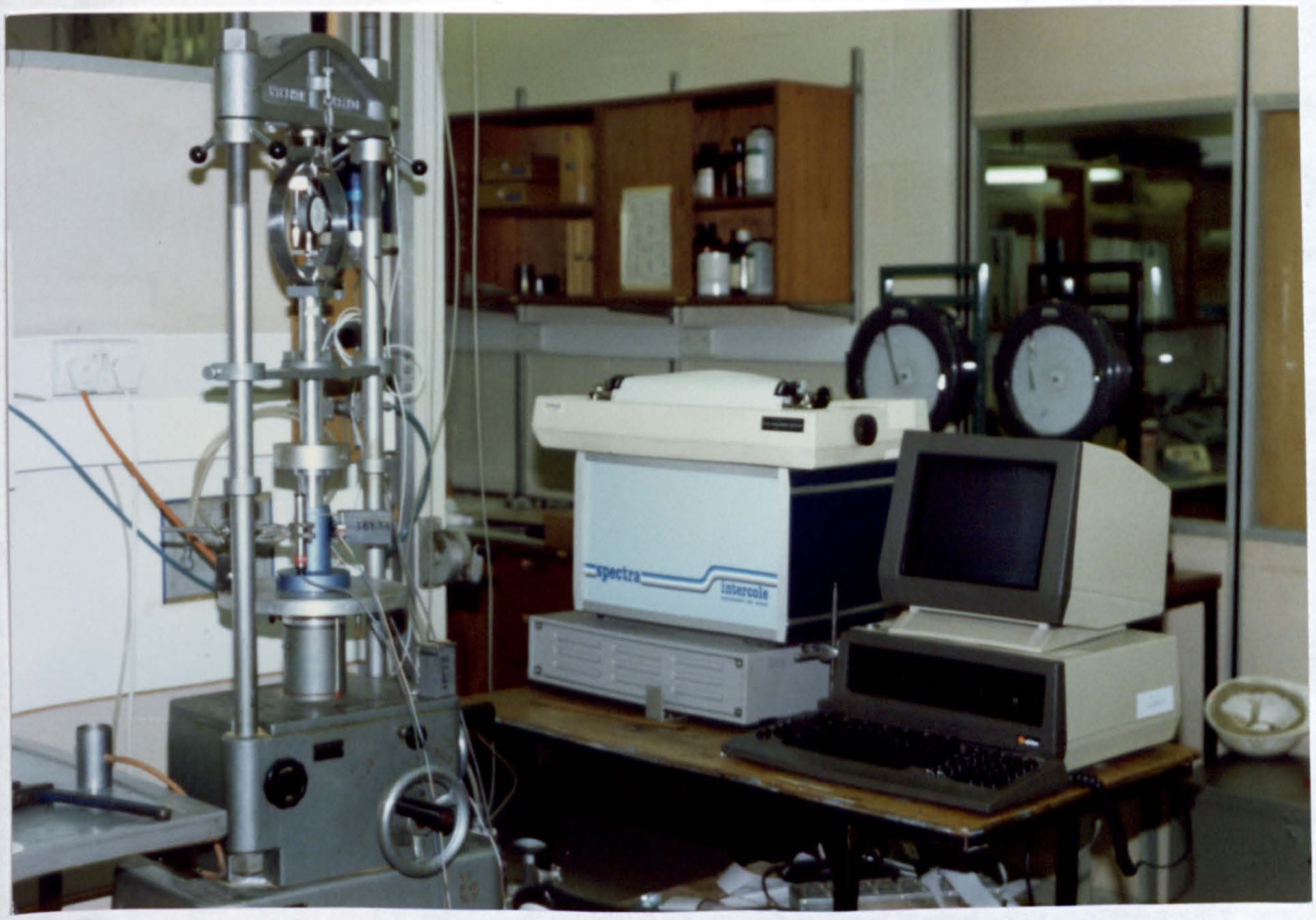

Plate 4.5.2 The setup of short bar fracture tests

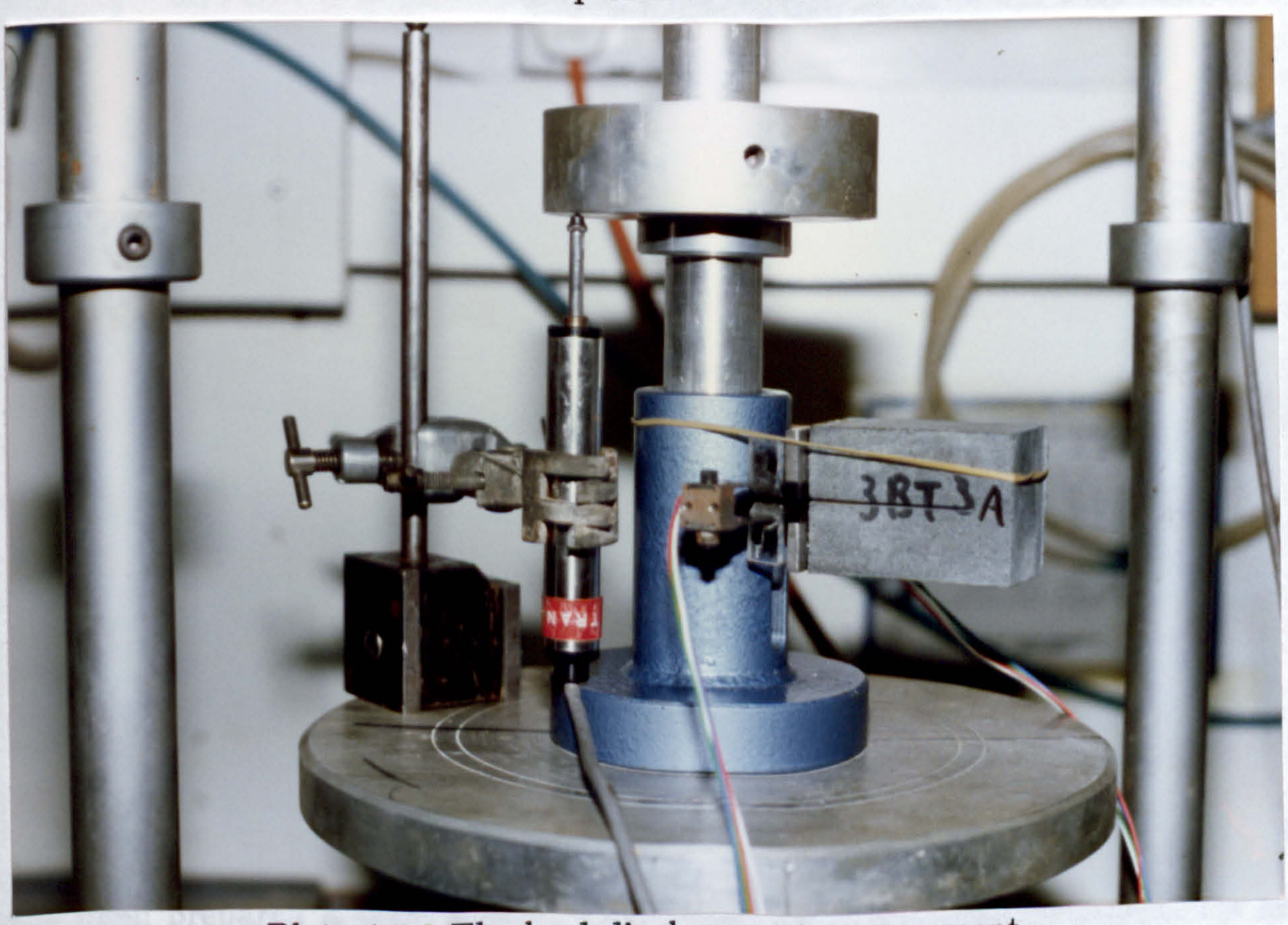

Plate 4.5.3 The load-displacement arrangement
for short bar specimens

sliding fit within the tube. There are two knifes fixed on the top of the tube and bottom of the bar, and the knife on the bar can move downward along a slot on the tube. The short bar specimen is loaded by putting the pressure on the bar. The equipment can be used in the compressive test machine which are available in most rock mechanics laboratories, instead of the tensile testing machines. The LVDT's gives the displacement, and the load cell gives the force on the specimen. The typical load versus displacement record, then, can be obtained using data-logger (Plate 4.5.3)

The critical stress intensity factor was determined from the short bar test using the following equation:

$$K_{\mathrm{Ic}} = \frac{P_{\mathrm{MAX}}}{B\sqrt{W}} Y_m \qquad 4.5.1$$

where

Y_m = minimum value of the dimensionless stress intensity factor coefficient.

Y_m was determined by Wang et al. (1984) as:

$$Y_m = [(11.304 + 2.121\frac{W}{H} + 0.664\frac{W}{H}) + (-80.428 + 17.533\frac{W}{H} -$$

$$0.336\frac{W}{H})\alpha_0 + (255.713 - 63.641\frac{W}{H} + 4.695\frac{W}{H})\alpha_0^2](\frac{\alpha_1 - \alpha_0}{1 - \alpha_0}). \qquad 4.5.2$$

for $3 \leq \frac{W}{H} \leq 4.5$.

Note: In Eq.(4.5.2), H defines half height, see Fig 4.5.1.

4.5.2 Results

The results for the short bar specimens are presented in Table 4.5.1. As the specimen prepared is from a part of the three point bend specimen, the first four columns of specimen identification number indicate the source of the specimen. The last column is for the short bar specimen number.

Table 4.4.1 Results of fracture tests using short bar specimens

Specimen iden. No.	a_0 m	a_1 m	W m	$Pmax$ kN	K_{Ic} $MPa\sqrt{m}$
1BT2A	0.0215	0.0552	0.0693	0.2196	0.58
1BT4B	0.0212	0.0549	0.0704	0.2187	0.57
1BT3B	0.0212	0.0549	0.0718	0.2053	0.53
					$\overline{X}\star = 0.56$
1BT4A	0.0213	0.0550	0.0722	0.2610	0.67
1BT2B	0.0213	0.0551	0.0721	0.2685	0.69
1BT3A	0.0212	0.0549	0.0724	0.2730	0.70
					$\overline{X} = 0.69$
2BT6A	0.0209	0.0546	0.0685	0.6330	1.66
2BT6B	0.0198	0.0535	0.0675	0.6360	1.63
2BT1B	0.0206	0.0546	0.0684	0.6456	1.69
					$\overline{X}\star = 1.66$
2BT2B	0.0203	0.0540	0.0682	0.7363	1.91
2BT1A	0.0201	0.0539	0.0685	0.7106	1.83
2BT2A	0.0198	0.0535	0.0688	0.7071	1.79
					$\overline{X} = 1.84$
3BT3A	0.0198	0.0535	0.0686	0.9040	2.30
3BT4B	0.0206	0.0540	0.0682	0.9531	2.48
3BT1B	0.0228	0.0565	0.0678	0.9880	2.79
					$\overline{X}\star = 2.52$
3BT1A	0.0212	0.0549	0.0682	0.9470	2.52
3BT4A	0.0214	0.0558	0.0683	0.9847	2.66
3BT3B	0.0219	0.0556	0.0679	1.0930	2.99
					$\overline{X} = 2.72$

Note:$\star$ fracture toughness obtained by pre-soaking specimens

4.5.3 Discussion

The $P - \delta$ curves for the short bar specimens in fracture tests, shown in Fig. 4.5.2 are very similar with those for the three point bend specimens. But the results listed in Table 4.5.1 have higher values than that given by both three point bend

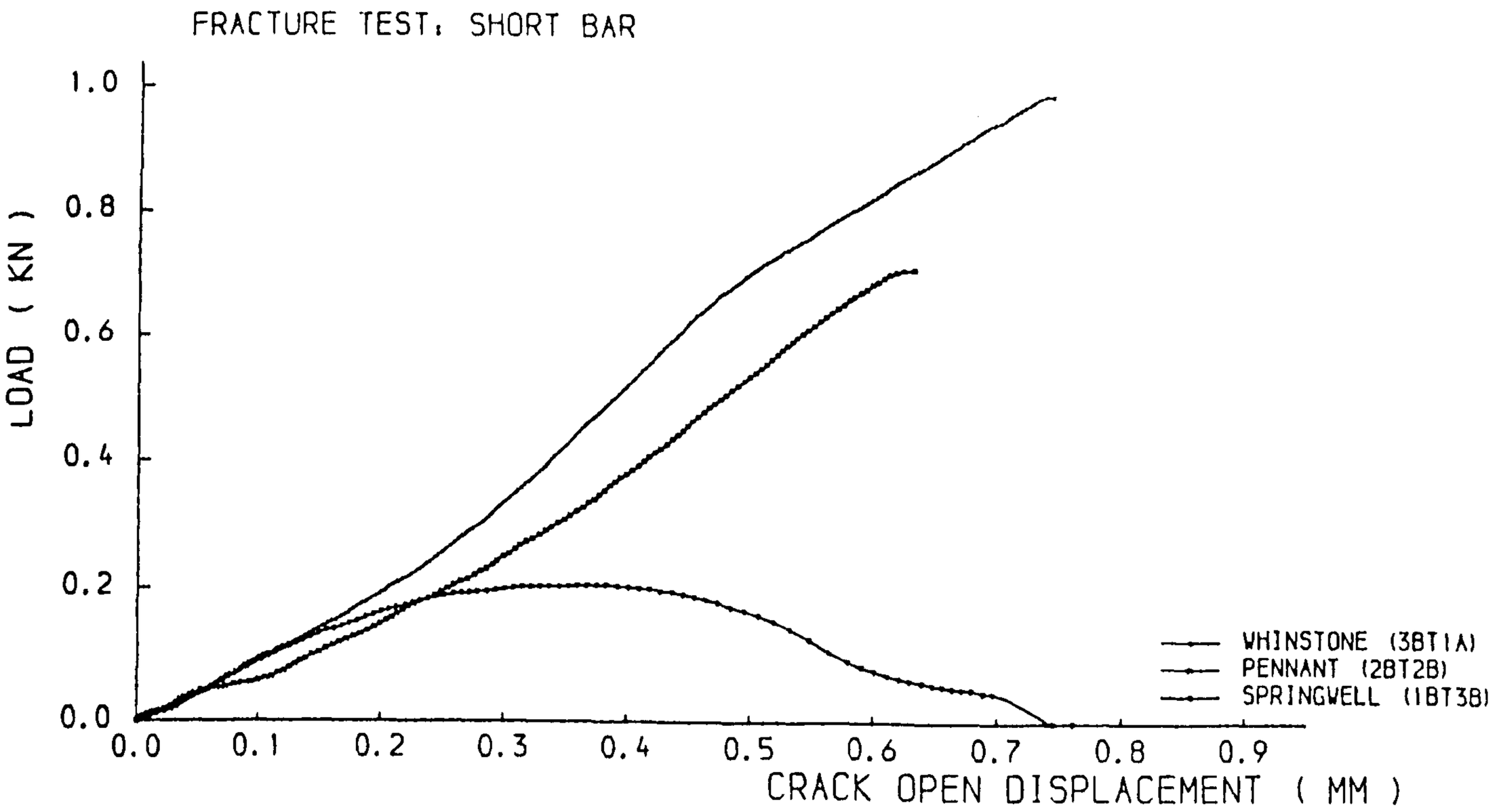

Fig. 4.5.2 Plots of load versus crack open displacements for short bar specimens

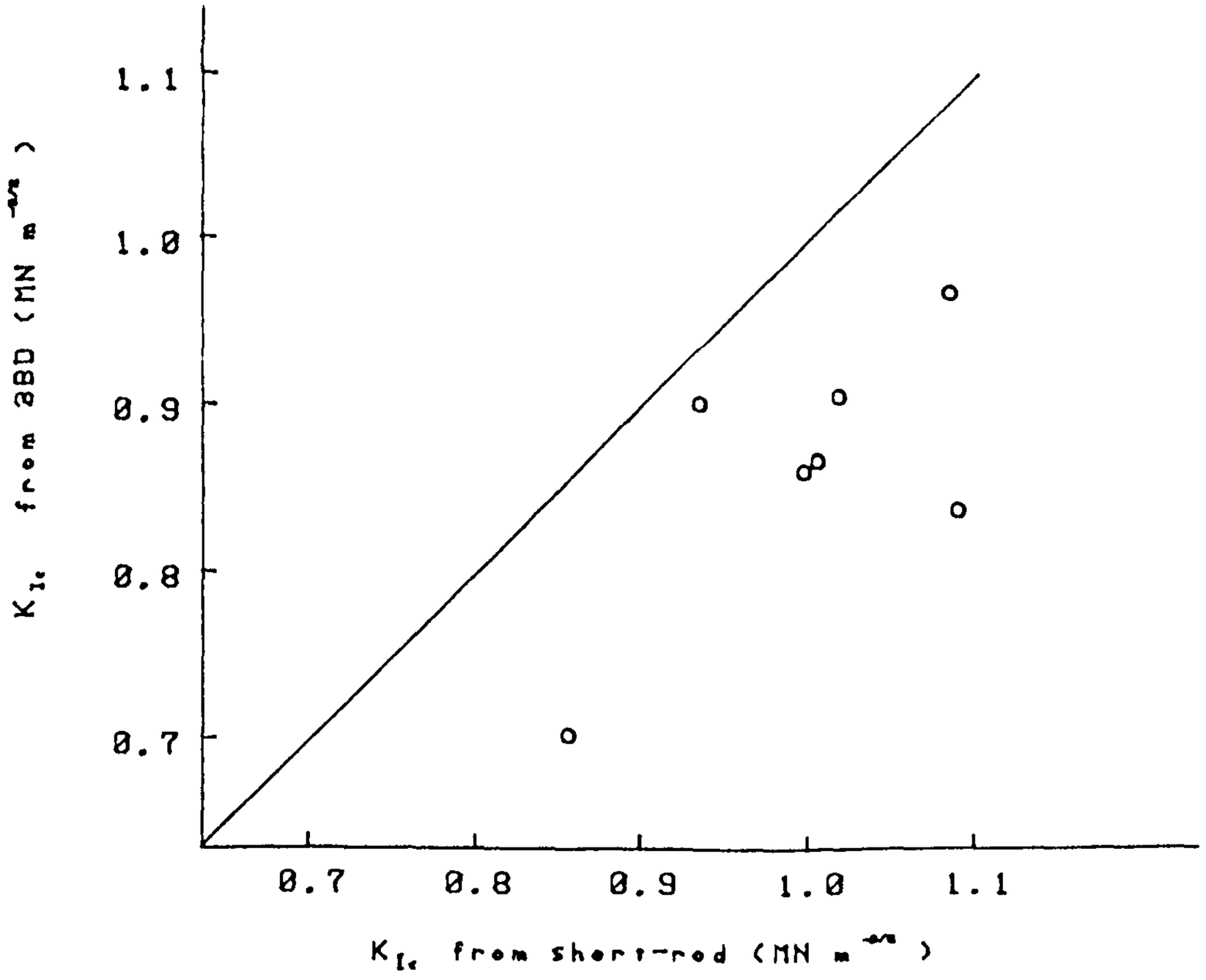

Fig. 4.5.3 Comparison of of three point bend and short rod results for Indiana limestone

specimens and radially cracked ring specimens. As the short bar specimens were cut from the rock block in a different direction from that used for the preparation of three point bend specimens and ring specimens, it is possible that the anisotropic properties of rocks affect the results to some degree. However, similar phenomena were observed by Ingraffea et al. (1982) using short rod specimens in rock fracture tests, see Fig. 4.5.3. Munz (1981) and Eschreiler et al. (1984) reported the higher values of fracture toughness obtained for short bar aluminum alloy specimens. They explained that it was due to the rising R-curve of the material and not a through thickness variation of K_{Ic}. Thus, it is considered that the difference may be attributed to the influence of the test method used.

Compared the results given by the short bar specimens in this study with the results obtained for the short rod specimens presented by Meretith (1983), the agreements are quite good. The fracture toughness for Pennant Sandstone as given by Meretith was 1.98 $MPa\sqrt{m}$, and for Whinstone 2.86 $MPa\sqrt{m}$.

The values of fracture toughness by pre-soaking specimens are lower than that cooled in air by 18.5% in Springwell Sandstone, by 9.7% in Pennant Sandstone and by 7.4% in Whinstone. This can be due to the effect of water. Water may affect crack propagation in rock chemically, by reacting with material at the crack tip and/or mechanically by reducing friction in the process zone (Barton,1983).

4.6 SUMMARY

Radially cracked ring specimens used in rock fracture tests give stable values of the fracture toughness for Pennant Sandstone and Whinstone. It seems that the sizes of specimens have some influence on the results, which depends on the rock materials. For example, the difference of the values of the measured fracture

toughness using the ring specimens with R_O 0.05mm and R_I 0.025mm and the specimens with R_O 0.0375mm and R_I 0.02275 is 25% for Springwell Sandstone, but only 9% for Pennant Sandstone. However, for specimens at the same size, the effects of crack lengths on the results are not significant.

The fracture toughness results obtained from the three point bend specimens agreed very well with those obtained from the ring specimens, but the results from the short bar specimens is significantly higher than that from the three point bend and the ring specimens. Similar phenomena were observed in rock and aluminum alloy fracture tests by other researchers, suggesting that although the anisotropic properties of rocks may influence the measured fracture toughness, the main factor considered is the test method used.

It has been found that the values of fracture toughness obtained from the pre-soaking specimens are lower than that from air-cooled specimens, — 18.5% in Springwell Sandstone, 9.7% in Pennant Sandstone and 7.4% in Whinstone in this study.

Chapter 5

INDENTATION TESTS

5.1 INTRODUCTION

The microcracking which occurs in the contact loading of brittle solids was first studied by Hertz in 1881. Central to the scientific evaluation of such phenomena is the indentation test, now widely adopted as a standard indicator of material "hardness".

The removal of material from rock during percussive drilling, full face boring and drag bit cutting, can in most cases be characterised by the indentation of a tool through a rock surface and has been studied by many authors. Some of the publications on the subject are mainly suggesting qualitative descriptions of the indentation process; others propose models of the indentation process which involve various stress-strain relationships. Different indenter shapes have been used in the indentation tests, which involve wedge (Reichmuth, 1963; Lindqvist et al., 1984), cone (Lundberg, 1974), sphere (Cood et al., 1984), as well as flat indenters.

It is a widely accepted point that the hydrostastic stress induced under the indenter is responsible for crushing in triaxial compression directly under the indenter (Hartman, 1959). Under the indenter stresses forming the crushed zone are larger than those forming the chip. Also such stresses are formed in advance of those forming a chip (Maurer, 1966).

Lindqvist et al (1984) observed the indentation fracture development in rock with a Scanning Electron Microscope. They found that:

1. cracks initiated mainly at the edge and corners of wedges but some crack initiation in the interior of the rock was also observed;

2. the first cracks to appear propagated in a stable manner thus dominated the progressive penetration process;

3. all such cracks were much longer than the actual depth of wedge penetration.

Lindqvist et al. (1983) also found that the crushed material could act as an extension to the cutting tool, and had the effect of distributing the indenter load over a wider area, thereby reducing its effectiveness.

Observations of crack propagation in hard rock loaded by an indenter were also given by Cood et al (1984). The fracture process of rock preceding failure can be divided into four stages:

1. closure of microcracks;
2. linear elastic deformation;
3. stable crack growth; and
4. unstable crack propagation.

A number of theoretical studies of bit and conical penetration in to brittle materials have been published which have their common origin in the wedge penetration model developed by Paul and Sikarskie (1965). The model assumed that the rock fails according to the Coulomb-Mohr failure criterion. Paul and Sikarskie predicted the orientation of the plane of failure and the load associated with shear failure, by using a two-dimensional analysis of the load associated with the indentation of a symmetrical wedge-shaped indenter. The way the force acting on an indenter is transmitted to solid rock depends on two parameters, namely, (a) the geometry of the indenter, and (b) the angle of friction which describes the indentation between the surface of the indenter, and the crushed and solid rock. This was modified by

Dutta (1972) who postulated that the way the force was transmitted depends on the rock material only. Another theoretical analysis of the penetration of an indenter into a non-isotropic material was presented by Benjamea and Sikarskie in 1969.

In recent studies of indentation fracture in brittle materials, the use of the cracks which form beneath a pointed indenter and which grow proportionally with load has been suggested as a simple technique for the determination of fracture toughness, K. The applicability of this technique has been assessed by performing tests on a number of ceramics, glass and rocks (Marion, 1979; Atkinson and Avdis, 1980). Two fracture mechanics theories of indentation fracture have been formulated by Lawn and Swain (1975), and Lawn and Fuller (1975). These theories provide a basis for obtaining the fracture toughness from tests using sharp indenters. The use of the theories is discussed in later Sections.

The indentation technique has been employed in one way or another in most mining and tunnelling machine projects, as a simple, usable method of boreability prediction. These tests are essentially very attractive, as they can be performed on small rock samples with a minimum of preparation and effort using conventional laboratory testing equipment. Generally speaking, such indenters can be of any geometry, although button shaped indenters have been used for most of investigations. Examples are the prediction of penetration rates in percussive drilling, raise boring and tunnel boring. However as pointed out by Ozdemir et al (1977), in order to predict field boreability from easily performed laboratory indentation tests, there are two major factors to consider. The first is the geometry of the indenter. This must be carefully selected as the geometry determines the relative magnitude of the force penetration constant. The second is results from these simple, independent indentation tests and their proper translation to the situation as represented by spaced cuts.

Instead of the indenters which are normally used to predict the performance of a field machine, Ozdemir et al. (1977) used the disc type cutters. They found that the ratios of the penetration induced for the static and rolling cases fluctuated between 1.8 and 2.1: the average being exactly two.

Work, done in the University of Newcastle upon Tyne, and carried out by Robson (1983) and McGann (1984) used the pencil-indenters on small rock samples. This simplified the core-grooving techniques which were used to predict the performance of pick cutting. Fauvel (1981) used an edge indenter to investigate the mechanism of rock breakage by disc cutter.

In this Chapter, the results of indentation tests using up to 25 disc cutters with different edge angles and diameters are presented and discussed. The application of These results to estimate the performance of cutting tests is discussed in Chapter 7.

5.2 INDENTATION FRACTURE

The crack configuration during indentation presents a complex elastic-plastic problem. It is possible to avoid most of the analytical complexities associated with the general indentation fracture problem by noting that the cracks tend, in the advanced stages of loading, to a certain geometrical similarity. This lends itself to a simple fracture mechanics analysis. As mentioned previously, the fracture mechanics analysis given by Lawn and Fuller (1975), and Lawn and Swain (1975) are based on the propagation of the penny-shaped median crack which forms beneath a pointed indenter. Swain and Lawn (1976) also investigated the equilibrium requirements for the indentation configurations of Fig. 5.2.1, in which P is the applied load, acting over a line L, i.e. $P = P_L \times L$, with P_L a line force per unit length. First of all, they considered the balance between the mechanical energy, U_m, and the surface

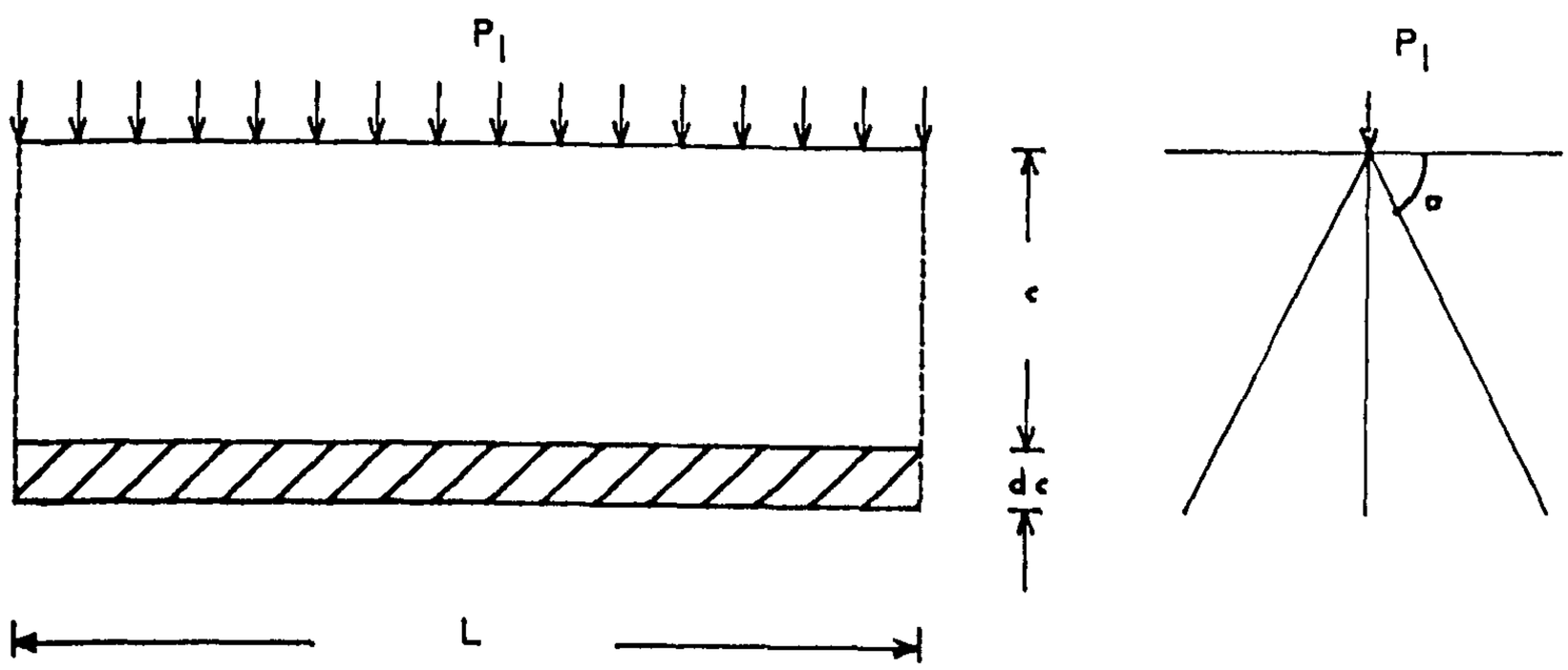

Fig. 5.2.1 Indentation — crack parameters for line-force configurations

energy, U_e, for a virtual displacement δc in the crack system. The appropriate surface energy change is immediately written in terms of incremental crack area,

$$\delta U_e \propto \Gamma(L\ \delta c) \qquad 5.2.1$$

where

$\Gamma = \frac{(1-\nu^2)K^2}{2E}$, the fracture surface energy.

To calculate mechanical energy change, it is assumed that the stress intensity of the indentation field is as the load divided by a characteristic area (taken as area of the surface everywhere distance c from the contact supporting the load, i.e. $\sigma \propto P/Lc$). Then, the strain energy density is determined by the stress squared divided by the appropriate elastic modulus ($\propto P/LcE$, where E is Young's modulus), and the volume of stressed material associated with the crack extension is that traced

out by the characteristic support area ($\propto Lc\ \delta c$). Thus,

$$\delta U_m \propto -\frac{P^2\ \delta c}{LcE} \qquad 5.2.2$$

Here the negative sign indicates that the mechanical energy diminishes as the crack extends. Therefore, to satisfy the Griffith-Irwin energy balance condition for crack equilibrium, the equation must be $\delta U_e = -\delta U_m$. Finally, Swain and Lawn obtained

$$c = k_l \frac{P^2}{2\Gamma E L^2} = k_l \frac{P_L^2}{2\Gamma E} \qquad 5.2.3$$

where

$k_l = \frac{1-\nu^2}{\pi \tan^2 \psi}$,

ψ = the wedging half angle of a sharp indenter.

5.3 DETERMINATION OF CONTACT PRESSURE

The contact pressure, or contact stress, is defined as:

$$\sigma_0 = \frac{P}{A} \qquad 5.3.1$$

where

σ_0 = mean contact pressure,

A = projected area,

P = load.

The problem of interpreting the mean contact pressure, σ_0, measured by a hardness indentation — in terms of the mechanical properties of the material being indented — has had considerable attention. Because of the complex nature of the strain field produced by an indentation, analytical solutions have been limited to rigid ideal plastic or ideal elastic-plastic materials. Tabor (1951) has shown that the mean contact pressure can be related to the yield stress of a material, σ_y, in

simple compression, by an expression based on the theory of indentation of a rigid perfectly-plastic solid:

$$\sigma_0 = C\sigma_y \qquad 5.3.2$$

The constraint factor C depends upon the geometry of the indenter. It was approximately three for all of the indenters considered. The origin and characteristics of the constraint factor C are the most important considerations in indentation hardness testing.

Johnson (1970) considered the indenter to be encased in a hemispherical core of radius a (Fig. 5.3.1) and assumed that a hydrostatic uniform pressure exists throughout the core. Furthermore, he assumed that pressure to be equal in magnitude to the applied pressure σ_0. Thus he obtained:

$$\frac{\sigma_0}{\sigma_y} = \frac{1}{\sqrt{3}}[1 + \ln(\frac{4E}{3\pi\sigma_y \tan\frac{\theta}{2}})] \qquad 5.3.3$$

where

θ = the angle of the indenter.

5.4 ARRANGEMENT AND PROCEDURE OF THE EXPERIMENT

5.4.1 Apparatus Description

The tests were carried out on the small cutting rig as used for the cutting tests (see Chapter 3).

The indenters used on the small cutting rig to investigate the effects of the size of discs were sharp edged discs with different edge angles and diameters. Twenty five disc cutters were used in the tests.

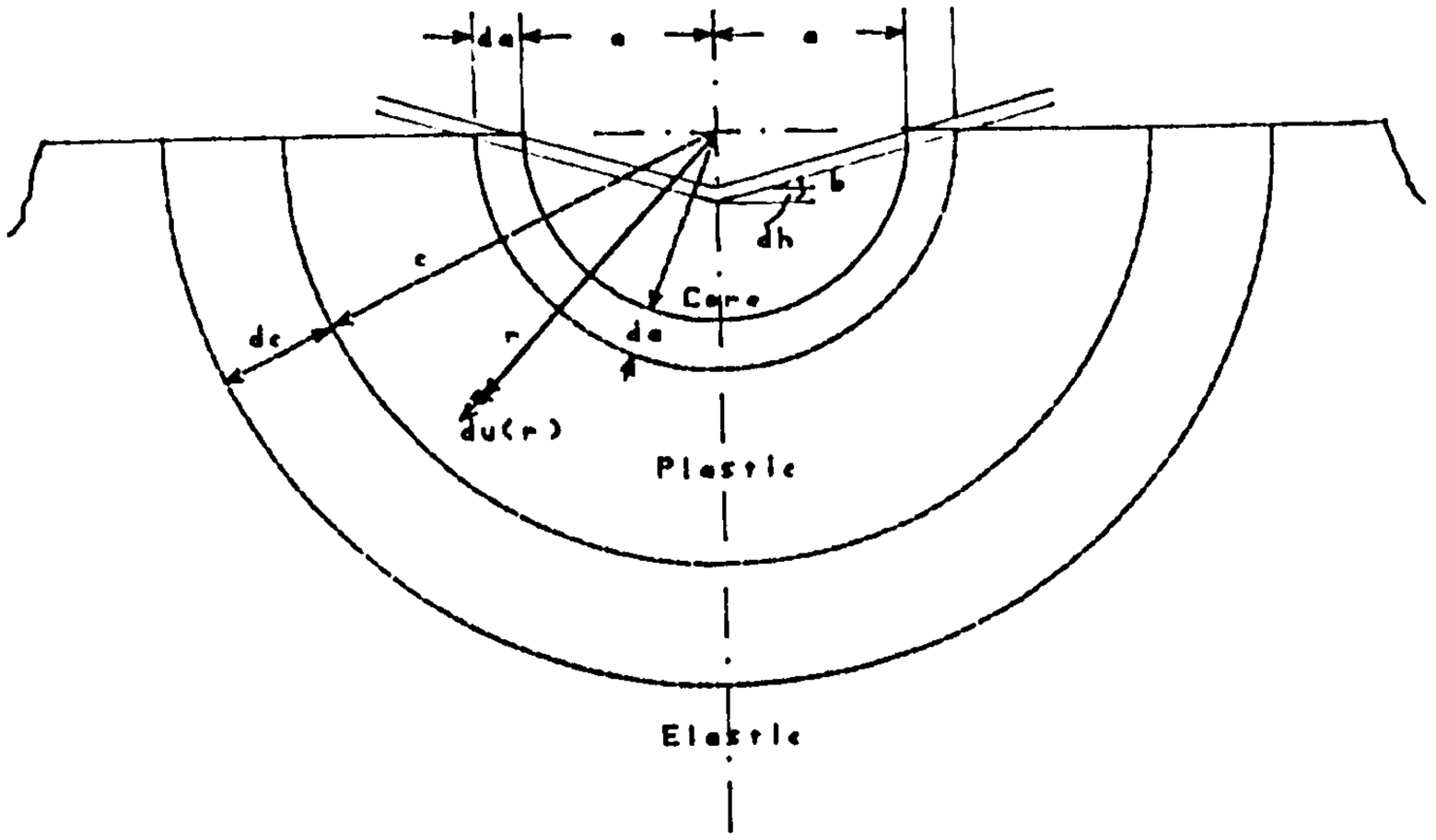

Fig. 5.3.1 Idealized model of an indentation

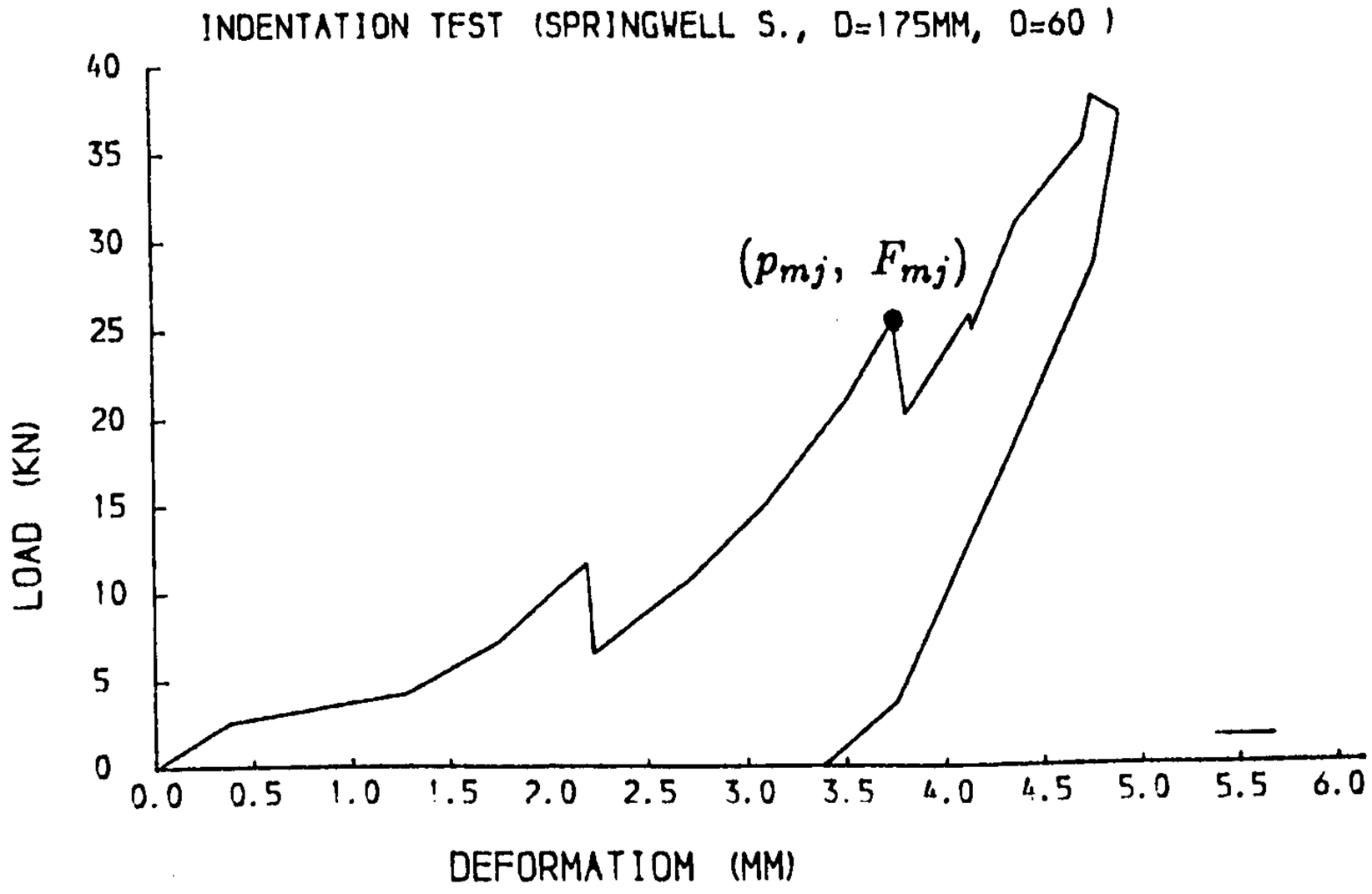

Fig. 5.4.1 Force versus penetration

5.4.2 Measurements of Force and Penetration

The force monitoring system comprised of a triaxial dynamometer, a deformation transducer , and an UV trace recorder. The triaxial dynamometer was used to measure the magnitude and direction of the thrust force on the disc, and the deformation transducer to measure the depth of the penetration. The dynamometer and transducer were calibrated before the indentation tests.

Continuous recording was facilitated by the SE 4000 system in conjunction with an Ultra-Violet (UV) chart recorder, as discribed in Chapter 3. Two traces were recorded, one for the thrust force and the other for the penetration.

5.4.3 Test Procedure

The thrust load was produced by raising the bed with a manual screw with a deformation transducer mounted between the disc holder and the rock block. The values of the load and penetration were recorded by UV chart recorder. Generally, when the penetration was reaching about 4mm, or the load was reaching about 80 kN, the disc tool was unloaded. Then the load point was changed to start the next run. At least three points at sufficient distance from each other to avoid interference, were chosen to be loaded by the same disc cutter. After all required points were loaded, the disc tool was changed.

Useful information concerning the failure process can be gained by recording the force-displacement curve during the indentation of rock. The standard load vs penetration curve, finally, can be drawn based on the data from UV chart recorder. A number of representative force vs penetration curves were obtained. Generally they are similar to the one depicted in Fig. 5.4.1 : p_m is the depth of penetration of the indenter into the rock, F_m is the measured force, and $(p_{mj},\ F_{mj})$ represents the jth point of chip formation. A set of $(p_{mj},\ F_{mj})$ values was collected from the

tests for each indenter. The average pressure can be obtained by:

$$\sigma_0 = \frac{1}{n}\sum_{j=1}^{n}\frac{F_{mj}}{A_{mj}} \qquad 5.4.1$$

where

A_{mj} = the contact area.

The first approach for determining the contact area assumes the shape of the area to be a pair of parabolas (see Fig. 2.1.1). This gives,

$$A_{mj} = \frac{8}{3}p_{mj}\sqrt{Dp_{mj} - p_{mj}^2}\tan\frac{\theta}{2} \qquad 5.4.2$$

where

θ = edge angle of the disc cutter.

5.5 EXPERIMENTAL RESULTS AND DISCUSSION

The results of indentation tests, in terms of the ratios of contact pressure/yield stress σ_0/σ_y with different disc cutters for Springwell Sandstone and Whinstone, are listed in Table 5.5.1 and Table 5.5.2. The theoretical analysis based on Eq. 5.3.2 is also given in the Tables. Note: for rock materials, $\sigma_y = \sigma_c$.

Figs 5.5.1 and 5.5.2 show the effects of the geometries of disc cutters to the ratios of σ_0/σ_y for Springwell Sandstone. The more stable results have been found in the tests with disc cutters which have either a diameter of 200mm or an edge angle of 100°. The indentation tests using a disc cutter with a smaller diameter and edge angle, give σ_0/σ_y ratios which are higher than those obtained by theoretical analysis. The values of the ratios of σ_0/σ_y fall as the disc diameter increases from 100mm to 200mm. This is equally true as the disc edge angle increases from 60° to 100°.

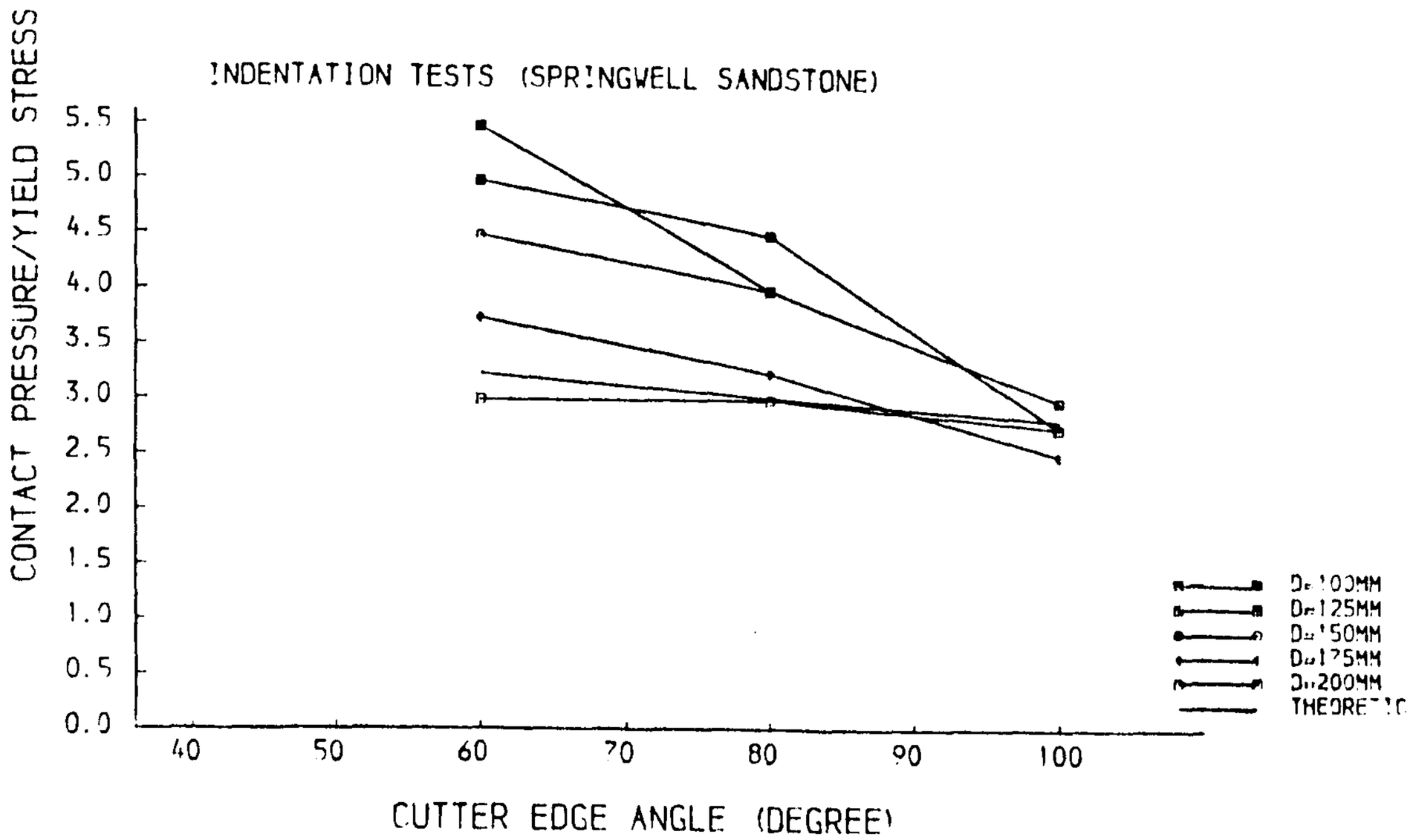

Fig. 5.5.1 Effect of cutter edge angle on σ_0/σ_y Springwell Sandstone

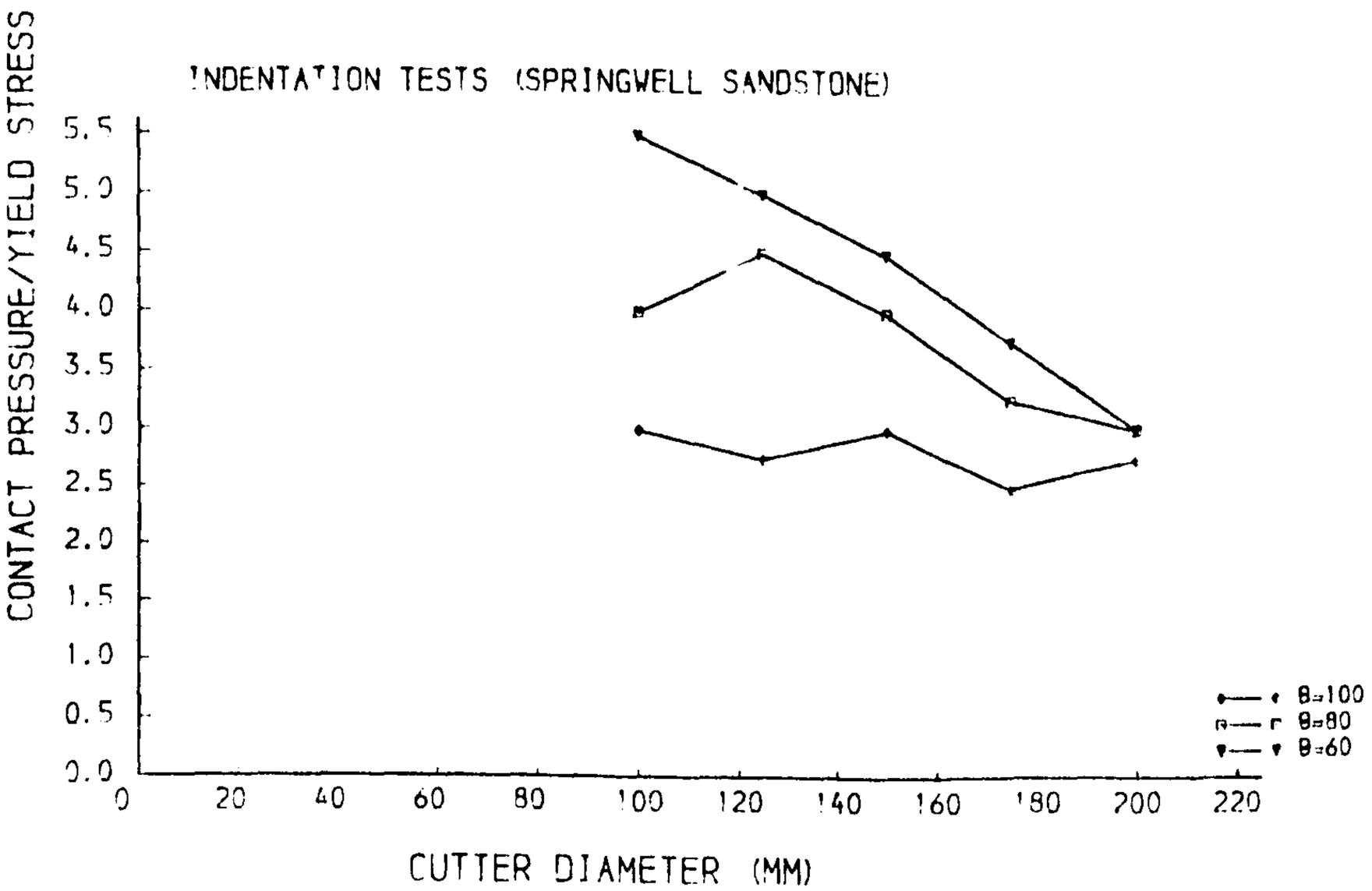

Fig. 5.5.2 Effect of cutter diameter on σ_0/σ_y Springwell Sandstone

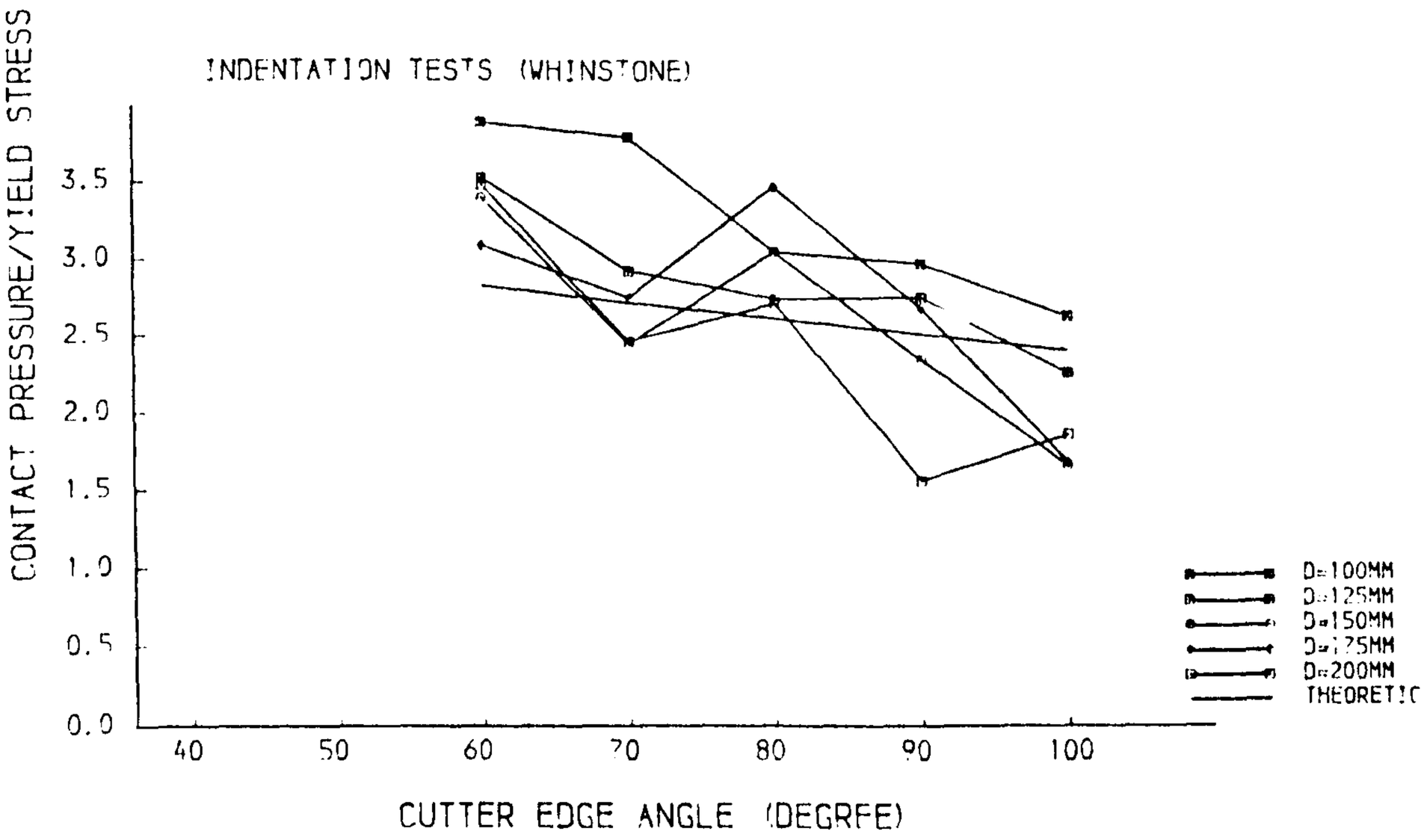

Fig. 5.5.3 Effect of cutter edge angle on σ_0/σ_y Whinstone

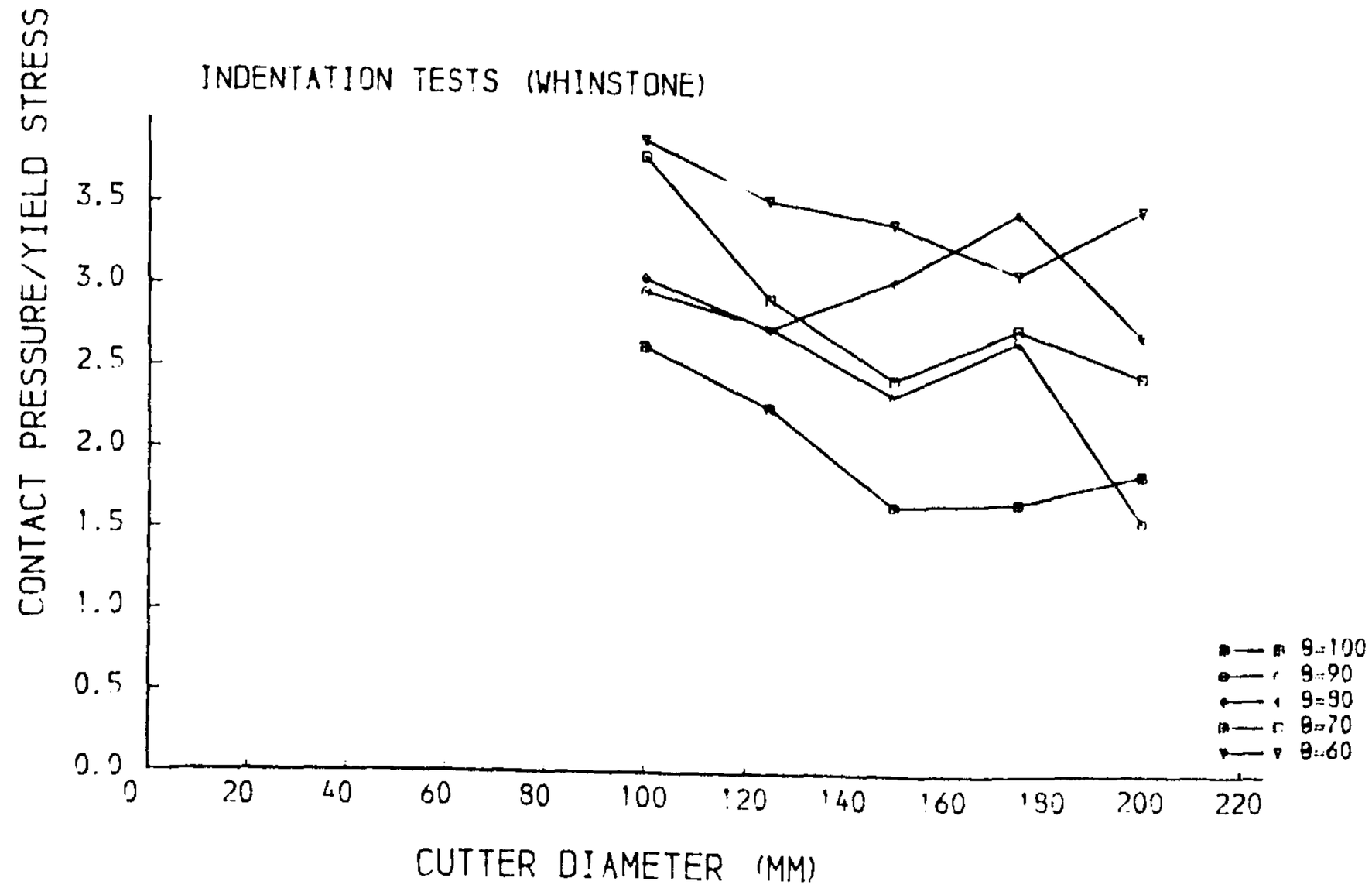

Fig. 5.5.4 Effect of cutter diameter on σ_0/σ_y Whinstone

Table 5.5.1 Experimental and theoretical results of indentation on Springwell Sandstone

θ	D	σ_0 / σ_y		D	σ_0 / σ_y	
degree	mm	exper.	theor.	mm	exper.	theor.
60.0	200.0	3.031	3.554	125.0	4.943	3.554
80.0	200.0	3.054	3.338	125.0	4.418	3.338
100.0	200.0	2.758	3.136	125.0	2.741	3.136
60.0	175.0	3.684	3.554	100.0	5.586	3.554
80.0	175.0	3.336	3.338	100.0	3.978	3.338
100.0	175.0	2.421	3.136	100.0	3.092	3.136
60.0	150.0	4.466	3.554			
80.0	150.0	3.864	3.338			
100.0	150.0	3.047	3.136			

Table 5.5.2 Experimental and theoretical results of indentation on Whinstone

θ	D	σ_0 / σ_y		D	σ_0 / σ_y	
degree	mm	exper.	theor.	mm	exper.	theor.
60.0	200.0	3.478	3.037	125.0	3.524	3.037
70.0	200.0	2.461	2.926	125.0	2.922	2.926
80.0	200.0	2.710	2.821	125.0	2.738	2.821
90.0	200.0	1.564	2.720	125.0	2.750	2.720
100.0	200.0	1.858	2.619	125.0	2.260	2.619
60.0	175.0	3.088	3.037	100.0	3.884	3.037
70.0	175.0	2.750	2.926	100.0	3.787	2.926
80.0	175.0	3.462	2.821	100.0	3.044	2.821
90.0	175.0	2.680	2.720	100.0	2.966	2.720
100.0	175.0	1.682	2.619	100.0	2.630	2.619
60.0	150.0	3.393	3.037			
70.0	150.0	2.446	2.926			
80.0	150.0	3.042	2.821			
90.0	150.0	2.345	2.720			
100.0	150.0	1.660	2.619			

Similar results for Whinstone are plotted in Figs 5.5.3 and 5.5.4, where the tendency of the geometry effect of disc cutters on the σ_0/σ_y ratio for Whinstone is not as clear as that for Springwell Sandstone. In addition, there seems to be an increased scatter in the results from Whinstone, although the results of the theoretical analysis are within the region covered by experimental tests.

The effective angle of an indenter plays a very important role in hardness testing. Fig. 5.5.5 gives the variation of constaint factor C with cone angle θ for metals (Shaw, 1973).

Most indenters used in engineering practice are nearly blunt and the constaint developed is essentially elastic. The effective angles θ for Brinell, Vickers and Knoop indenters (Fig.5.5.6) are listed in Table 5.5.3 (Shaw, 1973). Unless the friction is very large, the indenters listed in the Table 5.5.3 should be expected to show a small upward flow. In fact, the more blunt the indenter, the less will be the upward flow, and the less will be the influence of friction on the contact pressure or so called hardness.

Table 5.5.3 The effective angles for different indenters

Indenter type	θ $[degree]$
Brinell (d/D = 0.4)	132
Vickers	140
Knoop	144

For metal materials, nearly all practical indenters perform with some upward flow. However, it is fortunate that the constraint factor C is relatively insensitive to the mode of action (that is, whether a flow or elastic constraint pertains). In respect to rock materials, the flow is formed early in the process and then developed so fast as to form a chip. Consequently, the force is reduced and further increase of the force causes another chip, and so on. As only the loads at which the chip is

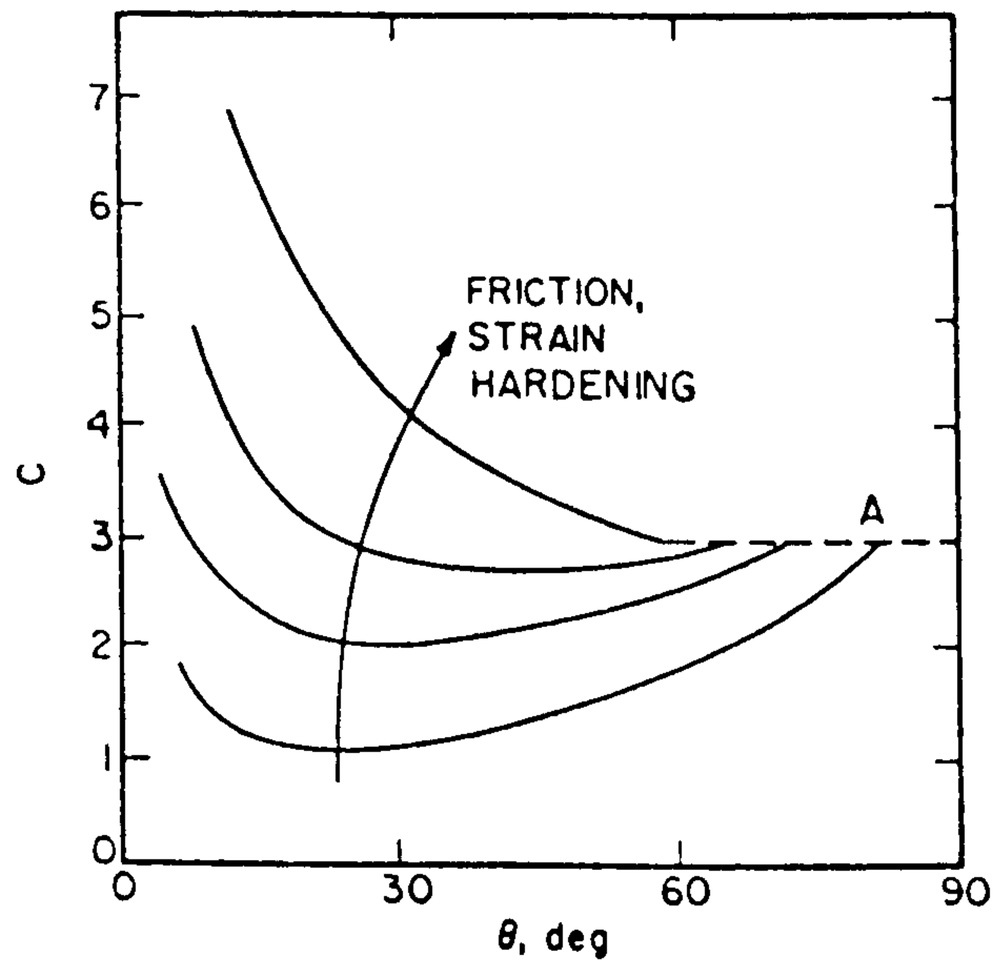

Fig. 5.5.5 Variation of constraint factor $C = \sigma_0/\sigma_y$ with cone angle θ for metal work hardened to different degrees and with different amounts of friction on the surface of the indenter

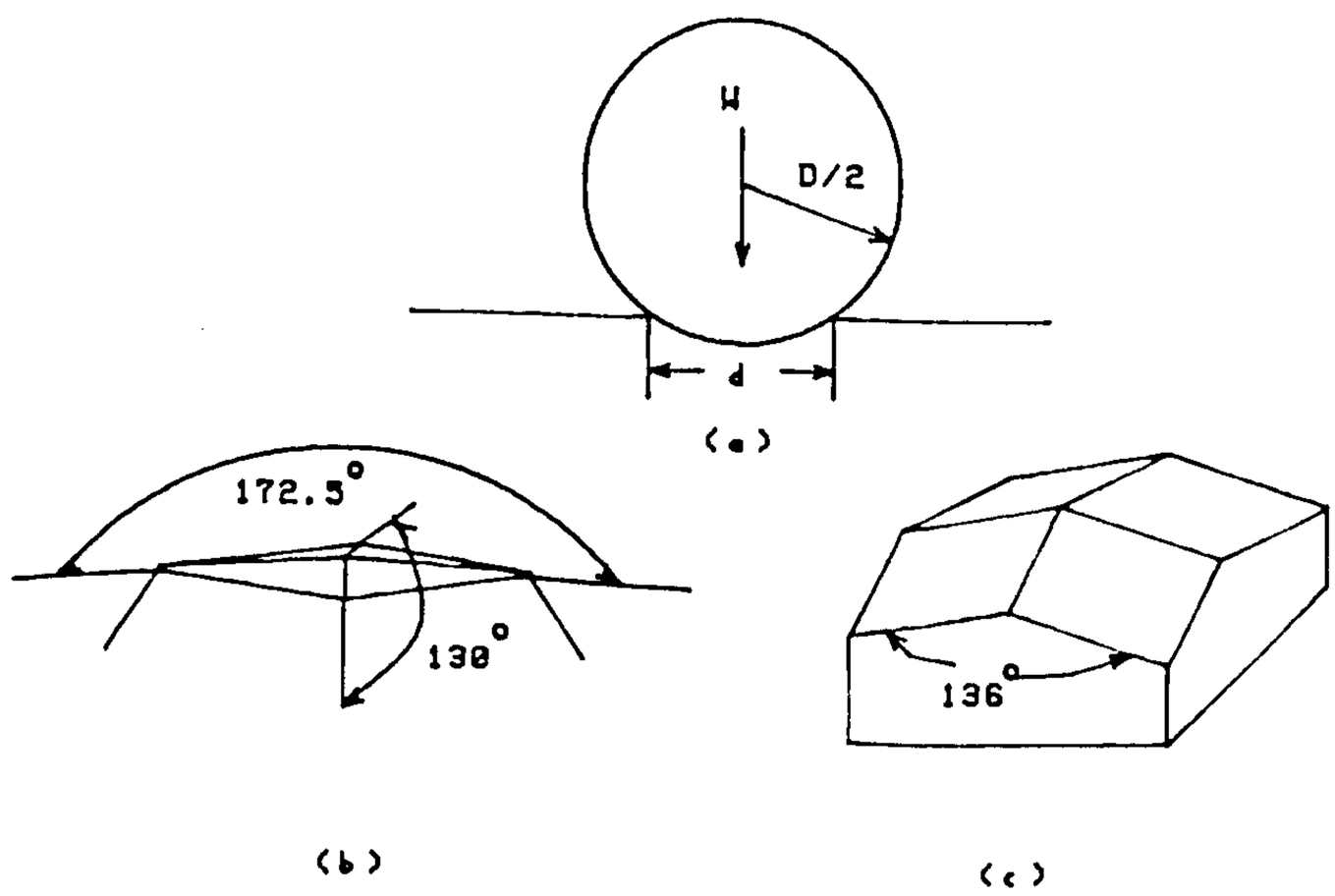

Fig. 5.5.6 (a) Brinell (b) Knoop (c) Vickers

formed are considered in this study, the influence of the upwards flow in this case can not be ignored.

As mentioned above, the diameter of the disc cutter also affects the values of mean contact pressure. However, this factor is less important than the effect of the edge angle of the cutter, unless the edge angle is small. With an edge angle of 60° in this study, for example, the ratios of σ_0/σ_y increases rapidly as the diameter of the disc cutter increases.

5.6 SUMMARY

Indentation tests with disc type indenters were carried out for use in the prediction of disc cutting and tunnel boring in this study. Twenty five sharp disc cutters with different edge angles and diameters were used. It was found that:

1. The contact pressure is affected by the edge angle and diameter of the disc cutter.

2. The agreement of theoretical results based on Johnson's analysis (1970) and experimental data are quite good for a disc cutter with a large edge angle and diameter.

The indentation fracture principle is introduced in this Chapter, and further use of the principle is discussed in Chapter 7.

Chapter 6

EXPERIMENTAL RESULTS AND DISCUSSION

6.1 INTRODUCTION

Following the recent development of high-pressure water jet technology, it is shown that the performance of TBM's could be enhanced with the assistance of water jets. The main advantages of water jet assisted cutting can dramatically solve the problems which characterize standard cutting. Also, it brings other benefits, such as, lower dust level, reduced fines, reduction in the weight of machines, and reduction in the wear of cutting tools.

As pointed out earlier in the Chapter 2, a considerable amount of research work aimed in investigating the efficiency of high pressure water jet assisted rotary cutting tools has been carried out. Results of several field tests have shown that TBM's equiped with high pressure water jets increased the penetration rates of the machines by up to 10% and reduced the cutting forces by up to 50% relative to normal TBM's. These results, however, were at conflict with a report by Schenck (1983). It stated that the power of the jets was largely dissipated without much increase in productivity and that the reliability of a TBM to which water jet equipment was added was much lower than for the same TBM without water jet assistance. As a result, the production of water jet equiped TBM's ceased. It is considered, however, that the problems outlined in Schenck may be overcome in two ways:

1. by use of more efficient pumping and sealing system, or,
2. by use of low pressure water jets.

Ozdemir (1984 and 1986) and Fenn et al. (1985) investigated the use of the low pressure water jets to assist disc cutting. The results given by Ozdemir (1984) indicate some improvement compared with unassisted cutting, however, the pressure of the water jet used in his study were in the range of 43.48MPa (5,000psi) to 96.53MPa (14,000psi), hardly a low pressure. Another report presented by the author in 1986 shows that the observed benefits were obtained in the water jet assisted cutting tests by using the jet at a pressure as low as 13.5 MPa, but the rocks used are sedimentary, not so called "hard" rocks. The lower pressure of 8MPa investigated by Fenn et al., used 4 nozzles arrangement, which seems too many. The results of the present study's investigation of a water jet, with the pressures in the range of 13.79 Mpa (2,000 psi) to 55.16 MPa (8,000 psi), assisted disc cutting are reported in this Chapter. The variables involved in this study were as follows:

a. test methods;

b. jet locations;

c. jet pressures;

d. cutting spacing distances and penetrations;

e. cutting speeds.

As the aim of the study is to investigate the possibility of using a low pressure water jet in disc cutting, the shape and geometry of disc tools and water jet nozzle diameters become less important than those listed above. The disc cutters and the jet nozzles used for different cutting machines have been mentioned earlier.

All the data presented here are the three components of the force acting at the rock-disc interface, i.e., thrust force, rolling force and side force. They represent the average values of each cut. At least three cuts were performed for each of the cutting condition. Cuts close to the edges of the rock block were excluded from the data to avoid boundary effects.

6.2 INITIAL EXPERIMENTS WITH SMALL CUTTING RIG

6.2.1 Experimental Plan

Rock: Springwell Sandstone, Whinstone

Test Methods: Single pass on level trimmed surface

Multiple pass on previous cutting surface

Tools: Sharp edged disc

Diameter: 150 mm

Edge Angle: 60°

Penetration Depths: 2 mm, 4 mm, 6 mm, 8 mm

Spacing Distance/Penetration: 2.5, 5, 10, 15, 20

Travel Speed: 68.8 mm/s

Jet Pressure: 34.48MPa (5,000 psi)

Jet location:

Stand-off Distance: 25 mm

Side-off Distance: 0 mm

Lead-on Distance: 110 mm

Nozzle Diameter: 0.68 mm

The multiple pass cutting on Springwell Sandstone was arranged. However, as the disc cutter was damaged during the multiple pass tests on Whinstone, this plan was abandoned.

6.2.2 Springwell Sandstone

A summary of the tool forces, yield and specific energies recorded when cutting are presented in Appendix C. Table 6.2.1 gives the percentage reduction in the cutting forces compared with unassisted disc cutter forces.

Table 6.2.1 Percentage reduction in cutting forces

p mm	s/p	MPTF %	MTF %	MPRF %	MRF %
2.0	2.50	83.11	81.14	61.02	66.04
	5.00	83.50	78.62	53.23	61.82
	10.00	82.36	81.77	62.03	60.71
	20.00	83.82	83.85	60.98	60.71
4.0	2.50	49.48	54.68	28.57	44.35
	5.00	66.03	75.26	28.92	45.52
	10.00	54.85	77.26	33.89	50.33
	20.00	57.87	78.89	28.64	44.67
6.0	2.50	35.99	31.95	22.83	54.18
	5.00	29.19	58.67	24.30	58.54
	10.00	29.12	58.70	26.17	53.31
	20.00	23.17	54.61	17.68	43.37
8.0	2.50	17.09	33.68	19.10	39.66
	5.00	37.54	44.11	19.23	38.46
	10.00	18.13	28.74	10.75	42.56

The depth of the slot cut by the water jet — which was put in front of the cutter — was measured. Before starting the water jet assisted cutting tests, a series of cuts was done with the water jet only to determine the relationship of the depth of the slot at the given jet pressure. For a water jet pressure of 34.48MPa, the slot cut by the water jet is 3.05 mm.

The effects of the s/p ratio on the thrust forces are illustrated in Figs 6.2.1 and 6.2.2. The forces increase linearly with spacing for each of the penetration values studied until an s/p of about 10, at which point they level off, indicating the end of the interactive zone. The effects of s/p ratio on the rolling force are illustrated in Figs 6.2.3 and 6.2.4.

The effects of cutting spacing on yield are illustrated in Fig. 6.2.5. Fig. 6.2.6 shows that the minimum specific energy occurs at an s/p value of 2.5 to 5 for each of the penetration conditions used during the unassisted cutting tests, and same

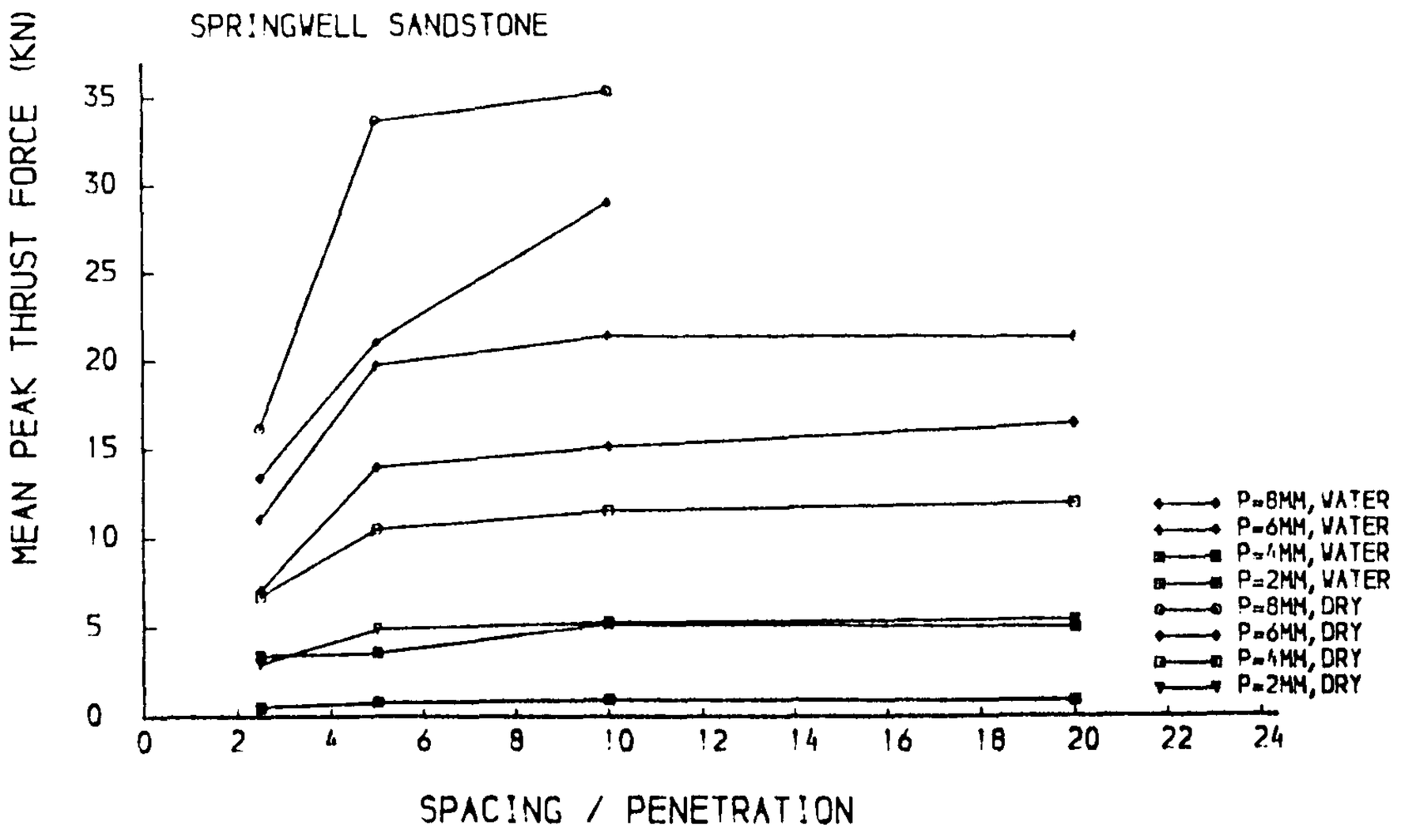

Fig. 6.2.1 Mean peak thrust force versus s/p ratio

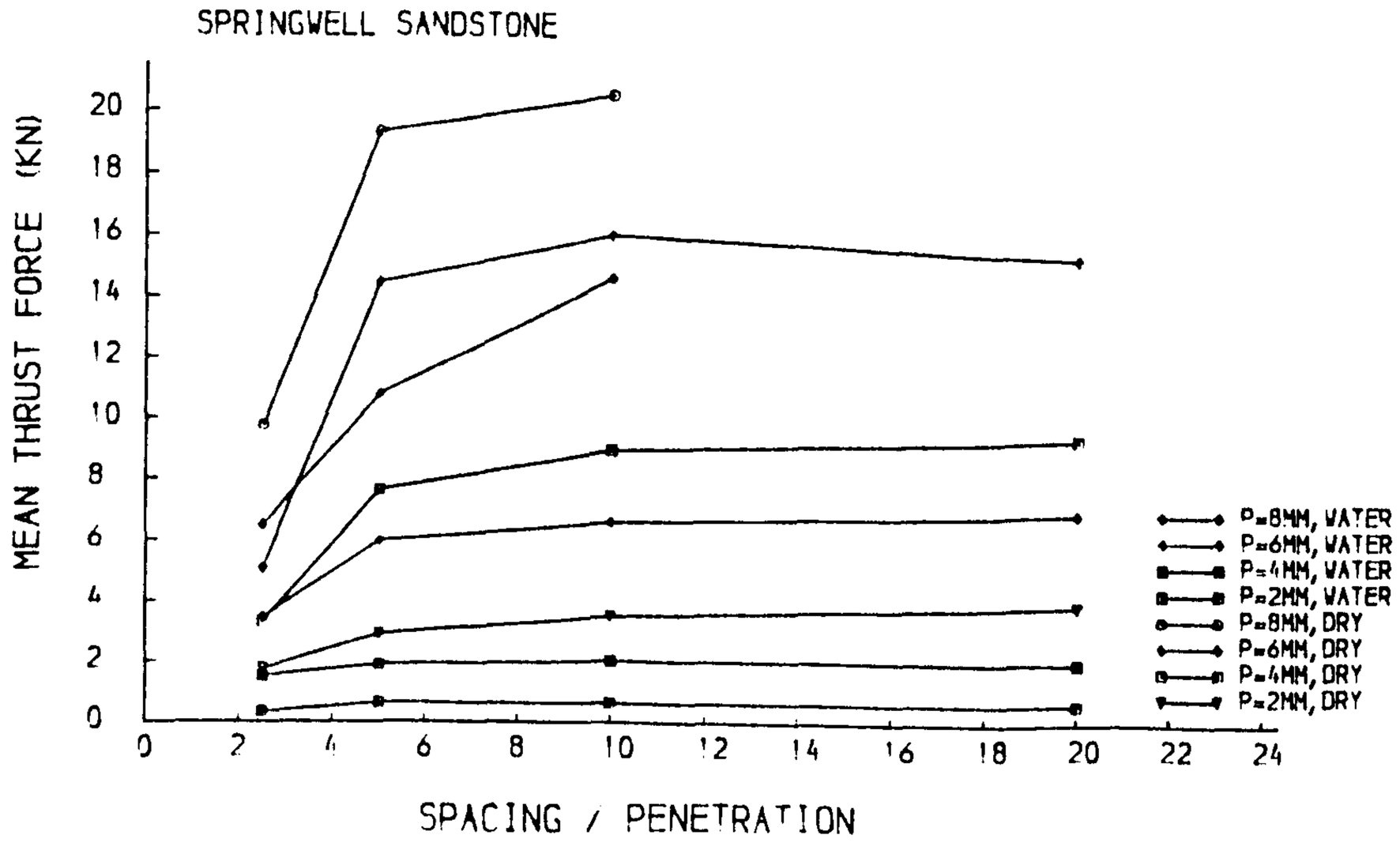

Fig. 6.2.2 Mean thrust force versus s/p ratio

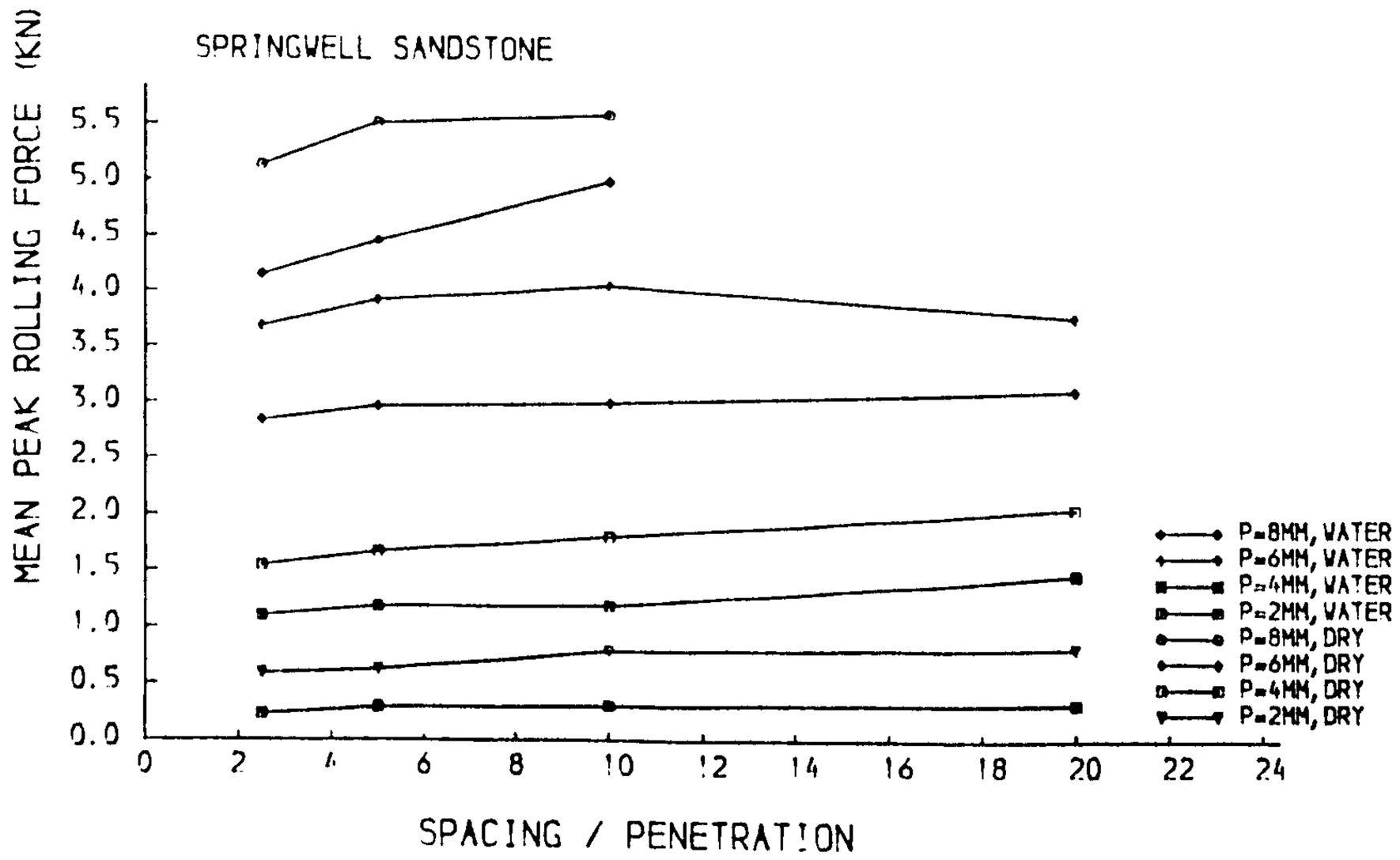

Fig. 6.2.3 Mean peak rolling force versus s/p ratio

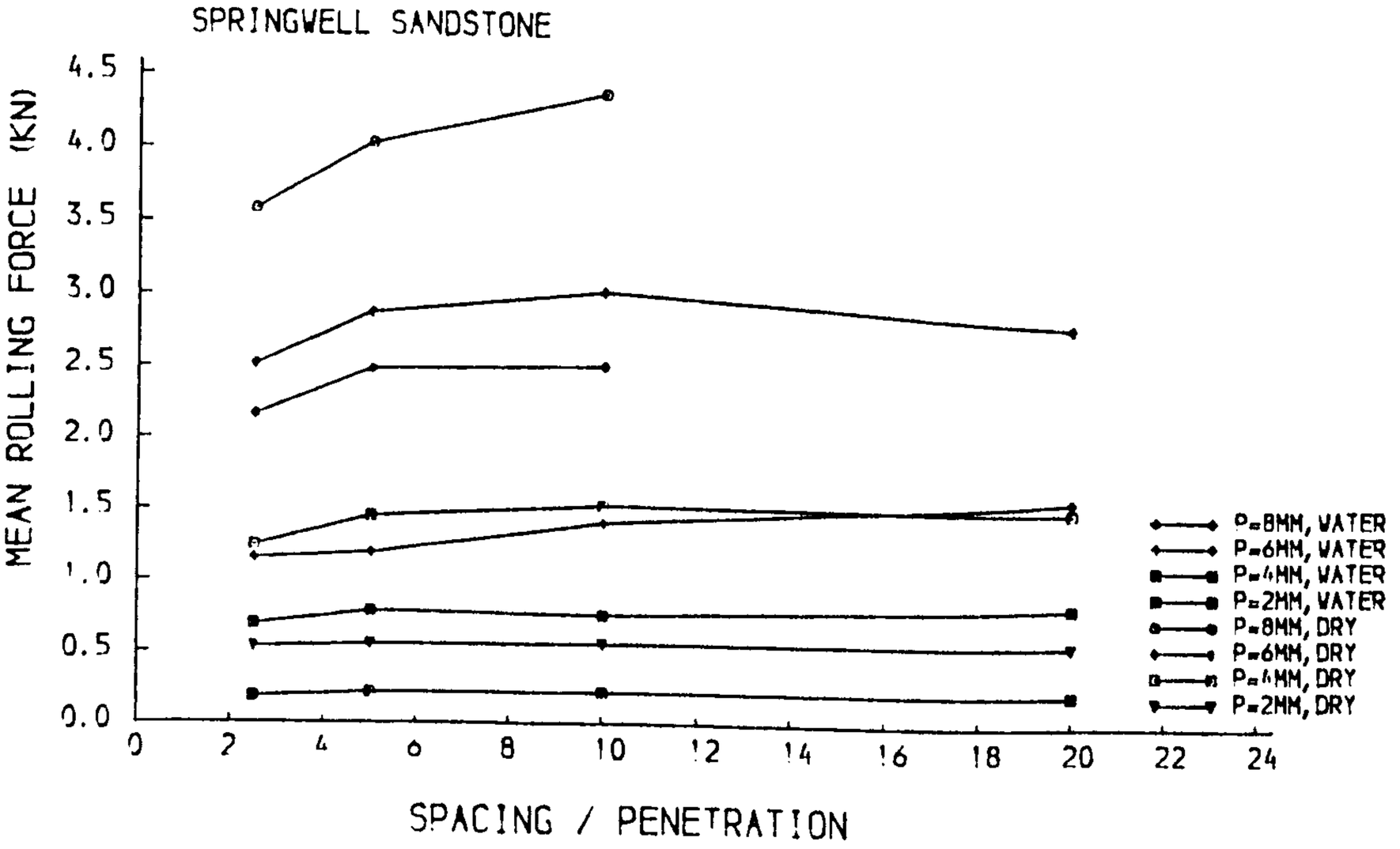

Fig. 6.2.4 Mean rolling force versus s/p ratio

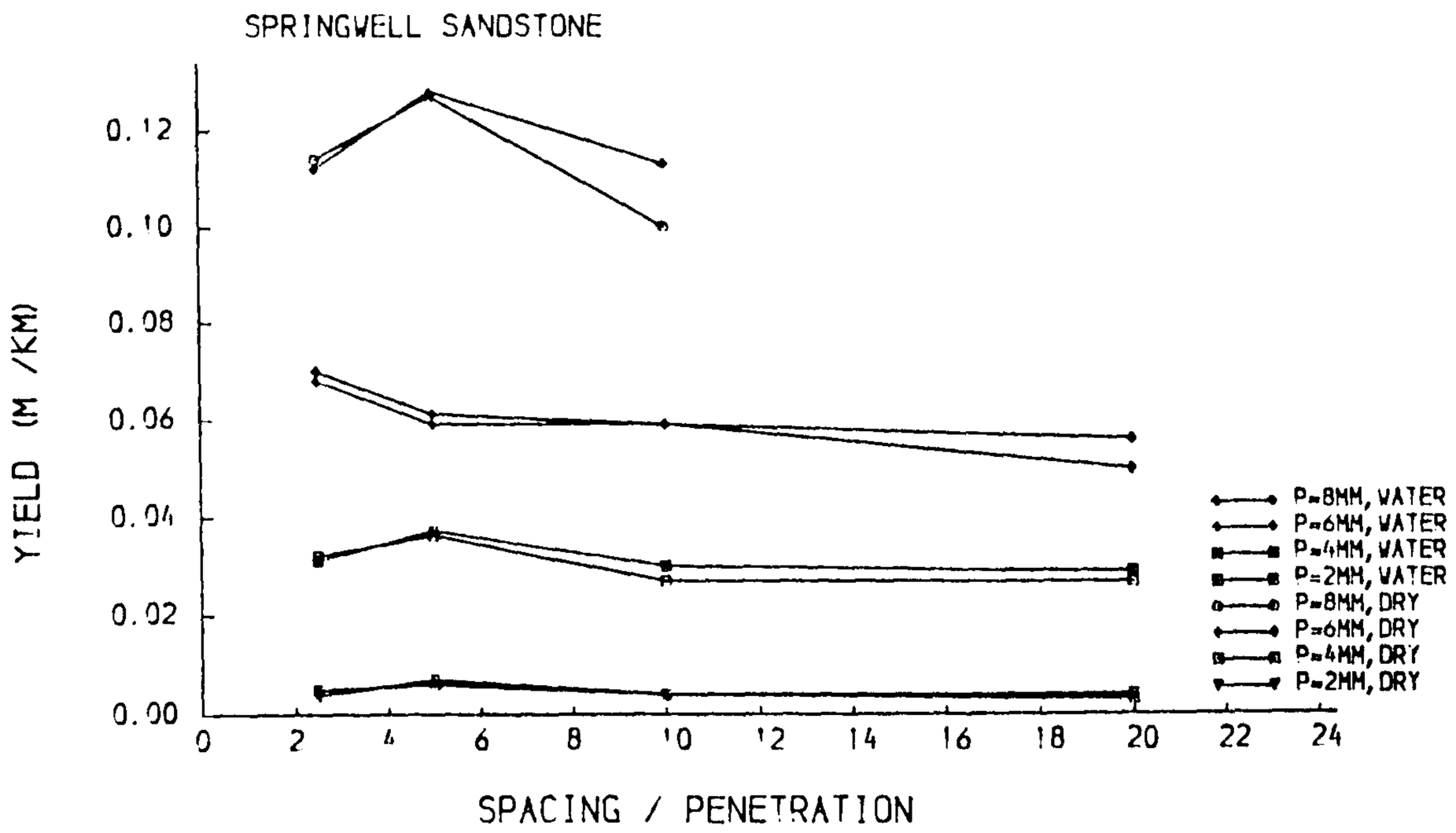

Fig. 6.2.5 Yield versus s/p ratio

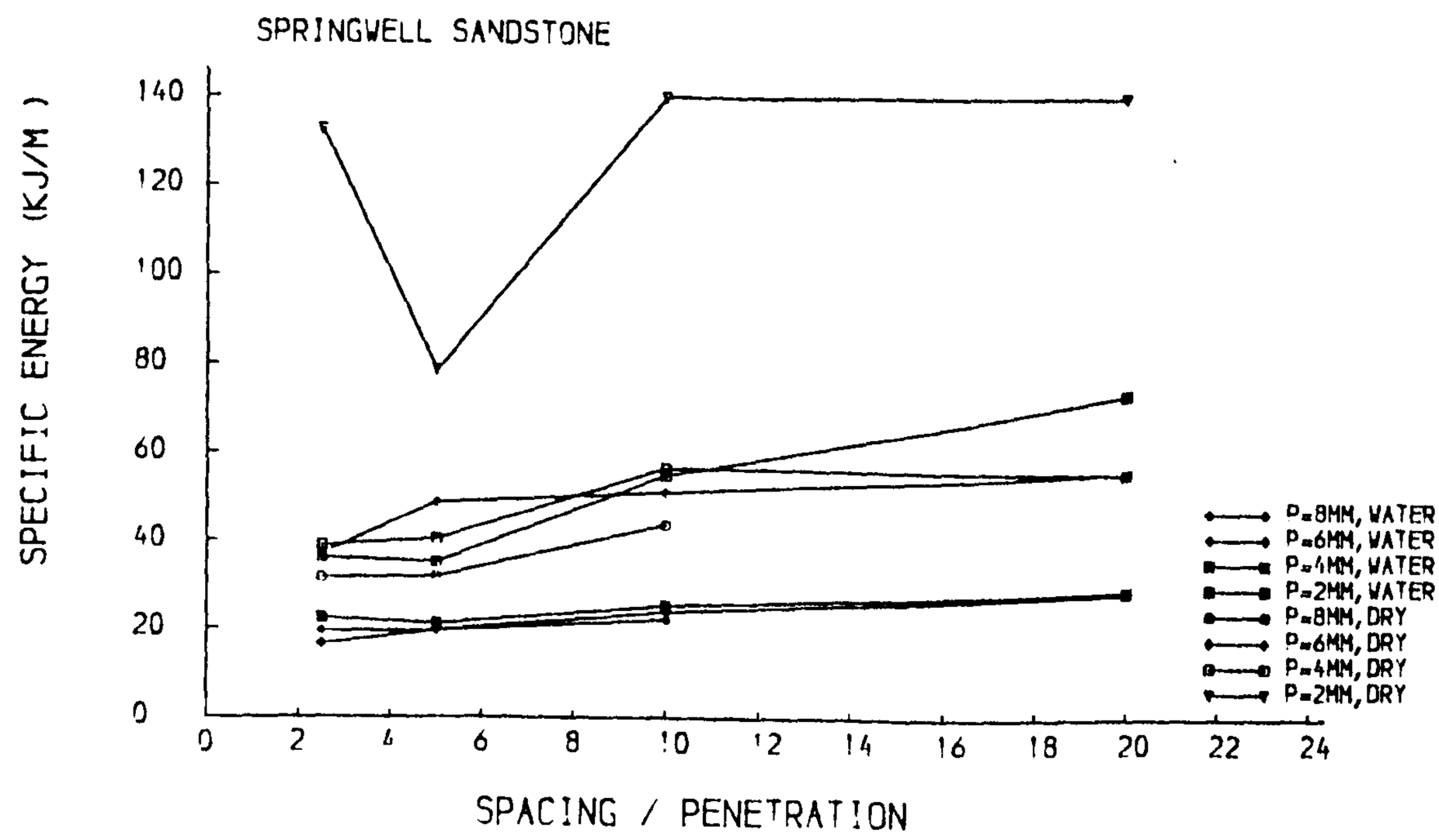

Fig. 6.2.6 Specific energy versus s/p ratio

conclusion can be drawn in the water jet assisted disc cutting tests.

6.2.3 Whinstone – Single Pass Cutting Tests

A summary of the disc cutter forces is presented in Appendix C.2 and includes the results recorded at a depth of cut of 2mm, 4mm and 6mm for single pass cutting tests. Table 6.2.2 shows the percentage reduction in the water jet assisted cutting forces compared with unassisted disc cutter forces on Whinstone by single pass method.

Table 6.2.2 Percentage reduction in cutting forces

p mm	s/p	MPTF %	MTF %	MPRF %	MRF %
2.0	2.50	-6.61	9.59	-0.93	10.59
	5.00	2.18	4.12	6.03	9.30
	10.00	-6.72	1.04	-3.36	16.83
	20.00	-6.49	0.46	-0.76	-5.26
4.0	2.50	6.46	2.99	29.74	33.85
	5.00	13.43	13.98	21.48	13.77
	10.00	15.09	9.09	20.61	15.46
	20.00	13.66	0.0	20.05	14.33
6.0	2.50	-4.56	-7.02	4.04	1.49
	5.00	10.16	1.46	14.59	7.09
	10.00	4.61	1.44	14.06	11.25
	20.00	14.36	6.66	19.27	6.15

The effects of the s/p ratio on the thrust and rolling force components are illustrated in Figs 6.2.7, 6.2.8, 6.2.9 and 6.2.10. As expected the force increase approximately linear with ratio of s/p until a value of 10, which is the same value obtained on Springwell Sandstone. Reference to previous chapter, i.e. Chapter 3, where explanation is given for this phenomenon.

The effects of s/p ratios on yield are illustrated in Fig. 6.2.11, and on specific

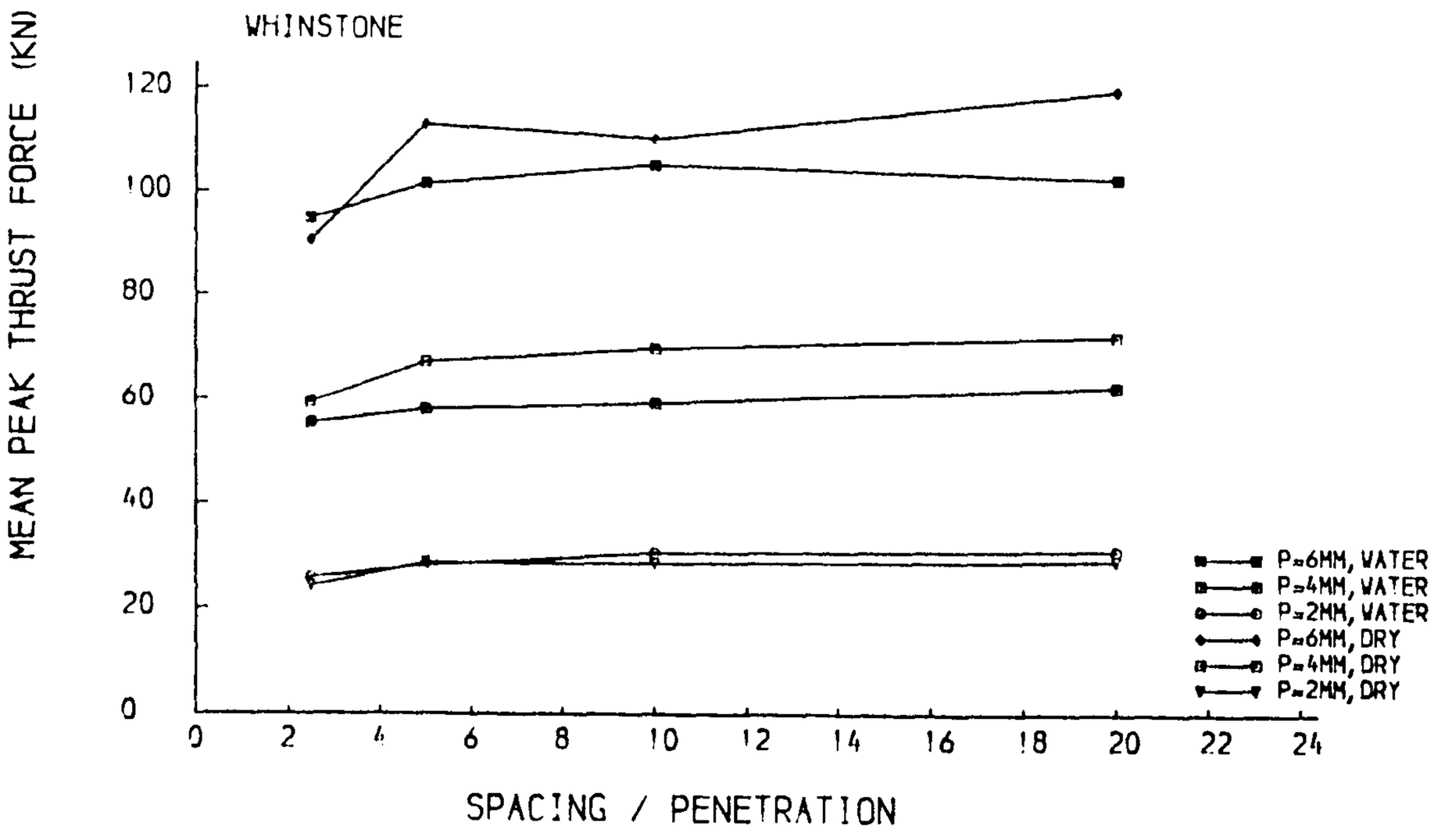

Fig. 6.2.7 Mean peak thrust force versus s/p ratio

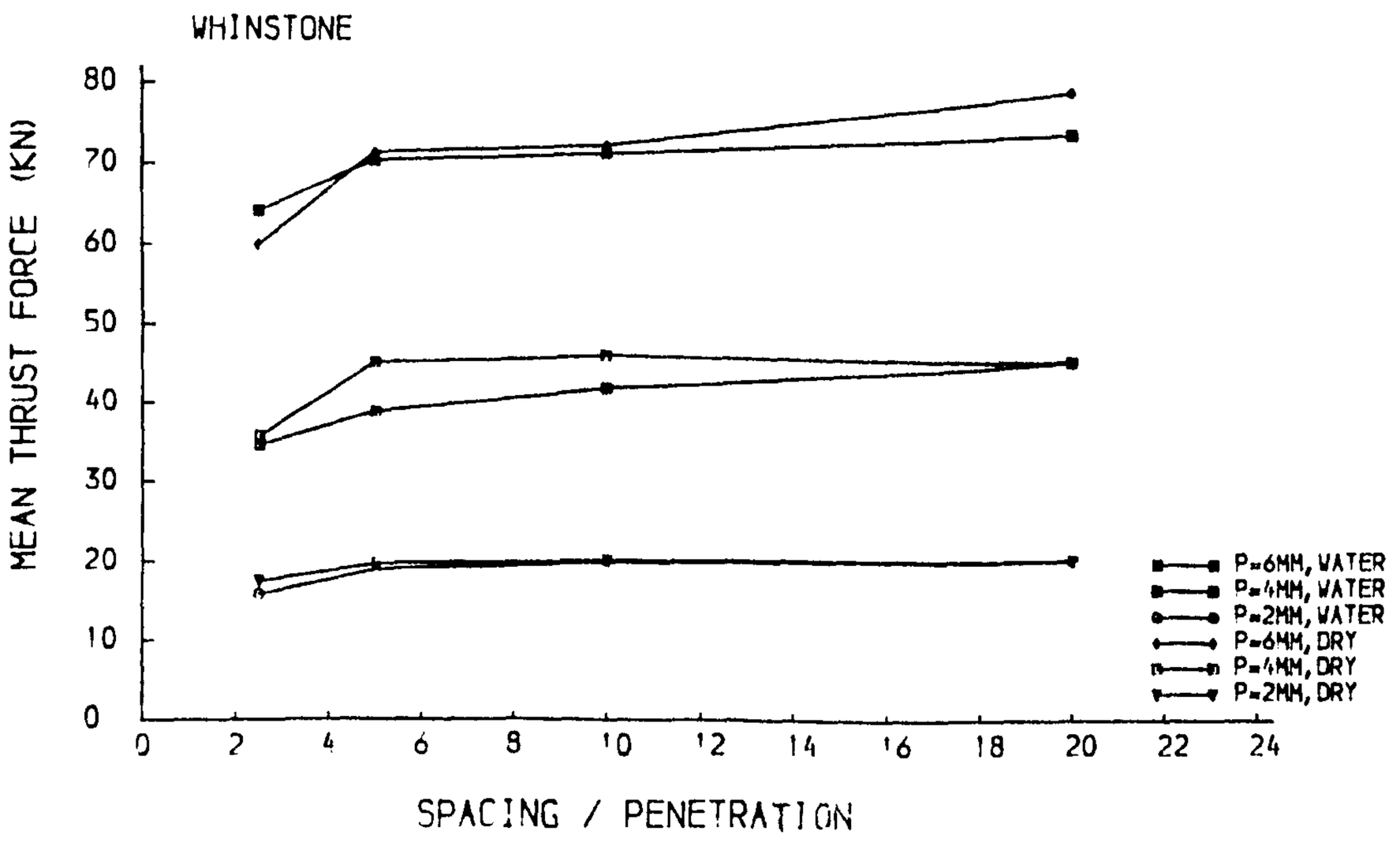

Fig. 6.2.8 Mean thrust force versus s/p ratio

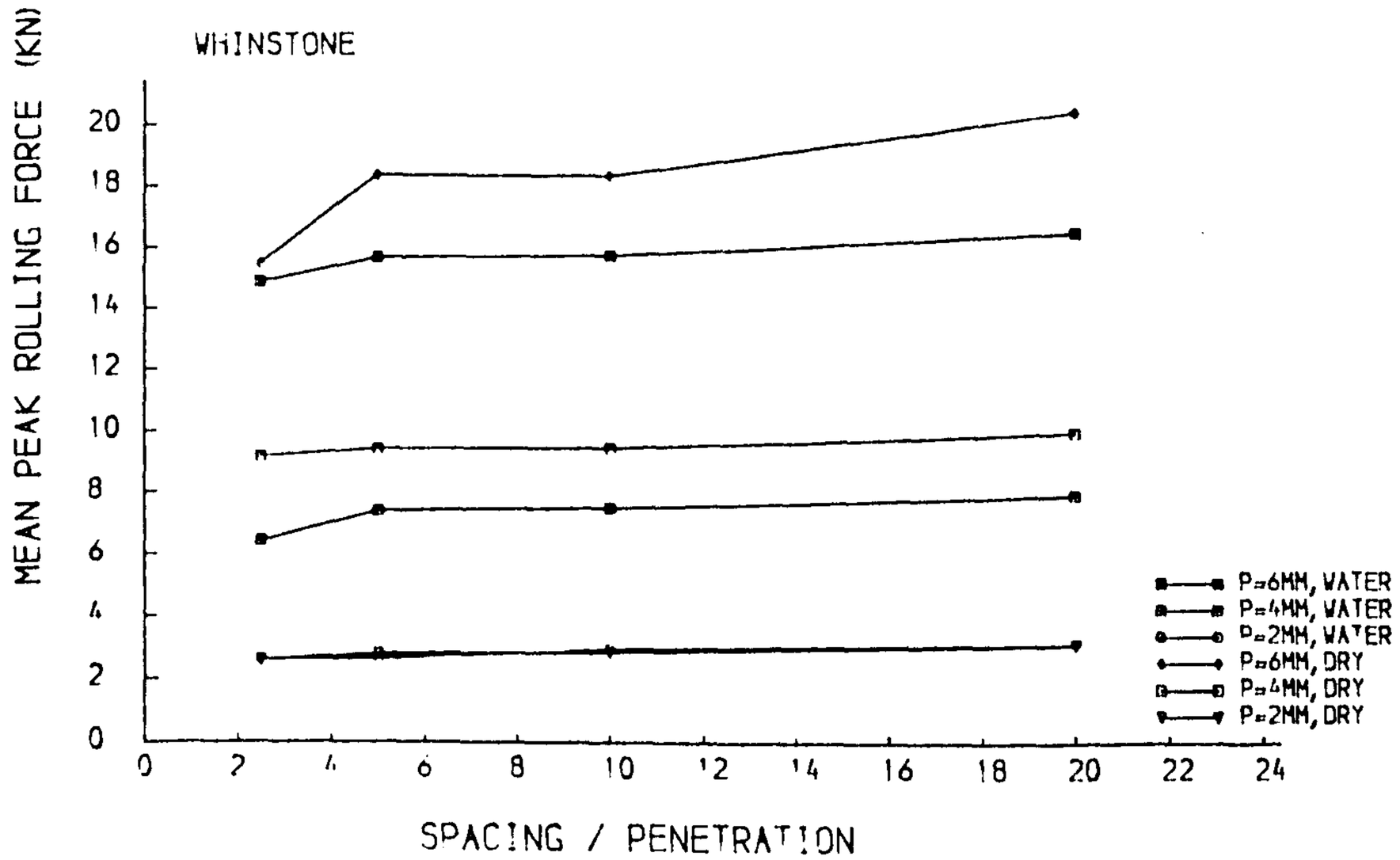

Fig. 6.2.9 Mean peak rolling force versus s/p ratio

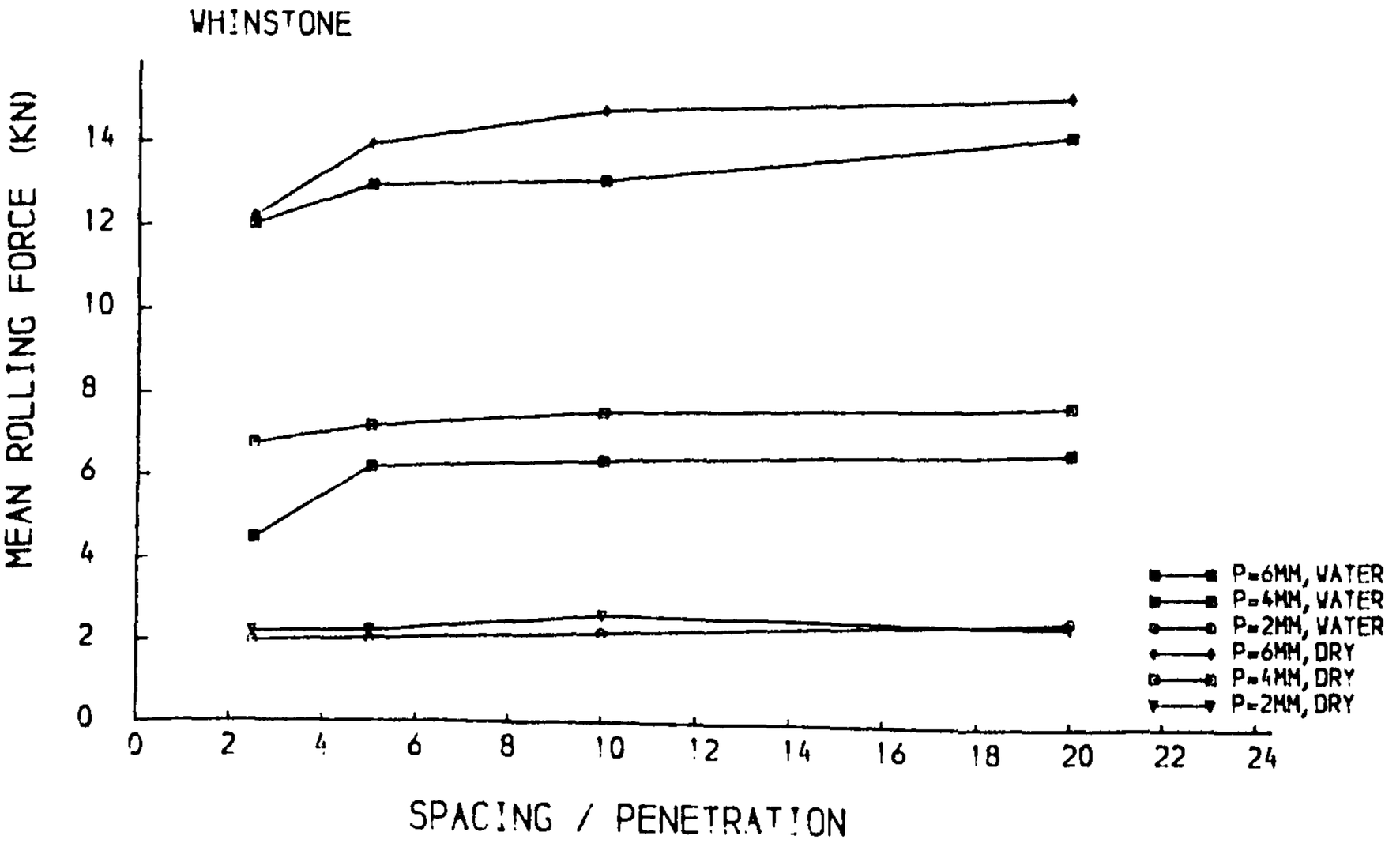

Fig. 6.2.10 Mean rolling force versus s/p ratio

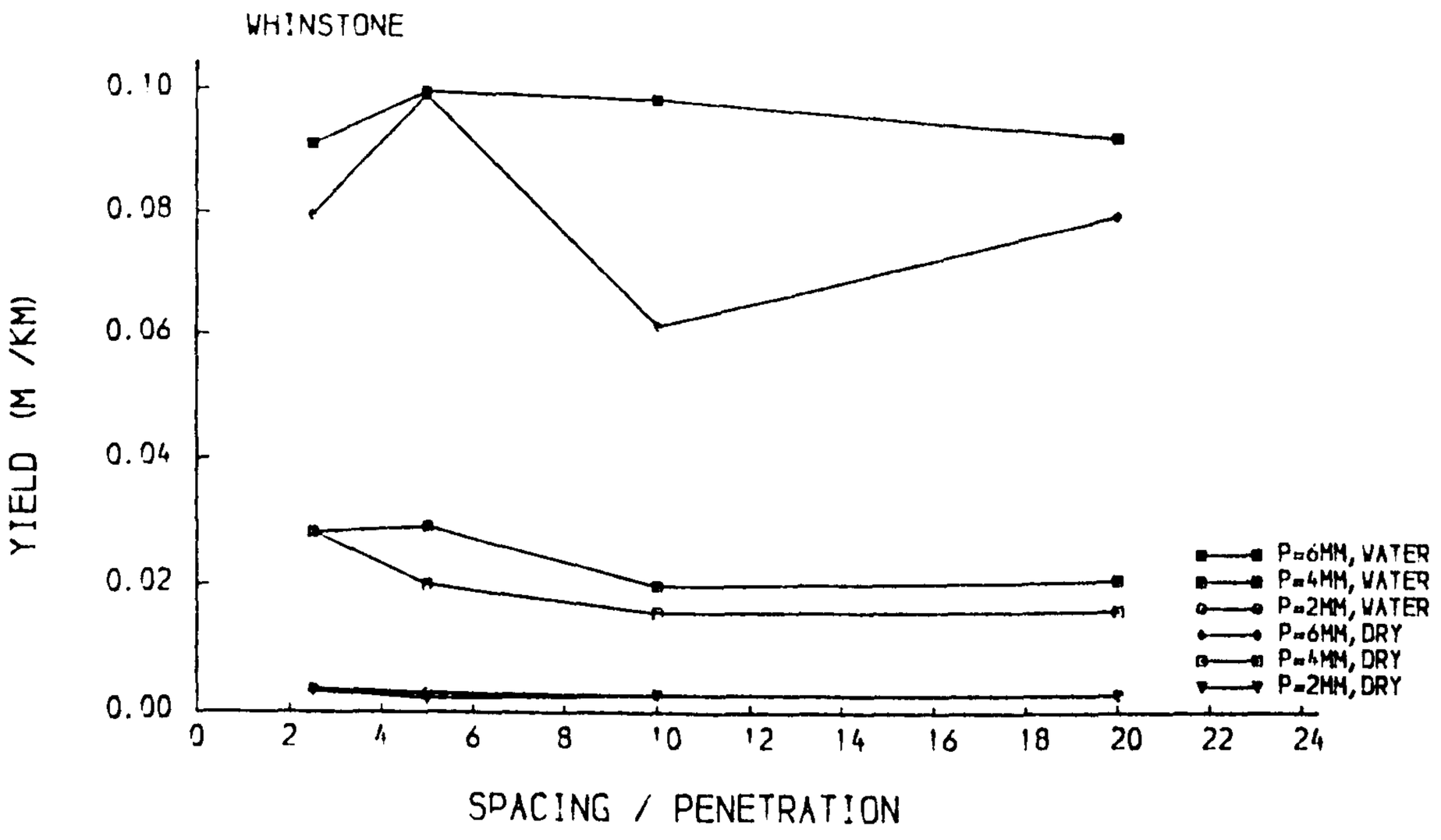

Fig. 6.2.11 Yield versus s/p ratio

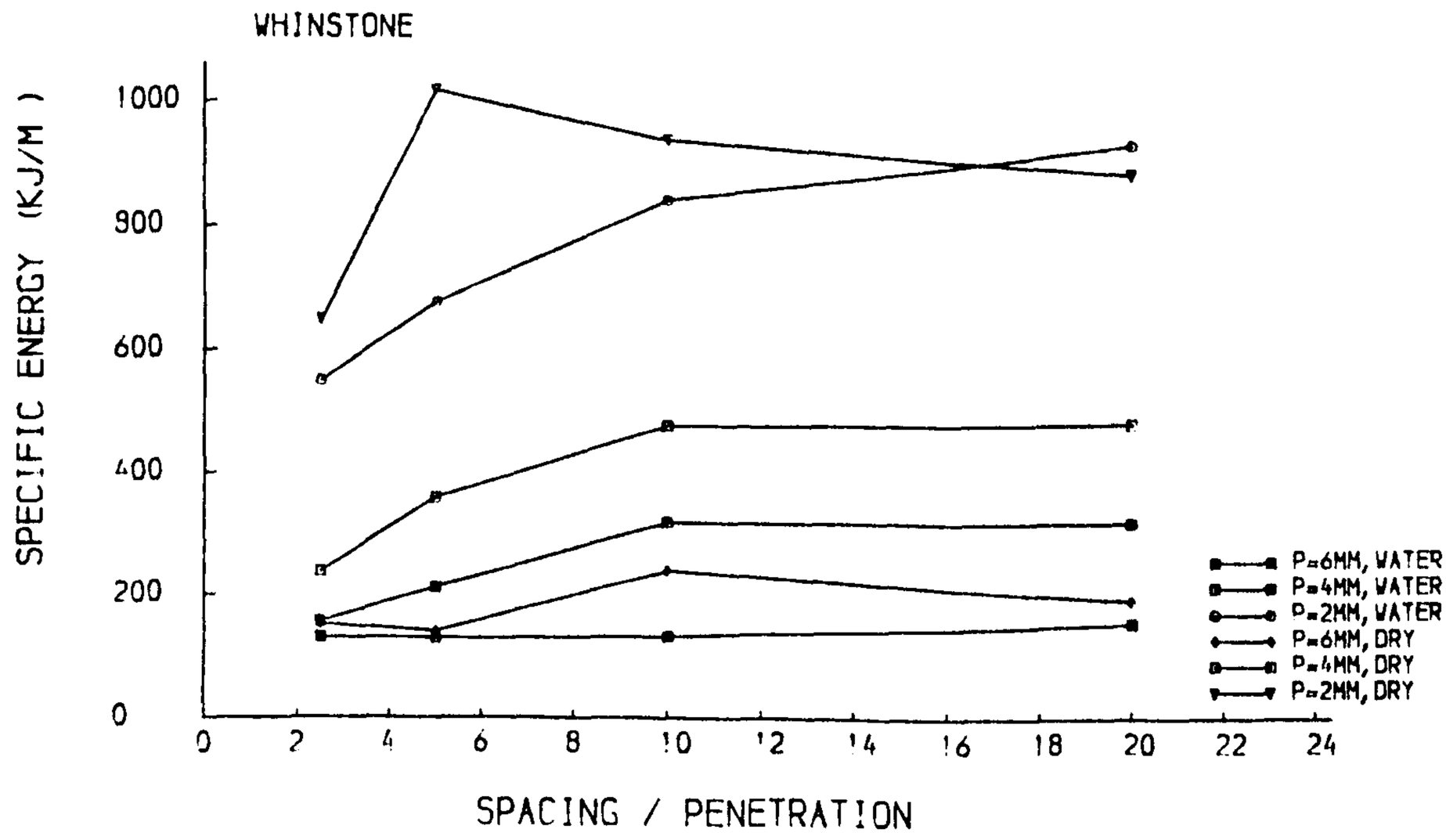

Fig. 6.2.12 Specific energy versus s/p ratio

Table 6.2.3 Percentage reduction in cutting forces

p mm	s/p	MPTF %	MTF %	MPRF %	MRF %
4.0	5.0	8.54	10.46	10.23	12.04
	10.0	3.86	-15.00	14.00	7.69

energy are shown in Fig. 6.2.12. Again, the minimum specific energy occurs at a s/p value of 2.5 or 5 for each of the penetration conditions used during the water jet assisted and unassisted cutting tests.

6.2.4 Whinstone – Multiple Pass Cutting Tests

Table 6.2.3 presents the percentage reduction in the cutting forces by the assistance of the water jet compared with unassisted disc cutter forces on Whinstone during the multiple cutting tests. A summary of the disc cutter forces is listed in Appendix C.3. Only few data were collected from the multiple cutting tests, as when a further series of cuts at s/p ratio of 20 were attempted, the disc cutter was badly damaged. As seen from Plate 6.2.1, the damage is caused by breakages rather than wear.

Compared with the results obtained by the single pass cutting tests, the cutting forces in the multiple cutting tests are higher. The reduction of the cutter forces by the assistance of a water jet in the multiple pass cutting tests is less than that in the single pass cutting tests. This suggests that the wear and the damage of the tool was an important factor affected the cutting performance, as the unassisted cutting tests was done before the water jet assisted cutting tests.

6.2.5 Summary

The laboratory test results obtained so far indicate that the use of a water jet directed in the disc cutter path offers a significant potential for improved cutting

performance. With a pre-cut slot of 3mm made by the water jet on Springwell Sandstone, the reductions of cutting forces decrease with increasing penetration depths. The changes in the cutting forces have shown the influence of the pre-cut slot on the cutting performance to be — for peak thrust forces — from over 80% reduction with a 2mm penetration, to less than 20% reduction with an 8mm penetration. For the cutting tests on Whinstone, the improvements are not as significant as on Springwell Sandstone, eg., only 0 - 15% reduction in peak thrust forces in the single pass cutting tests. However, without a pre-slot cut by a water jet on the rock surface, the reduction of cutting forces on Whinstone is still very encouraging.

Surprisingly, only about 4-9% reduction in peak thrust forces in the multiple pass cutting tests on Whinstone was achieved. This is much less than that obtained from same cutting conditions of single pass tests of 13.5-15%. The possible reason is the wear and damage of the tool.

6.3 PENNANT SANDSTONE

6.3.1 Experimental Plan

Rock: Pennant Sandstone

Test Method: Multiple pass on previous cutting surface

Tools: Disc cutter

Diameter (mm): 300

Edge Angle (degree): 60

Tip Radius (mm): 2.5

Penetration Depth (mm): 2, 4

Spacing Distance (mm): 20, 40, 60

Plate 6.2.1 The damaged disc cutter

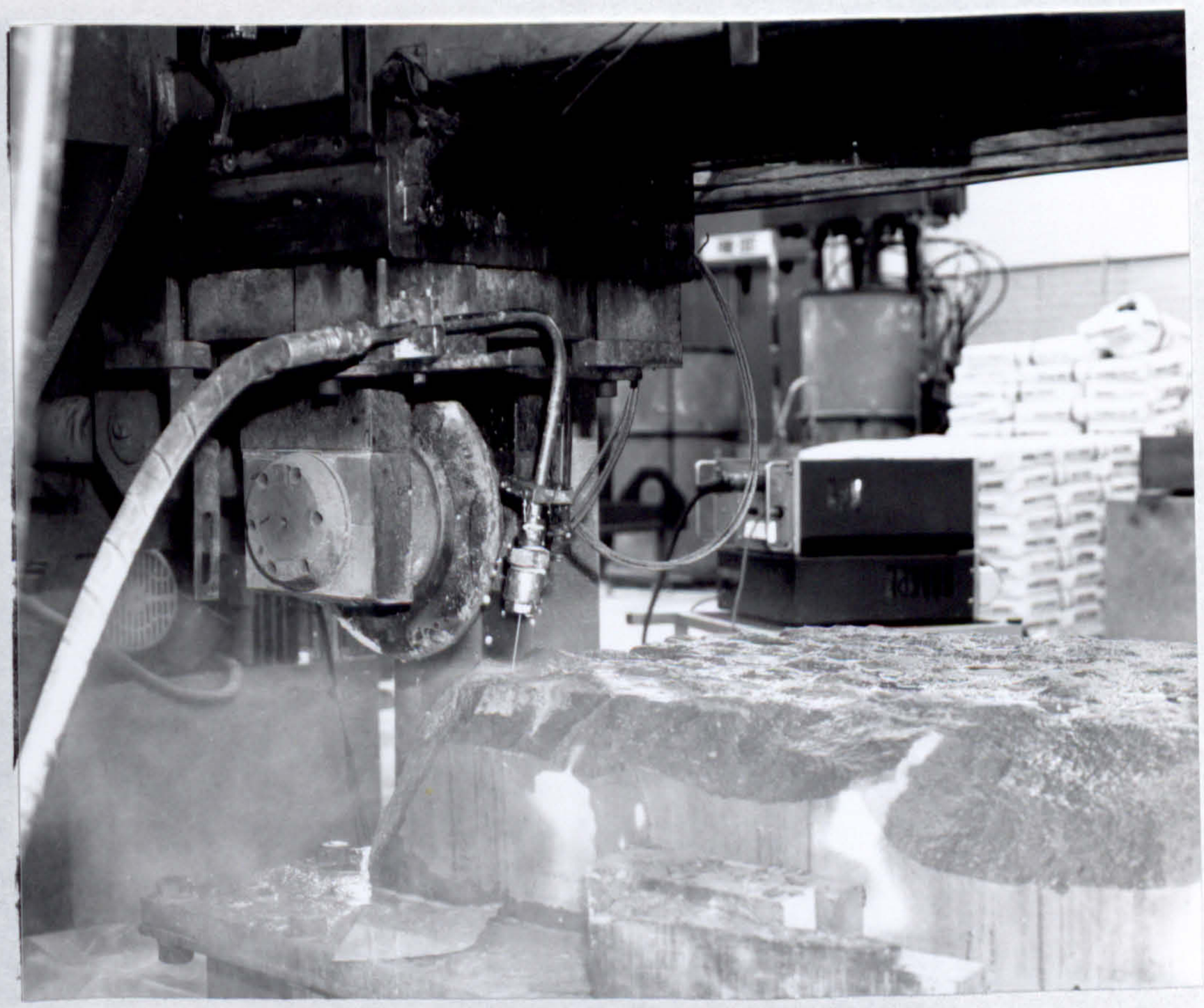

Plate 6.3.1 The nozzle location No. 1

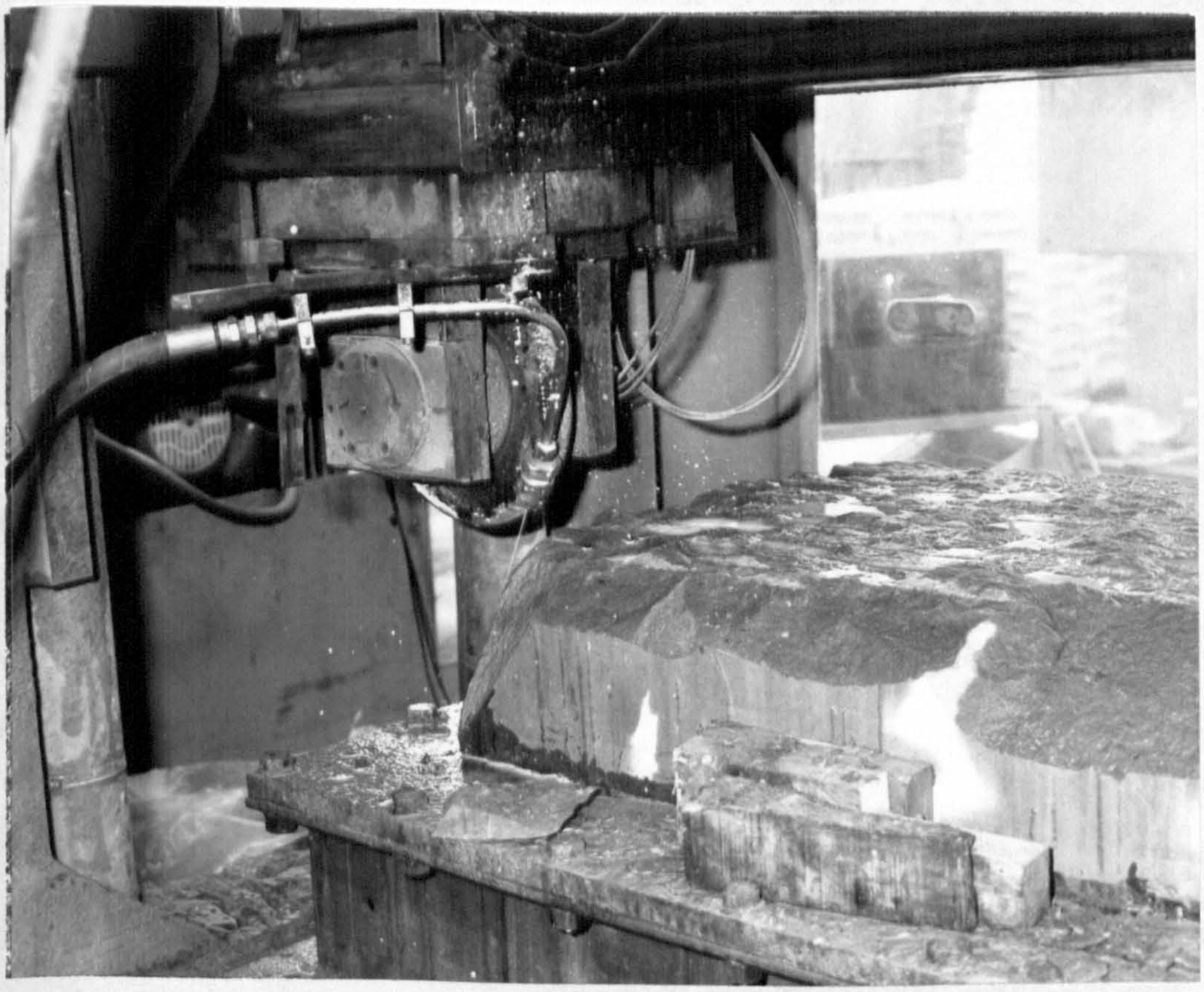

Plate 6.3.2 The nozzle location No. 2

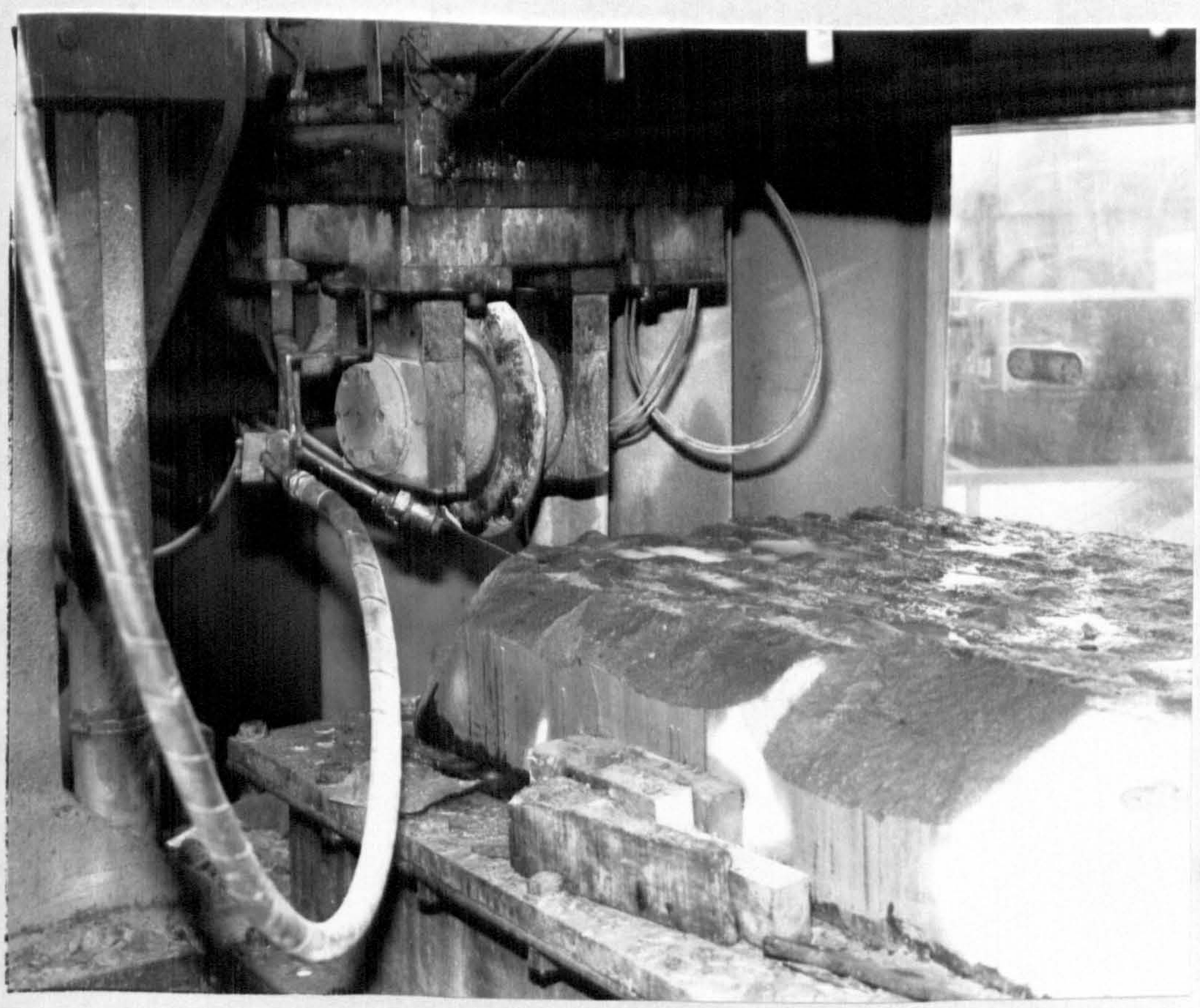

Plate 6.3.3 The nozzle location No. 3

Travel Speed (m/s): 0.25, 0.45, 0.6, 0.85, 1.0

Jet Pressure (MPa): 13.79 (2,000psi), 27.58 (4,000psi),

41.37 (6,000psi), 55.16 (8,000psi)

Jet Location: three different positions

Pattern 1: the water jet is in front of the disc cutter (Plate 6.3.1);

Pattern 2: the water jet is in front of and beside the disc cutter (Plate 6.3.2);

Pattern 3: the water jet is beside the disc cutter (Plate 6.3.3)

Nozzle Diameter: 0.68 mm

6.3.2 Unassisted Cutting

Unassisted cutting was done before water jet assisted cutting to avoid favouring the water jet assisted condition with an unworn cutter. Consequently, because the water jet assisted cutting tests used a "worn" tool, any improvement obtained is expected to be more conservative and as such, more reliable.

Fig. 6.3.1, Fig. 6.3.2 and Fig. 6.3.3 show respectively the variation of thrust force, rolling force and side force with spacing distance. The thrust force and rolling force initially increase rapidly with spacing from 20mm to 40mm but more gradually as the spacing is increased up to 60mm for the penetration of 2mm. For the penetration of 4mm, the thrust force and rolling force increase linearly with increased spacing from 20mm to 60mm. However, there is no regular relationship between spacing distance and side force can be found.

6.3.3 The Effects of Cutting Speed

The effects of cutting speed on water jet assisted disc cutting were investigated throughout all cutting tests on Pennant Sandstone.

1. Disc Cutter Thrust Force

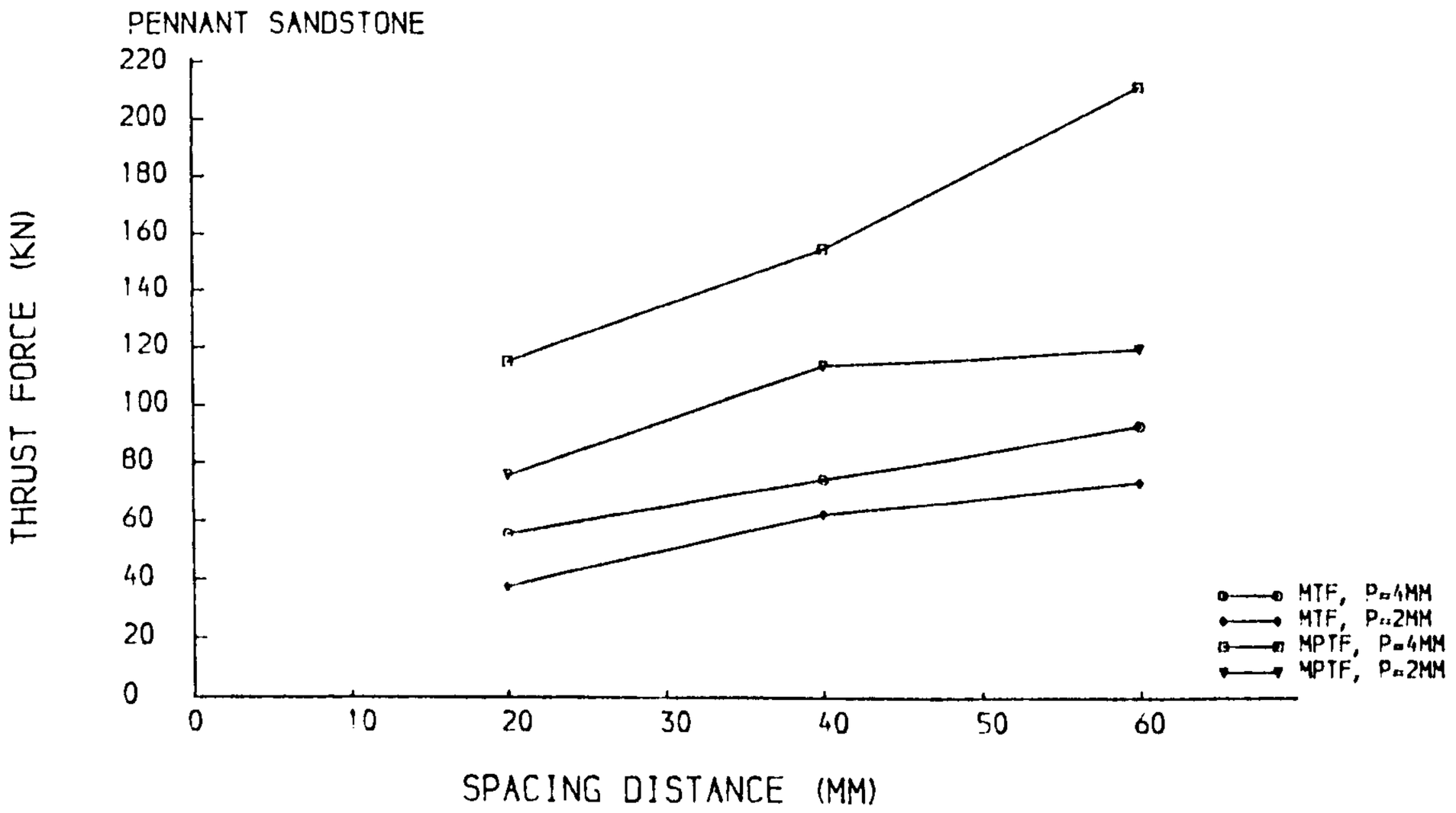

Fig. 6.3.1 Thrust force versus spacing distance

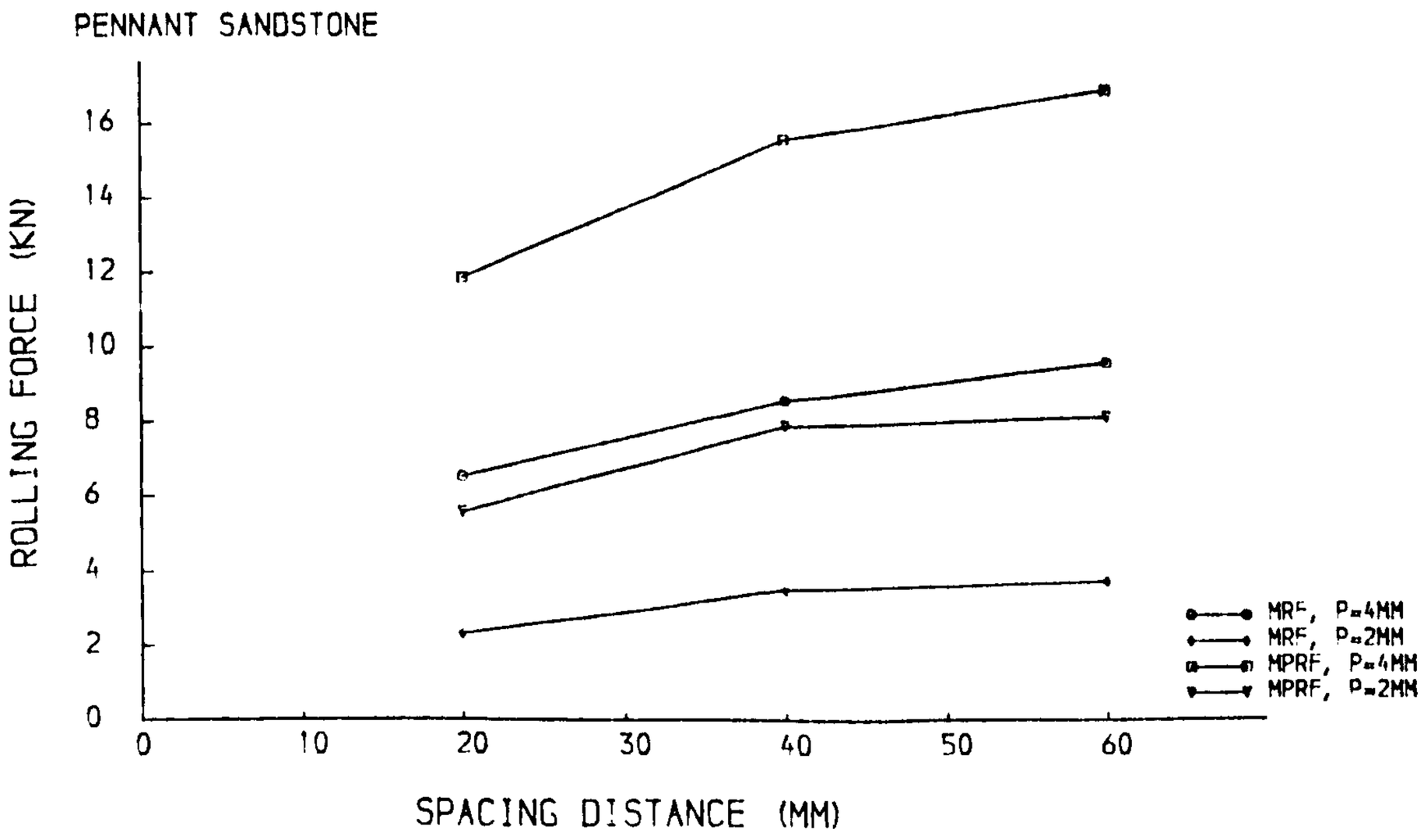

Fig. 6.3.2 Rolling force versus spacing distance

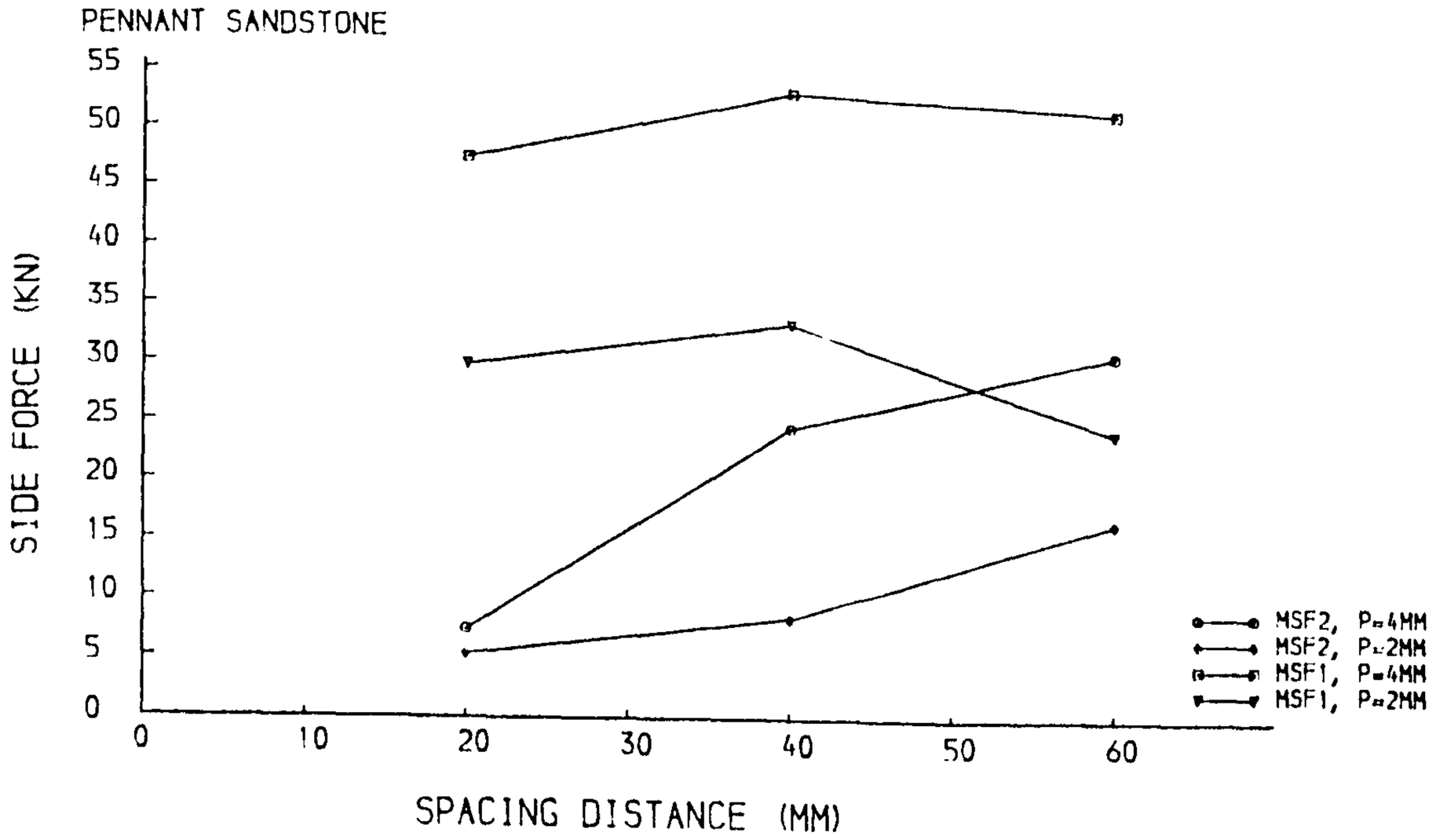

Fig. 6.3.3 Side force versus spacing distance

Considering Figs 6.3.4 and 6.3.5, the thrust forces — mean peak thrust force and mean thrust force — are either independent of cutting speed or rise slightly as the cutting speed increases. This is true for all three patterns of nozzle positions.

2. Disc Cutter Rolling Force

Considering Figs 6.3.6 and 6.3.7, there is no regular change in the rolling forces during the cutting speed increase from 0.2 m/s to 0.85 m/s.

3. Disc Cutter Side Force

Considering Figs 6.3.8 and 6.3.9, again, no significant effect of cutting speed on side force is apparent. That is true for all three nozzle locations at all speed conditions.

In fact, for a TBM, disc thrust force is provided by the machine thrust, and

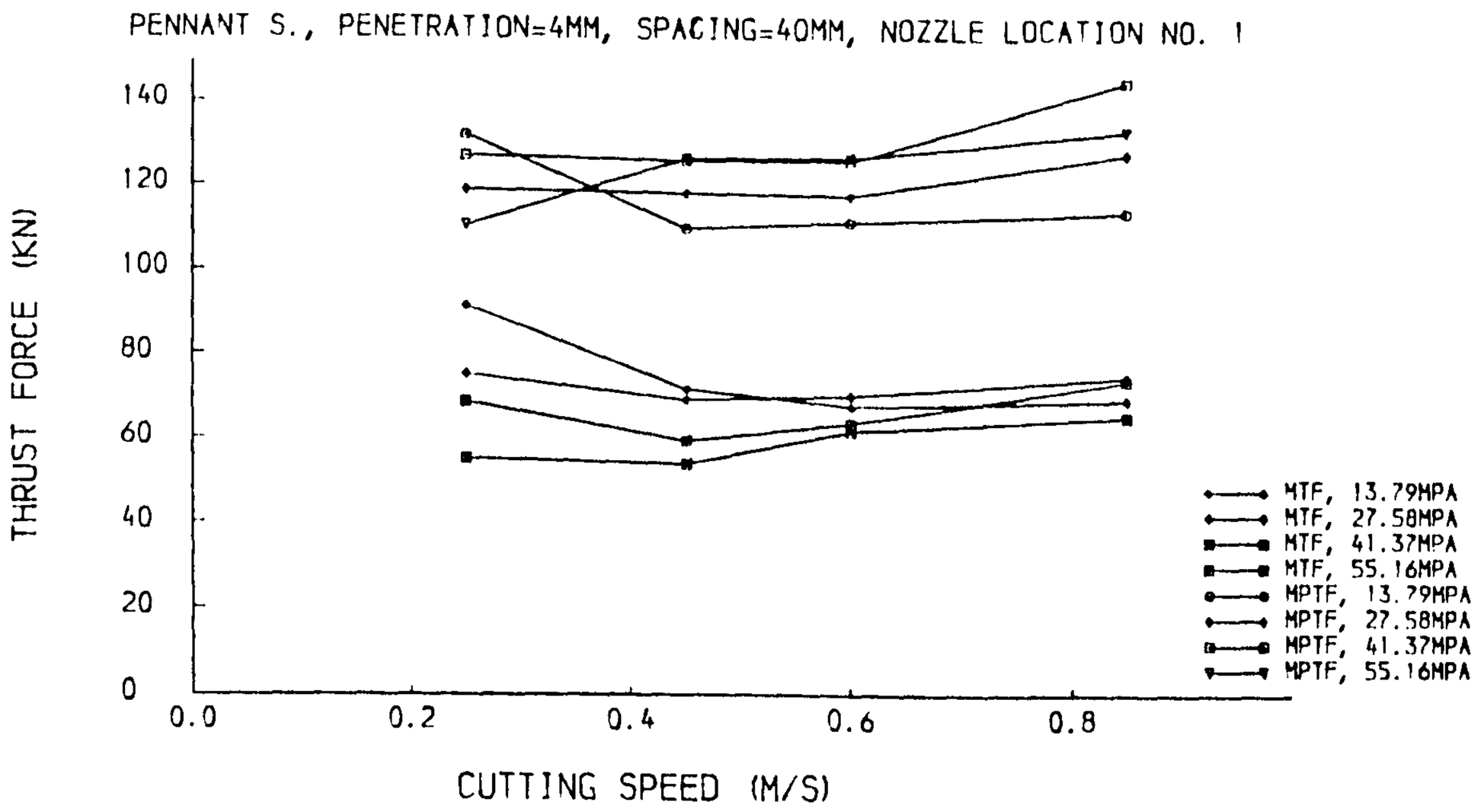

(a) $p = 4$mm, $s = 40$mm, Nozzle location No. 1

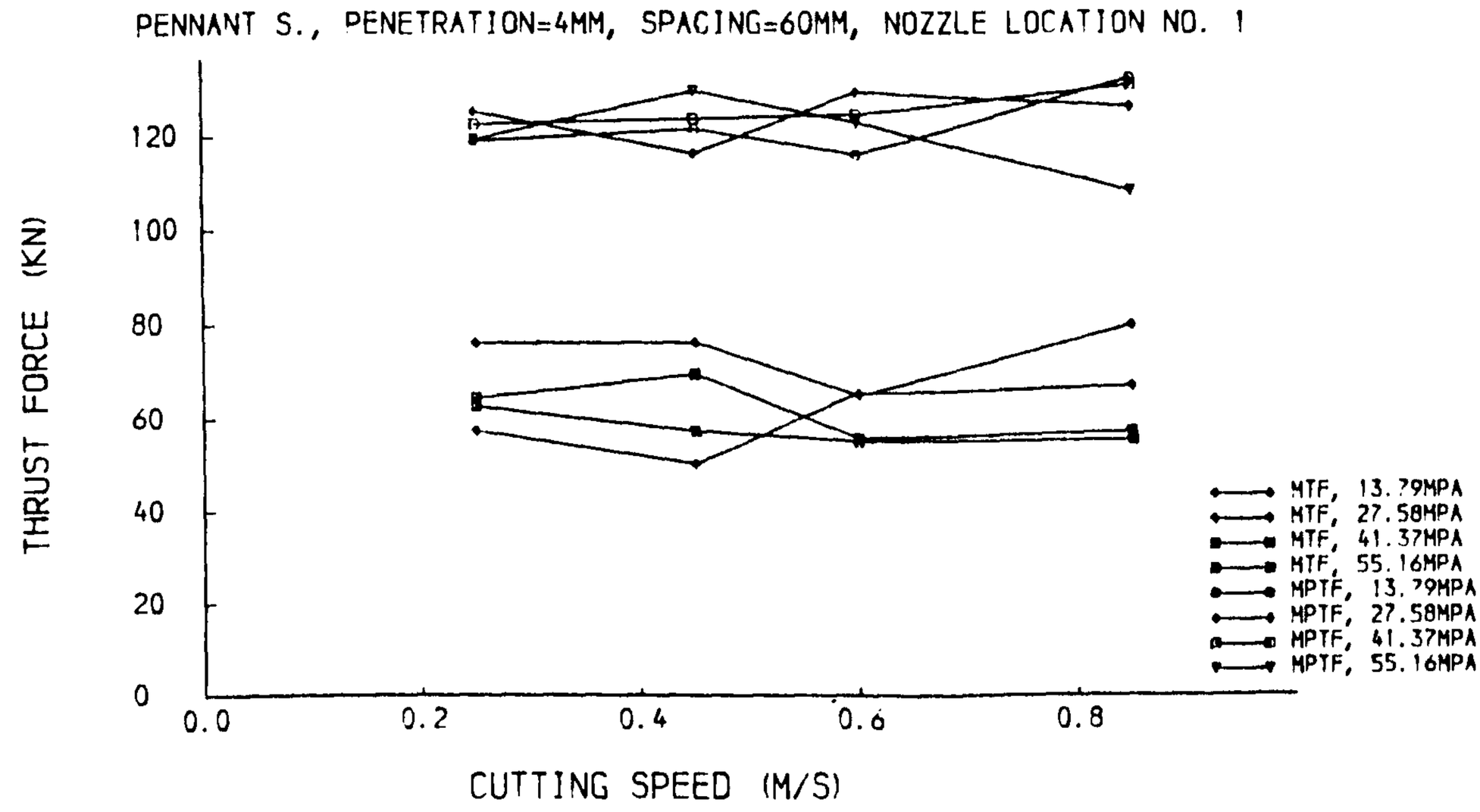

(b) $p = 4$mm, $s = 60$mm, Nozzle location No. 1

Fig. 6.3.4 Thrust force versus cutting speed

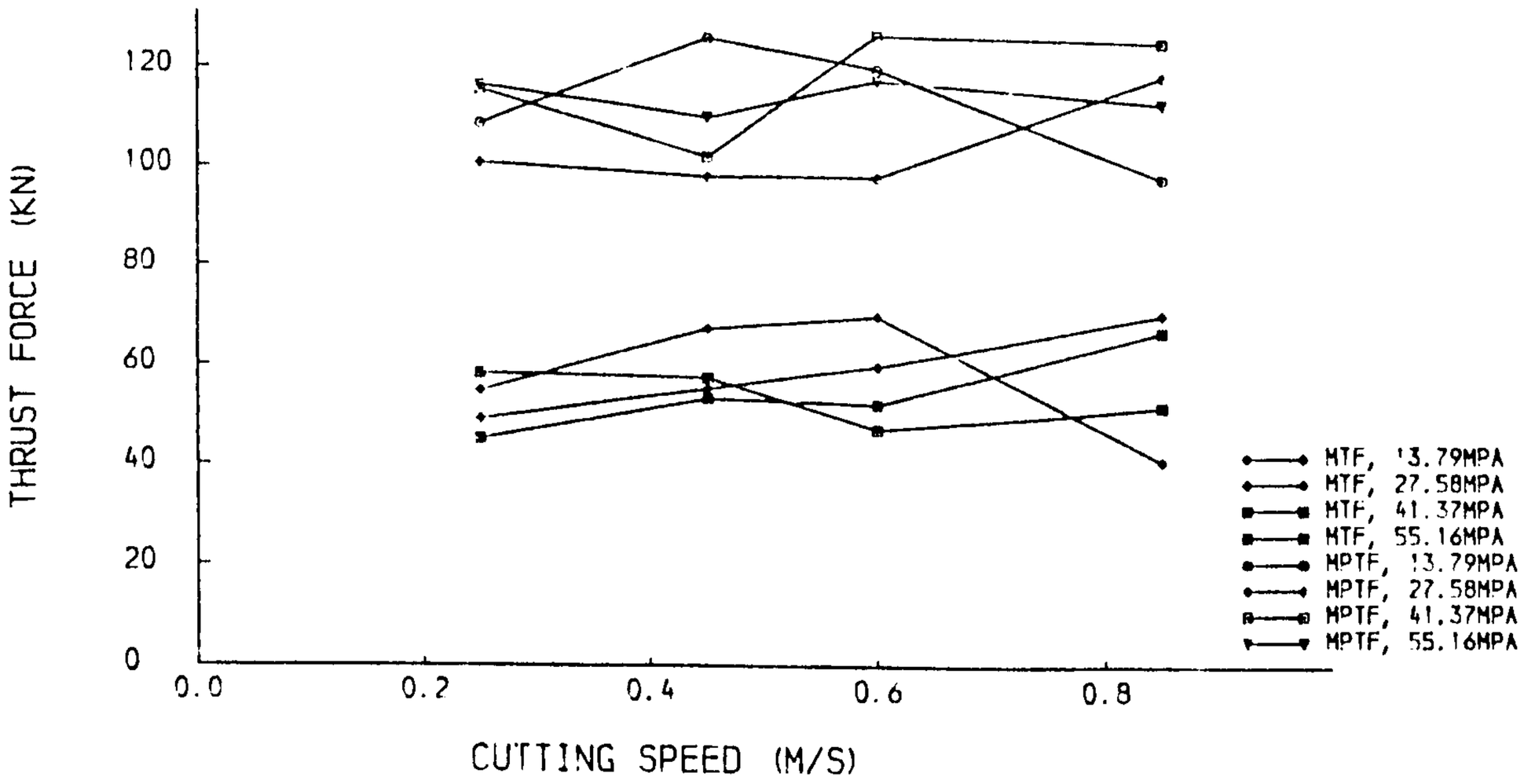

(a) $p = 4$mm, $s = 40$mm, Nozzle location No. 2

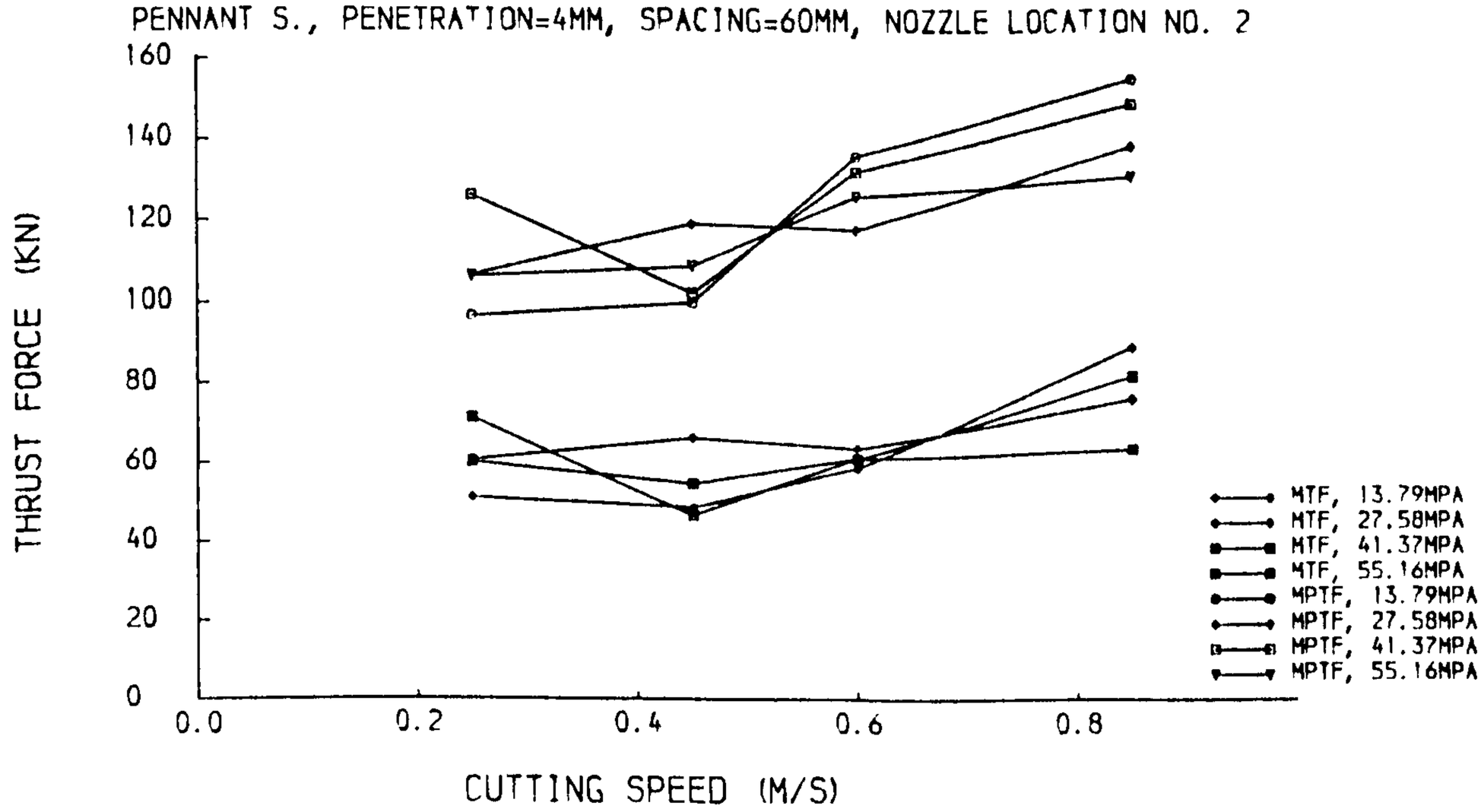

(b) $p = 4$mm, $s = 60$mm, Nozzle location No. 2

Fig. 6.3.5 Thrust force versus cutting speed

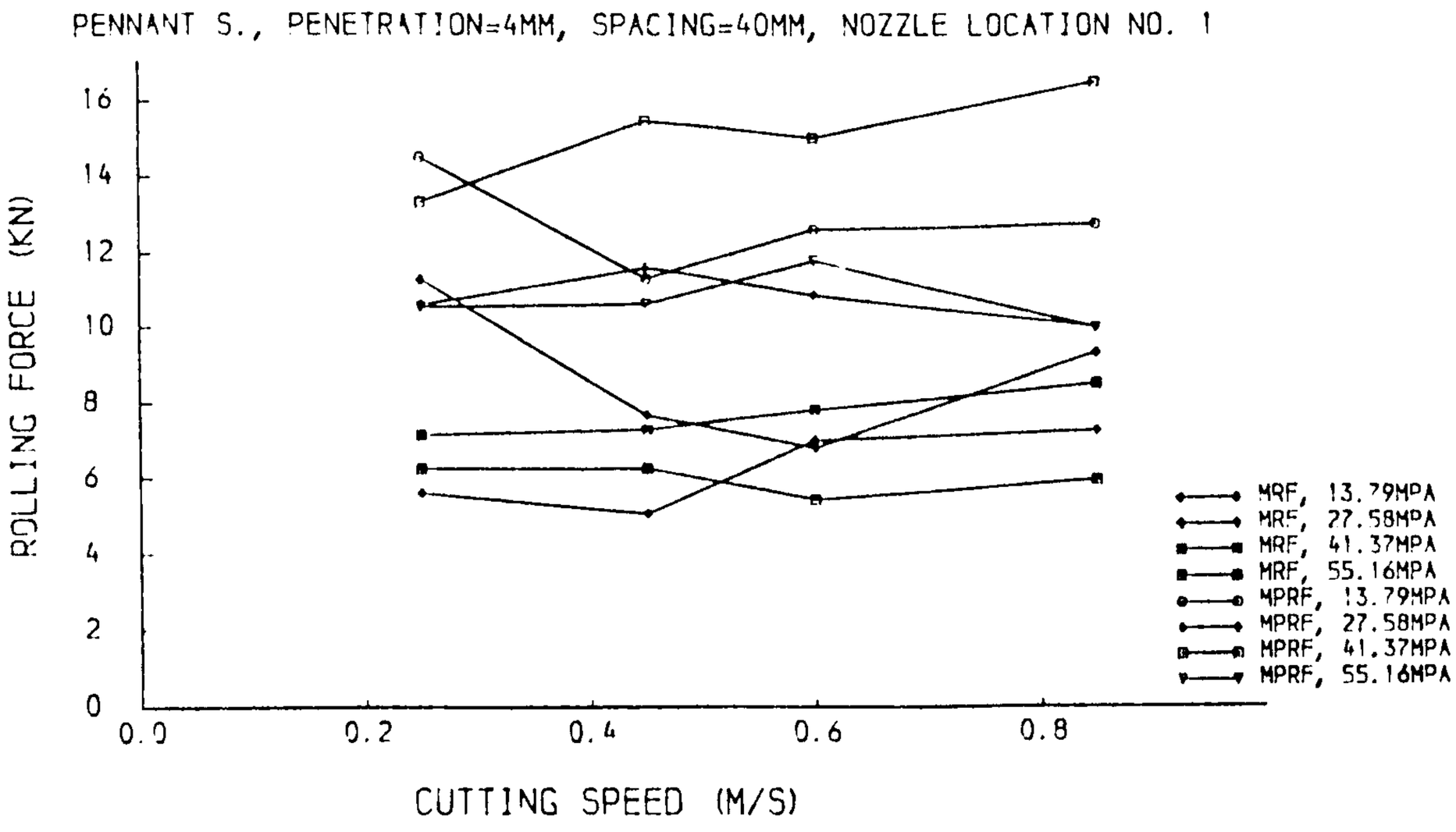

(a) $p = 4$mm, $s = 40$mm, Nozzle location No. 1

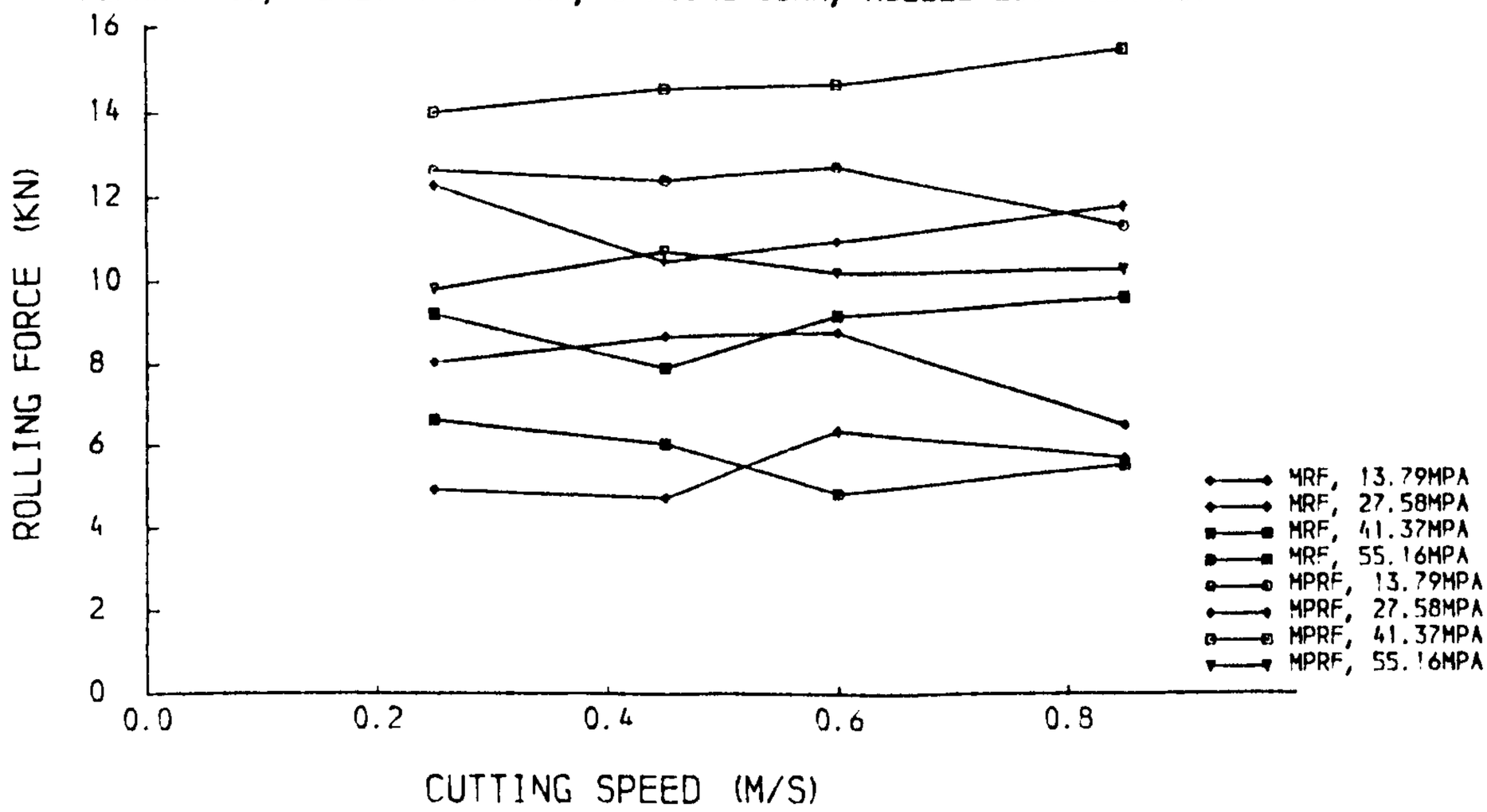

(b) $p = 4$mm, $s = 60$mm, Nozzle location No. 1

Fig. 6.3.6 Rolling force versus cutting speed

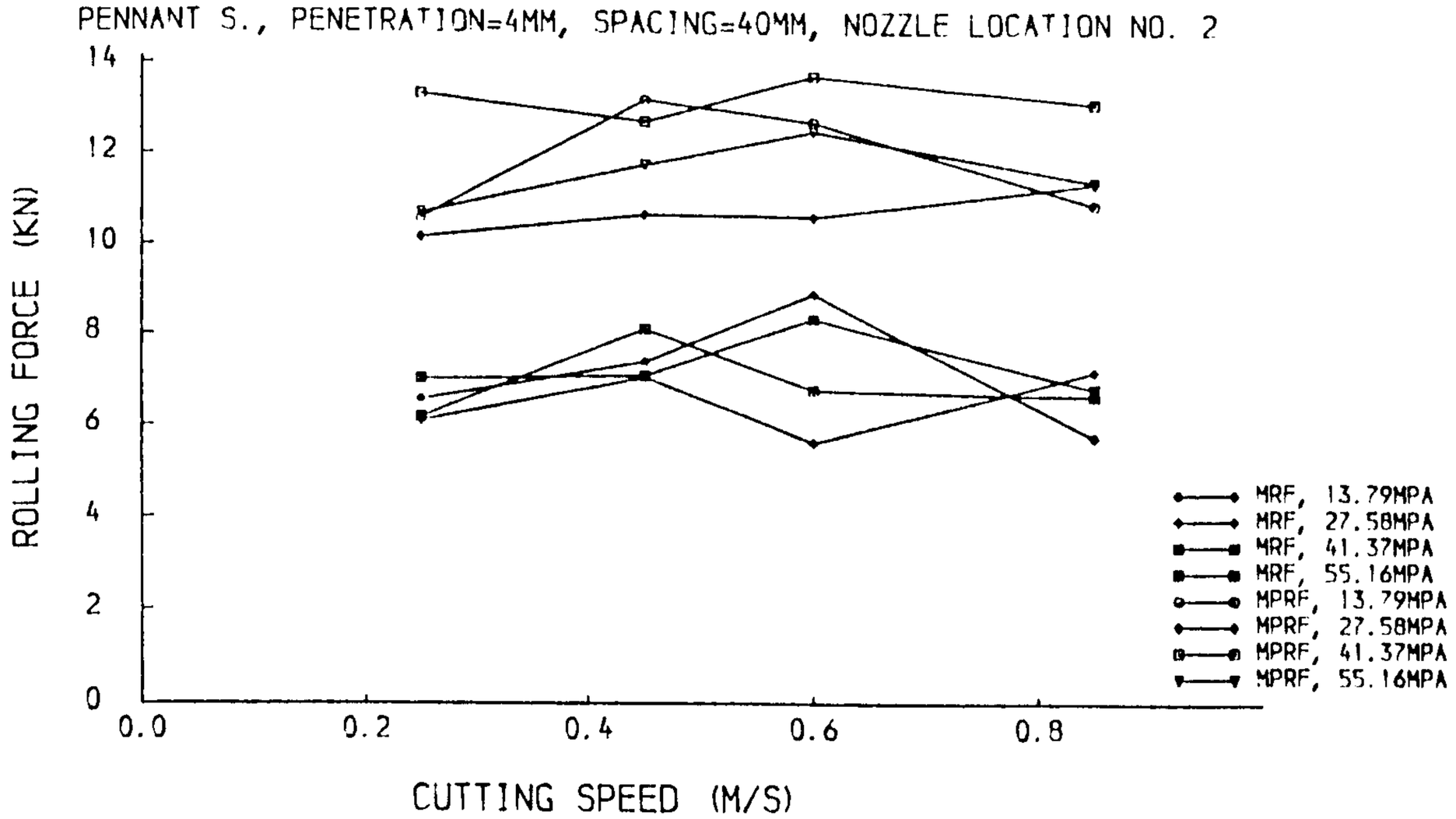

(a) $p = 4$mm, $s = 40$mm, Nozzle location No. 2

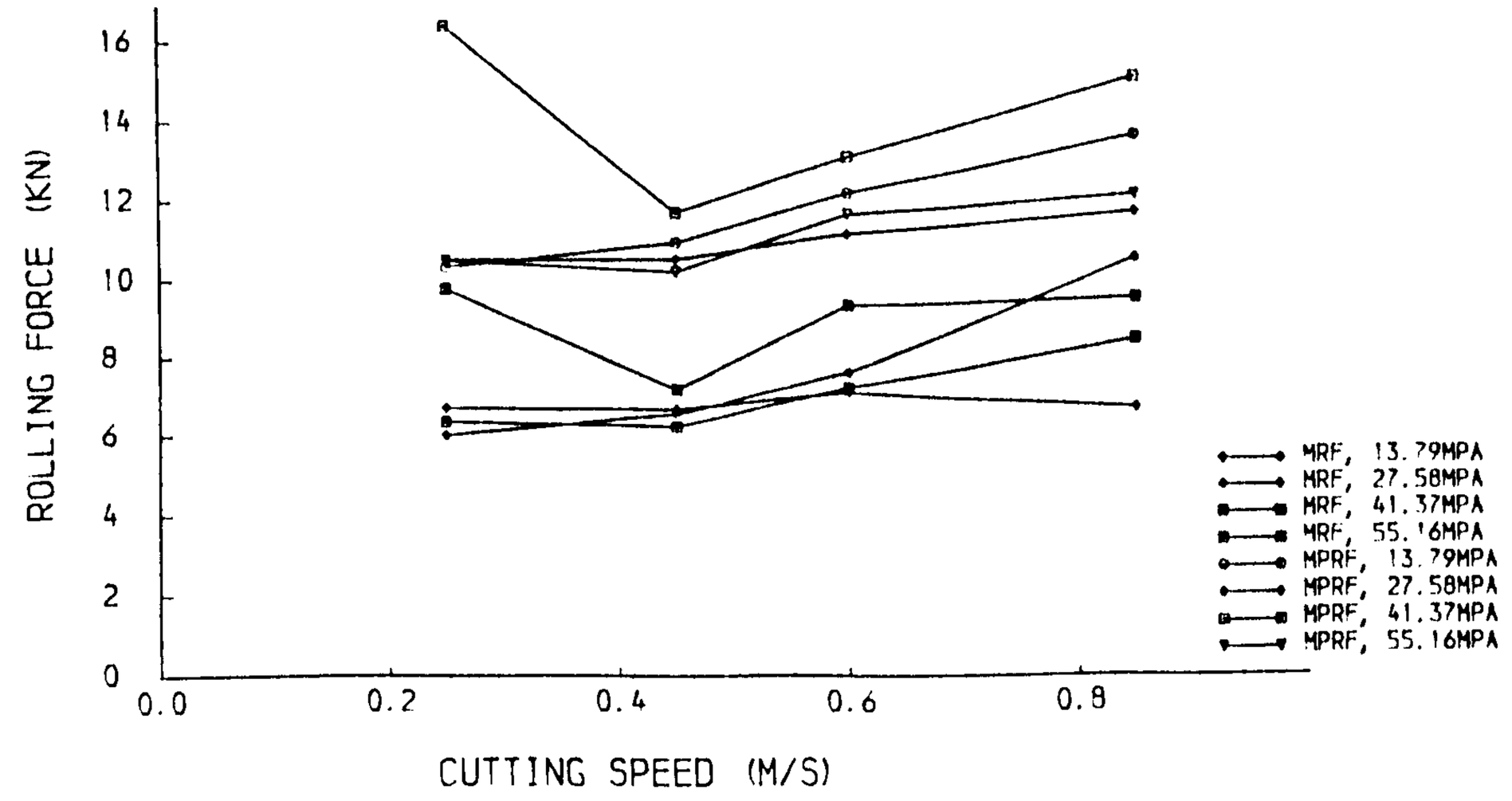

(b) $p = 4$mm, $s = 60$mm, Nozzle location No. 2

Fig. 6.3.7 Rolling force versus cutting speed

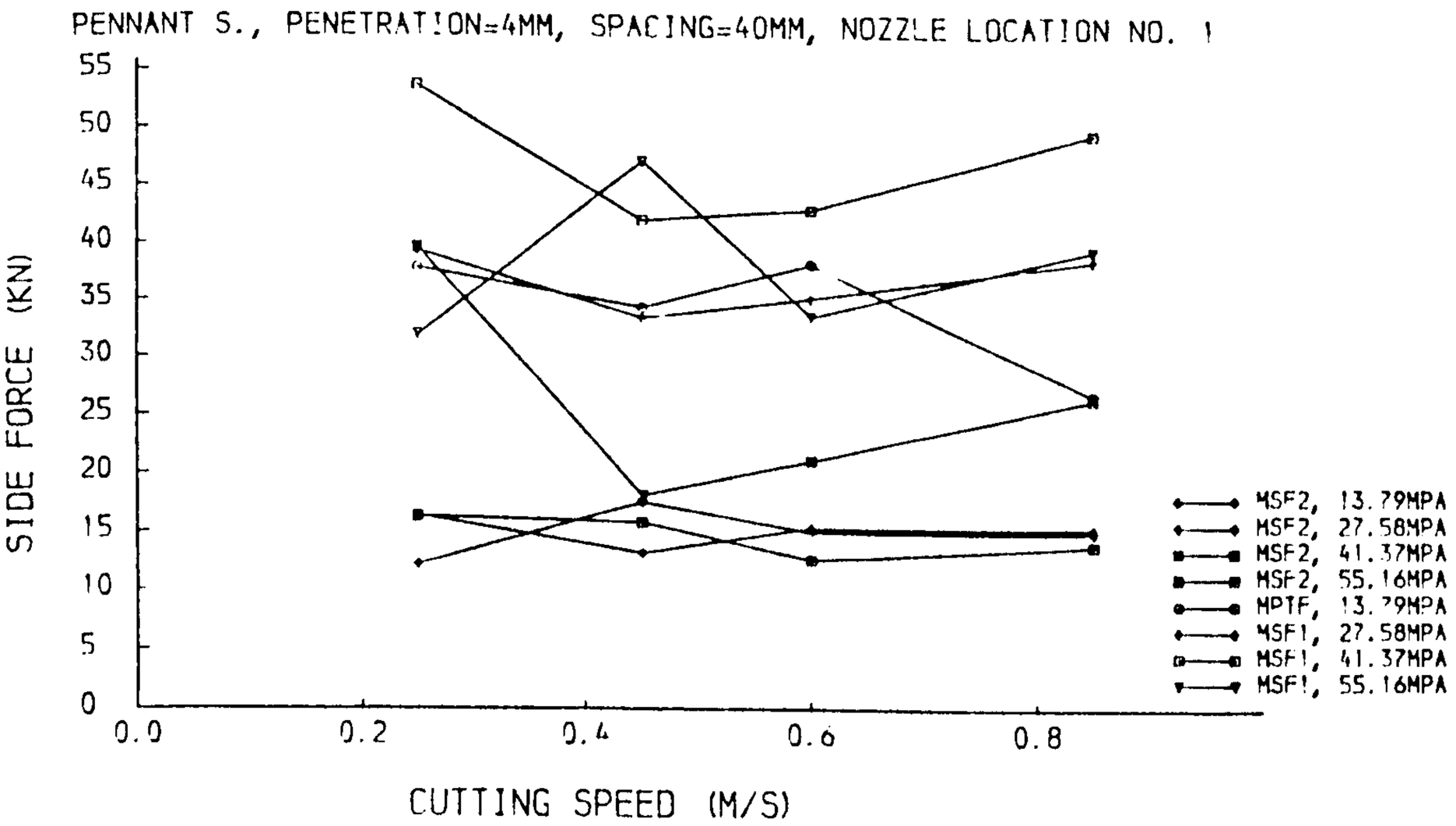

(a) $p = 4$mm, $s = 40$mm, Nozzle location No. 1

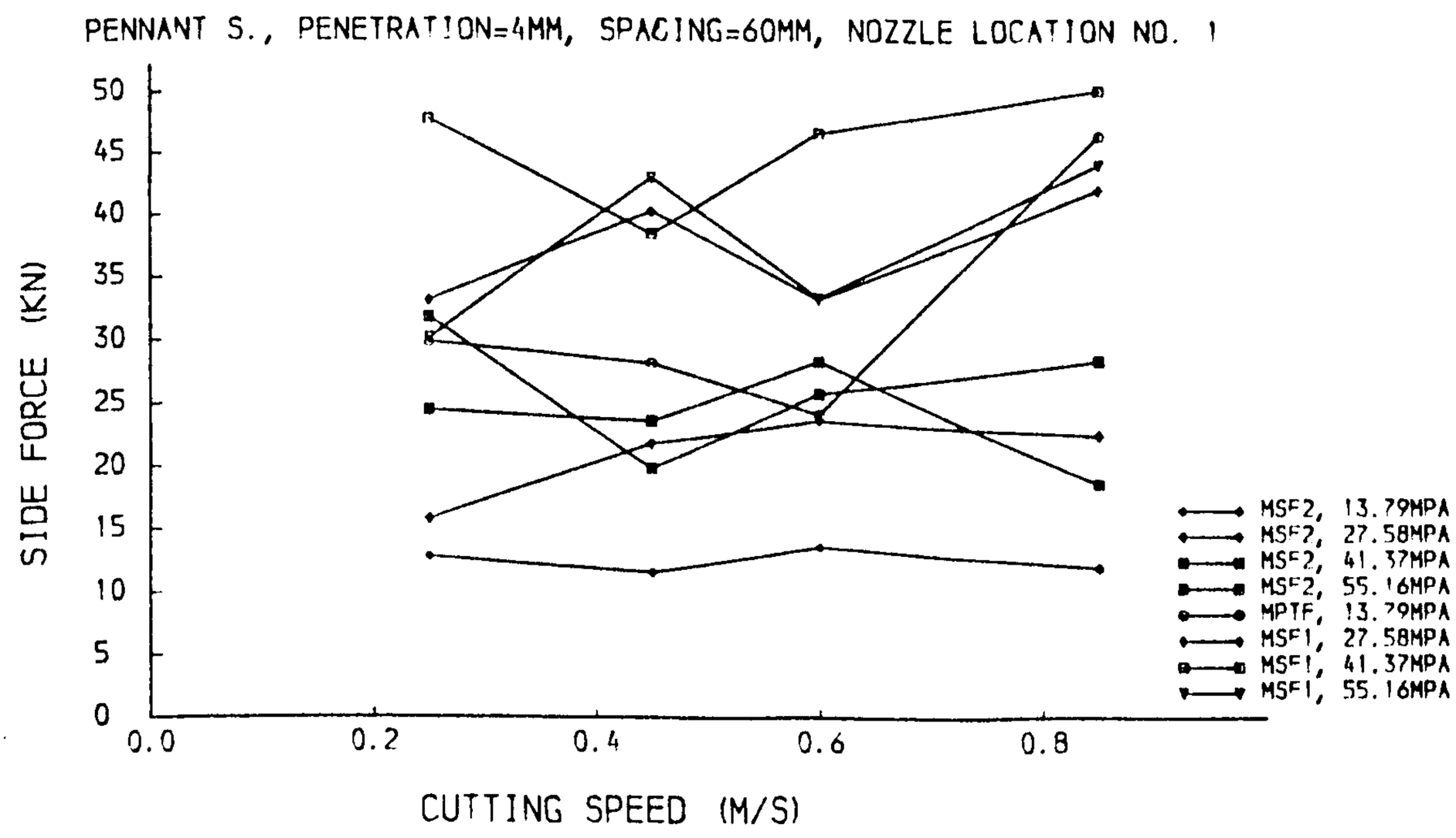

(b) $p = 4$mm, $s = 60$mm, Nozzle location No. 1

Fig. 6.3.8 Side force versus cutting speed

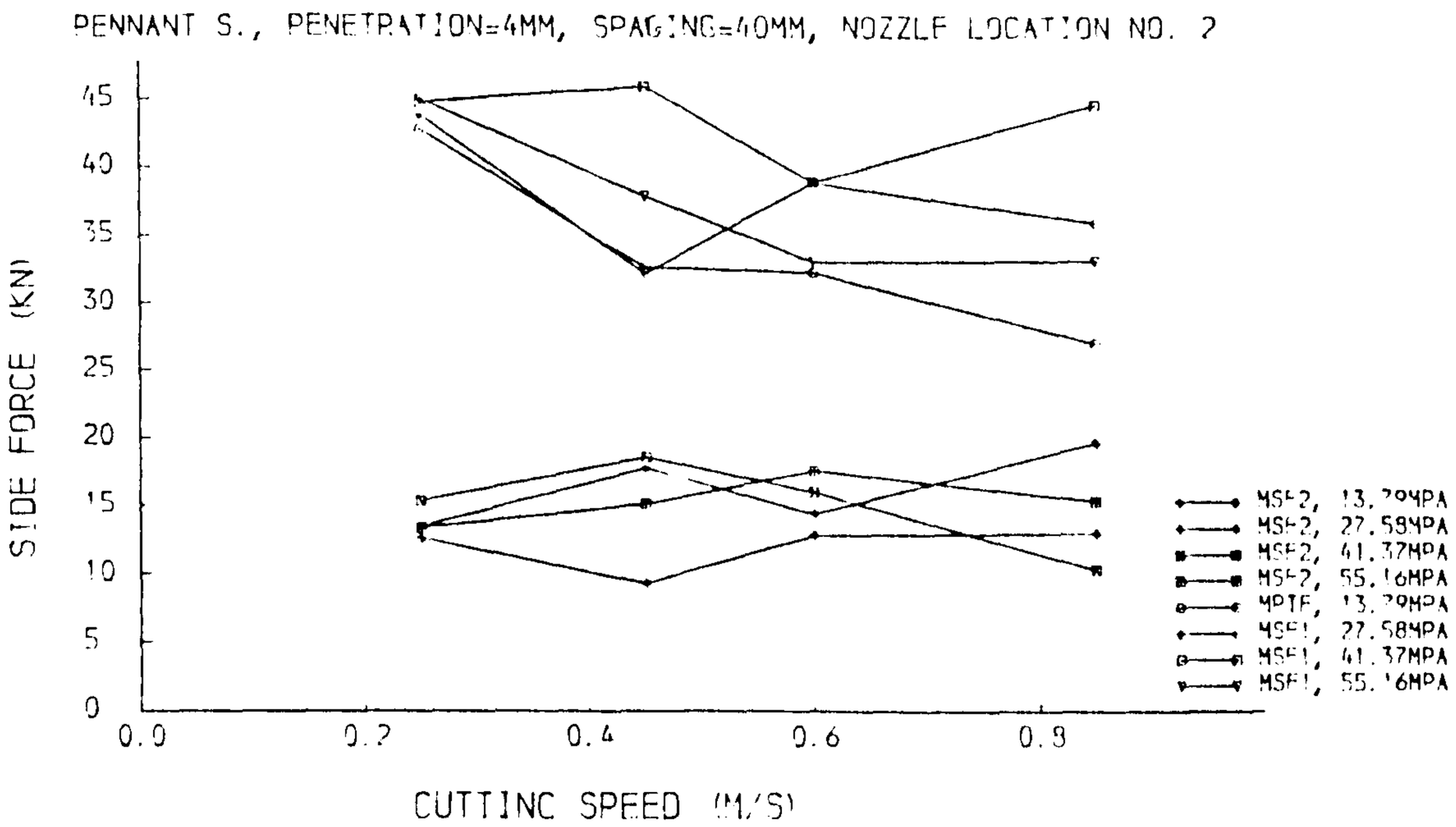

(a) $p = 4$mm, $s = 40$mm, Nozzle location No. 2

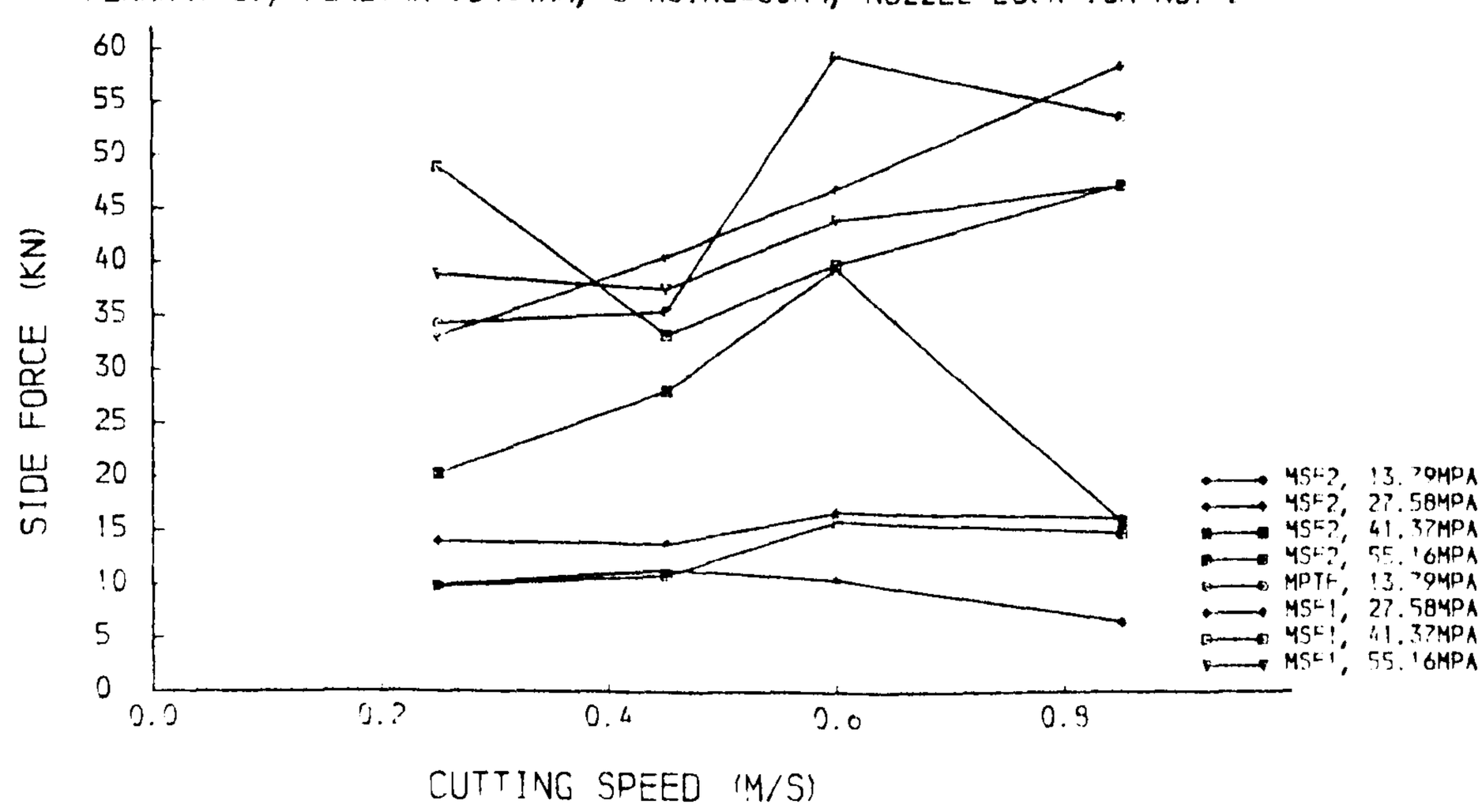

(b) $p = 4$mm, $s = 60$mm, Nozzle location No. 2

Fig. 6.3.9 Side force versus cutting speed

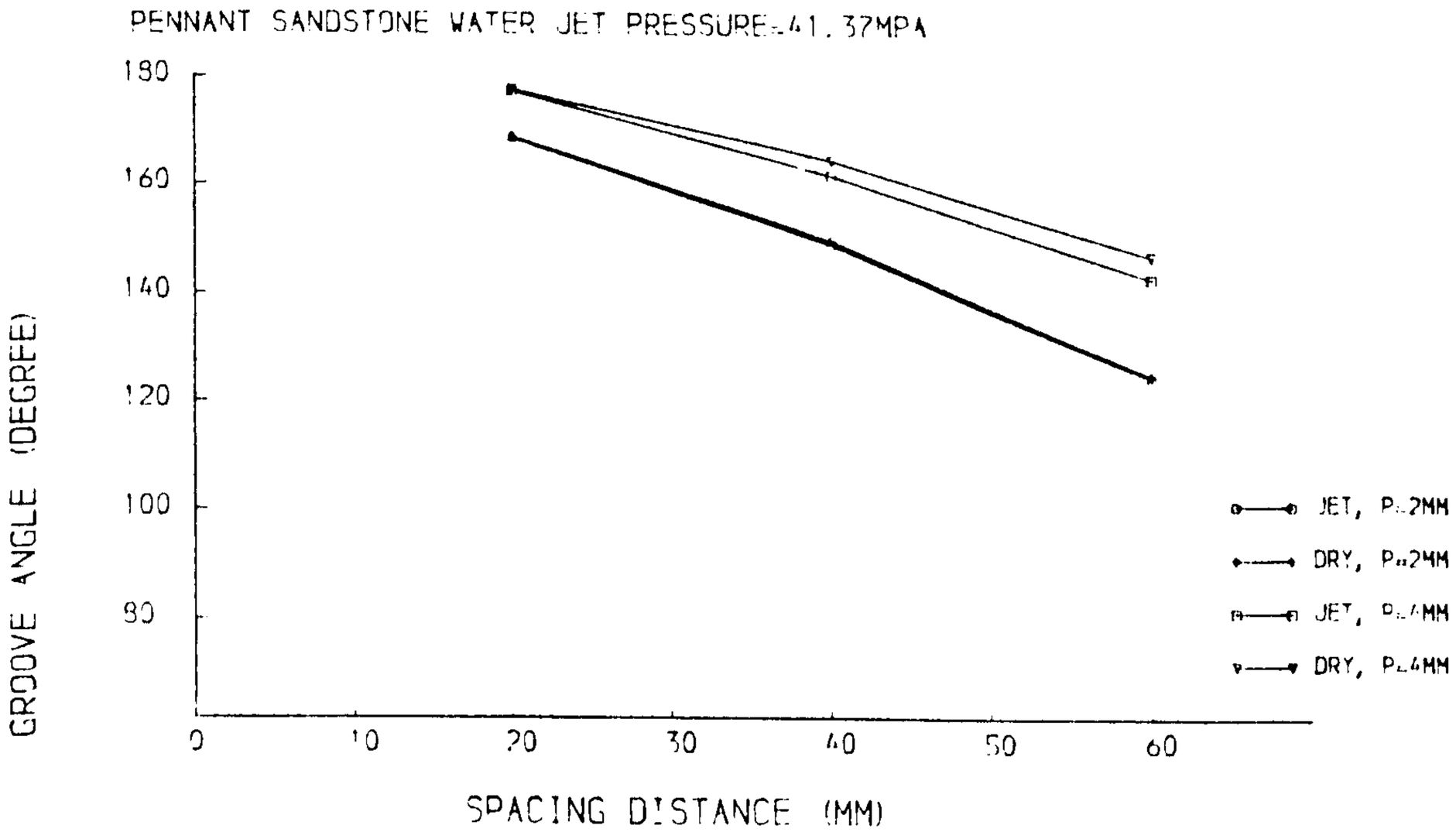

Fig. 6.3.10 Groove angle versus spacing distance

rolling force is provided by the machine torque. The side force, however, only depends on the geometry of the disc cutter. For this reason, it is considered less important than the thrust force and rolling force.

4. Specific Energy

Before calculating the specific energy, we consider the yield, ie., the mass of rock excavated by the disc per unit length of cut. As mentioned previously, measurement of the groove angle was used to establish the yield. Finally, it is found that for cutting in the same penetration and spacing, the groove angle is almost the same (Fig. 6.3.10). In other words, water jet assisted cutting at varied jet pressure and cutting speed does not affect the rock yield. This same conclusion is also reported by Fenn et al. (1985). In fact, subject to an analysis of the mechanism of rock breakage by water jet assisted disc cutting the conclusion is not surprising. The analysis is described in Section 6.5. Therefore, this conclusion is used to establish

any effect of cutting speed on specific energy.

As there is no change in rock yield during cutting with different speeds, the improvement of specific energies for water jet assisted cutting can only be related to the mean rolling force. This is because,

$$R = [1 - \frac{\text{MRF(assisted)/Yield(assisted)}}{\text{MRF(unassisted)/Yield(unassisted)}}] \times 100\% \qquad 6.3.1$$

Because Yield(assisted) = Yield(unassisted),

$$R = [1 - \frac{\text{MRF(assisted)}}{\text{MRF(unassisted)}}] \times 100\% \qquad 6.3.2$$

where

R = reduction of specific energy.

Since further analysis of the specific energy is the same as that of the mean rolling force, the study of the specific energy will not be discussed in the following sections.

6.3.4 The Effect of Water Jet Pressure

The percentage reductions of thrust force and rolling force with different water jet pressure are listed in Table 6.3.1 for Pattern 1 of the nozzle locations, and in Table 6.3.2 for Pattern 2. The Pattern 3 of the nozzle locations only used water pressure of 41.37MPa, as ribs between cutting grooves were so high that could damage the nozzle.

1. Disc Cutter Thrust Force

It is found from Table 6.3.1 and Table 6.3.2 that the effect of water jet pressure on thrust force is not very significant. It is very clear if we take the results of mean peak thrust force with a penetration of 4mm and a spacing distance of 60mm as an example. In the case of Pattern 1, the improvement of mean peak thrust force

Table 6.3.1 Percentage reduction in cutting forces

Nozzle Location Pattern 1

p mm	jet pre. MPa	s mm	MPTF %	MTF %	MPRF %	MRF %
4.	13.79	20.	-03	-01	-52	-34
		40.	25	18	00	-02
		60.	42	27	20	16
4.	27.58	20.	21	26	-02	27
		40.	23	31	04	28
		60.	41	32	35	43
4.	41.37	20.	16	09	09	06
		40.	16	03	21	10
		60.	41	13	38	06
4.	55.16	20.	15	25	02	27
		40.	20	31	12	30
		60.	43	39	33	40

assisted by a water jet at a pressure of 55.16MPa is 43%; at 41.37MPa, 41%; at 27.58MPa, 41%; and at 13.79MPa, 42%. In the case of Pattern 2, the improvement of mean peak thrust force assisted by a water jet at 55.16MPa pressure is 44%; at 41.37MPa, 40%; at 27.58MPa, 43% and at 13.79MPa, 42%. For most of the experimental conditions, the effect of water jet pressure on MPTF is not observable. For mean thrust force, again, when the penetration is 4mm and spacing distance is 60mm, stable results are given.

The effect of water jet pressure on the thrust forces is apparently absent as one may see in Figs 6.3.11 and 6.3.12.

2. Disc Cutter Rolling Force

Both mean peak rolling force and mean rolling force improved at different degree in different levels, at limiting of the penetration depth and spacing distance tested, not the pressures of the water jet (Figs 6.3.13 and 6.3.14).

Table 6.3.2 Percentage reduction in cutting forces

Nozzle Location Pattern 2

p mm	jet pre. MPa	*s* mm	MPTF %	MTF %	MPRF %	MRF %
2.	13.79	20.	16	00	-12	-08
		40.	35	28	21	28
		60.	35	25	36	33
2.	27.58	20.	16	22	18	29
		40.	25	27	23	42
		60.	19	18	19	26
2.	41.37	20.	28	01	35	-16
		40.	34	26	48	22
		60.	25	10	37	13
2.	55.16	20.	03	17	02	15
		40.	19	27	13	36
		60.	18	24	21	36
4.	13.79	20.	13	12	17	18
		40.	27	25	22	17
		60.	42	31	34	20
4.	27.58	20.	09	11	00	06
		40.	33	31	21	25
		60.	43	35	28	29
4.	41.37	20.	25	19	17	12
		40.	24	15	27	15
		60.	40	17	30	07
4.	55.16	20.	02	06	02	06
		40.	26	26	28	20
		60.	44	34	35	26

3. Disc Cutter Side Force

The same conclusions may be drawn for the disc cutter side forces from Figs 6.3.15 and 6.3.16.

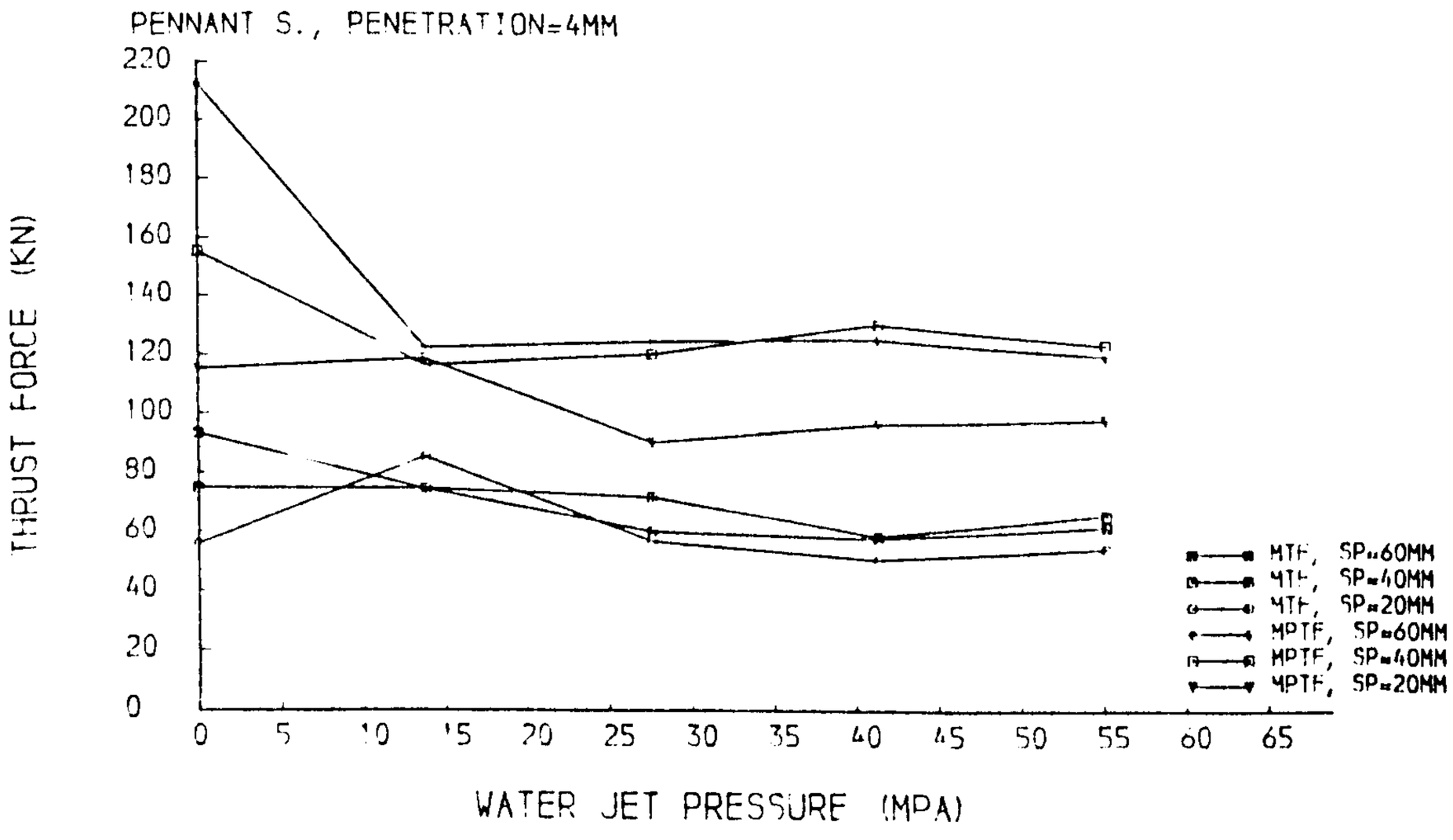

Fig. 6.3.11 Thrust force versus water jet pressure (location No.1)

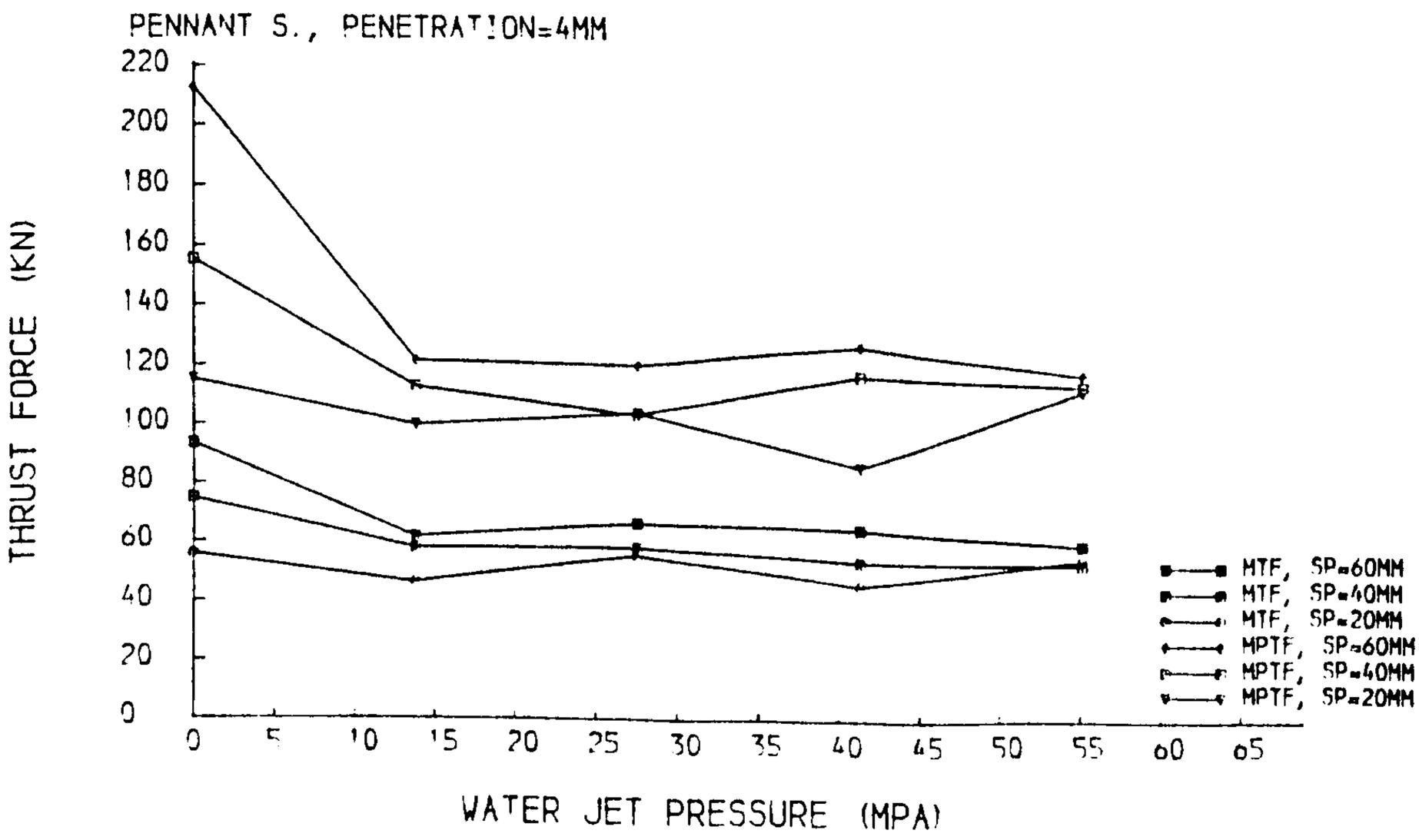

Fig. 6.3.12 Thrust force versus water jet pressure (location No.2)

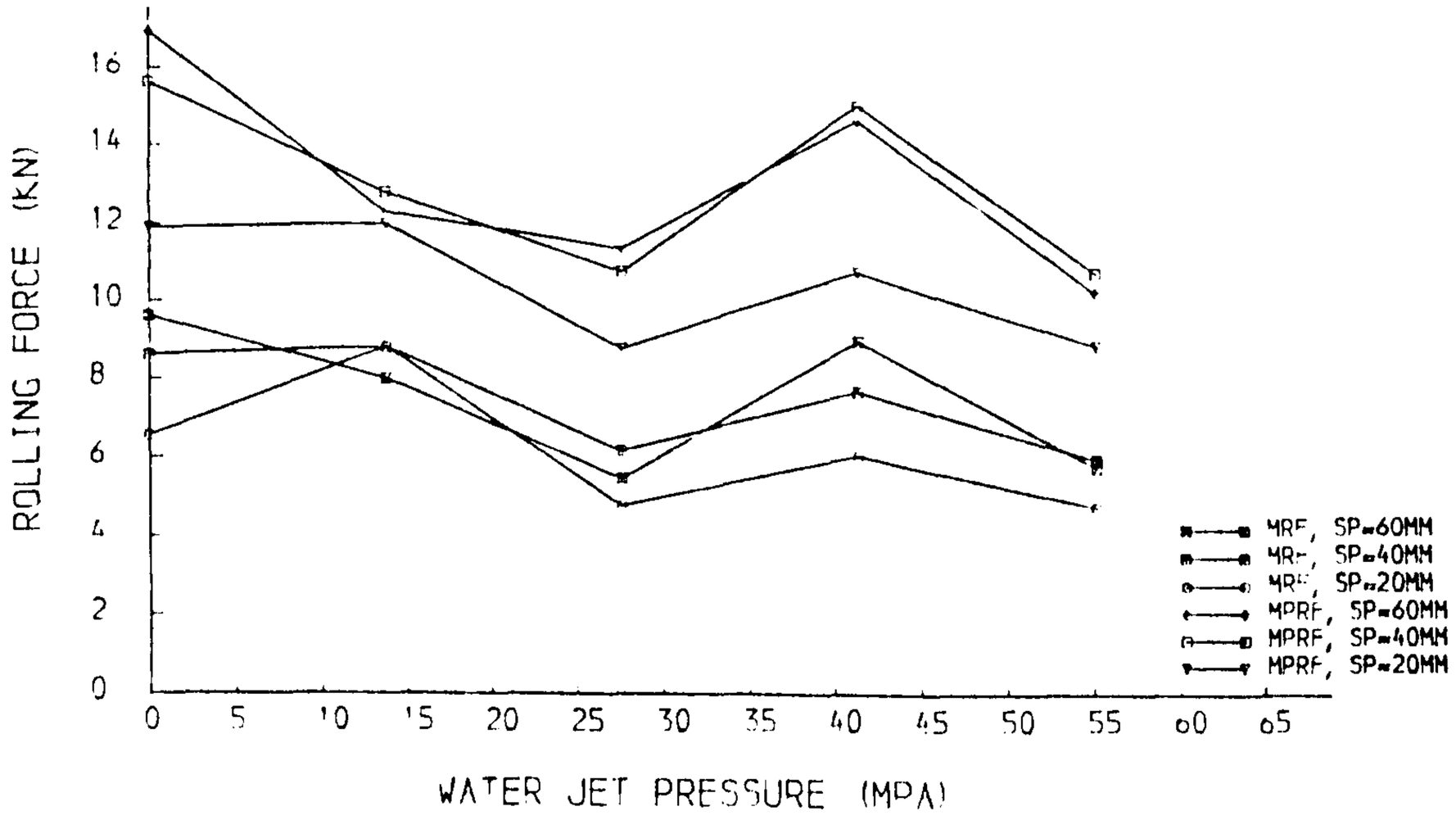

Fig. 6.3.13 Rolling force versus water jet pressure (location No.1)

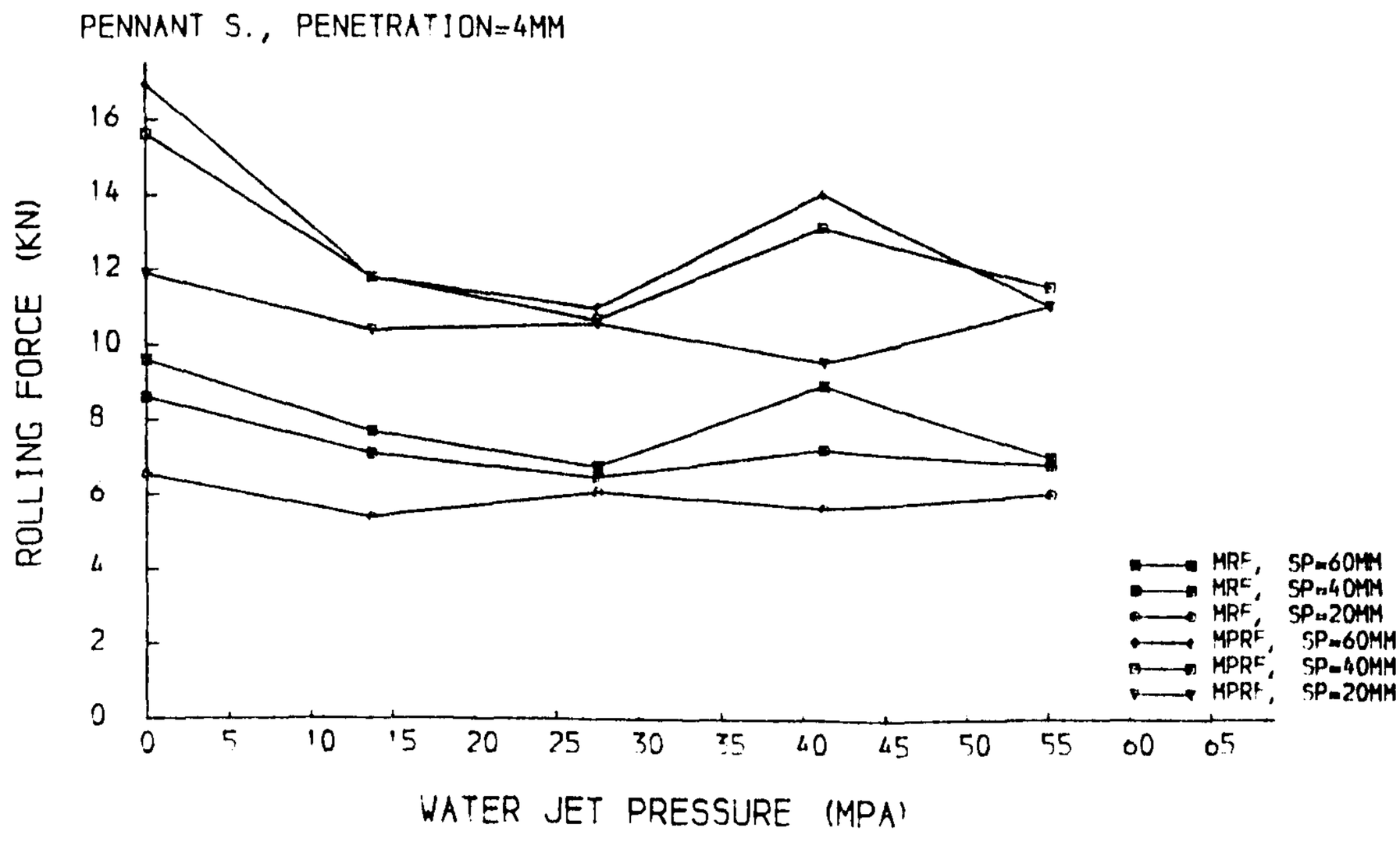

Fig. 6.3.14 Rolling force versus water jet pressure (location No.2)

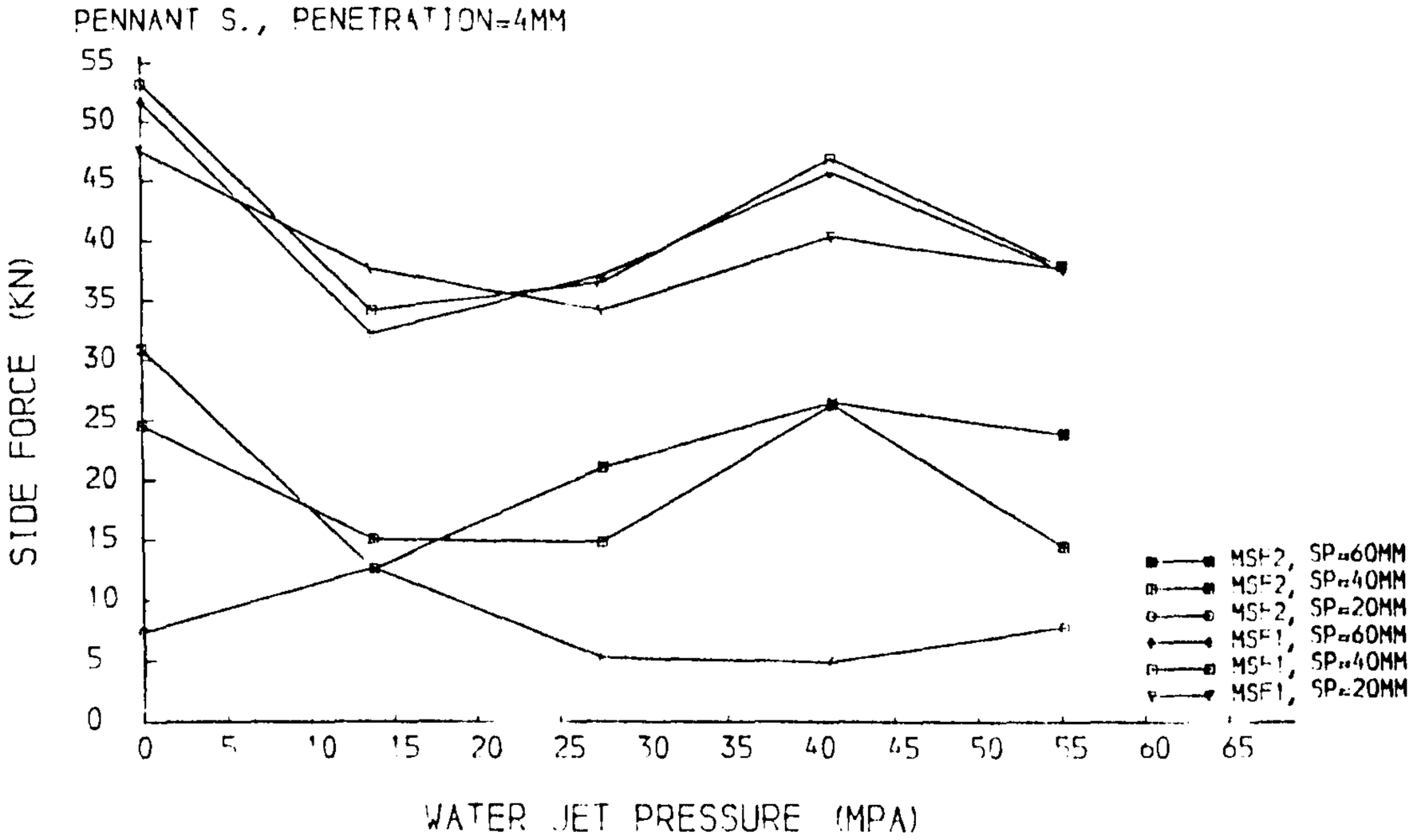

Fig. 6.3.15 Side force versus water jet pressure (location No.1)

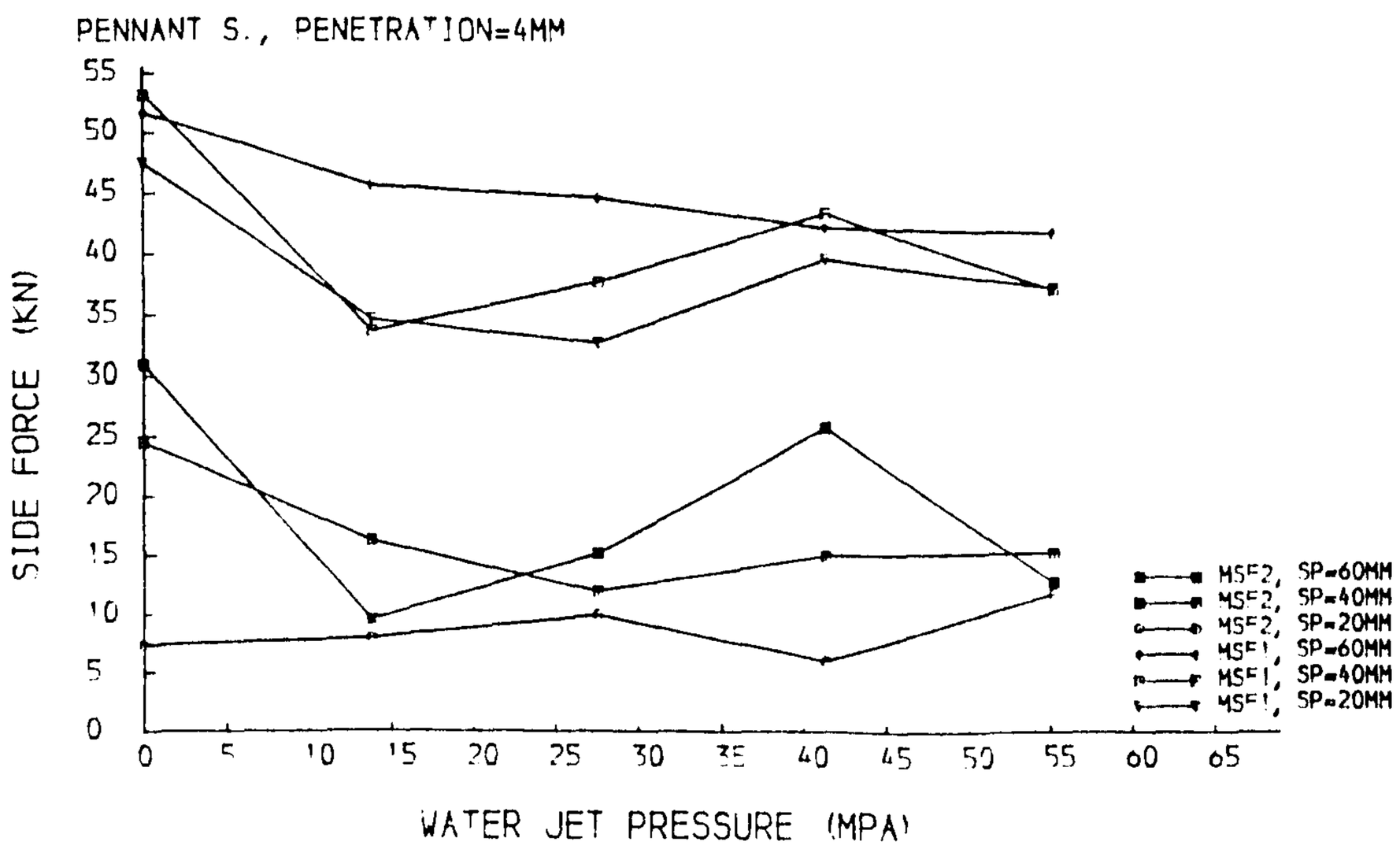

Fig. 6.3.16 Side force versus water jet pressure (location No.2)

6.3.5 The Effect of Spacing Distance and Penetration

For all nozzle position patterns, the effect of spacing is very observable. For the penetration depth of 4mm, the best results of improvements are give, generally, when the spacing is 60mm which is the biggest spacing distance in this study. For the penetration 2mm, Table 6.3.2 shows that better improvements appear in spacing distance of 40mm and 60mm. But, generally, the degree of the improvement in penetration of 2mm is less than that in penetration of 4mm. Figs 6.3.17, 6.3.18, 6.3.19, 6.3.20, 6.3.21 and 6.3.22 give an example of cutting test with 4mm penetration, all water jet pressure conditions for water jet locations in Pattern 1 and Pattern 2.

6.3.6 The Effect of Nozzle Location

Figs 6.3.23, 6.3.24, and 6.3.25 summarize the results of the tests aimed at investigating the effect of nozzle locations on cutting forces. With a water jet pressure of 41.37MPa, they show that the best results are given by putting the water jet nozzle by the side of the cutter, e.g. Pattern 3. This is in good agreement with the conclusion given by Fenn et al. (1985) who used four nozzles beside the cutter during cutting tests. Unfortunately, as previously mentioned, when the cutting tests were conducted at a spacing of 60mm, the ribs between grooves were so high that the nozzle was damaged. For this reason, the further tests with water jet nozzle in Pattern 3 were abandoned.

The results given for Pattern 1 and Pattern 2, although not as good as Pattern 3, are still very encouraging. With a water jet pressure of only 13.79MPa, The mean peak thrust force is reduced by more than 40%. Also, the nozzle was in a safer position in this case.

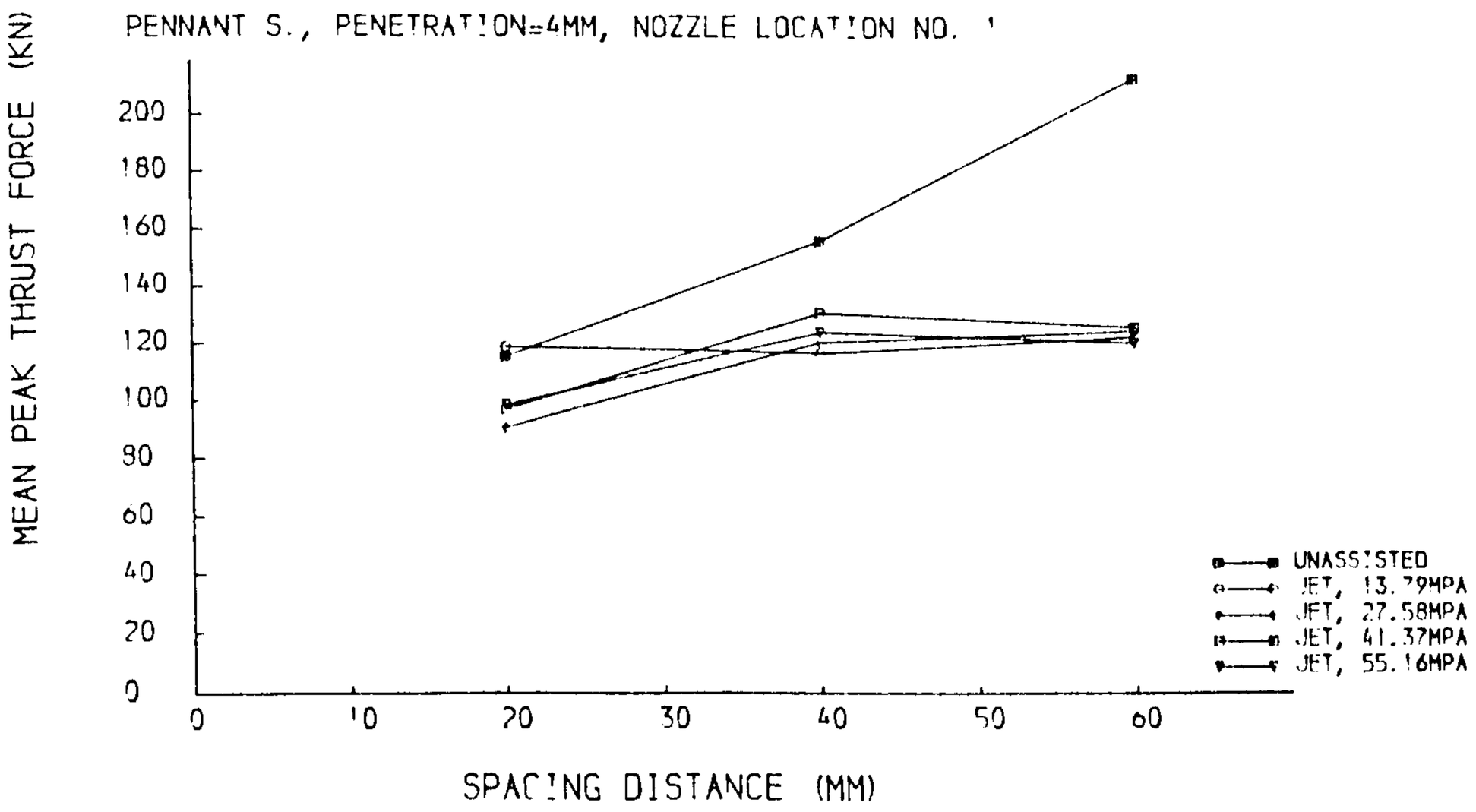

(a). Mean peak thrust force

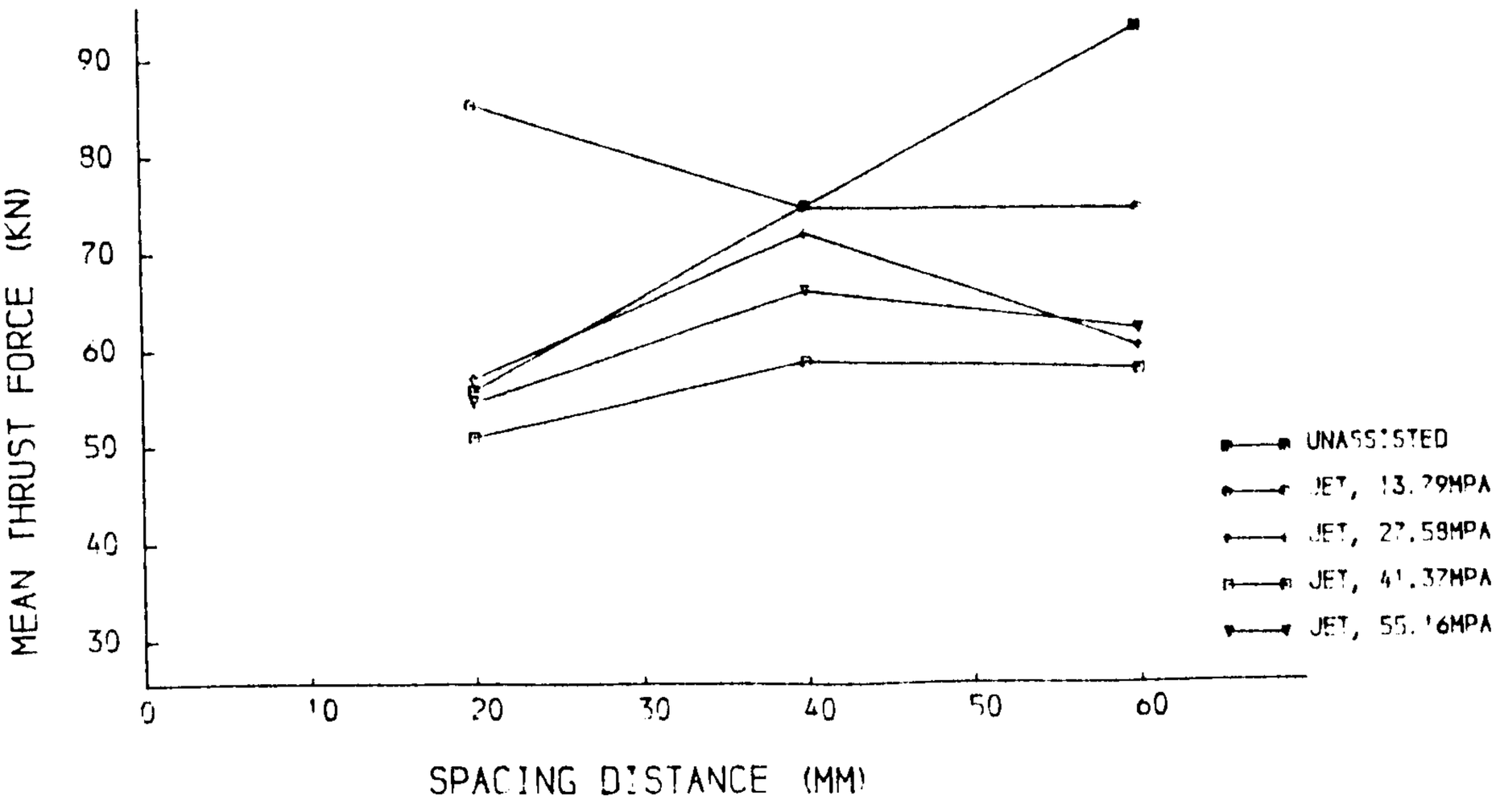

(b). Mean thrust force

Fig. 6.3.17 Thrust force versus spacing distance (location No.1)

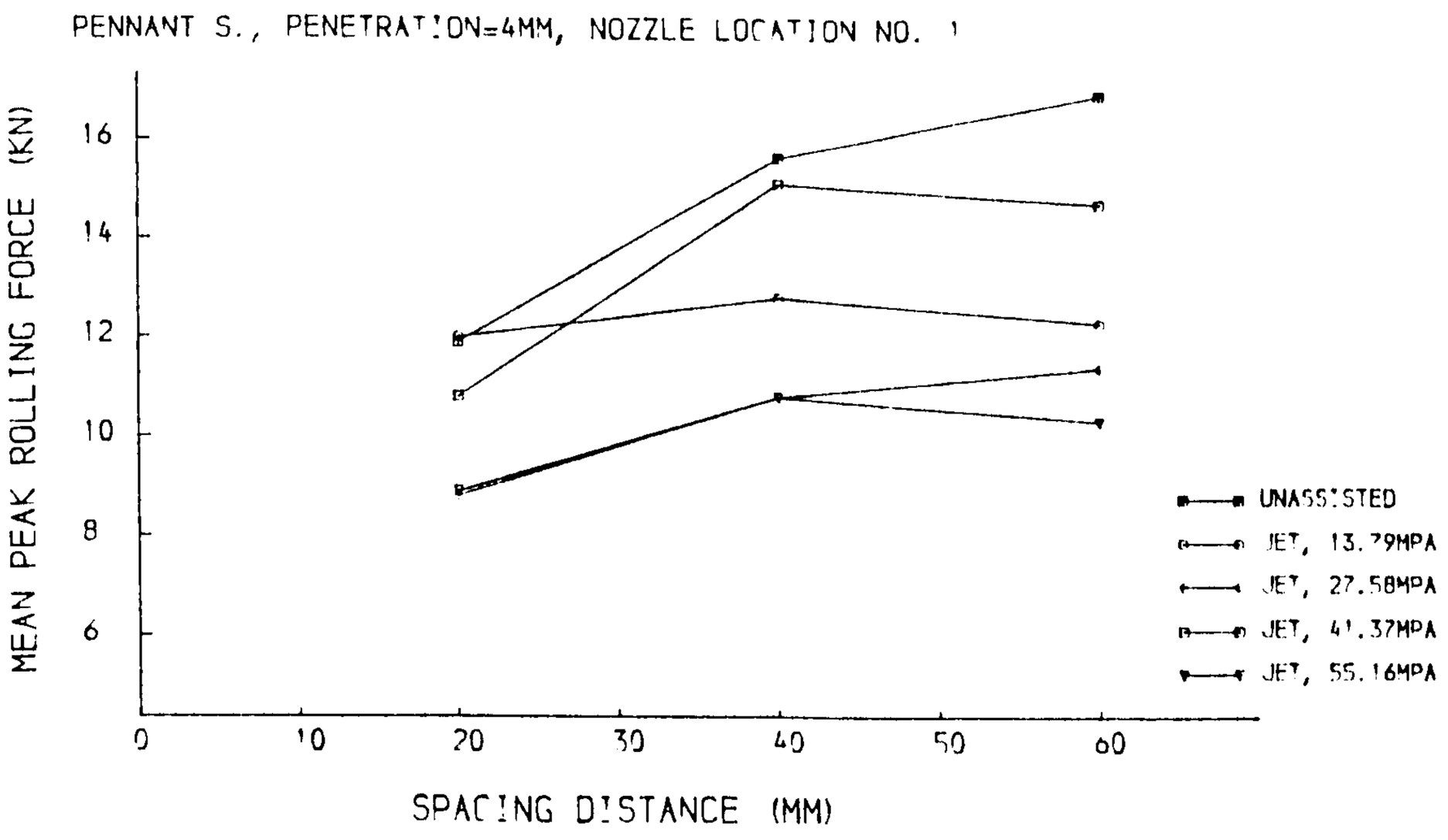

(a). Mean peak rolling force

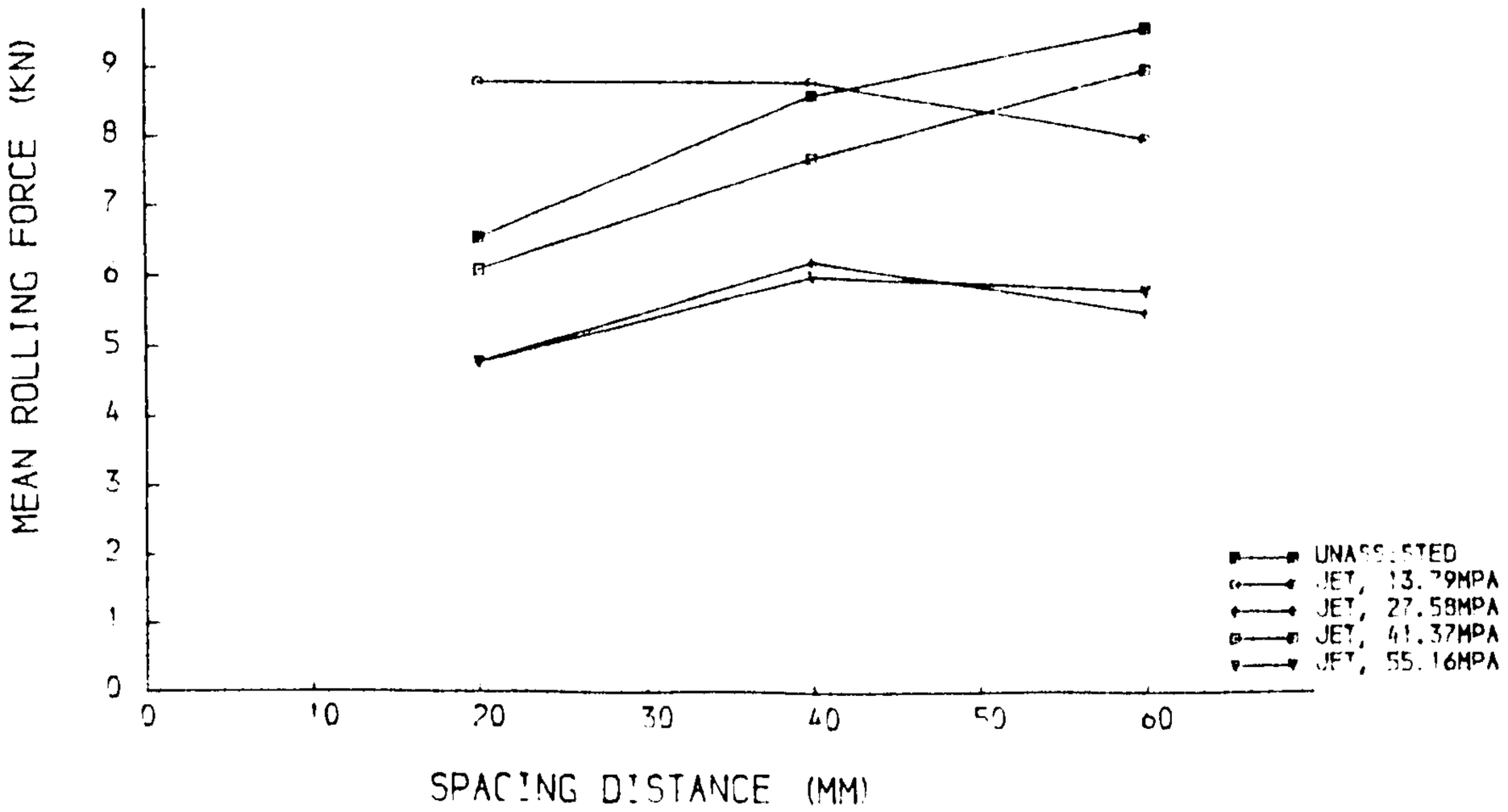

(b). Mean rolling force

Fig. 6.3.18 Rolling force versus spacing distance (location No.1)

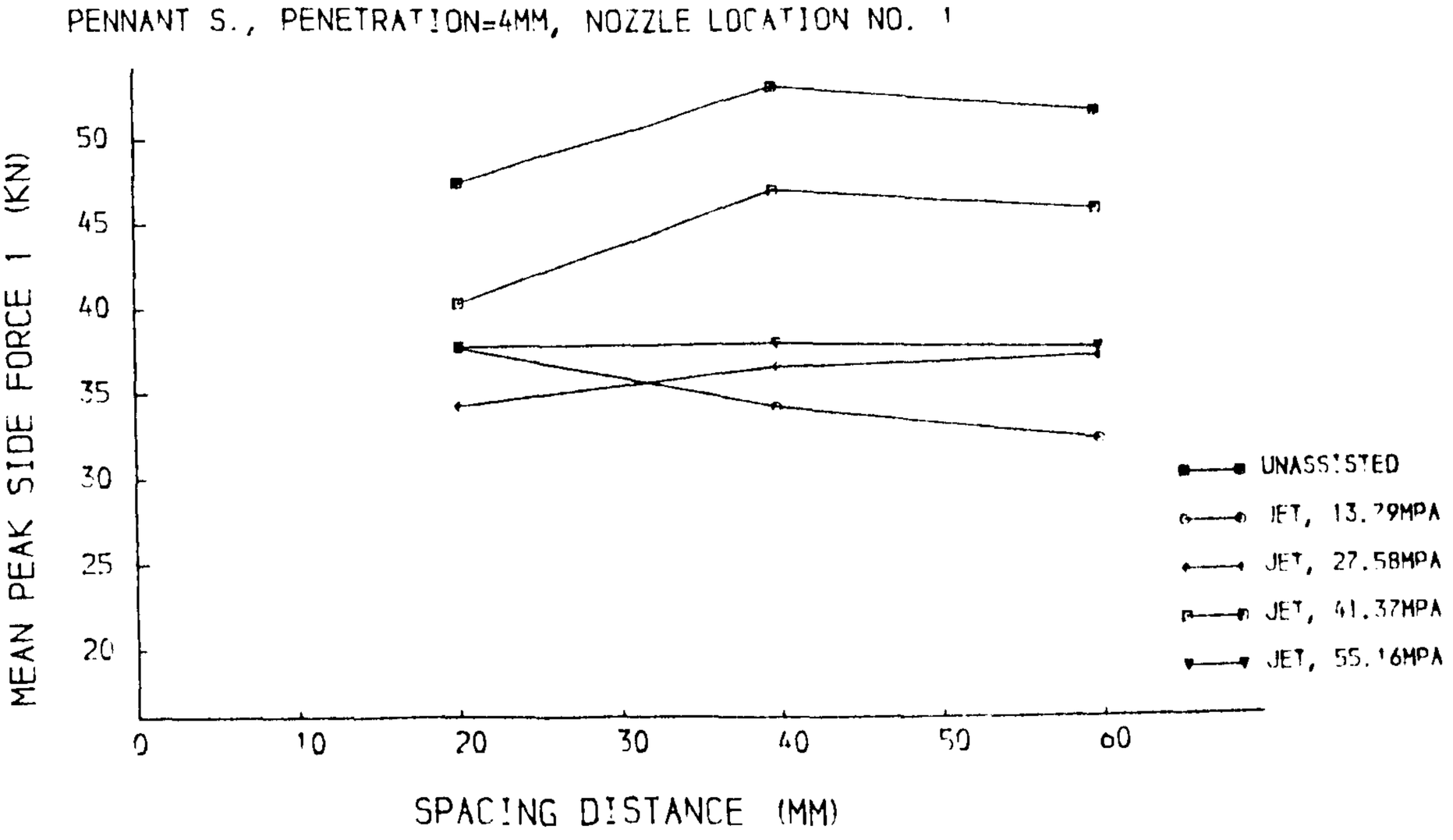

(a). Mean peak side force 1

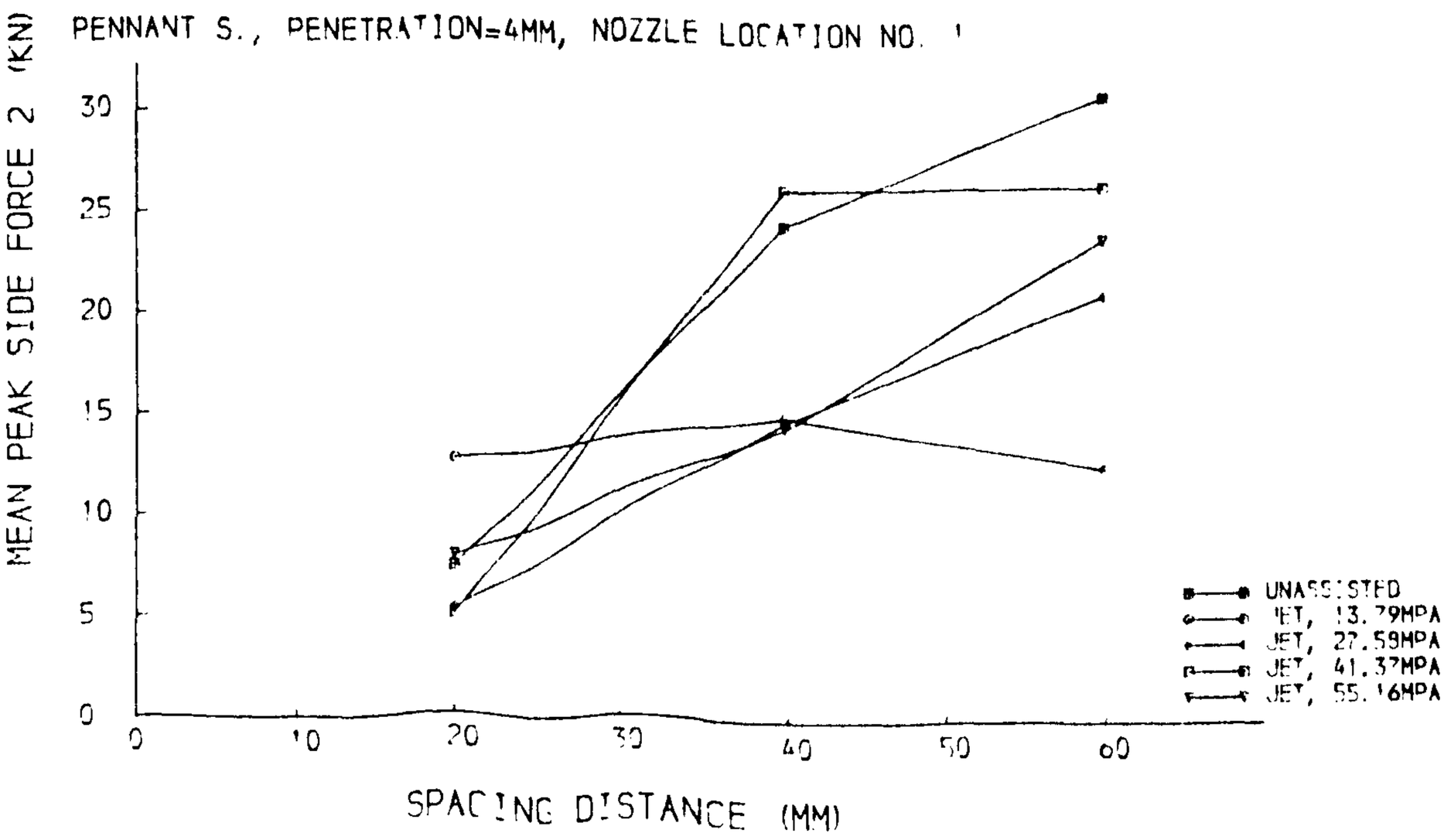

(a). Mean peak side force 2

Fig. 6.3.19 Side force versus spacing distance (location No.1)

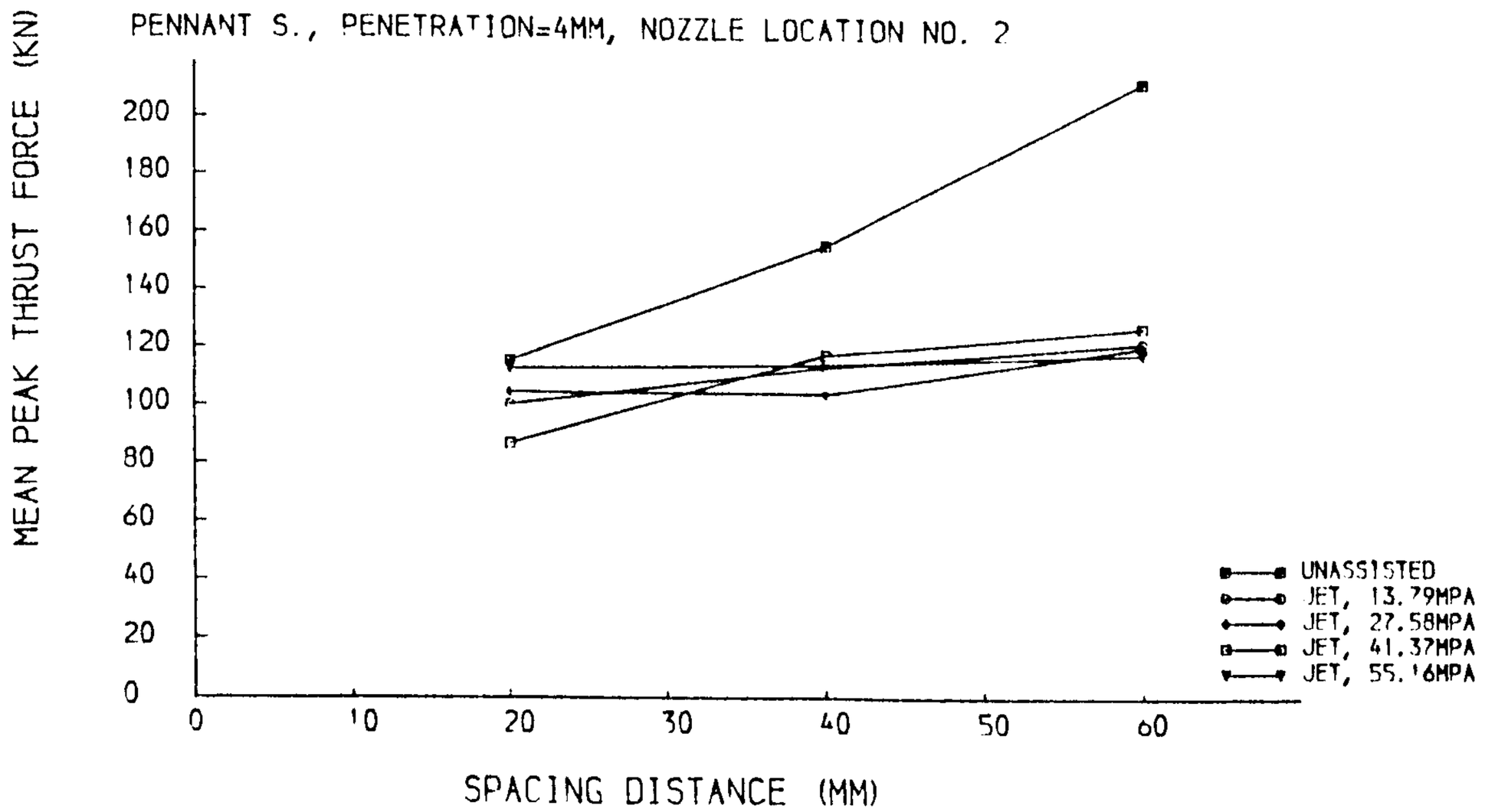

(a). Mean peak thrust force

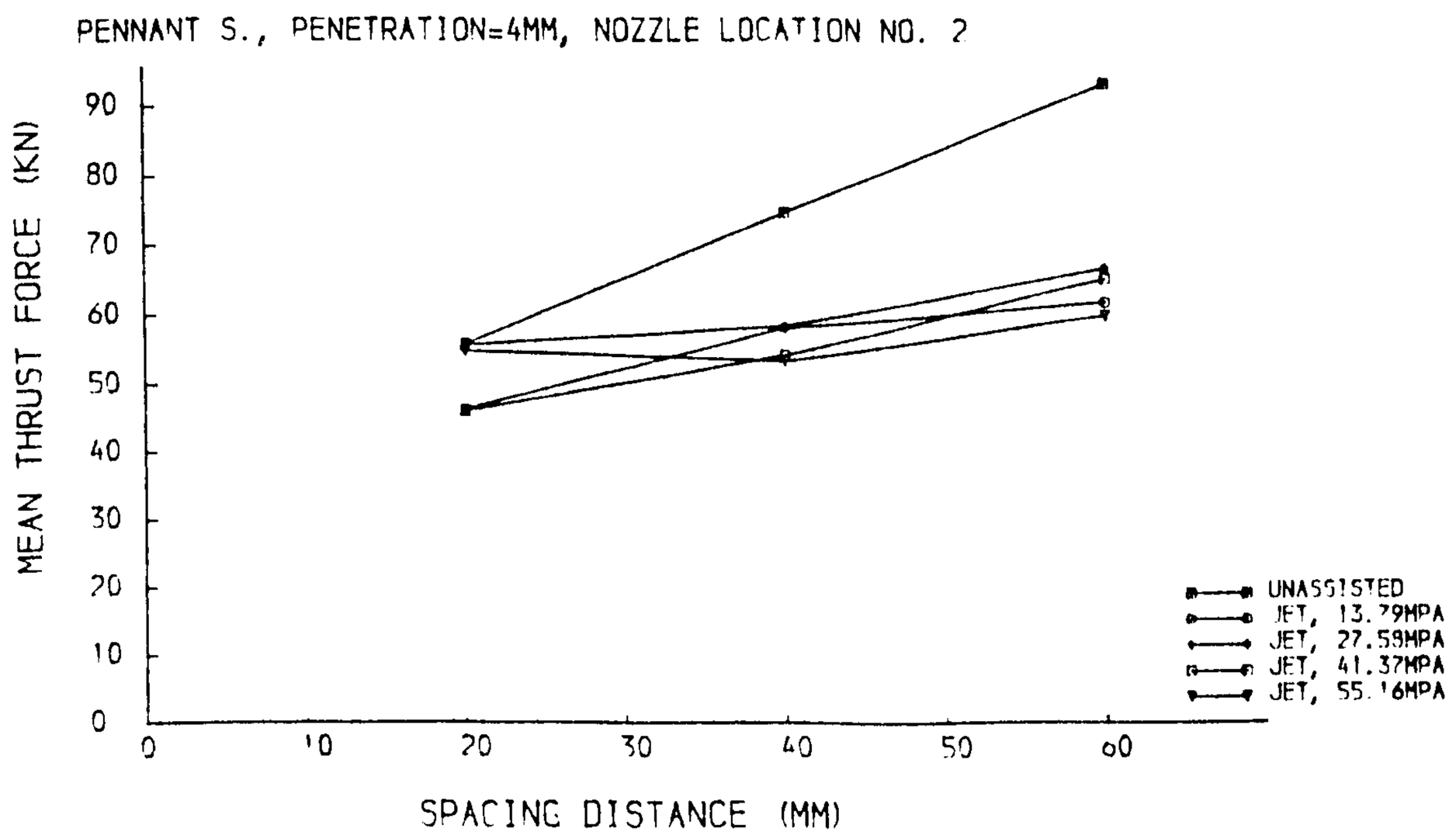

(b). Mean thrust force

Fig. 6.3.20 Thrust force versus spacing distance (location No.2)

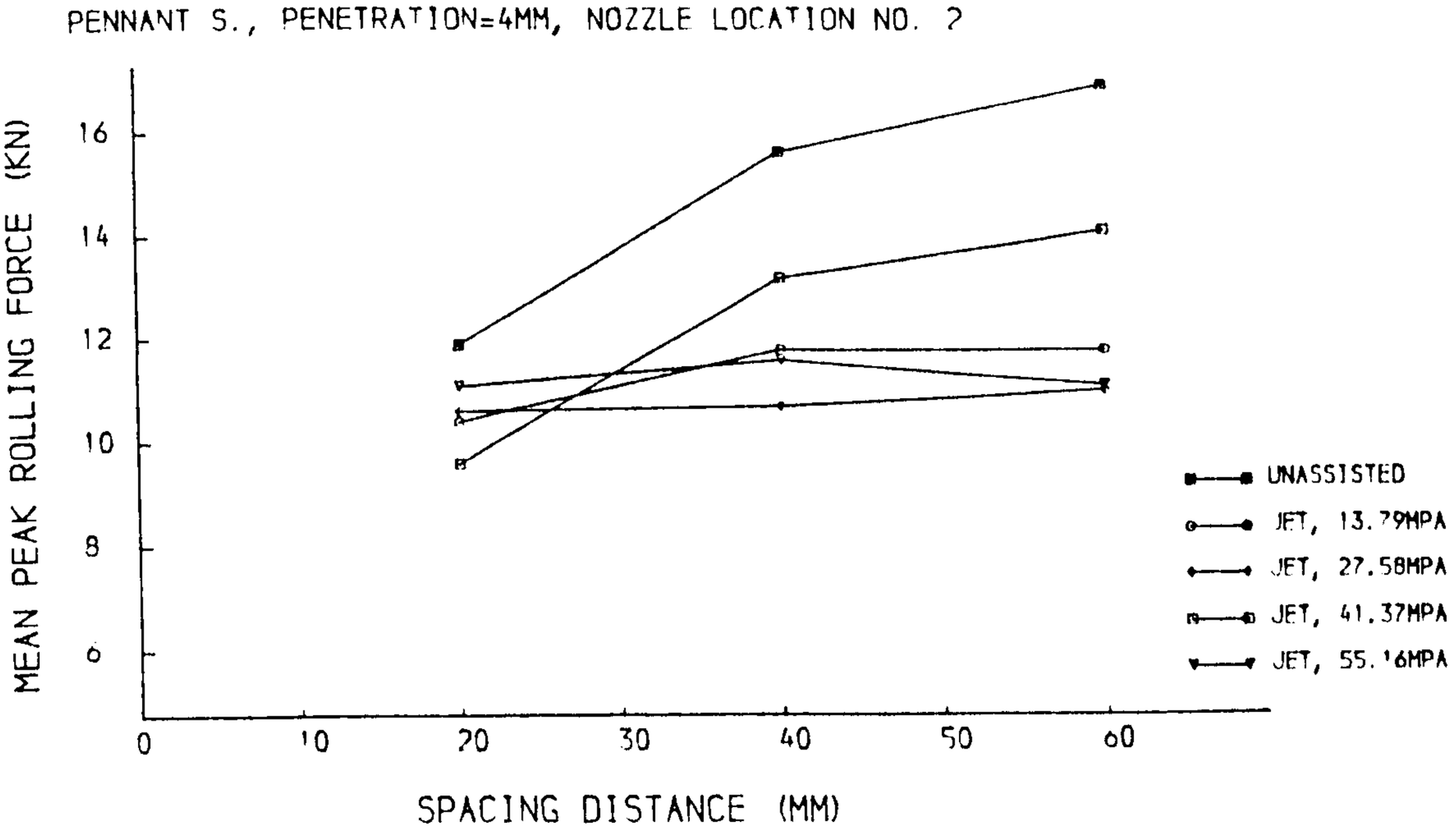

(a). Mean peak rolling force

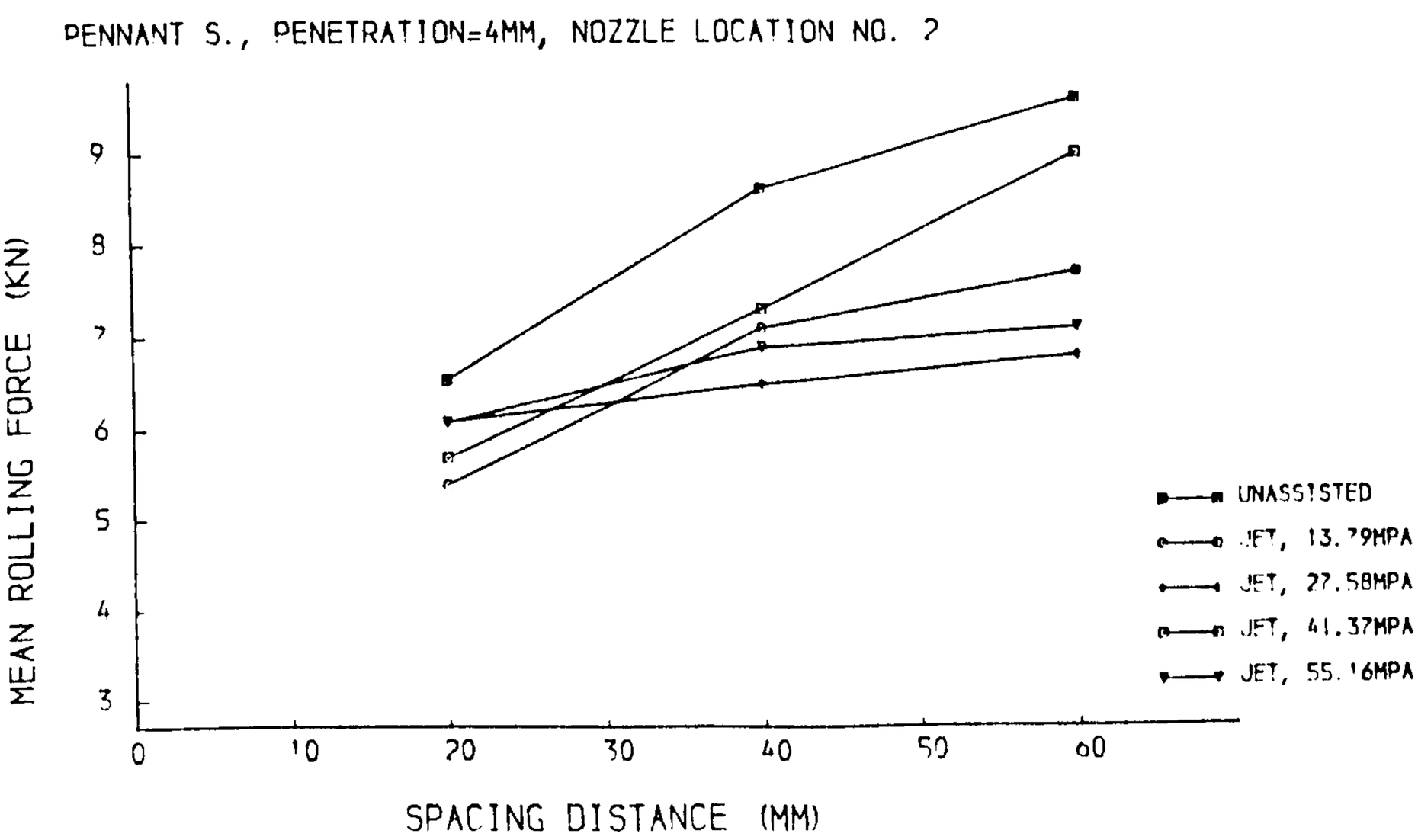

(b). Mean rolling force

Fig. 6.3.21 Rolling force versus spacing distance (location No.2)

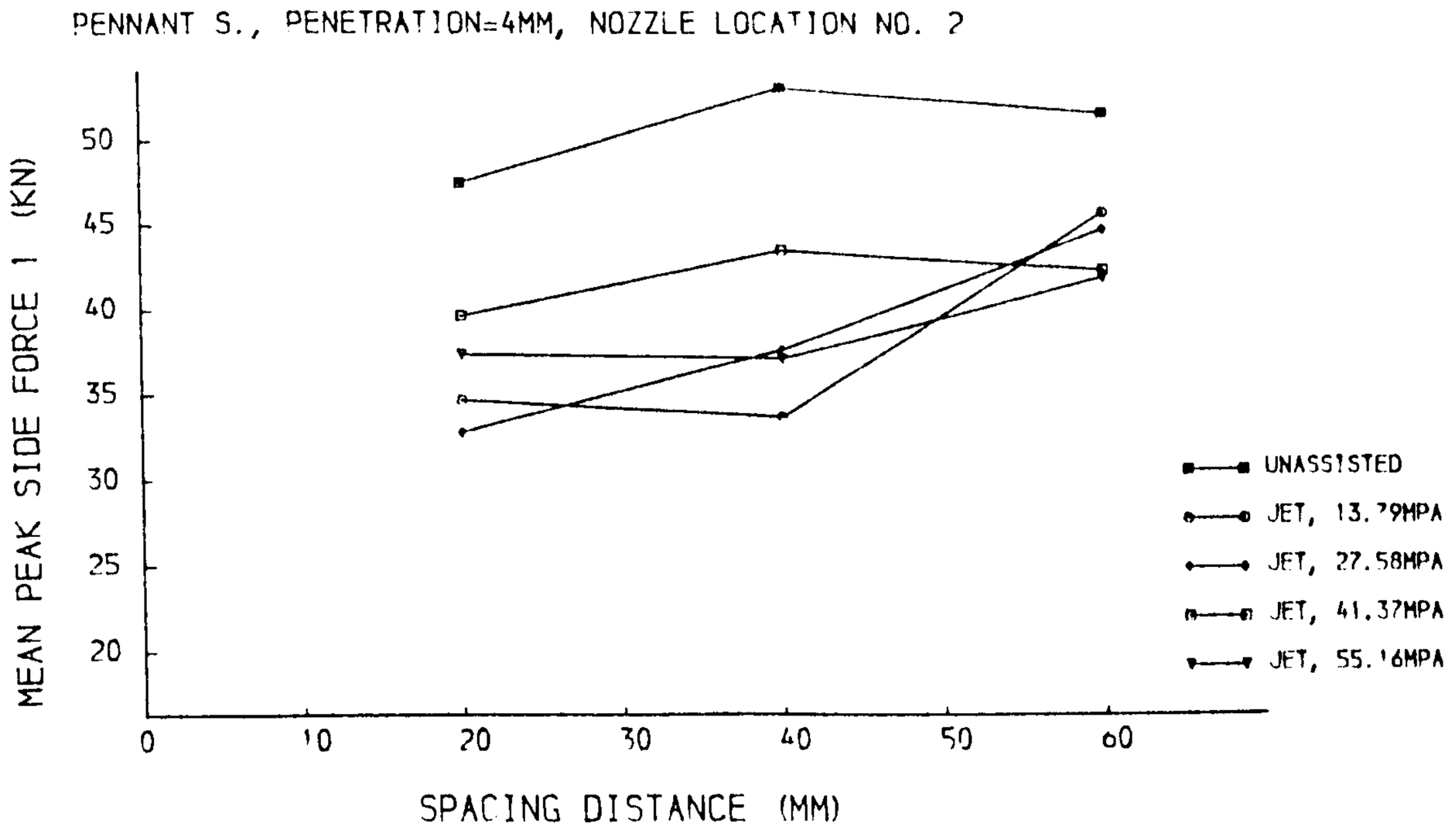

(a). Mean peak side force 1

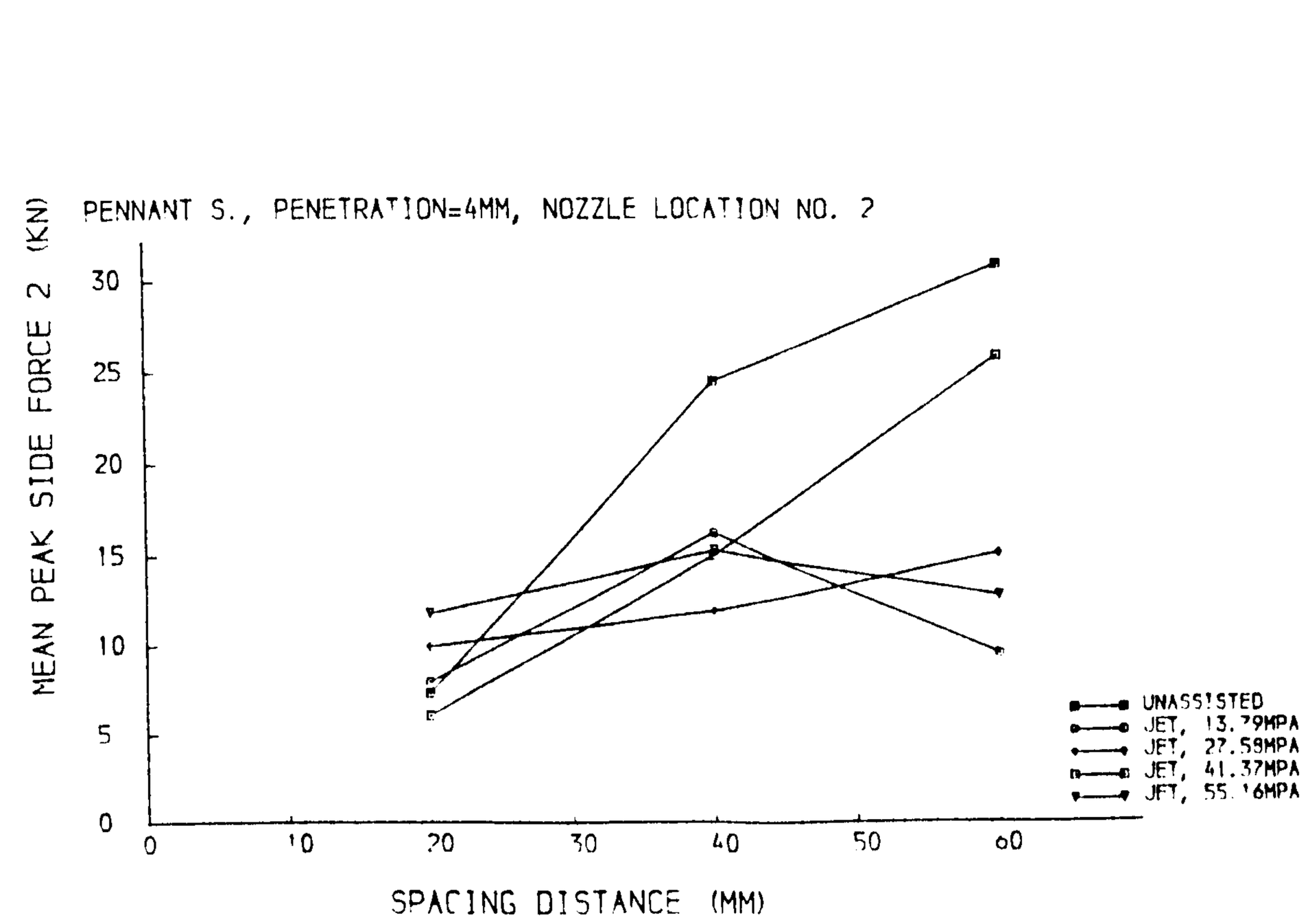

(a). Mean peak side force 2

Fig. 6.3.22 Side force versus spacing distance (location No.2)

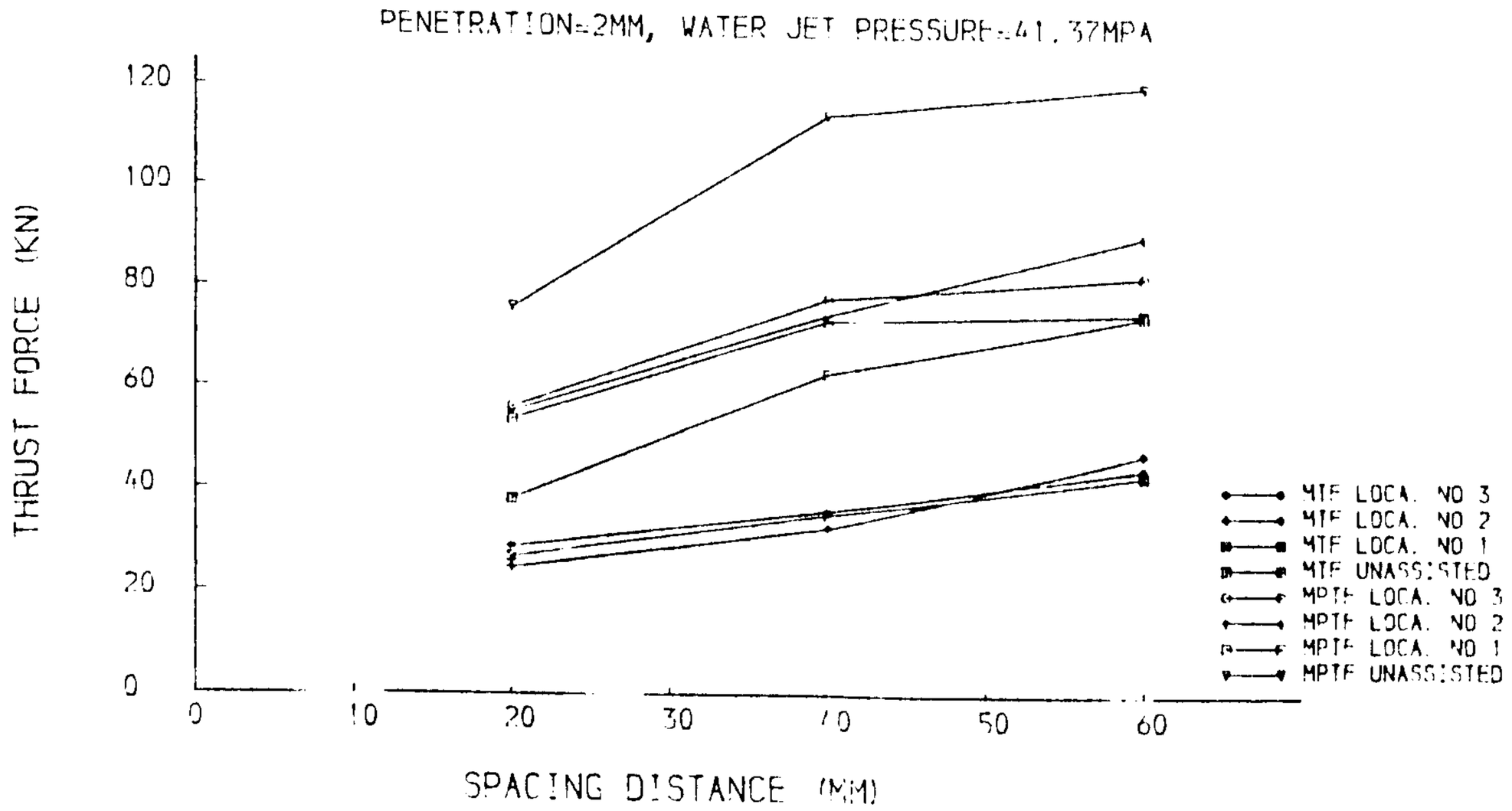

(a). p=2mm

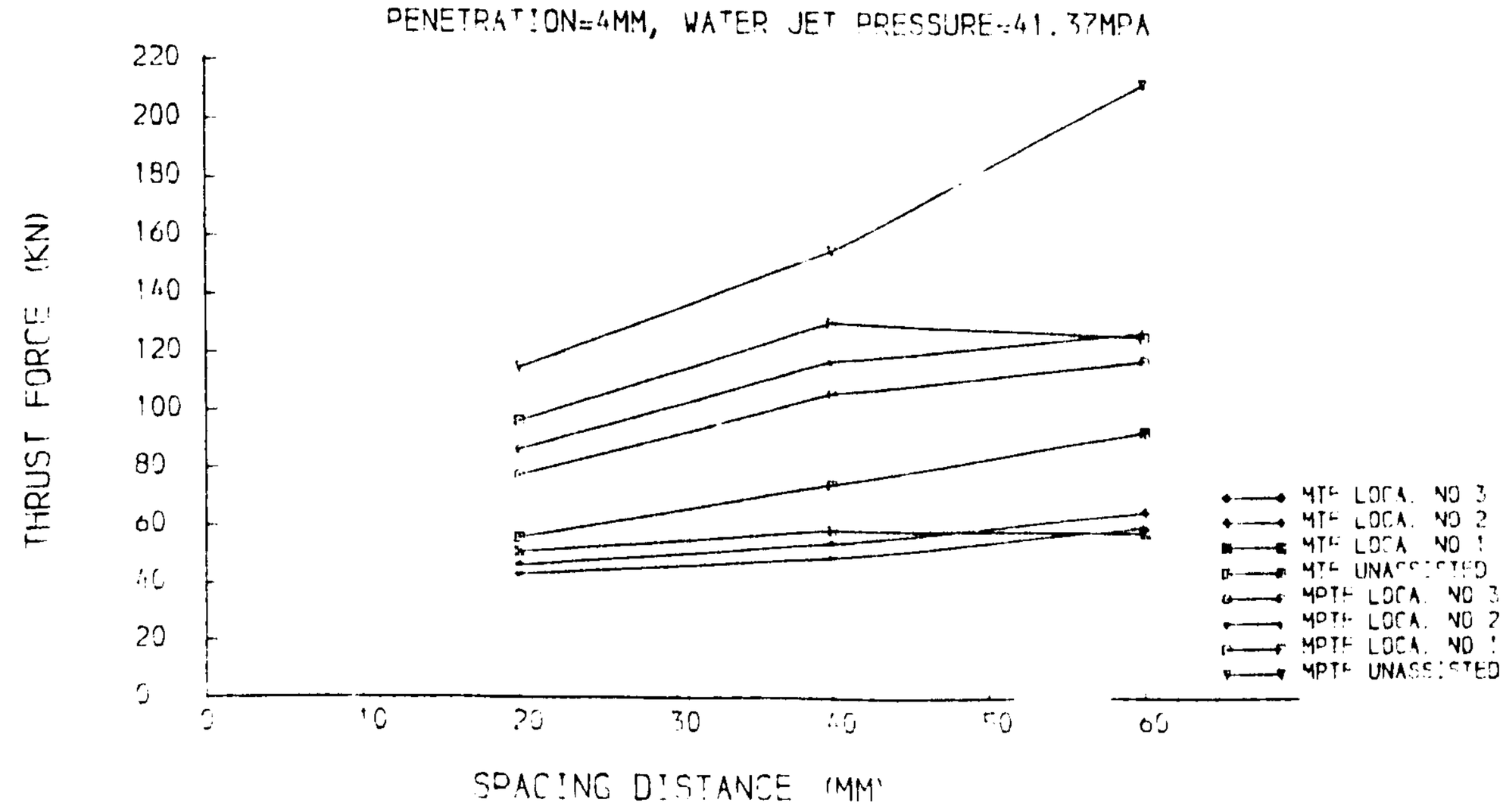

(b). p=4mm

Fig. 6.3.23 Thrust force versus spacing distance

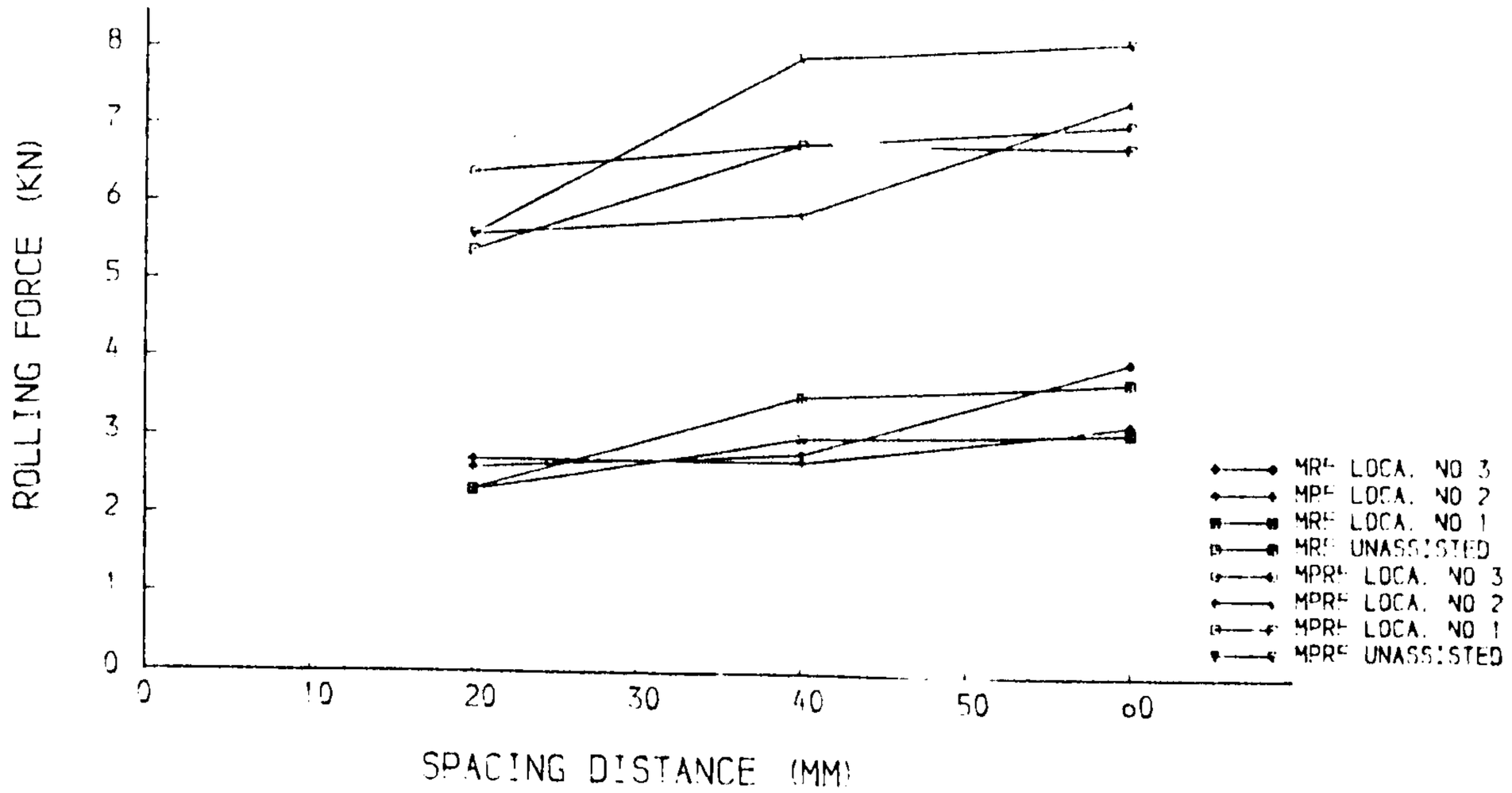

(a). p=2mm

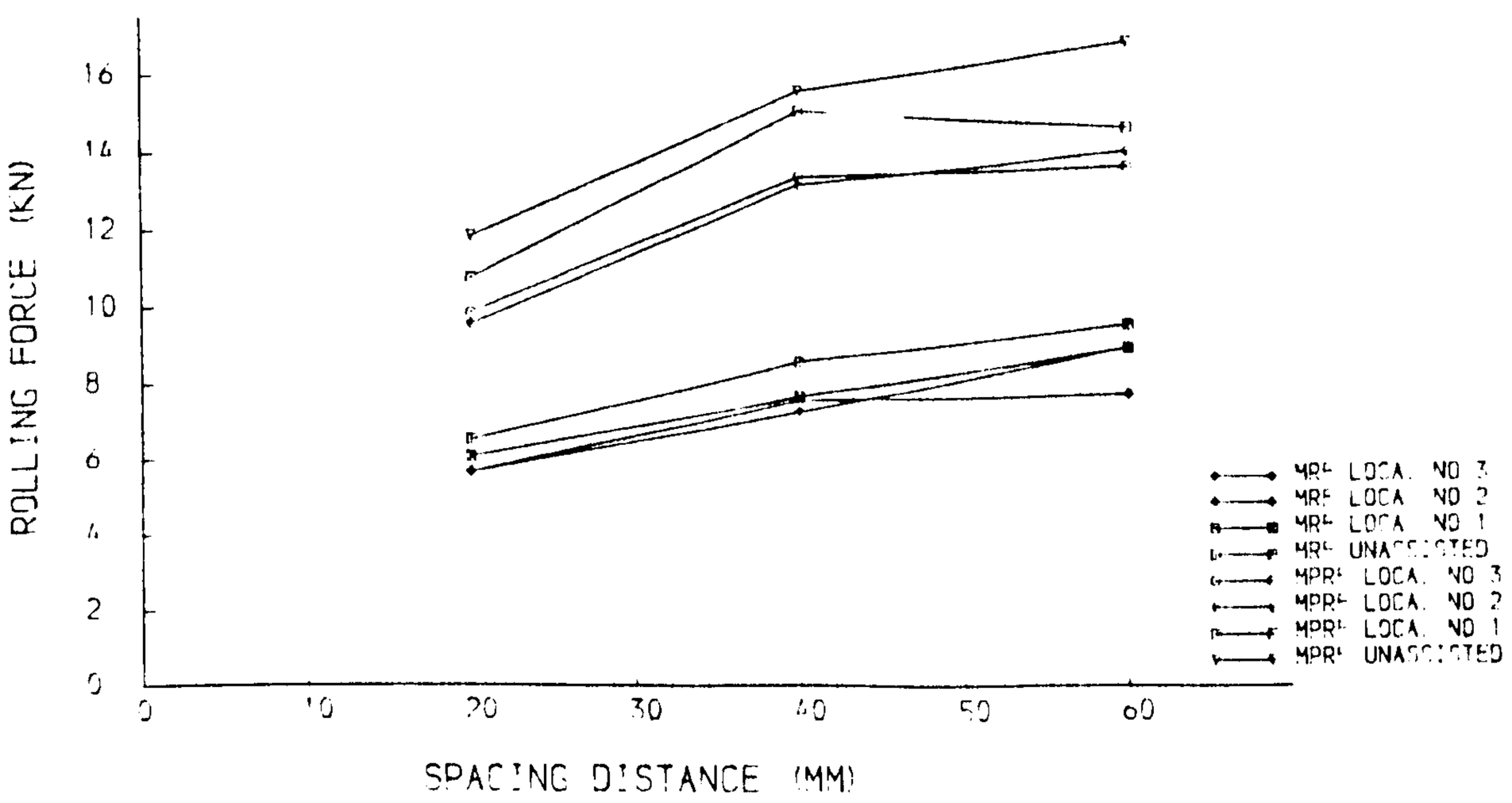

(b). p=4mm

Fig. 6.3.24 Rolling force versus spacing distance

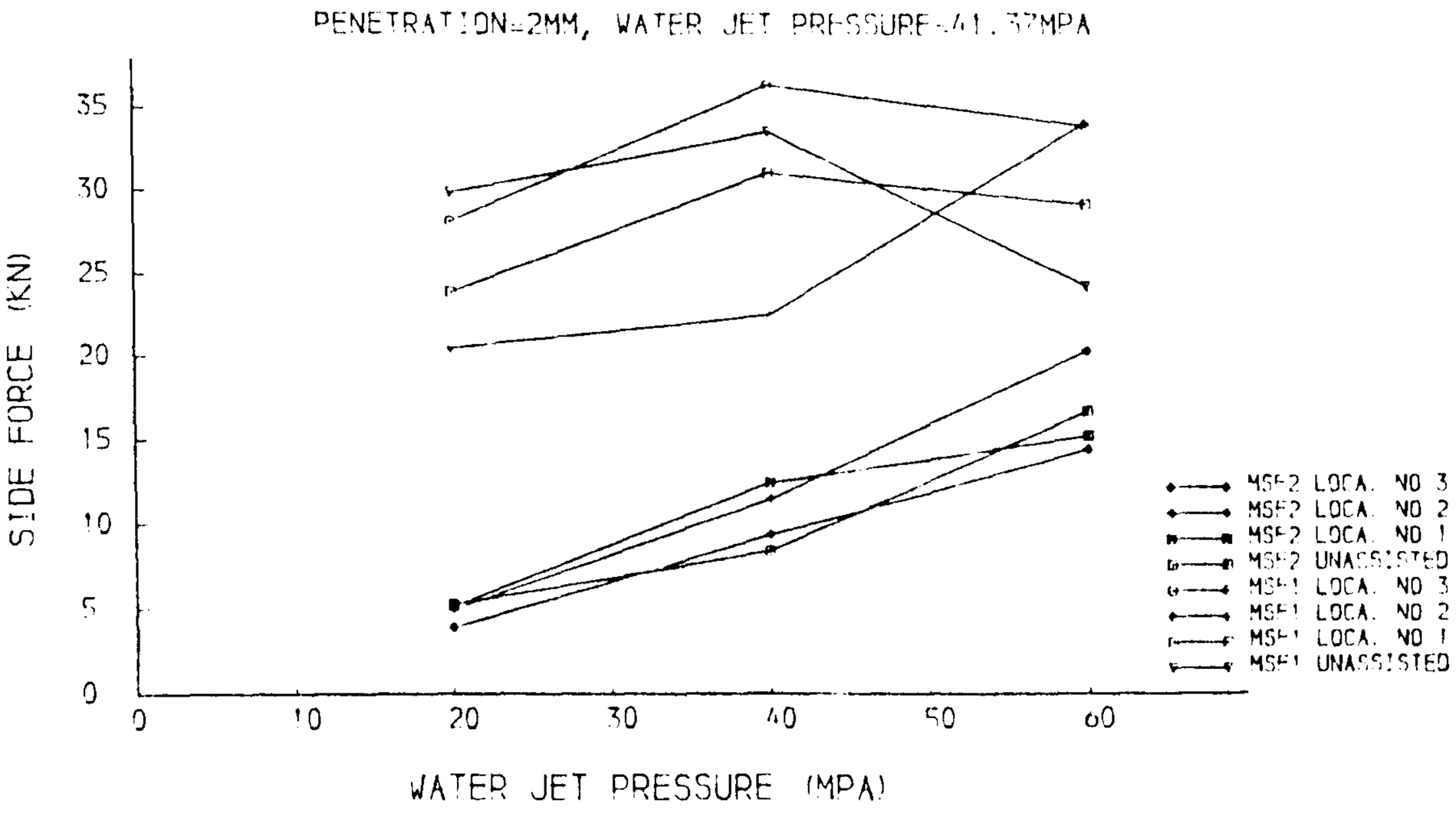

(a). p=2mm

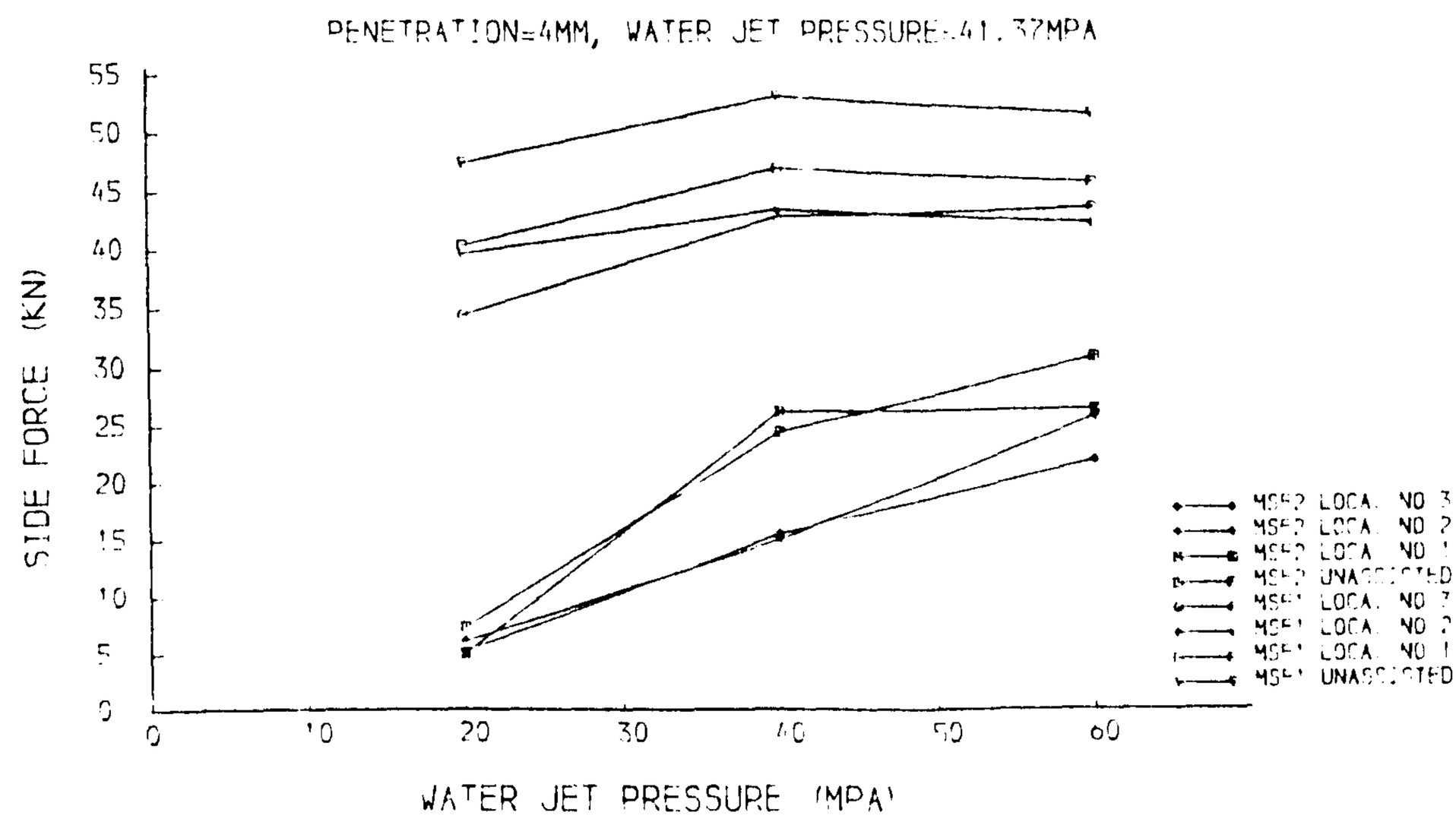

(b). p=4mm

Fig. 6.3.25 Side force versus spacing distance

6.3.7 Summary

It is readily seen that the water jet reduced the cutting force requirements on the cutter compared to unassisted cutting. The results from cutting speeds in the range of 0.25 - 0.85 m/s and water jet pressures in the range of 13.79 - 55.16 MPa have shown that the most important factors affecting the performance of water jet assisted disc cutting are penetration and spacing distance. The maximum benefit from water jet assisted disc cutting on Pennant Sandstone was obtained when the tests were undertaken at the deepest penetration and greatest spacing distance, e.g., at a penetration of 4 mm and spacing distance of 60 mm as in this study. At best the percentage reduction was 52% for the mean peak thrust force, 50% for the mean thrust force, 42% for the mean peak rolling force, and 49% for the mean rolling force.

6.4 WHINSTONE

6.4.1 Experimental Plan

Rock: Whinstone

Test Method: Multiple pass on previous cutting surface

Tools: Disc cutter

Diameter (mm): 300

Edge Angle (degree): 60

Tip Radius (mm): 2.5

Penetration Depths (mm): 2, 4

Spacing Distance (mm): 20, 40, 60

Travel Speed (m/s): 0.25, 0.45, 0.6, 0.85

Jet Pressure (MPa): 13.79 (2,000psi), 27.58 (4,000psi),

41.37 (6,000psi), 55.16 (8,000psi)

Jet Location: Pattern 2

Nozzle Diameter: 0.68 mm

6.4.2 Unassisted Cutting

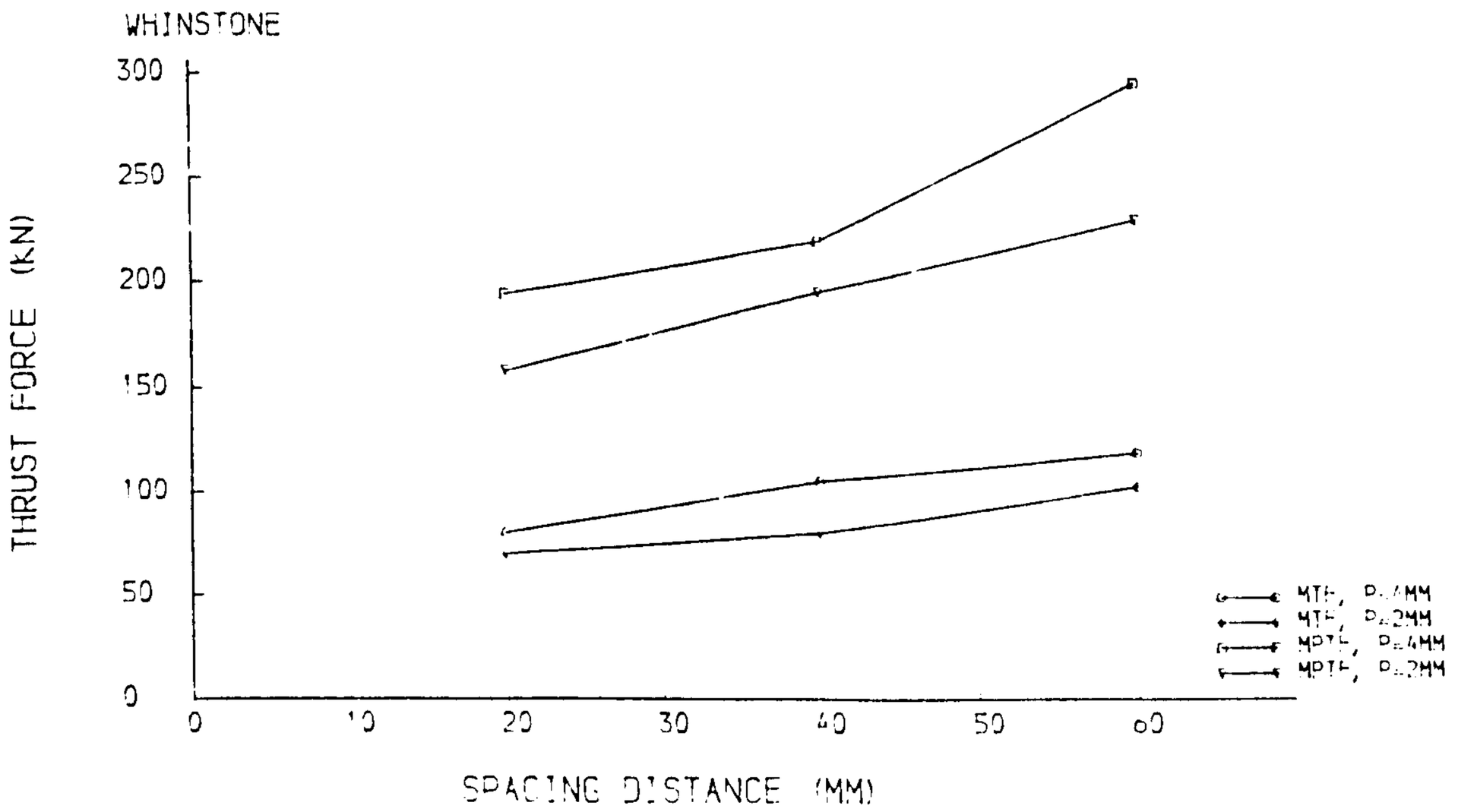

Fig. 6.4.1 Thrust force versus spacing distance

The results of unassisted cutting on Whinstone are shown in Figs 6.4.1, 6.4.2 and 6.4.3. For the 2mm penetration condition, the mean peak thrust force has a linear relationship with spacing distance, while for the 4mm penetration, the mean peak thrust force is characterised by a non-linear relationship. The curves of mean thrust forces against spacing distance are linear in both cases. The situations of mean peak rolling force and mean rolling force are similar with that of related thrust forces, but surprisingly, the mean peak rolling force for the 4mm penetration / 40mm spacing condition is less than that for the 20mm spacing condition. As a result, the low mean peak rolling force renders the action of water jet minimal for

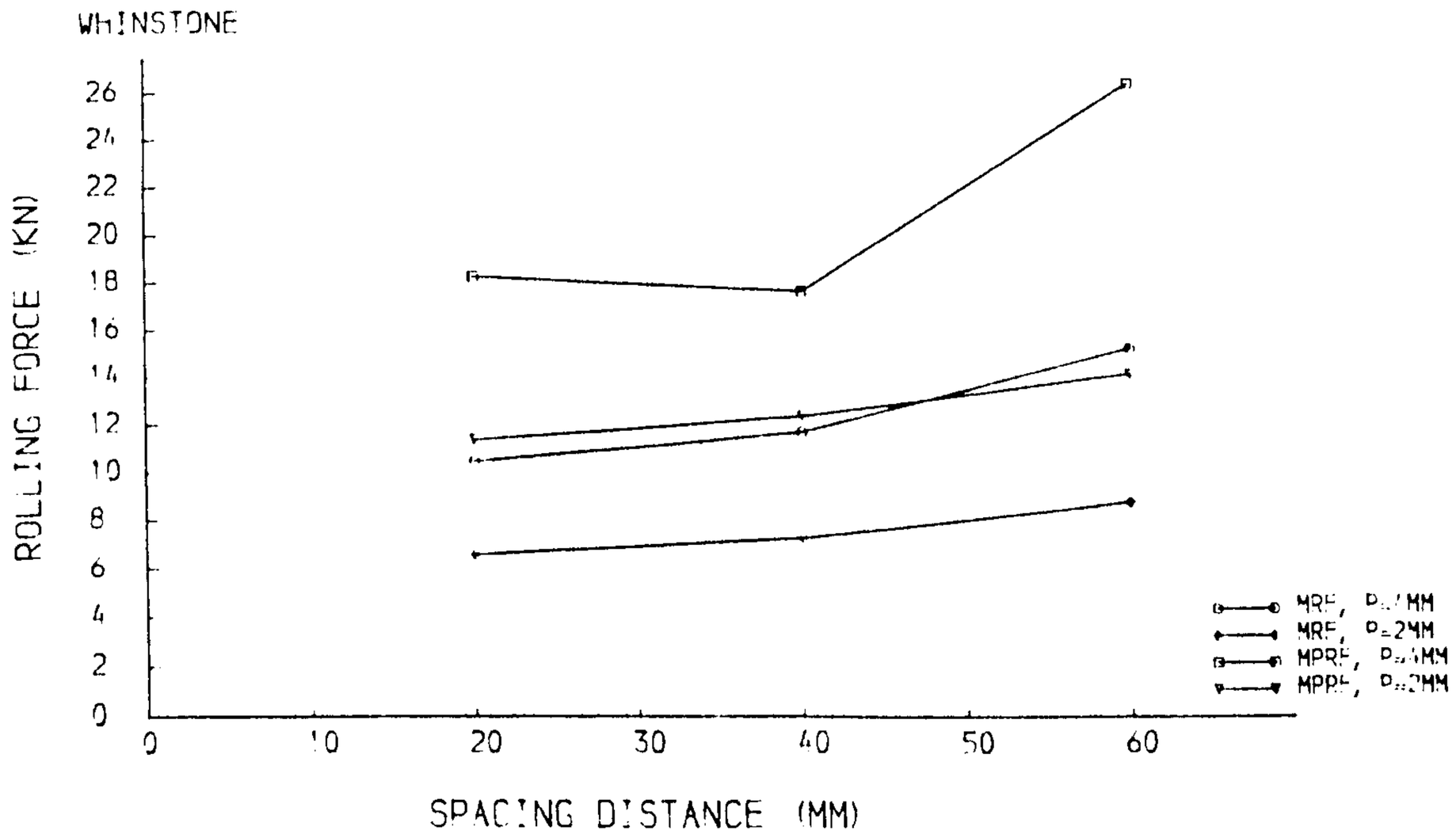

Fig. 6.4.2 Rolling force versus spacing distance

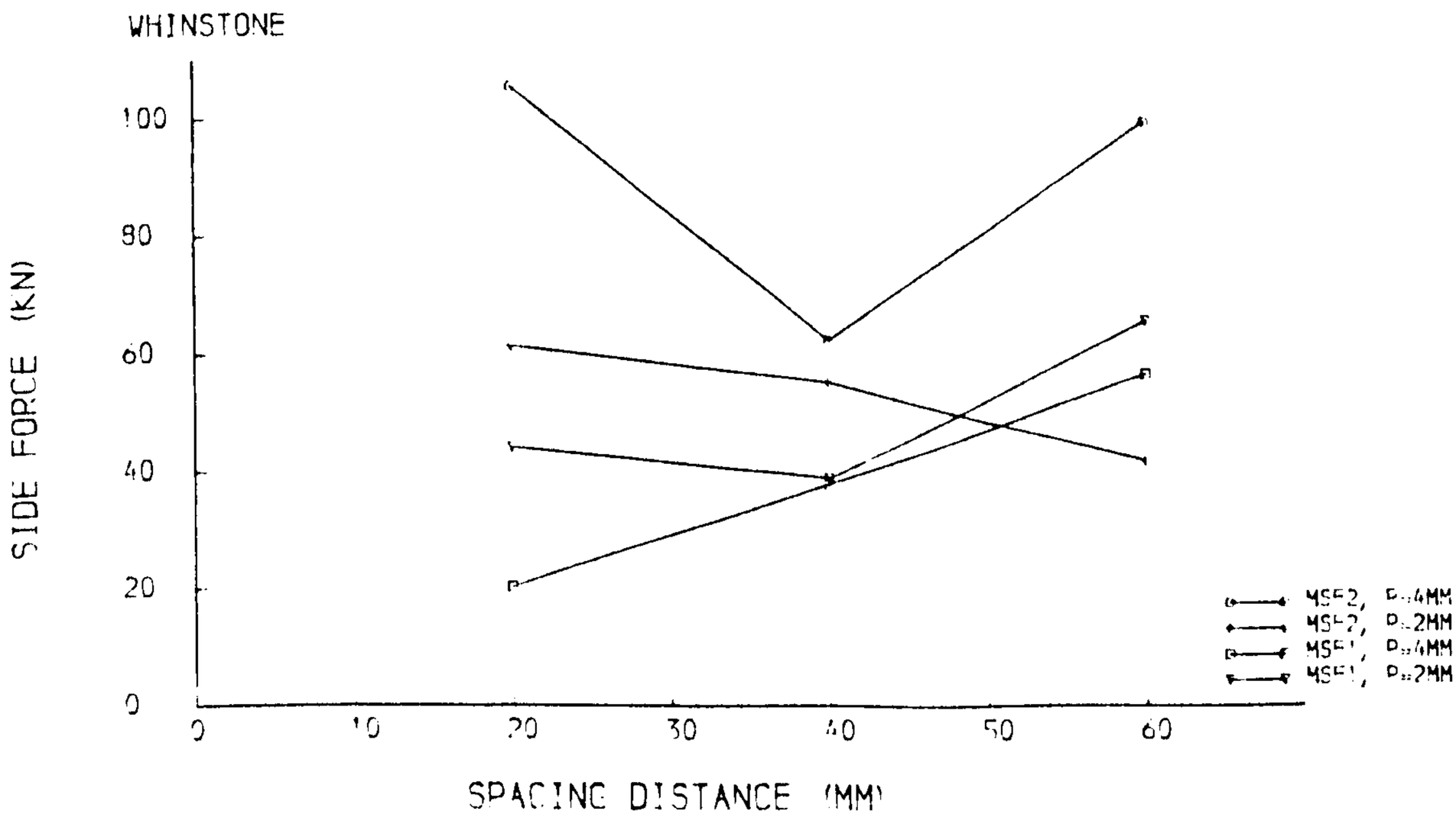

Fig. 6.4.3 Side force versus spacing distance

this condition.

6.4.3 The Effect of Cutting Speed

As indicated by Fig. 6.4.4, the thrust force shows no discernible change with cutting speed over the range 0.25-0.85 m/s. This fact is equally true for the rolling force as illustrated in Fig. 6.4.5 and for the side force as illustrated in Fig. 6.4.6.

These results, taken in conjunction with the wealth of data form cutting tests on Pennant Sandstone, encourages the general conclusion that the performance of a disc tool with the assistance of a water jet is not affected by the speed of cutting.

6.4.4 The Effect of Water Jet Pressure

In the previous section, attention was drawn to the effect of water jet pressure on cutting forces on Pennant Sandstone. Table 6.4.1 gives the percentage reduction of thrust force and rolling force during water jet assisted cutting on Whinstone for a range of water jet pressure conditions.

1. The Effect on Disc Cutter Thrust Force

Taking, again, as an example, the results using a spacing distance of 60mm, and a penetration of 4mm, it is found that the thrust force is reduced by 17% with an 55.16MPa water jet pressure; by 13% at 41.37MPa; by 15% at 27.58MPa and by 17% at 13.79MPa. With penetration 2mm, the reduction of mean peak thrust force for the different water jet pressure conditions are: 21% at 55.16MPa; 15% at 41.37MPa; 12% at 27.58MPa and 6% at 13.79MPa, – the greater benefit being obtained with higher water jet pressures. This is equally true for the spacing distances of 20mm and 40mm at a penetration of 2mm, but not for the case of the 4mm penetration. However, this does not mean that same tendency can be found with the mean thrust force.

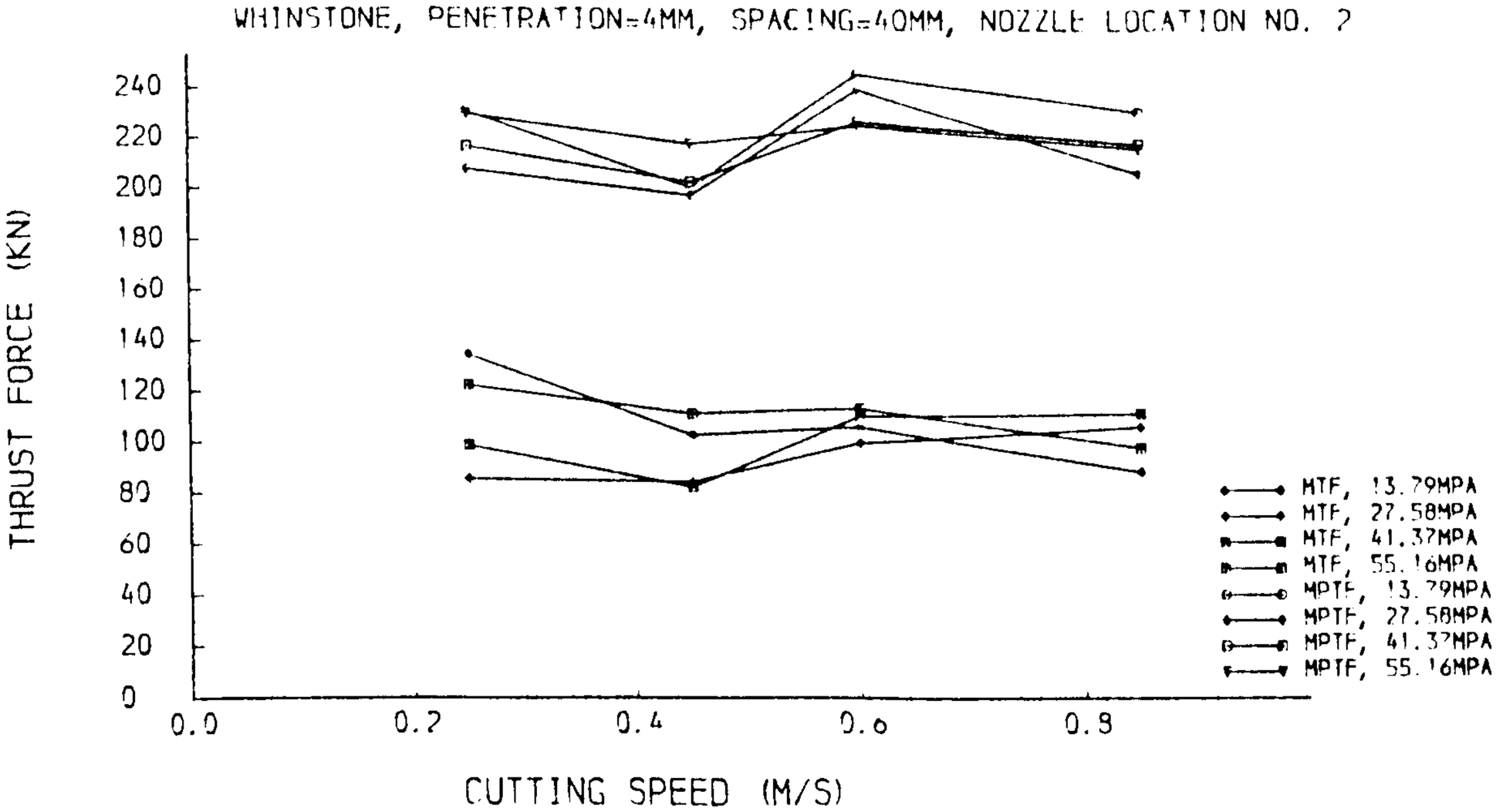

(a). p=4mm, s=40mm

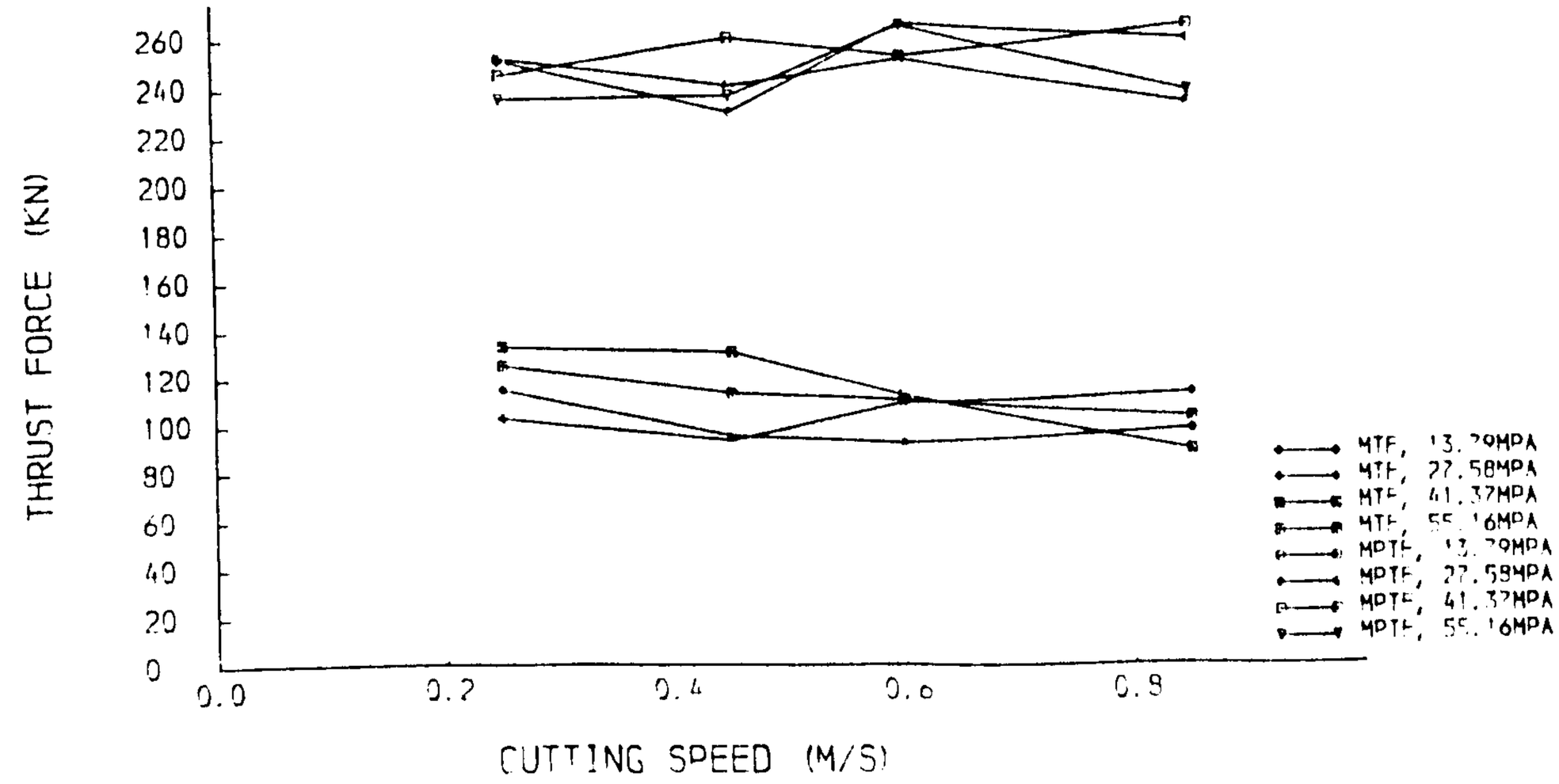

(b). p=4mm, s=60mm

Fig. 6.4.4 Thrust force versus cutting speed

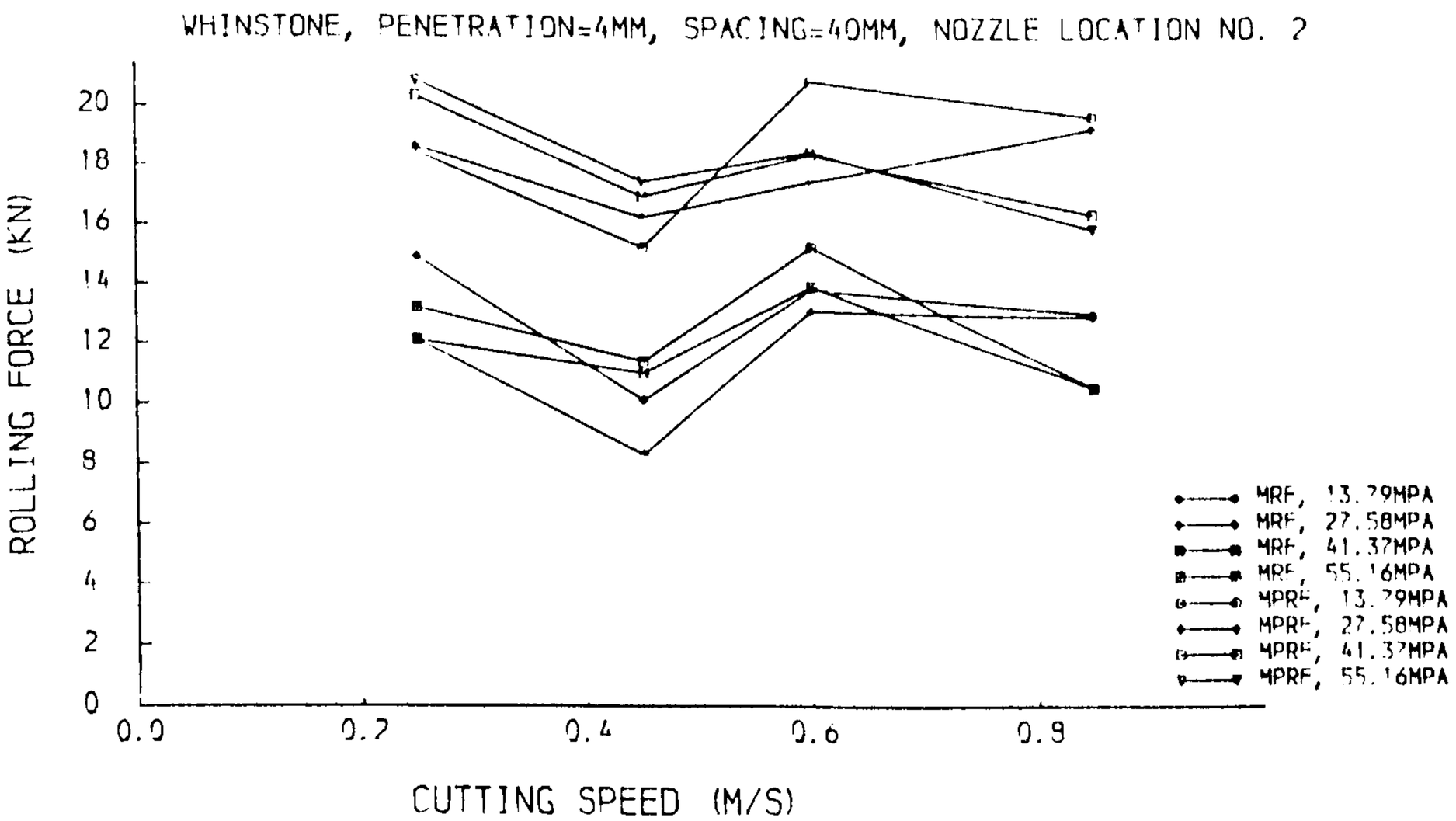

(a). p=4mm, s=40mm

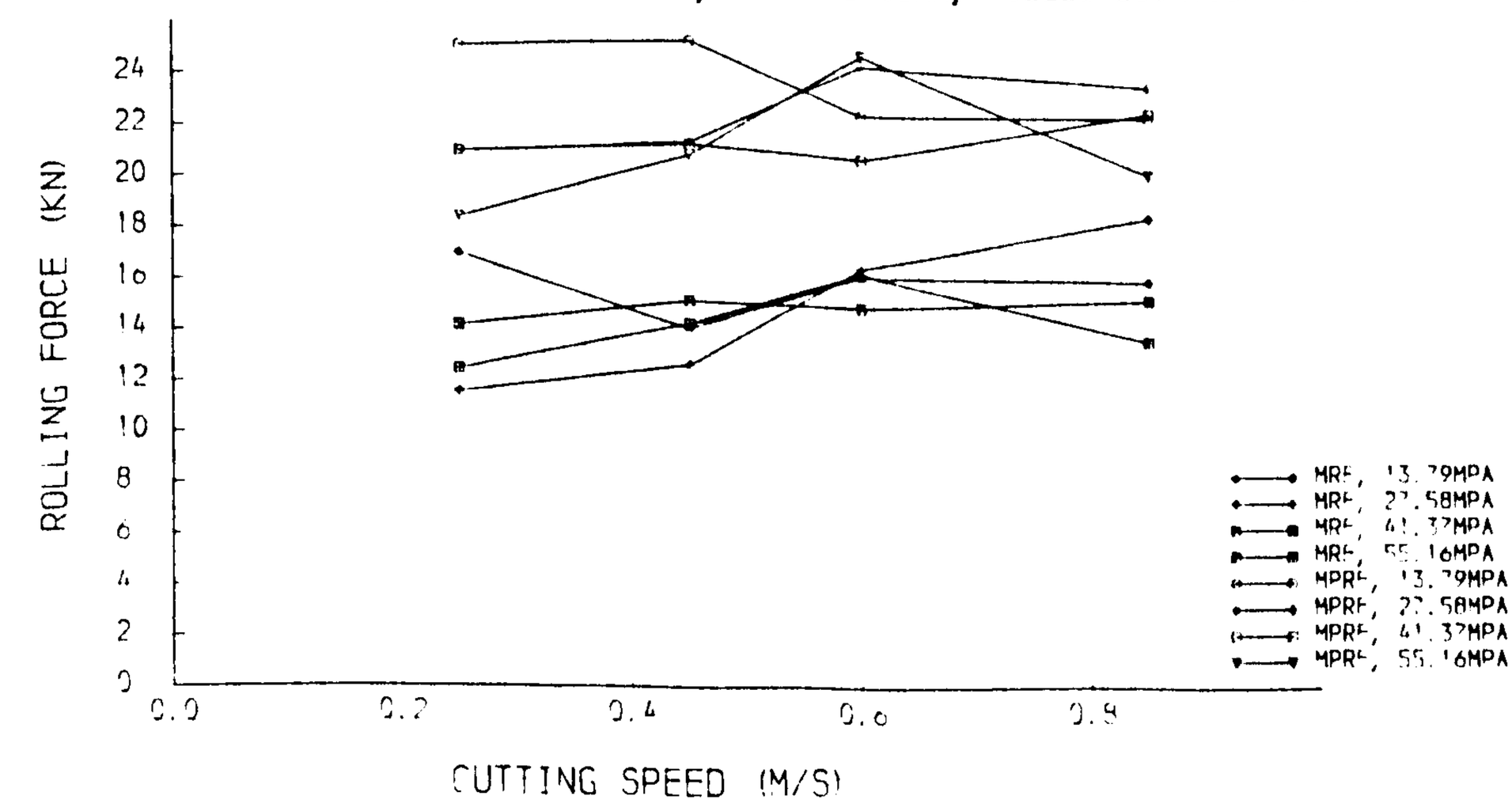

(b). p=4mm, s=60mm

Fig. 6.4.5 Rolling force versus cutting speed

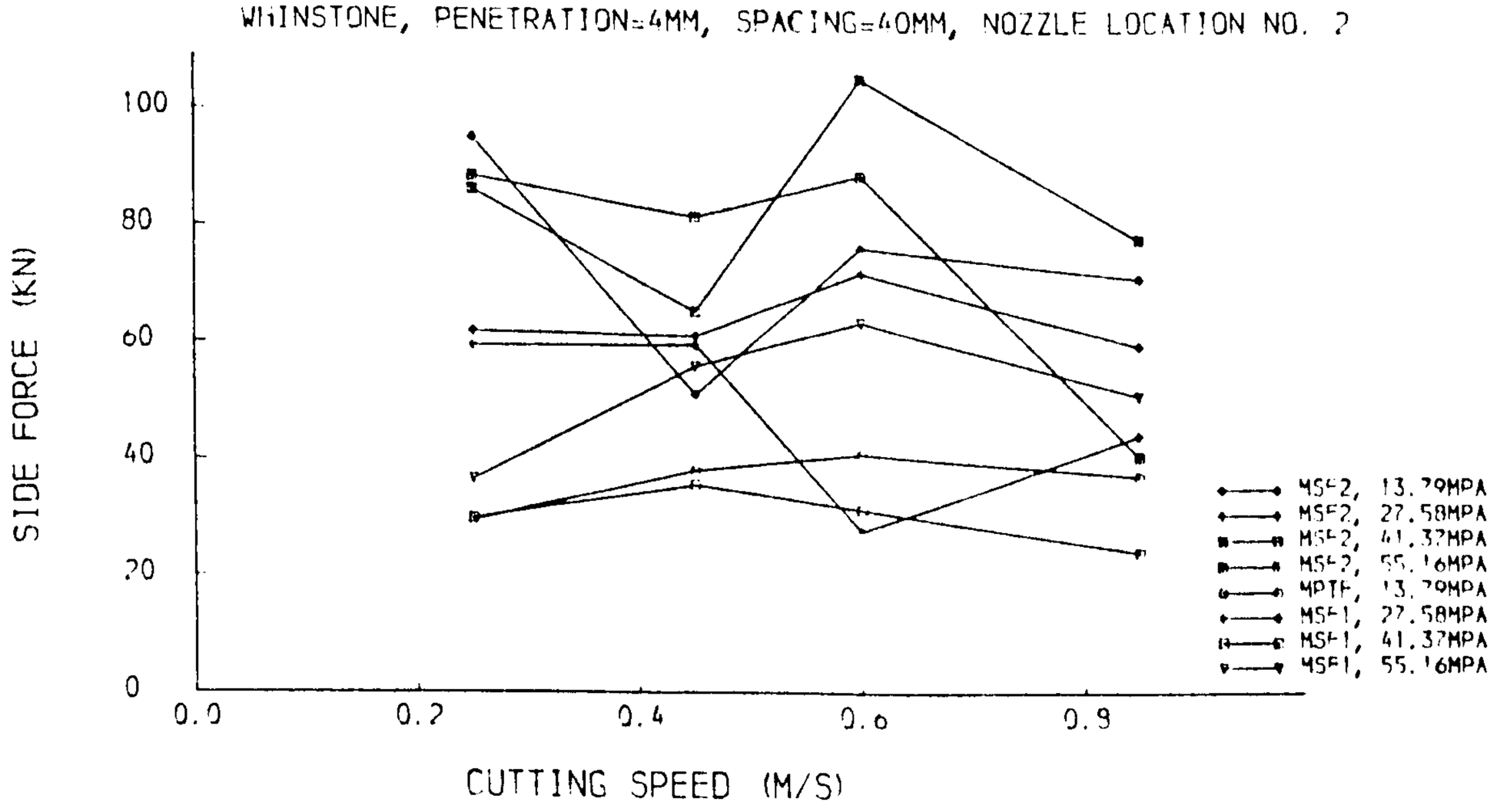

(a). p=4mm, s=40mm

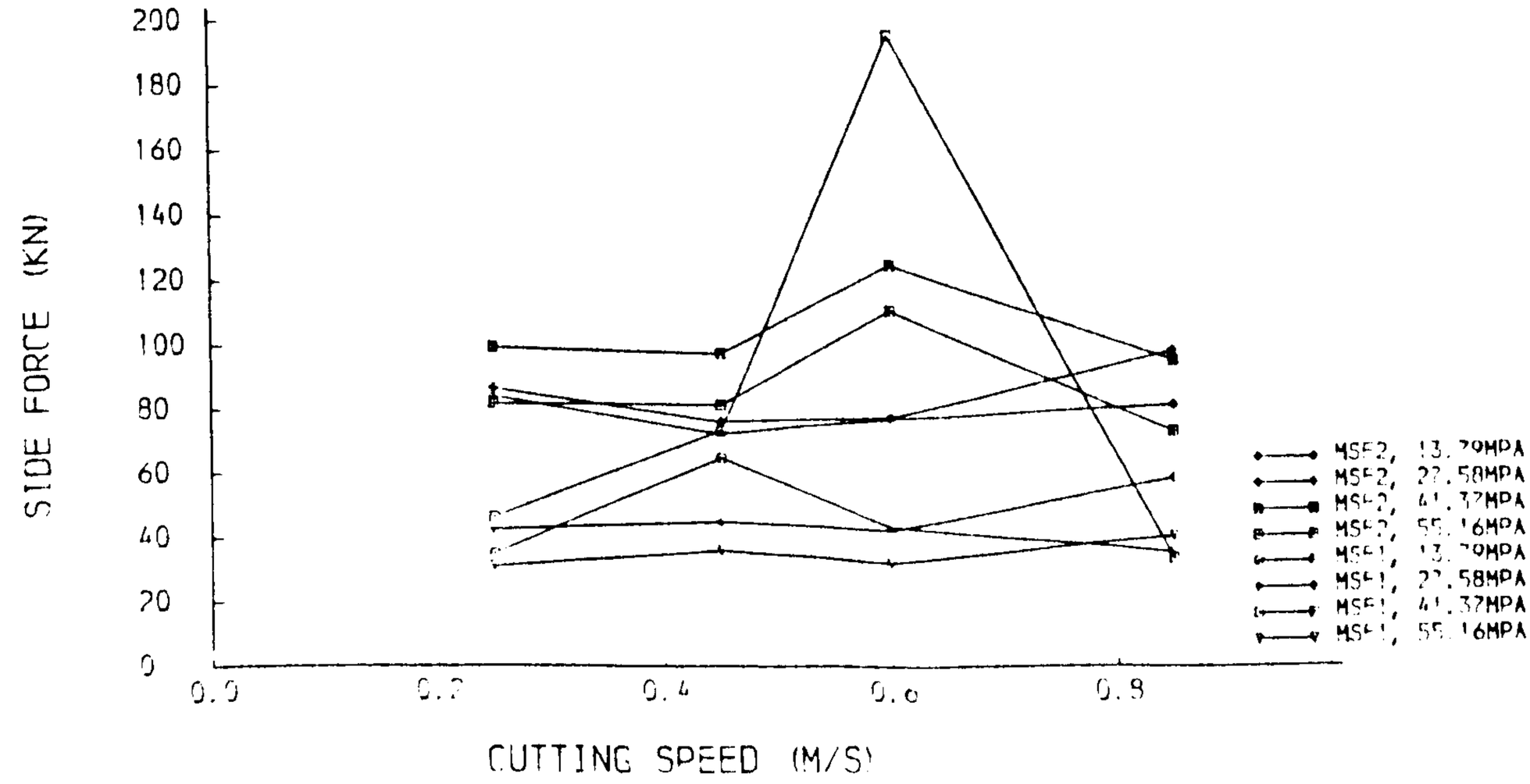

(b). p=4mm, s=60mm

Fig. 6.4.6 Side force versus cutting speed

Table 6.3.1 Percentage reduction in cutting forces

Nozzle Location Pattern 2

p mm	jet pre. MPa	*s* mm	MPTF %	MTF %	MPRF %	MRF %
2.	13.79	20.	10	14	10	03
		40.	13	09	-14	02
		60.	06	-03	-02	01
2.	27.58	20.	12	13	19	26
		40.	14	21	-23	10
		60.	12	10	-06	14
2.	41.37	20.	16	22	13	24
		40.	12	12	11	12
		60.	15	14	02	23
2.	55.16	20.	15	22	04	29
		40.	20	15	15	24
		60.	21	15	11	23
4.	13.79	20.	07	12	11	-01
		40.	-03	-05	-02	-10
		60.	17	10	15	-03
4.	27.58	20.	0	05	04	-03
		40.	03	-01	11	01
		60.	15	15	12	04
4.	41.37	20.	03	04	03	-01
		40.	02	-01	05	-01
		60.	13	19	02	03
4.	55.16	20.	09	11	-01	04
		40.	-01	-02	-05	-07
		60.	17	21	05	07

2. The Effect on Disc Cutter Rolling Force and Side force

Taking the same example as above, the same conclusion can be drawn for the mean peak rolling force and mean rolling force for the cutting tests with penetration of 2mm and 4mm, and spacing distance of 20, 40, and 60mm. Meanwhile, no effect on the disc cutter side force was found.

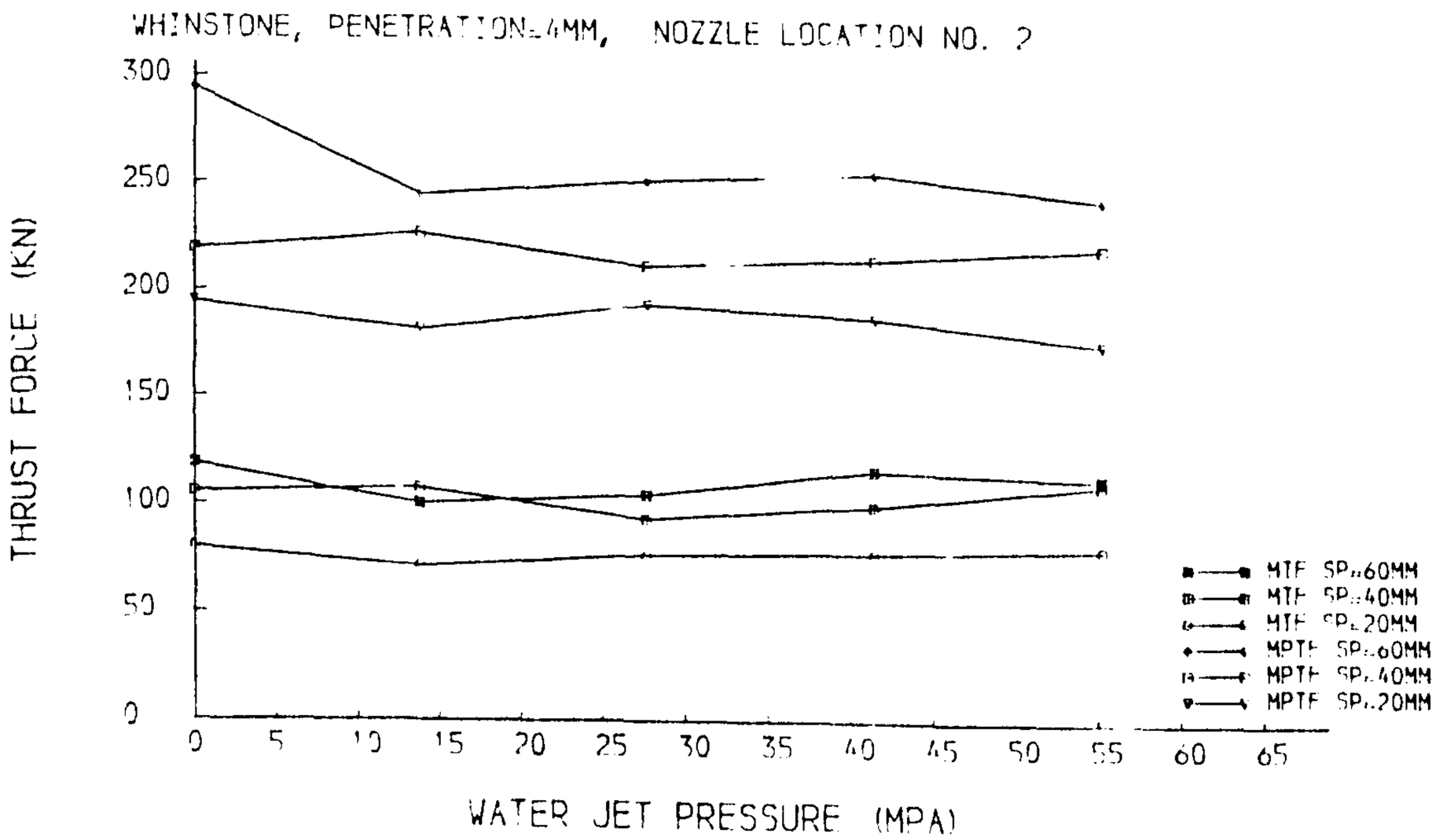

Fig. 6.4.7 Thrust force versus water jet pressure

The effect of the water jet pressure on the disc cutter forces with p=4mm is shown in Figs 6.4.7, 6.4.8 and 6.4.9.

6.4.5 The Effect of Spacing Distance and Penetration

The effect of the spacing distance to penetration ratio, s/p, on the cutting forces is shown in Figs 6.4.10, 6.4.11 and 6.4.12. The encouraging results achieved on Pennant Sandstone were not repeated in the cutting tests on Whinstone.

6.4.6 Summary

The improvement in performance of water jet assisted disc cutting on Whinstone is not as significant as that achieved on Pennant Sandstone. The mean peak thrust force is reduced by up to 21%, the mean thrust force by up to 19%, the mean peak rolling force by up to 21%, and the mean rolling force by up to 29%.

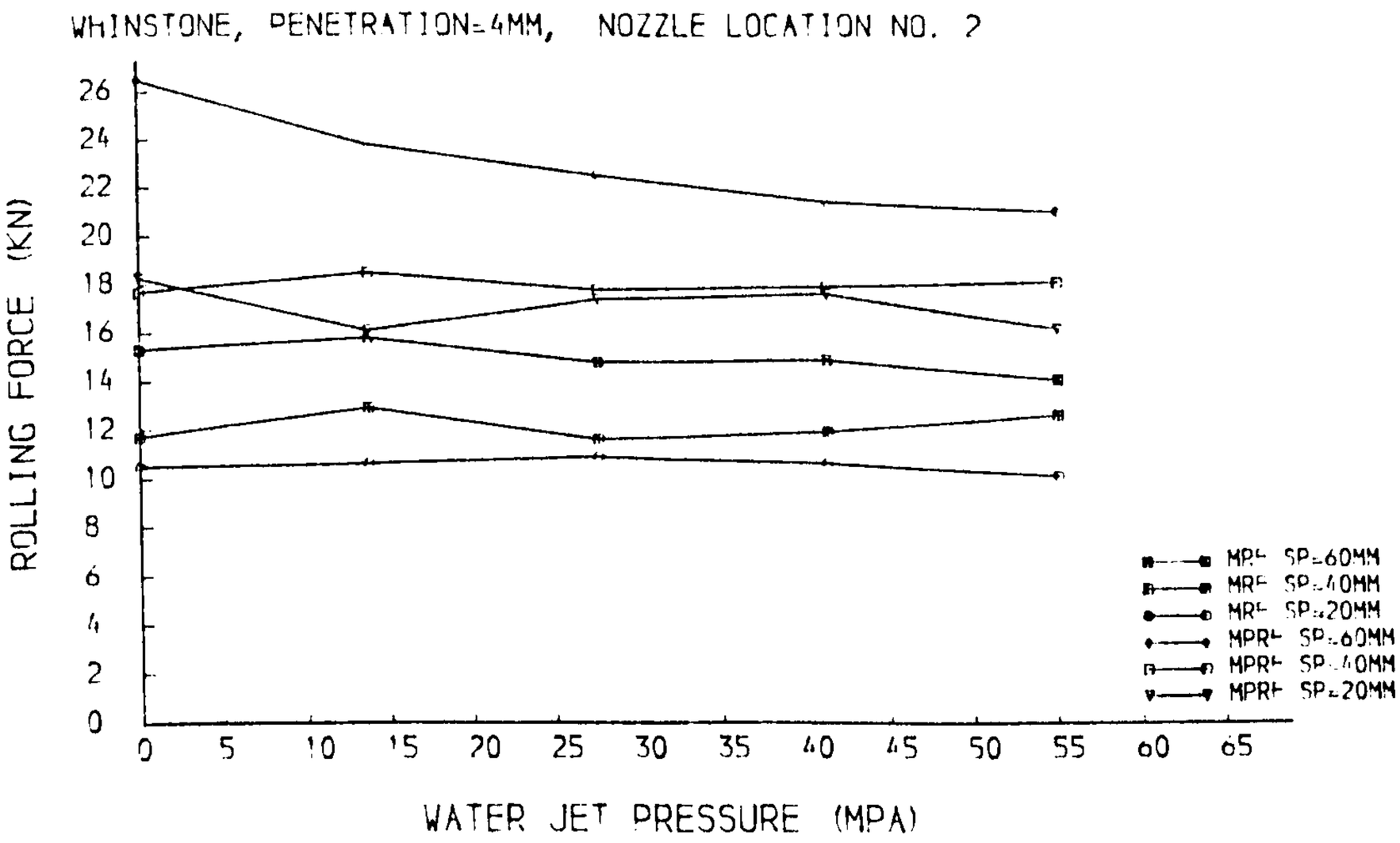

Fig. 6.4.8 Rolling force versus water jet pressure

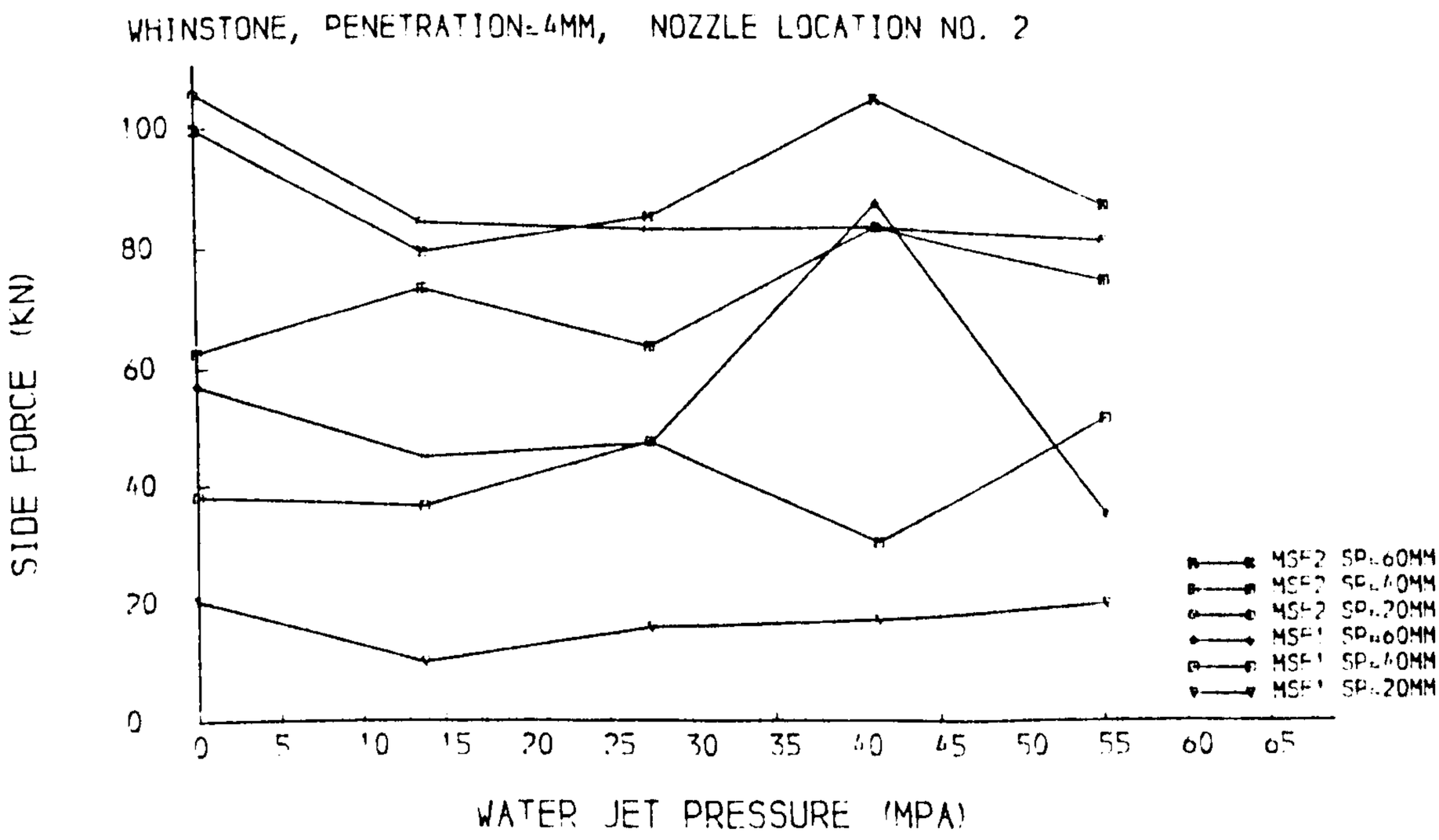

Fig. 6.4.9 Side force versus water jet pressure

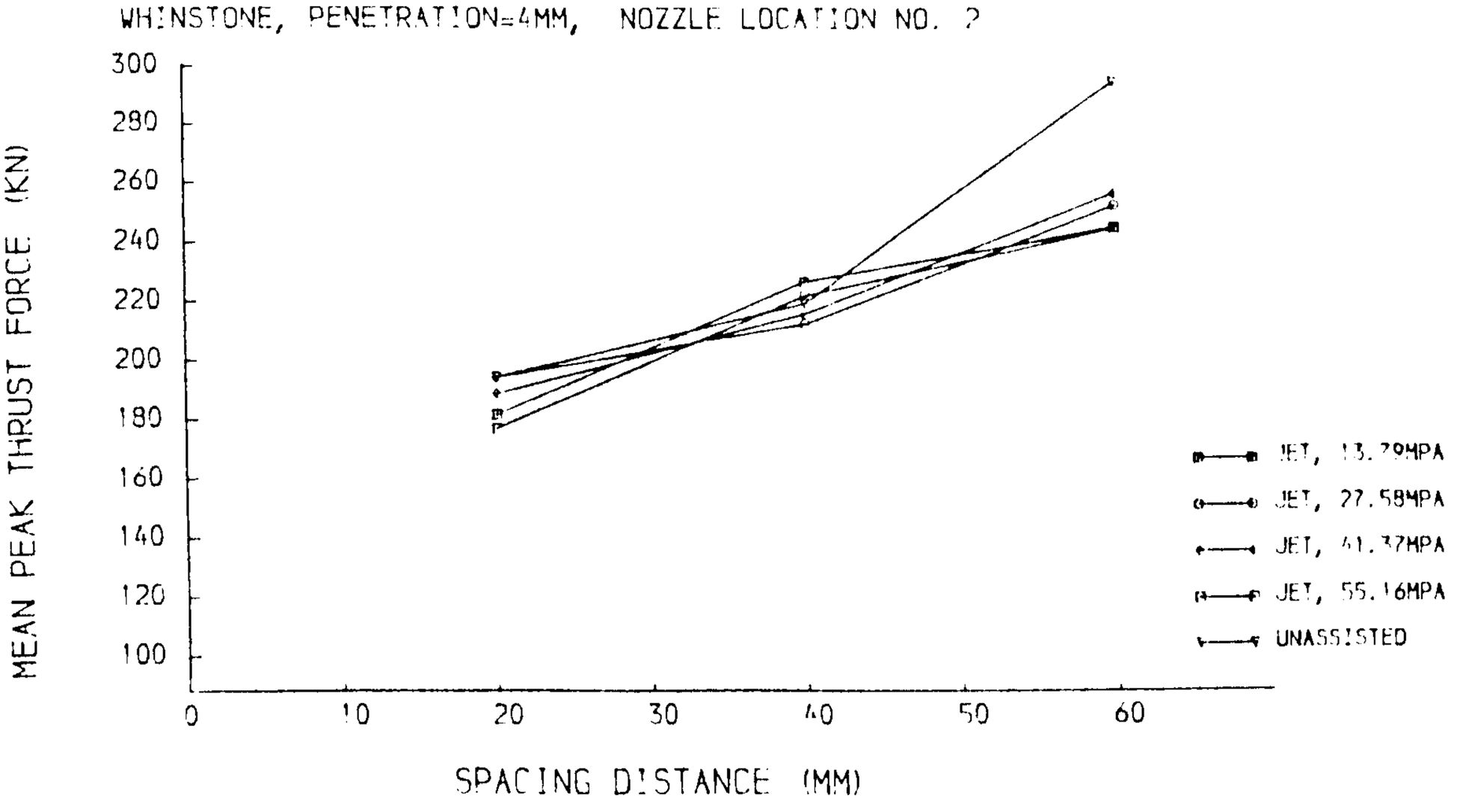

(a). Mean peak thrust force

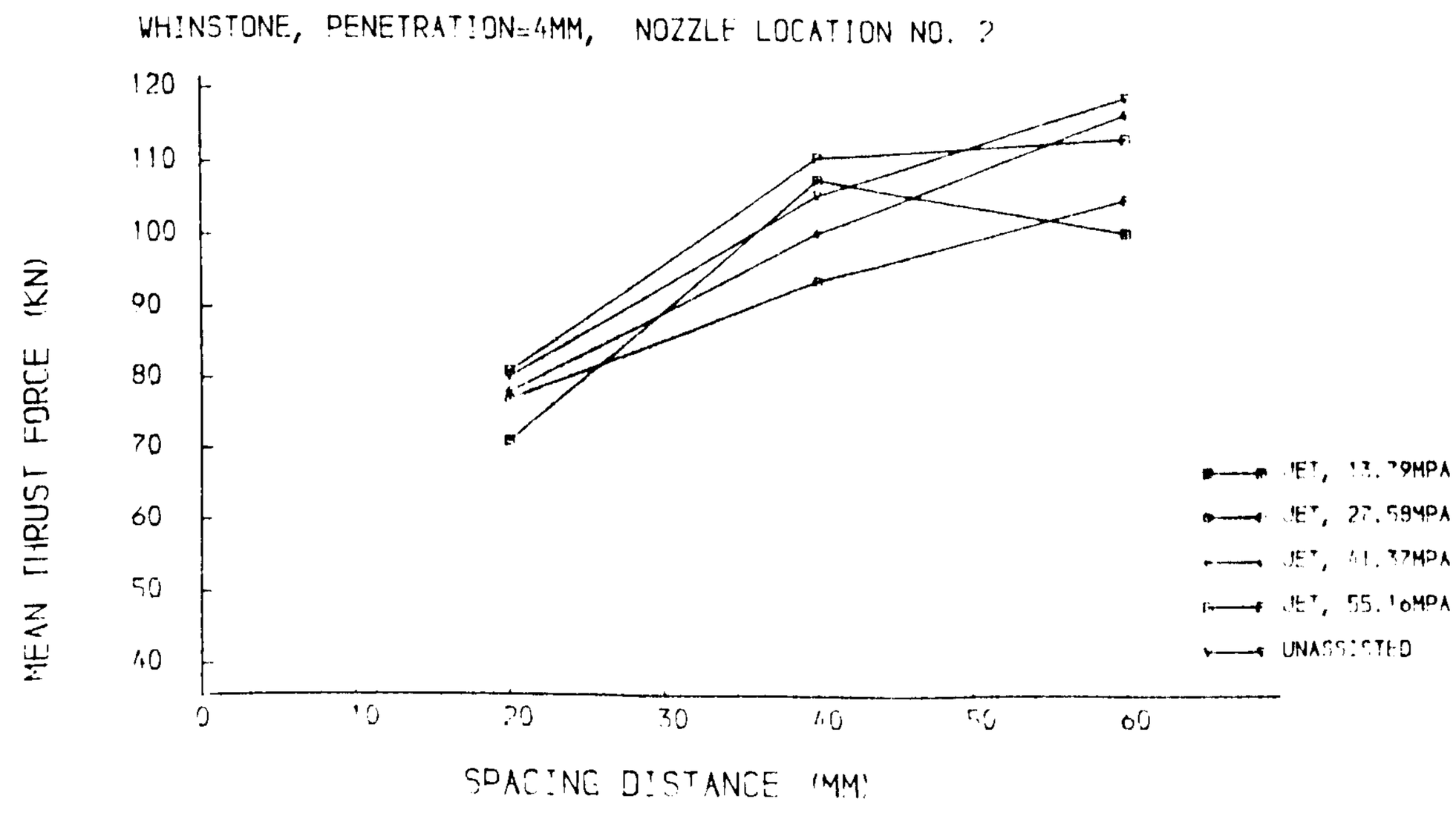

(b). Mean thrust force

Fig. 6.4.10 Thrust force versus spacing distance

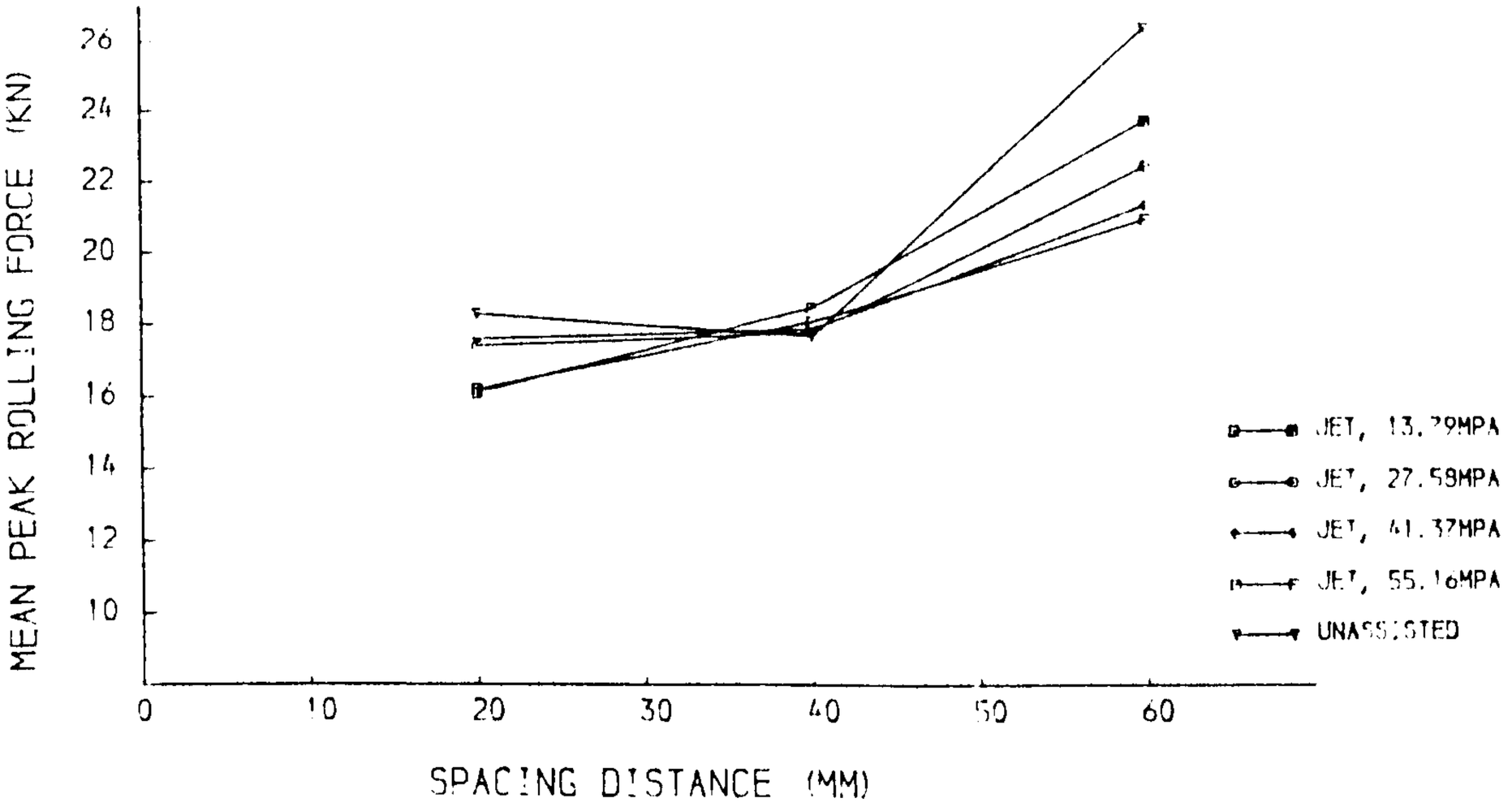

(a). Mean peak rolling force

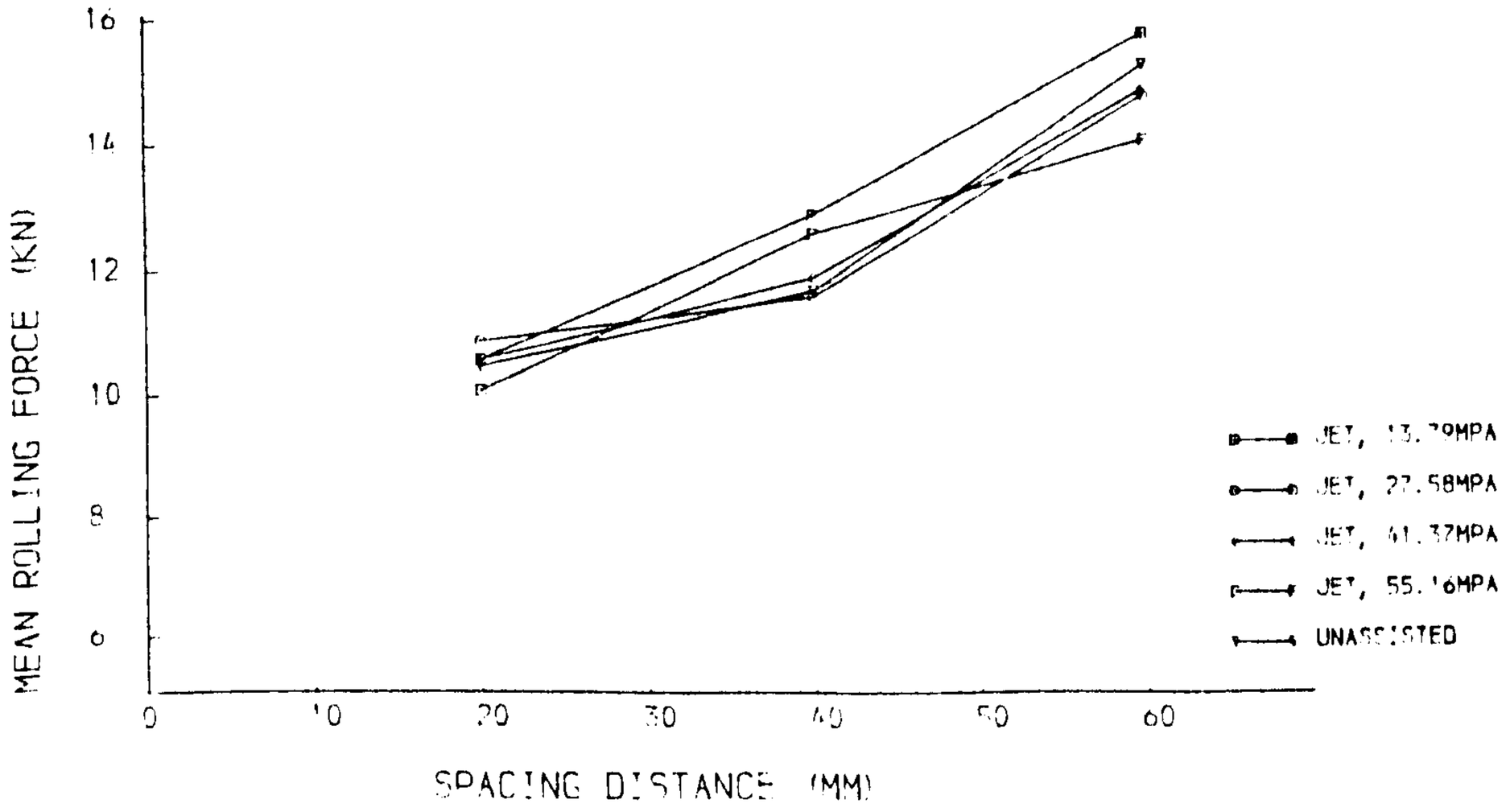

(b). Mean rolling force

Fig. 6.4.11 Rolling force versus spacing distance

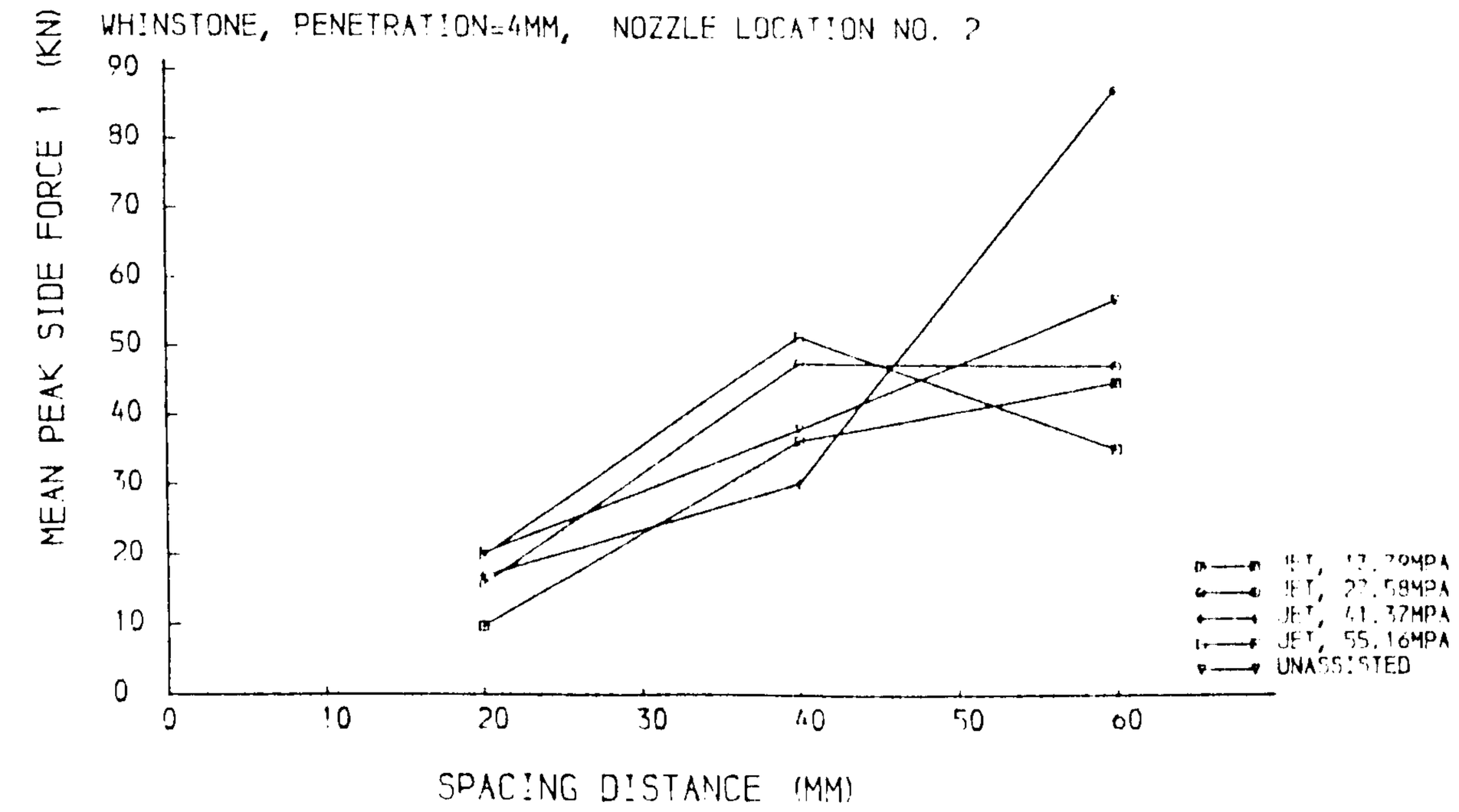

(a). Mean peak side force 1

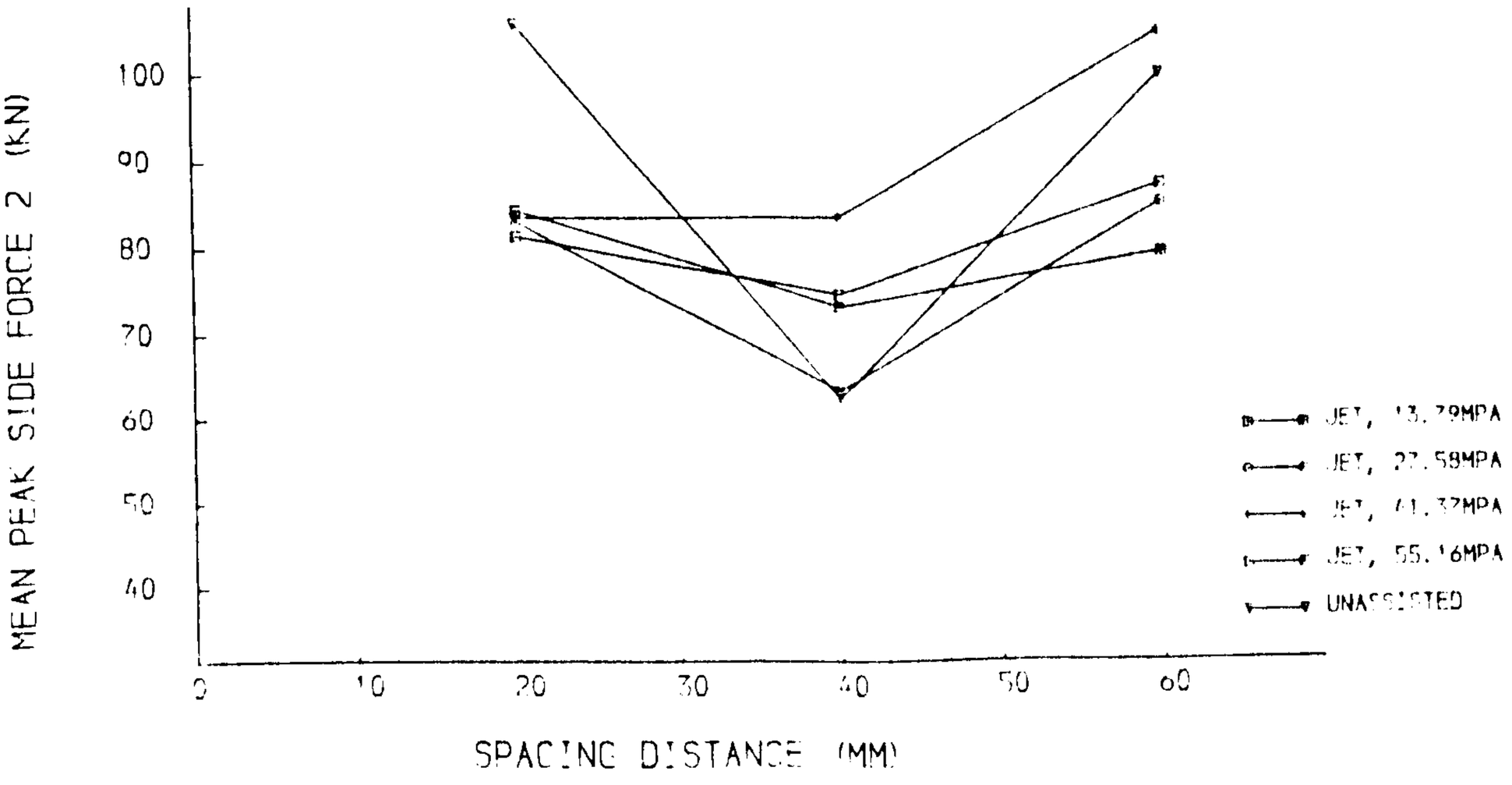

(b). Mean peak side force 2

Fig. 6.4.12 Side force versus spacing distance

No influence of cutting speed on cutting forces was indicated by the testing data, but the water jet pressures appeared to affect the testing performance to some degree. The maximum benefit was not determinable from the tests. This is quite different from the summary of the previous Section which concluded that the maximum benefit for rock cutting with water jet assistance on Pennant Sandstone obtains when the penetration is 4mm and spacing is 60mm. The possible reasons will be discussed in following sections.

6.5 THE MECHANISM OF ROCK BREAKAGE

6.5.1 The Mechanism of Rock Breakage by Mechanical Disc cutter

It is a widely accepted view that mechanical tunnel boring involves two separate rock breaking mechanisms. The first of these obtains at all cutter loads, and identifies with the crushing the rock beneath the cutter edges. The second, which occurs only after some critical load per cutter path is reached, identifies with the breaking of the rock out between the cutter paths (Dollinger, 1983). The method in which these two mechanisms of rock breakage function during every cutting cycle, is named "kerf cutting". In other circumstances, when the load on the edge is unable to break the rock between the cutter paths, the second mechanism only occurs after several cutting cycles. This method is called "multiple cutting".

The first rock breaking mechanism is very similar to the penetration of a cone indenter into a brittle material. Prediction of the failure of rock by disc cutter penetration, therefore, can be facilitated by first examining the type and nature of the stress field and the resulting failure produced beneath a wedge shaped indenter penetrating a rock surface with no nearby cuts or free faces. Below each cutter edge is an area of extremely high stress which produces a crushed zone formed by very fine rock powder just beneath the edge, as illustrated in Fig. 6.5.1. As the

crushed zone is in a state of triaxial compression which in turn produces a radial tensile stress field, it is believed that at least the failure surface is initiated as a tensile crack. This tensile crack can stop at a point on the failure surface, or reach the rock surface.

The penetration process for a disc cutter has been described by Snowdon et al. (1982), Farmer and Glossop (1980), and Law and Swain (1975) as follows:

1. during initial loading of the rock a zone of irreversible deformation occurs around the cutting edge of the disc;

2. at some critical load a crack, known as the "median vent", initiates from the edge of the disc in a direction parallel with the thrust force;

3. an increase in load causes further, stable growth of the median vent;

4. as the disc travels across the rock, initial unloading occurs which causes the madian vent to close.

5. just before unloading is completed, relaxation of the stress in the contact zone around the disc edge results in high tensile stresses which produce cracks, known as "lateral vents";

6. upon complete removal, the lateral vents tend to be concave in shape and travel upwards to intersect the rock surface, and may accordingly lead to chipping.

In fact, the actual failure of rock during cutting is not exactly as described above, because of the effects of spacing between cutter paths. Consequently, the failure surface does not always run from the crushed zone to the free surface, but to neighboring cutter paths. Thereby, assuming the force on the cutter is sufficiently high, much less energy is used per unit volume of rock removed than by other

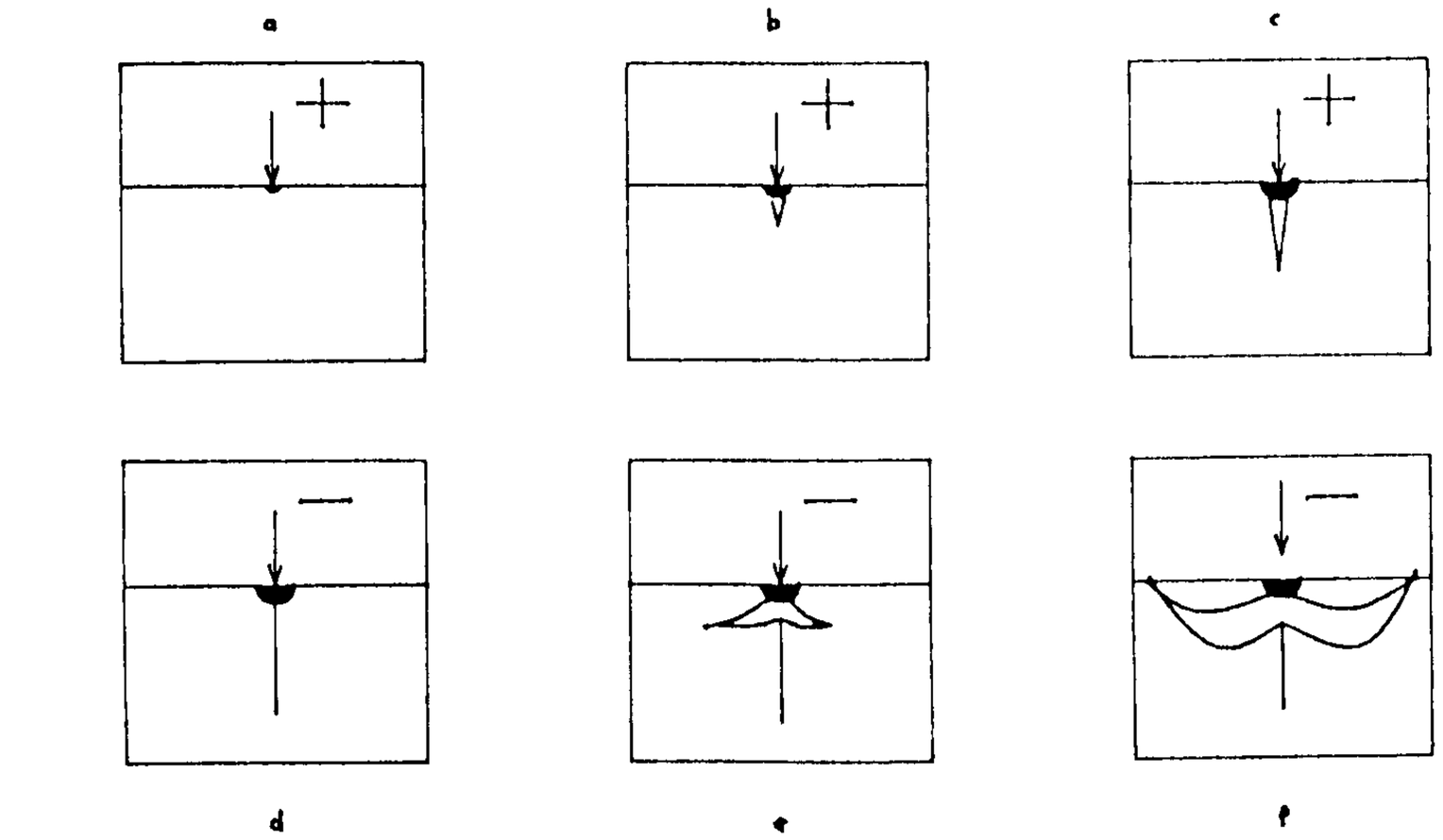

Median vent forms during loading (+) half-cycle; lateral vents during unloading (-) half-cycle. Fracture initiates from deformation zone (dark region).

Fig. 6.5.1 Schematic of vent crack formation under point indentation

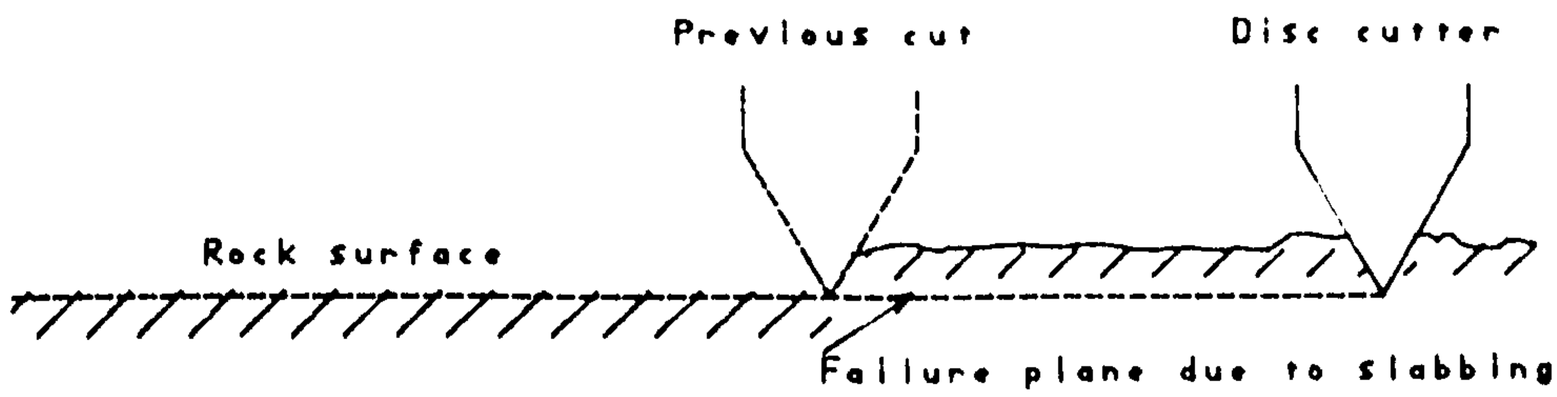

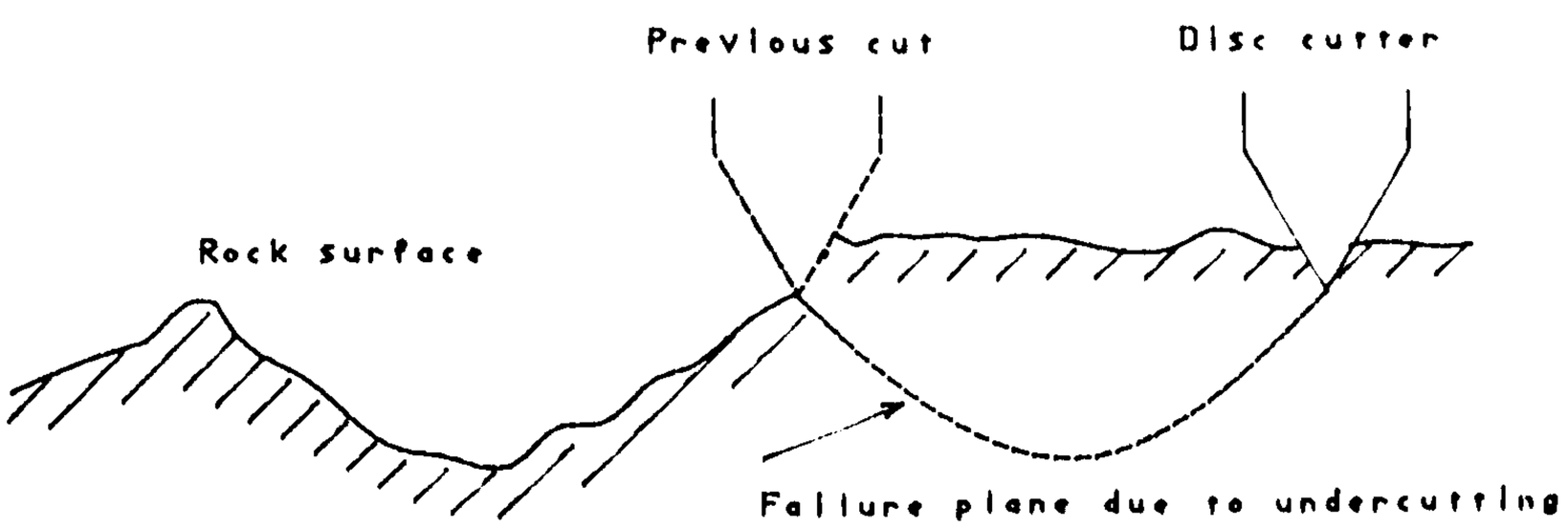

Fig. 6.5.2 Rock failure planes

methods.

Two different shapes have been observed in connection with the geometry of the breakout of rock between cutter paths. Considering the first of these, the breakout is roughly parallel to the rock surface creating a slab-like failure. For the second, the breakout is deeper, with the failure surface curving downwards from the bottom of each groove to leave a series of ridges at the position of each of the grooves (Fig. 6.5.2). With the first, the chip formation is considered as a shear failure, that is, the rock is simply crushed aside by the cutter edges, resulting in a lateral displacement of the interlying material, and failure. The second, on the other hand, is a tensile failure, caused by propagation of the initially radial cracks during unloading of the cutter tools.

Although the existence of a crushed zone and radial cracks have been visually observed in the rock cutting tests, the exact mechanism of chip formation is still not yet refined.

6.5.2 The Mechanism of Rock Breakage by High-pressure Water Jet Assisted Disc Cutter

Disc cutters are highly efficient at forming chips. But when the cutting is carried out on very hard rock formations, the tunnelling advance rate is limited by cutter wear and by the enormous thrust required to force the cutters into the tunnel face. High pressure water jets can be used to reduce these two problems.

Essentially, three types of jet nozzle patterns have been considered in water jet assisted tunnel boring tests (Wang, et al., 1976; Henneke and Knickmeyer, 1979). They are as follows:

1. jets between the cutters;

2. jets under the cutters;

3. jets both under and between the cutters.

Considering the first pattern, the water jets make kerfs and the following disc cutters, which travel between the water jet pre-cut slots, break out chips with comparatively little thrust and power. Furthermore, as the slots cut by water jets increase the free surfaces into rock, the rib between two grooves is removed by the shearing action of the cutter. As the compressive strengths for rock materials are much higher than their shear strengths the change in disc cutter attack on the rock from pressing / squeezing to a more shearing effect can reduce the required thrust forces.

Considering the second pattern with the water jets under the disc cutters, the kerfs made by the jets that coincide with the cutting paths. These kerfs reduce the mechanical penetration and thereby, the forces on the cutters. The failure of the rock is possible due to shear rather than tensile, because the consequence of crushed zone is less important in this case.

The third pattern with the jets both under and between cutters, simply combines the first two patterns.

In addition to cutting slots on the rock surface, there are several ways in which a water jet might affect the cutter forces. These possibilities are less important for high pressure water jet assisted disc cutting, but are playing very important roles in low pressure water jet assisted disc cutting. A detailed discussion is given in the next Section.

6.5.3 The Mechanism of Rock Breakage by Low-pressure Water Jet Assisted Disc Cutter

The mechanism of low-pressure water jet assisted disc cutting is rather different

from that of high-pressure water jet assisted disc cutting. The main difference is that the water jet pressure is not powerful enough to make a kerf into rock. Two mechanisms by which the water jet might act to reduce the cutting forces are proposed. They are as follows:

1. effective clearance of the rock particles from the region adjacent to the cutter.
2. chemical attack of rock by water, i.e. stress corrosion cracking (SCC);

In order to understand the effect of the low-pressure water jet on cutter forces, it is necessary to look at its action on the crushed zone. When the tools cut through the rock surface, a highly fractured zone is created beneath the disc cutters, as mentioned above. The zone formed by the rock powder has an inelastic characterization which subject to compression by a hydrostastic stress situation forms a new material with similar properties as intact rock (Lindqvist and Lai, 1983).

A very interesting observation of the sequence of events in hemispherical penetration was given by Lindqvist and Lai (1983). Fig. 6.5.3 illustrates the process forming the crushed zone due to hemispherical penetration tests. Similar phenomena occurs in the disc cutting tests. Plate 6.5.1 shows the cores of rock powders found in the bottom of cutting grooves. The thickness of the core can be up to 10 mm with only 4 mm depth of penetration.

The following analyses and comments of the first of the two mechanisms, considering three different nozzle locations:

1. As the water jet cuts through the crushed zone formed by previous cutting, and using the nozzle located vertically to the cutting groove, it is possible that only a kerf is made on the crushed zone with most of the powders in the zone still left in the groove. These powders have some effect on the thrust forces, as shown in Fig. 6.3.23. It is suggested that the crushed zone correspondly to the

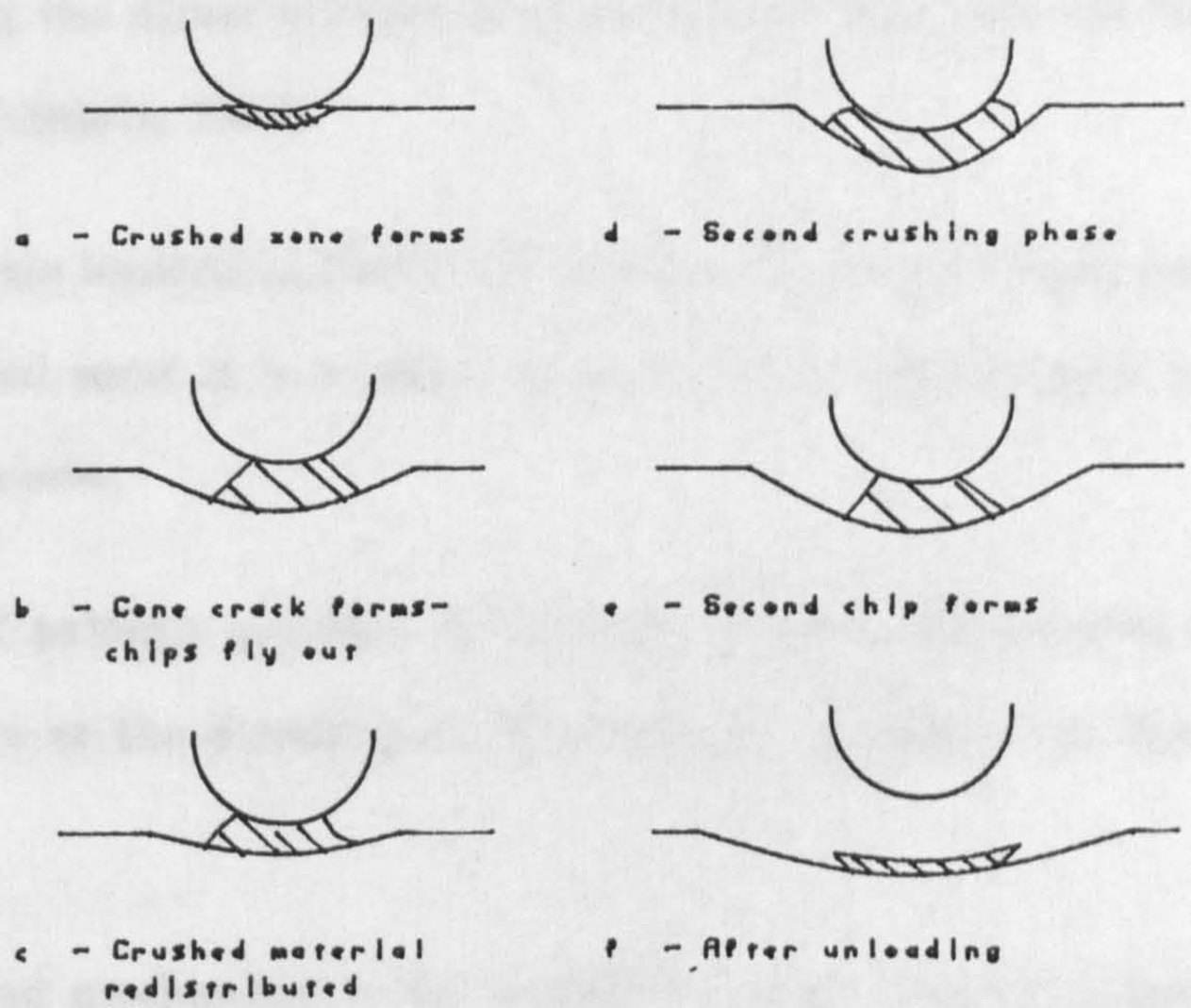

Fig. 6.5.3 The sequence of events in hemispherical penetration

Plate 6.5.1 Rock powder cores on the bottom of cutting grooves

presence of remained powder, is simply acting as a shock absorbing medium, preventing the direct transmission of cutting force into the rock material concerned (Passaris, 1988).

2. If the nozzle located in Pattern 2, because there is a "weak section" arounding the crushed zone, it is possible to easily move most of rock powders from the cutting groove.

3. The third pattern provides the easiest way for the removal of powders from the groove as the direction of the water jet is vertical to the direction of the cutting.

The second mechanism is the possibility that chemical attack of rock by the water will reduce cutter forces, i.e. stress corrosion cracking (Hood, 1985).

Stress corrosion cracking (SCC) can produce a significant reduction in the fracture strength of rock. But this effect might decrease as the velocity of the crack front increases, and there is a limiting crack velocity beyond which stress corrosion has no effect in the fracture process. For most brittle materials, including rock, the limiting velocity appears to be of the order of 0.0001 to 0.1 m/s (Barton, 1982). With a bit cutting speed of 0.06 m/s, the crack propagation velocity of about 80 m/s was determined by Hood (1985) from a series of high speed films of the cutting operation. Therefore, this hypothesis was rejected in water assisted bit cutting. In this study, the cutting experiments were undertaken with speeds up to 0.85m/s. It is evident that the velocity of the crack propagation would be far more than that in order to form the chips. From this point of view, this hypothesis would also be rejected in water jet assisted disc cutting. However, as the rock surface is in the wet conditions during the cutting tests, chemical attack of rock by the water could be in this way. Some rock fracture measurements do show the effect of moisture on

the fracture toughness, as mentioned in chapter 2.

6.6 DISCUSSION

6.6.1 Water Jet Pressure

From the testing results, it appears that the disc cutter forces are not affected as the water jet pressure changes between 14.79 and 55.16 MPa, implying that the low pressure water is capable of improving the disc cutting process. The advantages of the use of low pressure water jet have been discussed in Section 6.1.

6.6.2 Cutting Speed

As mentioned previously, the cutting speed is considered as an important factor in the high pressure water jet assisted drag pick cutting and disc cutting tests, as the travel speeds of the jets directly affect the depth of the slots cut by the the jets. This, plus the fact that the disc cutters on a cutterhead of a TBM have different cutting speeds, is the reason that more attention was paid in the study. The graphs of cutting forces with the assistance of a water jet against the cutting speeds within a region of 0.25 m/s to 1.0 m/s (Figs 6.6.1, 6.6.2, 6.6.3, 6.6.4, 6.6.5 and 6.6.6) have shown no regular tendency, which suggests that no significant influence of the cutting speeds to the cutting forces. The cutting forces in the figures are the average values of the forces in different water jet pressure conditions.

6.6.3 Mean Peak Forces and Mean Forces

The increase in the ratio of mean peak force to mean force results in a reduction of the vibrations caused by the changes of the thrust force in TBM boring, this implies that use of water jets may improve the stability of the TBM's. Table 6.6.1 lists a comparison analysis of the mean peak and mean forces. It indicates that

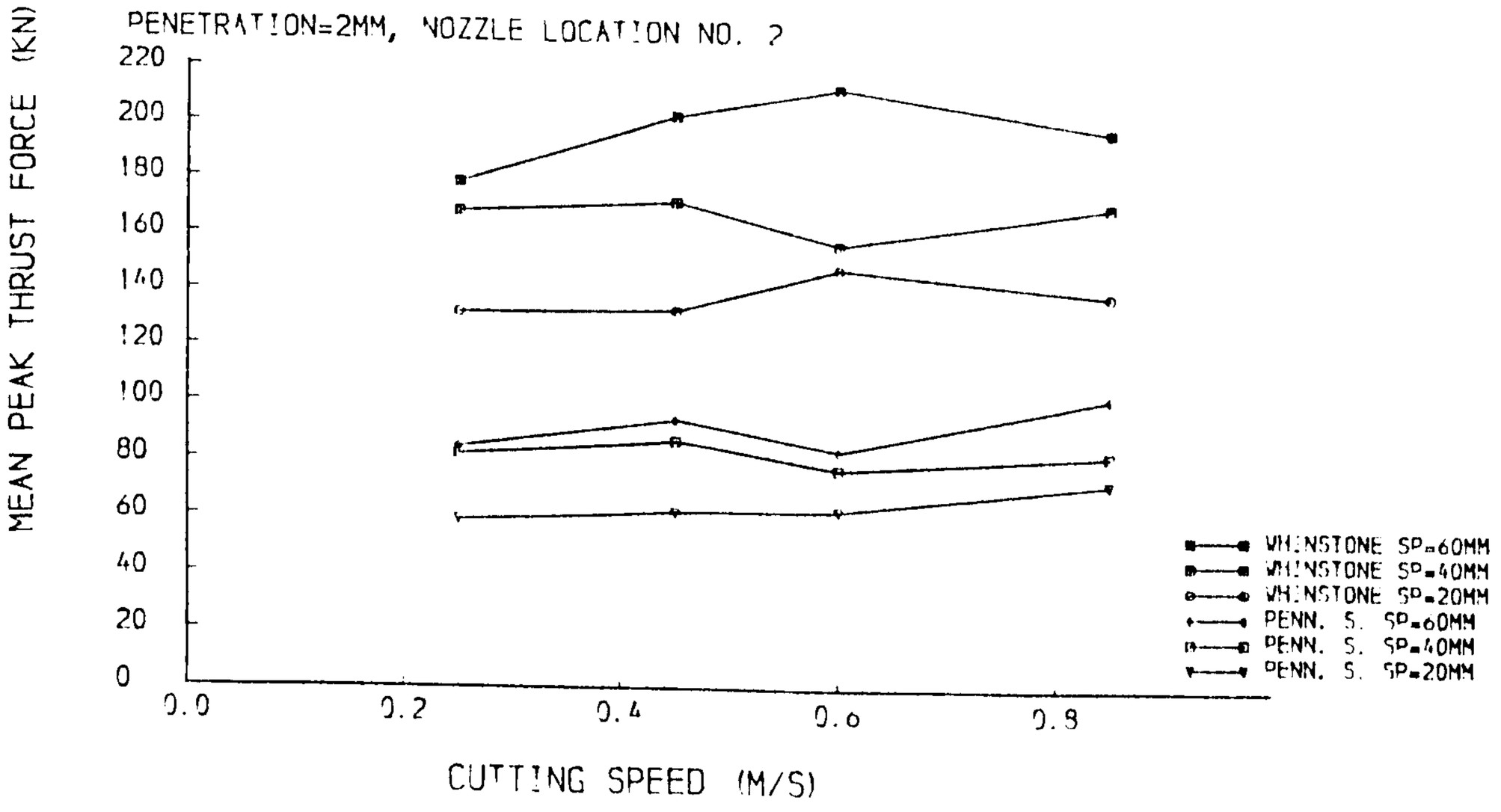

(a). p=2mm

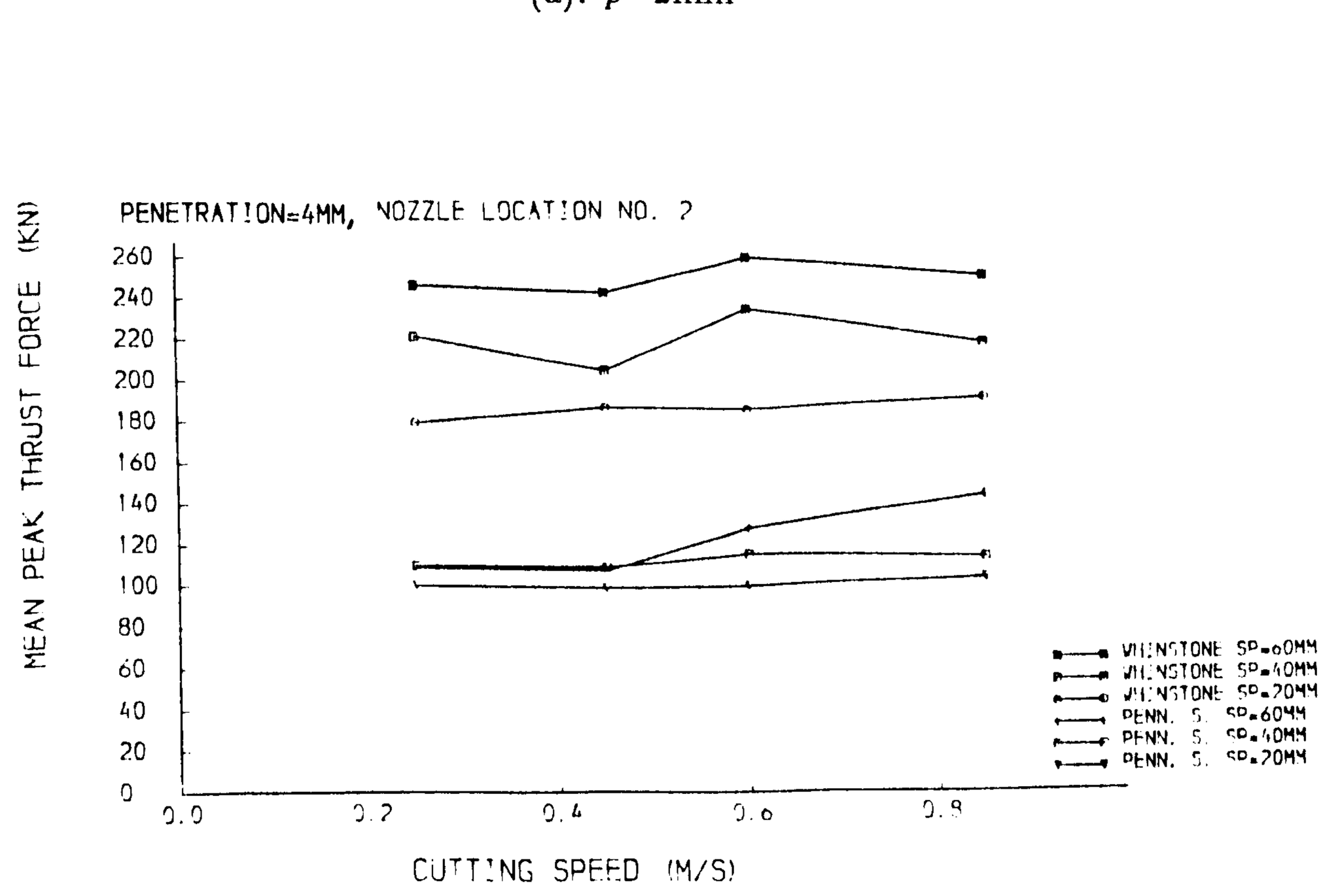

(b). p=4mm

Fig. 6.6.1 Mean peak thrust force versus cutting speed

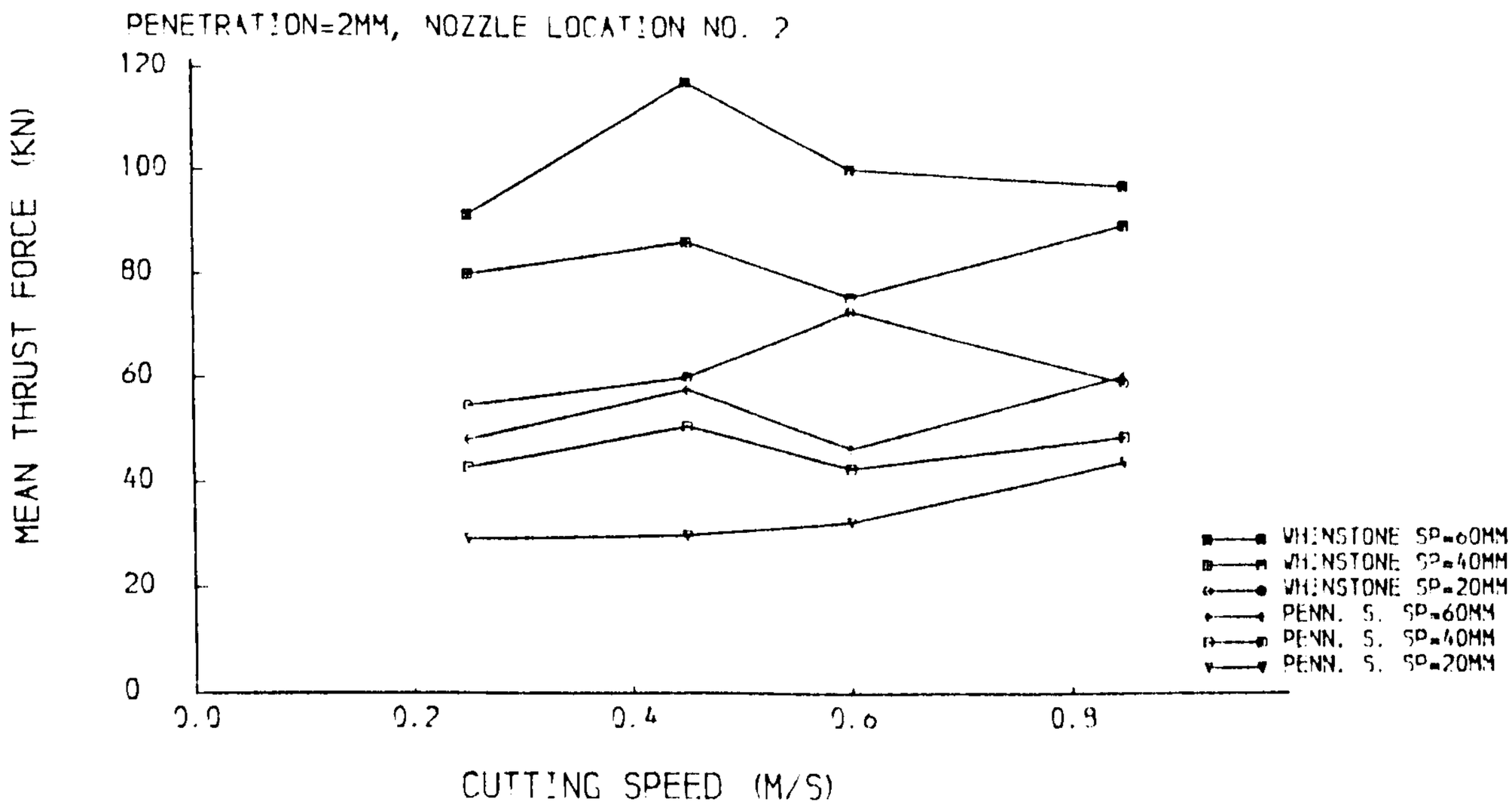

(a). p=2mm

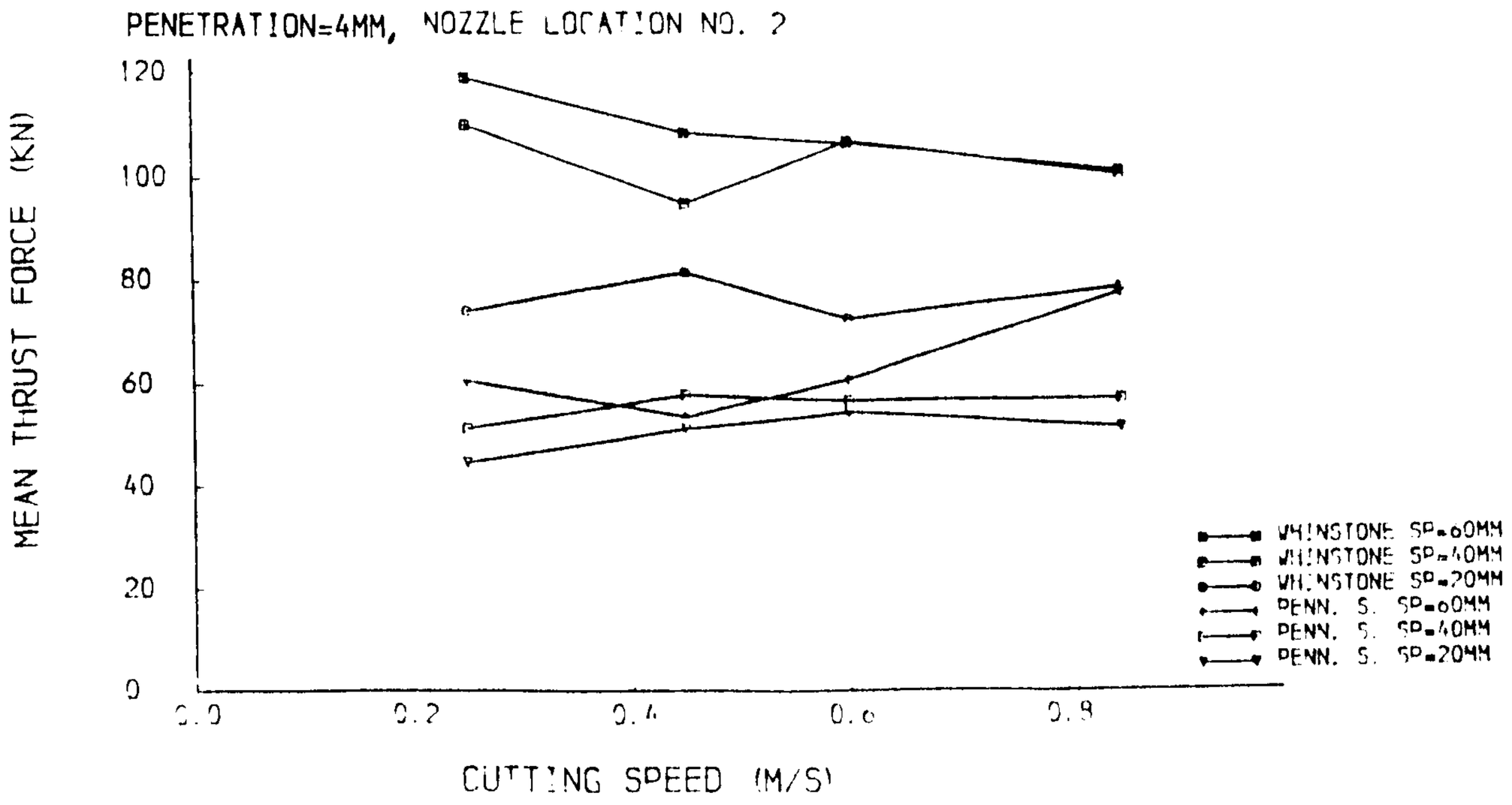

(b). p=4mm

Fig. 6.6.2 Mean thrust force versus cutting speed

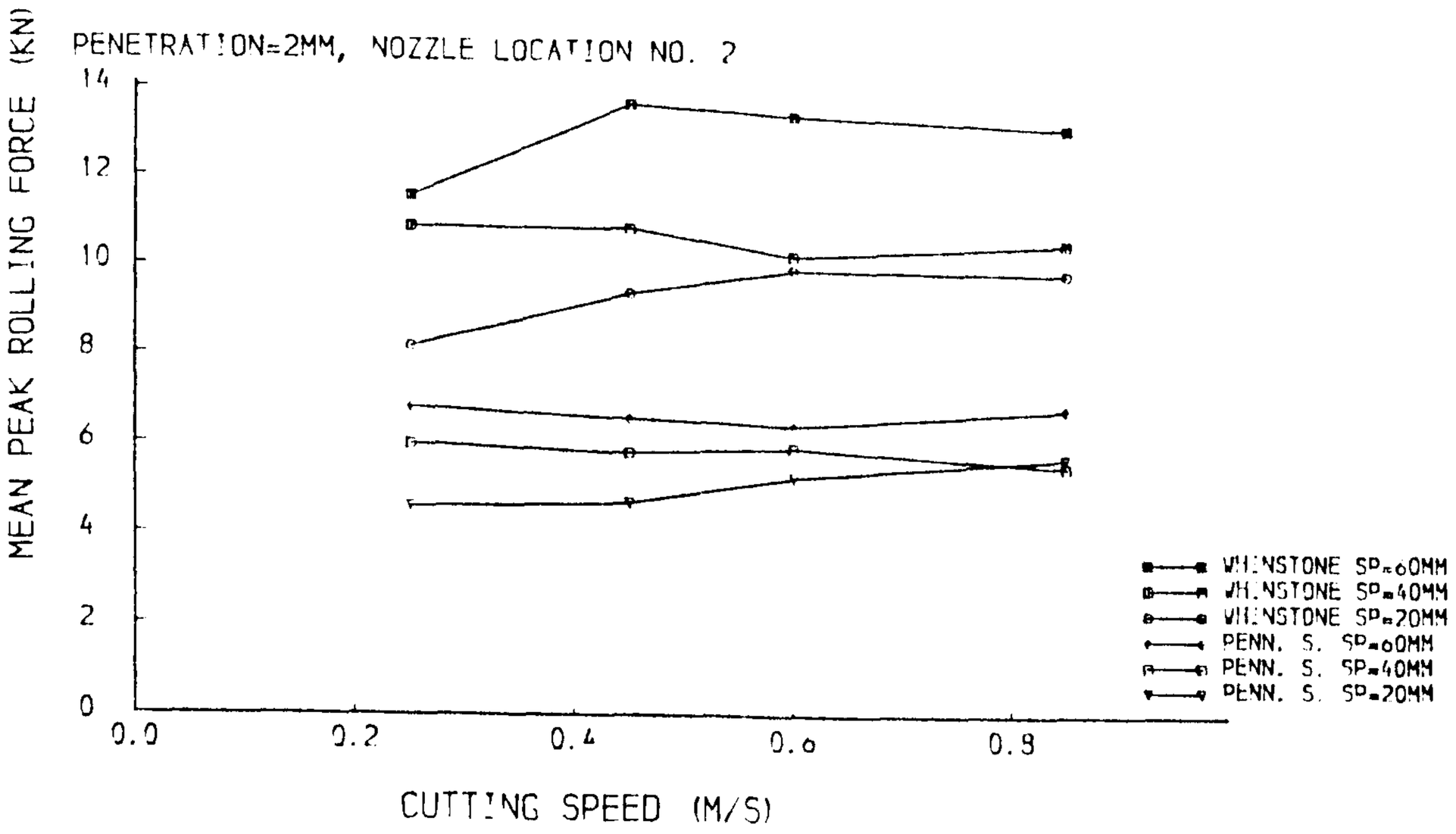

(a). p=2mm

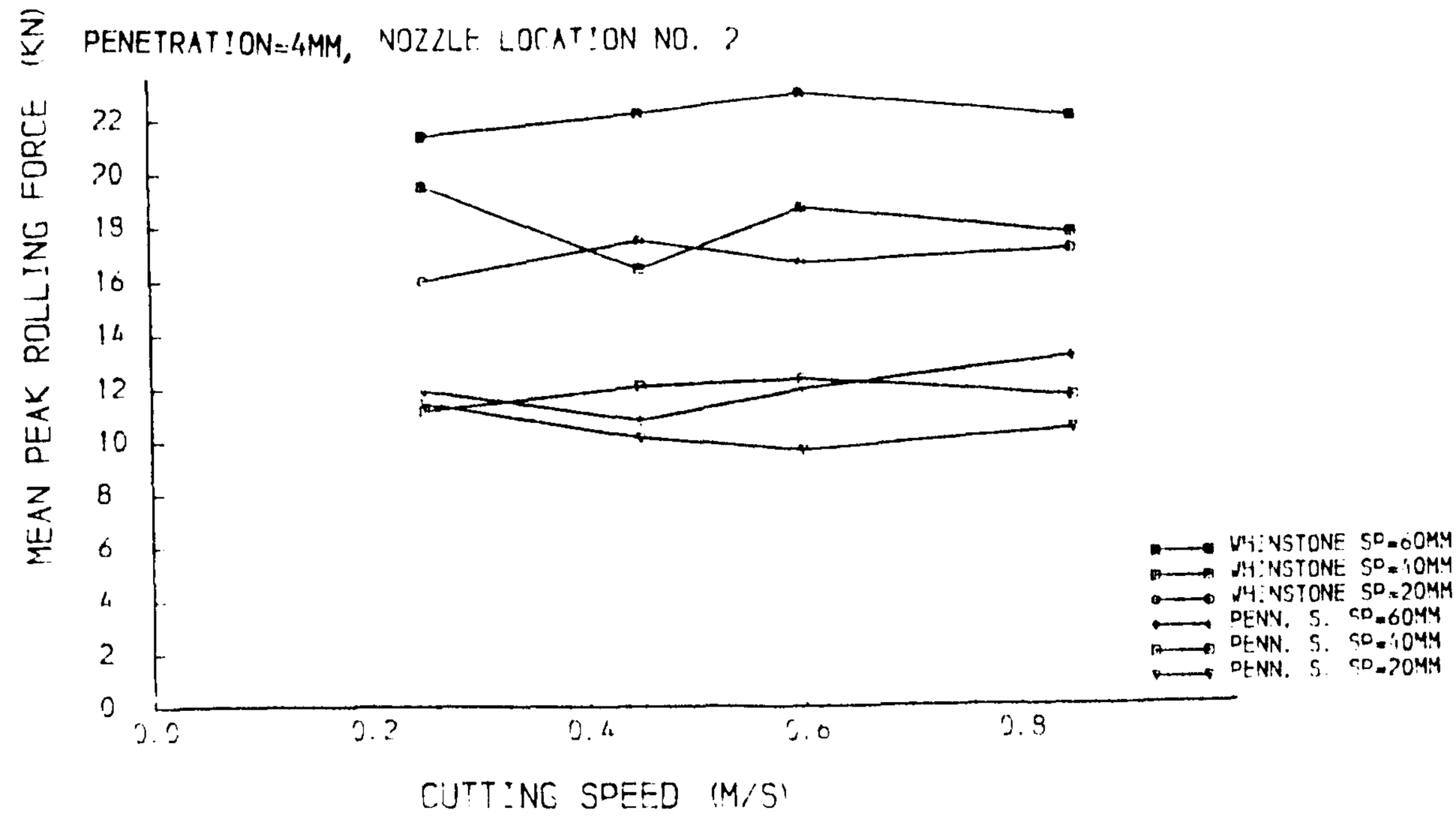

(b). p=4mm

Fig. 6.6.3 Mean peak rolling force versus cutting speed

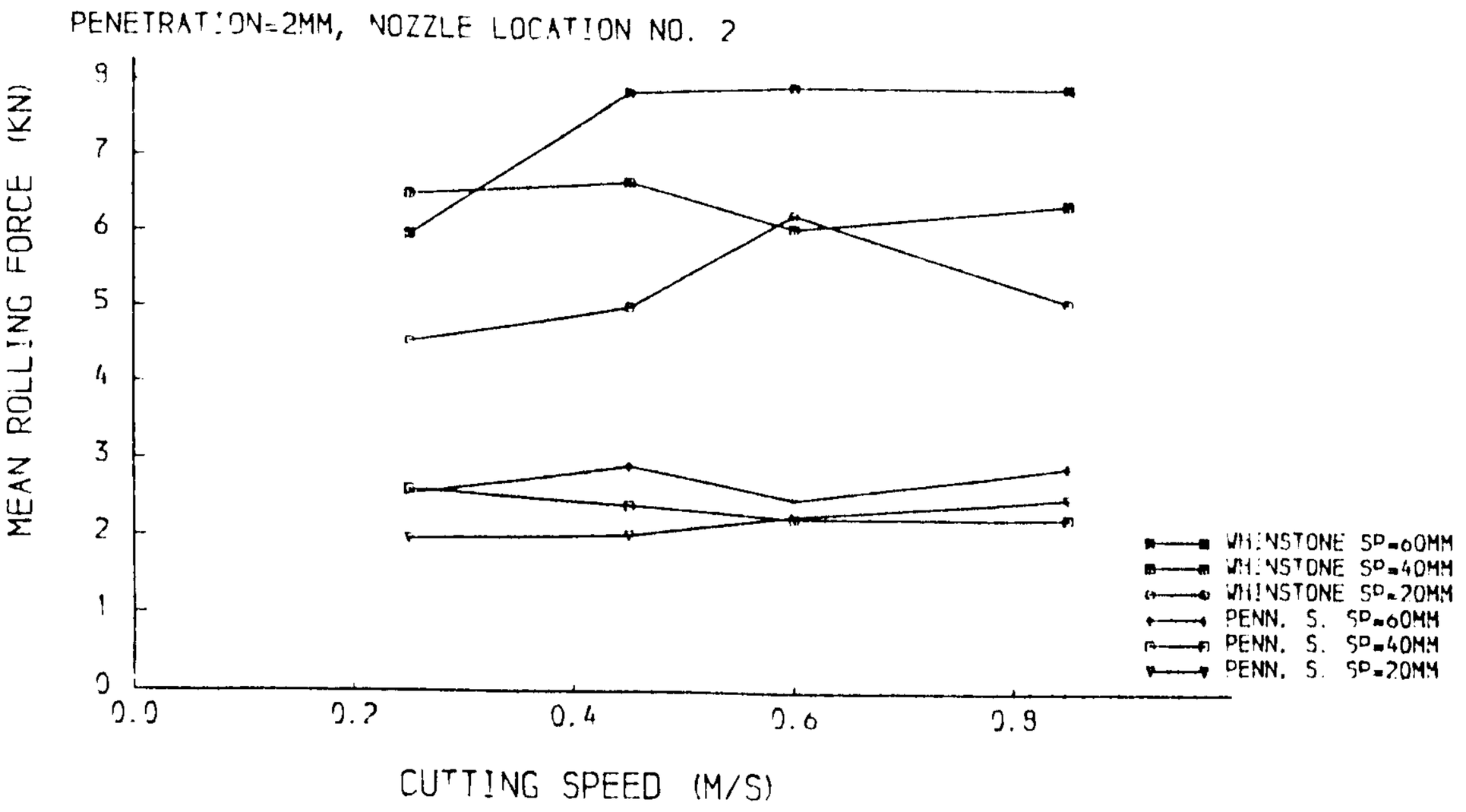

(a). p=2mm

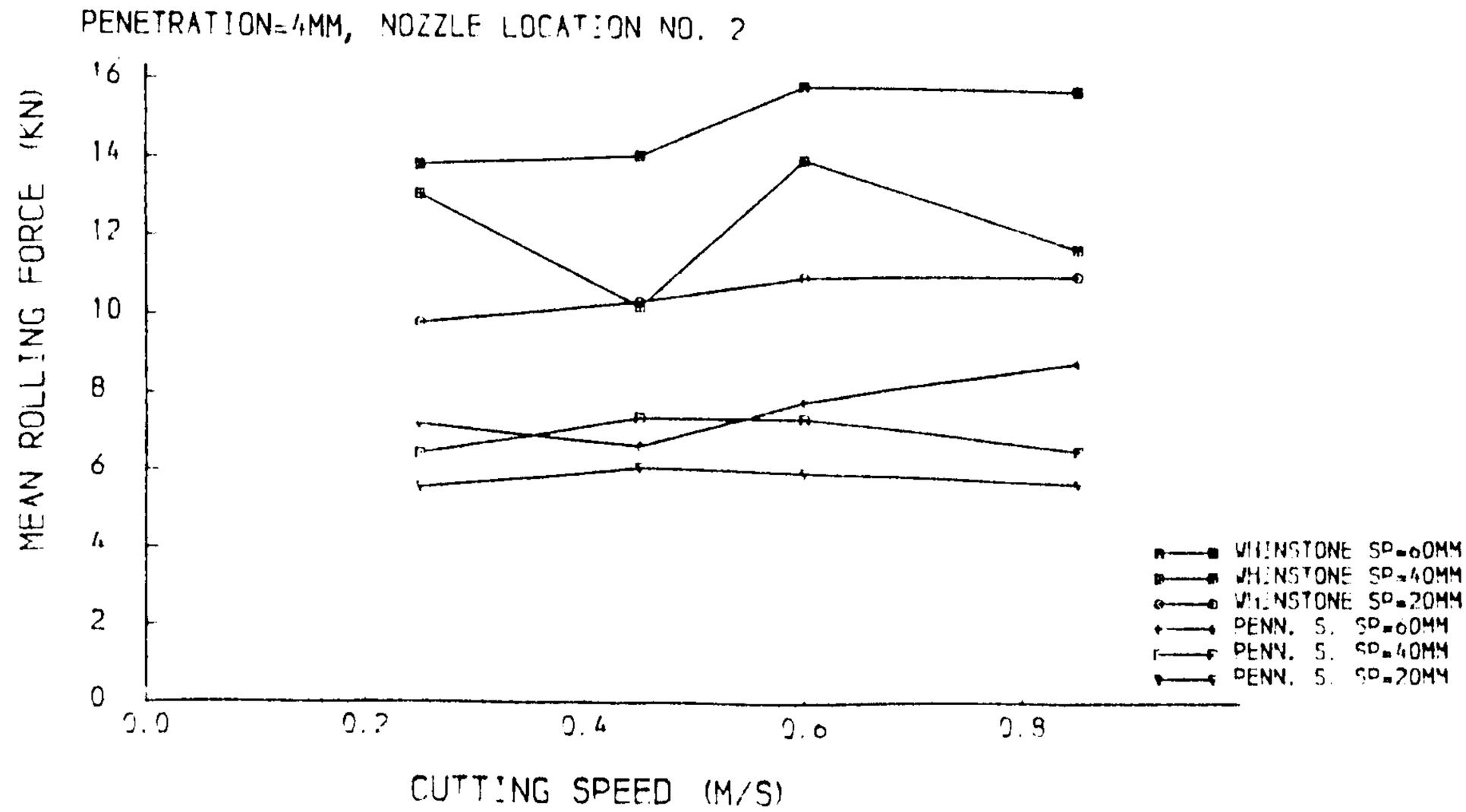

(b). p=4mm

Fig. 6.6.4 Mean rolling force versus cutting speed

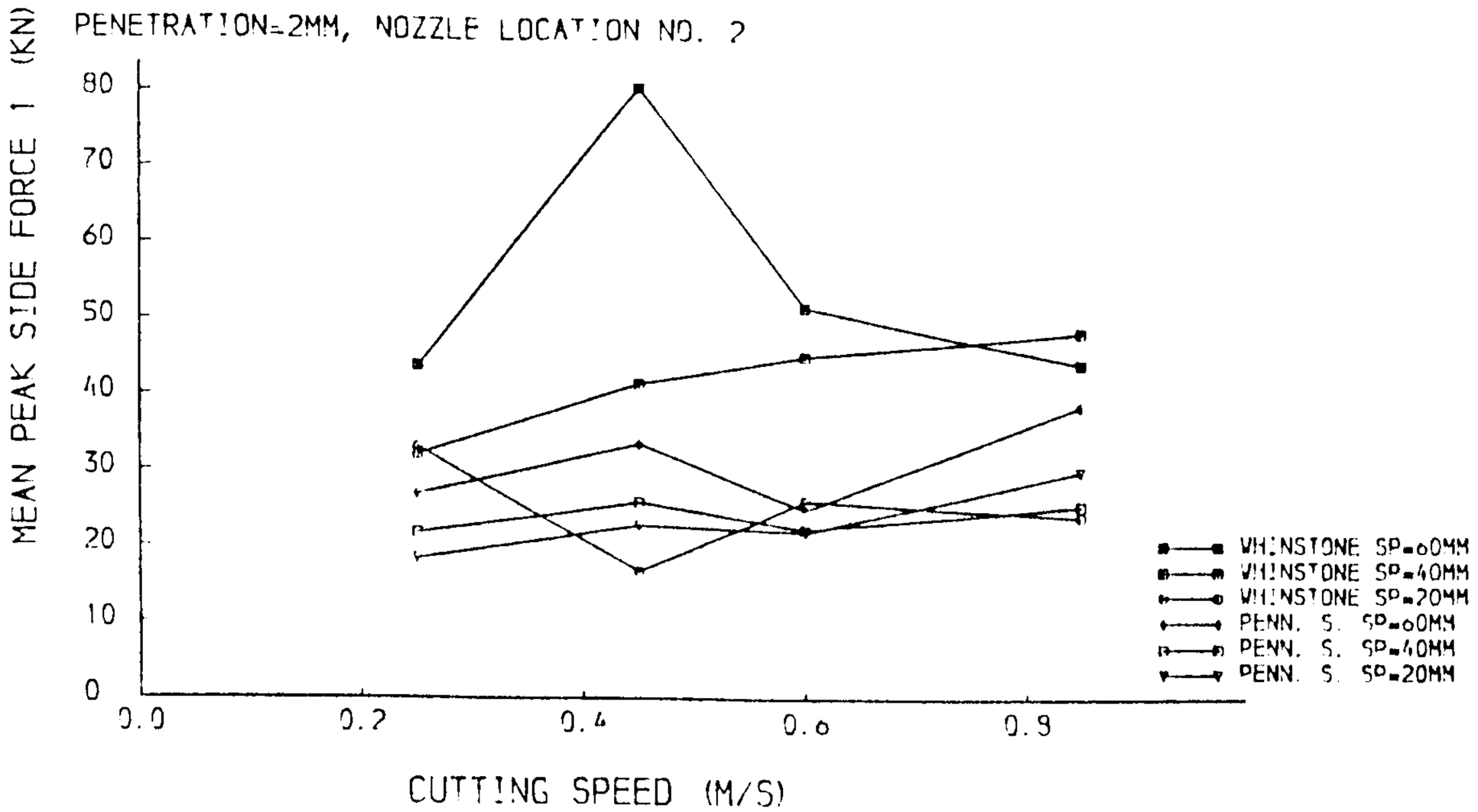

(a). p=2mm

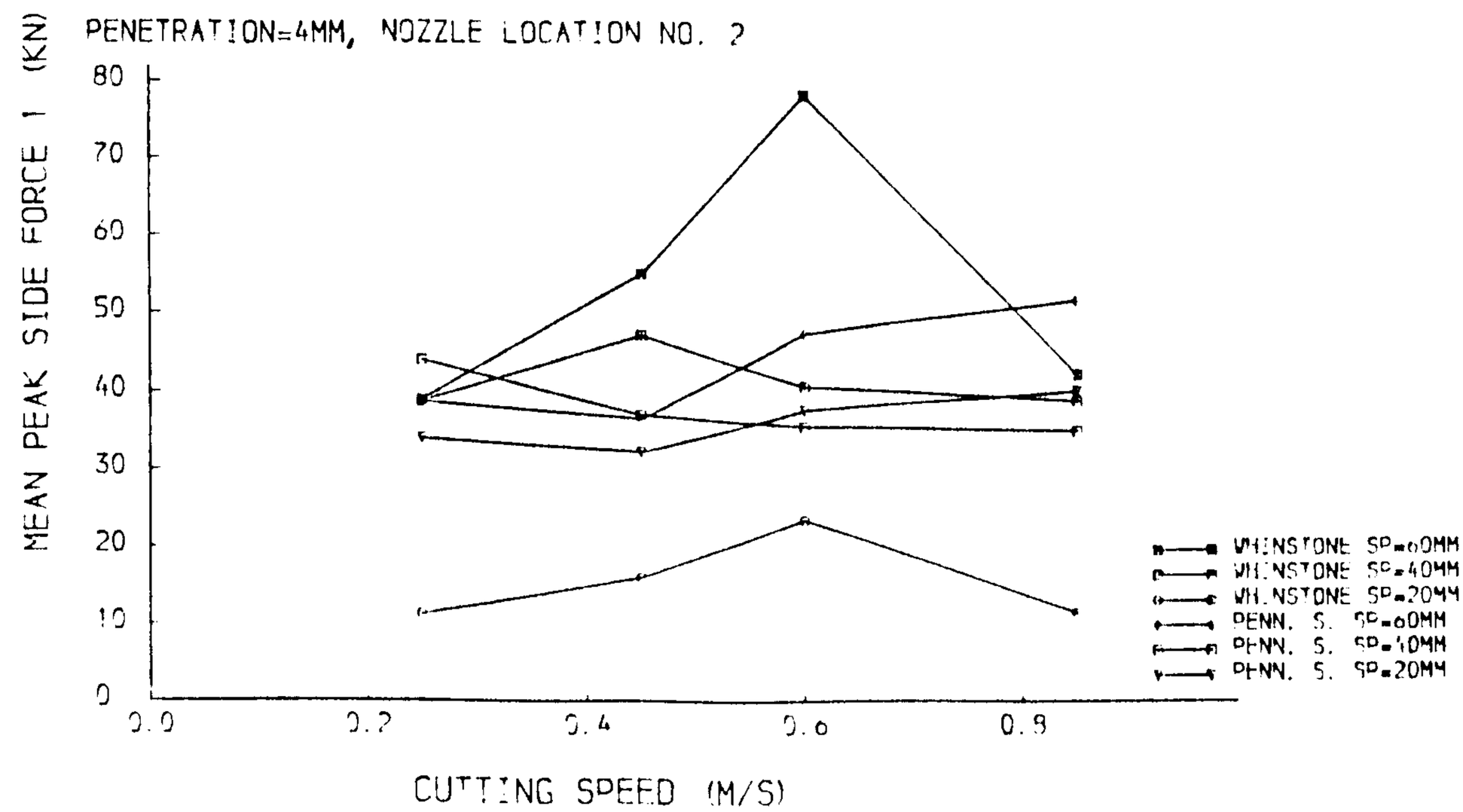

(a). p=4mm

Fig. 6.6.5 Mean peak side force 1 versus cutting speed

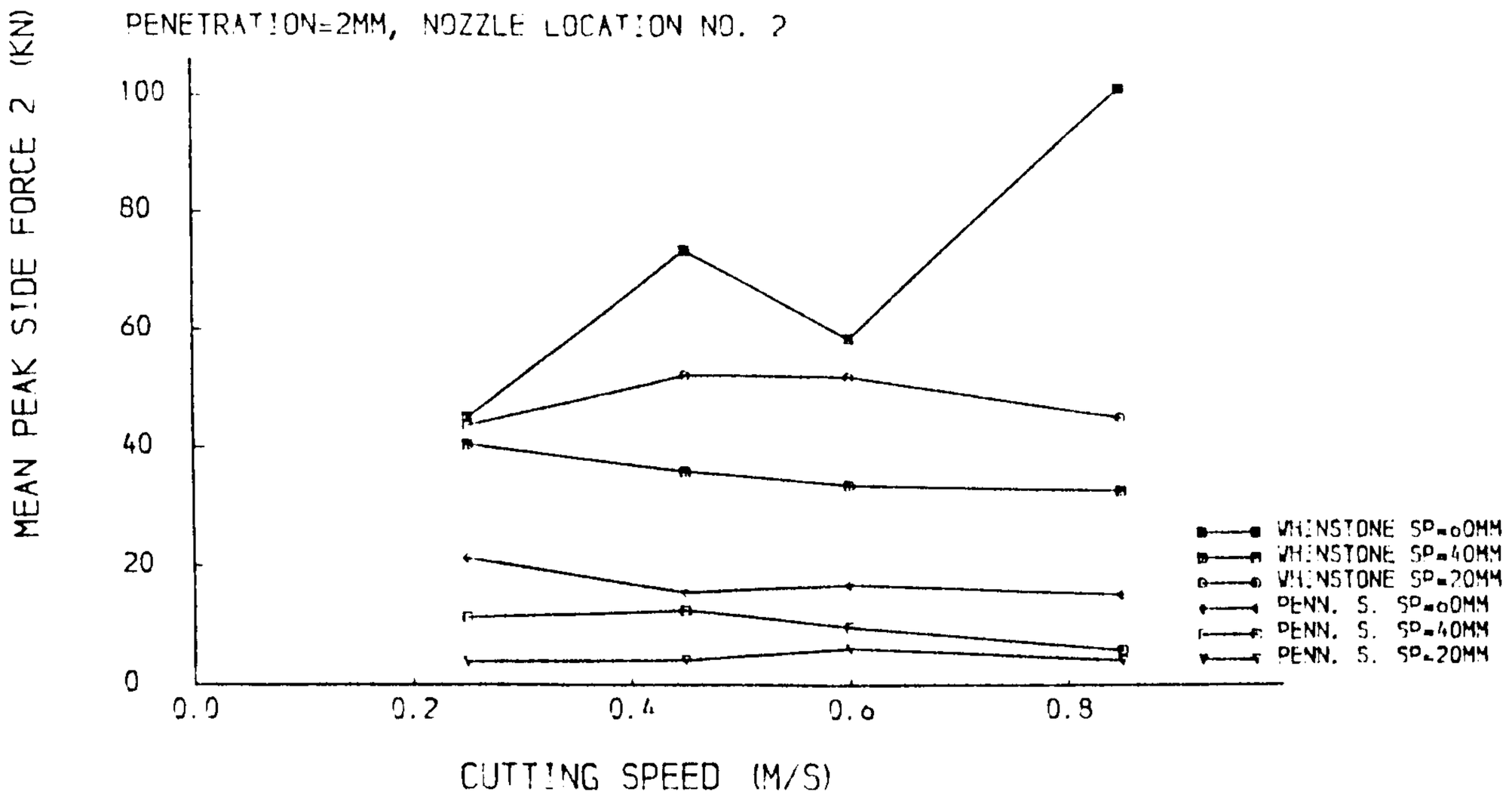

(a). p=2mm

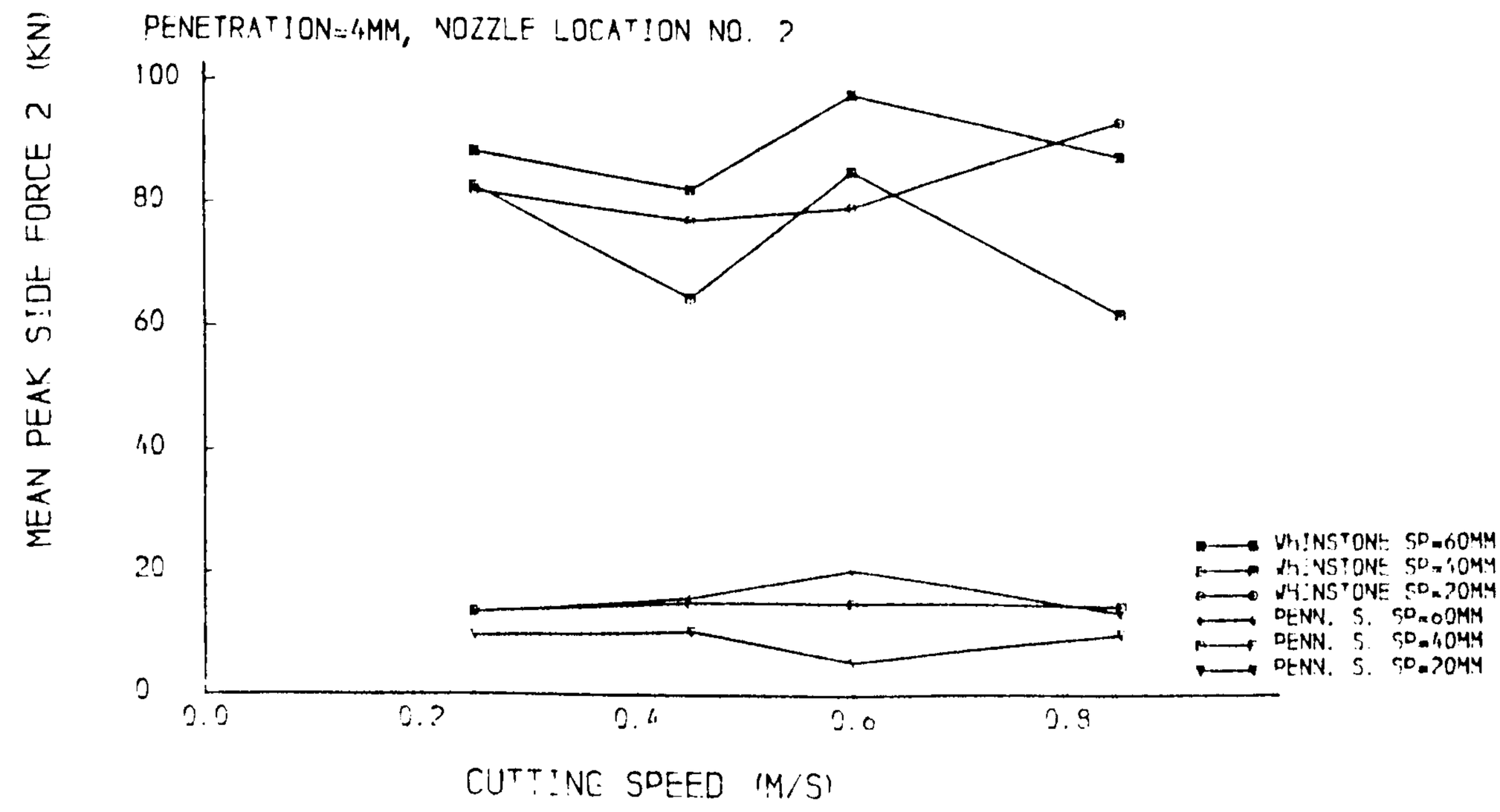

(b). p=4mm

Fig. 6.6.6 Mean peak side force 2 versus cutting speed

in the most of the cases, the improvements can be given by the use of the water jet. The forces of water jet assisted cutting is the average values of the forces with different cutting speed conditions and water jet pressure conditions.

Table 6.6.1 Comparison of mean peak and mean forces

			Pennant Sandstone			Whinstone		
	p	s	MTF / MPTF	MRF / MPRF	MPSF1 / MPSF2	MTF / MPTF	MRF / MPRF	MPSF1 / MPSF2
	mm	mm						
unassisted	2	20	0.50	0.41	5.63	0.44	0.58	0.72
	2	40	0.55	0.44	3.95	0.41	0.59	0.71
	2	60	0.62	0.46	1.45	0.45	0.62	1.56
unassisted	4	20	0.48	0.55	6.44	0.41	0.57	0.19
	4	40	0.48	0.55	2.17	0.48	0.66	0.61
	4	60	0.44	0.57	1.67	0.40	0.58	0.57
water jet	2	20	0.53	0.44	4.98	0.45	0.56	0.52
	2	40	0.57	0.41	2.39	0.50	0.61	1.17
	2	60	0.58	0.41	1.78	0.51	0.58	0.79
water jet	4	20	0.50	0.56	4.02	0.41	0.63	0.19
	4	40	0.50	0.59	2.59	0.47	0.68	0.56
	4	60	0.52	0.64	2.74	0.44	0.67	0.60

6.6.4 Cutter Spacing and Penetration

As the disc spacing in most TBM's is, effectively, fixed by the manufacturer, there is a minimum penetration that will permit disc interaction. For adequate interaction between adjacent discs a s/p ratio of at least six is needed (Poole, 1987). This is the situation of mechanical TBM design. As the water jet assisted TBM's are designed for the hard rock tunnelling, the limitation of the machine thrust can not keep the s/p ratio at about six. Therefore, the interaction may happen not in the every cutting pass, but after several pass, e.g. multiple pass, which is the cutting situation suggested in this study. Figs 6.6.7, 6.6.8, 6.6.9, 6.6.10, 6.6.11 and 6.6.12 illustrated the effect of spacing on the cutting forces. Surprisingly, one may notice that for the case of p=4mm, s=60mm, the thrust force falls to nearly the same

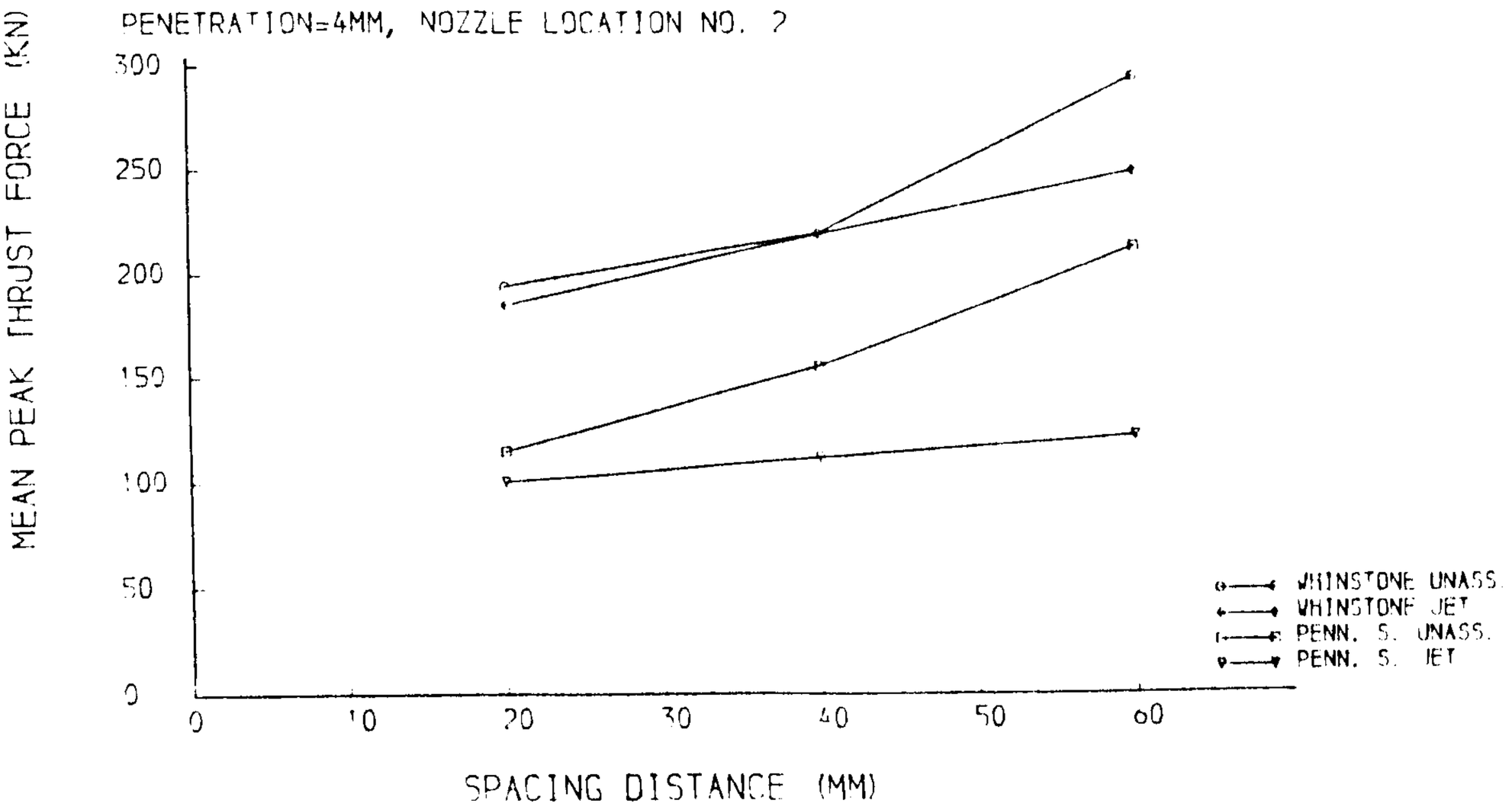

Fig. 6.6.7 Mean peak thrust force versus spacing distance

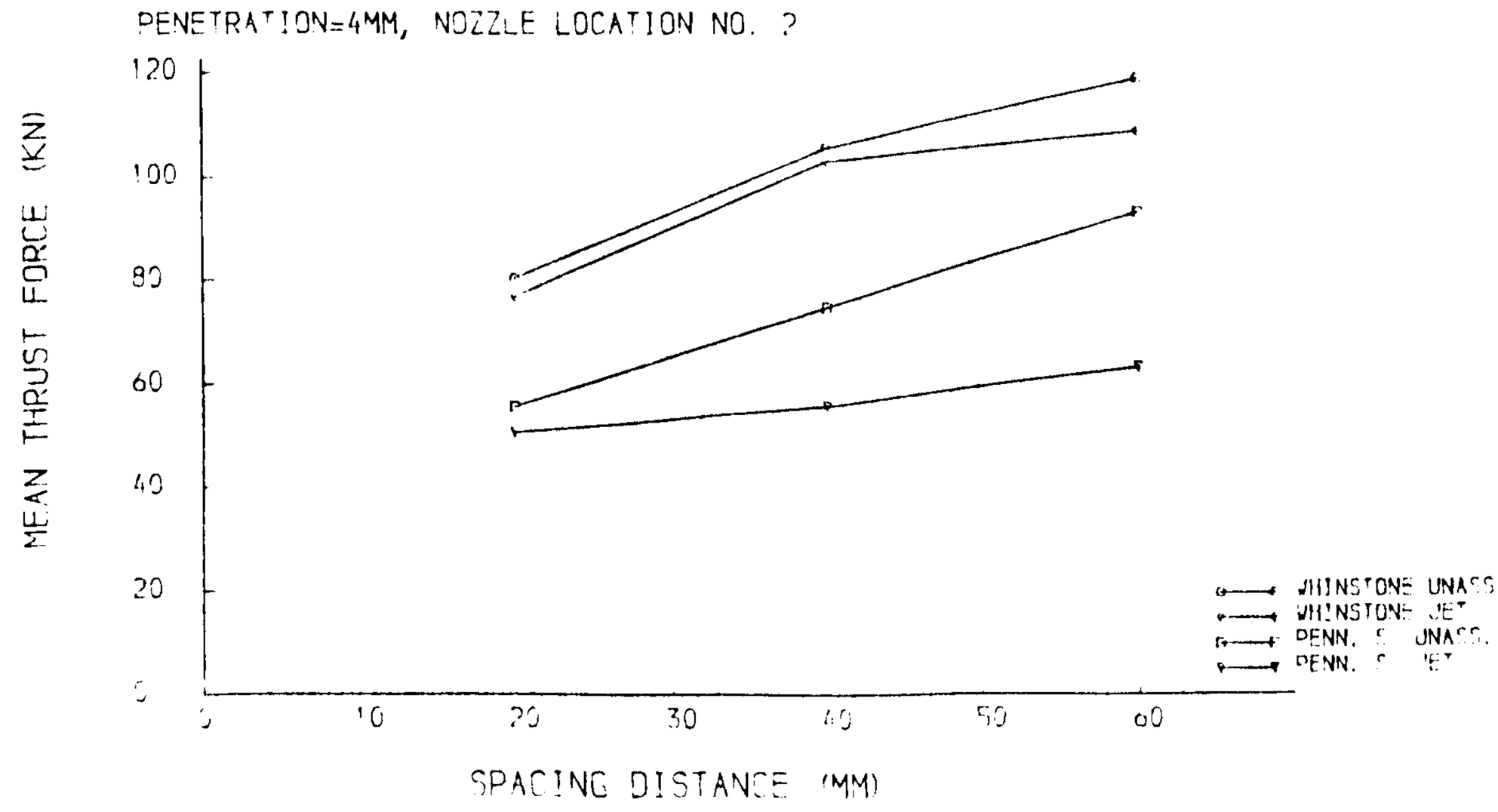

Fig. 6.6.8 Mean thrust force versus spacing distance

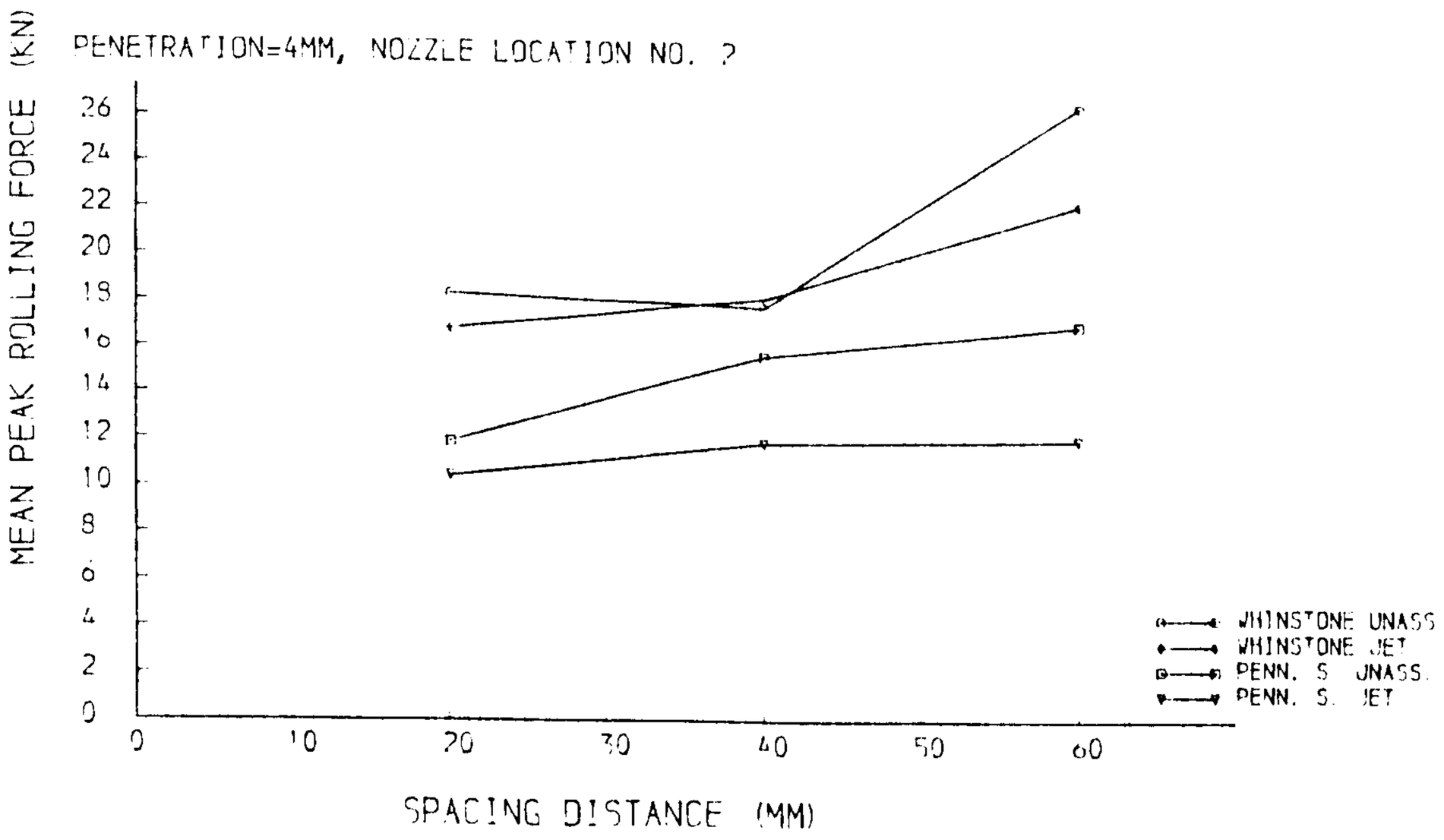

Fig. 6.6.9 Mean peak rolling force versus spacing distance

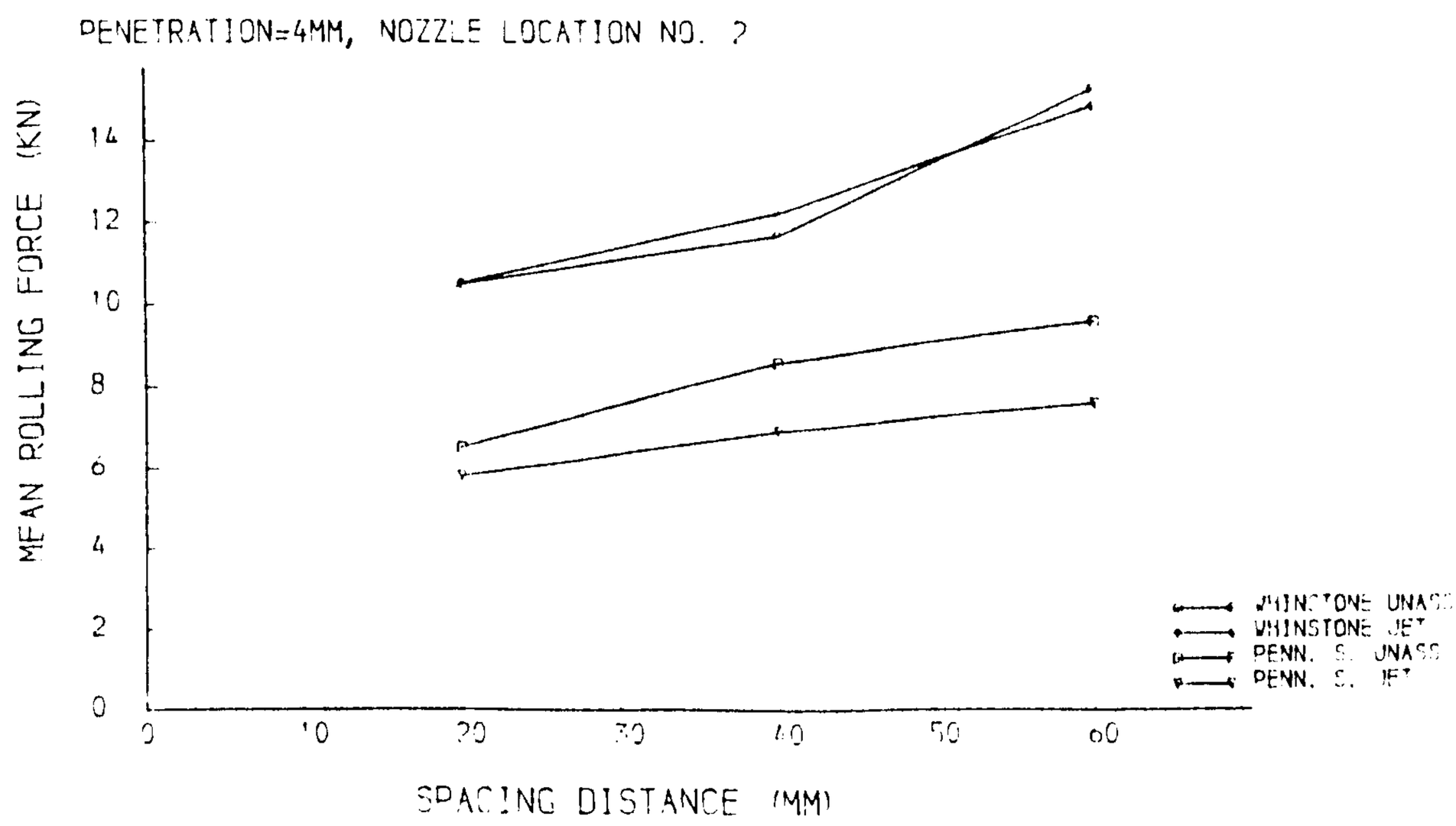

Fig. 6.6.10 Mean rolling force versus spacing distance

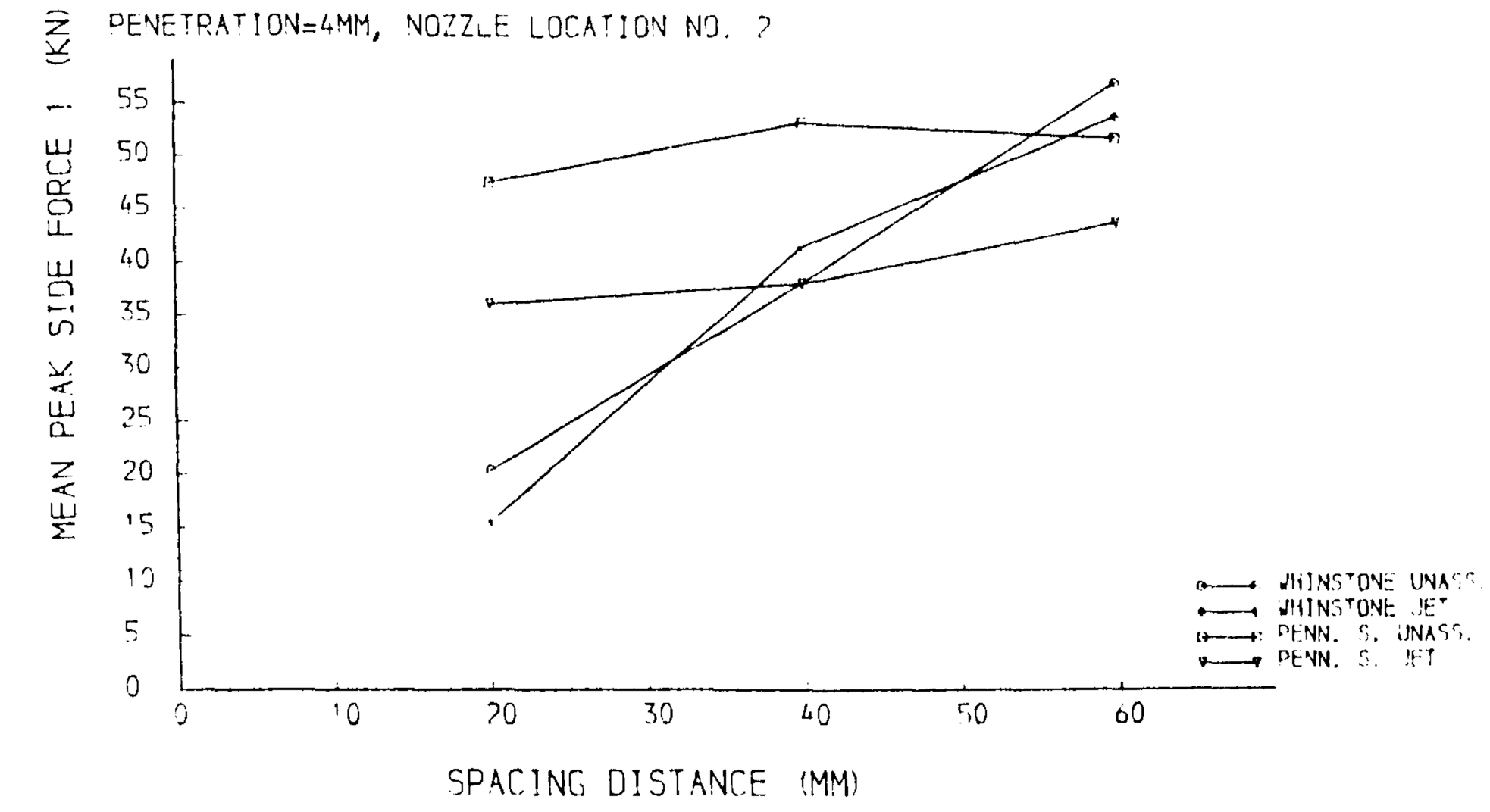

Fig. 6.6.11 Mean peak side force 1 versus spacing distance

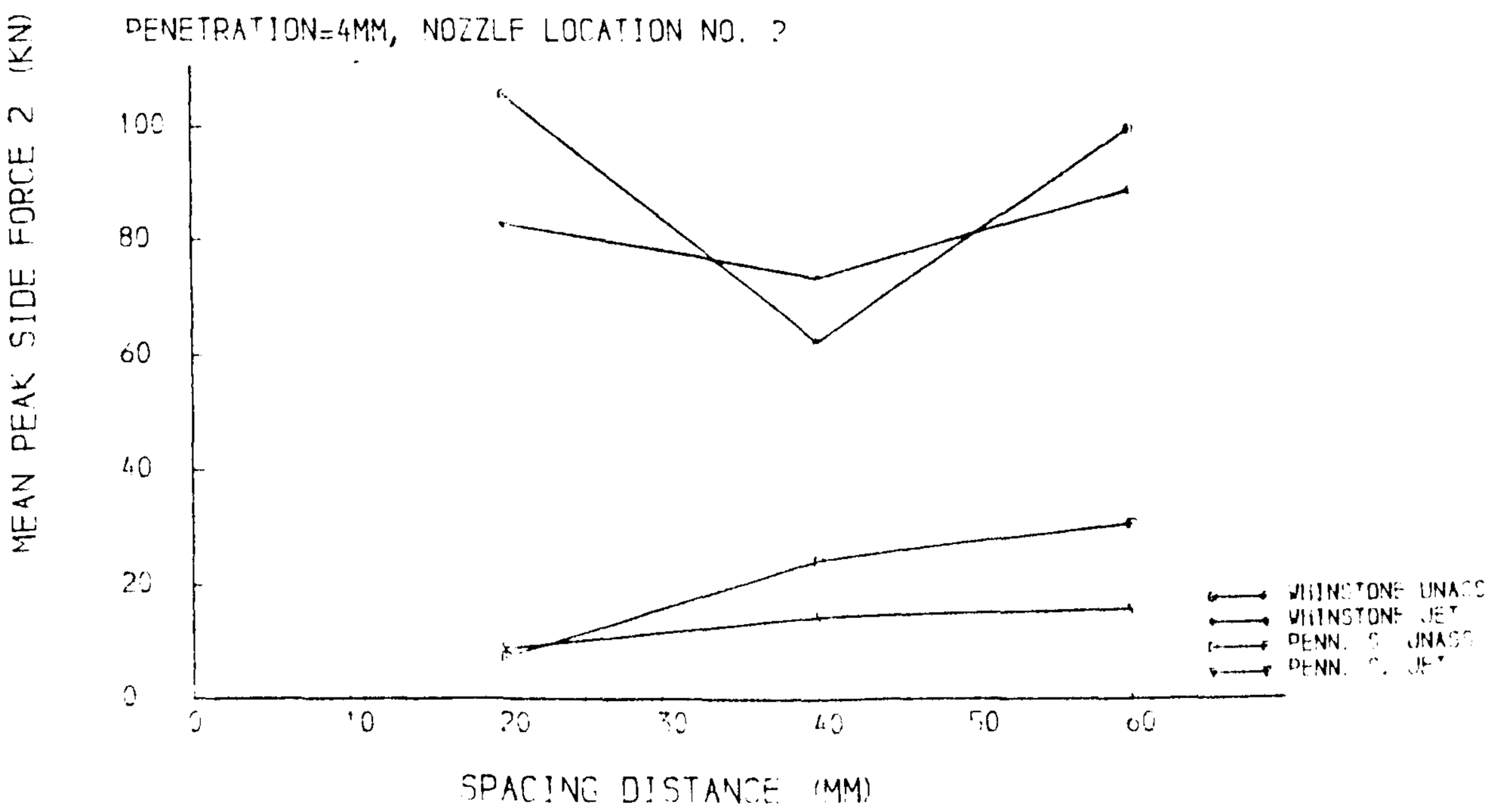

Fig. 6.6.12 Mean peak side force 2 versus spacing distance

level with the thrust force required for the case of s=40mm and s=20mm. This gives a possibility of improving machine cutting ability by use of larger spacing. Meanwhile, it also means that the cutter number can be reduced and with the same total machine thrust, the load on every cutter can be increased.

6.6.5 Specific Energy

Table 6.6.2 Percentage reduction in cutting forces

Rock type	p mm	s mm	MPTF %	MTF %	MPRF %	MRF %
Pennant S.	2.	20.	15.89	10.55	9.98	5.17
	2.	40.	28.37	26.35	27.24	32.39
	2.	60.	24.38	28.40	19.19	27.27
	4.	20.	12.35	8.93	12.20	10.69
	4.	40.	27.85	25.01	24.31	19.16
	4.	60.	42.61	32.01	29.32	20.60
Whinstone	2.	20.	13.23	11.79	18.33	20.76
	2.	40.	14.60	-2.55	14.68	12.19
	2.	60.	13.88	1.62	9.01	15.45
	4.	20.	4.67	4.35	8.09	-0.29
	4.	40.	0.11	2.36	-2.26	-4.70
	4.	60.	15.43	8.48	16.30	2.68

As mentioned in Section 6.3.3, the specific energy is only related to the mean rolling force, because the yield is almost the same for both mechanical cutting and water jet assisted cutting. However, in the hard rock excavation, the major problem faced by the TBM's is thrust limitation (Fig 6.6.19), not torque limitation. In some cases, the reduction of the thrust forces is of the same order with the rolling forces, but it is not true for some other cases, as we can see in Table 6.6.2. Furthermore, the specific energy for the water jet assisted cutting does not include the specific energy provided by the water jet itself, which is much higher than the mechanical specific energy. For such reasons, the specific energy seems not as important as it is in mechanical cutting tests.

6.6.6 Rock Properties

The reductions of disc cutter forces during the water jet assisted disc cutting tests on Whinstone are much less than that on Pennant Sandstone. A similar observation was reported by Ozdemir (1986) when he carried out the low pressure water jet assisted disc cutting tests using Sandstones and Limestones. He pointed out that jets were found to work best in Sandstones, because of their high porosity and granular structure.

In addition to above reasons given by Ozdemir, another possible reason is the brittlness of rock. For example, the rock powder observed during the tests on Pennant Sandstone (Plate 6.5.1) can not be found during the tests on Whinstone. However, as direct experimental confirmation is lacking at this stage, no further conclusion may be drawn.

Chapter 7

THEORETICAL ANALYSIS OF CUTTING FORCES

7.1 INTRODUCTION

The prediction of disc forces is a basic requirement of designers, manufacturers and users of the full-face tunnel boring machines (TBM's). Several reports and papers on the theoretical analysis of cutting forces have been presented since the 1970's (Crow, 1975; Roxborough and Phillips, 1975,a; Ozdemir et al., 1977; Sanio, 1985). All of these theories employed or partly dependent on the assumption that:
1. the rock is first crushed in a zone just beneath the tool;
2. the stresses discributed on the crushed zone are approximately hydrostatic.

In this Chapter, and based on the above widely accepted assumption, a simple mathematical derivation of disc cutting forces is undertaken. Then the effects of spacing and penetration of the cutting are considered. The theoretical predictions are compared with the results of this study and the published laboratory test data of other workers (Roxborough and Phillips, 1975,b; Ozdemir et al., 1977; Snowdon et al., 1982; Bilgin 1977; Moses, 1985).

7.2 THEORETICAL ANALYSIS

7.2.1 Analysis of Unrelieved Cutting

If only the contact zone is considered, the curve of any shape of cutting tool surface can be approximately expressed by a function — $f(X, Y, Z)$. Because of

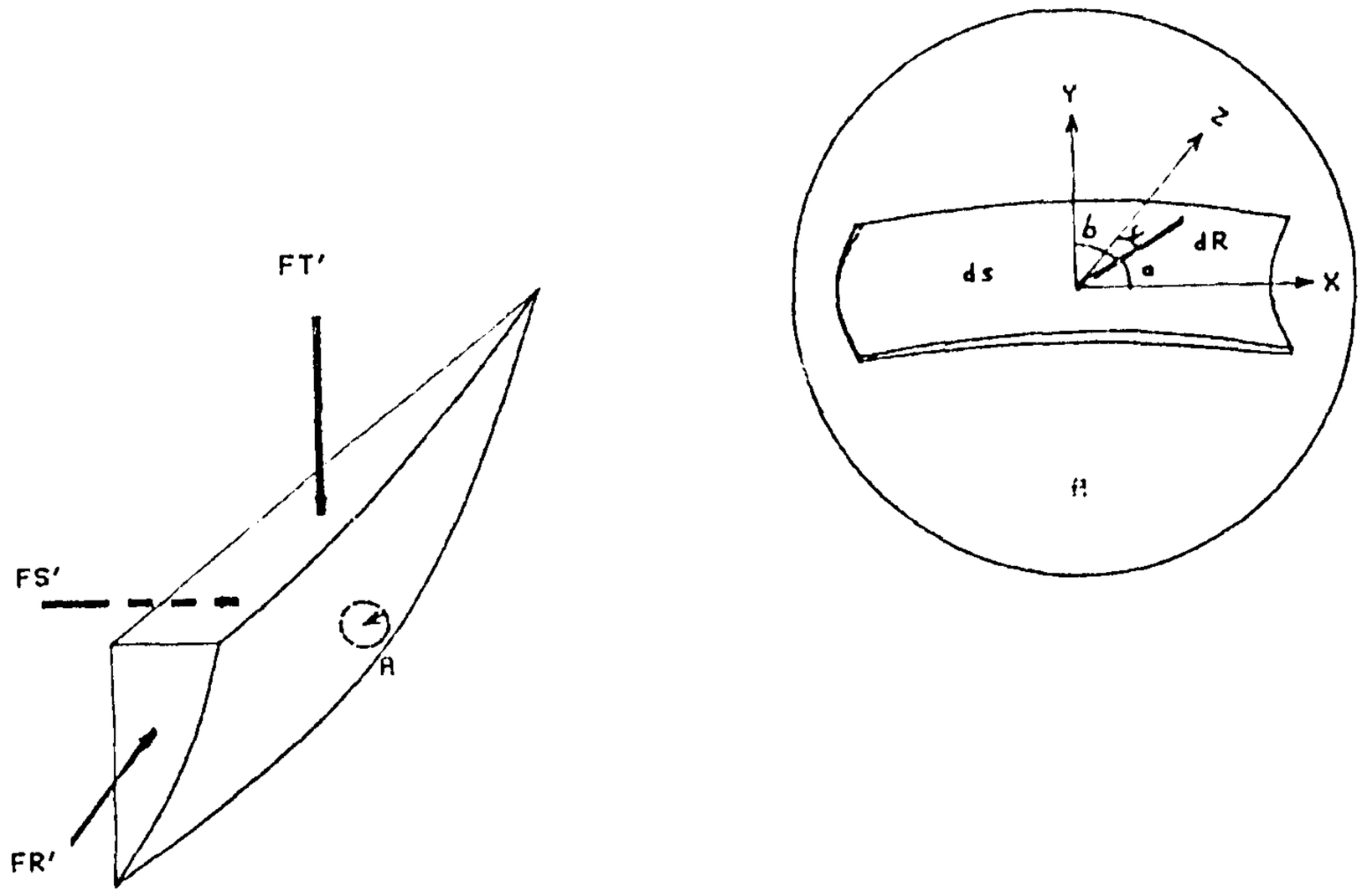

Fig. 7.2.1 Disc cutter forces

symmetry, only half of the crushed zone is considered in the analysis. As shown in Fig. 7.2.1, assuming that the forces from a cutting tool are thrust force FT', rolling force FR' and side force FS', acting on the projected areas of the three principle planes of the crushed zone, then the total thrust force, FT must be twice FT'. This is equally true for the total rolling force FR, but not for the total side force FS, $FS = FS'$. Thus, using the following procedure, all these forces may be determined:

Firstly, a small element with a surface area ds is separated from the crushed zone (Fig. 7.2.1). The forces acting on the element are the three components, acting in the directions X, Y and Z. Consequently, the resultant force dR can have a form:

$$dR = \sigma_0 ds \qquad 7.2.1$$

where

σ_0 = hydrostatic stress in the crushed zone.

The direction of the resultant force on the element should be normal to the surface of the element, if friction on the crushed zone is neglected.

The angles between resultant force and force components are as follows:

$$\left.\begin{aligned} \cos\alpha &= \frac{f_x}{\sqrt{f_x^2+f_y^2+f_z^2}} \\ \cos\beta &= \frac{f_y}{\sqrt{f_x^2+f_y^2+f_z^2}} \\ \cos\gamma &= \frac{f_z}{\sqrt{f_x^2+f_y^2+f_z^2}} \end{aligned}\right\} \qquad 7.2.2$$

where

$f_x = dF/dx$

$f_y = dF/dy$

$f_z = dF/dz$

Then the cutting forces on the element can be expressed as:

$$\left.\begin{aligned} dFT' &= \sigma_0 \cos\alpha ds \\ dFR' &= \sigma_0 \cos\beta ds \\ dFS' &= \sigma_0 \cos\gamma ds \end{aligned}\right\} \qquad 7.2.3$$

because

$$\left.\begin{aligned} ds\cos\alpha &= dA_t' \\ ds\cos\beta &= dA_r' \\ ds\cos\gamma &= dA_s' \end{aligned}\right\} \qquad 7.2.4$$

where

dA_t', dA_r', dA_s' are the projected areas of element ds.

Now, the forces acting on the principle plates can be obtained:

$$\left.\begin{aligned} dFT &= 2dFT' = 2\sigma_0 dA_t' \\ dFR &= 2dFR' = 2\sigma_0 dA_r' \\ dFS &= dFS' = \sigma_0 dA_s' \end{aligned}\right\} \qquad 7.2.5$$

Finally, integrating all forces in Eq(7.2.5) gives:

$$\left.\begin{aligned} FT &= \sigma_0 A_t \\ FR &= \sigma_0 A_r \\ FS &= \sigma_0 A_s \end{aligned}\right\} \qquad 7.2.6$$

where

A_t, A_r and A_s are the projected areas of the crushed zone.

If the edge of the disc cutter is sharp, the projected areas can be approximated as:

$$\left.\begin{aligned} A_t &= \tfrac{4}{3} p \tan\tfrac{\theta}{2} \sqrt{Dp - p^2} \\ A_r &= p^2 \tan\tfrac{\theta}{2} \\ A_s &= \tfrac{2}{3} p \sqrt{Dp - p^2} \end{aligned}\right\} \qquad 7.2.7$$

It is easy now to obtain the relationships of all forces:

$$\frac{FT}{FR} = \frac{A_t}{A_r} = \frac{4}{3}\sqrt{\frac{D}{p} - 1} \qquad 7.2.8$$

$$\frac{FT}{FS} = \frac{A_t}{A_s} = 2\tan\frac{\theta}{2}. \qquad 7.2.9$$

For a worn disc cutter with a tip radius r (Fig. 7.2.2), the projected area, Ar_t, acting against disc cutter thrust force becomes approximately:

$$Ar_t = \begin{cases} \tfrac{4}{3} p \sqrt{2r - p} \sqrt{D' - p}, & \text{when } p \le r(1 - \sin\tfrac{\theta}{2}); \\ \tfrac{4}{3} p' \tan\tfrac{\theta}{2} \sqrt{D'p' - p'^2}, & \text{when } p > r(1 - \sin\tfrac{\theta}{2}). \end{cases} \qquad 7.2.10$$

where

$$p' = p - r\left(1 - \frac{1}{\sin\frac{\theta}{2}}\right).$$

$$D' = D - 2r\left(1 - \frac{1}{\sin\frac{\theta}{2}}\right).$$

Ar_r, acting against the rolling force is:

$$Ar_r = \begin{cases} \tfrac{\phi}{2} r^2 - \sqrt{p}\sqrt{(r-p)^3}, & \text{when } p \le r(1 - \sin\tfrac{\theta}{2}); \\ (p'^2 - p''^2)\tan\tfrac{\theta}{2} + r^2\left(\tfrac{\phi'}{2} - \cos\tfrac{\theta}{2}\sin\tfrac{\theta}{2}\right), & \text{when } p > r(1 - \sin\tfrac{\theta}{2}). \end{cases} \qquad 7.2.11$$

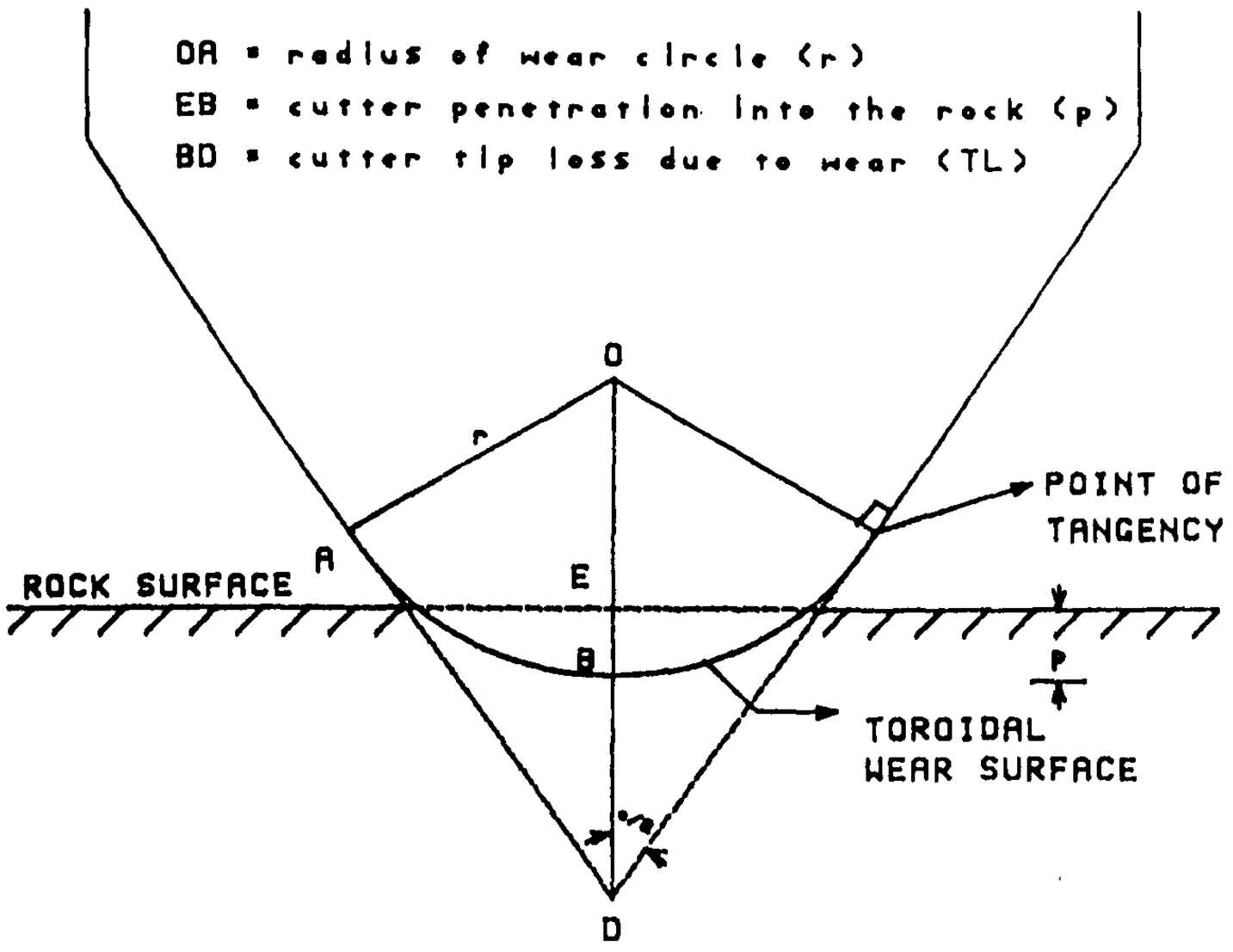

Fig. 7.2.2 The toroidal surface used for development of predictor equation for worn disc cutter (Ozdemir et al., 1977)

where

$$p'' = -r\left(\sin\frac{\theta}{2} - \frac{1}{\sin\frac{\theta}{2}}\right),$$

$$\phi = \tan^{-1}\sqrt{\frac{p}{r-p}}.$$

$$\phi' = \frac{\pi(180^\circ - \theta)}{180^\circ}$$

For the side force, Ar_s is:

$$Ar_s = \frac{2}{3}p\sqrt{D'p - p^2} \qquad 7.2.12$$

7.2.2 Analysis of Relieved Cutting

It is very important to note that the above formulae are only applicable to the unrelieved cutting condition. In fact, the spacing distance plays a very important role in both field experiments and laboratory tests of rock cutting.

At small s/p ratios, crack propagating from one groove interact with the cracks produced by indentation of the cutter in the neighbouring groove, and chip formation happens at lower cutter forces than would be required for chip release from grooves spread further apart. From the laboratory tests given by several workers (Ozdemir et al, 1977; Snowdon et al, 1982), it can be found that the effect of spacing is limited when the ratios of spacing and penetration (s/p) approach a critical value.

At s/p ratios larger than some critical value, grooves are too far apart for the interaction to occur, and chips form at applied force levels which are independent of further increases in groove spacing. Considering single pass tests on a smooth rock surface, the work of this study has shown the critical value of s/p ratio to be about 10, and for single pass tests on a previous cutting surface (see Snowdon et al., 1982) to be about 20. For multiple pass tests, the critical value could be more than 50, but equal to 20 when the independent thrust forces are the same as the thrust force in relieved cutting (see Ozdemir et al., 1977).

In order to determine the effects of s/p ratios on cutting forces, there are two ways which can be considered. The first is to find the relationship between the unrelieved cutting forces and the relieved cutting forces and the second is to use indentation fracture analysis.

The relieved cutting forces and unrelieved cutting forces are defined as follows, for the first method

$(FT)_{re}$= relieved thrust force

$(FT)_{un}$= unrelieved thrust force

$(FR)_{re}$= relieved rolling force

$(FR)_{un}$= unrelieved rolling force

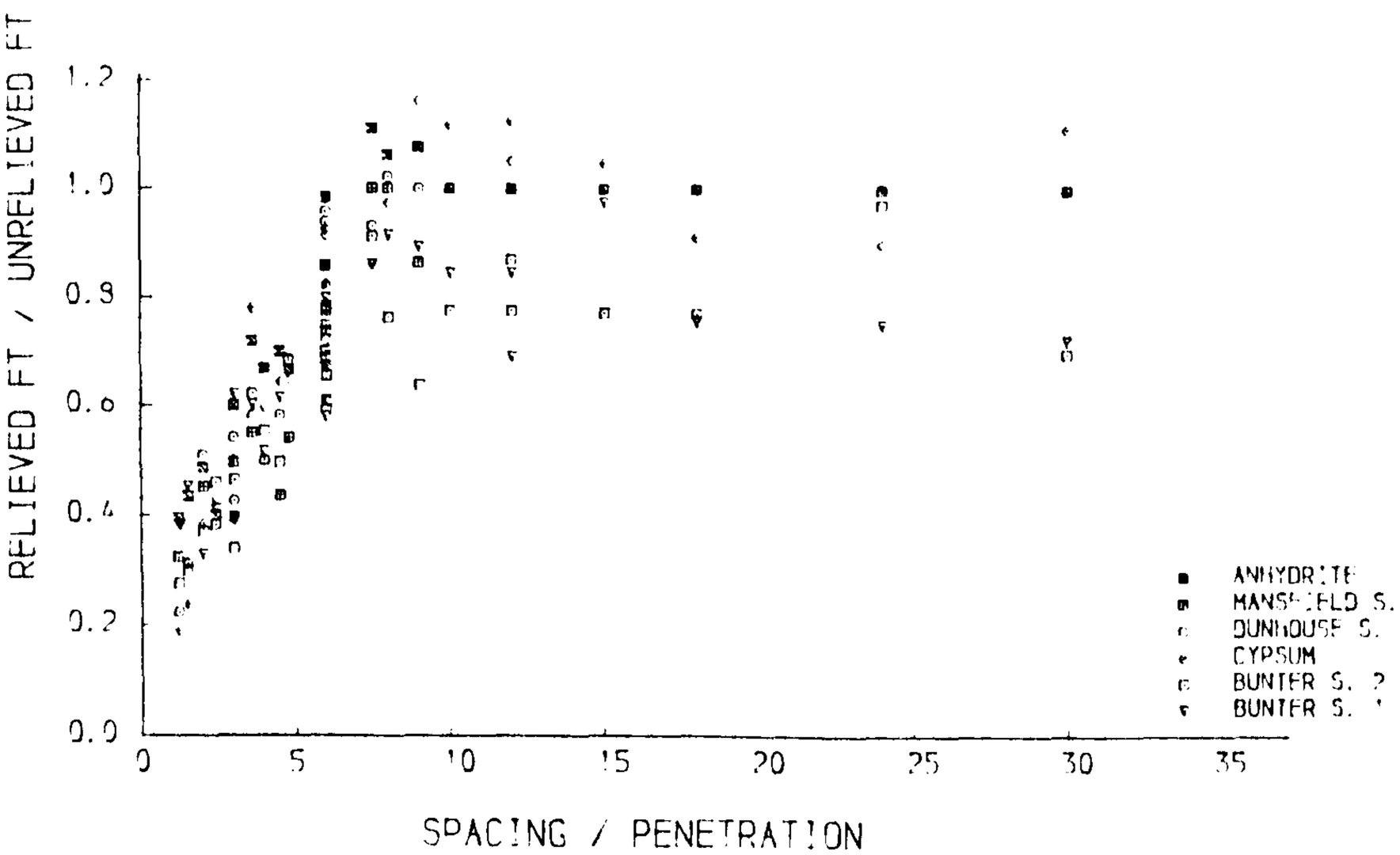

Fig. 7.2.3 $(FT)_{re}/(FT)_{un}$ versus s/p

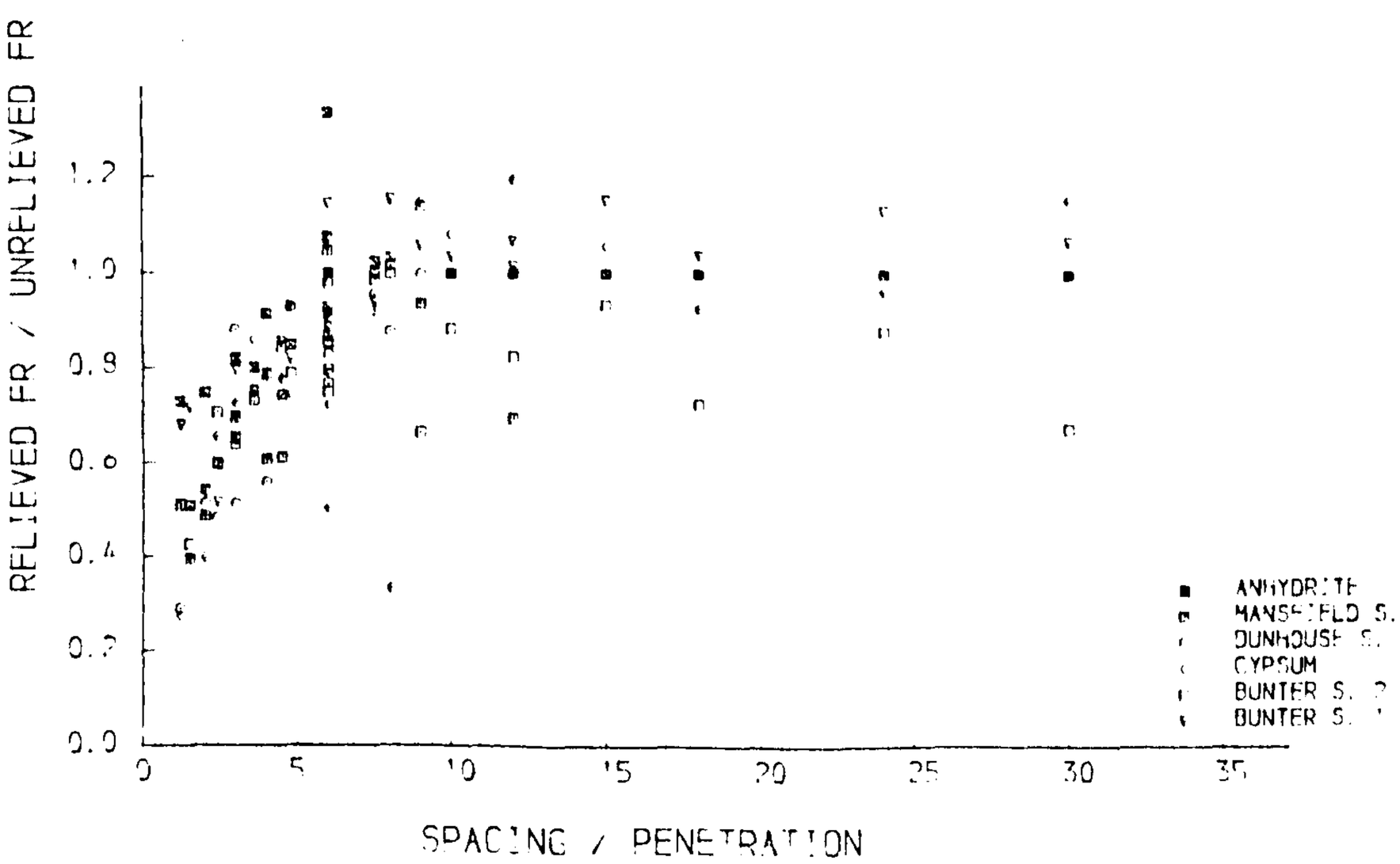

Fig. 7.2.4 $(FR)_{re}/(FR)_{un}$ versus s/p

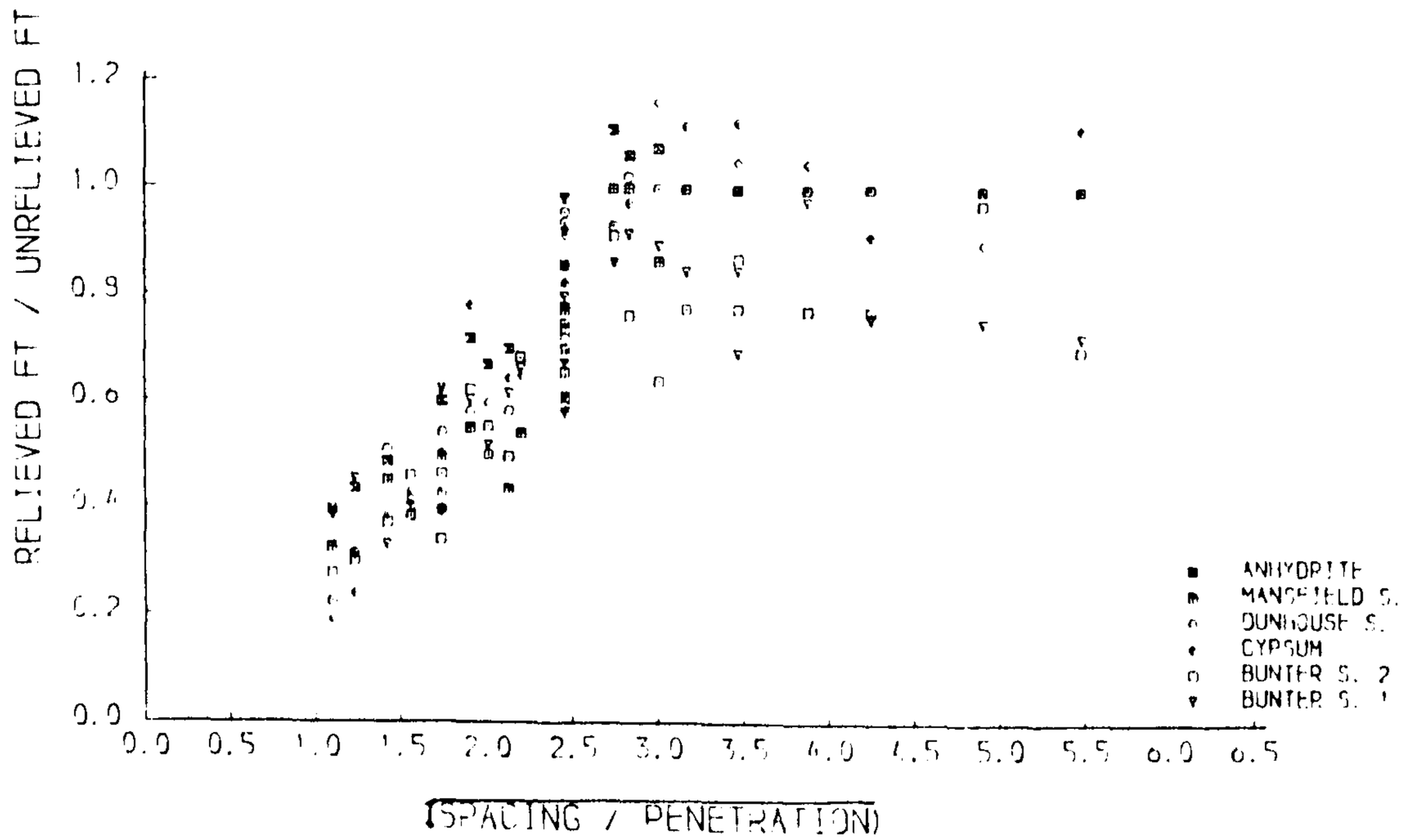

Fig. 7.2.5 $(FT)_{re}/(FT)_{un}$ versus $\sqrt{s/p}$

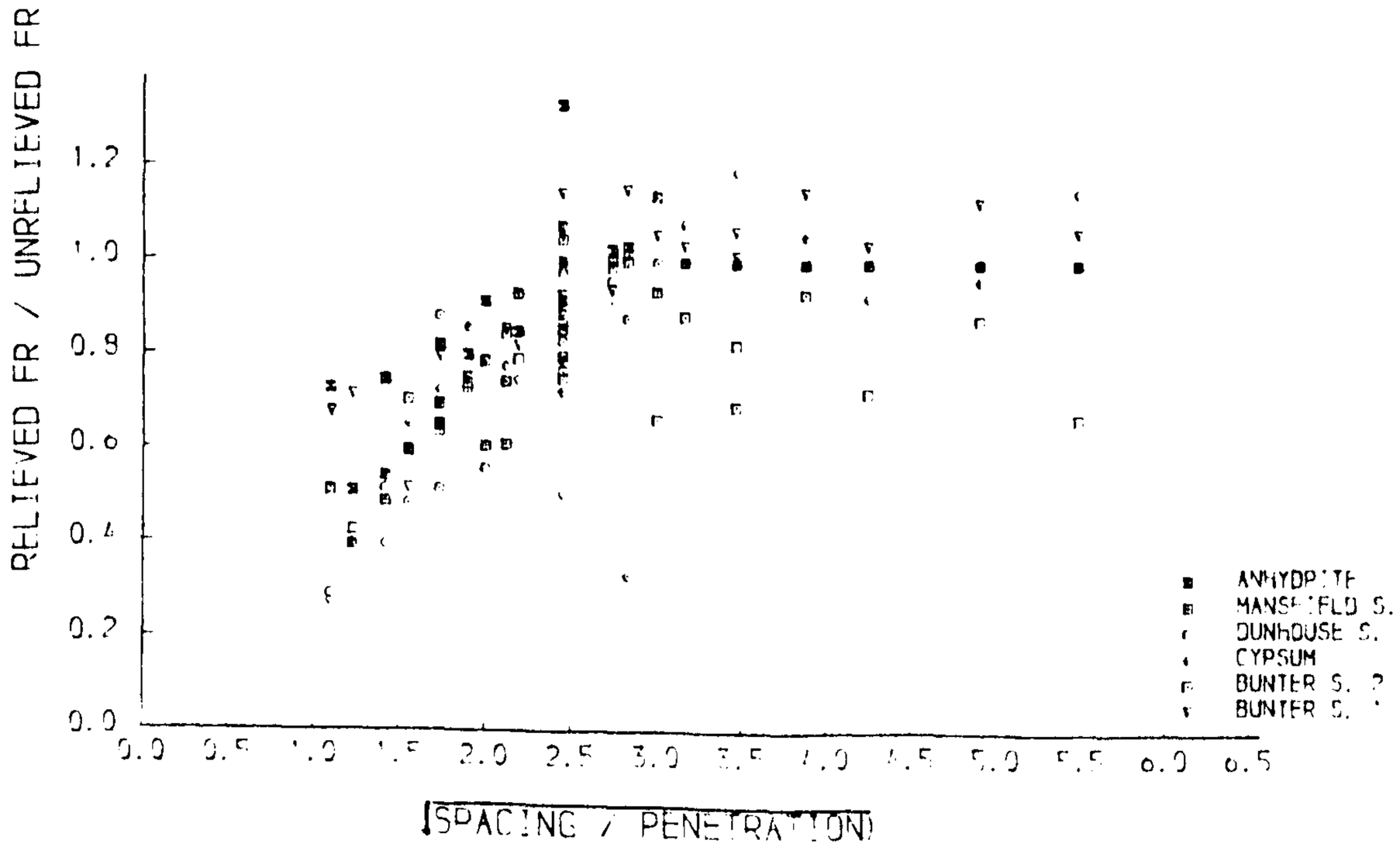

Fig. 7.2.6 $(FR)_{re}/(FR)_{un}$ versus $\sqrt{s/p}$

Plots of the ratios of $(FT)_{re}/(FT)_{un}$ and $(FR)_{re}/(FR)_{un}$ are drawn in Figs 7.2.3 and 7.2.4. Figs 7.2.5 and 7.2.6 show the relationships between the ratios of relieved and unrelieved forces and $\sqrt{s/p}$. This work is based on the collected data from single pass rock cutting tests by Bilgin (1977), and Roxborough and Phillips (1975,b) An analysis of the coefficient of determination (Table 7.2.1) has shown that there is a better linear relationship between the ratios of relieved cutting forces to unrelieved cutting forces and $\sqrt{s/p}$.

Table 7.2.1 The coefficient of determination

	unlimited	$s/p = 20$	$s/p = 15$	$s/p = 10$
$(FT)_{re}/(FT)_{un}$ to s/p	0.72	0.81	0.87	0.94
$(FR)_{re}/(FR)_{un}$ to s/p	0.68	0.76	0.82	0.90
$(FT)_{re}/(FT)_{un}$ to $\sqrt{s/p}$	0.93	0.95	0.97	0.98
$(FR)_{re}/(FR)_{un}$ to $\sqrt{s/p}$	0.91	0.93	0.95	0.97

This relation can be expressed as:

$$\frac{(FT)_{re}}{(FT)_{un}} = B\sqrt{\frac{s}{p}} \qquad 7.2.13$$

and,

$$\frac{(FR)_{re}}{(FR)_{un}} = B\sqrt{\frac{s}{p}} \qquad 7.2.14$$

where

B= dimensionless coefficient.

The dimensionless coefficient B can be determined by assuming the magnitude of the s/p ratio at the critical value. Therefore, for the single pass cutting tests on the smooth rock surface, and assuming that the relieved cutting forces are equal to

unrelieved cutting forces when $s/p = 15$, then,

$$B = \frac{1}{\sqrt{15}} \qquad 7.2.15$$

Thus,

$$(FT)_{re} = \sqrt{\frac{s}{15p}}(FT)_{un} \qquad 7.2.16$$

Combining Eqs (7.2.6), (7.2.7) and (7.2.16) gives:

$$(FT)_{re} = \frac{4}{3\sqrt{15}} \tan\frac{\theta}{2}\sqrt{sp}\sqrt{Dp - p^2}\ \sigma_0 \qquad 7.2.17$$

where

for single pass cutting tests,

when $s/p > 15, s = 15p$.

The second method is based on the work of Swain and Lawn (1975), in which the equilibrium requirements for the indentation configuration of Fig. 5.3.1 was investigated. In Fig. 5.3.1, P is the applied load, acting over a line L, i.e. $P = P_L L$, with P_L a line force per unit length, and c is a characteristic crack length. Considering the Griffith-Irwin energy-balance condition for crack equilibrium, Swain and Lawn found the relationship of the crack length, c, and fracture toughness, K as follow:

$$K = \frac{P_L}{\sqrt{\pi c}\tan\frac{\theta}{2}} \qquad 7.2.18$$

Thus,

$$P_L = \sqrt{\pi c}K\tan\frac{\theta}{2} \qquad 7.2.19$$

The action of a disc cutter can be considered as a group of small indenters of length dx, as shown in Fig 5.3.1. Therefore, the penetration force FT at the cutter is:

$$FT = \int_0^{\sqrt{Dp-p^2}} P_L dx \qquad 7.2.20$$

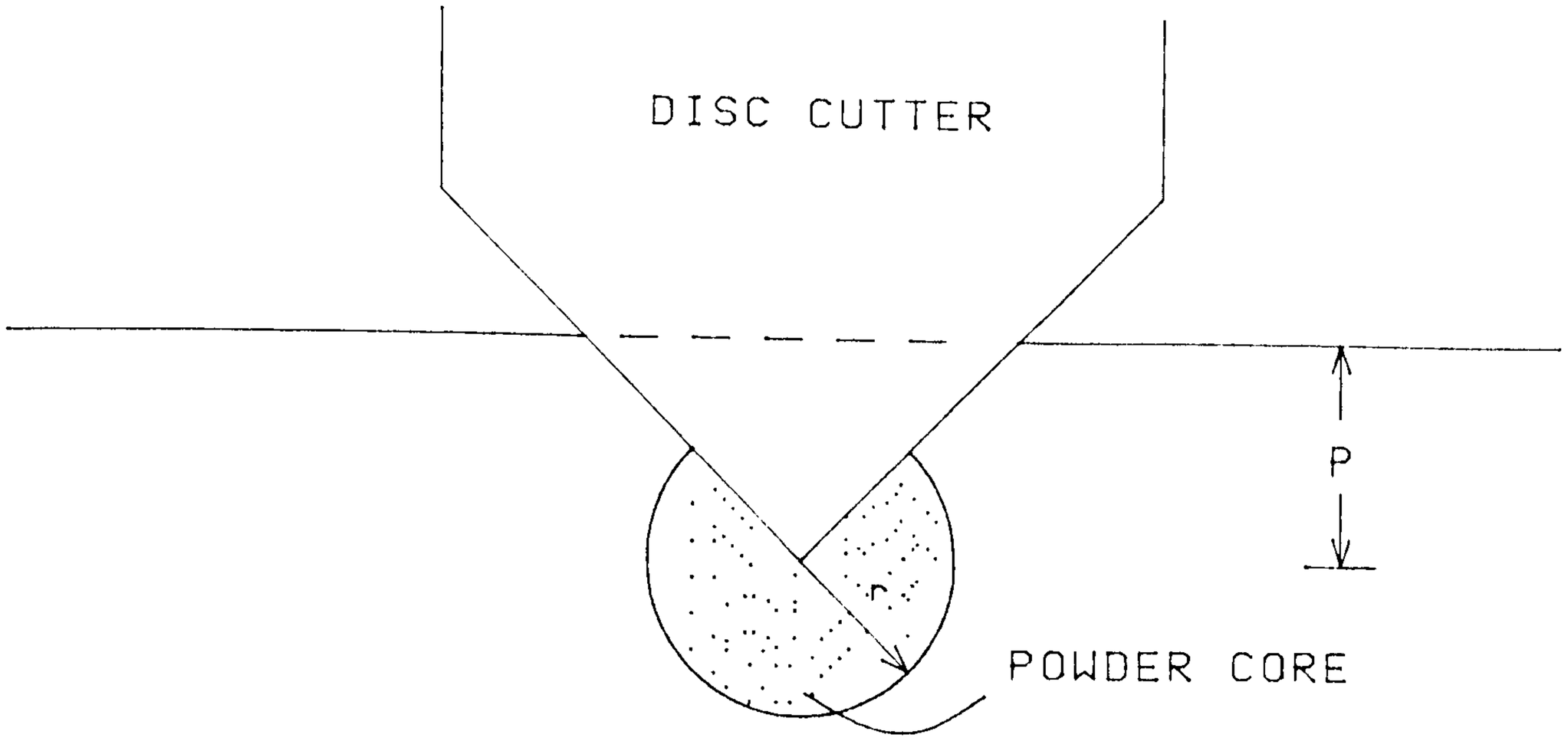

Fig. 7.2.7 A core of radius $r(c)$

If the cutting is conducted within the critical regions of s/p ratios, and assuming that the length of cracks increase approximately linearly with x (Sanio, 1985), then,

$$c(x) = \frac{s}{\sqrt{Dp - p^2}}x \qquad 7.2.21$$

Incorporating Eq. (7.2.21) into (7.2.20), and integrating gives:

$$FT = \frac{2}{3}\sqrt{\pi}K\sqrt{s}\sqrt{Dp - p^2}\tan\frac{\theta}{2} \qquad 7.2.22$$

From Eqs (7.2.8) and (7.2.9) for a sharp disc cutter, or Eqs (7.2.10), (7.2.11) and (7.2.12) for a worn disc cutter, the rolling force and the side force may be obtained.

7.2.3 The Determination of The Size of Fracture Zone

It is well known that the mechanisms of rock breakage by disc cutters can be seen the same as the discs thrust in to rock. That is to say that the disc cutting

can be considered as a action of the indentation. As the thrust force is increased the size of the crushed zone increases, until finally the whole of the material around the indentation is crushed.

A further analysis is based on the assumption that the indentation process is in an ideal elastic-plastic solid regarded as the expansion of a hemispherical core (Fig. 7.2.7). Within the core, a hydrostatic pressure is assumed, while outside the core, it is assumed that the stresses and displacements have radial symmetry in an infinite elastic perfectly-plastic body which contains a cylindrical or spherical cavity under pressure.

Based on a mode for a pressurized circular hole with cracks in a infinite plate as given by Ouchterlony (1974), Sanio (1985) introduced an equation to calculate the penetration force:

$$f_n = \frac{K}{q} \tan \frac{\theta}{2} \sqrt{c} \qquad 7.2.23$$

where

f_n = a line force per unite length,

c= the crack length,

$r(c)$ = the hemispherical core radius,

$q = r(c)/p$, a constant.

Compared with Eq. (7.2.19), we find:

$$q = \frac{1}{\sqrt{\pi}} = 0.56 \qquad 7.2.24$$

7.2.4 The Determination of Cutting Forces in Water Jet Assisted Cutting Tests

As mentioned in Chapter 6, the function of a low pressure water jet in cutting tests is to do no more than clear the debris in the cutting grooves which include

the powder core formed just beneath the disc cutter. If the core is moved from the groove, this means that the actual penetration is reduced. Thus we can obtain the actual penetration for the nth run:

$$p_{a_n} = p - qp_{a_{n-1}} \tag{7.2.25}$$

If $p_{a_1} = p$, it follows that,

$$p_{a_n} = p(1 + \sum_{i=2}^{n}(-1)^{i-1}q^{i-1}) \tag{7.2.26}$$

When $n > 7$, Eq. (7.2.26) gives:

$$p_a = 0.64p \tag{7.2.27}$$

Therefore, using p_a instead of p in the predicter equations, one can calculate the predicted cutting forces for water jet assisted cutting.

7.3 COMPARISON WITH EXPERIMENTAL RESULTS

7.3.1 Unrelieved Cutting

Unrelieved cutting tests were not involved in this study. The available data to compare with theoretical results were presented by Roxborough and Phillips (1975,b), and Bilgin (1977).

The predictor Eqs (7.2.6), (7.2.7) and (7.2.10) have considered many factors, such as disc diameter, disc edge angle, penetration depth, and contact stress. All factors can be obtained from the geometry of disc cutters and performance of cutting tests, except contact pressure, or thrust pressure, σ_0. In order to determine this factor, let us go back to Chapter 5 (Indentation Tests), in which the contact stress σ_0 were given in Eq. (5.2.1) as:

$$\sigma_0 = C\sigma_y \tag{7.3.1}$$

where $C = 3$, and $\sigma_y = \sigma_c$ for rock materials.

Combining Eqs (7.3.1), (7.2.6) and (7.2.7) gives:

$$FT = 4\sigma_c\sqrt{Dp^3 - p^4}\tan\frac{\theta}{2} \qquad 7.3.2$$

This equation is the same as Eq. (2.1.6) which was given by Roxborough and Phillips (1975,a). However, the derivation of Eq. (7.3.2) in this study is quite different from that by Roxborough and Phillips, in which they simply assumed that the projected areas against thrust force was a rectangle. A detail of the argument about this simplification was given by Meijer (1977).

Now, considering Eq. (5.3.2) which is:

$$\sigma_0 = \frac{1}{\sqrt{3}}[1 + \ln(\frac{4E}{3\pi\sigma_y \tan\frac{\theta}{2}})]\sigma_y \qquad 7.3.3$$

Furthermore, by combining Eqs (7.2.6) and (7.2.7) with Eq. (7.3.3), one obtains:

$$FT = \frac{4}{3\sqrt{3}}[1 + \ln(\frac{4E}{3\pi\sigma_c \tan\frac{\theta}{2}})]\sqrt{Dp^3 - p^4}\tan\frac{\theta}{2}\,\sigma_c \qquad 7.3.4$$

Theoretical and measured values of force FT are listed in Table 7.3.1 for five disc diameters, in Table 7.3.2 for five disc edge angles and in Table 7.3.3 for five penetration depths. Both theoretical results have shown very good agreement with the measured data: the difference between them being less than 10%.

The rolling forces can be determined by the Eq. (7.2.8), which this study gives as:

$$\frac{FT}{FR} = \frac{4}{3}\sqrt{\frac{D-p}{p}} \qquad 7.3.5$$

or by Roxborough and Phillips (1975,a), as

$$\frac{FT}{FR} = \sqrt{\frac{D-p}{p}} \qquad 7.3.6$$

Table 7.3.1 Thrust Force for Disc ($\theta = 80°; p$ =6mm)

D	Dry Bunter Sandstone			Wet Bunter Sandstone		
mm	Eq.(2)	Eq.(4)	measured	Eq.(2)	Eq.(4)	measured
100	25.6	23.3	25.4	22.6	19.5	24.4
125	28.8	26.2	27.3	24.8	21.9	23.0
150	31.7	28.8	30.8	27.3	24.1	30.2
175	34.3	31.2	29.7	29.5	26.1	25.2
200	36.8	33.4	32.6	31.7	28.0	28.5

Table 7.3.2 Thrust Force for Disc (D = 150mm; p = 6mm)

θ	Dry Bunter Sandstone			Wet Bunter Sandstone		
(degree)	Eq.(2)	Eq.(4)	measured	Eq.(2)	Eq.(4)	measured
60	23.2	19.9	18.5	19.9	16.7	17.3
70	27.3	24.2	23.9	23.5	20.3	20.1
80	31.7	29.0	28.7	27.3	24.3	24.9
90	36.6	34.6	35.1	31.5	29.0	30.9
100	42.5	41.2	39.5	36.4	34.5	37.9

Table 7.3.3 Thrust Force for Disc ($\theta = 80°$; D = 150mm)

p	Dry Bunter Sandstone			Wet Bunter Sandstone		
mm	Eq.(2)	Eq.(4)	measured	Eq.(2)	Eq.(4)	measured
2	6.2	5.7	8.2	5.3	4.8	6.9
4	17.4	15.9	18.8	15.0	13.4	16.0
6	31.7	29.1	29.5	27.3	24.4	27.0
8	48.5	44.5	36.3	41.6	37.4	35.7
10	67.3	61.7	53.0	57.8	51.8	45.6

Tables 7.3.4, 7.3.5 and 7.3.6 give predicted and measured FT/FR ratios. The much better fitting results was given by Eq. (7.3.5).

7.3.2 Relieved Cutting

Using the Eqs (7.2.17) and (7.2.7) for a sharp disc cutter, or (7.2.10) for a worn disc cutter, the theoretical cutting forces can be obtained. Compared with the experimental results provided by several workers (Roxborough and Phillips, 1975,b; Ozdemir et al., 1977; Bilgin, 1978; Snowdon et al., 1982; Moses, 1985), the agreement between theoretical and experimental results are very good: for single pass cutting on a smooth rock surface, with less 7% data, the difference is higher than 50%; for single pass cutting on a previous cutting surface, 10%; for multiple pass cutting, about 15%; and for worn disc cutting, about 20%. Some examples are listed in Appendix E.

Instead of Eq. (7.2.7), the contact pressure obtained in the indentation tests, Chapter 5, can be used in prediction of disc cutting. Figs 7.3.1 and 7.3.2 show that the agreements between predicted cutting forces and the experimental results are quite good.

Using the Eqs (7.2.21) and (7.2.22) presented in the theoretical analysis section, the theoretical force values were calculated and the thrust force vs s/p ratios were drawn in Fig. 7.3.3. While there is considerable scatter between the theoretical analysis and experimental results, the trend for both is almost the same.

There are many reasons to explain this problem. Firstly, the tests were performed on the very rough rock surfaces, while the Eq. (7.2.19) is only suitable for indentation tests on smooth surfaces. Secondly, the predictor equations were developed by assuming the cutter bearing friction force to be zero or negligible for mathematical simplicity in the theoretical derivations. A third possible explana-

Table 7.3.4 Thrust / rolling force ratio ($\theta = 80°$; $p = 6$mm)

D	Dry Bunter Sandstone			Wet Bunter Sandstone		
mm	Eq.(5)	Eq.(6)	measured	Eq.(5)	Eq.(6)	measured
100	5.3	4.0	5.8	5.3	4.0	6.1
125	5.9	4.5	6.1	5.9	4.5	5.8
150	6.5	4.9	7.0	6.5	4.9	6.9
175	7.1	5.3	6.9	7.1	5.3	6.6
200	7.6	5.7	7.6	7.6	5.7	7.1

Table 7.3.5 Thrust / rolling force ratio ($D = 150$mm; $p = 6$mm)

θ	Dry Bunter Sandstone			Wet Bunter Sandstone		
(degree)	Eq.(5)	Eq.(6)	measured	Eq.(5)	Eq.(6)	measured
60	6.5	4.5	5.6	6.5	4.5	5.8
70	6.5	4.5	6.1	6.5	4.5	5.7
80	6.5	4.5	6.4	6.5	4.5	5.9
90	6.5	4.5	7.3	6.5	4.5	6.9
100	6.5	4.5	7.5	6.5	4.5	7.4

Table 7.3.6 Thrust / rolling force ratio ($\theta = 80°$; $D = 150$mm)

p	Dry Bunter Sandstone			Wet Bunter Sandstone		
mm	Eq.(5)	Eq.(6)	measured	Eq.(5)	Eq.(6)	measured
2.0	11.5	8.6	10.3	11.5	8.6	8.6
4.0	8.1	6.0	8.5	8.1	6.0	7.6
6.0	6.5	4.9	6.9	6.5	4.9	6.8
8.0	5.6	4.2	6.0	5.6	4.2	6.3
10.0	5.0	3.7	6.1	5.0	3.7	5.8

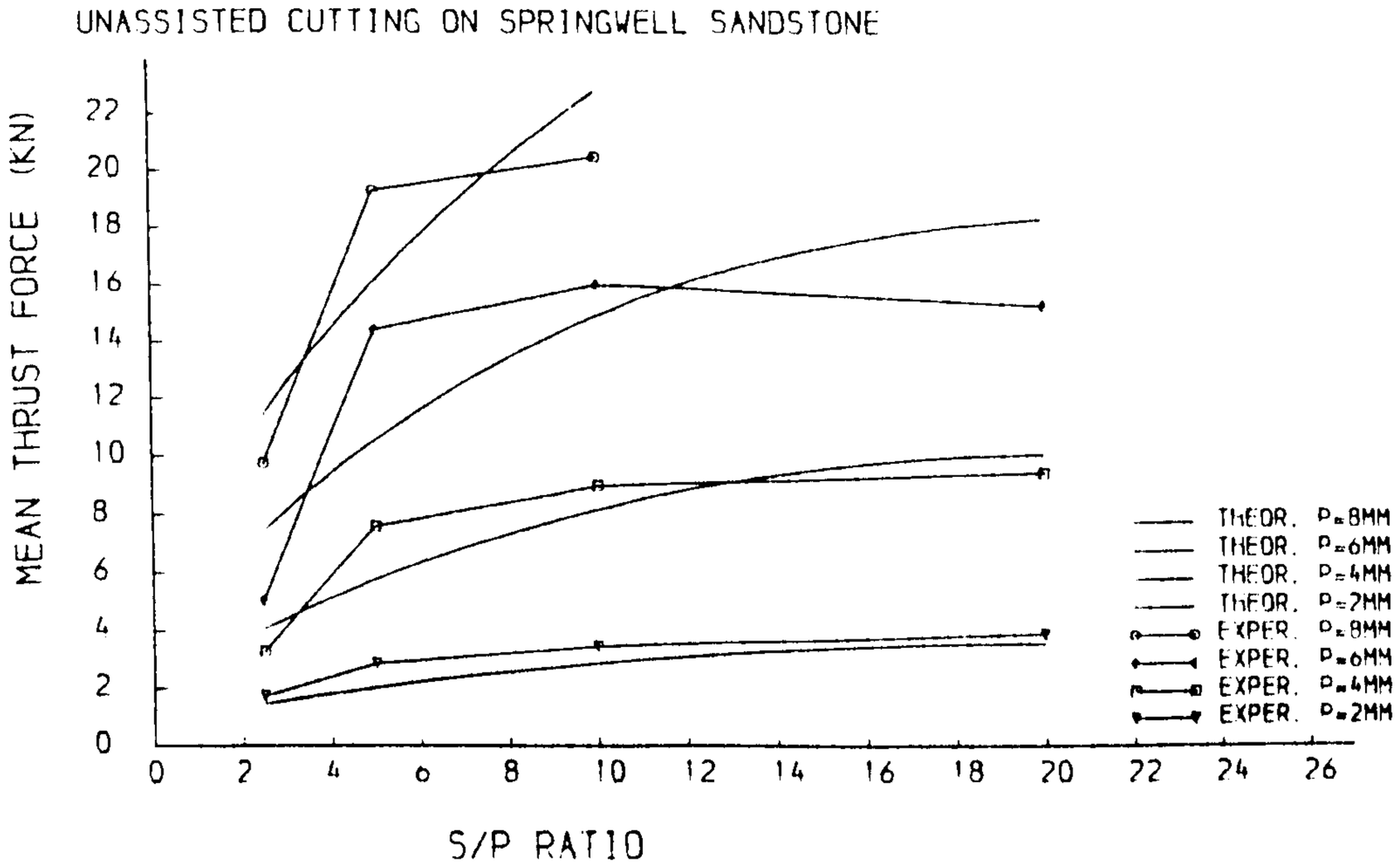

Fig. 7.3.1 Comparison of experimental and theoretical results (Springwell Sandstone)

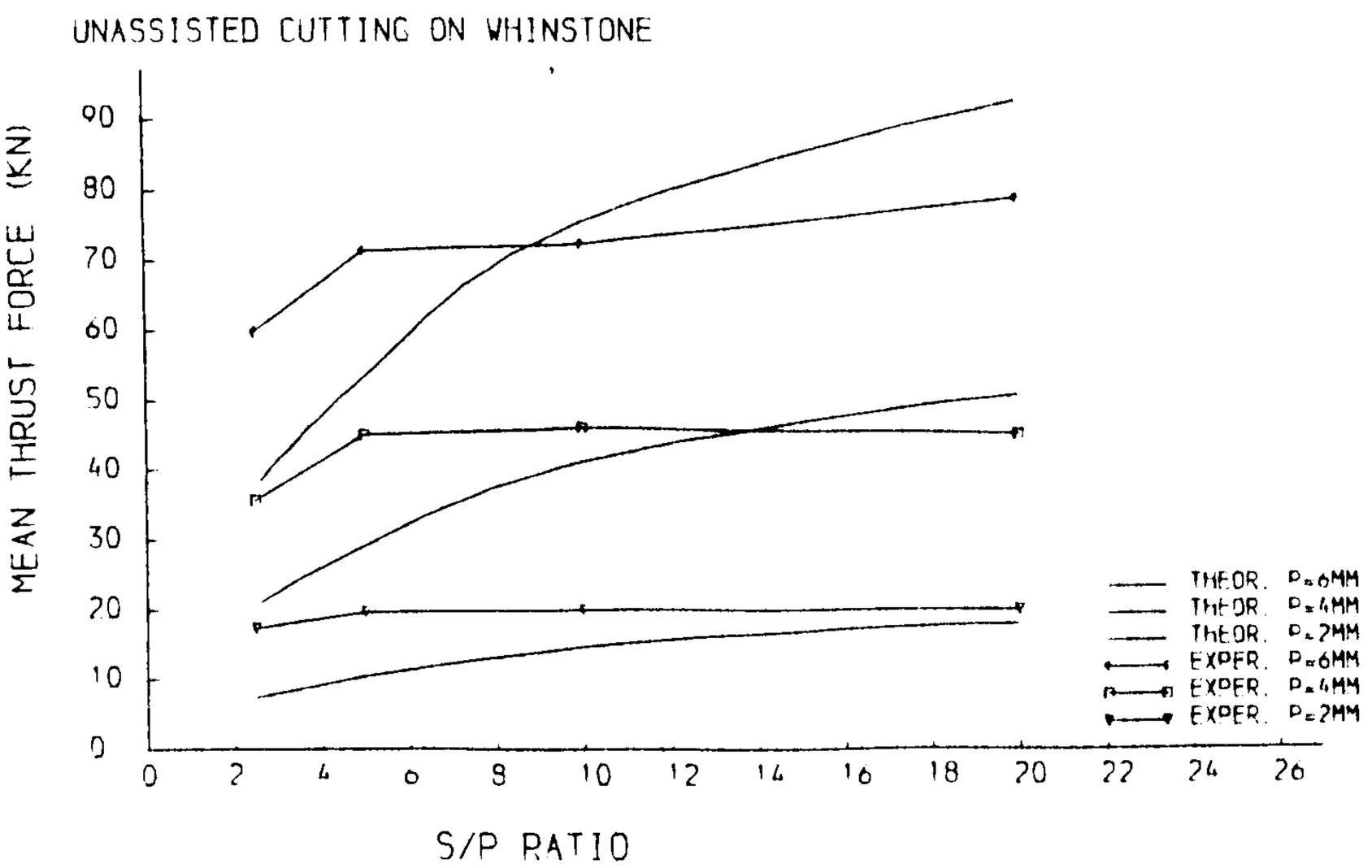

Fig. 7.3.2 Comparison of experimental and theoretical results (Whinstone)

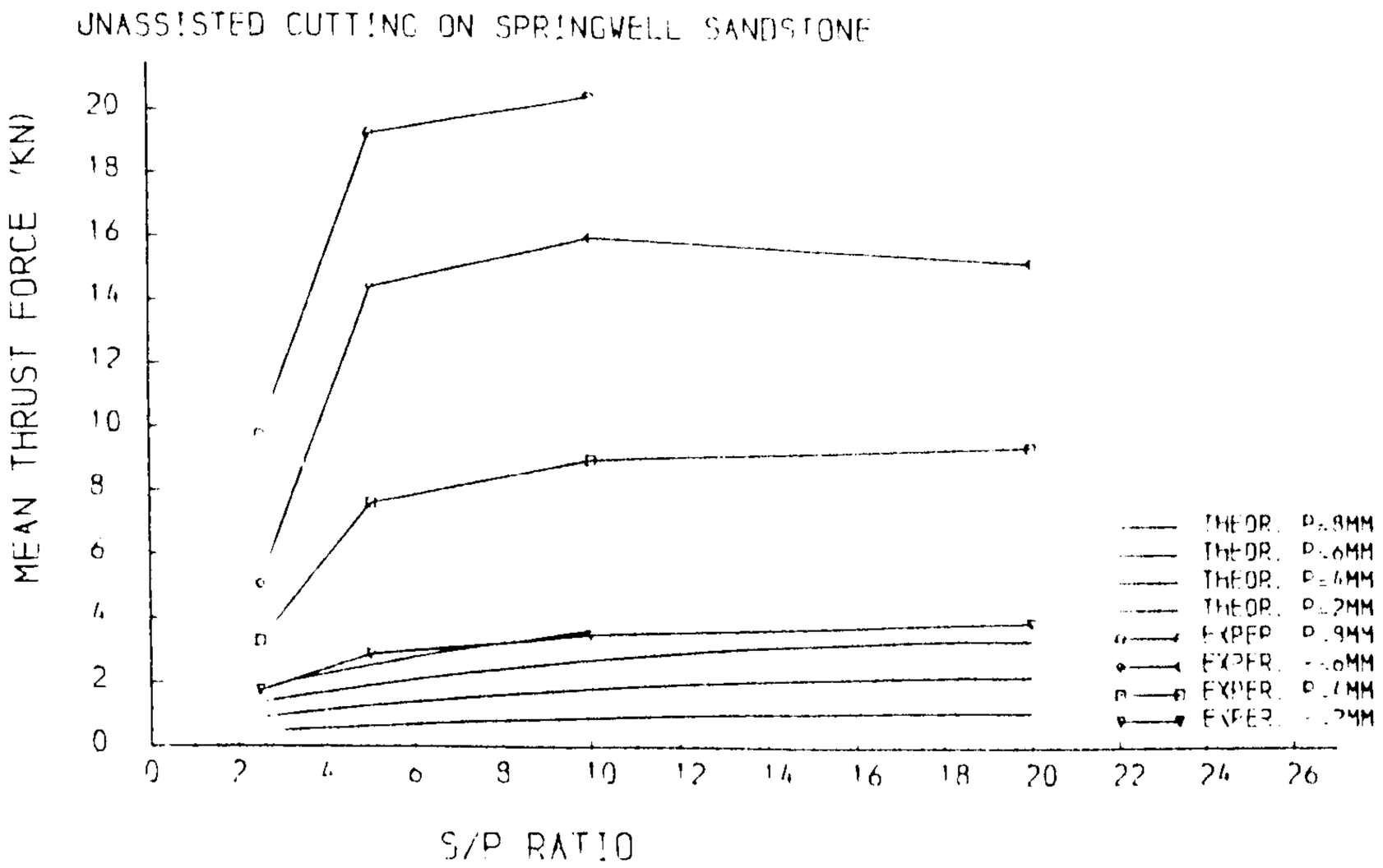

Fig. 7.3.3 Experimental and theoretical thrust forces versus s/p ratio

tion is that the disc cutters used were not as sharp as they could have been. The assumption that the penetration of a disc cutter into the rock is as the action of a group of wedge indenters maybe is the forth reason that caused the scatter between predicted values and experimental results. Furthermore, if the examples given by Swain and Lawn (1975) are considered, and even though a real wedge indenter was used in the tests, the predicted values of the load are still far lower than those obtained by the experiment. However, the correlation can be improved by using a factor, B_f, defined as:

$$B_f = \frac{3\ FT}{2\sqrt{\pi}K\sqrt{s}\sqrt{Dp - p^2}\tan\frac{\theta}{2}} \qquad 7.3.7$$

Averaged B_f values obtained from cutting tests were as follows:

for mean thrust force,

$$B_{f1} = \begin{cases} 9.12, & \text{for worn disc cutter;} \\ 5.26, & \text{for sharp disc cutter.} \end{cases}$$

and for peak thrust force,

$$B_{f2} = \begin{cases} 19.49, & \text{for worn disc cutter;} \\ 8.17, & \text{for sharp disc cutter.} \end{cases}$$

Thus, we have a predictor equation of relieved cutting as:

$$FT = \frac{2\sqrt{\pi}}{3} B_f K \sqrt{s} \sqrt{Dp - p^2} \tan\frac{\theta}{2} \qquad 7.3.8$$

Comparisons of the theoretical and experimental results are given in Figs 7.3.4 and 7.3.5.

From the Eqs (7.2.17) and (7.3.8), one can find that the predictor equations have a form of:

$$FT = C_p R_p \sqrt{s} \sqrt{Dp - p^2} \tan\frac{\theta}{2} \qquad 7.3.9$$

where

C_p = a constant or a function of penetration;

R_p = a parameter of rock properties.

As $D >> p$ for the cutting performed on hard rock formations, above equation can be rewritten as:

$$FT = C_p R_p \sqrt{Dps} \tan\frac{\theta}{2} \qquad 7.3.10$$

7.3.3 Water Jet Assisted Cutting

In connection with the present work, one may observe that the main effect that water jet has upon the disc cutting operation is the clearance of the powder cores from the grooves. Thus, when the cutter goes through the groove just after the water jet, the actual penetration depth influencing the following cut is reduced. From Eq. (7.2.26) we can find that the actual penetration for water jet assisted

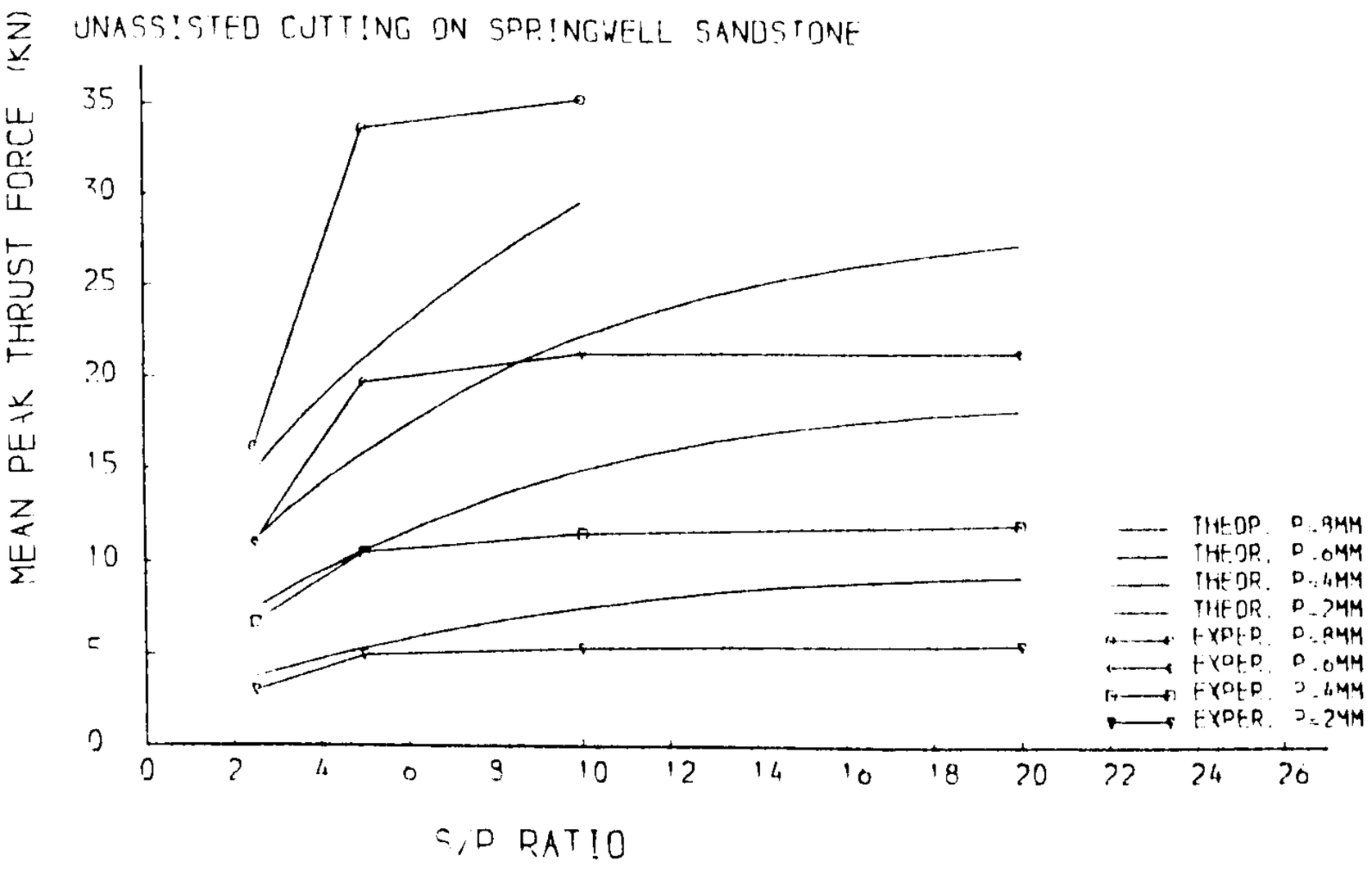

(a). Springwell Sandstone (MTF)

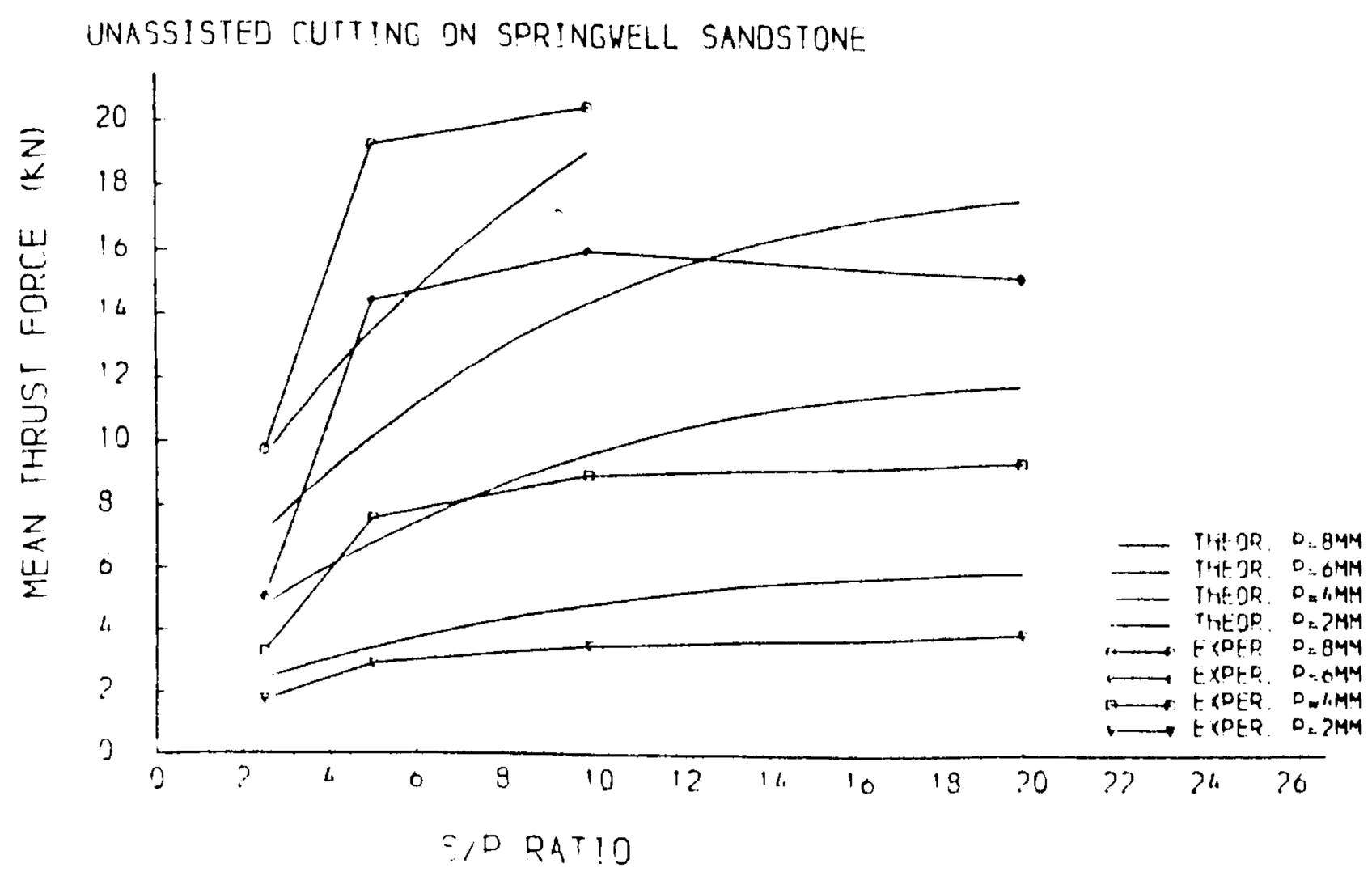

(b). Springwell Sandstone (MTF)

Fig. 7.3.4 A. Comparison of experimental and theoretical results (small cutting rig)

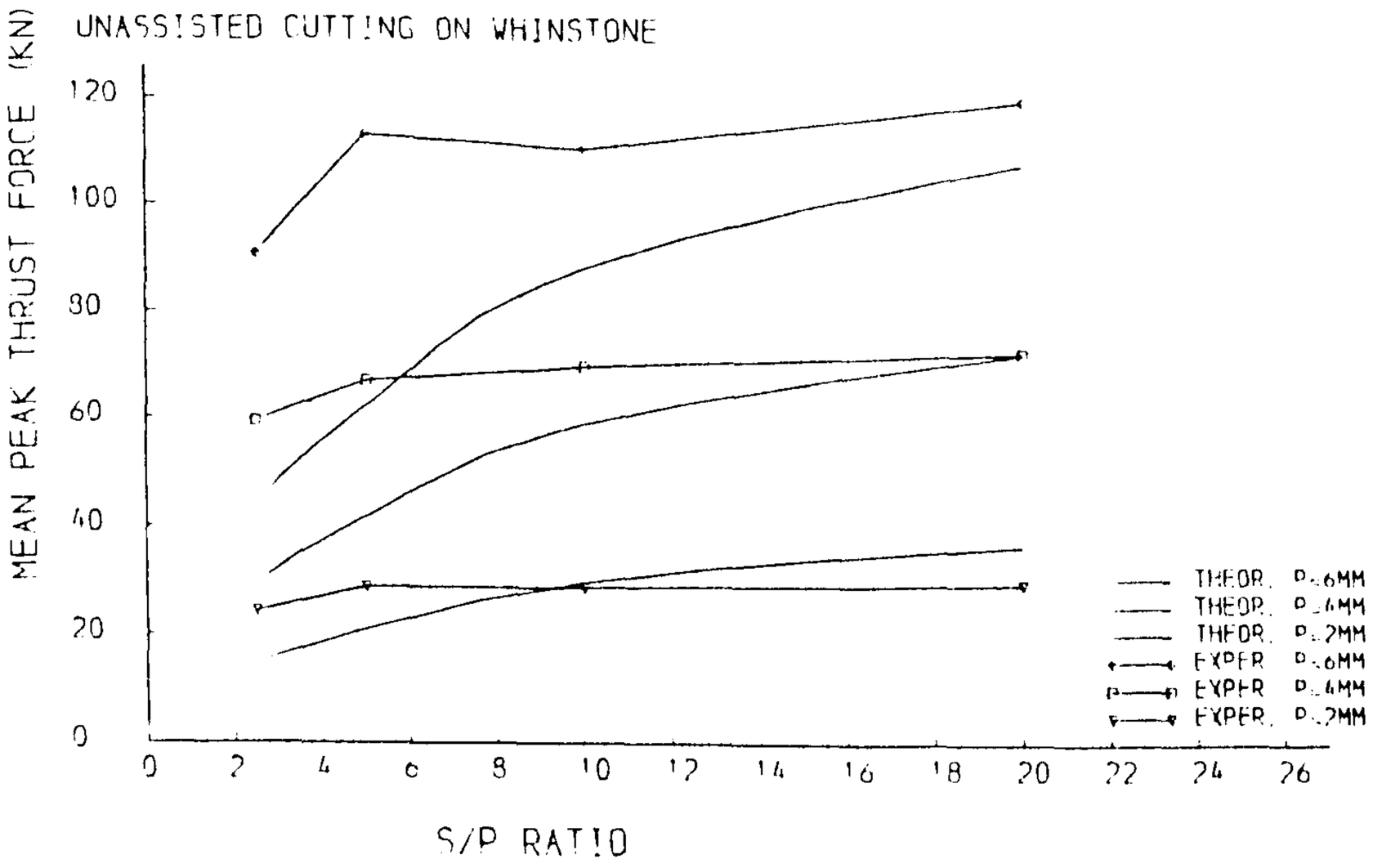

(c). Whinstone (MPTF)

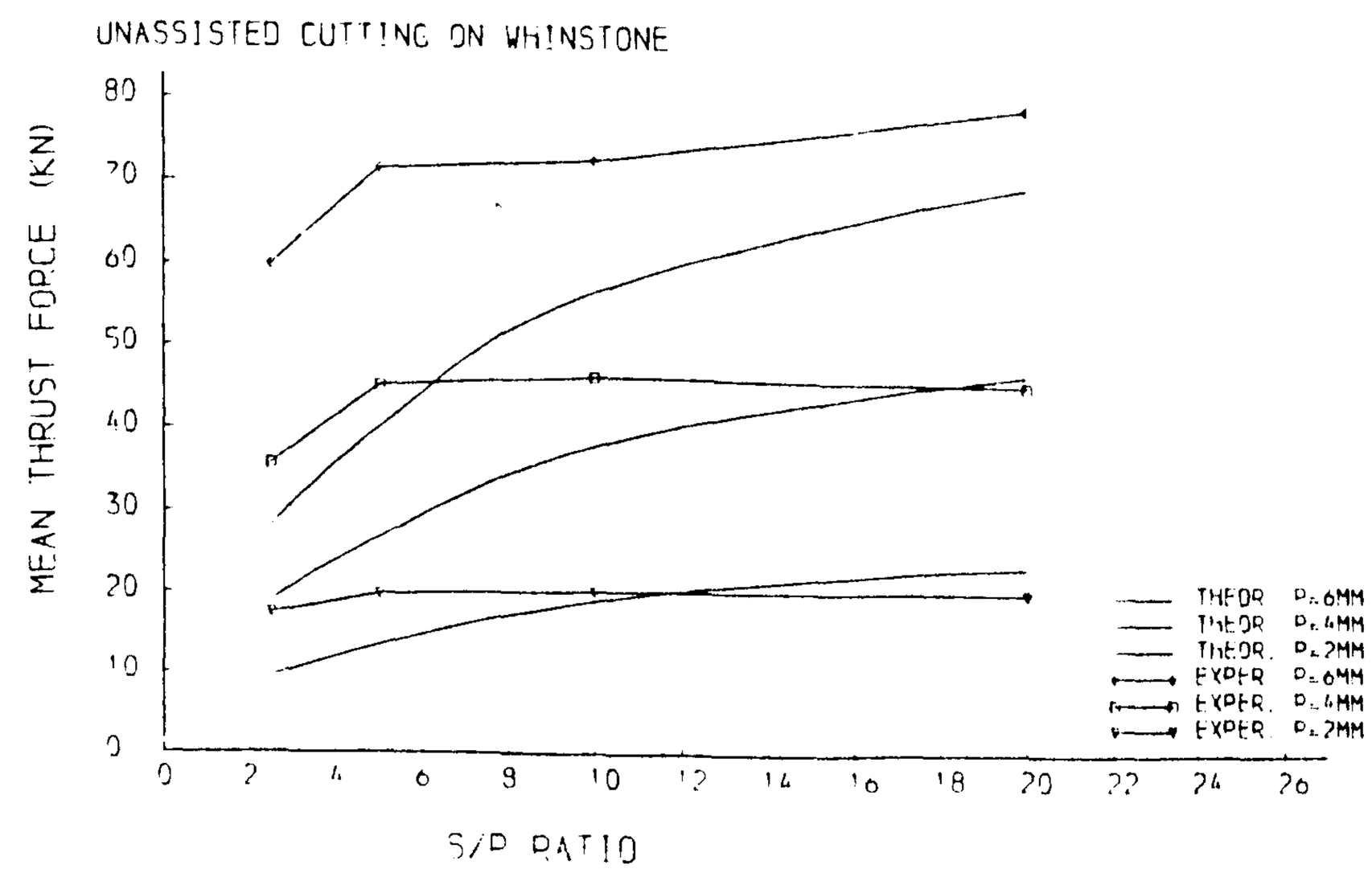

(d). Whinstone (MTF)

Fig. 7.3.4 B. Comparison of experimental and theoretical results (small cutting rig)

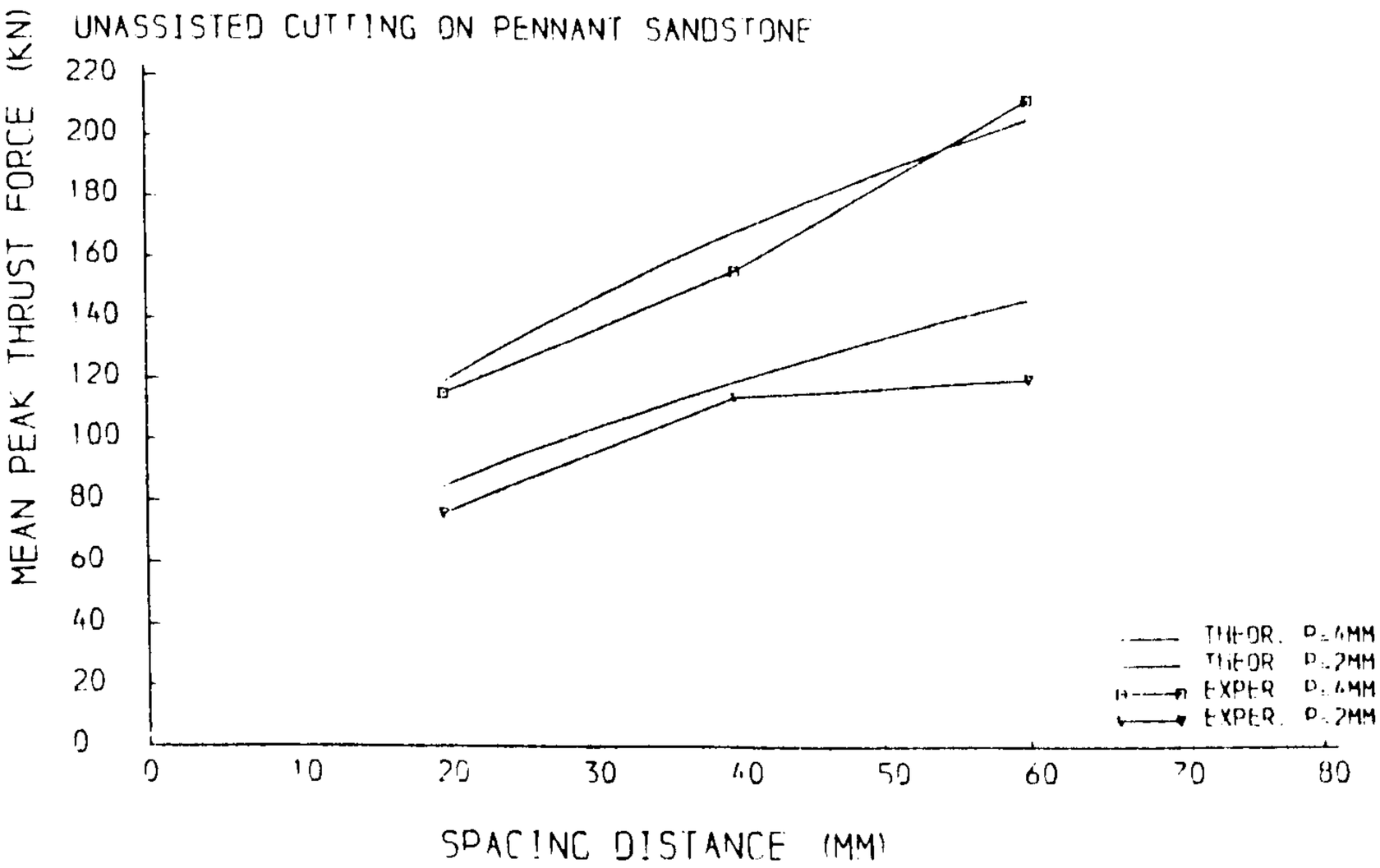

(a). Pennant Sandstone (MTF)

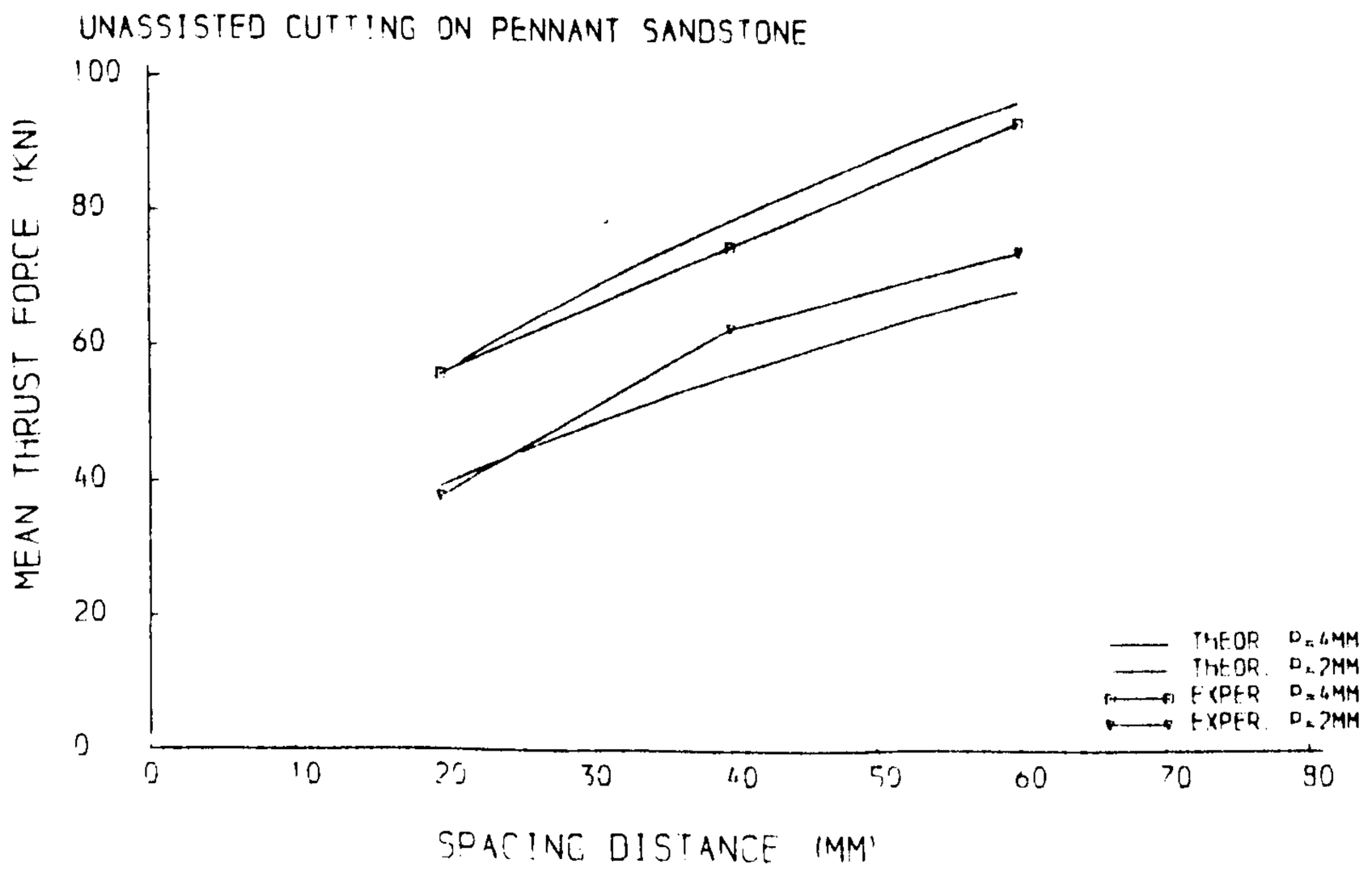

(b). Pennant Sandstone (MTF)

Fig. 7.3.5 A. Comparison of experimental and theoretical results (large cutting rig)

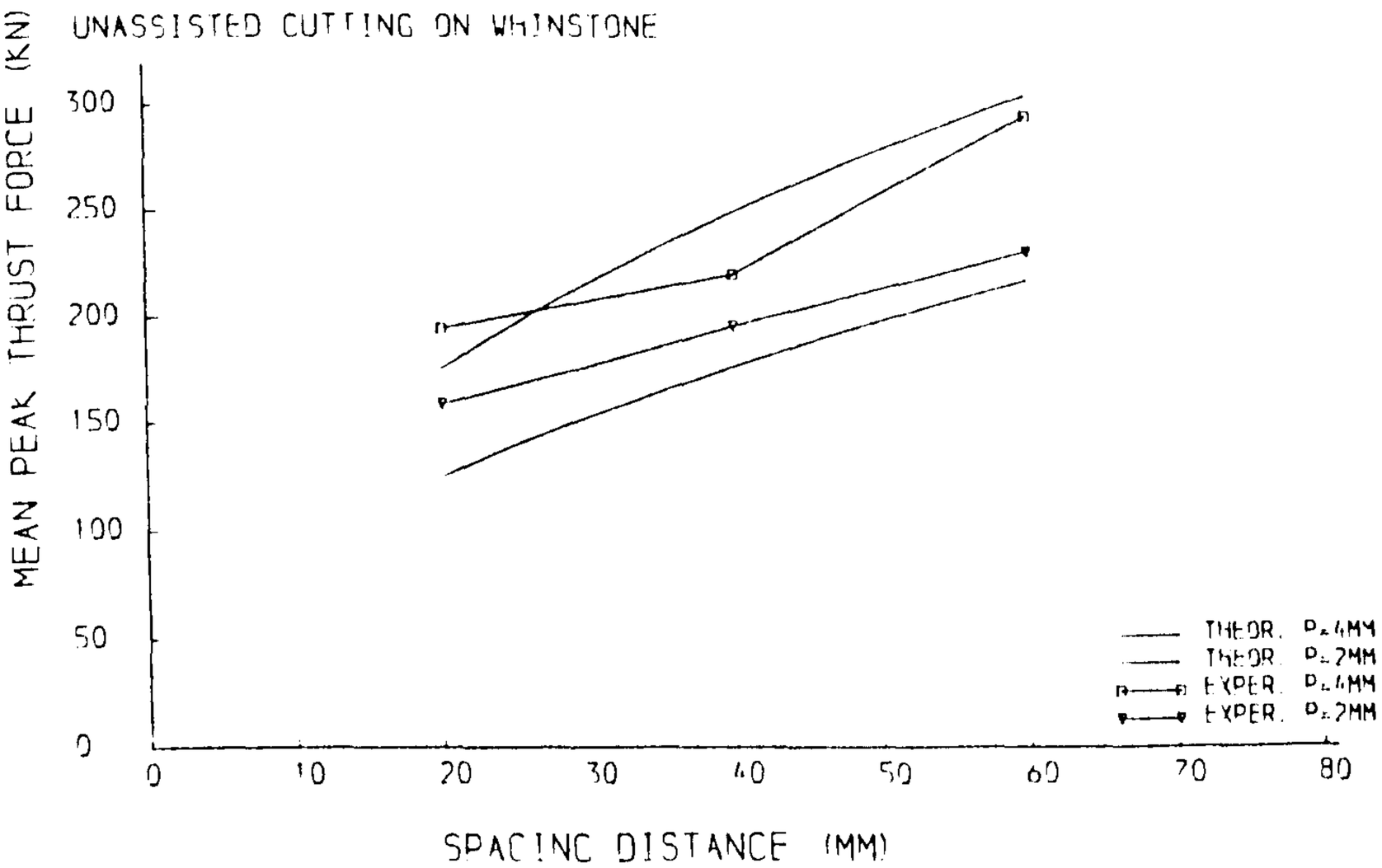

(c). Whinstone (MPTF)

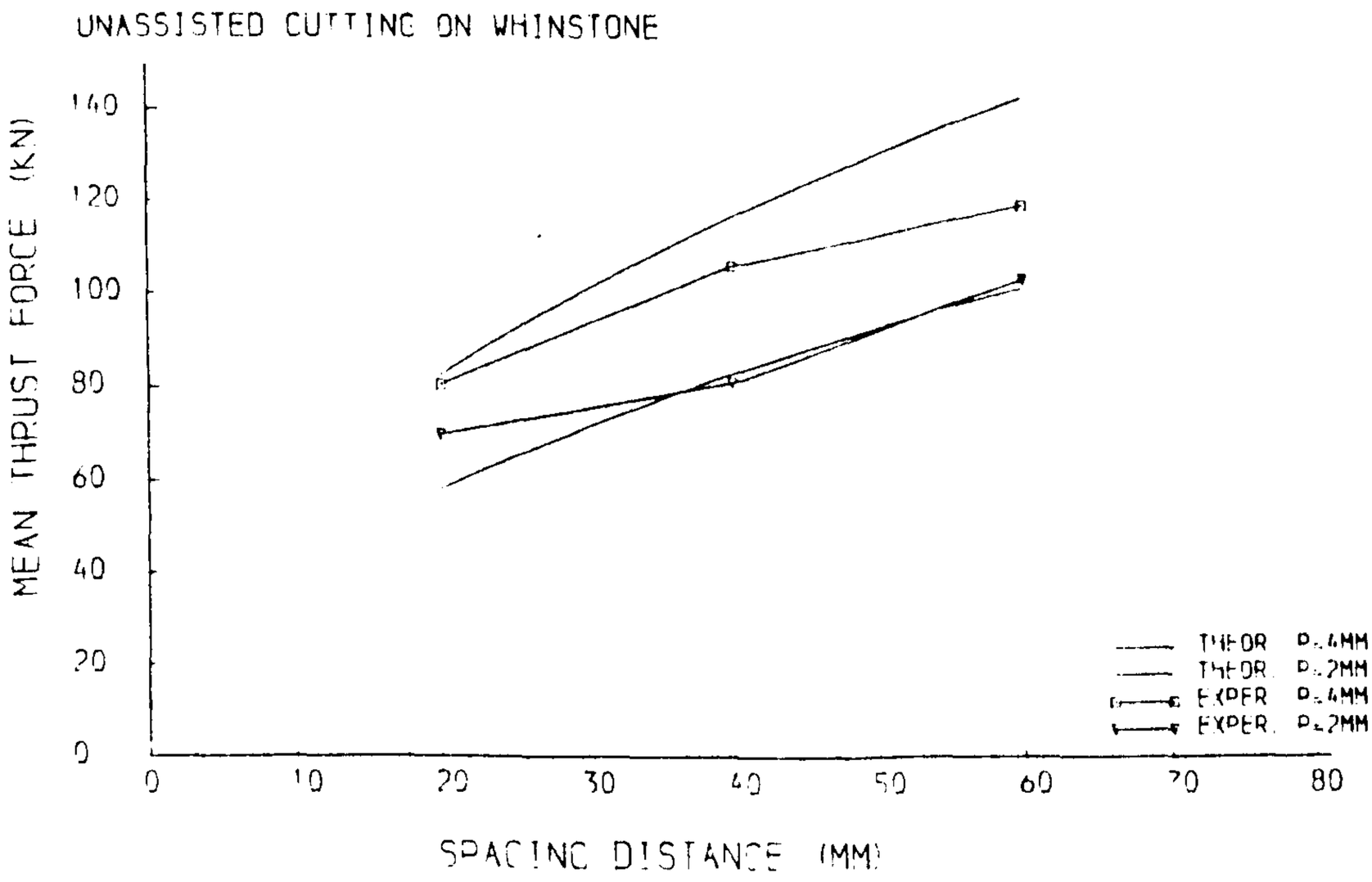

(d). Whinstone (MTF)

Fig. 7.3.5 B. Comparison of experimental and theoretical results (large cutting rig)

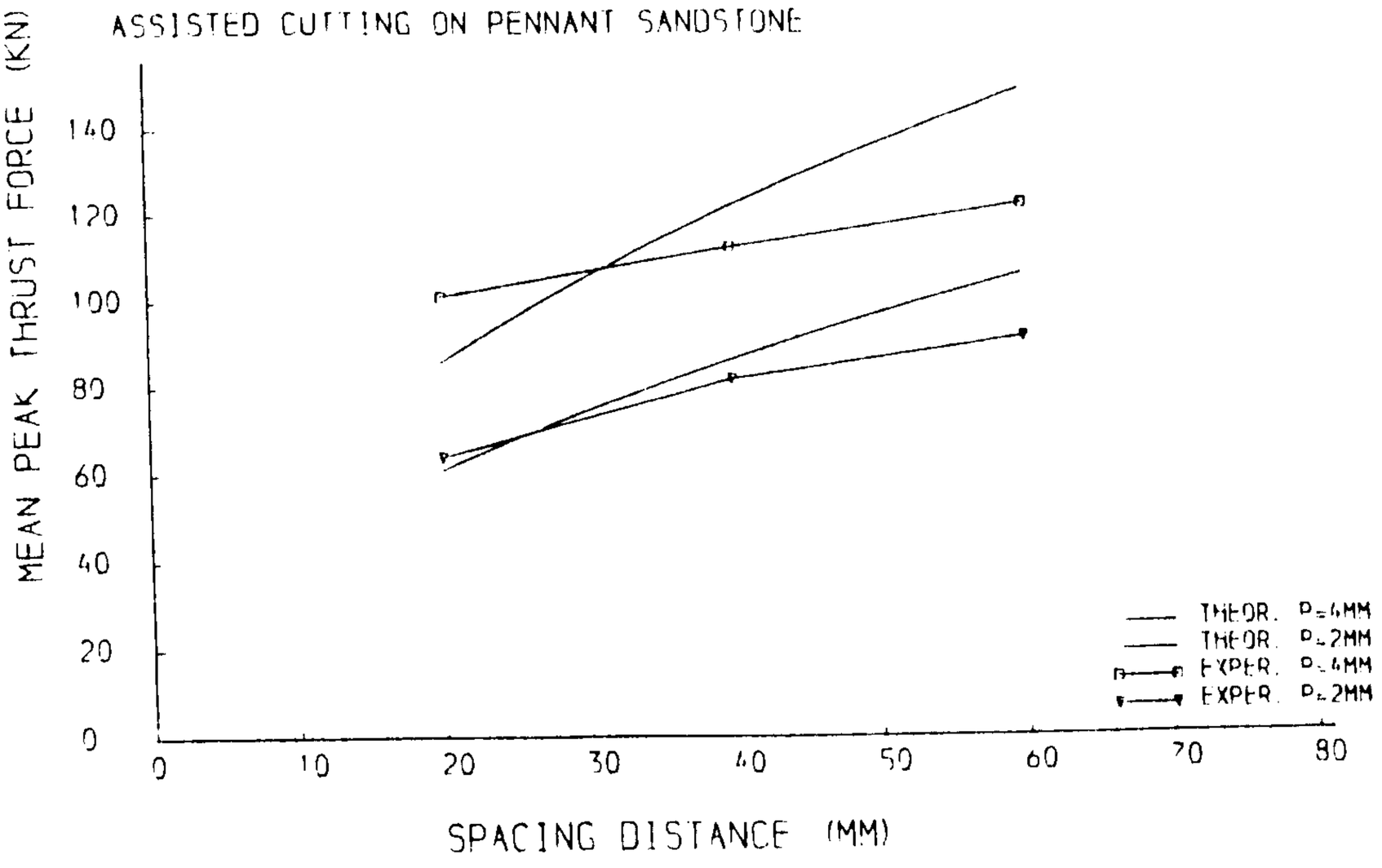

(a). MPTF

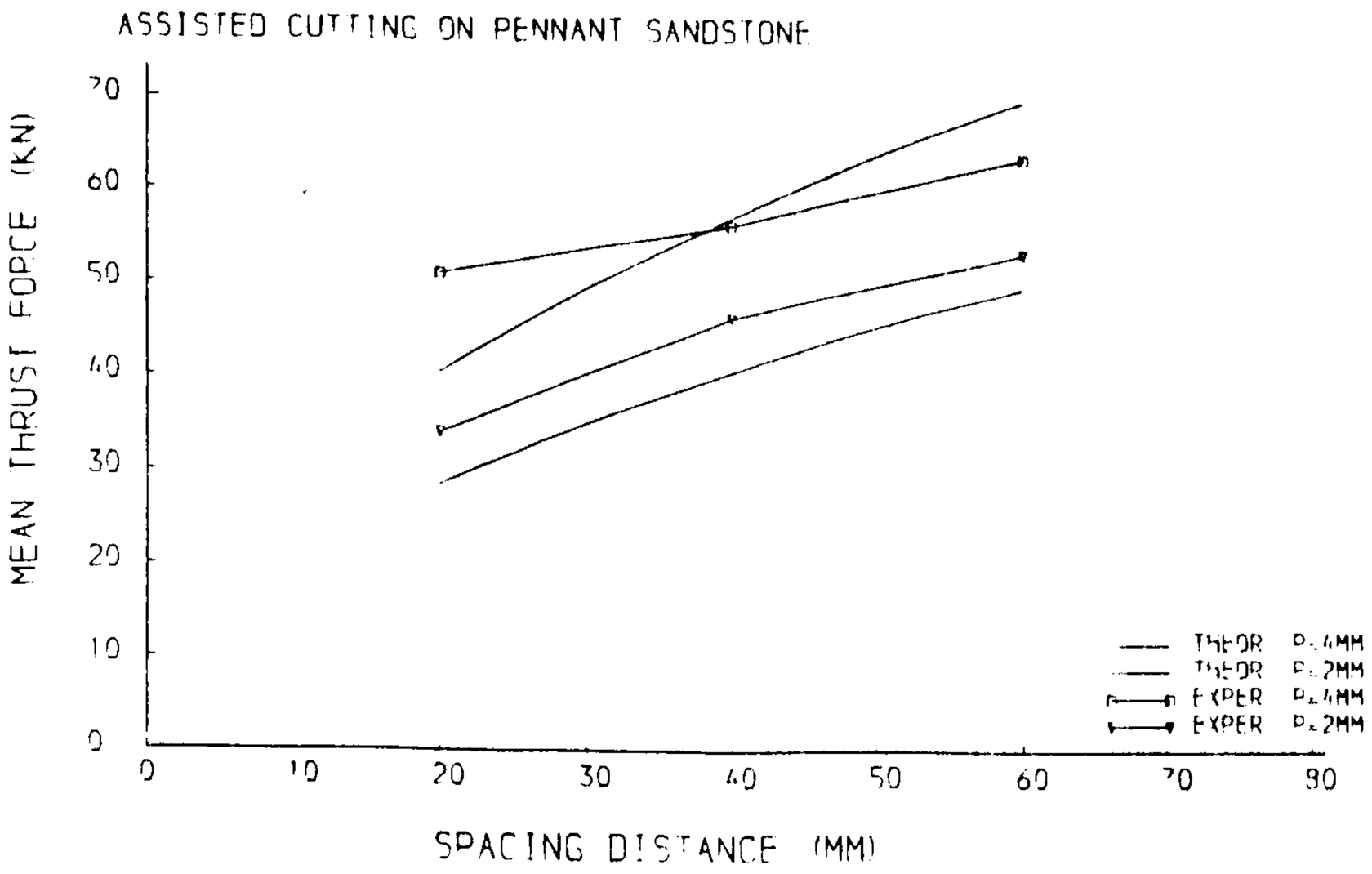

(b). MTF

Fig. 7.3.6 Comparison of experimental and theoretical results of water jet assisted cutting tests on Pennant Sandstone

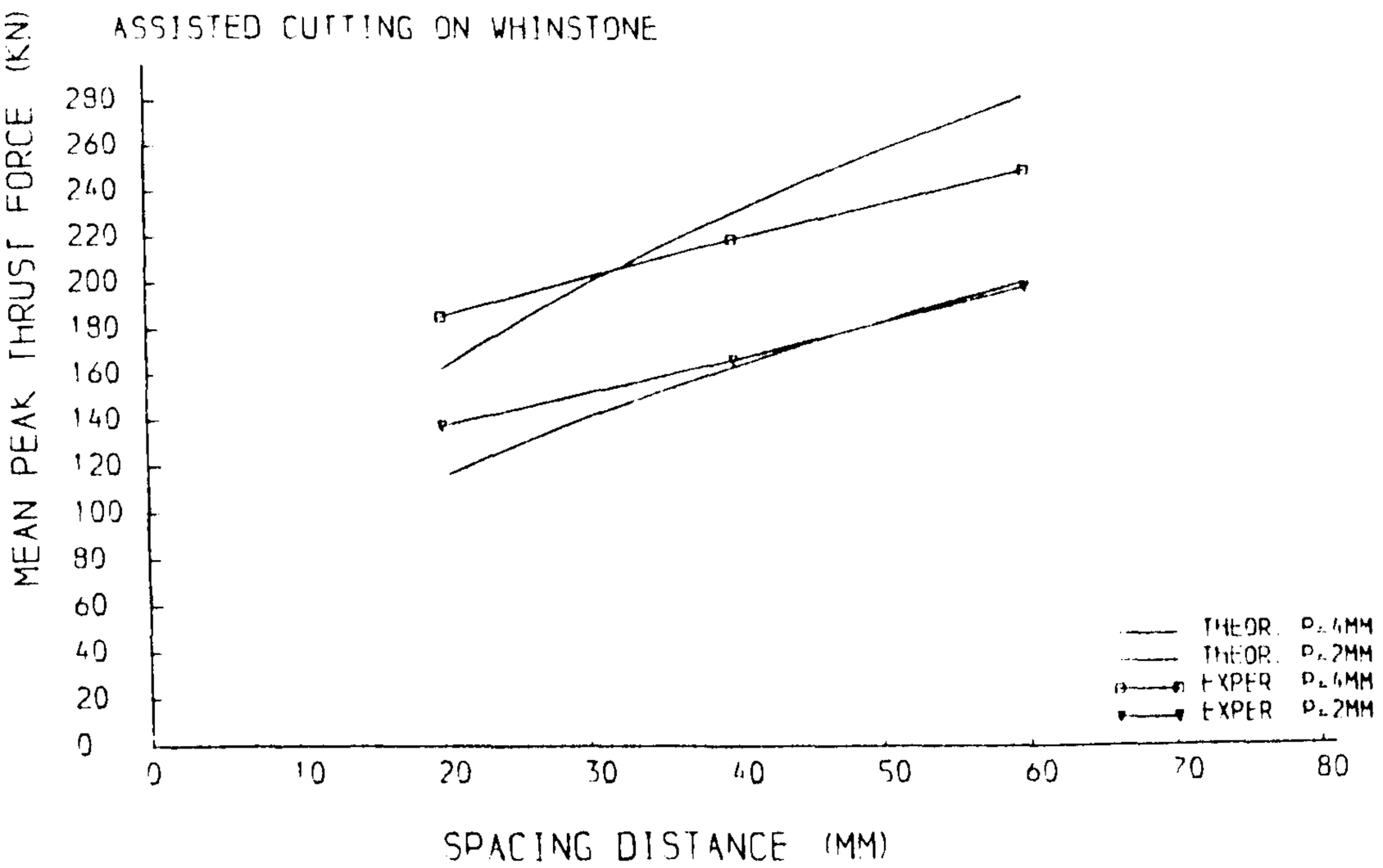

(a). MPTF

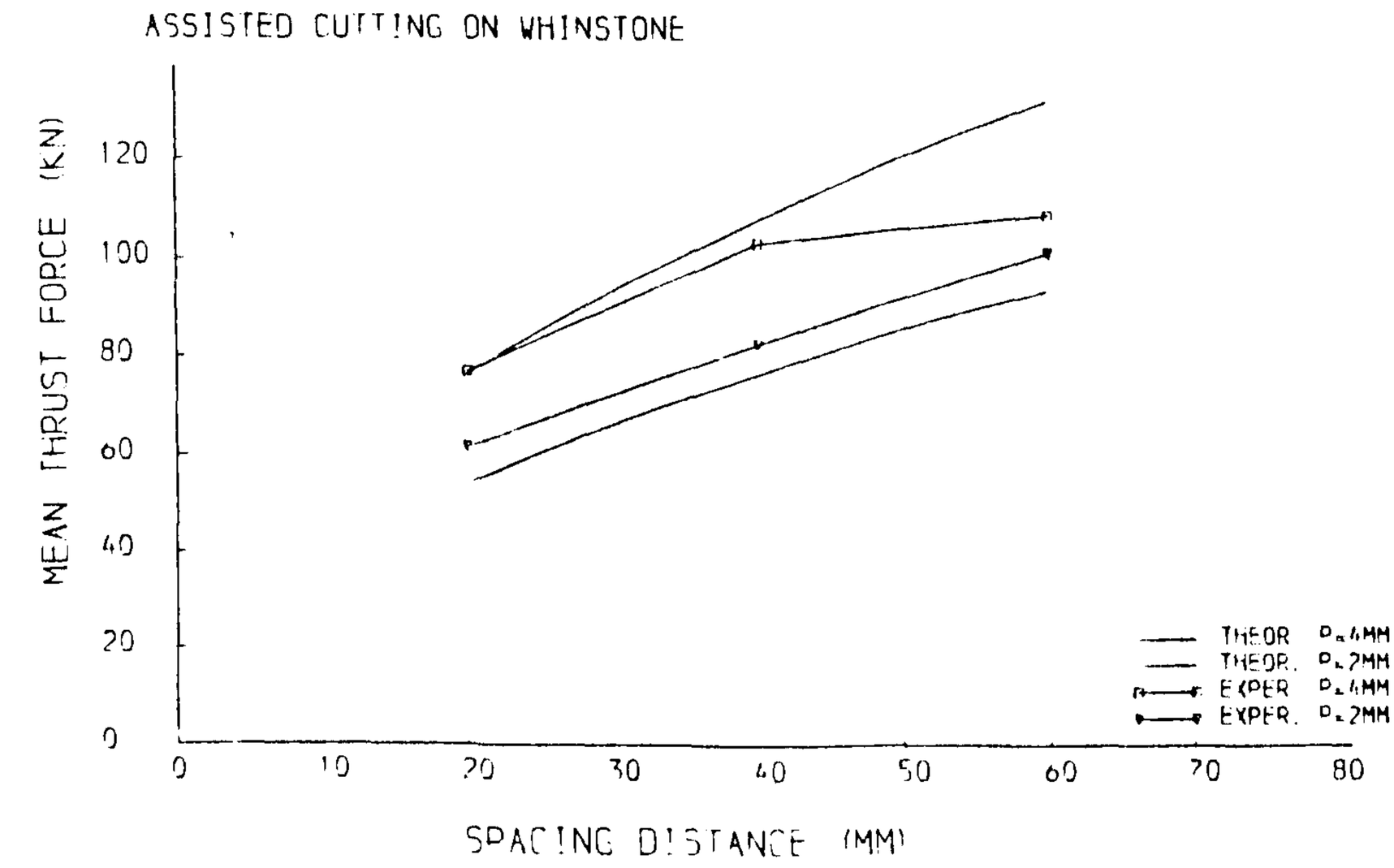

(b). MTF

Fig. 7.3.7 Comparison of experimental and theoretical results of water jet assisted cutting tests on Whinstone

cutting is only 36% of that for unassisted cutting. This gives an approximate 20% reduction in thrust forces, according to predictor equation (7.3.10). This, plus the reduction of fracture toughness due to the moisture, gives the total reduction in the forces during the water jet assisted cutting. So, the predicted water jet assisted disc cutter thrust force is:

$$FT^w = \frac{2\sqrt{\pi}}{3} B_f K^w \sqrt{s}\sqrt{Dp - p^2}\tan\frac{\theta}{2} \qquad 7.3.11$$

where

FT^w = water jet assisted disc thrust force,

K^w = fracture toughness of soaked rock.

However, the other factors, such as the rock microstructure, may affect the performance of rock cutting by the assistance of a low pressure water jet, which we can see from the different performance of two rocks used in this study, Pennant Sandstone and Whinstone. As mentioned in Chapter 6, the powder cores observed from Pennant Sandstone, can not be collected during the cutting tests on Whinstone. For such reason, the 20% reduction by clearing the powder core from the groove is not always true. Figs 7.3.6 and 7.3.7 give the comparison study of water jet assisted disc cutting tests on Pennant Sandstone and Whinstone. As no powder core was found during the cutting tests on Whinstone, $p_a = p$ in this case.

7.4 PREDICTION OF TBM PERFORMANCE

The primary objective of this study is to provide the manufacturers, designers, and users of TBM's with theoretically and experimentally derived machine performance mathematical model for use in field boreability and performance predictions.

There are considerable difficulties in attempting to relate rock fracture parameters to tunnel machine advance rates for reasons explained by Athorn et al. (1983).

Table 7.5.1 Summary description of tunnel projects and tunnelling equipment

Tunnel	Culver-Goodman	TARP 73-287-2H
Location	Rochester, New York	Chicago, Illinois
Contractor	Joint venture— J. F. Shea Inc. and Peter Kiewit Son Inc.	Traylor Brothers Inc.
Total tunnel length (m)	8597	7364
Excavated diameter (m)	5.8	6.5
TBM model	191-161	213-190
Number of cutters	45	47
Number of cutterhead motors	6	8
Motor rating (kW)	149	149
Cutterhead rotation rate(rpm)	4.61	5.66

Table 7.5.2 Summary of TBM performance parameters and rock property data

		TBM performance parameters		Rock property data		
Tunnel	Rock unit	Penetration per revolution (mm/rev)	Field penetration index, R_f (N/mm)	Fracture toughness, K_{Ic} ($MN\,m^{-1.5}$)	Critical energy relese rate, G_{Ic} (N/m)	Total hardness, H_t ($g^{-1.5}$)
Culver-Goodman	Reynales limestone	6.78	20.9	2.07	83	83
	Irondequoit limestone	7.67	15.4	1.36	44	46
TARP 73-287-2H	Markgraf dolostone	9.30	14.8	1.80	52	49
	Romeo dolostone	8.03	18.0	2.47	68	70

They are:

1. very little of the total energy available is utilised directly in cutting;
2. very little of the total available machine time is spent in cutting.

To solve these problems, only the optimum TBM performance is considered.

Recent work on rock cutting, incorporating the concept of fracture mechanics was reported by Nelson et al. (1985). The descriptive information on the tunnel projects and the tunnel boring machines for the study are listed in Table 7.5.1. Table 7.5.2 includes machine performance parameters and rock fracture property data for each rock unit selected. The results show that the critical energy release rate, G_{IC}, a property which includes the effects of rock strength and stiffness, can be correlated with optimum TBM performance, but no clear trend of field penetration index, R_f, with fracture toughness, K_{Ic} can be identified. This is not surprising as two of the most important factors which affect the performance of TBM's, the geometry of disc cutters and spacing distance, were not taken into the account. According to the predictor equation (7.3.10), the field penetration index is re-defined as

$$R_i = \frac{P}{\sqrt{Dsp}\tan\frac{\theta}{2}} = \frac{R_f\sqrt{p}}{\sqrt{Ds}\tan\frac{\theta}{2}} \qquad 7.4.1$$

where

s= excavated radius/number of cutters,

p= penetration per revolution,

P=total trust force per revolution,

$= R_f \times p$,

D= diameter of cutters,

θ= angle of disc cutters.

One finds that the coefficient of determinants have been improved from Nelson's figure of 0.34 to 0.47 using the newly defined penetration index vs fracture toughness,

and from 0.92 to 0.98 for the newly defined penetration index vs fracture surface energy. Note, as the diameter and angle of cutters were not given in the reference, $d = 400$ mm and $\theta = 60°$ were taken in both cases to calculate R_i.

It is obvious that more field performance predictions should be made in order to reach at a firm conclusion with regard to the applicability of the predictor equations. However, the acquisition of such data is usually a difficult and lengthy process. Also, as the standard rock fracture test methods have just been suggested, it is unfortunate that no data is available on fracture parameter measurements. Consequently, the prediction of tunnel boring performance using fracture parameters at present is difficult. In the near future, therefore, it is essential that fracture tests be conducted on rocks at excavation projects, to verify the new approach to performance prediction.

Chapter 8

THE STRESS DISTRIBUTION BENEATH THE DISC CUTTER

8.1 INTRODUCTION

The theoretical problem of determining the load needed for a wedge indenter (or roller cutter) to penetrate a rock surface has been under investigation for several decades. Generally, the theoretical elastic solution for a point load on a half space known classically as the Boussinesq solution (Timoshenko and Goodier, 1951) is used for understanding the indenter-rock behaviour. With the development of computing technology, numerical methods have been employed in the stress analysis. Using the finite element method, Wang and Lehnoff (1976) analysed the stress distribution for the bit penetration, and Ingraffea (1987) studied crack propagation under simulated cutter loading. Another similar work was undertaken by Pritchard and Reimer (1980), who consider the problem of water jet slotting on roller cutting forces.

In this Chapter, a boundary element method of stress analysis is described and the solution procedure used in a computer program for the analysis is presented. It is therefore possible to determine the stress distribution around a disc cutter for every possible condition.

8.2 PRECEPTS OF BOUNDARY ELEMENT METHOD

The governing differential equations for linear elasticity, for a homogeneous,

isotropic, two-dimensional body, are the following equilibrium equations

$$\sigma^*_{jk,j} + \Delta^i = 0 \qquad j = 1,2;\ k = 1,2 \tag{8.2.1}$$

The fundamental solution for a two-dimensional isotropic body is

$$u^*_{lk} = \frac{1}{8\pi G(1-\nu)}[(3-4\nu)\ln\frac{1}{r}\Delta_{lk} + \frac{\sigma_r}{\sigma_{x_l}}\frac{\sigma_r}{\sigma_{x_k}}] \tag{8.2.2}$$

$$p^*_{lk} = -\frac{1}{4\pi G(1-\nu)r}\{\frac{\sigma_r}{\sigma_n}[(1-2\nu)\Delta_{kl} + 2\frac{\sigma_r}{\sigma_{x_l}}\frac{\sigma_r}{\sigma_{x_k}}]$$
$$-(1-2\nu)(\frac{\sigma_r}{\sigma_{x_l}}n_k - \frac{\sigma_r}{\sigma_{x_k}}n_l)\} \tag{8.2.3}$$

where p^*_{lk} and u^*_{lk} represent the tractions and displacements in the k direction resulting from the unit force in the l direction.

The elements of p^* and u^* can be written in matrix form as

$$p^* = \begin{vmatrix} p^*_{11} & p^*_{12} \\ p^*_{21} & p^*_{22} \end{vmatrix}, \qquad u^* = \begin{vmatrix} u^*_{11} & u^*_{12} \\ u^*_{21} & u^*_{22} \end{vmatrix}. \tag{8.2.4}$$

The displacements, tractions, and body force vectors are now

$$u = \begin{vmatrix} u_1 \\ u_2 \end{vmatrix}, \quad p = \begin{vmatrix} p_1 \\ p_2 \end{vmatrix}, \quad b = \begin{vmatrix} b_1 \\ b_2 \end{vmatrix}, \tag{8.2.5}$$

The basic boundary equation can be written as,

$$c_i u_i + \int_\Gamma u p^* d\Gamma = \int_\Gamma p u^* d\Gamma + \int_Q b u^* dQ \tag{8.2.6}$$

Equation (8.2.6) applies for a point in the boundary and if $c = 1$ it also applies for an internal point. Once the displacements and tractions are known over all the surface, one can compute the internal displacements and stresses at any point using the displacements

$$u_i = \int_\Gamma p u^* d\Gamma - \int_\Gamma u p^* d\Gamma + \int_Q b u^* dQ \tag{8.2.7}$$

or

$$u_i = \int_\Gamma p_j u^*_{ij} d\Gamma - \int_\Gamma u_j p^*_{ij} d\Gamma + \int_Q b_j u^*_{ij} dQ \tag{8.2.8}$$

and the stresses

$$\sigma_{ij} = \int_{\Gamma} p_k u^*_{ijk} d\Gamma - \int_{\Gamma} u_k p^*_{ijk} d\Gamma + \int_{Q} b_k u^*_{ijk} dQ \qquad 8.2.9$$

8.3 PROBLEM CONFIGURATION

The macro flow chart for the rock cutting analysis program can be seen in Fig. 8.3.1. The basic program of the boundary element analysis is based on the work undertaken by Brebbia et al. (1984). The main program calls the following subroutines:

INPUT1 — Reads the rock properties, cutter geometry and criterion parameters.

INPUT — Reads the program input.

MATRX — Computes influence matrix A and vector F.

SLNPD — Solves the system of equations using Gauss elimination.

OUTPT — Outputs the boundary solution including computation and printout of boundary stresses and internal displacements and stresses.

CRITE — Checks the boundary nodes and internal points by Coulomb shear strength criterion.

This study was limited to a consideration of one individual disc cutter. The idealization of cutter-rock interface configuration is as shown in Fig. 8.3.2. The cutting is carried out by prescribing the disc cutter displacements. Forty six boundary nodes were used. Among them, twenty five nodes were located along the discretized

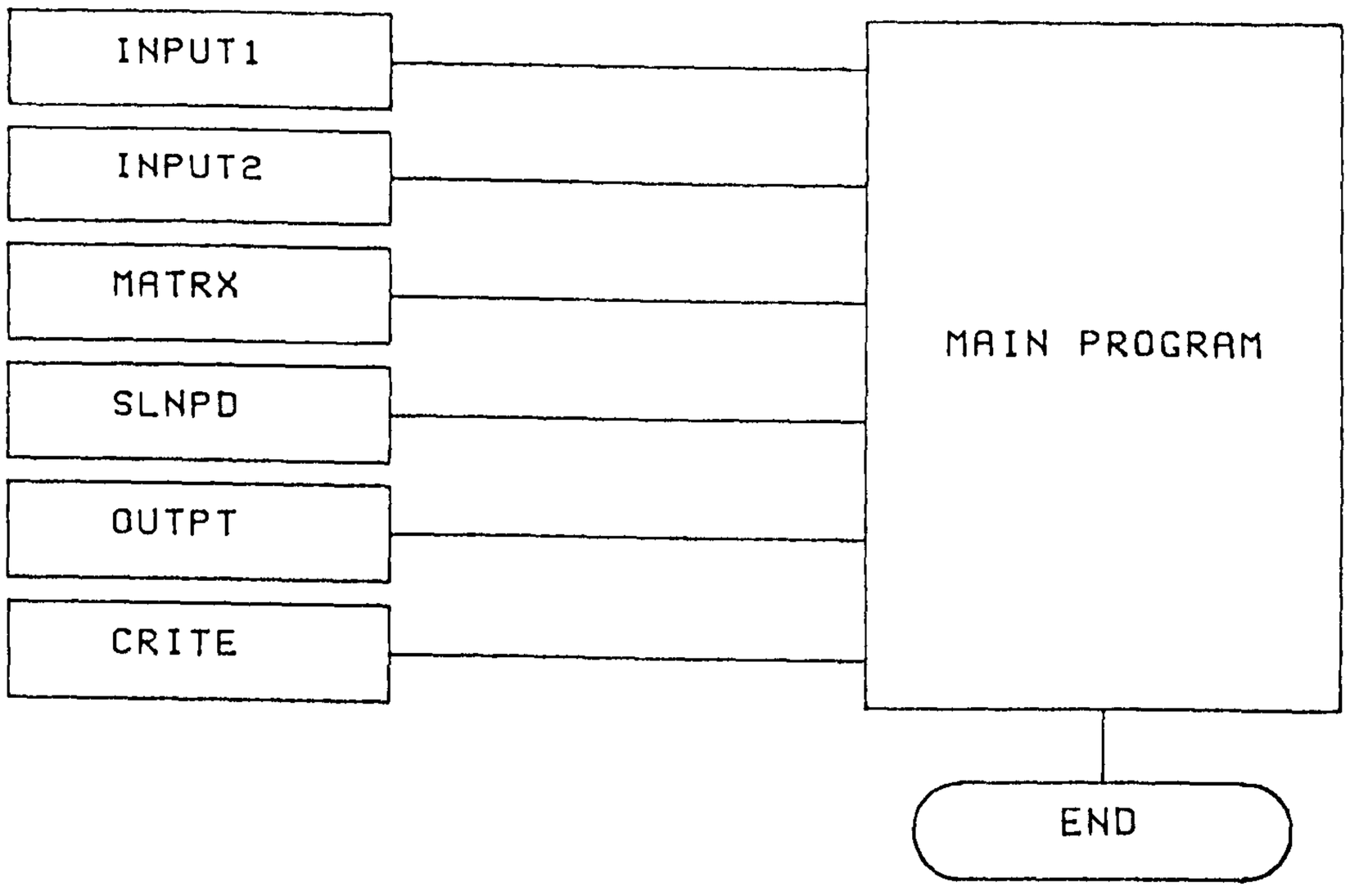

Fig. 8.3.1 Main flow chart

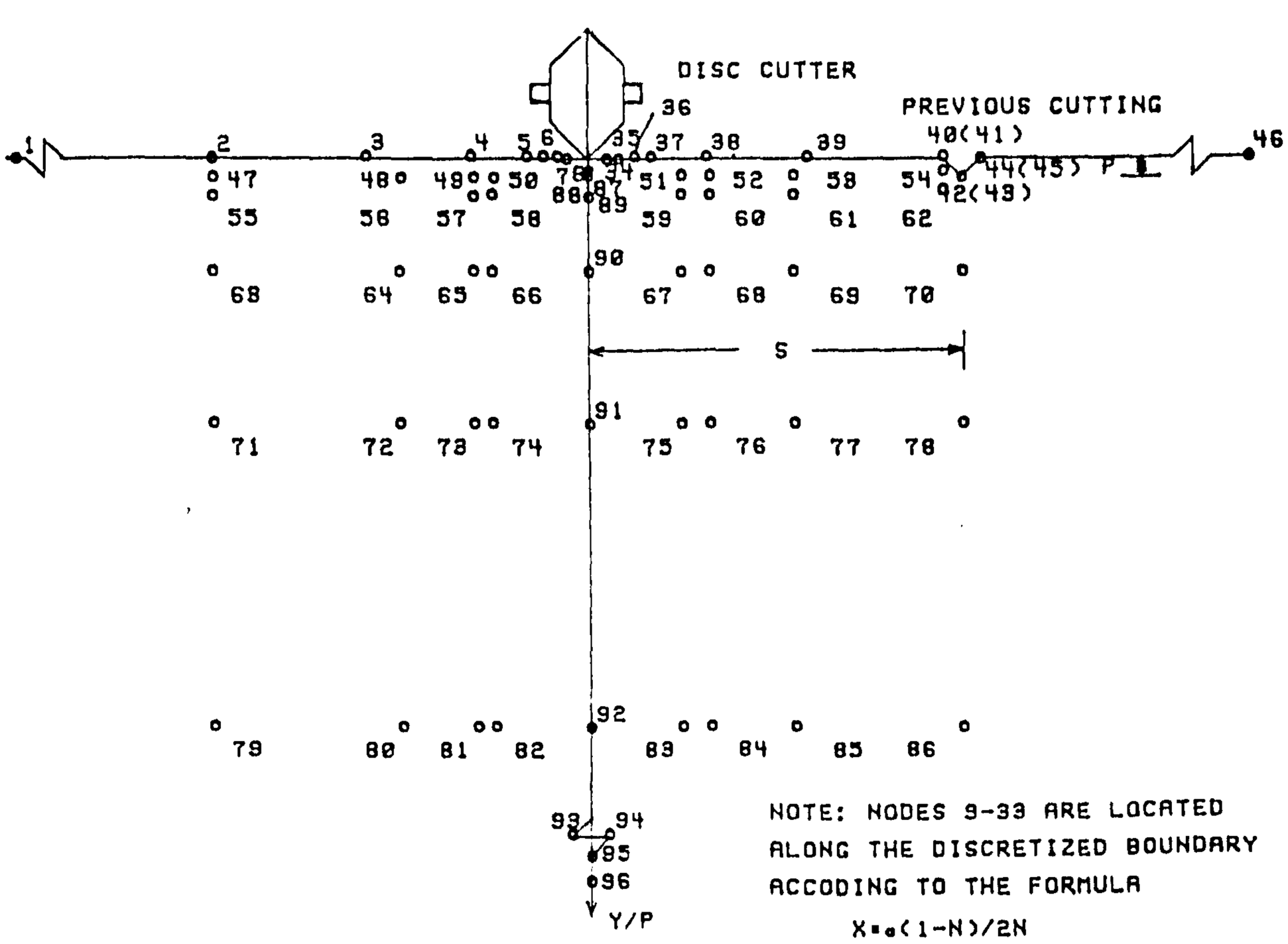

Fig. 8.3.2 The idealization of cutter-rock interface configuration and boundary element and internal points discretization

boundary according to the formula

$$X = \frac{a(1-N)}{2N} \qquad 8.3.1$$

where

a = the half length of the discretized boundary,

N = |nodes number − centre node number|.

Additional results were obtained at 50 internal points. The important information of the stress distribution under the disc cutter may be obtained from these points.

The data related with the geometry of the disc cutter, the rock properties and cutting penetration and spacing are input from Channel 5, simply by answering the questions shown on the screen. It allocates Channel 1 for output.

8.4 MATERIAL FAILURE MODEL

Coulomb shear strength criterion have been used in this study to determine the form of the yield surface. In the Coulomb model, the shear strength of rock is made up of two parts – a constant cohesion and a normal stress-dependent frictional component:

$$S = c + \sigma_n \tan\phi \qquad 8.4.1$$

where

c = cohesion,

ϕ = angle of internal friction.

Or, it can be expressed in form of principle stresses, as:

$$\sigma_1 = \frac{2c\cos\phi + \sigma_3(1+\sin\phi)}{1-\sin\phi} \qquad 8.4.2$$

The material compressive strength is related to c and ϕ by

$$\sigma_c = \frac{2c\cos\phi}{1-\sin\phi} \qquad 8.4.3$$

Thus

$$\sigma_1 = \sigma_c + \sigma_3\frac{1+\sin\phi}{1-\sin\phi} \qquad 8.4.4$$

The rock material modelled is Springwell Sandstone. The properties of Springwell Sandstone were reported in Chapter 3.

8.5 PARAMETER STUDY

As mentioned previously, the way of inputing data in this study is quite simple. Generally speaking, all cutting conditions can be considered with this program. The variables involved in this study are:

Edge angle of disc cutters (degree): 60, 70, 80, 90, 100

Tip radius of disc cutters (mm): 0, 1, 2, 3, 4, 5

Depth of penetration (mm): 2, 4, 6, 8, 10

s/p ratio: 2, 4, 6, 8, 10, 15, 20, 30, 50, 100

The reference parameters used in this study are:

Compressive strength (MPa): σ_c

Mean contact stress (MPa): $P(m)$

Half length of discretized boundary (mm): a

Penetration depth (mm): p

The mean contact stress is calculated by summarizing the normal stress along the discretized boundary and getting an average value. The thrust force, then, can be obtained as

$$FT = P(m)A \qquad 8.5.1$$

where

A= projected contact area.

8.6 RESULTS

8.6.1 The Effect of The Edge Angles

The sharp disc cutters of 150mm diameter with 2mm penetration depth and 40mm spacing distance were used for this study. Table 1.6.1 gives the comparative results of ratios of the peak contact stresses to compressive strength, $P(p)/\sigma_c$; the ratios of the peak contact stresses to mean contact stresses, $P(p)/P(m)$; the ratios of the mean contact stresses to compressive strength, $P(m)/\sigma_c$; and the thrust forces calculated by Eq. (8.5.1).

Table 8.6.1 Results of cutting with disc cutters at different edge angles

$p = 2mm,\ s = 40mm,\ r = 0mm,\ D = 150mm$

angle	$P(p)/\sigma_c$	$P(p)/P(m)$	$P(m)/\sigma_c$	FT
60	931.16	31.38	29.68	31.62
70	771.42	31.62	24.39	31.52
80	646.68	31.26	20.69	32.06
90	545.05	30.29	17.99	33.20
100	459.48	28.91	15.89	34.95

a. Contact stresses along the discretized boundary

The effects of the edge angles on the contact stresses along the discretized boundary are illustrated in Fig. 8.6.1. With the mean contact stress as a reference parameter, the differences between different edge angles are not significant (Fig. 8.6.1 (a)), while with the compressive strength as a reference parameter, the peak contact stress, which is at the centre of the boundary, is reduced as the edge angle

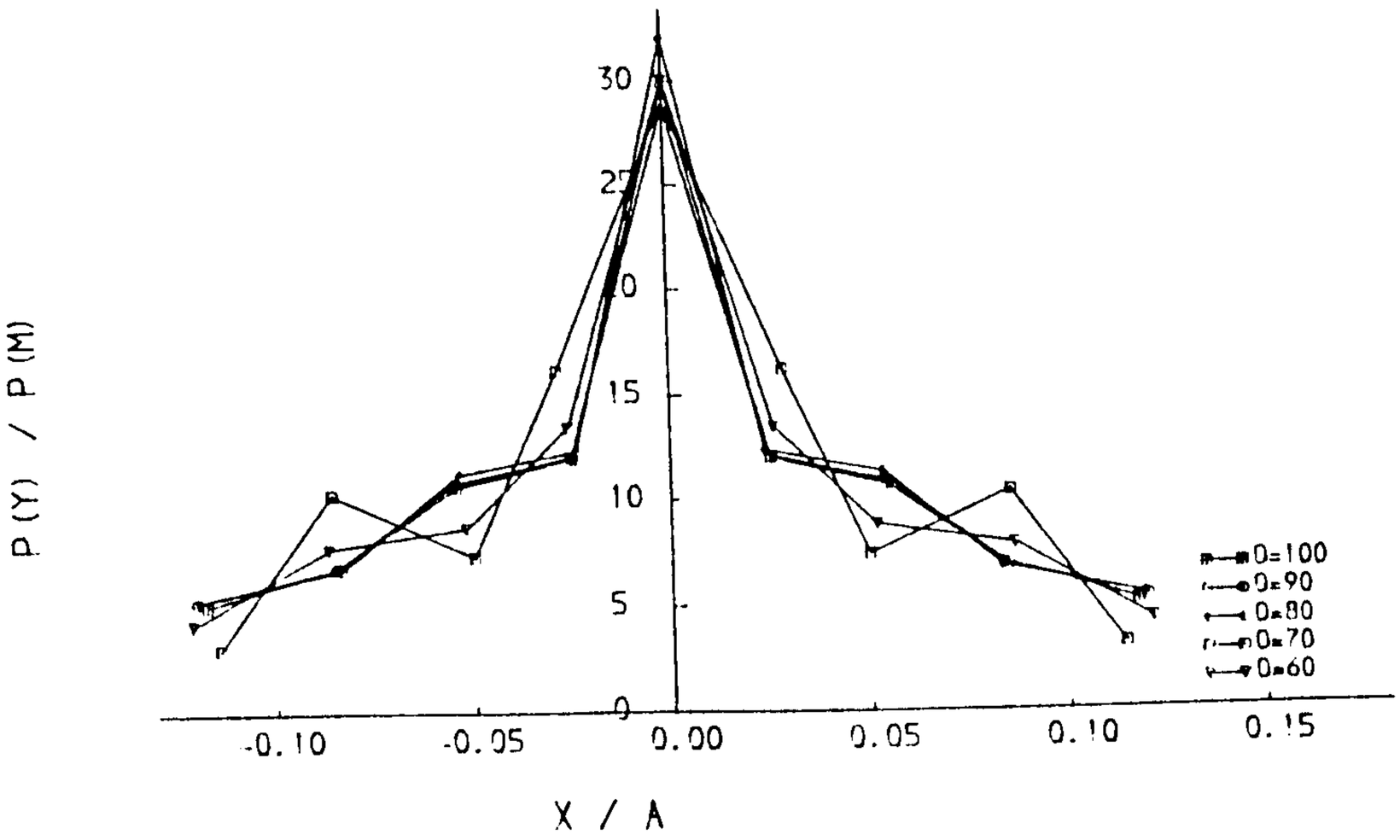

(a).

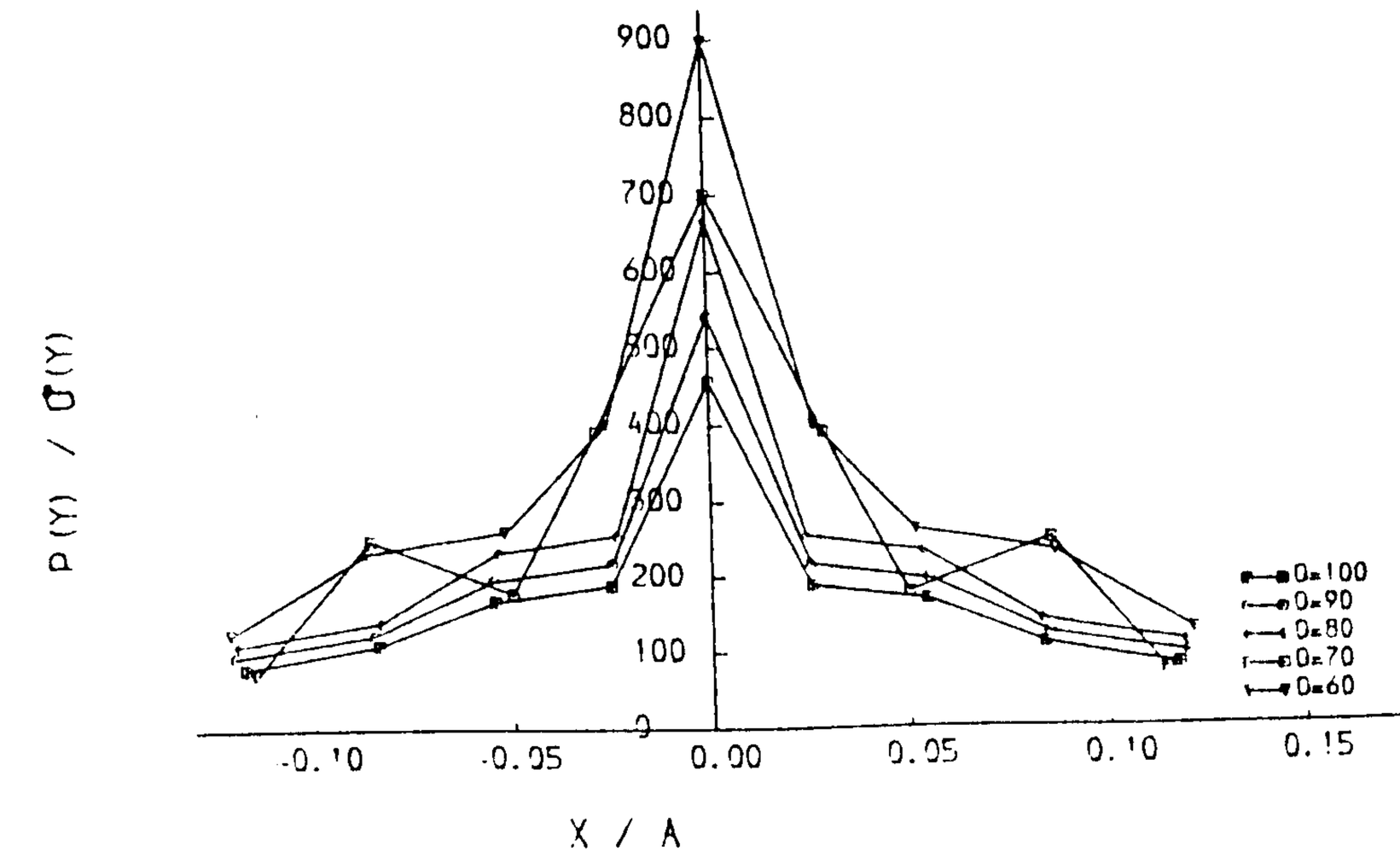

(b).

Fig. 8.6.1 The effects of the edge angles on the contact stresses along the discretized boundary

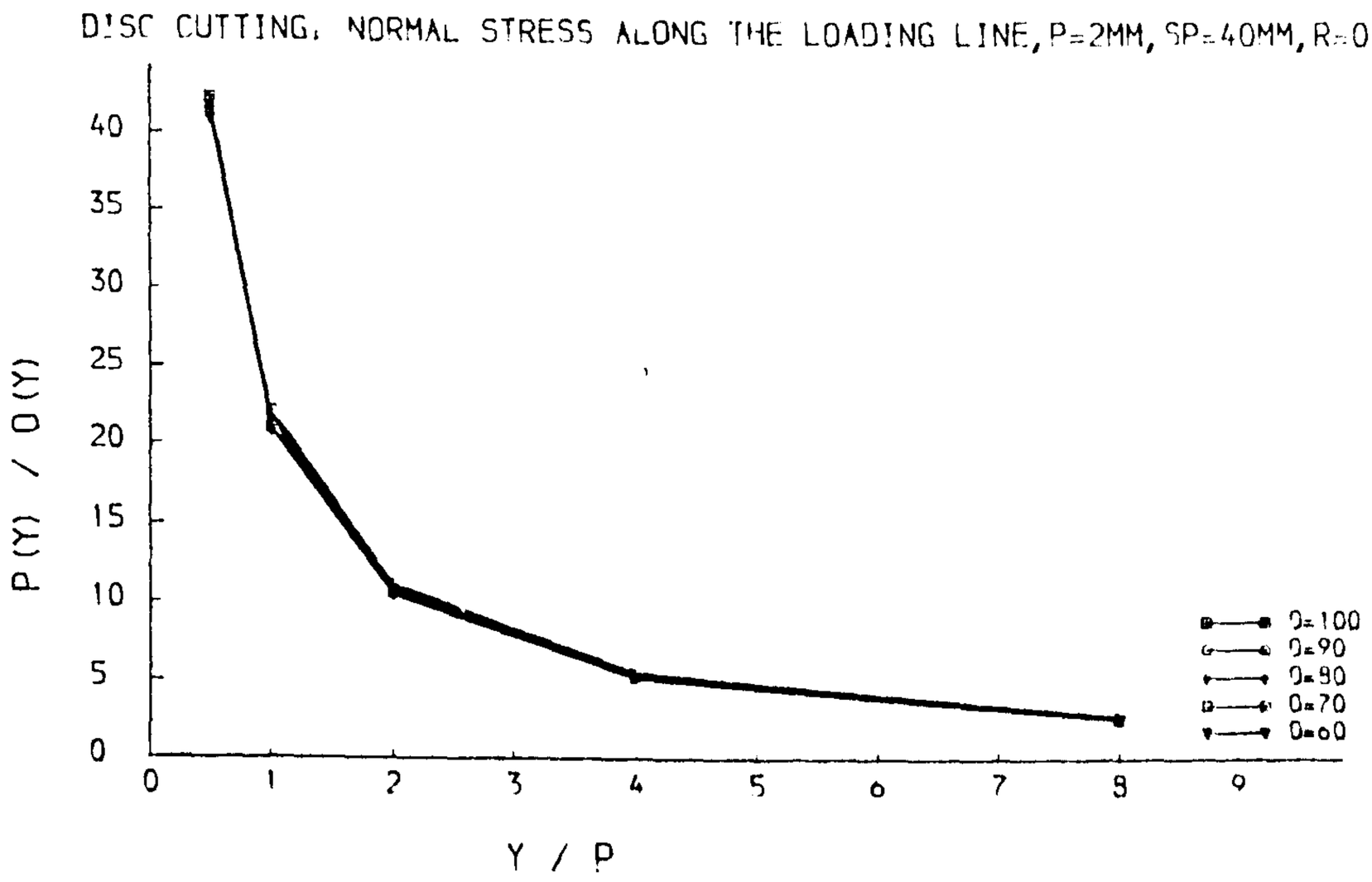

Fig. 8.6.2 The effects of the edge angles on the contact stresses along the loading line

increases. The ratio of the peak contact stress to compressive strength is reduced from 930 for edge angle of 60° to about 460 for edge angle of 100°.

b. Stresses along the centre loading line

Fig. 8.6.2 shows the effect of the edge angle on stresses along the centre loading line. It can be seen that the stress reduces rapidly as y/p ratio is increases. No significant difference in the ratio of $P(y)/\sigma_c$ can be found using disc cutters with different edge angles.

c. Mean contact stress and thrust force

The ratios of mean contact stress to compressive strength against edge angles are listed in the Table 8.6.1. A decline in the $P(m)/\sigma_c$ ratio is found as the edge angle increases.

As expected, the thrust forces calculated are reduced as the edge angle of the disc cutters is increased.

8.6.2 The Effect of Tip Radius

The disc cutter of 150mm diameter, 60° edge angle, at 2mm penetration depth and 40mm spacing distance was used in this study. The compared results of ratios of $P(p)/\sigma_c$, $P(p)/P(m)$, $P(m)/\sigma_c$ and FT are list in the Table 8.6.2 for a range of the radii from 0 to 5mm.

Table 8.6.2 Results of cutting with disc cutters of different tip radius

$p = 2mm,\ sp = 40mm,\ \theta = 60°,\ D = 150mm$

tip (r)	$P(p)/\sigma_c$	$P(p)/P(m)$	$P(m)/\sigma_c$	FT
0	931.16	31.38	29.68	31.62
1	115.78	3.97	29.14	56.85
2	82.32	3.41	24.14	72.23
3	67.67	3.29	20.54	85.62
4	58.21	3.36	17.27	94.32
5	53.44	3.47	15.38	104.37

a. Contact stresses along the discretized boundary

The ratios of $P(y)/P(m)$ to a/x plotted in Fig. 8.6.3 (a) for all conditions show little change. However, from the Fig. 8.6.3 (b), it can be seen that the ratio of $P(y)/\sigma_c$ reduced with increasing tip radii. The peak contact stresses reduce rapidly as the tip radius of the disc cutter increases (see Table 8.6.2)

b. Stresses along the centre loading line

From Fig. 8.6.4, it can be found that a significant difference is in the point of 0.5p for different tip radii. The maximum principle stress at these points decreases with increasing tip radius, while the rest of points concerned are almost at the same

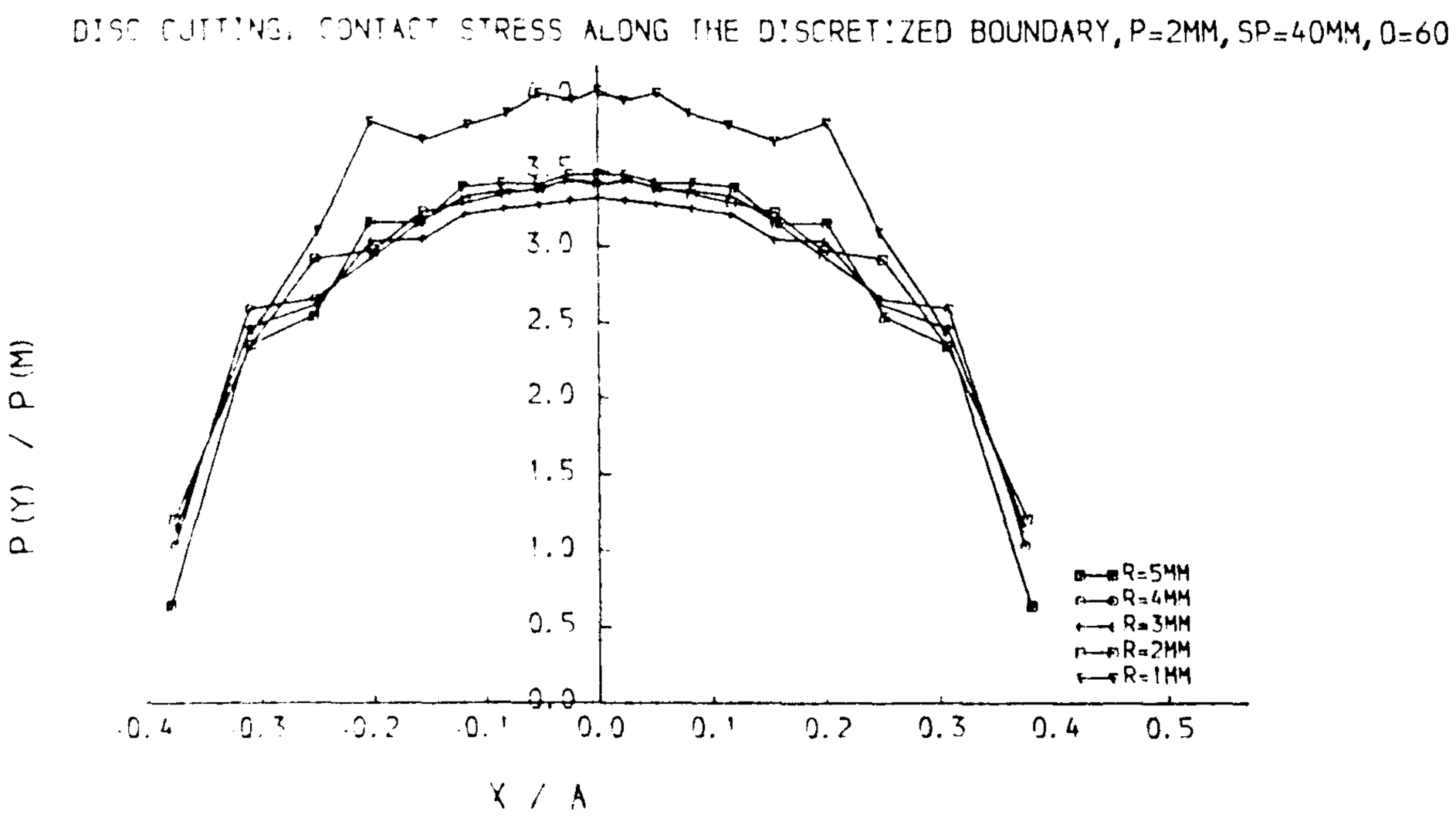

(a).

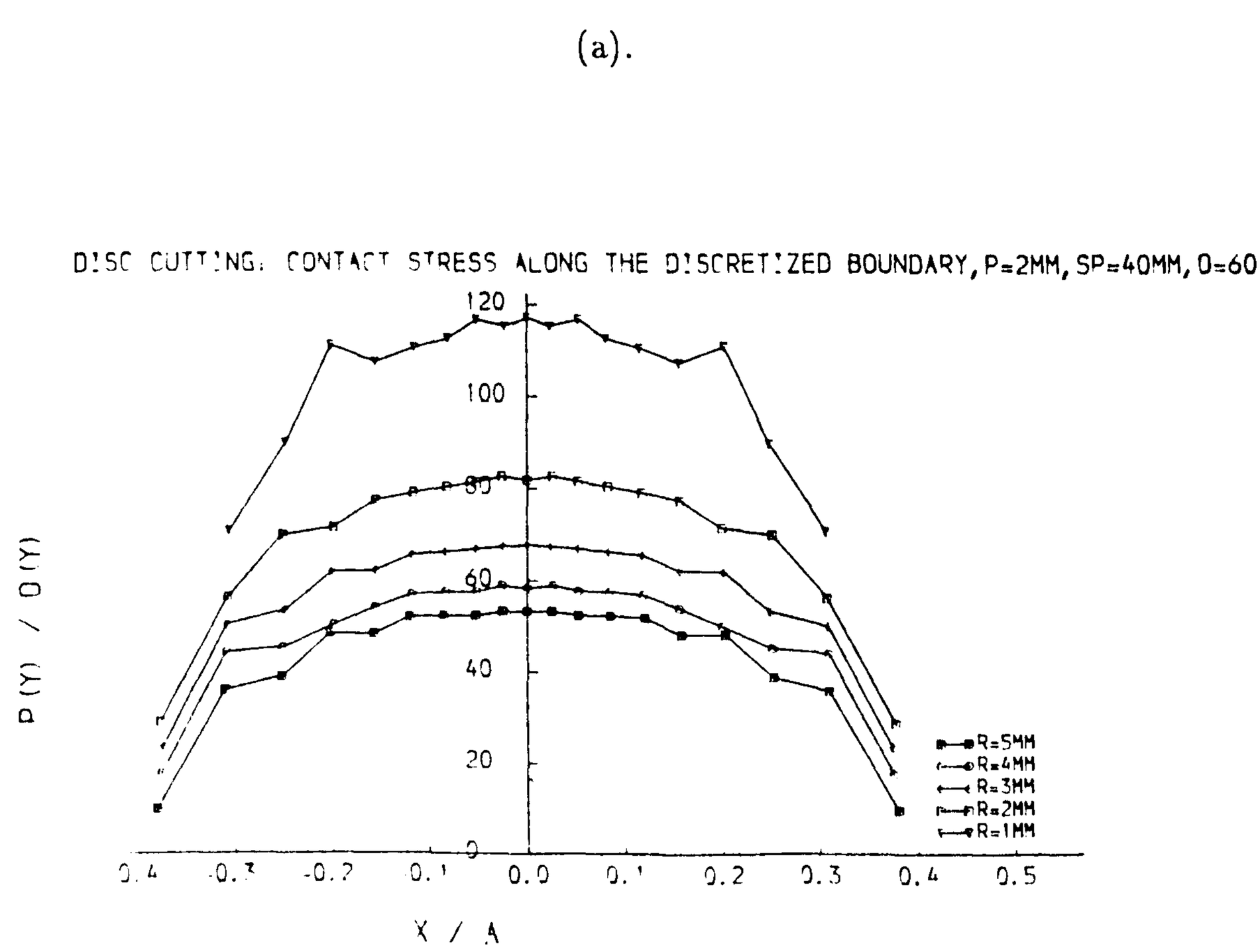

(b).

Fig. 8.6.3 The effects of the tip radius on the contact stresses along the discretized boundary

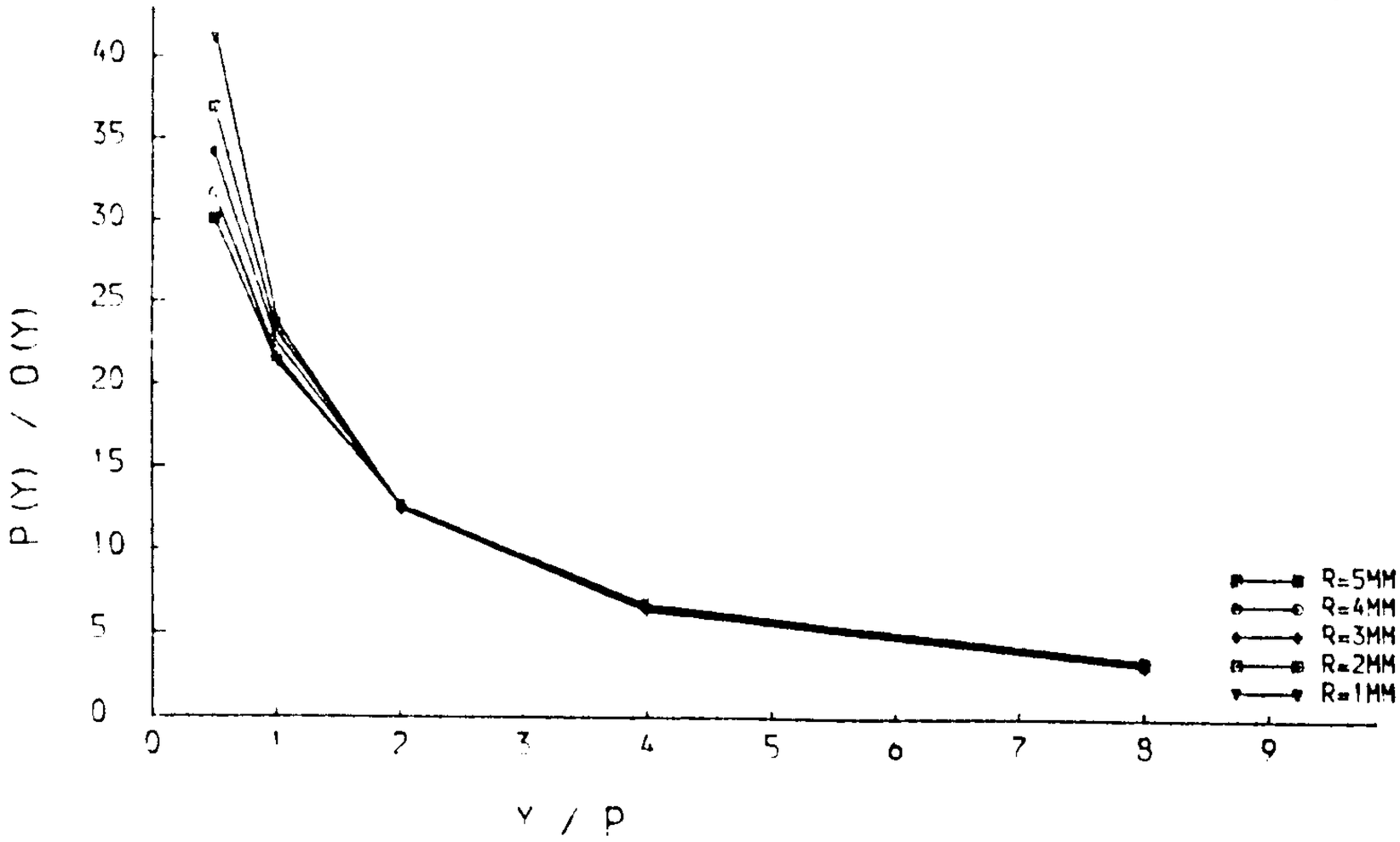

Fig. 8.6.4 The effects of the tip radius on the contact stresses along the loading line

level. This suggests that the change of tip radius has little effect on these points.

c. Mean contact stress and thrust force

Compared with the peak contact stresses, the mean contact stresses change slightly as the tip radius of the disc cutter increases, e.g., $P(p)/\sigma_c$ from about 30 for the sharp disc cutter to 15 for the cutter with a 5mm tip radius.

The thrust forces listed in Table 8.6.2 show, as expected, that much bigger thrust forces are needed for a disc cutter with a bigger tip radius.

8.6.3 The Effect of Penetration Depth

In this study, a sharp disc cutters of 150mm diameter and 60° edge angle with s/p ratio of 20 were considered. Using the sharp disc cutter, Table 8.6.3 lists the

Table 8.6.3 Results of cutting with disc cutters at different penetration depths

$s/p = 20,\ r = 0mm,\ \theta = 60°,\ D = 150mm$

penetr.	$P(p)/\sigma_c$	$P(p)/P(m)$	$P(m)/\sigma_c$	FT
2	931.16	31.38	29.68	31.62
4	946.89	29.10	32.54	97.40
6	958.02	27.79	34.48	188.27
8	966.03	26.84	35.99	300.42
10	972.78	26.12	37.24	431.45

results of cutting by penetrating the rock at different depths.

a. Contact stresses along the discretized boundary

Fig. 8.6.5 shows that the contact stresses along the discretized boundary increase with increasing penetration. The peak contact stress increases, but the ratio of $P(p)/P(m)$ decreases as the penetration depth increases.

b. Stresses along the centre loading line

From Fig. 8.6.6, it can be found that for the points deeper than penetration depth, the effect of penetration depth is not very significant. But for the points at depths less than the penetration, the influence of depth of penetration is considerable. The maximum principal stress increases with increasing penetration at these points.

c. Mean contact stress and thrust force

Table 8.6.3 shows that, as well as the thrust force, the ratios of $P(m)/\sigma_c$ increase with increasing penetration depth.

8.6.4 The Effect of s/p Ratios

a. Contact stresses along the discretized boundary

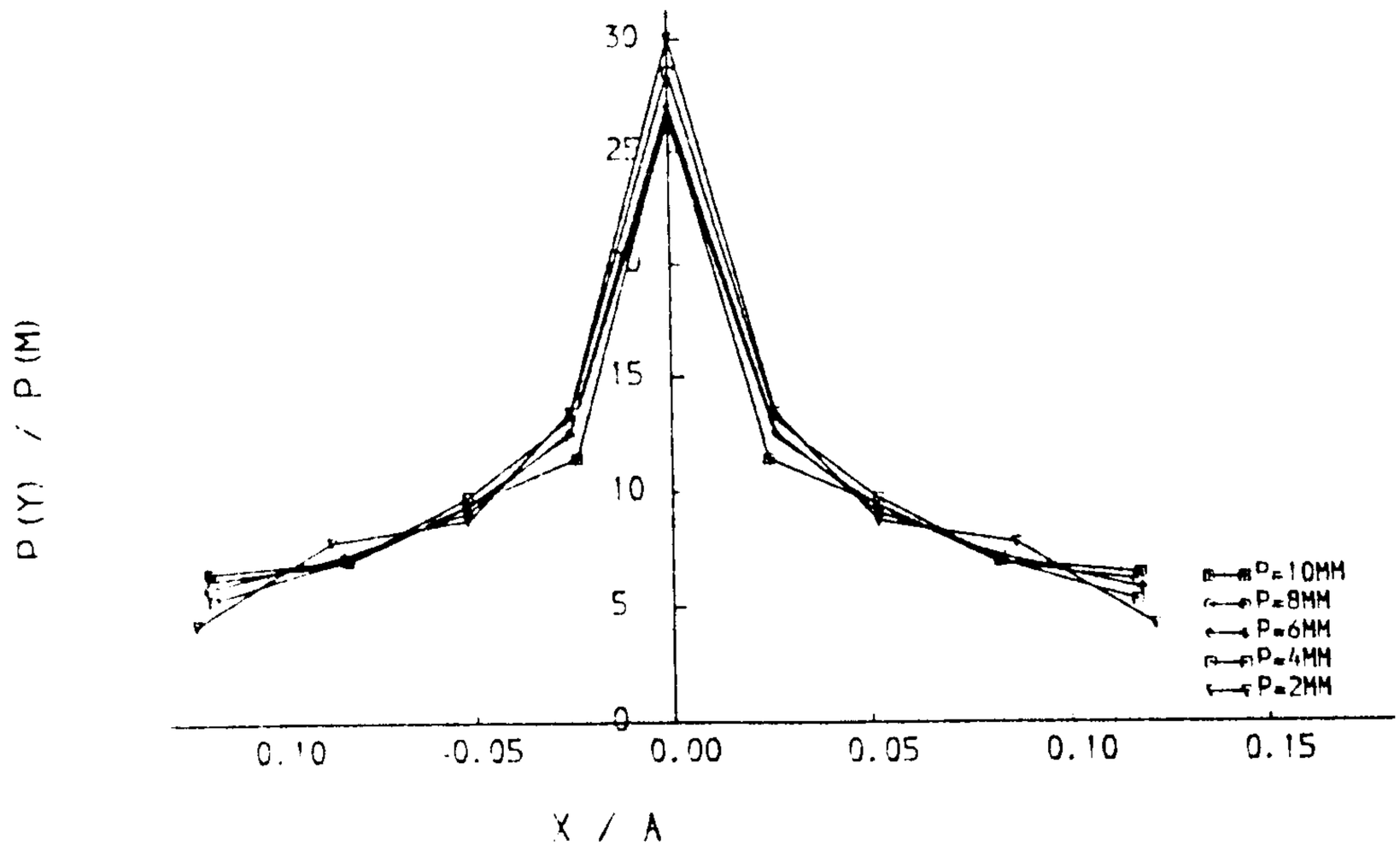

(a).

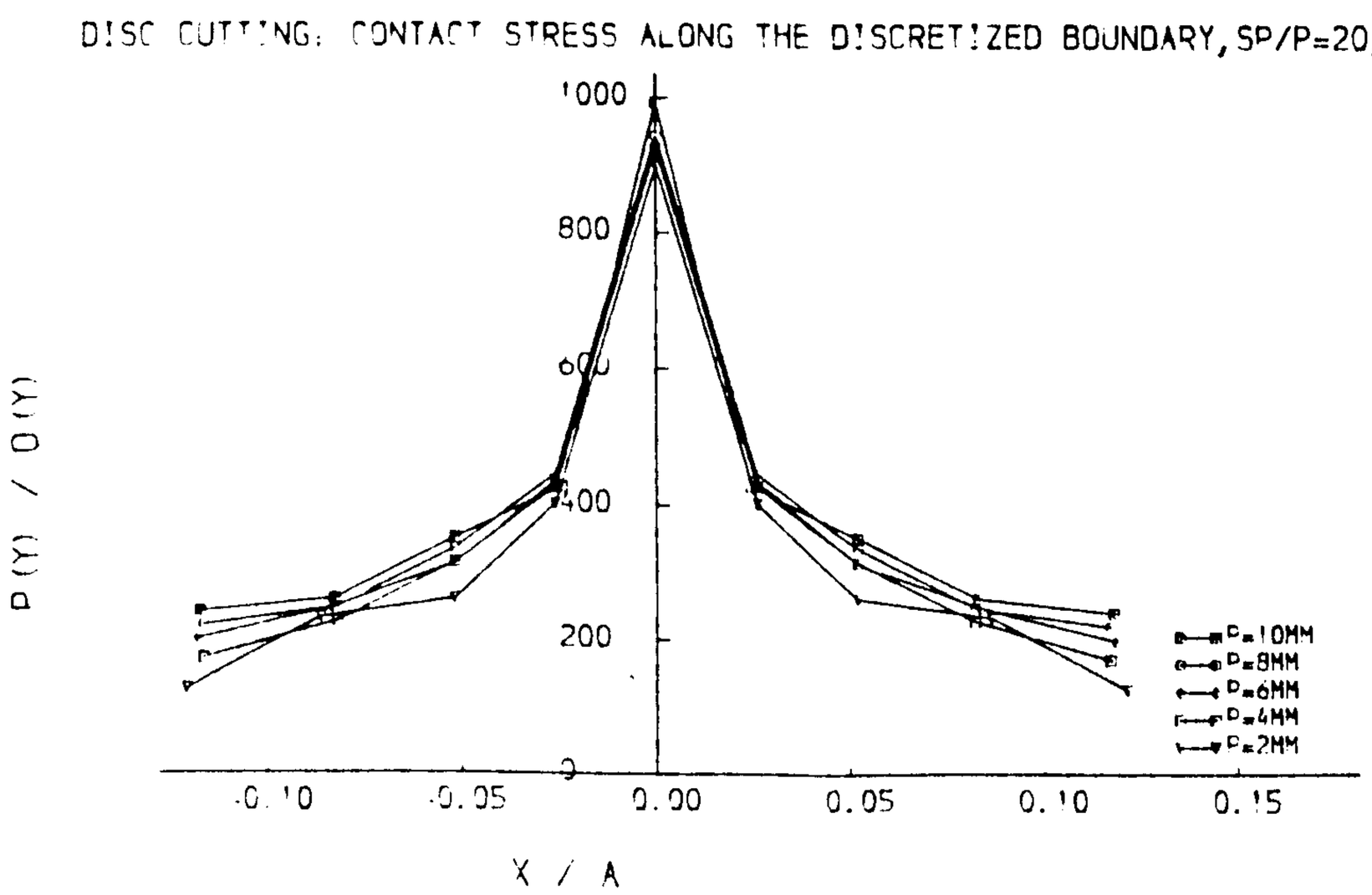

(b).

Fig. 8.6.5 The effects of the penetration on the contact stresses along the discretized boundary

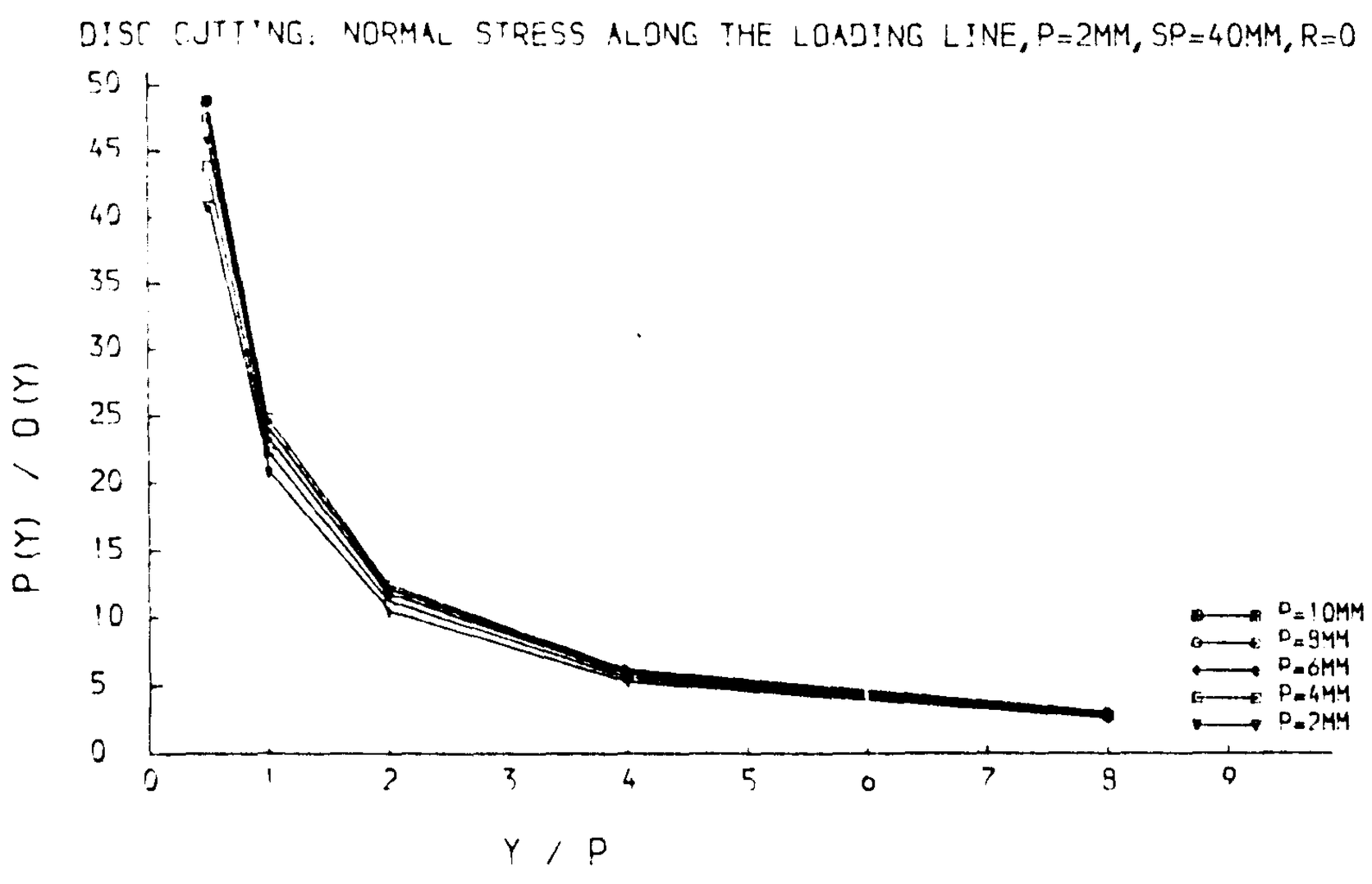

Fig. 8.6.6 The effects of the penetration on the contact stresses along the loading line

Table 8.6.4 Results of cutting with disc cutters at different s/p ratio

$p = 2mm,\ r = 0mm,\ \theta = 60°,\ D = 150mm$

s/p	$P(p)/\sigma_c$	$P(p)/P(m)$	$P(m)/\sigma_c$	FT
2	891.11	31.48	28.31	30.16
4	899.34	31.56	29.43	31.35
6	931.89	31.45	29.63	31.57
8	931.69	31.39	29.68	31.62
10	931.47	31.16	29.89	31.85
15	931.33	31.41	29.65	31.59
20	931.16	31.38	29.68	31.62
30	930.97	31.36	29.69	31.63
50	930.75	31.44	29.58	31.57
100	930.32	31.57	29.47	31.40

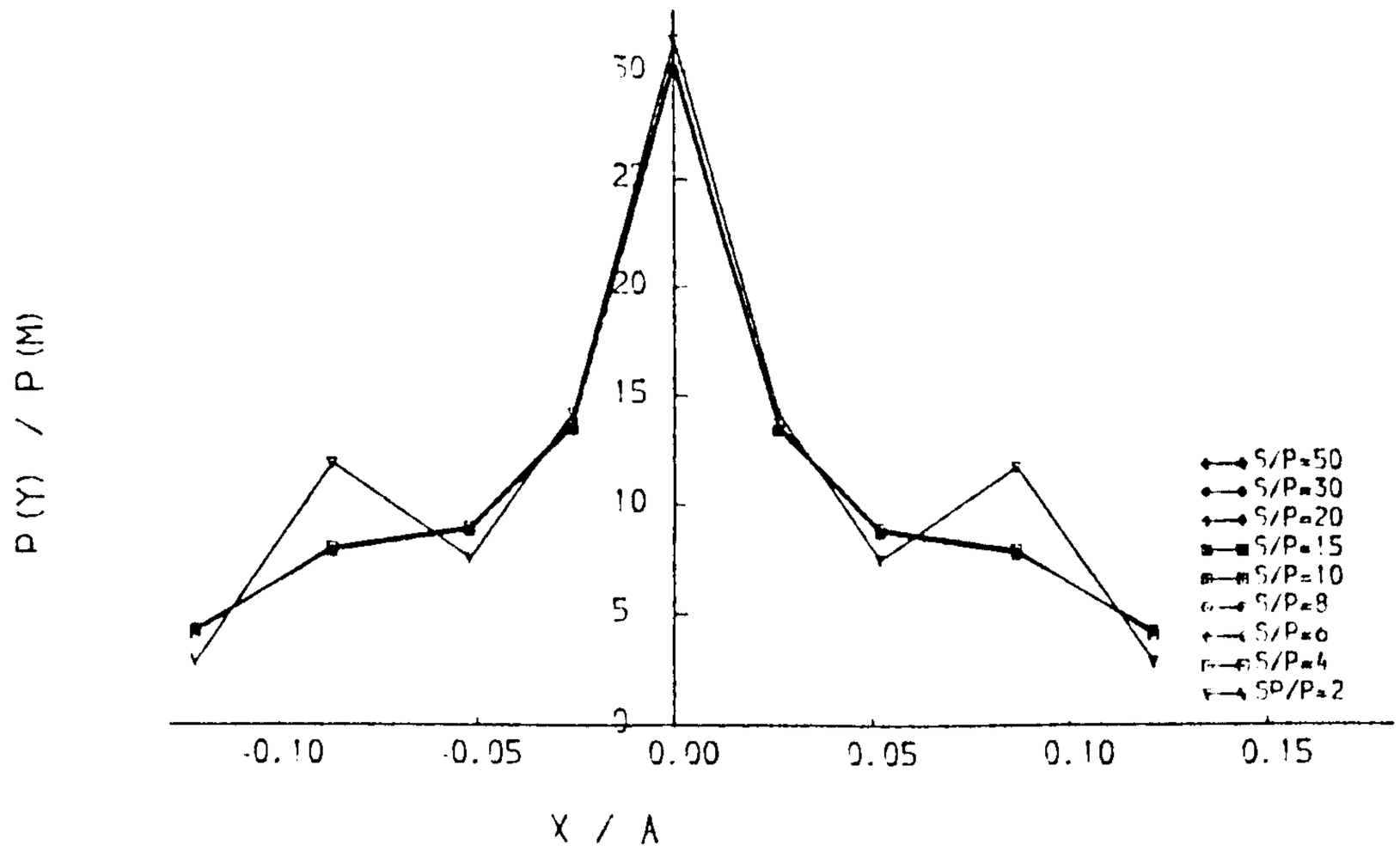

(a).

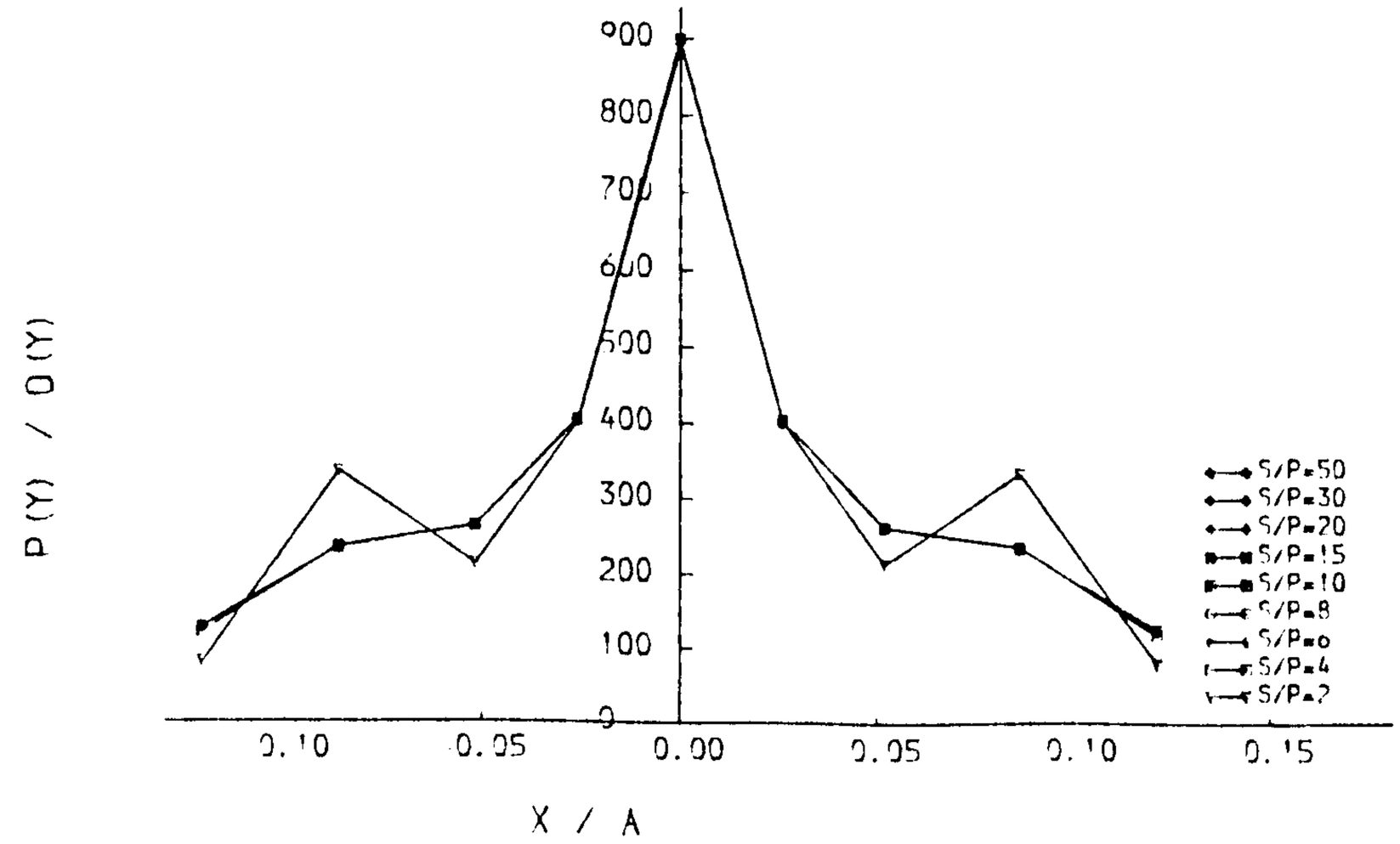

(b).

Fig. 8.6.7 The effects of the s/p ratio on the contact stresses along the discretized boundary

From Fig. 8.6.7, the distributions of the contact stresses along the discretized boundary are nearly constant when the s/p ratio is more than 6. For the s/p ratio of 2, the peak contact stress is much lower than that with higher s/p ratios.

b. Stresses along the centre loading line

The ratios of $P(y)/\sigma_c$ along the centre loading line for the disc cutting with different s/p ratios are plotted in Fig. 8.6.8. No significant changes can be found as the s/p ratios increase.

c. Mean contact stress and thrust force

Mean contact stress and thrust force increase as the s/p ratios increase up to 8. A further increasing s/p ratio has no influence on the mean contact stress and thrust force (Table 8.6.4).

8.6.5 The Crushed Zone

The crushed zone was determined by the Coulomb shear strength criterion mentioned in the Section 8.4. For all conditions, the crushed zones were found to be almost the same, as seen in Fig. 8.6.9. For the points at same penetration level, rock failure happened at depth less than y/p=8. For points with a y/p ratio of 8 and 18, the failure is found at the points within $|x/s|$ of 0.5. For points on the loading line, failure is observed up to y/p=18. An example of the failure points and their position is presented in Appendix F.

8.7 DISCUSSION

1. Tool wear

For a TBM excavating in hard rock formations, the running costs of the machine

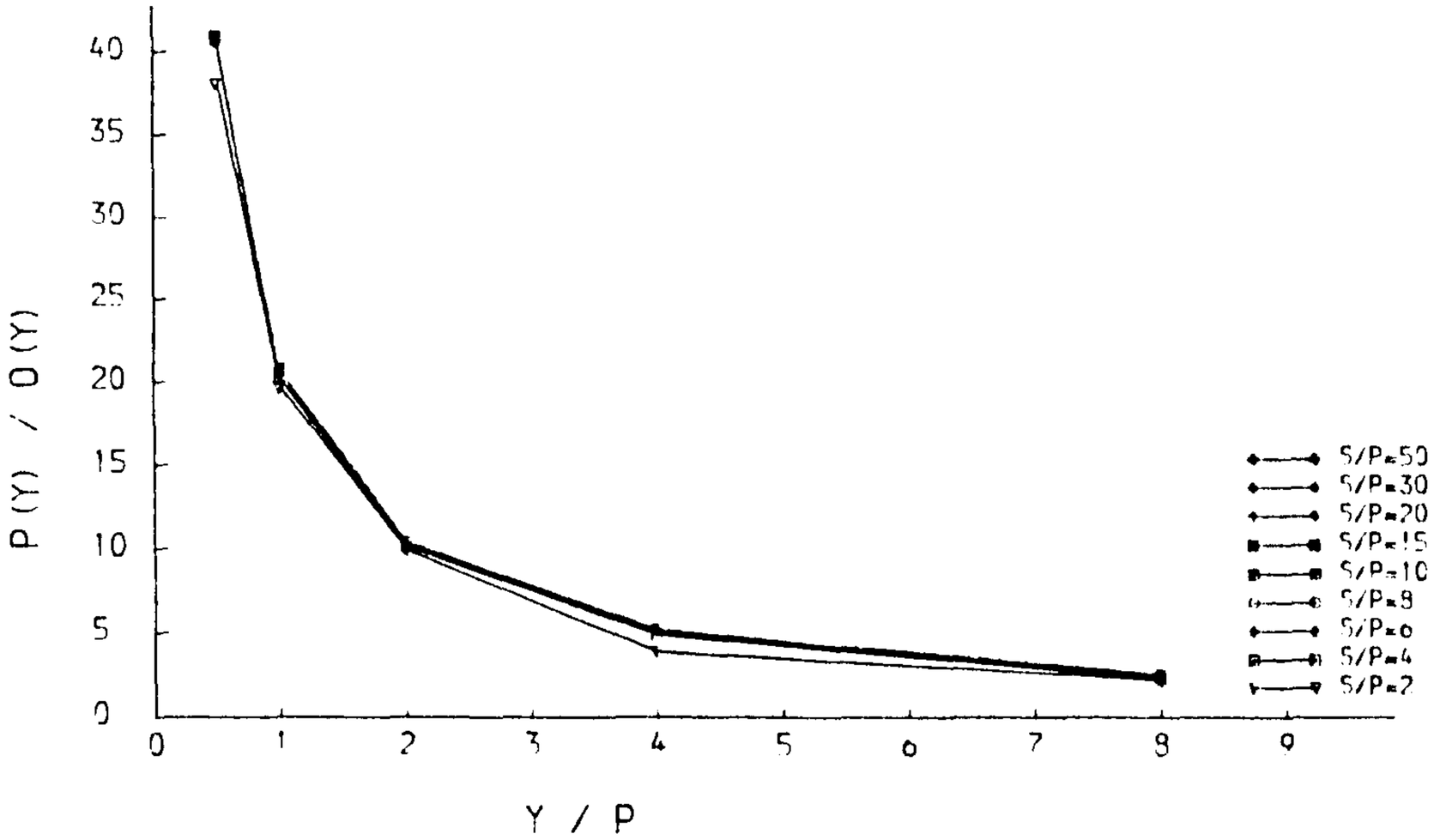

Fig. 8.6.8 The effects of the s/p ratio on the contact stresses along the loading line

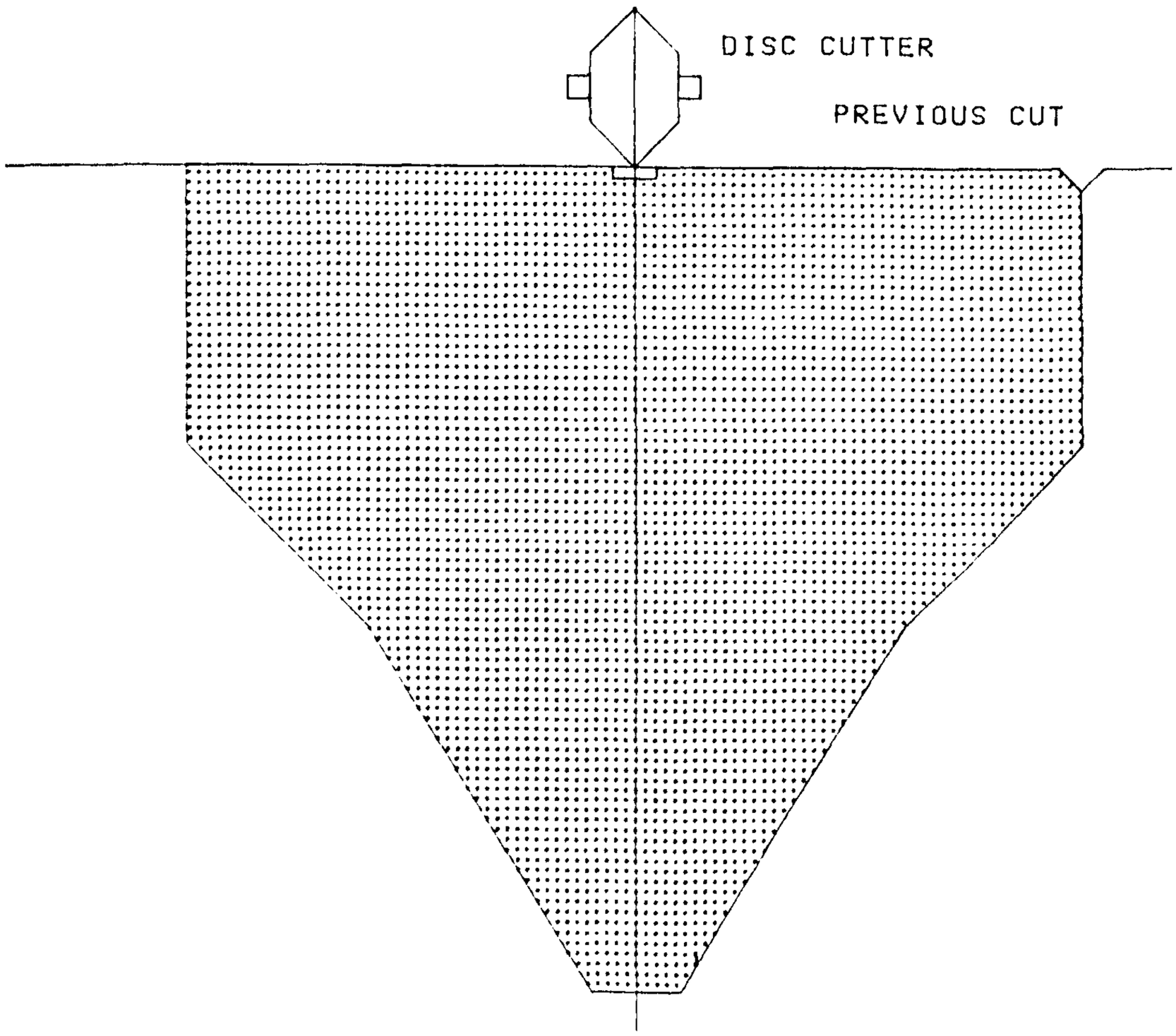

Fig. 8.6.9 The crushed zone under the disc cutter

is mainly from the wear of disc cutters, as latter being directly related to the force on the tool. This study shows that for a disc cutter of increased tip radius, the thrust forces increase rapidly, though the peak contact stress at the tip point is reduced. However, with an increased edge angle, the thrust forces on the disc cutter increase only a little, while the peak contact stress at the tip point is reduced a lot. This suggests that for a TBM excavating in very hard rock formations, the disc cutter with a larger edge angle would be more effective.

2. Thrust force

The thrust force has been found to be very sensitive to variation in the tip radius and depth of the penetration, but only slightly affected by the edge angle and s/p ratio. This suggests that TBM's can be designed with a bigger spacing distance and fewer disc cutters in the cutting header. This means, on the other hand, heavier loading of the remaining cutter. However, as the cutting condition in this study is only concerned with single pass cutting on smooth rock surfaces, untypical of what occurs in the field, a suitable spacing distance for the design of TBM's should be determined only after considering all such factors.

3. Comparison with laboratory tests

The results given by the boundary element analysis are much larger than that obtained from the laboratory tests. The possible reasons are:

a. The cutting process considered is indentation rather than cutting, as the stress analysis is based on the tool's displacements and the chipping of the rock is not taken into account.

b. The elastic model used in this analysis assumes that the material can withstand very high stresses.

c. The calculated forces are based on values of Young's modulus, which can not be measured accurately for rock materials.

8.8 SUMMARY

A primary study of the stress distribution beneath the disc cutter is given in this Chapter. The results of analysis show that

1. The peak contact stress is at the tip point of the cutter, which is more related with the edge angle and tip radius of the tools. For the disc cutter with a 60° edge angle, the peak contact stress is double that of the cutter with a 100° edge angle, as is the mean contact stress. For the sharp disc cutter, the peak contact stress is 10 to 20 times that for the worn disc cutter, with doubling of the mean contact stress. The peak contact stress is not very sensitive to the penetration depth and s/p ratio, but the mean contact stress is affected by the penetration depth but not the s/p ratio.

2. The stresses along the loading line are reduced quite rapidly until the depth of the point is more than the penetration depth. For all conditions considered in this study, the points with the same y/p ratio and far from the surface are nearly at same level.

3. The thrust forces calculated are much higher than the results given by the laboratory tests. The main reasons are that an elastic model is used in the study, and the accurate value of Young's modulus which is very important parameter for stress analysis, is very difficult to measure.

Chapter 9

CONCLUSIONS AND PROPOSALS FOR FURTHER STUDIES

The experimental work has led following conclusions:

9.1 ROCK FRACTURE MECHANICS

1. Fracture toughness can be obtained from radially cracked ring specimens, three point bend specimens, and short bar specimens for three different directions of a rock mass. As this project has been performed before the publication of "Suggested methods for determining the fracture toughness of rock" (Ouchterlony, 1988), the methods used are not the suggested one. However, compared with the data produced by the suggested methods, the results obtained indicate very good agreement between the short bar and the short rod methods.

2. The values given by ring specimens are affected by the size of the specimens used. There is, however, no effect with different lengths of cracks on specimens of the same size. As the main purpose of this study is the application of fracture mechanics to rock cutting, no further study was undertaken.

3. The values of fracture toughness given by short bar is higher that that obtained by ring specimens and three point bend specimens. Several other researchers have drawn attention to this point.

9.2 INDENTATION TESTS

1. Indentation testing is a useful method in predicting the performance of TBM's.

In this study, the disc cutters were used as a type of indenter. This has several advantages:

a. The geometry of the indenter is identical to that of a TBM tool;

b. The result given by the indentation tests can be easily transferred to those of spaced cuts.

2. The mechanism of rock cutting is more or less similar to the penetration of an indenter into rocks. Fracture mechanics analysis provides a new way of understanding rock breakage by an indenter.

3. The relationship between contact pressure and uniaxial compressive strength given by Tabor (1951) and by Johnson (1977) was used in this study. It is:

$$\sigma_0 = C\sigma_y \qquad 9.2.1$$

$$\frac{\sigma_0}{\sigma_y} = \frac{1}{\sqrt{3}}[1 + \ln(\frac{4E}{3\pi\sigma_y \tan\frac{\theta}{2}})] \qquad 9.2.2$$

Very good agreement between the theoretical analysis and experimental results is indicated, and this makes prediction of unrelieved cutting forces with simple uniaxial compressive strength possible.

9.3 MECHANICAL CUTTING

1. Though the unrelieved cutting tests were not included in this study, previous investigations have provided enough, useful data for comparison with the theoretical model developed in this study. Based on the assumption that there is no friction on the contact zone, and there is a uniform compressure around the zone, the thrust force FT, Rolling force FR and side force FS can be determined by the contact pressure times projected areas.

For the disc cutting with a sharp disc cutter, we have

$$\left.\begin{aligned} FT &= \tfrac{4}{3}p\tan\tfrac{\theta}{2}\sqrt{Dp-p^2}\;\sigma_0 \\ FR &= p^2\tan\tfrac{\theta}{2}\;\sigma_0 \\ FS &= \tfrac{2}{3}p\sqrt{Dp-p^2}\;\sigma_0 \end{aligned}\right\} \qquad 9.3.1$$

The contact pressure, σ_0, can be obtained from Eq. (3.2.1) or Eq. (3.2.2). The above analysis had been proved using the data given by Roxborough and Phillips (1975,b), and Bilgin (1977). For a worn disc cutter, the forces can be obtained as: when $p \leq r(1-\sin\frac{\theta}{2})$,

$$\left.\begin{aligned} FT &= \tfrac{4}{3}p\sqrt{2r-p}\sqrt{D'-p}\;\sigma_0 \\ FR &= \tfrac{\phi}{2}r^2-\sqrt{p}\sqrt{(r-p)^3}\;\sigma_0 \\ FS &= \tfrac{2}{3}p\sqrt{D'p-p^2}\;\sigma_0 \end{aligned}\right\} \qquad 9.3.2$$

when $p > r(1-\sin\frac{\theta}{2})$,

$$\left.\begin{aligned} FT &= \tfrac{4}{3}p'\tan\tfrac{\theta}{2}\sqrt{D'p'-p'^2}\;\sigma_0 \\ FR &= [(p'^2-p''^2)\tan\tfrac{\theta}{2}+r^2(\tfrac{\pi(180^\circ-\theta)}{360^\circ}-\cos\tfrac{\theta}{2}\sin\tfrac{\theta}{2})]\;\sigma_0 \\ FS &= \tfrac{2}{3}p\sqrt{D'p-p^2}\;\sigma_0 \end{aligned}\right\} \qquad 9.3.3$$

where

$D' = D - 2r(1-\frac{1}{\sin\frac{\theta}{2}})$.

$p' = p - r(1-\frac{1}{\sin\frac{\theta}{2}})$.

$p'' = -r(\sin\frac{\theta}{2}-\frac{1}{\sin\frac{\theta}{2}})$,

$\phi = \tan^{-1}\sqrt{\frac{p}{r-p}}$.

2. The relationship between thrust force and rolling force is specially important, as it is the same for both unrelieved cutting tests and the relieved cutting tests. The ratio of FT/FR obtained in this study is bigger than that provided by previous investigation. For a sharp disc cutter, it is:

$$\frac{FT}{FR} = \frac{4}{3}\sqrt{\frac{D-p}{p}} \qquad 9.3.4$$

Compared with FT/FR ratios provided by other investigators, Eq. (9.3.4) has a better agreement with the experimental results.

3. It is found that the ratios of unrelieved cutting forces to relieved cutting forces have a linear relationship with $\sqrt{s/p}$ rather than s/p ratios which were widely accepted at present. The relieved cutting force can be found as follows:

$$(FT)_{re} = B\sqrt{\frac{s}{p}}(FT)_{un} \qquad 9.3.5$$

where

$B = \frac{1}{\sqrt{15}}$;

when $s/p > 15$, $s = 15p$ for the single pass cutting test.

4. By using fracture mechanics analysis, the cutting forces predicted for the relieved cutting tests have following forms:

$$FT = \frac{2}{3}\sqrt{\pi}B_f K\sqrt{s}\sqrt{Dp - p^2}\tan\frac{\theta}{2} \qquad 9.3.6$$

where

for mean thrust force,

$$B_{f1} = \begin{cases} 9.12, & \text{for worn disc cutter,} \\ 5.26, & \text{for sharp disc cutter.} \end{cases}$$

for mean peak thrust force,

$$B_{f2} = \begin{cases} 19.49, & \text{for worn disc cutter,} \\ 8.17, & \text{for sharp disc cutter.} \end{cases}$$

And then using Equation (9.3.4), the rolling force can be easily calculated.

5. The predictor equations given by this author and other researchers have a general form:

$$FT = C_p R_p\sqrt{s}\sqrt{Dp - p^2}\tan\frac{\theta}{2} \qquad 9.3.7$$

or, as $D >> p$,

$$FT = C_p R_p\sqrt{Dsp}\tan\frac{\theta}{2} \qquad 9.3.8$$

where

C_p = a constant or a function of penetration depth,

R_p = a parameter of rock properties.

9.4 WATER JET ASSISTED CUTTING

1. For so called "hard rock" of compressive strength up to 260 MPa in this study, the improvements of water jet assisted rock cutting using pressure from 13.79 MPa (2,000 psi) to 55.16 MPa (8,000 psi) are significant. The reductions of cutting forces are up to 40% from all three patterns of water jet nozzle locations used in Pennant Sandstone, and about 20% in Whinstone.

2. The effects of cutting speed on the efficiency of low-pressure water jet assisted disc cutting were investigated. With cutting speeds in the regions of 0.25 m/s to 1 m/s, the cutting forces only change slightly. Therefore it can be said that cutting speed had little influence on the results of the disc cutting tests. Thus the findings indicate that improvement in the penetration rate of TBM's will be best served by the use of low pressure water jet.

3. Only little is gained by increasing the water jet pressure in the region from 13.79 to 55.16 MPa. The fact that water jet pressures of 13.79 MPa can still improve the cutting performance is very encouraging, as, besides improved performance, better machine safety and reliability is likely.

4. Nozzle locations have some effect on the improvement of cutting forces, but they are not very significant. A nozzle position put beside the cutter tool achieves the best results, but being much closer to the ridges which result in the course of cutting, they are susceptible to damage.

5. The results have shown that as the spacing distance increases, the improvement of water jet assisted disc cutting increases. Thus by increasing the spacing distance used in TBM's, it may be possible to reduce the number of disc cutters used. Also for the same thrust force and fewer disc cutters a deeper penetration will result; the larger resulting thrust force on each disc will increase the powder core dimension beneath the tools, which, subject to the water jet removing the powder, will improve the effectiveness of the following cutting.

6. The mechanism of water jet assisted cutting was studied in this thesis. The main action of water jet, unlike high pressure water jet assisted cutting, is to clear the cutting traces. As there is a crushed core beneath the cutter tool, clearing this core affects a decrease in cutting penetration.

7. The prediction of cutting performance can be done by assuming that the water jet only clears the cutting traces. Using fracture mechanics analysis, the dimension of the crushed core formed beneath the cutter can be determined as following:

$$q = \frac{r(c)}{p} = \frac{1}{\sqrt{\pi}} = 0.56 \qquad 9.4.1$$

where

$r(c)$ = the core radius.

Thus the actual penetration depth, p_a, for the water jet assisted cutting is:

$$p_a = 0.64p \qquad 9.4.2$$

Instead of p, and K for dry rocks, p_a and K^w (for water saturated rocks) are used in equation (9.3.6). This gives water jet assisted disc thrust force FT^w as:

$$FT^w = \frac{2}{3}\sqrt{\pi}B_f K^w \sqrt{s}\sqrt{Dp_a - p_a^2}\tan\frac{\theta}{2} \qquad 9.4.3$$

9.5 STRESS ANALYSIS OF DISC CUTTING

1. The stress distribution beneath the disc cutter is studied. The thrust forces calculated is found to be much higher than the results measured in the laboratory tests. The main reasons are that (i) an elastic model is used in the study, and (ii) an accurate value of Young's modulus, which is a very important parameter for the stress analysis, is very difficult to measure.

2. The peak contact stress for the disc cutter with a 60° edge angle is about double that of the cutter with a 100° edge angle. The same conclusion can find in the mean contact stress. As the tool wear is directly related to the force on the tip of the tool, this finding suggests that for a TBM excavating in very hard rock formations, the disc cutter with a larger edge angle would be more effective.

3. The crushed zone was determined by the Coulomb shear strength criterion. For all cutting conditions considered in the study, the shape of the crushed zone is almost the same.

9.6 FURTHER RESEARCH

Further research work should be carried out in the following areas:

1. Fracture toughness, as an important parameter, has been used in rock engineering. However, for some reasons, this parameter is not widely accepted in rock cutting. In this study an attempt is made to apply the principle of rock fracture mechanics to the disc cutting operations. However, due to the limitation of time and finance, it was not possible to investigate the use of fracture parameters for more than three types of rocks. It is suggested, therefore, to extend the same type of approach in this thesis, by employing other types of

rock with a wide region of mechanical properties.

2. Although the methods of measuring fracture toughness used in this study are not as suggested by the International Rock Mechanics Society, the values of fracture toughness obtained in this study agreed very well with that measured by the suggested method. However, since the I.S.A.M. suggested methods measure the fracture toughness only in two dimensions, it is proposed that future work may use cracked ring specimens, or cracked Brazilian disk specimens, see Fig. 9.6.1 (Shetty et al., 1987; Rosenfield and Duckworth, 1987), to assess the fracture toughness in the third dimension. For the ring specimen, the crack may be made very small, i.e. 2% of the width of the specimen, for which the finite element method may be used to calculate the fracture toughness. Furthermore for the Brazilian specimen with a Chevron crack, the calibration of the specimen can be done by using three dimension finite element analysis. It is interesting to note, that the aforementioned tests (cracked ring and cracked Brazilian disk) can be used not only to Mode 1 fracture test but also for Mode 2 (see §4.2.2).

3. Although many experimental tests results have been reported since the 1970s for mechanical rock cutting, the lack of measured fracture parameters makes prediction by the use of these parameters impossible. Therefore, as suggested methods of measuring fracture toughness in the rock have been published, it is proposed that use should be made of the measurement of these parameters in connecting with rock cutting assessment.

4. Compared with laboratory testing, theoretical work in the field of disc cutting is deficient. This is particularly so in the area of water jet assisted disc cutting. The mechanism of rock breakage by the disc cutters is still poorly understood. A theoretical study of fracture mechanics by disc cutting has been undertaken

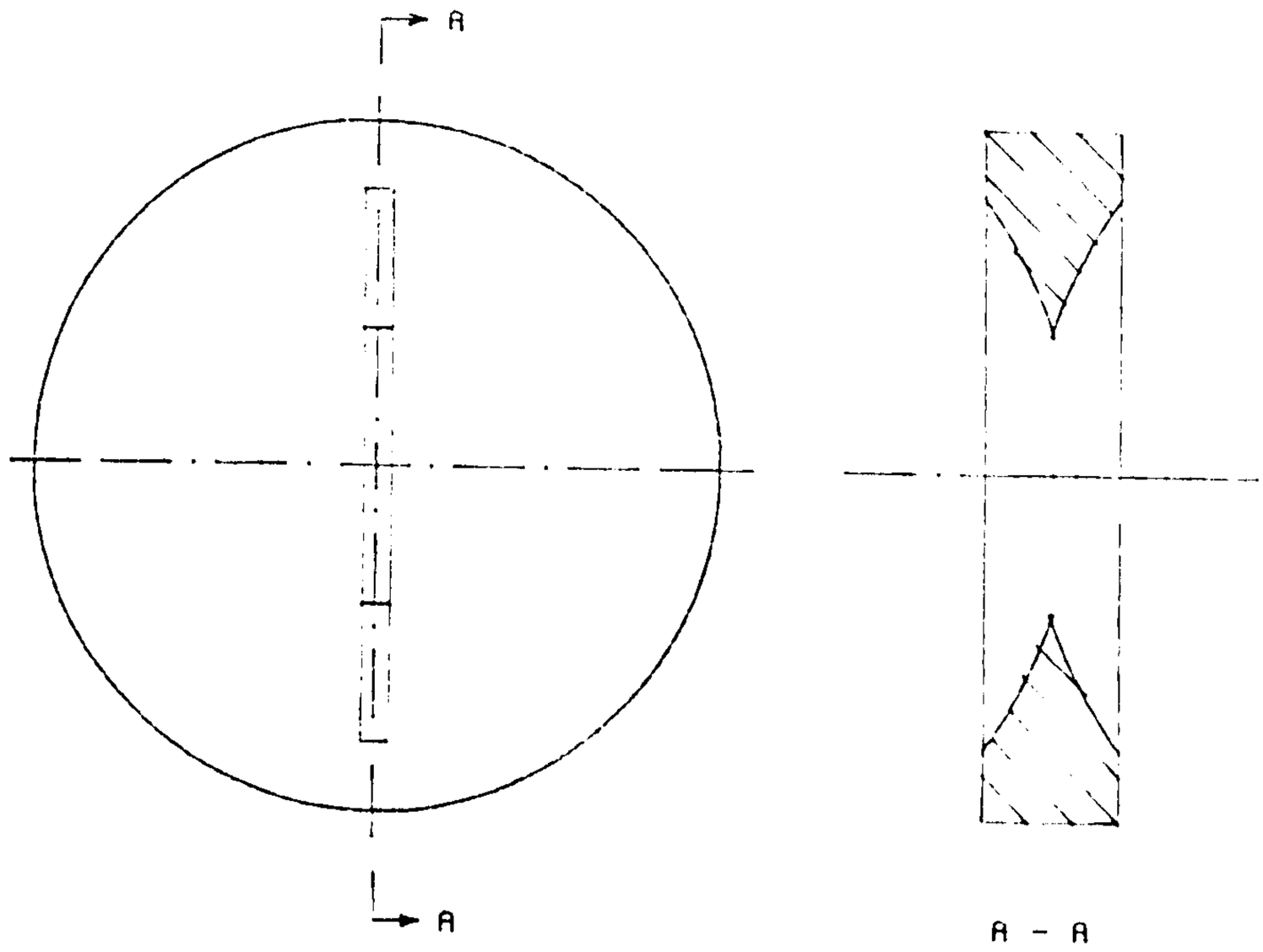

Fig. 9.6.1 Brazilian disk specimen

in this thesis, but further development is necessary to include rock parameters that define the transition of rock from the brittle state to the ductile state.

5. As we have seen that the performance of water jet assisted disc cutting on the different types of rocks are quite different. Therefore, a further investigation is suggested by performing the cutting tests on the rocks with different compressive strengths and different crystal structures. Micro-structure analysis of the rocks, may be required to understand the mechanism of low-pressure water jet assisted cutting.

6. An elastic-plastic model for the numerical analysis of stress distribution beneath a disc cutter during the cutting tests may correlate more closely to experimental data. The boundary element method is an ideal technique to do such a job.

REFERENCES

1. Ahmad J. and Ashbaugh N.E. (1982) *Constant K_I crack-propagation test specimens.* Int. J. of Fracture, Vol. 19, 115-129.

2. Athorn M., Farmer I.W. and Glossop N.H. (1983) *Performance of tunnelling machine in rock.* Proc. 24th U.S. Symp. on Rock Mechanics, 239-249.

3. Atkinson B.K. (1979) *Fracture toughness of Tennessee Sandstone and Carrara Marble using the double torsion testing method.* Int. J. Rock Mech. Min. Sci. & Geomech. Abstr. Vol. 16, 49-53.

4. Atkinson B.K. nd Avdis V.(1980) *Fracture mechanics parameters of some rock forming minerals determined using an indentation technique.* Int. J. Rock. Mech. Min. Sci. and Geomech. Abstr. Vol. 17, 383-386.

5. Bamford W.E. (1984) *Rock test indices are being successfully correlated with tunnel boring machine performance.* Fifth Australian Tunnelling Conference, October, 218-221.

6. Barker L.M. (1977) *A simplified method for measuring plate strain fracture toughness.* Eng. Fracture Mech. Vol. 9, 361-369.

7. Barton C.C. (1982) *Variables in fracture energy and toughness testing of rock.* Proc. 23rd U.S. Symp. on Rock Mech., 449-462.

8. Baumann L. and Heneke J. (1980) *Attempt of technical-economical optimization of high-pressure jet assistance for tunnelling machines.* 5th Int. Symp. on Jet Cutting Technology, paper C4, 119-139, June.

9. Benjumea R. and Sikarskie D.L. (1969) *A note on the penetration of a rigid wedge into a nonisotropic brittle material.* Int. J. Rock Mech. Min Sci. &

Geomech. Abstr., Vol. 6, 343-352.

10. Bilgin N. (1977) *Investigations in to the mechanical cutting characteristic of some medium and high strength rocks.* Ph.D thesis, University of Newcastle upon Tyne.

11. Brebbia C.A., Telles J.C.F. and Wrobel L.C. (1984) *Boundary element techniques: theory and application in engineering.* New York. p464.

12. Brown E.T. (Ed.) (1981) *Rock Characterization, Testing, and Monotoring - ISRM Suggested Methods.* p211. Pergamon press, New York.

13. Bruce W.E. and Morrell R.J. (1969) *Principles of rock cutting applied to mechanical boring machines.* 1969 RETC Proceedings, Sacremento, Calif., Oct.. P3 1-43.

14. Cassinelli F. (1982) *Power consumption and metal wear in tunnel-boring machines: analysis of tunnel-boring operation in hard rock.* Tunnelling'82, 73-81.

15. Cook N.G.W., Hood M. and Tsai F. (1984) *Observations of crack growth in hard rock loaded by an indenter.* Int. J. Rock Mech. Min. Sci & Geomech. Abstr., Vol. 21. 97-107.

16. Costin L.S. (1981) *Static and dynamic fracture behavior of oil shale.* Fracture Mech. for Ceramics, Rock, and Concrete. Freiman S.W. ed, STP 745, ASTM, 169-184.

17. Crabb G.I. and Hignett H.J. (1980) *A laboratory and pilot-scale study on the cutting of chalk containing flints.* Tunnels & Tunnelling, Vol. 12, 29-33.

18. Crow S.C. (1975) *Jet tunnelling machines - a guide for design.* Tunnels & tunnelling. 23-37. March.

19. Dobugnon O. and Barendsen P. (1985) *Small scale model testing: a new approach in TBM development.* 1985 RETC Proceedings, Vol. 1, Chapter 16, 245-263.

20. Dollinger G.L. (1983) *Hard rock tunnel boring: A summary of recent developments.* 1983 RETC Proceedings, Vol. 1, Chapter 6, 89-105.

21. Dutt P.K. (1972) *A theory of precussive drill bit penetration.* Int. J. Rock Mech. Min. Sci & Geomech. Abstr., Vol. 9, 543-567.

22. Eschweiler J., Marci G. and Munz D.G. (1984) *Fracture toughness of an aluminum alloy from short-bar and compact specimens.* Chevron-Notched Specimens: Testing and Stress Analysis. ASTM STP885, 255-269.

23. Evans A.G. (1979) *Fracture toughness: the role of indentation techniques.* Fracture Mechanics Applied to Brittle Materials, ASTM STP 678, Freiman S.W. ed., American Society for Testing and Materials, 112-135.

24. Ewalds H.L and Wanhill R.J.H (1984) *Fracture mechanics.* Edward Arnold (Publishers) Ltd., p304.

25. Farmer I.W. (1987) *Some considerations affecting the selection of tunnelling methods.* TRRL Report 51, p61.

26. Farmer I.W., Garritty P. and Glossop N.H. (1986) *Mechanical excavation of rock.* CIRIA project, Record PR 351, p46.

27. Farmer I.W., Glossop N.H. (1980) *Mechanics of disc cutter penetration.* Tunnels & tunnelling, Vol. 12, 22-25, July.

28. Fauvel O.R. (1981) *Implications of laboratory rock cutting for the design of a tunnel boring machine cutter head.* Ph.D thesis, University of Newcastle upon

Tyne.

29. Fenn O., Protherde B.E. and Joughin N.C. (1985) *Enhancement of roller cutting by means of water jets.* 1985 RETC Proceedings, Vol. 1, 341-356.

30. Fowell R.J., Johnson S.T. and Ip C.K. (1985) *Further studies in water jet assisted drag tool cutting in rock.* 3rd U.S. Water Jet Conference, 378-394.

31. Gaye F. (1972) *Efficient excavation: cutting head design of hard rock tunnelling machine.* Tunnels & Tunnelling, Vol. 4, No. 1, 39-48, Jan and No. 2, 135-143, March.

32. Graham P.C. (1976) *Rock exploration for machine manufacturers.* Proc. Symp. Exploration for Rock Engineering, Johannesburg, 173-180.

33. Griffith A.A. (1920) *The phenomena of rupture and flow in solids.* Proc. Trans. Royal Soc. A221, 163-198.

34. Hamilton W.H. and Dollinger G.L. (1979) *Optimizing tunnel boring machine and cutter design for greater boreability.* 1979 RETC Proceedings, Vol. 1, 280-296.

35. Hartman H.L. (1959) *Basic studies of percussion drill.* Trans. AIME(Mining), TP478, 68-75.

36. Henneke J. and Knickmeyer W. (1979) *Possibilities and limitations of water jet assisted tunnel boring in German coal mines.* 1979 RETC Proceedings, Vol. 2, 1013-1031.

37. Hertz H.J. (1887) Reine Angew. Math. 92-156.

38. Hewitt K.S. (1975) *Aspects of the design and applications of cutting systems in*

rock excavation. Ph.D Thesis, University of Newcastle upon Tyne.

39. Hignett H.J. and O'Reilly M.P. (1979) *The arrangement of rock cutting tools on full face tunnel boring machines.* Dept. of the Environment Department of Transport, TRRL Rept SR 376. TRRL, Crowthrone.

40. Hignett H.J., Snowdon R.A. and Temporal J. (1977) *Tunnelling in chalk: rock cutting experiments.* TRRL Rept 796. Dept of the Environment/transport.

41. Hoagland R.G., Hahn R.G. and Rosenfield A.R. (1973) *Influence of microstructure on fracture propagation in rock.* Rock Mechanics Vol. 5, 77-106.

42. Hood, M. (1976) *Cutting strong rock with a drag bit assisted by high-pressure water jets.* J. S. Afr. Inst. of Min. & Metal. Nov.

43. Hood, M. (1977) *Phenomena relating to the failure of hard rock adjacent to an indenter.* J. S. Afr. Inst. Min. & Metal. 77, 113-123.

44. Hood M. (1985) *Water jet-assisted rock cutting system — the present state of the art.* Int. J. of Mining Eng., Vol. 3, 91-111.

45. Hoshino K., Nagano T. and Tsuchishima H. (1972) *Rock cutting and breaking using high speed water jets together with "TBM" cutters.* 5th Int. Symp. on Jet Cutting Technology.

46. Howarth D.F. (1986) *Review of rock drillability and borability assessment methods.* Transations of Institution of Mining and Metallurgy, Vol. 195, A191-A202.

47. Howarth D.F. and Bridge E.J. (1988) *Microfracture beneath blunt disc cutters in rock.* Int. J Rock Mech. Min. Sci. & Geomech. Abstr., Vol. 25, No. 1, 35-38.

48. Hughes H.M. (1986) *The relative cuttability of Coal-Measures stone.* Min. Sci. Technol., Vol. 3, No. 2, 95-109.

49. Hustralid W.A.(1972) *A comparison of laboratory cutting results with actual tunnel boring performance.* Proc. N. American RETC Vol. 2, Chapter 74, 1299-1323.

50. Ingraffea A.R. (1981) *Mixed-mode fracture initiation in Indiana Limestone and Westerly Granite.* Proc. 22nd U.S. Symp. on Rock Mech..

51. Ingraffea A.R. (1987) *Theory of crack initiation and propagation in rock.* Fracture Mechanics of Rock. Atkinson B.K. ed. 71-110.

52. Ingraffea A.R., Gunsallus K.L., Beech J.F., Nelson P. (1982) *A fracture toughness testing system for prediction of tunnel boring machine performance.* Proc. 23rd U.S. Symp. on Rock Mech., 463-470.

53. Irwin (1957) *Analysis of stresses and strains near the end of a crack traversing a plate.* J. Appl. Mechanics, Vol. 24, 361-364.

54. Johnson K.L. (1970) *The correlation of indentation experiments.* J. Mech. Phys. Solids, Vol. 18, 115-126.

55. Jones A.T. (1974) *A radially cracked, cylindrical fracture toughness specimen.* Eng. Fracture Mech.,Vol. 6, 435-446.

56. Kenner V.H., Advani S.H. and Richard T.G. (1984) *A study of fracture toughness for an anisotropic shale.* Proc. 25th U.S. Symp. on Rock Mechanics. Chapter 48, 471-479.

57. Kirby G.C. and Mazur C.J. (1985) *Fracture toughness testing of coal.* Proc. 26th U.S. Symp. on Rock Mech., 497-504.

58. Klepaczko J.R., Bassim M.N. and Hsu T.R. (1984) *Fracture toughness of coal under quasi-static and impact loading.* Eng. Fracture Mech., Vol. 19, 306-316.

59. Knickmeyer W. and Banmann L. (1983) *High-pressure water jet-assisted tunnelling techniques.* Bergbau-Forschung GmbH, FRG.

60. Kutter H.K. and Sanio H.P. (1982) *Comparative study of performance of new and worn disc cutters on a full-face tunnelling machine.* Tunnelling'82, 127-133. IMM, London.

61. Kutter H.K. and Sanio H.P. (1983) *Discussion.* Int. J. Rock Mech. Min. Sci. & Geomech. Abstr., Vol. 20, No. 2, 103-104.

62. Kuzmich I.A., Goldin Ju.A., Ruthberg M.I. and Frolov V.S. (1982) *A combined method for rock breakage.* Proc. 6th Int. Symp. on Jet Cutting Technology, G3, 301-321.

63. Labuz J.F., Shah S.P. and Dowding C.H. (1985) *Experimental analysis of crack propagation in granite.* Int. J. Rock Mech. Min. Sci. & Geomech. Abstr., Vol. 22, 85-98.

64. Lai H.H, Lindqvist P.-A. and Ranman K.E. (1980) *Microcopic observations of the fragmentation in rock cutting.* Univ. of Lulea, Research report Tulea 1980:20, p25.

65. Lawn B.R. and Fuller E.R. (1975) *Equilibrium penny-like cracks in indentation fracture.* J. Mat. Sci., Vol. 10, 2016-2024.

66. Lawn B.R., Swain M.V. (1975) *Microfracture beneath point indentations in brittle solids.* J. Mat. Sci., Vol. 10, 113-122

67. Lawn B.R., Wilshaw T.R. (1975) *Review indentation fracture: principles and*

application. J. Mat. Sci.,Vol. 10, 1049-1081.

68. Lindqvist P.-A. (1984) *Stress fields and subsurface crack propagation of single and multiple rock indentation and disc cutting.* Rock Mech. & Rock Eng., Vol. 17, 97-112.

69. Lindqvist P.-A. and Lai H.H. (1983) *Behavior of crushed zone in rock indentation.* Rock Mech. & Rock Eng., Vol. 16, 199-207.

70. Lindqvist P.-A., Lai H.H. and Alm O. (9184) *Indentation fracture development in rock continuously observed with a scanning electron microscope.* Int. J. Rock Mech. Min. Sci & Geomech. Abstr., Vol. 21, No. 2, 97-107.

71. Lundberg B. (1974) *Penetration of rock by conical indenters.* Int. J. Rock Mech. Min. Sci. & Geomech. Abstr., Vol. 11, 209-213.

72. Marion R.H. (1979) *Use of indentation fracture to determine fracture toughness.* Fracture Mechanics Applied to Brittle Materials, ASTM STP 678, Freiman S.W. ed., ASTM, 103-111.

73. Maurer W.C. (1966) *The state of rock mechanics knowledge in drilling.* Proc. 8th Symp. on Rock Mech.

74. McGann E.A. (1984) *An investigation into rock hardness using a cone indenter method.* M.Sc Thesis. Dept. of Geotechnical Engineering, University of Newcastle upon Tyne.

75. Meijer K.L. (1976) *Discussion on paper by F.F. Roxborough and H.P. Phillips Rock excavation by disc cutter.* Int. J. Rock Mech. Min. Sci. & Geomech. Abstr., Vol. 13, 297.

76. Meredith P.G. (1983) *A fracture mechanics study of experimentally performed*

crushed rocks. Ph.D thesis, University of London. p350.

77. Morrell R.J., Bruce W.E. and Larson D.A. (1970) *Tunnel boring technology: disk cutter experiments in sedimentary and metamorphic rocks.* U.S. Bureau of Mines. RI7410, p32.

78. Morrell R.J. and Larson D.A. (1974) *Tunnel boring technology: disk cutter experiments in metamorphic and igneous rocks.* U.S. Bureau of Mines. RI7961, p50.

79. Moses D.M. (1985) *High pressure water jet assisted disc cutting.* M.Sc Dissertation, Dept. of Geotechnical Engineering, University of Newcastle upon Tyne.

80. Munz D. (1981) *Determination of fracture toughness of high strength aluminum alloys with Chevron notched short rod and short bar specimens.* Engineering Fracture Mechanics, Vol. 15, 231-236.

81. Munz D., Bubsey R.T. and Srawley J.E. (1980) *Compliance and stress intensity coefficient for short bar specimen with Chevron notches.* Int. J. of Fracture, Vol. 16.

82. Nelson P.P. and Fong F.L.C. (1986) *Charaterization of rock for boreability evaluation using fracture material properties.* Proc. 27th U.S. Symp. on Rock Mech., Chapter 120, 846-852. 227-237.

83. Nelson P.P., Ingraffea A.R. and O'Rourke T.D. (1985) *TBM performance prediction using rock fracture parameters.* Int. J. Rock Mech. Min. Sci. & Geomech. Abstr., Vol. 22, 189-192.

84. Nelson P.P., O'Rourke T.D. and Kulhawy F.H. (1983) *Factors affecting TBM*

penetration rates in sedimentary rocks. Proc. 24th U.S. Symp. on Rock Mech., 227-237.

85. Newman Jr. J.C. (1984) *A review of Chevron-notched fracture specimens.* Chevron-Notched Specimens: Testing and Stress Analysis, ASTM STP855, 5-31.

86. Nishimatsu Y. (1972) *The mechanics of rock cutting.* Int. J. Rock Mech. Min. Sci & Geomech. Abstr., Vol. 9, 261-270.

87. O'Reilly M.P. and Hignett H.J. (1977) *Rock cutting tools — their arrangement on full-face tunnel boring machines.* Chart. Mech. Engrs, Vol. 24, 47-51.

88. O'Rielly M.P., Roxborough F.F. and Hignett H.J. (1976) *Programme of laboratory, pilot and full-scale experiments in tunnel boring.* Proc. Tunnelling'76, 287-299.

89. Ouchterlony F. (1974) *Fracture mechanics applied to rock blasting.* Proc. 3rd Congr. ISRM Vol. 2. 1377-1383. Denver.

90. Ouchterlony F. (1982) *Review of fracture toughness testing of rock.* Solid Mech. Archive, 41.

91. Ouchterlony F. (1988) *Suggested methods for determining the fracture toughness of rock.* Int. J. Rock Mech. Min. Sci. & Geomech. Abstr., Vol. 25, 71-96.

92. Ozdemir L. (1984) *Water jet assisted tunnel boring.* Earth Mechanics Institute, CSM.

93. Ozdemir L. (1986) *Research and development of high speed, automated mechanical excavation system for underground construction.* Proc. 2nd International Conference on Innovative Mining Systems. Pennsyvania. 28-29.

94. Ozdemir L., and Dollinger G.L. (1984) *Recent developments in mechanical and water jet assisted tunnel boring technology for civil and mining engineering applications.* Design and Performance of Underground Excavations, ISRM/BGS, Cambridge.

95. Ozdemir, L., Evans, R.J., Miller, R.J. and Sharp, W. (1984) *CSM-USBM rotary cutting machine: Research capabilities and trials for improving the performance of tunnels, shafts and raise boring machines.* Earth Mechanics Institute, CSM Pittsburg Technology Center, USBM.

96. Ozdemir L., Miller R. and Wang F.D. (1977) *Mechanical tunnel boring prediction and machine design.* Annual Rept. NSF IRA-770199, Colorado School of Mines, Golden.

97. Pariseau W.G. and Fairnurst C. (1967) *The force-penetration characteristic for wedge penetration into rock.* Int. J. Rock Mech. Min. Sci. & Geomech. Abstr., Vol. 4, 165-180.

98. Passaris E.K.S. (1988) *Private communication.*

99. Paul B., Sikarskie D.L. (1965) *A preliminary theory of static penetration by a rigid wedge into a brittle material.* Trans. of the Soc. of Min. Eng. of AIME, 372-382, Dec.

100. Peng S. and Johson A.M. (1972) *Crack growth and faulting in Cylinderical specimens of Chelmsford granite.* Int. J. Rock Mech. Min. Sci. & Geomech. Abstr., Vol. 9, 37.

101. Phillips H.R. and Bilgin N. (1979) *Correlation of rock properties with the measured performance of disc cutters.* Proc. of Rock Engineering, Univ. of Newcastle upon Tyne.

102. Phillips H.R., Bilgin N. and Price D.L. (1978) *The influence of tyre tip geometry on the design of disc cutter arrays.* 3rd Australasian Tunnelling Conf., 48-52.

103. Plumpton N.A. and Tomlin M.G. (1982) *The development of a water jet system to improve the performance of a Boom-Type roadheader.* 6th Int. Symp. on Jet Cutting Technology.

104. Poole D. (1987) *The effectiveness of tunnelling machines.* Tunnel & Tunnelling, No.1, 66-67, Jan..

105. Pritchard and Reimer (1980) *Effects of waterjet slotting.* Proc. 21st U.S. Symp. on Rock Mechanics.

106. Rad P.F. (1975,a) *Importance of groove spacing in tunnel boring machine operations.* J. Geotechnical Engineering Division, ASCE, Vol 101, No. 9, 949-962.

107. Rad P.F. (1975,b) *Bluntness and wear of rolling disc cutters.* Int. J. Rock Mech. Min. Sci. & Geomech. Abstr., Vol. 12, 93-99.

108. Rad P.F. (1974) *Correlation of laboratory cutting data with tunnel boring machine performance.* U.S. Bureau of Mines. RI7883.

109. Rad P.F. and McGarry (1971) *Thermally assisted cutting of granite.* Proc. 12th U.S. Symp. on Rock Mechanics. 721-757.

110. Rad P.F. and Olson, R.C. (1974,a) *Tunneling machine research: interaction between disk-cutter grooves in rocks.* U.S. Bureau of Mines. RI7881, p21.

111. Rad P.F. and Olson R.C. (1974,b) *Tunneling machine research: size distribution of rock fragments produced by rolling disk cutters.* U.S. Bureau of Mines. RI7882, p40.

112. Reichmuth D.R. (1963) *Correlation of force displacement data with physical properties of rock for percussive drilling systems.* Proc. 5th U.S. Symp. on Rock Mechanics. 35-60.

113. Rice J.R. (1968) *Mathematical analysis in the mechanical of fracture.* Fracture: an advanced treatise. Academic Press, New York, p191.

114. Rispin A. and Bilgin N. (1977) *Prediction of disc cutter performance from laboratory rock cutting experiments.* Mining Industry, Vol 86, A28-A34.

115. Robson J.A. (1983) *Indentation testing as an aid to excavating performance prediction for boom-type tunnelling machines.* Dissertation for postgraduate diploma, Dept. of Geotechnical Engineering, University of Newcastle upon Tyne.

116. Roxborough F.F. (1976) *Rock excavation by machine: a comparative study of picks and discs.* 2rd Australasian Tunnelling Conf., 133-141.

117. Roxborough F.F. (1978) *Fundamental studies on the mechanics of cutting rock with discs.* 3rd Australian Tunnelling Conference, Sydney.

118. Roxborough F.F. (1985) *Research in mechanical rock excavation, progress and prospects.* 1985 RETC Proceedings, Vol. 1, Chapter 15, 225-244.

119. Roxborough F.F. and Phillips H.R. (1975,a) *Rock excavation by disc cutter.* Int. J. Rock Mech. Min. Sci. & Geomech. Abstr. 12, 361-366.

120. Roxborough F.F. and Phillips H.R. (1975,b) *The mechanical properties and cutting characteristics of selected rock formations.* Report to the TRRL. University of Newcastle upon Tyne.

121. Roxborough F.F and Phillips H.R. (1981) *The change in performance of disc*

cutters when stalled. 4th Australasian Tunnelling Conf., 361-368.

122. Roxborough F.F. and Rispin A. (1973) *The mechanical cutting characteristics of the Lower Chalk.* Tunnels & Tunnelling, 45-67, January.

123. Samuel A.E. and Seow L.P. (1984) *Disc force measurements on a full-face tunnelling machine.* Int. J. Rock Mech. Min. Sci & Geomech. Abstr., Vol. 21, 83-96.

124. Sanio H.P. (1985) *Prediction of the performance of disc cutters in anisotropic rock.* Int. J. Rock Mech. Min. Sci. & Geomech. Abstr., Vol. 22, No. 3, 153-161.

125. Schenck G.K. (1983) *Recent developments in high-pressure water-jet assisted cutting of rock and coal.* 1983 RETC Proceedings, Vol. 2, 663-682.

126. Schmidt R.A. (1976) *Fracture testing of Limestone.* Expl. Mech., Vol. 16, 166-167.

127. Schmidt R.A. (1977) *Fracture mechanics of oil shale unconfined fracture toughness, stress corrosion cracking, and tension test results.* Proc. 18th U.S. Symposium on Rock Mech., Paper2A2, 1-6.

128. Schmidt R.A. and Lutz T.J. (1979) K_{IC} *and* J_{IC} *of Weaterly Granite - Effects of thickness and in-plane dimensions.* Fracture Mechanics Applied to Brittle Materials. Freiman S.W. ed., ASTM STP 678, 166-182.

129. Shaw M.C. (1973) *Basis of hardness test.* The Science of Hardness Testing and As Research Applications. 1-15.

130. Shetty D.K., Rosenfield A.R. and Duchworth W.H. (1987) *Mixed-mode fracture in biaxial stress state: application of the diameteral-compressure (Brazilian*

Disk) test. Eng. Fracture Mech., Vol. 26, No. 6, 825-840.

131. Sikarskie D.L., Cheatheham Jr., J.B. (1973) *Penetration problems in rock mechanics.* Proc. 11th U.S. Symp. on Rock Mech., 41-47.

132. Smits, A.R. (1980) *The excavation of hard rock by disc & roller cutter.* Ph.D Thesis. University of South Wales, Australia.

133. Snowdon R.A. and Ryley M.D. (1983) *Single and multiple pass disc cutting in Shap Granite.* Tunnels & Tunnelling, November.

134. Snowdon R.A., Ryley M.D. and Temporal J. (1982) *A study of disc cutting in selected British rocks.* Int. J. Rock Mech. Min. Sci. & Geomech. Abstr., Vol. 13, 311-319.

135. Snowdon R.A., Ryley M.D. and Temporal J. (1983) *Author's Reply.* Int. J. Rock Mech. Min. Sci. & Geomech. Abstr., Vol. 20, 105.

136. Snowdon R.A., Ryley M.D., Temporal J. and Crabb G.I. (1983) *The effect of hydraulic stiffness on tunnel boring machine performance.* Int. J. Rock Mech. Min. Sci. & Geomech. Abstr., Vol. 20, 203-214.

137. Snowdon R.A., Temporal J. and Hignett H.J. (1981) *A linear rock cutting rig.* TRRL report 588.

138. Sun Z. and Ouchterlony F. (1986) *Fracture toughness of Stripa granite cores.* Int. J. Rock Mech. Min. Sci. & Geomech. Abstr., Vol. 23, No. 6, 339-409.

139. Swain M.V. and Lawn B.R. (1976) *Indentation fracture in brittle rocks and glasses.* Int. J. Rock Mech. Min. Sci. & Geomech. Abstr., Vol. 13, 311-319.

140. Tabor D. (1951) *The Hardness of Metals.* Clarendon, Oxford.

141. Takaoka S., Hayamizu H. and Misawa S. (1973) *Studies on the cutting of rock by rotary cutters - part 1. Rock cutting by disc cutters.* Tunnels & tunnelling, March.

142. Tarkoy P.J.,and Hendron A.J. (1975) *Rock hardness index properties and geotechnical parameters for predicting tunnel boring machine performance.* Report prepared for Univ. National Science Foundation, Grant No. GI-36468.

143. Teale R. (1964) *The mechanical excavation of rock — experiments with roller cutters.* Int. J. Rock Mech. Min Sci., & Geomech. Abstr., Vol. 1, 63-78.

144. Tecen, O. (1982) *High pressure water jet assisted drag tool cutting of rock materials.* Ph.D Thesis, Univ. of Newcastle upon Type.

145. Temporal J., Snowdon R.A. and O'Reilly (1983) *Laboratory disc cutting studies in medium and hard rocks.* 1983 RETC Proceedings, Vol. 1, 131-156.

146. Temporal J. and Snowdon R.A. (1982) *The effect of hydraulic stiffness on tunnel boring machine performance.* Tunnels & Tunnelling, Vol. 149, 11-13.

147. Thompson R.M., Andrasic C.P. and Parker A.P. (1984) *Comparison of two sets of results for radially cracked, point loaded ring specimens.* Eng. Fracture Mech., Vol. 19, No. 2, 383-386.

148. Timoshenko S. and Goodier J.N. (1951) *Theory of elasticity.* McGraw-Hill Publishing Company, New York.

149. Underwood J.H., Lasselle R.R., Scanlon R.D. and Hussain M.A. (1972) *A compliance K calibration for a pressurized thick wall cylinder.* Eng. Fracture Mech. Vol 8.

150. Wang C. Yuan M. and Chen T. (1984) *An investigation on the method for de-*

termination of fracture toughness K_{Ic} of materials with Chevron-notched short-rod and short-bar specimens. Chevron-notched Specimens: Testing and Stress Analysis. ASTM STP 855, 193-204.

151. Wang F.D., Robbins R. and Olsen J. (1976) *Water jet assisted tunnel boring.* 3rd Int. Symp. on Jet Cutting Technolgy.

152. Wang J.K. and Lehnhoff T.F. (1976) *Bit penetration into rock - A finite element study.* Int. J. Rock Mech. Min Sci., and Geomech. Abstr., Vol. 13, 11-16.

153. Wilkening W.W. (1978) *J-integral measurement in geological materials.* Proc. 19th U.S. Symp. on Rock Mechanics, Vol. 1, 254-258.

154. Williams J.G. (1984) *Fracture Mechanics of Polymers.* New York, p302.

155. Woodley J.N.L (1979) *Developments in hard rock tunnelling.* The Mining Engineer, October, 321-325.

156. Wu S. (1984) *Compliance and stress-intensity factor of Chevron-notched three-point bend specimens.* Chevron-notched Specimens: Testing and Stress Analysis. ASTM STP 855, 176-192.

157. Zhao X. (1984) *An investigation on the methods of measuring rock fracture toughness.* Fracture and Strength of Rock and Concrete, No. 1, 18-25; and Journal of Fuxin Mining Institute, Vol. 3, No. 4, 103-110 (in Chinese).

Appendix A

DYNAMOMETER CALIBRATION RESULTS

A.1 Load Cell

Load cell : Type 405, Serial No. 143
Calibration constant: 0.02323

Table A.1.1 The calibration of the load cell

Load kN	Strain Box Reading	Load kN	Strain Box Reading
5.0	197.0	30.0	1288.0
10.0	418.0	35.0	1514.0
15.0	628.0	40.0	1725.0
20.0	844.0	45.0	1954.0
25.0	1066.0		

Note: The strain box reading is the vertige values of three tests.

A.2 Dynamometer

Channel 1: Thrust force
Amplification setting: 0.02
Integrated amplification setting: 4

Table A.2.2 The calibration of the dynamometer

Strain Box Reading mV	MPTF Displ. mm	MTF Slope mm/s	Strain Box Reading mV	MPTF Displ. mm	MTF Slope mm/s
113.0	5.5	1.5	750.0	31.0	9.6
166.0	7.8	2.0	760.0	28.8	8.4
192.0	7.6	1.8	860.0	37.0	11.2
302.0	12.2	3.3	908.0	36.0	11.7
360.0	14.5	4.0	963.0	35.0	10.5
408.0	15.5	4.8	1014.0	41.7	13.0
476.0	18.0	6.0	1058.0	39.3	11.8
480.0	17.2	5.0	1283.0	52.6	16.7
532.0	20.5	5.6	1354.0	52.0	15.8
634.0	23.5	6.2	1377.0	54.2	16.0
650.0	23.5	6.5			

Channel 2: Rolling Force
Amplification setting: 0.1
Integrated amplification setting: 1

Table A.2.1 The calibration of the dynamometer

Strain Box Reading mV	MPRF Displ. mm	MRF Slope mm/s	Strain Box Reading mV	MPRF Displ. mm	MRF Slope mm/s
43.0	7.3	12.6	160.0	24.6	44.5
62.0	10.1	17.5	170.0	26.0	46.0
73.0	12.0	21.2	175.0	25.6	45.7
113.0	17.1	30.7	188.0	28.6	51.0
114.0	17.3	31.3	237.0	35.2	64.5
118.0	18.4	33.0	245.0	35.6	64.6
133.0	20.5	36.7	245.0	35.6	64.6
140.0	21.2	37.2			

A.3 Calibration Constants of Small Cutting Rig

Channel 1: Thrust Force

Table A.3.1 The calibration constants of thrust force

	Calibration Constants	
Channel Setting	MPTF (kN/mm)	MTF (kN/s)
0.02	0.5917	1.9490
0.05	1.3738	4.5252

Note: The integrated amplification setting is 4

Channel 2: Rolling Force

Table A.3.2 The calibration constants of rolling force

	Calibration Constants	
Channel Setting	MPRF (kN/mm)	MRF (kN/s)
0.02	0.1540	0.0858
0.05	0.3714	0.2233

Note: The integrated amplification setting is 1

A.4 Calibration Constants of Large Cutting Rig

Channel 1: Thrust Force

Table A.4.1 The calibration constants of thrust force

	Calibration Constants	
Channel Setting	MPTF (kN/mm)	MTF (kN/s)
0.02	0.2209	0.6301
0.05	0.5401	1.5185
0.1	1.0732	3.0537

Note: The integrated amplification setting is 4

Channel 2: Rolling Force

Table A.4.2 The calibration constants of rolling force

	Calibration Constants	
Channel Setting	MPRF (kN/mm)	MRF (kN/s)
0.1	0.0334	0.0179
0.2	0.0652	0.0394
0.5	0.1508	0.0876

Note: The integrated amplification setting is 1

Channel 3: Side Force

Table A.4.3 The calibration constants of side force

	Calibration Constants
Channel Setting	MPSF (kN/mm)
0.2	0.1795
0.5	0.4140
1.0	0.7685

Appendix B

RESULTS OF INDENTATION TESTS

B.1 INDENTATION TESTS ON SPRINGWELL SANDSTONE

Table B.1.1 Results of indentation tests on Springwell Sandstone

$D = 200.\text{mm}, \theta = 60°$

F_{mj} kN	p_{mj} mm	A_{mj} mm^2	σ_0 MPa	σ_0/σ_y
4.21	1.17	27.47	153.	3.80
13.02	3.39	134.74	97.	2.41
15.87	3.89	165.42	96.	2.39
19.94	4.69	218.54	91.	2.26
36.90	6.16	327.72	113.	2.81
22.52	4.26	189.39	119.	2.96
30.79	6.05	319.07	96.	2.39
4.88	1.01	22.04	221.	5.49
15.60	3.33	131.20	119.	2.96
31.33	5.46	273.97	114.	2.83
Mean Values			122.	3.03

$D = 175.\text{mm}, \theta = 60°$

F_{mj} kN	p_{mj} mm	A_{mj} mm^2	σ_0 MPa	σ_0/σ_y
16.55	2.99	104.40	159.	3.95
32.42	4.79	210.57	154.	3.83
35.81	5.21	238.57	150.	3.73
18.18	2.86	97.70	186.	4.62
23.60	3.54	134.27	176.	4.38
28.62	4.78	209.92	136.	3.38
10.85	2.21	66.49	163.	4.05
25.09	3.89	154.51	162.	4.03
36.62	4.79	210.57	174.	4.33
9.90	2.88	98.72	100.	2.49
18.58	3.83	150.98	123.	3.06
24.69	5.53	260.64	95.	2.36
Mean Values			148.	3.68

$D = 150.\text{mm}, \theta = 60°$

F_{mj} kN	p_{mj} mm	A_{mj} mm^2	σ_0 MPa	σ_0/σ_y
3.53	1.21	25.00	141.	3.51
14.24	3.10	101.85	140.	3.48
27.67	4.31	166.28	166.	4.13
28.62	5.02	208.51	137.	3.41
16.41	2.62	79.26	207.	5.15
25.23	3.63	128.82	196.	4.87
32.83	5.10	213.45	154.	3.83
5.70	1.31	28.15	202.	5.02
25.09	3.55	124.62	201.	5.00
40.02	4.93	202.99	197.	4.90
24.01	3.65	129.88	185.	4.60
34.18	4.51	177.87	192.	4.77
47.34	5.17	217.81	217.	5.40
Mean Values			180.	4.47

$D = 125.\text{mm}, \theta = 60°$

F_{mj} kN	p_{mj} mm	A_{mj} mm^2	σ_0 MPa	σ_0/σ_y
27.26	3.09	92.34	295.	7.33
32.28	4.55	163.99	197.	4.90
11.67	2.42	64.17	182.	4.53
21.97	3.67	119.23	184.	4.57
34.45	5.02	189.68	182.	4.53
12.62	2.14	53.42	236.	5.87
18.04	3.01	88.80	203.	5.05
35.27	5.10	194.17	182.	4.53
19.80	3.08	91.89	215.	5.35
26.59	4.64	168.82	158.	3.93
33.78	5.57	221.18	153.	3.80
Mean Values			199.	4.94

$D = 100.\text{mm}, \theta = 60°$

F_{mj} kN	p_{mj} mm	A_{mj} mm^2	σ_0 MPa	σ_0/σ_y
11.80	2.21	50.02	236.	5.87
36.62	4.87	161.38	227.	5.64
24.69	3.50	99.03	249.	6.19
37.85	5.34	184.84	205.	5.10
9.77	1.93	40.88	239.	5.94
21.70	3.12	83.51	260.	6.46
38.66	5.49	192.53	201.	5.00
13.16	2.72	68.12	193.	4.80
33.37	4.79	157.49	212.	5.27
Mean Values			225.	5.59

$D = 200.\text{mm}, \theta = 80°$

F_{mj} kN	p_{mj} mm	A_{mj} mm^2	σ_0 MPa	σ_0/σ_y
23.74	3.34	191.54	124.	3.08
31.74	3.81	233.08	136.	3.38
36.08	4.23	272.37	132.	3.28
39.74	4.52	300.64	132.	3.28
13.84	2.54	127.28	109.	2.71
20.21	3.34	191.54	106.	2.64
33.37	4.23	272.37	123.	3.06
23.60	3.67	220.43	107.	2.66
35.81	4.70	318.63	112.	2.78
30.25	3.46	201.89	150.	3.73
38.25	4.70	318.63	120.	2.98
Mean Values			123.	3.05

$D = 175.\text{mm}, \theta = 80°$

F_{mj} kN	p_{mj} mm	A_{mj} mm^2	σ_0 MPa	σ_0/σ_y
25.09	3.58	198.44	126.	3.13
32.69	4.17	249.04	131.	3.26
35.54	4.57	285.38	125.	3.11
20.35	2.74	133.20	153.	3.80
35.27	3.86	221.99	159.	3.95
39.74	4.09	241.96	164.	4.08
23.06	3.17	165.55	139.	3.46
33.64	4.01	234.96	143.	3.56
35.00	4.21	252.60	139.	3.46
18.99	3.31	176.56	108.	2.69
31.47	4.58	286.31	110.	2.73
37.44	5.04	330.07	113.	2.81
Mean Values			134.	3.34

$D = 150.\text{mm}, \theta = 80°$

F_{mj} kN	p_{mj} mm	A_{mj} mm^2	σ_0 MPa	σ_0/σ_y
30.11	3.34	165.41	182.	4.53
46.53	4.66	271.36	171.	4.25
16.28	3.03	143.07	114.	2.83
47.61	5.96	390.75	122.	3.03
35.81	3.85	204.35	175.	4.35
27.67	3.47	175.08	158.	3.93
37.30	4.11	225.19	166.	4.13
Mean Values			155.	3.86

$D = 125.\text{mm}, \theta = 80°$

F_{mj} kN	p_{mj} mm	A_{mj} mm^2	σ_0 MPa	σ_0/σ_y
11.12	1.91	65.53	170.	4.23
34.86	3.67	173.29	201.	5.00
47.20	4.66	246.93	191.	4.75
18.58	2.63	105.57	176.	4.38
49.65	4.66	246.93	201.	5.00
26.18	3.37	152.67	171.	4.25
42.86	4.55	238.34	180.	4.48
13.97	2.36	89.84	156.	3.88
38.79	4.47	232.16	167.	4.15
49.38	5.32	300.37	164.	4.08
Mean Values			178.	4.42

$D = 100.\text{mm}, \theta = 80°$

F_{mj} kN	p_{mj} mm	A_{mj} mm^2	σ_0 MPa	σ_0/σ_y
21.70	3.42	139.08	156.	3.88
36.49	4.77	227.48	160.	3.98
21.84	3.14	122.53	178.	4.43
36.90	4.38	200.57	184.	4.57
44.49	5.20	258.34	172.	4.28
20.75	3.59	149.45	139.	3.46
35.95	4.99	243.12	148.	3.68
26.32	4.00	175.39	150.	3.73
43.41	5.54	283.58	153.	3.80
Mean Values			160.	3.98

$D = 200.\text{mm}, \theta = 100°$

F_{mj} kN	p_{mj} mm	A_{mj} mm^2	σ_0 MPa	σ_0/σ_y
5.70	1.27	64.12	89.	2.21
30.25	2.93	223.75	135.	3.36
33.64	3.20	255.21	132.	3.28
36.08	3.29	265.99	136.	3.38
7.05	1.52	83.90	84.	2.09
23.06	2.83	212.45	109.	2.71
33.78	3.73	320.73	105.	2.61
14.79	2.07	133.16	111.	2.76
23.33	3.04	236.40	99.	2.46
29.84	3.39	278.14	107.	2.66
36.76	3.77	325.87	113.	2.81
Mean Values			111.	2.76

$D = 175.\text{mm}, \theta = 100°$

F_{mj} kN	p_{mj} mm	A_{mj} mm^2	σ_0 MPa	σ_0/σ_y
10.44	2.04	121.78	86.	2.14
16.14	2.83	198.52	81.	2.01
24.01	3.39	259.85	92.	2.29
26.45	3.80	308.02	86.	2.14
31.20	4.14	349.93	89.	2.21
12.62	1.74	96.01	131.	3.26
28.21	2.99	215.49	131.	3.26
31.88	3.47	269.04	118.	2.93
5.56	1.28	60.66	92.	2.29
11.12	2.14	130.80	85.	2.11
33.10	4.02	334.94	99.	2.46
9.77	2.11	128.07	76.	1.89
25.09	3.31	250.77	100.	2.49
Mean Values			97.	2.42

$D = 150.\text{mm}, \theta = 100°$

F_{mj} kN	p_{mj} mm	A_{mj} mm^2	σ_0 MPa	σ_0/σ_y
8.27	1.52	72.57	114.	2.83
24.28	2.72	173.01	140.	3.48
32.28	3.31	231.79	139.	3.46
28.89	3.09	209.23	138.	3.43
32.28	3.45	246.53	131.	3.26
8.82	1.53	73.28	120.	2.98
24.14	2.99	199.22	121.	3.01
34.32	4.19	329.13	104.	2.59
8.00	1.47	69.03	116.	2.88
25.64	3.31	231.79	111.	2.76
29.71	3.58	260.48	114.	2.83
Mean Values			123.	3.05

$D = 125.\text{mm}, \theta = 100°$

F_{mj} kN	p_{mj} mm	A_{mj} mm^2	σ_0 MPa	σ_0/σ_y
10.17	1.82	86.60	117.	2.91
21.97	2.76	161.11	136.	3.38
27.13	3.20	200.77	135.	3.36
29.57	3.34	213.97	138.	3.43
11.26	2.48	137.38	82.	2.04
18.72	3.34	213.97	87.	2.16
25.37	4.17	297.47	85.	2.11
7.60	1.85	88.74	86.	2.14
22.92	3.50	229.37	100.	2.49
32.96	4.26	307.04	107.	2.66
9.50	1.94	95.26	100.	2.49
29.30	3.14	195.20	150.	3.73
Mean Values			110.	2.74

$D = 100.\text{mm}, \theta = 100°$

F_{mj} kN	p_{mj} mm	A_{mj} mm^2	σ_0 MPa	σ_0/σ_y
5.02	1.27	45.19	111.	2.76
21.97	2.78	145.24	151.	3.75
34.05	3.56	209.63	162.	4.03
12.21	1.99	88.32	138.	3.43
26.86	3.38	194.12	138.	3.43
9.63	1.81	76.68	126.	3.13
15.46	2.74	142.15	109.	2.71
35.27	4.21	268.68	131.	3.26
4.75	1.32	47.88	99.	2.46
19.40	3.14	174.03	111.	2.76
24.42	4.18	265.86	92.	2.29
Mean Values			124.	3.09

B.2 INDENTATION TESTS ON WHINSTONE

Table B.2.1 Results of indentation tests on Whinstone

$D = 200.\text{mm}, \theta = 60°$

F_{mj} kN	p_{mj} mm	A_{mj} mm^2	σ_0 MPa	σ_0/σ_y
13.00	0.80	16.13	809.	3.02
47.10	1.70	46.79	1007.	3.76
65.90	2.00	60.82	1084.	4.04
80.20	2.30	74.53	1077.	4.02
11.40	0.70	12.19	935.	3.49
39.60	1.40	37.10	1066.	3.98
52.80	1.80	51.91	1016.	3.79
66.20	2.10	65.44	1012.	3.78
13.30	0.90	18.55	719.	2.68
44.20	2.00	61.73	716.	2.67
68.00	2.50	83.49	815.	3.04
Mean Values			932.	3.48

$D = 200.\text{mm}, \theta = 70°$

F_{mj} kN	p_{mj} mm	A_{mj} mm^2	σ_0 MPa	σ_0/σ_y
12.40	0.70	15.77	785.	2.93
49.30	1.90	67.75	728.	2.72
64.20	2.30	92.17	696.	2.60
77.90	2.60	113.16	688.	2.57
39.30	1.80	63.48	619.	2.31
61.80	2.30	92.17	671.	2.50
38.60	1.90	69.37	557.	2.08
61.80	2.70	115.72	534.	1.99
Mean Values			660.	2.46

$D = 200.\text{mm}, \theta = 80°$

F_{mj} kN	p_{mj} mm	A_{mj} mm^2	σ_0 MPa	σ_0/σ_y
44.10	1.40	51.12	862.	3.22
60.90	1.70	71.69	849.	3.17
83.10	2.10	94.43	880.	3.28
11.70	0.60	16.56	705.	2.63
47.40	1.60	65.59	723.	2.70
63.70	2.00	86.41	738.	2.75
11.10	0.70	19.70	565.	2.11
41.90	1.70	72.31	580.	2.16
69.00	2.30	108.32	637.	2.38
Mean Values			727.	2.71

$D = 200.\text{mm}, \theta = 90°$

F_{mj} kN	p_{mj} mm	A_{mj} mm^2	σ_0 MPa	σ_0/σ_y
57.60	1.80	92.93	619.	2.31
31.90	1.00	37.06	860.	3.21
11.00	1.00	38.75	283.	1.06
48.90	2.70	162.52	301.	1.12
64.30	3.40	229.29	280.	1.04
30.00	1.90	94.45	317.	1.18
51.90	2.50	149.02	349.	1.30
70.40	3.10	204.24	344.	1.28
Mean Values			419.	1.56

$D = 200.\text{mm}, \theta = 100°$

F_{mj} kN	p_{mj} mm	A_{mj} mm^2	σ_0 MPa	σ_0/σ_y
11.80	0.50	16.83	702.	2.62
47.10	1.60	92.29	511.	1.91
63.20	1.90	118.99	531.	1.98
82.60	2.30	155.87	530.	1.98
42.90	1.60	94.00	456.	1.70
78.60	2.40	165.07	476.	1.78
40.00	1.70	96.59	414.	1.54
68.70	2.30	159.93	429.	1.60
78.50	2.50	180.78	434.	1.62
Mean Values			498.	1.86

$D = 175.\text{mm}, \theta = 60°$

F_{mj} kN	p_{mj} mm	A_{mj} mm^2	σ_0 MPa	σ_0/σ_y
36.40	1.50	36.88	987.	3.68
65.10	2.30	71.03	917.	3.42
10.70	0.90	16.20	662.	2.47
35.20	1.70	43.74	804.	3.00
70.90	2.60	83.78	846.	3.16
15.80	1.00	19.40	814.	3.04
57.10	2.40	74.74	765.	2.85
Mean Values			828.	3.09

$D = 175.\text{mm}, \theta = 70°$

F_{mj} kN	p_{mj} mm	A_{mj} mm^2	σ_0 MPa	σ_0/σ_y
36.70	1.40	42.51	863.	3.22
51.40	1.90	66.89	768.	2.87
66.50	2.30	86.71	767.	2.86
78.70	2.60	99.85	788.	2.94
43.10	1.60	50.70	851.	3.17
68.60	2.30	83.38	822.	3.07
40.10	2.20	78.47	511.	1.91
63.70	2.90	120.97	527.	1.97
Mean Values			737.	2.75

$D = 175.\text{mm}, \theta = 80°$

F_{mj} kN	p_{mj} mm	A_{mj} mm^2	σ_0 MPa	σ_0/σ_y
41.10	1.20	40.24	1021.	3.81
59.20	1.50	55.77	1062.	3.96
84.80	1.90	76.50	1108.	4.13
48.50	1.40	49.36	983.	3.67
80.80	1.90	78.32	1031.	3.85
23.80	1.00	31.30	760.	2.84
38.90	1.50	53.07	733.	2.73
51.20	1.80	70.53	727.	2.71
Mean Values			928.	3.46

$D = 175.\text{mm}, \theta = 90°$

F_{mj} kN	p_{mj} mm	A_{mj} mm^2	σ_0 MPa	σ_0/σ_y
39.00	1.50	63.25	617.	2.30
72.80	2.20	112.84	645.	2.41
83.10	2.40	131.07	634.	2.37
51.20	1.40	55.73	919.	3.43
84.20	2.10	105.19	801.	2.99
38.30	1.40	55.73	688.	2.57
51.90	1.60	71.73	724.	2.70
Mean Values			718.	2.68

$D = 175.\text{mm}, \theta = 100°$

F_{mj} kN	p_{mj} mm	A_{mj} mm^2	σ_0 MPa	σ_0/σ_y
53.70	2.00	115.59	465.	1.73
70.10	2.30	149.48	469.	1.75
82.40	2.60	175.94	468.	1.75
100.00	3.00	218.73	457.	1.70
63.90	2.20	138.18	462.	1.72
104.00	3.10	225.24	462.	1.72
50.50	2.10	128.98	392.	1.46
101.90	3.20	236.23	431.	1.61
Mean Values			451.	1.68

$D = 150.\text{mm}, \theta = 60°$

F_{mj} kN	p_{mj} mm	A_{mj} mm^2	σ_0 MPa	σ_0/σ_y
31.90	1.40	30.10	1059.	3.95
67.60	2.20	62.32	1085.	4.05
10.20	0.60	9.63	1060.	3.95
37.30	1.80	46.02	811.	3.03
65.10	2.40	71.72	907.	3.38
29.00	1.70	41.92	692.	2.58
48.50	2.30	64.42	753.	2.81
Mean Values			910.	3.39

$D = 150.\text{mm}, \theta = 70°$

F_{mj} kN	p_{mj} mm	A_{mj} mm^2	σ_0 MPa	σ_0/σ_y
11.80	0.80	16.63	711.	2.65
40.70	1.90	59.98	678.	2.53
57.00	2.50	89.11	640.	2.39
66.50	2.80	103.33	644.	2.40
10.20	0.80	16.01	635.	2.37
48.80	2.20	75.08	650.	2.42
56.00	2.50	91.79	611.	2.28
15.10	1.00	23.48	644.	2.40
36.50	1.70	51.74	706.	2.63
54.00	2.40	84.34	640.	2.39
Mean Values			656.	2.45

$D = 150.\text{mm}, \theta = 80°$

F_{mj} kN	p_{mj} mm	A_{mj} mm^2	σ_0 MPa	σ_0/σ_y
12.00	0.70	16.70	716.	2.67
50.30	1.70	61.46	818.	3.05
58.50	2.00	74.71	784.	2.92
72.00	2.30	96.09	749.	2.79
12.20	0.70	15.00	816.	3.04
33.90	1.20	37.68	900.	3.36
54.50	1.70	62.00	880.	3.28
69.80	2.10	85.77	814.	3.04
76.70	2.30	97.33	788.	2.94
11.30	0.60	13.03	864.	3.22
50.20	1.70	60.93	823.	3.07
62.20	2.00	75.85	820.	3.06
79.10	2.30	95.47	829.	3.09
Mean Values			815.	3.04

$D = 150.\text{mm}, \theta = 90°$

F_{mj} kN	p_{mj} mm	A_{mj} mm^2	σ_0 MPa	σ_0/σ_y
10.60	0.60	15.15	699.	2.61
26.90	1.10	38.05	708.	2.64
44.60	1.50	60.89	733.	2.73
63.60	1.90	82.99	767.	2.86
78.00	2.20	107.95	723.	2.70
51.00	1.80	76.45	667.	2.49
73.90	2.30	113.78	650.	2.42
9.90	0.80	24.63	402.	1.50
36.10	1.80	79.05	457.	1.70
61.40	2.50	127.26	483.	1.80
Mean Values			629.	2.35

$D = 150.\text{mm}, \theta = 100°$

F_{mj} kN	p_{mj} mm	A_{mj} mm^2	σ_0 MPa	σ_0/σ_y
41.10	1.60	75.44	544.	2.03
55.20	1.90	101.29	545.	2.03
74.30	2.40	146.24	508.	1.90
14.70	1.20	50.33	292.	1.09
47.10	2.10	114.29	412.	1.54
66.50	2.70	168.29	395.	1.47
12.90	0.90	35.93	359.	1.34
46.30	1.90	98.12	472.	1.76
68.70	2.40	144.45	475.	1.77
Mean Values			445.	1.66

$D = 125.\text{mm}, \theta = 60°$

F_{mj} kN	p_{mj} mm	A_{mj} mm^2	σ_0 MPa	σ_0/σ_y
12.00	0.80	11.60	1031.	3.85
50.30	1.80	41.61	1209.	4.51
66.10	2.30	59.49	1111.	4.14
78.30	2.70	75.12	1042.	3.89
12.20	0.90	13.68	894.	3.34
34.80	1.80	41.61	835.	3.12
73.40	2.60	73.46	999.	3.73
11.40	1.00	16.13	707.	2.64
46.00	2.30	57.95	794.	2.96
61.60	2.70	74.71	824.	3.07
Mean Values			945.	3.52

$D = 125.\text{mm}, \theta = 70°$

F_{mj} kN	p_{mj} mm	A_{mj} mm^2	σ_0 MPa	σ_0/σ_y
10.70	0.80	16.02	670.	2.50
45.60	1.80	50.88	896.	3.34
65.70	2.10	65.24	1006.	3.75
10.80	0.90	16.30	665.	2.48
37.40	1.70	46.77	799.	2.98
65.00	2.40	75.92	856.	3.19
78.80	2.70	90.60	870.	3.25
35.30	2.00	59.45	594.	2.22
60.30	2.60	87.10	693.	2.59
Mean Values			783.	2.92

$D = 125.\text{mm}, \theta = 80°$

F_{mj} kN	p_{mj} mm	A_{mj} mm^2	σ_0 MPa	σ_0/σ_y
23.90	1.10	28.35	844.	3.15
39.40	1.40	41.21	957.	3.57
60.40	1.80	60.48	999.	3.73
10.40	0.80	18.51	564.	2.10
22.70	1.40	42.54	533.	1.99
60.60	2.30	83.67	724.	2.70
11.30	0.80	16.20	695.	2.59
31.50	1.50	47.51	662.	2.47
45.10	2.00	71.77	628.	2.34
Mean Values			734.	2.74

$D = 125.\text{mm}, \theta = 90°$

F_{mj} kN	p_{mj} mm	A_{mj} mm^2	σ_0 MPa	σ_0/σ_y
10.00	0.60	12.80	784.	2.92
48.90	1.40	51.75	945.	3.53
77.80	2.00	82.40	944.	3.52
11.80	0.80	19.31	612.	2.28
55.40	1.90	76.88	720.	2.69
65.40	2.10	93.18	702.	2.62
9.80	0.60	12.80	762.	2.84
47.00	2.00	81.79	575.	2.15
72.40	2.60	122.27	592.	2.21
Mean Values			737.	2.75

$D = 125.\text{mm}, \theta = 100°$

F_{mj} kN	p_{mj} mm	A_{mj} mm^2	σ_0 MPa	σ_0/σ_y
12.40	0.70	21.20	584.	2.18
25.30	1.20	44.76	565.	2.11
47.40	1.60	68.80	689.	2.57
60.70	1.90	94.53	642.	2.40
15.70	0.80	24.87	630.	2.35
32.60	1.30	49.41	659.	2.46
57.60	1.90	90.18	638.	2.38
12.10	0.70	21.20	571.	2.13
32.80	1.40	59.15	555.	2.07
47.80	1.90	90.90	526.	1.96
Mean Values			606.	2.26

$D = 100.\text{mm}, \theta = 60°$

F_{mj} kN	p_{mj} mm	A_{mj} mm^2	σ_0 MPa	σ_0/σ_y
12.80	0.90	12.87	992.	3.70
33.20	1.80	38.07	873.	3.26
38.80	2.10	46.69	830.	3.10
55.00	2.60	62.97	873.	3.26
11.30	0.70	9.18	1227.	4.58
27.10	1.30	22.67	1194.	4.45
39.70	1.80	37.76	1051.	3.92
11.40	0.70	9.37	1216.	4.54
30.80	1.50	28.07	1096.	4.09
57.30	2.30	54.12	1058.	3.95
Mean Values			1041.	3.88

$D = 100.\text{mm}, \theta = 70°$

F_{mj} kN	p_{mj} mm	A_{mj} mm^2	σ_0 MPa	σ_0/σ_y
20.50	1.20	24.09	850.	3.17
47.00	2.00	51.12	919.	3.43
10.20	0.70	10.66	954.	3.56
37.20	1.50	34.38	1083.	4.04
56.30	1.90	49.20	1145.	4.27
25.30	1.20	24.09	1049.	3.91
45.60	1.70	41.40	1102.	4.11
Mean Values			1015.	3.79

$D = 100.\text{mm}, \theta = 80°$

F_{mj} kN	p_{mj} mm	A_{mj} mm^2	σ_0 MPa	σ_0/σ_y
27.20	1.20	30.34	897.	3.35
50.50	1.80	53.55	944.	3.52
12.10	0.80	15.65	773.	2.88
35.00	1.50	40.39	867.	3.23
57.30	2.10	69.78	821.	3.06
11.50	0.70	14.19	813.	3.03
25.10	1.40	35.25	713.	2.66
47.20	2.10	67.38	701.	2.62
Mean Values			816.	3.04

$D = 100.\text{mm}, \theta = 90°$

F_{mj} kN	p_{mj} mm	A_{mj} mm^2	σ_0 MPa	σ_0/σ_y
11.10	0.70	16.23	685.	2.56
42.90	1.70	57.58	744.	2.78
52.80	2.00	76.90	686.	2.56
76.00	2.60	108.45	701.	2.62
13.00	0.80	18.65	700.	2.61
37.00	1.40	42.93	861.	3.21
54.80	2.00	73.56	745.	2.78
19.20	0.80	20.44	940.	3.51
49.60	1.50	48.62	1020.	3.81
70.40	2.10	80.87	870.	3.25
Mean Values			795.	2.97

$D = 100.\text{mm}, \theta = 100°$

F_{mj} kN	p_{mj} mm	A_{mj} mm^2	σ_0 MPa	σ_0/σ_y
19.30	0.80	22.65	851.	3.17
41.60	1.50	57.94	717.	2.67
11.10	0.50	11.21	994.	3.71
35.80	1.70	69.84	512.	1.91
49.00	1.80	76.05	644.	2.40
23.00	1.00	31.62	727.	2.71
39.90	1.70	69.84	572.	2.13
50.80	1.80	76.05	669.	2.50
59.00	2.00	88.98	663.	2.47
Mean Values			705.	2.63

Appendix C

CUTTING TEST RESULTS — SMALL CUTTING RIG

C.1 Results of Disc Cutting Tests on Springwell Sandstone

Table C.1.1 Results of unassisted cutting tests

p mm	s/p	MPTF kN	MTF kN	MRTF kN	MRF kN	YIELD m^3/km	SE kJ/m^3
2.0	2.5	3.02	1.75	0.59	0.53	0.004	132.50
	5.0	4.91	2.90	0.62	0.55	0.007	78.57
	10.0	5.33	3.51	0.79	0.56	0.004	140.00
	20.0	5.50	3.90	0.82	0.56	0.004	140.00
4.0	2.5	6.75	3.31	1.54	1.24	0.032	38.75
	5.0	10.48	7.60	1.66	1.45	0.036	40.28
	10.0	11.54	8.97	1.80	1.53	0.027	56.67
	20.0	12.01	9.38	2.06	1.50	0.027	55.56
6.0	2.5	11.06	5.07	3.68	2.51	0.068	36.91
	5.0	19.70	14.42	3.91	2.87	0.059	48.64
	10.0	21.36	15.98	4.05	3.02	0.059	51.19
	20.0	21.41	15.20	3.79	2.79	0.050	55.80
8.0	2.5	16.15	9.74	5.13	3.58	0.114	31.40
	5.0	33.61	19.27	5.51	4.03	0.127	31.73
	10.0	35.35	20.46	5.58	4.37	0.100	43.70

Table C.1.2 Results of water jet assisted cutting tests

p mm	s/p	MPTF kN	MTF kN	MRTF kN	MRF kN	YIELD m^3/km	SE kJ/m^3
2.0	2.5	0.51	0.33	0.23	0.18	0.005	36.00
	5.0	0.81	0.62	0.29	0.21	0.006	35.00
	10.0	0.94	0.64	0.30	0.22	0.004	55.00
	20.0	0.89	0.63	0.32	0.22	0.003	73.33
4.0	2.5	3.41	1.50	1.10	0.69	0.031	22.26
	5.0	3.56	1.88	1.18	0.78	0.037	21.08
	10.0	5.21	2.04	1.19	0.76	0.030	25.33
	20.0	5.06	1.98	1.47	0.83	0.029	28.62
6.0	2.5	7.08	3.45	2.84	1.15	0.070	16.43
	5.0	13.95	5.96	2.96	1.19	0.061	19.51
	10.0	15.14	6.60	2.99	1.41	0.059	23.90
	20.0	16.45	6.90	3.12	1.58	0.056	28.21
8.0	2.5	13.39	6.46	4.15	2.16	0.112	19.29
	5.0	20.99	10.77	4.45	2.48	0.128	19.37
	10.0	28.94	14.58	4.98	2.51	0.113	22.21

C.2 Results of Cutting Tests on Whinstone

Table C.2.1 Results of unassisted cutting tests

p mm	s/p	MPTF kN	MTF kN	MRTF kN	MRF kN	YIELD m^3/km	SE kJ/m^3
2.0	2.5	24.24	17.44	2.60	2.21	0.0034	650.00
	5.0	28.70	19.74	2.80	2.24	0.0022	1018.18
	10.0	28.70	20.18	2.87	2.63	0.0028	939.29
	20.0	29.35	20.08	3.16	2.47	0.0028	882.14
4.0	2.5	59.32	35.73	9.16	6.77	0.0284	238.38
	5.0	67.05	45.18	9.43	7.18	0.0200	359.00
	10.0	69.86	46.23	9.48	7.57	0.0158	479.11
	20.0	72.42	45.18	9.98	7.81	0.0162	482.10
6.0	2.5	90.60	59.88	15.51	12.21	0.0796	153.39
	5.0	112.91	71.44	18.35	13.95	0.0990	140.91
	10.0	110.35	72.49	18.35	14.81	0.0616	240.42
	20.0	119.94	78.80	20.52	15.23	0.0796	191.33

Table C.2.2 Results of water jet assisted cutting tests

p mm	s/p	MPTF kN	MTF kN	MRTF kN	MRF kN	YIELD m^3/km	SE kJ/m^3
2.0	2.5	25.84	15.77	2.63	1.98	0.0036	550.00
	5.0	28.07	18.92	2.63	2.03	0.0030	676.67
	10.0	30.62	19.97	2.97	2.19	0.0026	842.31
	20.0	31.25	19.99	3.18	2.60	0.0028	928.57
4.0	2.5	55.49	34.66	6.44	4.48	0.0284	157.75
	5.0	58.04	38.87	7.40	6.19	0.0292	211.99
	10.0	59.32	42.02	7.52	6.40	0.0200	320.00
	20.0	62.53	45.18	7.98	6.69	0.0210	318.57
6.0	2.5	94.73	64.08	14.88	12.02	0.0910	132.09
	5.0	101.44	70.40	15.68	12.96	0.0996	130.12
	10.0	105.27	71.44	15.77	13.14	0.0984	133.54
	20.0	102.72	73.55	16.57	14.29	0.0924	154.65

C.3 Results of Multiple Cutting Tests on Whinstone

Table C.3.1 Results of unassisted cutting tests

p mm	s/p	MPTF kN	MTF kN	MRTF kN	MRF kN	YIELD m^3/km	SE kJ/m^3
4.0	5.0	56.33	30.32	9.77	6.73	0.080	84.13
	10.0	67.59	48.40	12.36	8.71	0.163	53.44

Table C.3.2 Results of water jet assisted cutting tests

p mm	s/p	MPTF kN	MTF kN	MRTF kN	MRF kN	YIELD m^3/km	SE kJ/m^3
4.0	5.0	51.52	27.15	8.77	5.92	0.081	73.09
	10.0	64.98	55.66	10.63	8.04	0.154	52.20

Appendix D

CUTTING TEST RESULTS — LARGE CUTTING RIG

D.1 CUTTING TESTS ON PENNANT SANDSTONE

Table D.1.1 Unassisted cutting forces

p mm	s mm	MPTF MPa	MTF MPa	MPRF MPa	MRF MPa	MPSF1 MPa	MPSF2 MPa
2.	20.	75.95	38.00	5.61	2.32	29.85	5.30
2.	40.	114.18	62.76	7.93	3.52	33.48	8.47
2.	60.	120.21	74.23	8.18	3.74	24.20	16.66
4.	20.	115.26	55.88	11.89	6.55	47.49	7.37
4.	40.	155.49	74.86	15.63	8.61	53.20	24.55
4.	60.	212.58	93.39	16.95	9.61	51.67	30.93

Table D.1.2 Average values of assisted cutting forces

p mm	s mm	MPTF MPa	MTF MPa	MPRF MPa	MRF MPa	MPSF1 MPa	MPSF2 MPa
2.	20.	63.88	33.99	5.05	2.20	23.23	4.66
2.	40.	81.79	46.22	5.77	2.38	23.78	9.95
2.	60.	90.90	53.15	6.61	2.72	30.86	17.31
4.	20.	101.02	50.89	10.44	5.85	36.15	8.99
4.	40.	112.19	56.14	11.83	6.96	38.03	14.67
4.	60.	121.99	63.50	11.98	7.63	43.65	15.93

Table D.1.3 Water jet assisted disc cutter forces

Noz. L. No.	p mm	s mm	W. p. MPa	C. sp. m/s	MPTF MPa	MTF MPa	MPRF MPa	MRF MPa	MPSF1 MPa	MPSF2 MPa
1	2.	20.	41.37	0.25	36.34	17.01	3.05	1.14	16.12	1.01
1	2.	20.	41.37	0.60	68.10	36.10	7.06	3.11	33.03	6.32
1	2.	20.	41.37	0.85	57.96	28.04	6.58	2.83	24.88	8.54
1	2.	20.	41.37	1.00	51.23	26.15	4.77	1.94	21.52	5.01
1	2.	40.	41.37	0.25	50.50	22.37	4.35	1.23	21.11	8.02
1	2.	40.	41.37	0.60	87.39	38.00	8.55	3.67	37.84	15.54
1	2.	40.	41.37	0.85	98.63	46.50	9.15	4.94	42.74	16.84
1	2.	40.	41.37	1.00	57.01	33.71	5.16	2.01	22.13	9.44
1	2.	60.	41.37	0.25	53.33	29.80	5.08	1.97	26.89	9.59
1	2.	60.	41.37	0.60	80.23	46.82	6.93	3.79	27.09	12.91
1	2.	60.	41.37	0.85	86.11	52.80	8.78	3.84	30.14	20.61
1	2.	60.	41.37	1.00	79.48	41.27	6.55	2.65	32.42	17.79
1	4.	20.	55.16	0.25	85.39	41.00	7.61	5.00	36.97	7.29
1	4.	20.	55.16	0.45	96.89	55.73	9.14	4.78	41.44	7.49
1	4.	20.	55.16	0.60	105.59	55.12	9.26	4.90	32.75	7.82
1	4.	20.	55.16	0.85	105.21	66.81	9.50	4.51	39.87	8.82
1	4.	40.	55.16	0.25	110.50	68.33	10.57	6.26	31.92	16.27
1	4.	40.	55.16	0.45	126.38	59.22	10.65	6.28	47.07	15.77
1	4.	40.	55.16	0.60	126.55	63.32	11.79	5.45	33.58	12.67
1	4.	40.	55.16	0.85	133.08	73.34	10.01	5.97	39.29	13.87
1	4.	60.	55.16	0.25	119.63	64.84	9.85	6.64	30.26	24.55
1	4.	60.	55.16	0.45	129.89	69.85	10.74	6.05	43.10	23.76
1	4.	60.	55.16	0.60	123.09	56.18	10.23	4.86	33.41	28.40
1	4.	60.	55.16	0.85	108.51	57.70	10.31	5.56	44.17	18.75
1	4.	20.	41.37	0.25	93.11	48.59	10.27	6.09	40.32	3.35
1	4.	20.	41.37	0.45	95.49	52.39	10.69	5.93	40.16	6.75
1	4.	20.	41.37	0.60	89.87	50.57	10.17	5.59	39.95	2.69
1	4.	20.	41.37	0.85	108.51	52.39	12.11	6.93	41.36	7.12
1	4.	40.	41.37	0.25	126.98	55.12	13.33	7.16	53.70	39.58
1	4.	40.	41.37	0.45	125.79	53.91	15.48	7.30	41.94	18.09
1	4.	40.	41.37	0.60	125.79	61.50	15.02	7.81	42.81	21.07
1	4.	40.	41.37	0.85	144.80	64.99	16.50	8.50	49.43	26.29
1	4.	60.	41.37	0.25	122.76	63.02	14.02	9.24	47.86	31.84
1	4.	60.	41.37	0.45	124.01	57.70	14.58	7.93	38.54	20.00
1	4.	60.	41.37	0.60	124.87	55.43	14.69	9.20	46.74	25.87
1	4.	60.	41.37	0.85	131.19	55.88	15.52	9.62	50.26	28.48

Noz. L. No.	p mm	s mm	W. p. MPa	C. sp. m/s	MPTF MPa	MTF MPa	MPRF MPa	MRF MPa	MPSF1 MPa	MPSF2 MPa
1	4.	20.	27.58	0.25	82.42	65.75	9.07	6.30	34.69	2.73
1	4.	20.	27.58	0.45	88.63	48.59	8.98	3.82	33.91	5.84
1	4.	20.	27.58	0.60	87.06	52.08	8.32	4.28	30.10	3.81
1	4.	20.	27.58	0.85	103.65	61.80	8.78	4.84	38.42	8.82
1	4.	40.	27.58	0.25	118.82	74.86	10.62	5.61	39.33	12.17
1	4.	40.	27.58	0.45	117.80	68.79	11.61	5.07	33.41	17.51
1	4.	40.	27.58	0.60	117.36	69.85	10.87	7.00	35.11	15.03
1	4.	40.	27.58	0.85	127.52	74.41	10.03	7.25	38.38	14.95
1	4.	60.	27.58	0.25	125.47	57.70	12.30	4.93	33.20	15.86
1	4.	60.	27.58	0.45	116.45	50.57	10.48	4.74	40.36	21.98
1	4.	60.	27.58	0.60	129.57	65.75	10.97	6.40	33.24	23.76
1	4.	60.	27.58	0.85	126.49	67.27	11.81	5.74	42.10	22.65
1	4.	20.	13.79	0.25	110.02	79.42	10.69	7.94	34.94	11.22
1	4.	20.	13.79	0.45	123.03	88.53	11.57	9.69	33.08	19.17
1	4.	20.	13.79	0.60	118.50	87.01	13.20	8.96	40.03	11.76
1	4.	20.	13.79	0.85	123.74	86.10	12.63	8.61	42.77	8.61
1	4.	40.	13.79	0.25	131.95	91.11	14.52	11.30	37.80	16.35
1	4.	40.	13.79	0.45	109.48	71.37	11.32	7.67	34.32	13.21
1	4.	40.	13.79	0.60	111.15	67.27	12.59	6.80	38.05	15.40
1	4.	40.	13.79	0.85	113.48	68.79	12.73	9.33	26.62	15.28
1	4.	60.	13.79	0.25	119.20	76.38	12.65	8.07	29.93	12.83
1	4.	60.	13.79	0.45	121.68	76.38	12.41	8.69	28.28	11.63
1	4.	60.	13.79	0.60	116.07	65.30	12.75	8.81	24.26	13.70
1	4.	60.	13.79	0.85	132.70	80.02	11.34	6.54	46.49	12.05
2	2.	20.	55.16	0.25	57.50	27.72	3.42	1.60	20.79	2.28
2	2.	20.	55.16	0.45	74.95	39.51	4.71	2.21	27.82	4.02
2	2.	20.	55.16	0.60	75.04	33.21	5.11	2.05	28.52	3.52
2	2.	20.	55.16	0.85	85.36	48.96	5.45	1.99	31.92	3.28
2	2.	40.	55.16	0.25	87.72	46.19	5.79	2.18	18.79	13.98
2	2.	40.	55.16	0.45	95.03	55.45	5.82	2.14	28.20	9.21
2	2.	40.	55.16	0.60	89.86	52.11	5.79	2.22	23.32	10.72
2	2.	40.	55.16	0.85	99.29	63.20	5.66	2.40	29.99	9.01
2	2.	60.	55.16	0.25	92.09	51.23	6.64	2.51	26.39	25.06
2	2.	60.	55.16	0.45	100.91	66.98	5.77	2.22	30.46	12.83
2	2.	60.	55.16	0.60	101.86	56.27	6.60	2.58	24.18	18.90
2	2.	60.	55.16	0.85	100.00	58.79	5.76	2.28	32.24	12.15

Noz. L. No.	p mm	s mm	W. p. MPa	C. sp. m/s	MPTF MPa	MTF MPa	MPRF MPa	MRF MPa	MPSF1 MPa	MPSF2 MPa
2	2.	20.	41.37	0.25	56.22	17.83	5.44	2.02	19.37	5.21
2	2.	20.	41.37	0.45	49.42	17.45	4.95	2.39	17.18	6.80
2	2.	20.	41.37	0.60	51.18	25.83	5.33	2.72	16.78	4.27
2	2.	20.	41.37	0.85	63.22	37.81	6.49	3.62	28.72	3.59
2	2.	40.	41.37	0.25	79.41	35.47	6.70	3.14	27.46	11.94
2	2.	40.	41.37	0.45	78.40	34.21	5.87	2.70	20.01	17.05
2	2.	40.	41.37	0.60	68.77	28.80	5.63	2.63	17.95	13.59
2	2.	40.	41.37	0.85	71.79	31.50	5.34	2.49	24.52	3.34
2	2.	60.	41.37	0.25	76.94	38.88	7.28	2.52	26.78	21.09
2	2.	60.	41.37	0.45	98.52	48.08	8.11	3.82	35.70	22.15
2	2.	60.	41.37	0.60	67.11	35.98	6.02	2.69	17.03	16.59
2	2.	60.	41.37	0.85	117.17	64.27	8.00	3.92	56.43	21.43
2	2.	20.	27.58	0.25	54.85	30.06	3.73	1.61	18.96	3.14
2	2.	20.	27.58	0.45	64.81	27.91	4.14	1.47	25.69	2.33
2	2.	20.	27.58	0.60	65.23	29.61	4.99	1.75	22.11	5.38
2	2.	20.	27.58	0.85	70.67	37.81	4.70	1.75	32.63	2.10
2	2.	40.	27.58	0.25	82.04	35.47	5.15	1.58	23.01	6.03
2	2.	40.	27.58	0.45	87.68	52.30	5.67	2.02	27.45	5.89
2	2.	40.	27.58	0.60	79.63	47.07	6.02	2.13	22.04	10.12
2	2.	40.	27.58	0.85	92.49	59.04	6.22	2.36	29.53	5.82
2	2.	60.	27.58	0.25	95.36	54.82	7.08	2.76	30.17	28.06
2	2.	60.	27.58	0.45	102.56	71.39	6.39	3.03	41.75	19.44
2	2.	60.	27.58	0.60	92.16	52.30	6.83	2.42	28.92	21.97
2	2.	60.	27.58	0.85	97.81	62.38	6.64	2.83	30.14	19.57
2	2.	20.	13.79	0.25	66.69	42.03	5.83	2.64	14.54	5.33
2	2.	20.	13.79	0.45	57.57	35.29	4.97	2.00	20.43	3.72
2	2.	20.	13.79	0.60	59.51	42.03	5.58	2.65	20.62	11.90
2	2.	20.	13.79	0.85	69.85	50.85	5.99	2.74	25.65	7.66
2	2.	40.	13.79	0.25	78.71	54.82	6.20	3.56	17.91	13.80
2	2.	40.	13.79	0.45	83.85	60.49	5.75	2.77	27.30	18.13
2	2.	40.	13.79	0.60	69.74	42.85	6.13	2.02	25.96	5.06
2	2.	40.	13.79	0.85	64.22	40.52	4.64	1.80	17.05	5.56
2	2.	60.	13.79	0.25	73.32	47.89	6.16	2.39	24.32	11.22
2	2.	60.	13.79	0.45	73.16	44.30	5.89	2.61	25.24	8.22
2	2.	60.	13.79	0.60	72.04	40.96	6.06	2.31	29.29	10.39
2	2.	60.	13.79	0.85	93.40	55.89	6.56	2.64	34.81	7.84

Noz. L. No.	p mm	s mm	W. p. MPa	C. sp. m/s	MPTF MPa	MTF MPa	MPRF MPa	MRF MPa	MPSF1 MPa	MPSF2 MPa
2	4.	20.	55.16	0.25	110.77	47.53	13.24	5.95	31.84	19.33
2	4.	20.	55.16	0.45	114.12	62.26	10.64	7.28	41.98	12.71
2	4.	20.	55.16	0.60	109.37	57.70	9.74	6.09	37.63	7.49
2	4.	20.	55.16	0.85	116.99	52.69	10.95	5.24	38.13	8.16
2	4.	40.	55.16	0.25	116.34	58.16	10.70	6.18	45.00	13.37
2	4.	40.	55.16	0.45	110.13	57.25	11.76	8.10	37.84	15.15
2	4.	40.	55.16	0.60	117.69	47.07	12.51	6.75	33.00	17.59
2	4.	40.	55.16	0.85	113.04	51.63	11.38	6.63	33.08	15.32
2	4.	60.	55.16	0.25	106.56	60.28	10.50	6.36	38.87	9.85
2	4.	60.	55.16	0.45	108.88	54.67	10.19	6.23	37.47	10.89
2	4.	60.	55.16	0.60	126.11	61.20	11.63	7.24	43.93	16.02
2	4.	60.	55.16	0.85	131.03	63.78	12.15	8.48	47.28	14.90
2	4.	20.	41.37	0.25	77.07	35.99	8.78	5.31	35.89	4.06
2	4.	20.	41.37	0.45	77.40	42.97	9.22	5.82	28.15	8.57
2	4.	20.	41.37	0.60	83.01	49.65	9.92	5.80	33.91	4.02
2	4.	20.	41.37	0.85	109.53	56.18	10.61	6.07	60.78	7.62
2	4.	40.	41.37	0.25	115.42	45.10	13.32	7.01	44.75	15.36
2	4.	40.	41.37	0.45	102.08	53.15	12.72	7.07	45.95	18.55
2	4.	40.	41.37	0.60	126.82	52.08	13.72	8.34	38.87	16.02
2	4.	40.	41.37	0.85	125.52	66.81	13.11	6.79	44.63	10.35
2	4.	60.	41.37	0.25	126.28	71.37	16.41	9.78	48.93	20.33
2	4.	60.	41.37	0.45	102.24	46.62	11.67	7.19	33.24	28.11
2	4.	60.	41.37	0.60	132.05	61.20	13.09	9.33	39.74	39.29
2	4.	60.	41.37	0.85	148.96	82.00	15.10	9.53	47.28	16.06
2	4.	20.	27.58	0.25	101.16	42.97	10.67	5.12	23.47	11.84
2	4.	20.	27.58	0.45	111.53	65.75	10.74	6.26	37.47	7.74
2	4.	20.	27.58	0.60	106.29	58.77	10.52	6.83	34.36	9.31
2	4.	20.	27.58	0.85	98.57	55.73	10.43	6.28	36.06	11.14
2	4.	40.	27.58	0.25	100.67	49.05	10.16	6.10	43.88	12.63
2	4.	40.	27.58	0.45	98.08	55.12	10.64	7.03	32.13	9.36
2	4.	40.	27.58	0.60	98.03	59.68	10.59	5.61	38.83	12.88
2	4.	40.	27.58	0.85	118.61	70.31	11.34	7.17	35.89	13.04
2	4.	60.	27.58	0.25	106.78	60.74	10.53	6.71	33.08	13.99
2	4.	60.	27.58	0.45	119.09	66.36	10.49	6.68	40.41	13.79
2	4.	60.	27.58	0.60	117.69	63.78	11.13	7.12	46.86	16.89
2	4.	60.	27.58	0.85	138.54	76.38	11.71	6.75	58.58	16.27

Noz. L. No.	p mm	s mm	W. p. MPa	C. sp. m/s	MPTF MPa	MTF MPa	MPRF MPa	MRF MPa	MPSF1 MPa	MPSF2 MPa
2	4.	20.	13.79	0.25	113.53	53.60	13.16	5.90	45.46	3.93
2	4.	20.	13.79	0.45	94.03	35.99	10.05	5.03	22.15	13.29
2	4.	20.	13.79	0.60	102.84	53.60	8.61	5.29	45.25	1.53
2	4.	20.	13.79	0.85	90.14	42.97	9.85	5.28	25.96	13.08
2	4.	40.	13.79	0.25	108.56	54.67	10.57	6.56	42.81	13.45
2	4.	40.	13.79	0.45	126.22	67.27	13.19	7.38	32.58	17.76
2	4.	40.	13.79	0.60	119.96	69.85	12.70	8.89	32.21	14.45
2	4.	40.	13.79	0.85	97.87	41.00	10.86	5.73	27.03	19.58
2	4.	60.	13.79	0.25	96.79	51.17	10.33	6.02	34.32	9.98
2	4.	60.	13.79	0.45	99.97	48.59	10.92	6.56	35.40	11.38
2	4.	60.	13.79	0.60	135.73	58.77	12.16	7.63	59.37	10.56
2	4.	60.	13.79	0.85	155.17	89.14	13.63	10.53	53.70	6.58
3	2.	20.	41.37	0.25	49.33	25.20	7.13	2.94	23.64	4.45
3	2.	20.	41.37	0.60	50.25	21.86	7.32	2.63	21.18	5.28
3	2.	20.	41.37	0.85	48.80	29.80	4.93	2.13	23.96	5.24
3	2.	20.	41.37	1.00	75.42	37.81	6.39	2.88	43.62	0.79
3	2.	40.	41.37	0.25	79.83	31.32	7.30	2.20	34.19	7.16
3	2.	40.	41.37	0.60	72.96	31.69	6.09	2.65	31.56	13.50
3	2.	40.	41.37	0.85	57.94	28.80	4.54	2.04	24.50	11.20
3	2.	40.	41.37	1.00	99.94	51.98	9.34	4.47	54.87	5.94
3	2.	60.	41.37	0.25	78.84	45.56	6.51	3.47	32.33	15.96
3	2.	60.	41.37	0.60	78.73	36.55	6.90	3.41	29.94	16.96
3	2.	60.	41.37	0.85	86.81	46.19	7.29	4.70	35.56	15.80
3	2.	60.	41.37	1.00	83.50	47.57	7.53	4.27	37.52	8.71
3	4.	20.	41.37	0.25	77.72	34.93	10.10	6.01	32.83	3.35
3	4.	20.	41.37	0.45	83.82	42.97	10.44	5.44	37.72	5.42
3	4.	20.	41.37	0.60	74.80	47.07	9.81	5.92	32.79	7.16
3	4.	20.	41.37	0.85	74.21	47.07	9.26	5.56	34.53	4.93
3	4.	40.	41.37	0.25	106.13	53.15	12.90	9.02	46.41	10.64
3	4.	40.	41.37	0.45	102.02	44.04	12.84	6.60	42.60	17.97
3	4.	40.	41.37	0.60	104.83	47.53	13.77	7.29	40.03	16.81
3	4.	40.	41.37	0.85	112.39	52.08	14.07	7.45	42.64	16.85
3	4.	60.	41.37	0.25	117.26	61.80	13.57	7.78	43.93	19.09
3	4.	60.	41.37	0.45	110.45	58.77	13.63	6.79	39.79	16.02
3	4.	60.	41.37	0.60	125.47	62.26	13.72	7.70	54.36	20.45
3	4.	60.	41.37	0.85	117.26	58.16	13.97	8.97	36.35	32.71

D.2 CUTTING TESTS ON WHINSTONE

Table D.2.1 Unassisted cutting forces

p mm	s mm	MPTF MPa	MTF MPa	MPRF MPa	MRF MPa	MPSF1 MPa	MPSF2 MPa
2.	20.	158.90	69.90	11.40	6.60	44.40	61.60
2.	40.	195.10	80.70	12.40	7.30	39.20	55.50
2.	60.	229.80	103.10	14.20	8.80	65.90	42.30
4.	20.	194.50	80.40	18.30	10.50	20.40	105.80
4.	40.	219.40	105.80	17.70	11.70	38.10	62.60
4.	60.	294.70	119.10	26.50	15.30	57.00	99.90

Table D.2.2 Average values of assisted cutting forces

p mm	s mm	MPTF MPa	MTF MPa	MPRF MPa	MRF MPa	MPSF1 MPa	MPSF2 MPa
2.	20.	137.88	61.66	9.31	5.23	24.87	48.15
2.	40.	166.62	82.76	10.58	6.41	41.70	35.63
2.	60.	197.91	101.43	12.92	7.44	54.98	69.57
4.	20.	185.41	76.90	16.82	10.53	15.63	83.05
4.	40.	219.15	103.30	18.10	12.25	41.46	73.71
4.	60.	249.22	109.00	22.18	14.89	53.71	89.09

Table D.2.3 Water jet assisted disc cutter forces

Noz. L. No.	p mm	s mm	W. p. MPa	C. sp. m/s	MPTF MPa	MTF MPa	MPRF MPa	MRF MPa	MPSF1 MPa	MPSF2 MPa
2	2.	20.	55.16	0.25	112.00	39.00	6.80	2.90	11.30	26.40
2	2.	20.	55.16	0.45	130.30	54.70	9.20	4.50	19.50	45.50
2	2.	20.	55.16	0.60	144.50	94.70	9.50	6.20	39.00	23.80
2	2.	20.	55.16	0.85	152.80	80.00	9.80	5.00	36.90	26.90
2	2.	40.	55.16	0.25	155.00	66.30	10.00	4.70	34.30	59.80
2	2.	40.	55.16	0.45	164.80	80.50	11.60	6.50	58.70	32.90
2	2.	40.	55.16	0.60	161.40	66.80	9.80	5.80	51.20	43.30
2	2.	40.	55.16	0.85	144.00	59.80	10.60	5.30	40.70	31.00
2	2.	60.	55.16	0.25	168.00	93.00	9.90	5.10	38.60	62.00
2	2.	60.	55.16	0.45	175.10	105.30	12.90	7.00	37.70	88.00
2	2.	60.	55.16	0.60	187.30	75.90	12.10	7.00	34.70	42.90
2	2.	60.	55.16	0.85	191.20	90.60	13.20	7.90	41.20	53.80
2	2.	20.	41.37	0.25	129.80	53.30	7.60	4.20	7.80	44.90
2	2.	20.	41.37	0.45	132.30	71.30	8.70	5.20	16.00	56.40
2	2.	20.	41.37	0.60	145.50	64.80	10.10	5.90	22.60	55.50
2	2.	20.	41.37	0.85	124.70	52.50	8.90	4.70	19.30	45.10
2	2.	40.	41.37	0.25	182.90	71.30	11.80	6.40	36.20	32.50
2	2.	40.	41.37	0.45	156.70	68.40	10.00	5.90	47.10	29.00
2	2.	40.	41.37	0.60	160.90	75.90	11.90	6.20	44.40	31.60
2	2.	40.	41.37	0.85	190.20	70.90	9.90	7.10	45.30	32.10
2	2.	60.	41.37	0.25	158.40	76.40	11.10	5.00	42.00	28.80
2	2.	60.	41.37	0.45	196.30	107.70	12.50	7.70	35.60	73.50
2	2.	60.	41.37	0.60	219.60	109.90	12.60	7.00	43.30	76.70
2	2.	60.	41.37	0.85	205.40	108.20	12.70	7.30	31.40	88.70
2	2.	20.	27.58	0.25	141.10	56.60	9.10	4.30	18.40	45.10
2	2.	20.	27.58	0.45	131.50	54.20	9.70	4.90	11.30	53.30
2	2.	20.	27.58	0.60	147.40	64.30	9.70	5.20	22.80	65.90
2	2.	20.	27.58	0.85	140.30	50.10	10.90	5.00	23.60	53.80
2	2.	40.	27.58	0.25	172.40	97.60	10.50	7.70	32.50	32.50
2	2.	40.	27.58	0.45	174.60	97.10	10.40	6.90	33.80	48.60
2	2.	40.	27.58	0.60	135.70	84.60	8.10	5.90	32.90	28.80
2	2.	40.	27.58	0.85	184.40	117.40	9.90	5.60	36.60	32.90
2	2.	60.	27.58	0.25	197.60	109.90	12.10	7.40	42.00	46.00
2	2.	60.	27.58	0.45	221.00	134.20	13.40	8.00	186.20	86.50
2	2.	60.	27.58	0.60	210.30	99.30	12.80	7.00	70.90	58.70
2	2.	60.	27.58	0.85	180.00	92.50	13.10	7.90	65.30	209.20

Noz. L. No.	p mm	s mm	W. p. MPa	C. sp. m/s	MPTF MPa	MTF MPa	MPRF MPa	MRF MPa	MPSF1 MPa	MPSF2 MPa
2	2.	20.	13.79	0.25	146.00	69.90	9.20	6.80	94.30	58.10
2	2.	20.	13.79	0.45	137.40	60.20	9.90	5.50	20.00	53.30
2	2.	20.	13.79	0.60	154.30	67.70	10.30	7.70	19.70	62.60
2	2.	20.	13.79	0.85	136.20	53.30	9.60	5.70	15.40	53.80
2	2.	40.	13.79	0.25	162.10	85.10	11.10	7.20	25.10	37.10
2	2.	40.	13.79	0.45	189.70	98.30	11.30	7.40	25.80	32.90
2	2.	40.	13.79	0.60	168.00	74.90	11.00	6.40	52.20	30.80
2	2.	40.	13.79	0.85	163.10	109.40	11.50	7.60	70.40	34.20
2	2.	60.	13.79	0.25	189.70	86.00	13.10	6.40	52.70	43.10
2	2.	60.	13.79	0.45	217.40	121.50	15.80	8.80	62.60	45.10
2	2.	60.	13.79	0.60	235.90	115.90	16.10	10.90	57.20	56.10
2	2.	60.	13.79	0.85	213.40	96.60	13.40	8.80	38.40	54.00
2	4.	20.	55.16	0.25	165.90	89.50	15.60	10.20	14.30	76.50
2	4.	20.	55.16	0.45	165.30	70.20	16.60	8.50	11.00	74.30
2	4.	20.	55.16	0.60	186.00	72.20	16.60	11.20	39.90	64.20
2	4.	20.	55.16	0.85	191.00	92.70	15.90	10.50	14.30	110.30
2	4.	40.	55.16	0.25	229.30	122.10	20.80	13.20	36.60	88.40
2	4.	40.	55.16	0.45	217.60	111.00	17.40	11.40	55.70	81.30
2	4.	40.	55.16	0.60	224.90	113.00	18.40	15.20	63.30	88.40
2	4.	40.	55.16	0.85	215.80	97.70	15.80	10.50	50.70	40.50
2	4.	60.	55.16	0.25	235.50	125.30	18.40	12.50	31.40	82.20
2	4.	60.	55.16	0.45	236.90	114.00	20.90	14.30	36.20	81.90
2	4.	60.	55.16	0.60	265.50	111.00	24.70	16.20	32.30	111.20
2	4.	60.	55.16	0.85	239.00	103.80	20.10	13.60	40.80	73.70
2	4.	20.	41.37	0.25	181.40	70.20	16.10	9.90	12.40	81.30
2	4.	20.	41.37	0.45	191.70	86.50	18.50	10.90	35.60	59.80
2	4.	20.	41.37	0.60	185.00	82.50	17.70	11.10	9.10	103.20
2	4.	20.	41.37	0.85	196.70	73.20	18.10	10.50	11.00	89.80
2	4.	40.	41.37	0.25	216.40	98.70	20.30	12.10	29.90	86.10
2	4.	40.	41.37	0.45	202.50	82.50	16.90	11.00	35.60	65.20
2	4.	40.	41.37	0.60	226.50	110.00	18.30	13.90	31.40	105.10
2	4.	40.	41.37	0.85	217.60	111.00	16.30	10.50	24.10	77.60
2	4.	60.	41.37	0.25	245.00	133.30	21.00	14.20	46.60	99.90
2	4.	60.	41.37	0.45	260.50	131.30	21.30	15.20	73.70	98.00
2	4.	60.	41.37	0.60	253.00	113.00	20.70	14.90	195.80	125.10
2	4.	60.	41.37	0.85	266.10	89.70	22.50	15.20	33.80	96.00

Noz. L. No.	p mm	s mm	W. p. MPa	C. sp. m/s	MPTF MPa	MTF MPa	MPRF MPa	MRF MPa	MPSF1 MPa	MPSF2 MPa
2	4.	20.	27.58	0.25	188.20	69.20	16.00	9.80	10.00	82.80
2	4.	20.	27.58	0.45	203.90	93.70	19.10	12.10	4.80	98.00
2	4.	20.	27.58	0.60	201.10	69.20	17.90	11.20	37.10	70.90
2	4.	20.	27.58	0.85	184.20	76.40	16.70	10.40	11.30	80.40
2	4.	40.	27.58	0.25	207.40	85.50	18.60	12.10	59.40	61.80
2	4.	40.	27.58	0.45	197.10	84.50	16.20	8.30	59.40	60.90
2	4.	40.	27.58	0.60	239.20	99.70	17.40	13.10	27.70	71.80
2	4.	40.	27.58	0.85	205.90	105.80	19.20	12.90	44.00	59.40
2	4.	60.	27.58	0.25	250.80	102.80	21.00	11.60	42.90	87.10
2	4.	60.	27.58	0.45	230.30	93.70	21.40	12.70	45.10	76.50
2	4.	60.	27.58	0.60	266.50	110.00	24.30	16.40	42.30	78.00
2	4.	60.	27.58	0.85	260.10	114.00	23.50	18.40	59.00	98.90
2	4.	20.	13.79	0.25	181.80	68.20	16.30	9.30	8.50	87.40
2	4.	20.	13.79	0.45	184.20	76.40	15.70	9.80	12.80	77.00
2	4.	20.	13.79	0.60	169.90	67.20	14.50	10.50	8.50	79.80
2	4.	20.	13.79	0.85	190.40	73.20	17.80	12.70	9.50	93.20
2	4.	40.	13.79	0.25	230.30	134.30	18.40	14.90	29.50	95.00
2	4.	40.	13.79	0.45	200.30	102.80	15.20	10.10	38.10	50.90
2	4.	40.	13.79	0.60	245.40	105.80	20.80	13.80	40.80	76.10
2	4.	40.	13.79	0.85	230.30	88.50	19.60	13.00	37.10	70.90
2	4.	60.	13.79	0.25	251.80	115.00	25.10	17.00	35.30	84.60
2	4.	60.	13.79	0.45	240.80	95.70	25.30	14.10	65.20	72.60
2	4.	60.	13.79	0.60	251.80	92.70	22.40	16.10	43.30	77.60
2	4.	60.	13.79	0.85	233.90	98.70	22.30	15.90	35.60	82.20

Appendix E

THE COMPARISON OF THEORETICAL ANALYSIS WITH EXPERIMENTAL RESULTS

E.1 CUTTING TESTS WITH SHARP DISC CUTTERS

Table E.1.1 Cutting tests on Bunter Sandstone (Dry)
[Roxborough and Phillips (1975,b)]

			Unrelieved				Relieved		
θ	D	p	MTF_u	MTF_1	MTF_2	s	MTF_r	MTF_3	MTF_4
deg.	mm	mm	kN	kN	kN	mm	kN	kN	kN
60.0	100.0	10.0	29.42	29.68	25.57	12.0	11.33	8.39	7.23
60.0	125.0	6.0	15.35	15.86	13.66	48.0	14.04	11.58	9.98
60.0	150.0	2.0	5.35	3.40	2.93	24.0	3.71	3.04	2.62
60.0	175.0	8.0	28.96	28.93	24.92	60.0	24.94	20.46	17.62
60.0	200.0	4.0	13.66	11.08	9.54	36.0	12.20	8.58	7.39
70.0	125.0	8.0	26.78	28.43	25.30	24.0	16.67	12.71	11.31
70.0	150.0	4.0	13.94	11.23	9.99	60.0	13.61	11.23	9.99
70.0	175.0	10.0	43.31	47.18	41.98	36.0	26.10	23.11	20.57
70.0	200.0	6.0	29.89	23.78	21.16	12.0	9.89	8.68	7.73
70.0	100.0	2.0	5.77	3.25	2.89	48.0	4.34	4.11	3.66
80.0	150.0	6.0	29.49	23.79	21.84	36.0	19.82	15.04	13.81
80.0	175.0	2.0	8.11	5.02	4.61	12.0	4.70	3.17	2.91
80.0	200.0	8.0	34.48	42.29	38.83	48.0	33.80	26.75	24.56
80.0	100.0	4.0	14.12	10.57	9.71	24.0	11.28	6.69	6.14
80.0	125.0	10.0	57.51	45.74	42.00	60.0	35.10	28.93	26.56
90.0	175.0	4.0	24.14	16.29	15.44	48.0	20.44	14.57	13.81
90.0	200.0	10.0	71.69	67.89	64.34	24.0	29.55	27.16	25.73
90.0	100.0	6.0	28.82	22.19	21.03	60.0	24.37	18.12	17.17
90.0	125.0	2.0	8.70	4.89	4.63	36.0	6.59	5.35	5.07
90.0	150.0	8.0	42.19	42.00	39.80	12.0	19.17	13.28	12.59
100.0	200.0	2.0	13.19	7.15	7.00	60.0	9.55	10.11	9.90
100.0	100.0	8.0	49.06	39.00	38.18	36.0	30.18	21.36	20.91
100.0	125.0	4.0	27.92	15.81	15.48	12.0	10.99	7.07	6.92
100.0	150.0	10.0	63.11	67.23	65.82	48.0	41.78	38.03	37.23
100.0	175.0	6.0	43.99	34.33	33.61	24.0	22.77	17.73	17.36

Table E.1.2 Cutting tests on Bunter Sandstone (Wet)
[Roxborough and Phillips (1975,b)]

			Unrelieved				Relieved		
θ	D	p	MTF_u	MTF_1	MTF_2	s	MTF_r	MTF_3	MTF_4
deg.	mm	mm	kN	kN	kN	mm	kN	kN	kN
60.0	100.0	10.0	28.68	25.47	21.29	12.0	7.95	7.20	6.02
60.0	125.0	6.0	16.31	13.61	11.38	48.0	12.46	9.94	8.31
60.0	150.0	2.0	4.53	2.92	2.44	24.0	3.52	2.61	2.18
60.0	175.0	8.0	23.92	24.82	20.75	60.0	21.81	17.55	14.67
60.0	200.0	4.0	13.09	9.51	7.95	36.0	8.36	7.37	6.16
70.0	125.0	8.0	26.16	24.42	21.06	24.0	12.18	10.92	9.42
70.0	150.0	4.0	11.43	9.64	8.32	60.0	8.84	9.64	8.32
70.0	175.0	10.0	35.15	40.53	34.96	36.0	21.87	19.85	17.13
70.0	200.0	6.0	23.90	20.42	17.62	12.0	8.89	7.46	6.43
70.0	100.0	2.0	3.97	2.79	2.41	48.0	3.86	3.53	3.05
80.0	150.0	6.0	25.34	20.45	18.19	36.0	17.07	12.94	11.50
80.0	175.0	2.0	6.68	4.31	3.84	12.0	4.05	2.73	2.43
80.0	200.0	8.0	38.00	36.36	32.34	48.0	27.97	23.00	20.45
80.0	100.0	4.0	12.52	9.09	8.08	24.0	7.41	5.75	5.11
80.0	125.0	10.0	42.14	39.33	34.97	60.0	28.94	24.87	22.12
90.0	175.0	4.0	19.75	14.02	12.86	48.0	17.18	12.54	11.50
90.0	200.0	10.0	55.38	58.43	53.58	24.0	25.56	23.37	21.43
90.0	100.0	6.0	29.12	19.10	17.51	60.0	22.61	15.60	14.30
90.0	125.0	2.0	7.29	4.21	3.86	36.0	5.62	4.61	4.22
90.0	150.0	8.0	43.11	36.15	33.14	12.0	12.96	11.43	10.48
100.0	200.0	2.0	12.14	6.16	5.83	60.0	8.49	8.71	8.24
100.0	100.0	8.0	47.45	33.60	31.79	36.0	23.61	18.40	17.41
100.0	125.0	4.0	22.93	13.62	12.89	12.0	7.82	6.09	5.76
100.0	150.0	10.0	66.46	57.93	54.81	48.0	45.43	32.77	31.00
100.0	175.0	6.0	40.42	29.58	27.99	24.0	22.39	15.27	14.45

Note:
MTF_u = experimental unrelieved thrust force,
MTF_1 = theoretical thrust force (Eq. 9.2.2 + 9.3.1),
MTF_2 = theoretical thrust force (Eq. 9.2.1 + 9.3.1),
MTF_r = experimental relieved thrust force,
MTF_3 = theoretical thrust force (Eq. 9.2.2 + 9.3.2 + 9.3.3),
MTF_4 = theoretical thrust force (Eq. 9.2.1 + 9.3.2 + 9.3.3),

Table E.1.3 Cutting tests on Gypsum [Bilgin (1977)]

			Unrelieved				Relieved		
θ	D	p	MTF_u	MTF_1	MTF_2	s	MTF_r	MTF_3	MTF_4
deg.	mm	mm	kN	kN	kN	mm	kN	kN	kN
60.0	100.0	10.0	35.86	34.68	23.38	12.0	6.81	9.81	6.61
60.0	125.0	6.0	19.49	18.53	12.50	48.0	18.96	13.53	9.13
60.0	150.0	2.0	6.11	3.98	2.68	24.0	6.88	3.56	2.40
60.0	175.0	8.0	34.21	33.80	22.79	60.0	29.48	23.90	16.12
60.0	200.0	4.0	12.75	12.95	8.73	36.0	14.82	10.03	6.76
70.0	125.0	8.0	30.94	33.45	23.14	24.0	19.06	14.96	10.35
70.0	150.0	4.0	14.38	13.21	9.14	60.0	15.07	13.21	9.14
70.0	175.0	10.0	44.75	55.52	38.40	36.0	34.96	27.20	18.81
70.0	200.0	6.0	26.70	27.98	19.35	12.0	10.31	10.22	7.07
70.0	100.0	2.0	6.32	3.83	2.65	48.0	5.68	4.84	3.35
80.0	150.0	6.0	29.43	28.19	19.98	36.0	24.27	17.83	12.64
80.0	175.0	2.0	7.48	5.95	4.21	12.0	6.91	3.76	2.67
80.0	200.0	8.0	45.56	50.11	35.52	48.0	41.58	31.69	22.46
80.0	100.0	4.0	14.25	12.53	8.88	24.0	12.17	7.92	5.62
80.0	125.0	10.0	48.92	54.20	38.41	60.0	45.19	34.28	24.30
90.0	175.0	4.0	21.95	19.45	14.12	48.0	23.09	17.40	12.63
90.0	200.0	10.0	78.76	81.04	58.85	24.0	33.97	32.42	23.54
90.0	100.0	6.0	24.81	26.49	19.24	60.0	27.75	21.63	15.71
90.0	125.0	2.0	10.44	5.83	4.23	36.0	9.51	6.39	4.64
90.0	150.0	8.0	51.31	50.13	36.40	12.0	12.23	15.85	11.51
100.0	200.0	2.0	11.24	8.60	6.40	60.0	12.52	12.17	9.06
100.0	100.0	8.0	47.66	46.91	34.92	36.0	30.68	25.69	19.13
100.0	125.0	4.0	23.61	19.02	14.16	12.0	11.87	8.51	6.33
100.0	150.0	10.0	75.38	80.87	60.20	48.0	48.82	45.75	34.05
100.0	175.0	6.0	46.89	41.30	30.74	24.0	28.02	21.33	15.87

Note:
MTF_u = experimental unrelieved thrust force,
MTF_1 = theoretical thrust force (Eq. 9.2.2 + 9.3.1),
MTF_2 = theoretical thrust force (Eq. 9.2.1 + 9.3.1),
MTF_r = experimental relieved thrust force,
MTF_3 = theoretical thrust force (Eq. 9.2.2 + 9.3.2 + 9.3.3),
MTF_4 = theoretical thrust force (Eq. 9.2.1 + 9.3.2 + 9.3.3),

Table E.1.4 Cutting tests on Dunhouse Sandstone [Bilgin (1977)]

			Unrelieved				Relieved		
θ	D	p	MTF_u	MTF_1	MTF_2	s	MTF_r	MTF_3	MTF_4
deg.	mm	mm	kN	kN	kN	mm	kN	kN	kN
60.0	100.0	10.0	25.07	33.85	29.02	12.0	5.61	9.58	8.21
60.0	125.0	6.0	14.09	18.09	15.51	48.0	14.39	13.21	11.32
60.0	150.0	2.0	4.71	3.88	3.33	24.0	4.71	3.47	2.98
60.0	175.0	8.0	23.01	33.00	28.28	60.0	21.41	23.33	20.00
60.0	200.0	4.0	12.62	12.64	10.83	36.0	12.62	9.79	8.39
70.0	125.0	8.0	25.26	32.43	28.71	24.0	13.68	14.50	12.84
70.0	150.0	4.0	12.74	12.81	11.34	60.0	12.74	12.81	11.34
70.0	175.0	10.0	40.52	53.82	47.65	36.0	23.56	26.37	23.34
70.0	200.0	6.0	18.48	27.12	24.01	12.0	9.44	9.90	8.77
70.0	100.0	2.0	4.45	3.71	3.28	48.0	4.46	4.69	4.15
80.0	150.0	6.0	24.98	27.14	24.79	36.0	17.14	17.17	15.68
80.0	175.0	2.0	6.11	5.73	5.23	12.0	5.84	3.62	3.31
80.0	200.0	8.0	37.12	48.25	44.07	48.0	26.83	30.52	27.87
80.0	100.0	4.0	12.86	12.06	11.02	24.0	12.05	7.63	6.97
80.0	125.0	10.0	36.11	52.19	47.67	60.0	29.63	33.01	30.15
90.0	175.0	4.0	9.13	18.59	17.52	48.0	9.13	16.63	15.67
90.0	200.0	10.0	62.90	77.48	73.02	24.0	24.18	30.99	29.21
90.0	100.0	6.0	23.41	25.33	23.87	60.0	23.41	20.68	19.49
90.0	125.0	2.0	8.10	5.58	5.25	36.0	8.10	6.11	5.76
90.0	150.0	8.0	34.23	47.93	45.17	12.0	10.69	15.16	14.28
100.0	200.0	2.0	12.53	8.16	7.95	60.0	12.53	11.54	11.24
100.0	100.0	8.0	38.37	44.51	43.33	36.0	22.37	24.38	23.73
100.0	125.0	4.0	25.47	18.05	17.57	12.0	10.89	8.07	7.86
100.0	150.0	10.0	55.74	76.74	74.70	48.0	38.39	43.41	42.26
100.0	175.0	6.0	37.65	39.18	38.14	24.0	18.89	20.23	19.70

Note:
MTF_u = experimental unrelieved thrust force,
MTF_1 = theoretical thrust force (Eq. 9.2.2 + 9.3.1),
MTF_2 = theoretical thrust force (Eq. 9.2.1 + 9.3.1),
MTF_r = experimental relieved thrust force,
MTF_3 = theoretical thrust force (Eq. 9.2.2 + 9.3.2 + 9.3.3),
MTF_4 = theoretical thrust force (Eq. 9.2.1 + 9.3.2 + 9.3.3),

Table E.1.5 Cutting tests on Mansfield Sandstone [Bilgin (1977)]

			Unrelieved				Relieved		
θ	D	p	MTF_u	MTF_1	MTF_2	s	MTF_r	MTF_3	MTF_4
deg.	mm	mm	kN	kN	kN	mm	kN	kN	kN
60.0	100.0	7.5	20.16	34.32	24.40	9.0	6.56	9.71	6.90
60.0	125.0	4.5	14.47	18.20	12.94	36.0	14.47	13.29	9.45
60.0	150.0	1.5	4.32	3.89	2.76	18.0	4.32	3.48	2.47
60.0	175.0	6.0	20.05	33.19	23.60	45.0	20.05	23.47	16.68
60.0	200.0	3.0	10.42	12.67	9.01	27.0	9.00	9.81	6.98
70.0	125.0	6.0	22.65	32.89	24.01	18.0	11.26	14.71	10.74
70.0	150.0	3.0	10.54	12.92	9.44	45.0	10.54	12.92	9.44
70.0	175.0	7.5	34.05	54.53	39.81	27.0	18.74	26.71	19.50
70.0	200.0	4.5	20.42	27.38	19.99	9.0	9.25	10.00	7.30
70.0	100.0	1.5	4.48	3.74	2.73	36.0	4.48	4.73	3.45
80.0	150.0	4.5	22.30	27.58	20.67	27.0	16.69	17.45	13.07
80.0	175.0	1.5	5.85	5.80	4.34	9.0	4.53	3.67	2.75
80.0	200.0	6.0	34.83	49.04	36.74	36.0	24.39	31.01	23.24
80.0	100.0	3.0	11.99	12.26	9.19	18.0	7.85	7.75	5.81
80.0	125.0	7.5	37.12	53.34	39.96	45.0	28.97	33.73	25.27
90.0	175.0	3.0	18.70	18.96	14.58	36.0	18.70	16.96	13.04
90.0	200.0	7.5	62.68	79.30	60.96	18.0	24.00	31.72	24.38
90.0	100.0	4.5	24.77	25.96	19.95	45.0	24.77	21.20	16.29
90.0	125.0	1.5	7.69	5.68	4.37	27.0	7.69	6.22	4.78
90.0	150.0	6.0	38.85	49.08	37.72	9.0	12.20	15.52	11.93
100.0	200.0	1.5	12.48	8.36	6.60	45.0	12.48	11.82	9.33
100.0	100.0	6.0	44.03	46.03	36.32	27.0	19.26	25.21	19.90
100.0	125.0	3.0	22.08	18.54	14.63	9.0	8.78	8.29	6.54
100.0	150.0	7.5	65.19	79.20	62.50	36.0	35.28	44.80	35.36
100.0	175.0	4.5	39.90	40.26	31.77	18.0	20.00	20.79	16.41

Note:
MTF_u = experimental unrelieved thrust force,
MTF_1 = theoretical thrust force (Eq. 9.2.2 + 9.3.1),
MTF_2 = theoretical thrust force (Eq. 9.2.1 + 9.3.1),
MTF_r = experimental relieved thrust force,
MTF_3 = theoretical thrust force (Eq. 9.2.2 + 9.3.2 + 9.3.3),
MTF_4 = theoretical thrust force (Eq. 9.2.1 + 9.3.2 + 9.3.3),

Table E.1.6 Cutting tests on Anhydrite [Bilgin (1977)]

			Unrelieved				Relieved		
θ	D	p	MTF_u	MTF_1	MTF_2	s	MTF_r	MTF_3	MTF_4
deg.	mm	mm	kN	kN	kN	mm	kN	kN	kN
60.0	100.0	5.0	21.62	31.05	21.31	6.0	8.55	8.78	6.03
60.0	125.0	3.0	11.18	16.35	11.22	24.0	11.87	11.94	8.20
60.0	150.0	1.0	2.93	3.48	2.39	12.0	2.93	3.11	2.14
60.0	175.0	4.0	17.64	29.80	20.46	30.0	19.59	21.07	14.47
60.0	200.0	2.0	4.60	11.34	7.78	18.0	4.95	8.78	6.03
70.0	125.0	4.0	18.58	29.63	20.87	12.0	11.15	13.25	9.33
70.0	150.0	2.0	9.39	11.59	8.16	30.0	9.39	11.59	8.16
70.0	175.0	5.0	28.58	49.08	34.57	18.0	20.56	24.05	16.94
70.0	200.0	3.0	15.83	24.56	17.30	6.0	7.72	8.97	6.32
70.0	100.0	1.0	3.66	3.35	2.36	24.0	3.66	4.24	2.99
80.0	150.0	3.0	23.09	24.80	17.91	18.0	18.00	15.68	11.32
80.0	175.0	1.0	4.54	5.19	3.75	6.0	4.46	3.28	2.37
80.0	200.0	4.0	26.05	44.08	31.83	24.0	22.33	27.88	20.13
80.0	100.0	2.0	10.45	11.02	7.96	12.0	8.95	6.97	5.03
80.0	125.0	5.0	35.08	48.21	34.81	30.0	28.01	30.49	22.02
90.0	175.0	2.0	16.36	17.03	12.60	24.0	16.36	15.23	11.27
90.0	200.0	5.0	50.19	71.45	52.88	12.0	20.13	28.58	21.15
90.0	100.0	3.0	17.65	23.42	17.33	30.0	17.65	19.12	14.15
90.0	125.0	1.0	3.93	5.10	3.77	18.0	3.93	5.58	4.13
90.0	150.0	4.0	29.01	44.24	32.74	6.0	12.63	13.99	10.35
100.0	200.0	1.0	7.73	7.50	5.69	30.0	7.73	10.61	8.05
100.0	100.0	4.0	30.91	41.68	31.64	18.0	21.64	22.83	17.33
100.0	125.0	2.0	17.69	16.68	12.66	6.0	10.61	7.46	5.66
100.0	150.0	5.0	42.49	71.59	54.35	24.0	28.33	40.50	30.74
100.0	175.0	3.0	34.61	36.24	27.51	12.0	23.16	18.71	14.21

Note:
MTF_u = experimental unrelieved thrust force,
MTF_1 = theoretical thrust force (Eq. 9.2.2 + 9.3.1),
MTF_2 = theoretical thrust force (Eq. 9.2.1 + 9.3.1),
MTF_r = experimental relieved thrust force,
MTF_3 = theoretical thrust force (Eq. 9.2.2 + 9.3.2 + 9.3.3),
MTF_4 = theoretical thrust force (Eq. 9.2.1 + 9.3.2 + 9.3.3),

Table E.1.7 Cutting tests on Colorado Red Granite [Ozdemir et al. 1977)]

θ deg.	D in	p in	s in	MTF_t lb	MTF_1 lb	MTF_2 lb	R	R_1	R_2
120.0	8.0	0.25	1.0	23102.	19593.	18675.	11.79	7.42	5.57
75.0	10.0	0.15	1.0	7075.	6748.	5596.	8.72	10.80	8.10
105.0	12.0	0.05	1.0	6001.	3852.	3490.	13.34	20.61	15.46
60.0	14.0	0.20	1.0	10435.	8377.	6645.	15.93	11.08	8.31
90.0	16.0	0.10	1.0	8058.	7134.	6177.	18.23	16.81	12.61
75.0	8.0	0.05	1.5	6417.	2475.	2053.	27.90	16.81	12.61
105.0	10.0	0.20	1.5	20860.	17091.	15482.	11.70	9.33	7.00
60.0	12.0	0.10	1.5	10472.	4764.	3779.	13.22	14.54	10.91
90.0	14.0	0.25	1.5	21605.	20314.	17589.	11.27	9.89	7.42
120.0	16.0	0.15	1.5	27639.	20591.	19625.	29.72	13.71	10.28
105.0	8.0	0.10	2.0	15851.	8859.	8025.	21.54	11.85	8.89
60.0	10.0	0.25	2.0	15442.	12448.	9874.	8.42	8.33	6.24
90.0	12.0	0.15	2.0	17701.	13065.	11313.	8.33	11.85	8.89
120.0	14.0	0.05	2.0	20769.	7435.	7087.	37.09	22.27	16.70
75.0	16.0	0.20	2.0	26393.	16116.	13365.	14.02	11.85	8.89
60.0	8.0	0.15	2.5	13509.	7492.	5943.	12.04	9.65	7.23
90.0	10.0	0.05	2.5	13766.	4462.	3863.	21.99	18.81	14.11
120.0	12.0	0.20	2.5	37955.	30582.	29148.	17.57	10.24	7.68
75.0	14.0	0.10	2.5	14190.	8450.	7008.	15.59	15.72	11.79
105.0	16.0	0.25	2.5	43429.	34964.	31672.	12.71	10.58	7.94
90.0	8.0	0.20	3.0	23270.	17310.	14988.	9.63	8.33	6.24
120.0	10.0	0.10	3.0	31822.	15342.	14623.	19.57	13.27	9.95
75.0	12.0	0.25	3.0	22076.	21277.	17644.	10.00	9.14	6.86
105.0	14.0	0.15	3.0	38696.	21550.	19521.	14.74	12.81	9.61
60.0	16.0	0.05	3.0	10684.	3900.	3094.	19.86	23.81	17.86

Note:

MTF_u = experimental unrelieved thrust force,

MTF_1 = theoretical thrust force (Eq. 9.2.2 + 9.3.1),

MTF_2 = theoretical thrust force (Eq. 9.2.1 + 9.3.1),

MTF_r = experimental relieved thrust force,

MTF_3 = theoretical thrust force (Eq. 9.2.2 + 9.3.2 + 9.3.3),

MTF_4 = theoretical thrust force (Eq. 9.2.1 + 9.3.2 + 9.3.3),

Table E.1.8 Cutting tests on Charcoal Grey granite [Ozdemir et al. 1977)]

θ deg.	D in	p in	s in	MTF_t lb	MTF_1 lb	MTF_2 lb	R	R_1	R_2
60.0	16.0	0.25	1.0	14347.	17670.	14199.	9.63	10.58	7.94
75.0	10.0	0.15	1.0	11829.	10653.	8954.	10.38	10.80	8.10
90.0	14.0	0.05	1.0	7452.	5271.	4629.	33.27	22.27	16.70
105.0	8.0	0.20	1.0	17007.	19628.	18044.	10.21	8.33	6.24
120.0	12.0	0.10	1.0	14718.	15300.	14810.	20.70	14.54	10.91
60.0	10.0	0.05	1.5	5771.	3440.	2764.	11.78	18.81	14.11
75.0	14.0	0.20	1.5	16597.	20591.	17307.	10.09	11.08	8.31
90.0	8.0	0.10	1.5	11309.	9717.	8533.	14.88	11.85	8.89
105.0	12.0	0.25	1.5	25519.	36881.	33904.	8.59	9.14	6.86
120.0	16.0	0.15	1.5	28678.	32439.	31400.	31.58	13.71	10.28
60.0	14.0	0.10	2.0	12441.	9390.	7545.	18.32	15.72	11.79
75.0	8.0	0.25	2.0	18562.	22272.	18720.	8.46	7.42	5.57
90.0	12.0	0.15	2.0	18622.	20613.	18100.	12.25	11.85	8.89
105.0	16.0	0.05	2.0	16672.	9923.	9122.	33.01	23.81	17.86
120.0	10.0	0.20	2.0	40025.	39271.	38014.	19.39	9.33	7.00
60.0	8.0	0.15	2.5	13194.	11835.	9510.	11.14	9.65	7.23
75.0	12.0	0.05	2.5	12348.	6184.	5198.	14.32	20.61	15.46
90.0	16.0	0.20	2.5	47059.	35481.	31157.	21.02	11.85	8.89
105.0	10.0	0.10	2.5	29642.	17482.	16071.	16.30	13.27	9.95
120.0	14.0	0.25	2.5	53613.	65009.	62928.	12.47	9.89	7.42
60.0	12.0	0.20	3.0	18881.	21193.	17029.	8.36	10.24	7.68
75.0	16.0	0.10	3.0	23176.	15629.	13136.	26.10	16.81	12.61
90.0	10.0	0.25	3.0	42727.	38165.	33514.	10.91	8.33	6.24
105.0	14.0	0.15	3.0	37030.	33976.	31234.	16.55	12.81	9.61
120.0	8.0	0.05	3.0	26280.	10830.	10483.	29.10	16.81	12.61

Note:

MTF_u = experimental unrelieved thrust force,
MTF_1 = theoretical thrust force (Eq. 9.2.2 + 9.3.1),
MTF_2 = theoretical thrust force (Eq. 9.2.1 + 9.3.1),
MTF_r = experimental relieved thrust force,
MTF_3 = theoretical thrust force (Eq. 9.2.2 + 9.3.2 + 9.3.3),
MTF_4 = theoretical thrust force (Eq. 9.2.1 + 9.3.2 + 9.3.3),

E.2 CUTTING TESTS WITH WORN DISC CUTTERS

Table E.2.1 Cutting tests on Colorado Red Granite [Ozdemir et al. (1977)]

θ deg.	D in	p in	s in	r in	MTF_t lb	MTF_1 lb	MTF_2 lb	R	R_1	R_2
60.0	12.0	0.050	1.0	0.06250	6611.	4396.	3487.	21.53	20.61	15.46
75.0	12.0	0.100	1.0	0.15625	14597.	9952.	8253.	18.38	14.54	10.91
75.0	12.0	0.100	2.0	0.06250	17670.	9819.	8142.	18.41	14.54	10.91
90.0	12.0	0.050	1.0	0.15625	10495.	7115.	6160.	31.24	20.61	15.46
60.0	12.0	0.100	2.0	0.15625	15629.	14188.	11255.	16.26	14.54	10.91
75.0	12.0	0.050	1.0	0.25000	12466.	8501.	7050.	35.82	20.61	15.46
90.0	12.0	0.150	2.0	0.15625	32719.	18753.	16238.	16.22	11.85	8.89
60.0	12.0	0.050	3.0	0.15625	16560.	6785.	5382.	24.53	20.61	15.46
90.0	12.0	0.150	1.0	0.25000	21224.	15684.	13581.	19.19	11.85	8.89
90.0	12.0	0.150	3.0	0.06250	38176.	18784.	16264.	17.96	11.85	8.89
75.0	12.0	0.100	3.0	0.25000	28530.	22476.	18639.	21.29	14.54	10.91
60.0	12.0	0.050	2.0	0.25000	16560.	8952.	7101.	28.55	20.61	15.46
75.0	12.0	0.050	2.0	0.15625	15806.	6461.	5358.	29.06	20.61	15.46
75.0	12.0	0.050	3.0	0.06250	18332.	7752.	6428.	30.10	20.61	15.46
90.0	12.0	0.100	2.0	0.25000	23820.	17844.	15451.	23.80	14.54	10.91
75.0	12.0	0.150	1.0	0.06250	14080.	9400.	7795.	11.91	11.85	8.89
60.0	12.0	0.150	3.0	0.25000	29134.	27173.	21555.	14.63	11.85	8.89
75.0	12.0	0.150	3.0	0.15625	28302.	21493.	17824.	15.80	11.85	8.89
90.0	12.0	0.050	3.0	0.25000	21241.	8104.	7017.	24.39	20.61	15.46
60.0	12.0	0.150	2.0	0.06250	16001.	11695.	9277.	10.81	11.85	8.89
90.0	12.0	0.100	3.0	0.15625	27584.	17657.	15289.	20.42	14.54	10.91
75.0	12.0	0.150	2.0	0.25000	21896.	21827.	18100.	17.64	11.85	8.89
60.0	12.0	0.100	3.0	0.06250	17490.	10976.	8707.	15.89	14.54	10.91
60.0	12.0	0.100	1.0	0.25000	15111.	16845.	13363.	20.96	14.54	10.91
90.0	12.0	0.050	2.0	0.06250	12113.	6645.	5754.	27.22	20.61	15.46
90.0	12.0	0.100	1.0	0.06250	14275.	7778.	6735.	21.83	14.54	10.91
60.0	12.0	0.150	1.0	0.15625	13571.	11965.	9491.	12.46	11.85	8.89

Note:
MTF_t = experimental thrust force,
MTF_1 = theoretical thrust force(Eqs 9.2.2 + 9.3.2 + 9.3.3),
MTF_2 = theoretical thrust force(Eqs 9.2.1 + 9.3.2 + 9.3.3),
R = experimental FT/FR,
R_1 = theoretical FT/FR (Eq. 7.3.5),
R_2 = theoretical FT/FR (Eq. 7.3.6),

Table E.2.2 Cutting tests on Charcoal Gray Granite [Ozdemir et al. (1977)]

θ deg.	D in	p in	s in	r in	MTF_t lb	MTF_1 lb	MTF_2 lb	R	R_1	R_2
75.0	12.0	0.050	2.0	0.06250	13930.	9992.	8398.	30.28	20.61	15.46
75.0	12.0	0.050	1.0	0.15625	15484.	10199.	8573.	31.28	20.61	15.46
75.0	12.0	0.100	1.0	0.06250	14928.	10960.	9212.	15.39	14.54	10.91
90.0	12.0	0.050	1.0	0.06250	15087.	7413.	6510.	29.30	20.61	15.46
60.0	12.0	0.050	1.0	0.25000	14934.	14139.	11361.	37.71	20.61	15.46
75.0	12.0	0.150	3.0	0.06250	22280.	25701.	21602.	10.78	11.85	8.89
60.0	12.0	0.100	3.0	0.25000	27052.	26608.	21380.	15.94	14.54	10.91
75.0	12.0	0.150	1.0	0.25000	28109.	24364.	20478.	15.28	11.85	8.89
60.0	12.0	0.050	2.0	0.15625	14154.	10717.	8612.	34.27	20.61	15.46
90.0	12.0	0.100	1.0	0.25000	22907.	19907.	17481.	20.01	14.54	10.91
60.0	12.0	0.150	2.0	0.25000	28647.	35045.	28160.	15.67	11.85	8.89
60.0	12.0	0.150	3.0	0.15625	24687.	32734.	26303.	11.39	11.85	8.89
75.0	12.0	0.050	3.0	0.25000	23754.	13420.	11280.	24.12	20.61	15.46
90.0	12.0	0.150	1.0	0.15625	28347.	20921.	18371.	13.62	11.85	8.89
90.0	12.0	0.100	3.0	0.06250	25380.	21255.	18665.	17.95	14.54	10.91
90.0	12.0	0.150	2.0	0.06250	30425.	24196.	21248.	14.97	11.85	8.89
75.0	12.0	0.100	3.0	0.15625	25260.	27212.	22872.	17.31	14.54	10.91
75.0	12.0	0.100	2.0	0.25000	32447.	28970.	24350.	18.55	14.54	10.91
75.0	12.0	0.150	2.0	0.15625	27429.	27704.	23285.	15.86	11.85	8.89
60.0	12.0	0.100	1.0	0.15625	15063.	15846.	12733.	18.62	14.54	10.91
60.0	12.0	0.150	1.0	0.06250	13529.	13062.	10496.	10.69	11.85	8.89
60.0	12.0	0.050	3.0	0.06250	15514.	12028.	9665.	20.77	20.61	15.46
60.0	12.0	0.100	2.0	0.06250	12336.	14156.	11375.	15.75	14.54	10.91
90.0	12.0	0.100	2.0	0.15625	29031.	22745.	19973.	20.34	14.54	10.91
90.0	12.0	0.050	3.0	0.15625	23695.	19441.	17072.	24.28	20.61	15.46
90.0	12.0	0.050	2.0	0.25000	29937.	12785.	11227.	28.84	20.61	15.46
90.0	12.0	0.150	3.0	0.25000	60295.	42859.	37636.	17.99	11.85	8.89

Note:
MTF_t = experimental thrust force,
MTF_1 = theoretical thrust force(Eqs 9.2.2 + 9.3.2 + 9.3.3),
MTF_2 = theoretical thrust force(Eqs 9.2.1 + 9.3.2 + 9.3.3),
R = experimental FT/FR,
R_1 = theoretical FT/FR (Eq. 7.3.5),
R_2 = theoretical FT/FR (Eq. 7.3.6),

Table E.2.3 Cutting tests on Tennessee Marble [Ozdemir et al. (1977)]

θ deg.	D in	p in	s in	r in	MTF_t lb	MTF_1 lb	MTF_2 lb	R	R_1	R_2
75.0	12.0	0.050	1.0	0.06250	6157.	4035.	3136.	28.77	20.61	15.46
60.0	12.0	0.050	1.0	0.15625	6701.	6101.	4548.	20.81	20.61	15.46
60.0	12.0	0.100	1.0	0.06250	6576.	5698.	4248.	10.32	14.54	10.91
60.0	12.0	0.050	2.0	0.06250	8171.	5590.	4168.	29.18	20.61	15.46
90.0	12.0	0.100	1.0	0.15625	12325.	9217.	7459.	25.31	14.54	10.91
90.0	12.0	0.100	2.0	0.06250	14782.	9945.	8048.	22.40	14.54	10.91
90.0	12.0	0.050	2.0	0.15625	12835.	9097.	7362.	30.27	20.61	15.46
75.0	12.0	0.100	1.0	0.25000	14054.	11700.	9093.	27.72	14.54	10.91
75.0	12.0	0.150	1.0	0.15625	15725.	11188.	8696.	17.11	11.85	8.89
75.0	12.0	0.050	3.0	0.15625	13450.	5825.	4527.	23.35	20.61	15.46
90.0	12.0	0.050	1.0	0.25000	9066.	7327.	5929.	32.15	20.61	15.46
60.0	12.0	0.150	1.0	0.25000	16528.	14106.	10516.	15.76	11.85	8.89
60.0	12.0	0.150	3.0	0.06250	15326.	12879.	9601.	10.57	11.85	8.89
75.0	12.0	0.100	3.0	0.06250	15085.	10842.	8427.	15.00	14.54	10.91
75.0	12.0	0.150	2.0	0.06250	14942.	11985.	9315.	12.57	11.85	8.89
75.0	12.0	0.050	2.0	0.25000	10685.	7665.	5957.	29.11	20.61	15.46
75.0	12.0	0.100	2.0	0.15625	11236.	12690.	9863.	19.99	14.54	10.91
60.0	12.0	0.050	3.0	0.25000	11900.	8049.	6000.	24.34	20.61	15.46
60.0	12.0	0.100	3.0	0.15625	14624.	15624.	11647.	17.75	14.54	10.91
60.0	12.0	0.150	2.0	0.15625	14281.	15214.	11342.	12.63	11.85	8.89
60.0	12.0	0.100	2.0	0.25000	14996.	15146.	11291.	21.03	14.54	10.91
90.0	12.0	0.150	1.0	0.06250	15866.	9805.	7935.	16.91	11.85	8.89
90.0	12.0	0.050	3.0	0.06250	12164.	7358.	5955.	17.60	20.61	15.46
90.0	12.0	0.150	2.0	0.25000	23704.	20054.	16229.	13.94	11.85	8.89
90.0	12.0	0.150	3.0	0.15625	26522.	20766.	16805.	13.20	11.85	8.89
90.0	12.0	0.100	3.0	0.25000	24985.	19759.	15990.	13.80	14.54	10.91
75.0	12.0	0.150	3.0	0.25000	24204.	24102.	18732.	10.76	11.85	8.89

Note:
MTF_t = experimental thrust force,
MTF_1 = theoretical thrust force(Eqs 9.2.2 + 9.3.2 + 9.3.3),
MTF_2 = theoretical thrust force(Eqs 9.2.1 + 9.3.2 + 9.3.3),
R = experimental FT/FR,
R_1 = theoretical FT/FR (Eq. 7.3.5),
R_2 = theoretical FT/FR (Eq. 7.3.6),

Appendix F

OUTPUT OF BOUDARY ELEMENT ANALYSIS

F.1 AN OUTPUT FILE OF BOUNDARY ELEMENT ANALYSIS

```
* * * STRESS FIELDS OF ROCK INDENTATION * * *

* * *              AND DISC CUTTING              * * *


    * MATERIAL PROPERTIES *


YOUNGS MODULUS (MPa) = 5510.

POISSONS RATIO = 0.275

COMPRESSIVE STRENGTH (MPa) = 40.220

TENSILE STRENGTH (MPa) = 3.020

ANGLE OF INTERNAL FRICTION (degree) = 36.2


    * DISC CUTTER GEOMETRY, SPACING AND PENETRATION *


DISC CUTTER ANGLE (degree) = 60.

DISC DIAMETER (mm) = 150.

DISC CUTTER TIP RADIUS (mm) = 0.

SPACING DISTANCE (mm) = 40.

PENETRATION DEPTH (mm) = 2.
```

DISPLACEMENTS AND STRESSES AT NODES AND INTERNAL POINTS

No	U	V	SX	SXY	SY	SZ
1	0.00003	0.00031	-0.1	-0.0	-0.0	-0.0
2	0.00003	0.00062	-1.3	-0.0	-0.0	-0.4
3	0.00004	0.00070	-1.8	-0.0	-0.0	-0.5
4	0.00004	0.00084	-1.6	-0.0	-0.0	-0.5
5	0.00004	0.00095	-2.1	-0.0	-0.0	-0.6
6	0.00004	0.00104	-2.0	-0.0	-0.0	-0.5
7	0.00004	0.00112	-3.2	-0.0	-0.0	-0.9
8	0.00005	0.00118	3.6	-0.0	-0.0	1.0
9	0.00004	0.00131	24.6	-0.0	-0.0	6.8
10	0.00004	0.00143	44.1	-0.0	-0.0	12.1
11	0.00004	0.00147	76.4	-0.0	-0.0	21.0
12	0.00004	0.00151	130.5	-0.0	-0.0	35.9
13	0.00004	0.00154	212.9	-0.0	-0.0	58.5
14	0.00003	0.00159	374.7	-0.0	-0.0	103.0
15	0.00003	0.00164	811.4	-0.0	-0.0	223.1
16	0.00002	0.00170	1892.7	-0.0	-0.0	520.5
17	0.0	0.00176	3266.3	-4711.0	5124.3	2307.4
18	0.0	0.00183	3571.2	-2030.2	9415.0	3571.2
19	0.0	0.00189	4003.0	-1998.2	10553.4	4003.0
20	0.0	0.00195	6145.4	-2273.6	16201.6	6145.4
21	0.0	0.00200	13703.0	1.4	36126.2	13703.0
22	0.0	0.00195	6145.4	2277.3	16201.5	6145.4
23	0.0	0.00189	4003.0	2001.6	10553.3	4003.0
24	0.0	0.00183	3571.1	2034.2	9414.8	3571.1
25	0.0	0.00176	3267.8	4719.5	5122.3	2307.3

26	-.00002	0.00170	1896.8	-0.0	-0.0	521.6
27	-.00003	0.00164	814.4	-0.0	-0.0	224.0
28	-.00003	0.00159	376.6	-0.0	-0.0	103.6
29	-.00004	0.00154	214.3	-0.0	-0.0	58.9
30	-.00004	0.00151	131.7	-0.0	-0.0	36.2
31	-.00004	0.00147	77.2	-0.0	-0.0	21.2
32	-.00004	0.00143	44.7	-0.0	-0.0	12.3
33	-.00004	0.00131	25.0	-0.0	-0.0	6.9
34	-.00005	0.00118	3.8	-0.0	-0.0	1.1
35	-.00004	0.00112	-3.1	-0.0	-0.0	-0.8
36	-.00004	0.00104	-1.9	-0.0	-0.0	-0.5
37	-.00004	0.00095	-2.0	-0.0	-0.0	-0.5
38	-.00004	0.00084	-1.6	-0.0	-0.0	-0.4
39	-.00004	0.00070	-1.6	-0.0	-0.0	-0.4
40	-.00003	0.00063	-2.1	-0.0	-0.0	-0.6
41	-.00003	0.00063	0.4	0.6	1.1	0.4
42	-.00003	0.00062	0.4	0.6	1.1	0.4
43	-.00003	0.00062	-5.2	4.5	-3.9	-2.5
44	-.00003	0.00061	-5.2	4.5	-3.9	-2.5
45	-.00003	0.00061	-0.1	-0.0	-0.0	-0.0
46	-.00003	0.00031	-0.1	-0.0	-0.0	-0.0
47	0.00000	0.00080	-149.9	-482.1	-104.0	-69.8
48	0.00006	0.00092	173.1	39.5	-1151.2	-269.0
49	0.00002	0.00127	-385.5	-369.4	553.8	46.3
50	0.00004	0.00131	368.0	-202.5	-552.9	-50.9
51	-.00004	0.00131	368.2	202.3	-553.0	-50.8
52	-.00002	0.00127	-385.4	369.6	553.7	46.3
53	-.00006	0.00092	173.3	-39.6	-1151.1	-268.9

54	-.00006	0.00094	344.2	59.6	-177.9	45.7
55	0.00002	0.00082	-42.1	-183.3	-187.3	-63.1
56	0.00005	0.00107	253.2	40.6	-446.8	-53.2
57	0.00003	0.00125	24.5	-67.5	-26.8	-0.6
58	0.00002	0.00134	33.5	-25.0	-7.0	7.3
59	-.00003	0.00134	33.6	25.0	-7.0	7.3
60	-.00003	0.00125	24.6	67.5	-26.8	-0.6
61	-.00005	0.00107	253.4	-40.8	-446.7	-53.2
62	-.00005	0.00093	-21.0	-7.9	26.3	1.4
63	0.00005	0.00088	64.3	-43.1	-149.1	-23.3
64	0.00002	0.00113	30.6	-7.8	-21.5	2.5
65	0.00001	0.00126	26.9	-17.1	3.7	8.4
66	-.00001	0.00134	39.5	-31.6	12.5	14.3
67	0.00001	0.00134	39.6	31.6	12.5	14.3
68	-.00001	0.00126	27.0	17.1	3.8	8.5
69	-.00003	0.00113	30.8	7.7	-21.5	2.6
70	-.00003	0.00091	-8.4	41.3	-20.2	-7.9
71	0.00004	0.00094	26.6	24.1	-18.7	2.2
72	-.00001	0.00114	19.2	-16.1	7.0	7.2
73	-.00003	0.00126	31.7	-30.6	18.5	13.8
74	-.00005	0.00133	37.6	-45.8	36.4	20.4
75	0.00005	0.00133	37.7	45.7	36.5	20.4
76	0.00003	0.00126	31.8	30.5	18.6	13.8
77	0.00001	0.00114	19.3	16.0	7.1	7.3
78	-.00003	0.00093	19.8	2.4	-19.7	0.0
79	-.00001	0.00094	6.5	-5.1	8.6	4.2
80	-.00005	0.00113	18.6	-23.2	18.2	10.1
81	-.00006	0.00123	17.1	-32.5	39.0	15.4

82	-.00006	0.00128	12.1	-35.2	56.3	18.8
83	0.00006	0.00128	12.1	35.2	56.4	18.8
84	0.00006	0.00123	17.1	32.5	39.1	15.4
85	0.00005	0.00113	18.6	23.2	18.4	10.2
86	0.00001	0.00094	9.1	4.8	4.9	3.9
87	-.00000	0.00218	-145.6	0.0	1642.0	411.5
88	-.00000	0.00198	-75.8	-0.0	835.3	208.9
89	-.00000	0.00178	-39.1	-0.0	420.6	104.9
90	-.00000	0.00158	-19.8	-0.0	210.5	52.4
91	-.00000	0.00138	-9.9	-0.0	105.2	26.2
92	0.00000	0.00114	-4.2	0.0	46.7	11.7
93	0.00000	0.00101	-2.6	0.0	30.1	7.6
94	0.00000	0.00092	-1.9	0.0	22.4	5.6
95	0.00000	0.00085	-1.7	0.0	18.0	4.5
96	0.00000	0.00079	-1.6	0.0	15.1	3.7

PRINCIPAL STRESSES AT NODES AND INTERNAL POINTS

No	X	Y	PS1	PS12	PS2	θ
1	-.20000	0.0	-0.0	0.0	-0.1	0.0
2	-.04000	0.0	0.0	0.6	-1.3	0.0
3	-.02705	0.0	0.0	0.9	-1.8	0.0
4	-.01281	0.0	0.0	0.8	-1.6	0.0
5	-.00737	0.0	0.0	1.0	-2.1	0.0
6	-.00462	0.0	0.0	1.0	-2.0	0.0
7	-.00311	0.0	0.0	1.6	-3.2	0.0
8	-.00226	0.0	3.6	1.8	0.0	0.0
9	-.00115	0.0	24.6	12.3	0.0	0.0

*	10	-.00064	0.0	44.1	22.0	0.0	0.0
*	11	-.00052	0.0	76.4	38.2	0.0	0.0
*	12	-.00043	0.0	130.5	65.3	0.0	0.0
*	13	-.00036	0.0	212.9	106.4	0.0	0.0
*	14	-.00029	0.0	374.7	187.3	0.0	0.0
*	15	-.00023	0.0	811.4	405.7	0.0	0.0
*	16	-.00018	0.0	1892.7	946.3	0.0	0.0
*	17	-.00014	0.0	8997.0	4801.7	-606.4	39.42
	18	-.00010	0.0	10051.0	3558.0	2935.1	17.40
	19	-.00006	0.0	11114.8	3836.6	3441.6	15.69
	20	-.00003	0.0	16691.8	5518.2	5655.3	12.17
	21	0.0	0.0	36126.2	11211.6	13703.0	-0.00
	22	0.00003	0.0	16693.2	5519.7	5653.7	-12.18
	23	0.00006	0.0	11116.5	3838.3	3439.8	-15.72
	24	0.00010	0.0	10053.2	3560.2	2932.8	-17.42
*	25	0.00014	0.0	9004.8	4809.7	-614.6	-39.44
*	26	0.00018	0.0	1896.8	948.4	0.0	0.0
*	27	0.00023	0.0	814.4	407.2	0.0	0.0
*	28	0.00029	0.0	376.6	188.3	0.0	0.0
*	29	0.00036	0.0	214.3	107.1	0.0	0.0
*	30	0.00043	0.0	131.7	65.8	0.0	0.0
*	31	0.00052	0.0	77.2	38.6	0.0	0.0
*	32	0.00064	0.0	44.7	22.3	0.0	0.0
	33	0.00115	0.0	25.0	12.5	0.0	0.0
	34	0.00226	0.0	3.8	1.9	0.0	0.0
	35	0.00311	0.0	0.0	1.5	-3.1	0.0
	36	0.00462	0.0	0.0	0.9	-1.9	0.0
	37	0.00737	0.0	0.0	1.0	-2.0	0.0

	38	0.01281	0.0	0.0	0.8	-1.6	0.0
	39	0.02705	0.0	0.0	0.8	-1.6	0.0
	40	0.03885	0.0	0.0	1.1	-2.1	0.0
	41	0.03885	0.0	1.4	0.7	-0.0	-29.90
	42	0.04000	0.00200	1.4	0.7	-0.0	-29.90
	43	0.04000	0.00200	0.0	4.5	-9.1	-40.89
	44	0.04231	0.0	0.0	4.5	-9.1	-40.89
	45	0.04231	0.0	0.0	0.1	-0.1	0.0
	46	0.20000	0.0	0.0	0.0	-0.1	0.0
*	47	-.04000	0.00100	355.7	482.7	-609.6	43.64
*	48	-.02000	0.00100	174.2	663.3	-1152.3	1.71
*	49	-.01333	0.00100	681.6	597.5	-513.4	19.09
*	50	-.01000	0.00100	410.6	503.0	-595.5	-11.87
*	51	0.01000	0.00100	410.7	503.1	-595.5	11.86
*	52	0.01333	0.00100	681.7	597.6	-513.4	-19.10
*	53	0.02000	0.00100	174.5	663.4	-1152.3	-1.71
*	54	0.03885	0.00100	350.9	267.8	-184.6	6.43
*	55	-.04000	0.00200	82.5	197.2	-311.9	-34.20
*	56	-.02000	0.00200	255.6	352.3	-449.1	3.31
*	57	-.01333	0.00200	71.0	72.2	-73.3	-34.59
*	58	-.01000	0.00200	45.4	32.2	-18.9	-25.50
*	59	0.01000	0.00200	45.5	32.2	-18.9	25.46
*	60	0.01333	0.00200	71.1	72.2	-73.3	34.56
*	61	0.02000	0.00200	255.7	352.4	-449.1	-3.32
*	62	0.03885	0.00200	27.6	24.9	-22.3	9.24
*	63	-.04000	0.00400	72.7	115.1	-157.4	-11.00
*	64	-.02000	0.00400	31.8	27.2	-22.7	-8.28
*	65	-.01333	0.00400	36.0	20.7	-5.4	-27.97

*	66	-.01000	0.00400	60.3	34.4	-8.4	-33.45
*	67	0.01000	0.00400	60.4	34.4	-8.4	33.42
*	68	0.01333	0.00400	36.1	20.7	-5.3	27.93
*	69	0.02000	0.00400	31.9	27.2	-22.6	8.21
*	70	0.04000	0.00400	27.4	41.7	-56.1	40.94
*	71	-.04000	0.00800	37.0	33.1	-29.1	23.36
*	72	-.02000	0.00800	30.3	17.2	-4.1	-34.66
*	73	-.01333	0.00800	56.4	31.3	-6.2	-38.91
*	74	-.01000	0.00800	82.8	45.8	-8.7	-44.63
*	75	0.01000	0.00800	82.8	45.7	-8.7	44.63
*	76	0.01333	0.00800	56.4	31.2	-6.1	38.90
*	77	0.02000	0.00800	30.4	17.1	-3.9	34.61
*	78	0.04000	0.00800	20.0	19.9	-19.9	3.50
	79	-.04000	0.01600	12.7	5.2	2.4	39.35
*	80	-.02000	0.01600	41.6	23.2	-4.8	-44.74
*	81	-.01333	0.01600	62.4	34.3	-6.3	35.69
*	82	-.01000	0.01600	75.8	41.6	-7.4	28.94
*	83	0.01000	0.01600	75.8	41.6	-7.4	-28.90
*	84	0.01333	0.01600	62.4	34.3	-6.2	-35.64
*	85	0.02000	0.01600	41.6	23.2	-4.7	44.87
	86	0.04000	0.01600	12.2	5.2	1.8	33.08
*	87	0.0	0.00100	1642.0	893.8	-145.6	-0.00
*	88	0.0	0.00200	835.3	455.5	-75.8	0.00
*	89	0.0	0.00400	420.6	229.8	-39.1	0.00
*	90	0.0	0.00800	210.5	115.2	-19.8	0.00
*	91	0.0	0.01600	105.2	57.6	-9.9	0.01
*	92	0.0	0.03600	46.7	25.5	-4.2	-0.00
	93	0.0	0.05600	30.1	16.4	-2.6	-0.03

94	0.0	0.07600	22.4	12.2	-1.9	-0.05
95	0.0	0.09600	18.0	9.8	-1.7	-0.06
96	0.0	0.11600	15.1	8.3	-1.6	-0.07

*** AVERAGE CONTACT PRESSURE (MPa) = 1202.22 ***

*** TOTAL THRUST FORCE (kN) = 31.84 ***